AD-A253 108

AGARD-CP-512

AGARD

ADVISORY GROUP FOR AEROSPACE RESEARCH & DEVELOPMENT

7 RUE ANCELLE 92200 NEUILLY SUR SEINE FRANCE

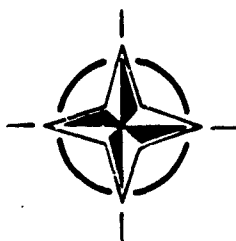### AGARD CONFERENCE PROCEEDINGS 512

Combat Aircraft Noise

(Le Bruit Généré par les Avions de Combat)

NORTH ATLANTIC TREATY ORGANIZATION

Published April 1992

Distribution and Availability on Back Cover

COMPONENT PART NOTICE

THIS PAPER IS A COMPONENT PART OF THE FOLLOWING COMPILATION REPORT:

TITLE: Combat Aircraft Noise held in Bonn, Germany on 23-25 October 1991

____(Le Bruit Genere par les Avions de Combat)____

_____

TO ORDER THE COMPLETE COMPILATION REPORT, USE ___AD-A253 108___.

THE COMPONENT PART IS PROVIDED H⁻RE TO ALLOW USERS ACCESS TO IND⁻'IDUALLY
AUTHORED SECTIONS OF PROCEEDING, ANNALS, SYMPOSIA, ETC. HOWEVER, THE COMPONENT
SHOULD BE CONSIDERED WITHIN THE CONTEXT OF THE OVERALL COMPILATION REPORT AND
NOT AS A STAND-ALONE TECHNICAL REPORT.

THE FOLLOWING COMPONENT PART NUMBERS COMPRISE THE COMPILATION REPORT:

AD#:_____PO07 512___thru___AD#__PO07 533_____

AD#:_____ AD#:_____

AD#:_____ AD#:_____

Accession For

NTIS GRA&I	☑
DTIC TAB	☐
Unannounced	☐
Justification	

By_____
Distribution/
Availability Codes

Dist	Avail and/or Special
A-l	21

AGARD

ADVISORY GROUP FOR AEROSPACE RESEARCH & DEVELOPMENT

7 RUE ANCELLE 92200 NEUILLY SUR SEINE FRANCE

AGARD CONFERENCE PROCEEDINGS 512

Combat Aircraft Noise

(Le Bruit Généré par les Avions de Combat)

North Atlantic Treaty Organization
Organisation du Traité de l'Atlantique Nord

92-15450

92 6 1? ∩┌┐

The Mission of AGARD

According to its Charter, the mission of AGARD is to bring together the leading personalities of the NATO nations in the fields of science and technology relating to aerospace for the following purposes:

— Recommending effective ways for the member nations to use their research and development capabilities for the common benefit of the NATO community;

— Providing scientific and technical advice and assistance to the Military Committee in the field of aerospace research and development (with particular regard to its military application);

— Continuously stimulating advances in the aerospace sciences relevant to strengthening the common defence posture;

— Improving the co-operation among member nations in aerospace research and development;

— Exchange of scientific and technical information;

— Providing assistance to member nations for the purpose of increasing their scientific and technical potential;

— Rendering scientific and technical assistance, as requested, to other NATO bodies and to member nations in connection with research and development problems in the aerospace field.

The highest authority within AGARD is the National Delegates Board consisting of officially appointed senior representatives from each member nation. The mission of AGARD is carried out through the Panels which are composed of experts appointed by the National Delegates, the Consultant and Exchange Programme and the Aerospace Applications Studies Programme. The results of AGARD work are reported to the member nations and the NATO Authorities through the AGARD series of publications of which this is one.

Participation in AGARD activities is by invitation only and is normally limited to citizens of the NATO nations.

Recent Publications of
the Propulsion and Energetics Panel

Theme

The noise emission from combat aircraft is increasingly perceived by the public as a nuisance, particularly in the densely populated areas of Central Europe. Besides procedural measures with respect to military flight missions, it will be necessary in the future to take other steps towards the reduction of military flight noise at the sources of the noise emission themselves. This is also dictated by the uninterrupted trends to higher military flight performance of combat aircraft, which is inevitably connected with still higher noise.

Other than for civil aircraft the physics of noise generation and reduction of military aircraft and propulsion systems is not well understood, and one has to admit the existence of important gaps in our basic understanding.

Despite this situation one can think of conceivable technical measures towards noise reduction which concern on the one hand the propulsion system itself such as low noise nozzle concepts or noise-reduced turbomachine and afterburner designs, and on the other hand possibilities for reduced noise emission on a system design level, such as non-afterburning variable cycle propulsion systems, aircraft with reduced drag by internal weapon stores or aircraft with shielded noise sources.

The purpose of this meeting was to report the present state of knowledge on fixed wing aircraft noise emission and its remedies.

Identification of the main noise sources and mechanisms of noise generation and propagation, particularly arising in the propulsion system, and the possibilities for noise reduction was the main focus of the meeting.

Thème

L'émission de bruit par les avions de combat est de plus en plus considérée par le public comme une nuisance, en particulier dans les zones de l'Europe centrale à forte densité de population. En plus des procédures qu'il conviendrait d'adopter pour les missions aériennes militaires à l'avenir, il faudra réduire le niveau de bruit à la source. Le problème est du reste aggravé par les efforts soutenus pour l'amélioration des performances de vol des avions de combat, amélioration qu i engendre, inévitablement, des niveaux de bruit toujours plus élevés.

Le cas des avions civils mis à part, la physique de la génération et de la réduction du bruit des propulseurs n'est pas encore bien comprise et il existe d'importantes lacunes dans nos connaissances de base dans ce domaine.

Certaines mesures techniques ont pourtant été envisagés dans le sens de la réduction du bruit: d'une part en ce qui concerne le système de propulsion lui-même avec les études de tuyères à dispositifs atténuateurs de bruit, ainsi que les turbomachines et les réchauffes à bruit réduit: et d'autre part l'examen des possibilités de réduction du bruit au niveau de la conception des systèmes, avec des propulseurs sans réchauffe à cycle variable, la réduction de la traînée par l'intégration de la soute d'armes et le blindage des sources de bruit.

La réunion avait pour objet de présenter l'état de l'art sur les connaissances en matière de bruit émis par les aéronefs à voilure fixe et d'examiner les remèdes envisageables.

L'accent était mis sur l'identification des principales sources de bruit, les mécanismes de génération et de propagation du bruit, en particulier au sein des systèmes de propulsion, et les différentes possibilités en ce qui concerne la réduction du bruit.

Propulsion and Energetics Panel

Chairman: Prof. Dr A. Üçer
Middle East Technical University
O D T Ü
Makina Müh. Bölümü
Ankara
Turkey

Deputy Chairman: Mr R.E. Henderson
Deputy for Technology
Aero Propulsion & Power Laboratory
WL/POT
Wright Patterscn Air Force Base
OHIO 45433-6563
United States

PROGRAMME COMMITTEE

Prof. Dr-Ing. L. Fottner (Chairman)
Universität der Bundeswehr München
Institut für Strahlantriebe
Werner Heisenberg-Weg 39
W-8014 Neubiberg
Germai.y

Ir W.B. de Wolf
National Aerospace Laboratory
PO Box 153
8300 AD Emmeloord
The Netherlands

Dr Enrique Fraga Fernandez Cuevas
Director del departamento de
   Motopropulsion y Energia
INTA
Crta. de Torrejon a Ajalvir, Km.4
28850 Torrejon de Ardoz
Madrid
Spain

M. Ing. Princ. Arm. Philippe Ramette
DGT-Chef de Departement Propulsion
Dassault Aviation
78 quai Marcel Dassault
92214 Saint-Cloud
France

Mr Gregory M. Reck
Director, Space Technology
Office of Aeronautics, Exploration and
   Technology
NASA Headquarters, Code RS
Washington DC 20546
United States

Mr David J. Way
Superintendent Turbomachinery
Propulsion Department
Defence Research Agency (Aerospace Division)
RAE Pyestock, Farnborough
Hants GU14 0LS
United Kingdom

HOST NATION COORDINATOR

Regierungsdirektor F. Günther

PANEL EXECUTIVE

Dr E. Riester

Mail from Europe:
AGARD—OTAN
Attn: PEP Executive
7, rue Ancelle
F-92200 Neuilly-sur-Seine
France

Mail from US and Canada:
AGARD—NATO
Attn: PEP Executive
Unit 21551
APO AE 09777

Tel: 33 (1) 47 38 57 85
Telex: 610176F
Telefax: 33 (1) 47 38 57 99

ACKNOWLEDGEMENT

Contents

Reference

SESSION I — USER'S DEMAND, EXPERIENCE ON NOISE EFFECTS

SESSION II — MECHANISMS OF NOISE GENERATION

SESSION III — NOISE MEASUREMENTS, PREDICTION METHODS

SESSION IV — NOISE REDUCTION

TECHNICAL EVALUATION REPORT
W.B. de Wolf
National Aerospace Laboratory NLR,
P.O. Box 90502, 1006 BM Amsterdam

SUMMARY

A technical evaluation is presented of the AGARD-
PEP Specialists' Meeting on Combat Aircraft Noise
at Bonn, October 1991. The meeting concentrated on
the noise from combat aircraft on low-altitude
high-speed training missions.
Considerable improvement was reported on the
understanding and prediction of various noise
components. One of the main conclusions was that
the overall effectiveness of reduction of engine
based noise critically depends on the airframe
noise level at high flight speeds and more work is
required in this area to clarify the situation.

1   INTRODUCTION

The annoyance of aircraft noise in the vicinity of
military airfields has been reduced by operational
measures and by sound insulation of dwellings where
certain noise levels still are exceeded. The noise
situation around those airfields is still of
concern but seems to be more or less accepted.
In contrast, the noise from combat aircraft on low-
altitude, high-speed training missions over
populated areas has led to massive complaints,
particularly in Germany. This, and a few accidents,
led to the decision that from September 1990 all
flying below 1000 ft (300 m) above ground level
over Germany became forbidden. The Luftwaffe is now
carrying out its training for low-altitude flight
missions in Canada. In other European countries and
in the U.S. the noise from low flying combat
aircraft has not led so far to similar massive
public reactions.

In a number of NATO countries studies were
performed during the last few years specifically on
the noise from low flying combat aircraft. These
studies related to the character of the noise
impact, including the 'startle' effect, the
identification and prediction of the various
contributing noise sources and their possible
reduction by technical measures.

The purpose of this meeting on Combat Aircraft
Noise was "to report the present state of knowledge
on fixed-wing aircraft noise emissions and its
remedies". This scope is wider than the noise from
low flying combat aircraft only and is reflected in
the variety of presented papers, about 8 of the 26
papers being of a more general character.

Topics of these more general papers were on the noise from an outdoor engine test facility (6), airframe noise from transport aircraft (7), pressure fluctuations in cavities (7), the sonic boom from supersonic aircraft (12), fan noise generation and reduction (15), combustion noise (18), theory of noise generation in subsonic jets (24) and supersonic elliptic jets (20), experiments on jet screech related to acoustic fatigue problems of the airframe (20) and the prospects of reducing propeller noise by active control (29). Most of the papers were of good to outstanding quality However the present technical evaluation will be confined to the noise from low flying combat aircraft at high speed.

2 THE NOISE FROM LOW FLYING COMBAT AIRCRAFT

From the meeting it emerged that:
1) The noise from low flying combat aircraft tends to be no longer accepted by the public.
2) Its annoyance is not only caused by the high noise levels but also by its unexpected sudden occurrence ('startle' effect).
3) Analysis of recent flight test data has considerably improved our understanding and prediction of the various noise components.
4) Prospects for the reduction of overall noise levels by treatment of the engine based sources critically depend on the airframe noise levels and may thus range from a few to more than 10 decibels.
5) More work is required on the contribution and reduction of the airframe noise levels at high flight speeds and their possible reduction and on the weight and performance penalties of jet noise silencer systems together with their consequences for operational flexibility and cost of implementation.

These five items will be elucidated briefly in the following sections, each ending with a concluding remark. Numbers between parentheses refer to the numbers of the papers in the proceedings.

3 ACCEPTABILITY

The effectiveness of air forces heavily depends on their ability to penetrate through hostile air defence environments. Under these conditions flying extremely low and very fast, combined with additional measures is the best way to maximize operational effectiveness and survivability (1). To be useful, training for these conditions requires flying below 500 ft (3). In fact an actual military operation would require a penetration at 100 ft altitude and as fast as possible, typically 480-600 kts. The present training in Europe is already compromising this situation by mostly flying at 250

ft altitude and 420 kts, with no effective training possibilities in Germany, see the introduction. In three NATO countries, Canada, UK and US, training down to 100 ft is allowed in specially designated areas (3).

The philosophy in the UK is to allow training at 250 ft throughout the country, except over densely populated areas, in order to spread the noise burden as widely as practicable. It was suggested that concentration of the noise in a few areas has been at the heart of the problems in Germany (3).

Flight simulators could help to a limited extent to compensate for the decrease in actual flight training hours which tends to be imposed by budgetary reasons. However for low altitude flights the technology for realistic simulation is still not available and the absence of physical danger strongly influences the training results (2).

It was stressed that further limitations of the possibilities for low altitude training will significantly degrade the capability and survivability of the NATO air forces in an actual wartime situation (1). The operation "Desert Storm" where penetrations at night below 100 ft were performed with remarkably low losses of aircraft owed a great deal of its success to the skill and professionalism of the pilots, acquired on low altitude training missions in peace time (3).

It is concluded that operational measures to significantly reduce the noise from low flying combat aircraft now have virtually come to an end and technical measures at the source are desired.

4   ANNOYANCE

For many combat aircraft noise level data are now available relating to the high-speed fly-over situation at low altitude between 250 ft/75 m and 1000 ft/300 m. These measurements were performed in Germany (9,27), France (10), the UK (22,23) and the USA (4).

As an example, one configuration of a Tornado aircraft flying at an altitude of 250 ft and 420 kts generates a maximum level on the ground of around 110 dBA and this increased at a rate of 1 dBA per 10 kts.

However it is not only the high noise level that matters, but also the onset rate as defined in (4) and expressed in dBA per second. When the Tornado flies over at 250 ft altitude and 420 kts the dBA level increases from the background to the peak at a rate of about 30 dB/sec (27). At lower flight altitudes and higher flight speeds onset rates of

up to 90 dBA/sec are possible (23) with potentially very strong 'startle' effects.

The USAF is presently conducting various laboratory studies to determine the key psychoacoustic parameters associated with the noise exposure from low-flying combat aircraft (4). These suggest that onset rates below 15 dBA/sec do not increase the annoyance while at 30 dBA/sec the penalty to be added to the Sound Exposure Level is 5 dB. For higher onset rates more study is required to determine the penalty. The onset rates quickly diminish with lateral offset.

Concerning the width of the annoyed area, in case of the Tornado (250 ft/75 m) altitude, 460 kts) the corridor where 80 dB(A) is exceeded is about 900 m wide (27). If the aircraft increases its flight altitude from 250 ft/75 m to 1500 ft/450 m the width of this corridor is the same due to the loss in ground attenuation. However the peak level below the aircraft is reduced by about 10 dB.

The noise from low flying aircraft further differs from the airfield environment situation by its single event character. In a typical case 90 dBA may be exceeded every 4 hours while 105 dBA is only exceeded every 60 hours (9). Still a 10 log N event factor seems to apply for a few hundred or a few events per day to calculate the Sound Exposure Levels (4). Additional work on prediction of reactions to individual overflights at some distance to the flight track is underway (19) together with how the audibility is affected by the terrain.

With respect to possible hearing damage it is not the maximum dBA level that counts but again the Sound Exposure Level, which takes also the exposure time into account. Even under the most severe conditions with regular overflights of say 50 per day, of combat aircraft at 250 ft/75 m altitude, hearing damage is very unlikely even after many years of exposure (4).

It is concluded that the sound levels from low flying combat aircraft are now well documented. The effect of the onset rate ('startle' effect) and the effect of the sparse events on human response is under study and good progress is being made.

5   SOURCE ANALYSIS AND PREDICTION

Until recently far field diagnostic measurements and research on aircraft noise have been limited to relatively low forward speeds, say Mach 0.35 because these were aimed at take-off and climb-out situations (5,7,14) through the need to comply with civil noise certification requirements.

For combat aircraft flying at high subsonic flight speeds no meaningful diagnostic measurements were available so far. The structured experimental program of high speed light tests in the UK (22) has provided new understanding. For a Tornado aircraft steady flights were performed at different power settings by allowing the aircraft to ascend or descend. The aircraft was flown with a full stores complement and a 45 degree wing sweep. The measurements revealed the importance of the noise generated by the air flowing past the airframe. This airframe noise yields a significant contribution to the dBA level in the time before overhead and to the peak dBA level and it is sometimes the dominant component. This was concluded after adjusting the data to typical conditions for horizontal steady flight. Diagnostic measurements of this type are mandatory to predict the effect of reductions in the engine noise based on the overall noise of a particular aircraft and configuration.

Significant improvement was also reported on the prediction of jet noise at high subsonic flight speeds (21) using fly-over noise data of four different military aircraft (8). Here it was assumed that the noise was dominated by the jet, producing mixing noise and broadband shock associated noise. The latter occurs if the jet is supersonic and different from the nozzle design Mach number, see also (16). No conclusive indication for the importance of airframe or combustion noise was observed from the frequency spectra in the high flight speed cases examined in (8) and (21). One of the aircraft was a Tornado, but in a cleaner configuration than the configuration measured in the UK (22). It is suggested however in (22) that the measured airframe noise of the Tornado is possibly dominated by the wing trailing edge noise which should be the same for both configurations.

Based on the noise data of (8) an improvement to the classical SAE jet noise prediction method was developed (21). This should considerably improve the prediction accuracy for high speed flight conditions, the difference with the measured fly-over levels being generally less than 2 dB. Differences with the earlier SAE method amount up to 10 dB.

The method contains an empirical factor σ_1 which describes the increase of the turbulence in the jet due to flight, for instance due to the effect of the boundary layer from the rear fuselage. The measurements of (22) showed some 10 dB difference between the "installed" jet noise level and a prediction which includes the effect of forward speed (ESDU-method). This may be attributed to the same phenomenon. More analysis is required to sort out the role of σ_1 and the mixing process in the

jet as affected by the flow around the afterbody. In addition, the twin nozzle configuration of the Tornado may show additional phenomena compared to a single jet and could possibly also affect the airframe noise phenomena in that area (22).

It is concluded that targetted research is required to establish the level of airframe noise in a specific situation. This question remains a critical issue as benefits from jet noise reduction may well bottom on the airframe noise floor at high speed flight conditions. A considerable improvement of the prediction of jet noise at high speed flight conditions was presented but questions concerning installation effects still remain.

6   PROSPECTS FOR NOISE SOURCE REDUCTION

A number of papers (5,14,15,28) reviewed the various options for jet noise silencing. Most of these referred to techniques developed for the earlier subsonic jet transport aircraft with low bypass ratio engines and the Concorde supersonic transport. The best suppressor nozzles at that time, offering significant reductions, show a trade-off of about 0,5 percent loss in gross thrust for each dB jet noise reduction (14) together with an increase in all-up weight.

The Concorde aircraft has engine exhaust conditions similar to combat aircraft. In spite of an extensive research programme no simple universal jet noise silencer was found. Some silencers developed on static ground test rigs were found to be ineffective in flight and were discarded (4). For reduction of the fly-over noise increasing the area of the primary nozzle combined with the power cut-back procedure proved to be effective in reducing the jet noise by some 5 EPNdB (5).

Squeezing of the jet in one direction as used by Concorde (5) (14) or by using elliptic nozzles (16) may reduce the noise from supersonic jets in the region around the major axis. For elliptic nozzles static tests showed reductions of 6 to 7 PNdB along the major axis with little impact on performance (16).

All this work however related to the reduction of jet noise at take-off and climb conditions and not to high subsonic cruise flight. For the latter conditions the trade-off between jet noise reduction and performance losses is not yet known.

For the present problem of jet noise reduction for low-altitude high-speed combat aircraft missions, the simplest option seems to be to open up the engine exhaust nozzle, providing the same thrust with increased mass flow but with lower jet velocity and noise. This procedure is likely to

increase the specific fuel consumption and cause the engine to operate closer to its limits (e.g. shaft speed, choking of bypass duct).

For the Tornado aircraft details were presented how this option might work out (26,27). For the low weight, clean configuration a reduction in the jet noise of about 5 dBA is predicted at Mach 0.7 by opening up the nozzle. It is estimated that the aircraft fuel consumption will hardly be affected in this case because the increase in specific fuel consumption will be compensated by lower intake and afterbody drag. However for the heavy weight aircraft, a higher power setting is required and the nozzle cannot be opened very much without exceeding the engine limits.

This has led to a proposal for flying low altitude training flights of the Tornado in a clean low-weight configuration only. Combined with an open nozzle this might lead to a noise reduction of 8 dBA compared to the standard configuration (27), assuming that the jet noise reduction does not bottom on the airframe noise floor of the clean configuration. Modification of the nozzle control schedule requires only a software change in the engine control unit. More drastic measures like a proposal for a low noise training version of the Tornado with an ejector silencer nozzle (27), need to be considered very cautiously, with all the issues addressed.

Besides, for low-altitude high-speed overflights not only the maximum dB(A) level is important but also the 'startle' effect, caused by the high onset rates. An interesting, but maybe fancy, possibility for reducing this 'startle' effect was identified in (22). It was suggested to decrease the onset rate by adding a powerful sound source, radiating in the forward arc and serving as a warning device.

It is concluded that for the reduction of the noise from the present combat aircraft, flying low-altitude training missions, opening up of the exhaust nozzle and a clean configuration whenever possible is the first thing to consider. For more drastic measures like suppressor nozzles the effects on weight, performance and operational flexibility should be evaluated carefully. The airframe noise floor is likely to be of critical importance.

7 CONCLUDING REMARKS

Very useful work has been done recently to get a
better picture on the possibilities for reduction
of the noise from low flying combat aircraft. More
work is required on the assessment of the airframe
noise levels and their possible source reductions.
Furthermore, not only more information is required
on the weight and performance penalties of jet
noise silencer systems at these high flight speeds,
but also their effects on multi-mission
flexibility, logistics and cost as these aspects
have been identified as possible show stoppers.

For moderate noise reductions by changing the
nozzle schedule, discussions with the operators
should be continued.

For significant reductions of the noise from low
flying combat aircraft at high speed, while
retaining their mission capability, the prospects
are presently unclear.
In response to the public concern and the need for
military alertness, further work should be
performed along the lines identified by this
specialists' meeting. Then it can justifiably be
argued that all reasonable measures have been
pursued to the end, in order to minimize the noise
from low flying, high performance combat aircraft,
without sacrificing their operational capabilities.

8 ACKNOWLEDGEMENT

COMBAT AIRCRAFT OPERATIONS: TRAINING REQUIREMENTS FOR THE GERMAN AIR FORCE TACTICAL FLYING UNITS AND THE NOISE PROBLEM

Oberst i.G. W. Jertz
BMVg-FÜ L III 3
Postfach 1328, 5300 Bonn 1

Summary

Deterrence potential of Air Forces and by that the capability to fulfil their mission in times of war, rests to a high degree with a threat oriented training in peacetime.
Low level flying is a major tactical means to help aircrews reduce the anticipated threat imposed to them by enemy air defence systems to an acceptable degree. The demand for this capability applies also to air defence tasks against attacking fighter bombers.

Military low level flying requires a high degree of proficiency, only to be reached and maintained by constant training. A high performance level is then the key to air power.

The possibilities for this kind of necessary training are restricted by superior demands concerning, amongst others, flying safety and environmental reasons.
Too intensive restrictions might reduce the fighting capability of the wings to such an extent, that mission fulfilment could be seriously endangered.

1   Introduction

In all political endeavors to prevent war such as
- disarmament,
- relaxation of tensions,
- improvement of economic relations,
- reduction of confrontation and
- confidence building measures,
armed forces do continue to play an important role. This is in accordance with the strategy of NATO alliance directed to prevent war by deterrence and by the capability to defend against aggression.

Because of their special characteristics, such as range, speed and by their capability to concentrate fire power, air forces are particularly suited to prevent surprise and to respond rapidly and effectively. Deterrence potential of Air Forces, i.e. their capability to fulfil their missions in times of tension and war, rests to a high degree with an efficient, threat oriented training in peacetime.
The density of air defence systems likely to be expected anywhere in well armed countries do pose significant potential threats and must be considered in any risk assessment.

The effectiveness of air forces heavily depends on their penetration ability through hostile air defence environment. Despite the improvement of ground based air defense weapon and the rising number of aircraft with look-down/shoot-down capabilities, air to ground weapon/systems must be able to fly very fast and very low in order to shorten reaction time available to enemy air defence as well as to escape detection and engagement.
For the near future many air-delivered weapons will continue to be limited to line-of-sight operations. Weapons which do meet key parameters like
- stand off capability
- adaptability
- versatility
- precision (to minimise collateral damage)
- reliability
- maintainability
are all very costly. Therefore present air-to-ground weapons held in stock will continue to influence delivery tactics for the immediate future.

Flying extremely low and very fast combined with additional measures like jinking, terrain masking, dropping chaff and flares and using the onboard electronic counter measure equipment results in a high degree of survivability and operational effectiness which is unattainable by any other manner of operation under present conditions.

In other terms, flight crews must be enabled not only to fly aircraft at altitudes of 100 feet but also to perform their wartime mission.
In order to meet the standard aircrews require a high degree of proficiency, only to be reached and maintained by continued training. The amount and frequency of low-level flying training is dependent on a number of important factors, such as aircrew experience level, aircraft type, role and operating area and topographical conditions.
Complete confidence in all aspects of low level flying and a high level of competence in tactical operations can only be achieved if aircrews have enough opportunities to train their wartime missions already in peacetime.
Restrictions on low flying training opportunities at realistic heights and speeds have already resulted in a decline in the ability of flying personnel. Thus, if NATO air forces are to meet the operational demands, it is essential that each nation develops training programmes which

ensure a high degree of competence and combat effectiveness for aircrews. Based on current ACE FORCES STANDARDS the Luftwaffe has designed a threat orientated TACTICAL COMBAT TRAINING PROGRAM (TCTP) to achieve the required operational readiness and effectiveness of their aircrews within its operational wings. It contains guidelines and annual minimum requirements for the tactical training of aircrews, having successfully completed the initial weapon system training. It can be used to assess the training/combat capabilities of the individual aircrew as well as the combat status of whole squadrons or wings.

At the same time the TCTP serves as an administrative vehicle for data collection and reporting to facilitate effective control over the training standards within the wings and by superior Headquarters.

Type and number of the required tactical missions and events reflect the national ideas on how to optimize operational training within the limitations and restrictions imposed by material, money and environment.

2 Structure of the Tactical Training Program (TCTP)

Basically, the TCTP for flying units is structured into the following areas:

A General
General requirements for flying units like flying hour calculations and areas of special emphasis or interest.

B Tactical
Governs the tactical training requirements in terms of missions, events and runs according to weapon system and role.

C Theory
Lays out the required lessons, which have to be covered during each year. The lessons encompass areas like
- aerial tactics
- weapons and sensors
- ground tactics
- intelligence
- aircraft compontents and procedures
- flying safety and
- electronic warfare.

D Qualifications
Describes the weapons qualification criteria for all types of aircraft and roles

E Combat Status
Contains detailed instructions, how each specific operational status of the individual crew members have to be achieved, tested and maintained.

G Reporting
Covers in detail the upline reporting. Basically quarterly results are to be forwarded to the headquarters containing all pertinent information on flying hours, percentage of missions and events flown, and special problems encountered.

3 General Flying Program

The annual minimum flying time per squadron crew members is set at 180 hours, for crew member assigned to staff positions 90 hours, and crews in currency status (war reserve crews) 70 hours, which is as well the minimum for any pilot holding an instrument rating. Within this program minimum requirements are set to ensure safe aircraft handling in Visual and Instrument Meteorological Conditions at day and at night; e.g. simulator training, instrument and formation flying, flights at aerodynamical and structural limits of the aircraft such as high performance maneuvers, aircraft handling characteristics and confidence maneuvers, as well as long range navigation flights.

4 Tactical Training Program

The tactical training program is structured as close as possible to the operational requirements deducted from the threat potential posed by countries outside NATO territory. Nevertheless, the program always had to be a compromise because of the numerous peacetime limitations caused by flying safety, financial and environmental constraints including noise abatement procedures.

Despite these limitations the Luftwaffe considers the tactical training program to be sufficient realistically structured to enhance mission orientated training.

To get the best efficiency out of the available sorties, several tactical events have to be combined in one operational training mission, which - whenever possible - should be embedded in a tactical scenario. The training program puts special emphasis on this aspect and reflects this requirement for combat-oriented training in a high number of equivalent combat missions to be flown per year.

The Luftwaffe seeked for different ways in minimizing this noise burden:

5 Training outside Germany

Permanent tactical training facilities are established at DECIMOMANNU/Italy, BEJA/Portugal and GOOSE BAY/Canada.

At these facilities we conduct an essential part of our tactical training.

5.1 DECIMOMANNU

The training facility in DECIMOMANNU which is mainly shared by Germany, Italy, United Kingdom and USA, is primarily used for air/ground gunnery, life air-to-air-firing and for air combat training in the Air Combat Maneouvering Installation (ACMI), a computerized instrumented range, which allows replay and assessment of all tactical movements and simulated weapons delive-

ries. All our TORNADO and F-4F wings are
detached with about 22 aircraft for an
average of 6 weeks/year.

5.2   BEJA

At BEJA we have a permanent detachment
equipped with own ALPHA JETs, so that
training is done there on a personnel-
exchange basis by the ALPHA JET wings.
Additional deployments to Beja are con-
ducted by reconnaissance wings.

The main training embraces air-to-ground
weapons delivery and tactical low level
flying down to 250 feet Above Ground
Level (AGL).

5.3   GOOSE BAY

Most important for our tactical training
is the training center at GOOSE BAY,
because there our crews can extensively
be trained in lowest level flying down to
100 feet AGL. Attacks on tactical targets
with delivery of training weapons are
also included. Another big advantage is
the fact, that there are always two
different tactical aircraft types (e.g.
TORNADO and F-4 or Royal Netherland Air
Force F-16) in GOOSE BAY at the same
time. This facilitates extensive combined
training, either together in combined air
operations or against each other in
attacker/defender roles.

Our wings deploy to GOOSE BAY either by
air-to-air-refuelling direct or, as
generally for the ALPHA JET, with "island
hopping" via Scotland - Iceland - Green-
land.

5.4   Assessment

All together, the external training faci-
lities contribute essentially to the
fulfilment of the tactical training pro-
gram:
- About 50 % of the weapons qualification
  and
- 25 % of the low flying program is
  achieved there, but - more important
- 100 % of the essential lowest level
  flying and
- 100 % of the high quality air combat
  training in the ACMI is conducted at
  these facilities.

We know, that this training would be more
beneficial if done in a probable combat
area, but with todays peacetime restric-
tions all over in Europe we wouldn't be
able to conduct these essential training
parts at all.

Besides the transfer of tactical flying
to unpopulated or rare populated areas -
which is not a new subject for the German
Air Force, since almost from the very
beginning, parts of the gunnery training
was shifted to DECIMOMANNU - some other
ways for further noise relief of the
environment and society were called into
being at home.

6   Environmental Constraints in Germany

The airspace overhead Germany is very
crowded looking at the following figures
(1990):
. Annually a total number of about
  5.200.000 flights
. 83 % associated to civil aviation
. 17 % (875.000) to military aviation
. From these 17 % or 875.000 military
  flights a total number of about 42.000
  hours were flown as low-level-flights
. 13.500 hours of these by the Luftwaffe
  and
. 28.500 hours by the Allies.

6.1   Annual Noon Break

From May until October low-level flying is
prohibited between 12.30 and 13.30 local
time, not to mention the fact that the
low-level flying is generally restricted
to a certain time frame which lasts from
7 o'clock a.m. to 5 o'clock p.m.

6.2   Night Low Level

Nite-low-level flying is restricted to a
minimum altitude of 1000' AGL up to
12 o'clock p.m.
All nite-flying-route-systems are posi-
tioned so, as to avoid dense populated
areas. This fact holds also true for low-
level flying in general.

6.3   Avoidance of Dense Populated Areas

Dense populated areas, e.g. towns with
more than 100.000 inhabitants are to be
avoided or overflown at an altitude of
minimum 1.500' AGL.

6.4   Maximum Low Level Speed

In general the maximum flying speed over
Germany is restricted to subsonic (.96
Mach) between 10.000' - 38.000', whereas
supersonic flights have to be flown above
38.000 feet. The maximum low level flying
speed was recently reduced to 420 KIAS
(540 KIAS only during the attack phase),
and the use of afterburner is prohibited
at altitudes below 3000' AGL unless for
take-off and landing (go arounds) or
dictated by flying safety.

The report of the assembly of the WEU on
"The future of low flying" published in
April 1991 states:
"The reduction to 420 KIAS means where
noise is concerned:
- the lower engine speed greatly reduces
  the noise emitted - by up to 25 %, de-
  pending on the type of aircraft. Peak
  noise levels considered critical in
  research on aircraft noise are not as a
  rule reached at this speed.
- owing to its lower speed, the aircraft's
  appearance is less of a surprise. The
  shock is greatly reduced, and the audi-
  tory system is better able to adjust to
  the volume of noise."

This measure undoubtedly having some positive effects on the environmantal impact of low flying jet operations has considerably degraded the operational capability/flexibility of combat aircraft operating in the low level environment. Any further restriction in the operating speed would adversely effect flying safety.

6.5   Air-to-Air Training

Low altitude interception training is carried out at altitudes of 1.000-1.500' AGL. As several high powered airecraft are normally simultaneously present in a small area for a fairly long time in this type of training, the noise level and stress are particularly high because of frequency of overflights at high airspeeds. With the advance of pulse doppler radar this training can be increasingly carried out at altitudes above 1.500', weather conditions permitting. Installation of pulse-doppler-radar in Luftwaffe aircraft will begin in 1992.

Unlike low altitude interceptions, areal combat training over land is always carried out at altitudes above 10.000' AGL. In the future 86 % of German Air Force training of this kind will be performed over the sea or abroad, leaving only 14 % over Germany.

6.6   Low Level Attack Profile

In the sixties and seventies low level flying was timewise not restricted. About 1980 the maximum low-level-flying-time was restricted to 50 minutes per sortie. Then some years later the attack phase, when flown in the 250' low-level-areas was limited to about 90 seconds; this is between initial attack point and target.

Effective 17 September 1990 all low flying below 1.000' AGL over Germany was banned. This contributed on one side to a noticeable reduction of the environmental impact caused by fast flying jet aircraft, but as well changed the training capabilities in Germany to an extent, that realistic low level combat training nearly became impossible. This development was further aggrevated by the fact, that all neighbouring allies as well prohibited low level flying below 1.000' for Luftwaffe jet aircraft.

However, now as before low level flying is the most effective possibility, to secure survivability and fighting capability to a satisfactory extent.

In the meantime, some exemptions have been authorized in Germany for flights below 1.000' AGL, providing some opportunities on a case by case basis at or above 500' AGL for the NATO Tactical Leadership Programme stationed at Florennes, Belgium and down to 250' AGL for our ALPHA JET squadron holding an ACE Mobile Force assignment.

7   Low Level Flying Manamgenet Systems

The Luftwaffe is presently testing a computer assisted Low Level Flying Management System for all low level flight operations of its units. At present this system is capable of recording and depicting low altitude movements with the aid of the flight plan data inputs by the operational squadrons. Concentrations both on individual days and over longer periods can be analysed and recommendations for mission planning can be issued. Weekly "LOW FLYING DIRECTIVES" are dissiminated to all units concerned at present.

As soon as this system is fully operational timely adjustments to the daily low flying operations can be achieved to avoid areas of high traffic density and by this lower the noise level and reduce the risk of collisions, thus further improving air safety.
The aim is to incorporate all airspace users in this system.
A further step ahead would be a NATO-wide airspace coordination system to provide sufficient training airspace by minimizing environmental inpacts.

8   Summary

As you are well aware, all these selfimposed restrictions, their disciplined utilization by our aircrews and last but not least the use of the technical improved simulators could not prevent, that military flying and especially the noise intensive low level flying has become in the past a leading issue in public and political discussions.

However, no current developments indicate that low-altitude operations can be completely abandoned in the near or even distant future, unless roles are reallocated.

Operational measures to reduce the noise caused by low-altitude flying in the short term may, however, be joined in the medium term by a number of technical measures that can be taken on equipment already in use. For the most part they consist of modifications to the source of noise itself, e.g. the aircraft or its engines.

Specifically, they may consist of changes in configuration leading to reduced air resistance and thus to reduced engine thrust requirements, or changes to the engine itself, ranging from the removal of the afterburner through the use of sound absorbers to the development of new jet designs.

As the political situation in Central Europe has changed, the reunion of Germany being executed and the Warszawa Pact being cracked, the increase of low level flying minimum altitude of military jet to a height of 1000' AGL the TCTP had to be retailored, to try to maintain the required skills and fullfil the requirements for the necessary states of readiness in the future. However, substitus for the low level parts are presently not in sight.

All the mentioned limitations in Europe definitely decrease the noise problem caused by low level fast flying jet aircraft but as well dramatically degrade the combat training of the aircrews to an extent, that the required combat capability is at stake.

There are signs of technological and conceptual developments which are likely to have positive implications in the future on tactical operational concepts and overall strategy and so not least on the nature and scale of low-altitude flying with the associated noise problem.

Discussion

QUESTION BY: G. Winterfeld, DLR, Germany

The figures on low-level flying hours executed by the NATO Air Force given in your paper concern the former western part of Germany. Since one year we have to worry also about its eastern part. Can you give some figures for the low-level flying hours executed by the Russian or Warsaw Pact Air Force over Eastern Germany?
Are there similar altitude limitations for low level flying in Eastern-Germany?

AUTHOR'S RESPONSE:

Presently only the 1990 figures are available. USSR aircraft did fly approximately a total number of 168.000 hours. Round about 42.000 hours were flown in lower altitude (min. altitude 2000 feet Above Ground Level)
In 1991 only very limited low level flying was done by USSR military aircraft. Since 02 Sept. 1991 Luftwaffe also flies low level sorties in the new Bundesländer with 10 sorties per day at altitudes of 1000 feet AGL·

QUESTION BY: W.B. de Wolf, NLR, The Netherlands

Could you comment on the difference between the training environment in Goose Bay and in a highly populated industrialized area with e.g. chimneys and electricity lines?

AUTHOR'S RESPONSE:

At 100 feet there is not much difference between high trees and industry chimneys. Topographically the northern training area of Goose Bay has a lot of valleys which do allow good training for terrain masking flights. In a broad sense wherever we can fly lower than 1000 feet (present restriction in most European countries) it increases combat efficiency of our aircrews.

QUESTION BY: G. Krishnappa, National Research Council, Canada

You showed in your diagram the peak noise complaint during 1990 and also a steady increase of noise complaints over the years. Is it because of the increase in the number of flights or due to higher sensitivity to noise among the population?

AUTHOR'S RESPONSE:

Fact is, already briefed, that the amount of military low level flying was already decreasing in the mentioned time frame. My personal opinion is that the rise in noise complaints is a result of an increased sensitivity of the German population. Another reason could be seen in the fact that in the time prior to GE government election (02 Dec. 90) noise -created by low flying military jet aircraft- was one of the important preelection topics.

POSSIBILITIES AND LIMITATIONS OF FLYING
TRAINING IN THE GERMAN AIR FORCE

by

H. Rüggeberg
German Air Force Planning Division
FMOD
Postfach 1328
5300 Bonn 1
Germany

I. **Summary**

Training is the most important task of
our Air Force in peacetime and simula-
tion must be seen as an integral part
of it.

The rapid progress made in improving
and advancing simulation techniques
leads to a broader use of simulation
in combat aircrew training.

Pilots concern about reduction in fly-
ing hours in exchange for simulation
missions has changed somewhat due to
the fact that the total annual flying
hours were reduced anyway and low
level flying was restricted to 300
meters AGL without having any adequate
substitute.

Simulators are therefore more and more
accepted as a necessary add-on for
optimum combat proficiency training
in which the simulator training por-
tion will have to grow to approximate-
ly 30 to 35 percent of the future live
flying training program.

The German Air Force has used simula-
tors for all types of aircraft for
many years and managed to install one
special-to-aircraft type simulator in
every wing. The experience gained
with those systems should be investi-
gated thoroughly to improve our know-
ledge of the possible application of
simulators in combat training.
But before we identify the principle
interrelationships and longterm per-
spectives in a new training and simu-
lation concept, we should collect all
available data and analyse the finding
from the evaluation and flight testing
of the ongoing TORNADO simulator up-
grade program.

We should identify the shortfalls and
initiate the neccessary follow on
program and improve first the proto-
type simulator before we come to any
decision for the simulators in our
TORNADO wings.
Urged by our politicians we have pro-
bably asked for too much too early.
Let me finally quote a NATO paper on
lessons learned from the Golf War:
"Pilot training must be carried out
in peacetime under severe conditions:
night, bad weather, high speed, low
level, crew fatique etc. Simulation
can provide a little but not enough.

AGENDA

II.   **Introduction**

The public pressure to cut the jet
noise of low flying aircraft still
exists and the associated problems
were just discussed in our defence
committee last week.

You will still find noise complaints
about low flying military jet air-
craft in our newspapers, and not too
many people took note of the result
of a very recent study summarizing,
that noise emission from yet air-
craft flying as high as 300 meters
is unlikely to hurt anybody - the
study was presented in Berlin during
a symposium on "Noise and Health" a
few weeks ago -.

Nevertheless we have to avoid or at
least reduce the environmental
impact of operational flying as
much as possible and I think there
is no doubt that simulation is an
important tool in noise reduction
besides other possibilities you are
going to talk about during the next
days.

The ability of piloted simulators
and their contribution to a wide
range of tasks - including the use
and potential of simulation in full
mission training for military roles -
was presented in Brussels last week
during a symposium of the "Flight
Mechanics Panel" on "Piloted Simu-
lation Effectiveness". I could not
attend that meeting but I am afraid
that one of the results was that we
still have to wait for modern simu-
lation techniques to become part of
a fully integrated approach to
training and combine optimum combat
readiness with crew motivation and
minimum environmental impact.

Simulation in flying training is
constantly gaining in importance
but whatever requirements or im-
proved simulator features we come
up with will build on systems we
have in use today.

92-17416

I shall therefore start my presentation with a definition of todays conditions and influencing factors and go on to describe the status of simulation capabilities in the German Air force. From this I will deduce our objectives with regard to future requirements, give a short presentation on our simulator improvement programs and describe the Air Force planning concept and assess its feasibility.

Definition

**Computer assisted reproduction
of technical, physical,
economic and tactical
processes by means of real
or abstract models**

It's the artificial duplication of natural situations with adequate fidelity.
Although simulators are used in almost all Air Force elements for a wide variety of purposes, my paper will focus on simulation for pilot training as a result of the dramatic changes in our political environment and the associated diminished public acceptance of low level flights with there environmental and safety risks. The resulting question is not any longer: "can flying hours be substituted?" Our major problem today is how to compensate for the decrease in flying hours per pilot per year and the restricted training opportunities especially at low level and not let practical flying experience become a variable.

III. **Conditions and Influencing Factors**
Training is the most important task of Armed Forces in peacetime and must be oriented along its operational missions. To exploit the capacities and capabilities of command, control, reconnaissance and weapon systems completely, continuous realistic training with the operating equipment is necessary. But safety regulations, environmental restrictions and limited availability of training areas and funds more and more limit the capability to provide training in a near-realistic war scenario and thus the use of simulators is of paricular importance.

The mission of the Air Force Flying Units is to train aircrews for the fighter weapons systems TORNADO and F-4F PHANTOM, for transport aircraft like the C-160 TRANSALL and for helicopters.
This initial and proficiency aircrew training is subject to parameters which are primarily derived from the political situation, the changing public perception of defence constraints and the demographic development in the Federal Republic of Germany. The following factors and trends to be deduced from these parameters will have a restrictive effect on training.

1. **Reduced Personal Strength**
Due to the demographic development and the force reduction already agreed upon, the personnel strength in the Air Force will be reduced decisively and in consequence, additional flying hours can hardly be provided.

2. **Limited Funds**
Under the current defence budget expectations the limitation of operating costs will become one of the most important criteria of future planning. In regard to the selection of training aids, personnel and operating cost savings must therefore be considered more strongly.

3. **Lack of Realistic Training Conditions**
A number of training objectives cannot be achieved due to the lack of realistic training prerequisites. Because of security and costs, certain tactical missions may be trained only to a limited extend and for peacetime flying operations, safety is another very important limiting factor. This training deficits will be further aggravated by the technological developments and introduction of more sophisticated aircraft and ordnance.

4. **Growing Environmental Consciousness**
A growing public interest in the preservation of the natural environment, greater awarness of risks, greater sensitivity and the need to reduce the noise strain was already mentioned and they cause additional limitations to training programs.
Any major transfer of training to the neighbouring European countries or overseas beyond the extent currently planned appears hardly practicable in view of the reduced operational readiness, the high absence rate of aircrews and the problem of future acceptance of such transfers by host nations.

5. **Availability of Weapon Systems**
Finally, and in view of the high development and procurement costs, advanced weapon systems must be designed for long in-service live. As a matter of principle, training missions with operational equipment contribute to material fatique and should therefore be restricted to an extent to be defined on a case-by-case basis.

In summary, beside the general reduction in actual tactical flight training, increasingly restrictive conditions demand a permanent revision of

the training concept of the Air Force for their flight crews and the need to consider more and more advanced simulation facilities as training support and not as live flying replacement tool.

IV. Status of Flight Simulation

Apart from the fact that simulation provides both relief from environmental strain and the necessary protection of the real system against material fatigue, it has a number of further advantages to offer

- Operating costs of simulators are lower than those of weapon systems. Thus, the average flying-hour-to-simulator-hour cost ratio is about 10 to 1.
- Simulators make it possible to record and reproduce the training sequence and offer means for a quantitative control of the training success.
- Simulators make it possible to train the behaviour required in hazardous situations without endangering man and material.
- Simulators premet training of weapon employment even in cases where the limited availability of training areas, weapons or funds rule out live firing.
- Simulators shorten the training time during initial and proficiency training. Investigations made in the US revealed a time saving factor of between 10 and 20 % in comparison with conventional training without simulators.

On the other hand, simulators have basic disadvantages
- the limited reproduction of reality and the resulting reservations our pilots have and
- the adsense of physical and psychical stress of our aircrews.

Simulator Training Requirements
The requirements for simulator training for aircrews are laid down in the "Simulator-based Flying and Tactical Training Program" within the Tactical Combat Training Program (TCTP).

Tactical Combat Training Program
TCTP

Weapon System	Flying Hours	Simulator Mission
TORNADO	150	12
F-4F	150	10
C-160	200	-
UH-1D	150	20

According to this program, the annual requirement for flying hours and simulator missions per aircrew is 10 to 1 as an average. Simulator hours are to be seen in addition to the maximum possible flying hours a pilot can fly per year.

This will change with the increasing complexity of simulators and their ability to include environmental effects and a close to full realism technique particularly with advances in visual systems.

We have three simulator generations in use in our Air Force, each having been up to the latest standard of technology when introduced. But with every new weapon system higher quality simulator training will be required. For example, important mission elements of the ECR-TORNADO in the area of electronic warfare and suppression of enemy air defence cannot be trained life for security and cost reasons and have to be carried out primarily in a simulator.

Evaluation of Simulators
Our C-160 TRANSALL simulator is a first-generation device. Due to its analogous technology, it is no longer suited to meet the present or future training requirements. It's a procedure and instrument flight simulator and tactical procedures can only be trained to a very limited extent. We will procure a new simulator for the training of our transport crews next year.

A 2nd-generation system is our F-4F PHANTOM simulator. It will be considered a good training aid once it is retrofitted with a fiber-optics helmed mounted display for an texternal visual system and modified and equipped with electronic warfare components. I am going to talk more about our ongoing simulator improvement programs in a minute.

We hope, that the F-4F simulator will provide an environment closer to reality and may be used to train limited air combat maneuvers against computer generated targets.

The TORNADO simulator is a third generation full mission simulator with still considerable limitations
- it is equipped with a visual system whose ground resolution and topographic display capabilities are unsatisfactory. Therefore, visual low-level flying is not possible
- due to its limited field of view in battlefield missions and ground attack operations, it allows for visual final attacks only and
- finally, it has no external visual aerial target display so that evasive maneuvers to escape fighter attacks cannot be trained.

Simulators

	1st Generation
C-160 TRANSALL	
	(analog)
	2nd Generation
F-4F PHANTOM	
	(Air Combat-FOHMD)
	3rd Generation
PA-200 TORNADO	**(Visual System-FOHMD)**
	6-DoF Motion
	System)

What we need is a full-mission simula-
tor capable of providing
- air-to-air combat
- electronic warfare
- high speed, low level visual and
  radar missions and
- air-to-ground attack
training capabilities.

TORNADO Simulator Improvement Program
The Air Force therefore initiated a
TORNADO simulator improvement program
in 1990 which mainly consits of
- a visual system upgrade with a Fibre-
  Optic Helmet Mounted Display (FOHMD)
  and
- a six degrees of freedom (DOF) motion
  system.

Since the basic simulator had to be
changed to support the new elements CAE
built a prototype simulator in Stolberg
including the FOHMD, the Evans & Suther-
land ESIG 1000 image generator, a motion
and a recording and air target system.

The evaluation program was scheduled
from the 8th of July until the 11th
of October this year and more than 250
low-level sorties were flown.

The Air Force is going to flight-test
the improved system between the 5th of
November and the 17th of December.

Although it's to early to draw final
conclusions from the results already
in hand, we have today a better under-
standing of the interaction of the se-
veral elements and some indications in
what direction further developments
should go.

With the present simulator configuration
three TORNADO missions per day can be
flown. This is sufficient to meet to-
days annual requirements per pilot. We
managed to get full-time instructor
personnel in our training facilities in
every wing and the employment of former
combat ready pilots as civilian instruc-
tors proved to be successful.

In summary, it may be stated that, for
the time being, simulator training of
aircrews still has limitations prima-
rily due to the fact that

- the technology for realistic simula-
  tion is still not available and the
  absense of physical danger influen-
  ces the training results and
- simulation systems available do not
  allow to train combined air combat
  and tactical formation.

V. Objectivies of the German Air Force
What objectives may be derived from
the above statements for the future
employment of simulators in the Air
Force?

Objectives

Support of Training
High Degree of Reality
Acceptance
Overall Training Concept

In view of the limiting and unfavou-
rable conditions under which life
flying training has to be conducted,
the improved performance characteris-
tics that are emerging in future simu-
lation systems must consistently be
utilized.

The aim of simulation must be the
support of the reduced actual flying
training of fully qualified aircrews
with a detectable contribution to
their proficiency.
With in the interrelationship between
theoretical knowledge, simulation and
practical flying, simulation has to
fulfil a supplementary function to
prepare aircrews for their missions,
and to maintain and, if possible, to
increase their proficiency in a safe,
comprehensive, fast and cost effective
manner.

Combined air operations involving
several trainees in a tactical sce-
nario can only be established by
netting simulators and transfer a lot
of data or by setting up a centrali-
zed tactical simulation center for
the training of highvalue missions
only.
As the effectiveness of simulation is
primarily determined by the degree of
reality and the subconscious acceptance
by the aircrews and since most low
level high speed missions are flown
under visual conditions, the develop-
ment of a high-quality visual system
must be given first priority.

A realistic aircrew training corres-
ponding to the performance characte-
ristics of the weapon system and de-
signated to improve or optimise the
interaction of tactics and technology
requires a continuous improvement of
in-service simulators. A still open
question is to what extent such an im-
provement program should be executed.

The investment in an advanced simulator
is substantial and a simulator can
cost more than the aircraft itself.
With the growing complexity of simula-

tors with their high-tech subsystems, it may become impossible to have a full-mission simulator available in every wing due to the enourmous high cost of procuring, operating and maintaining these systems.

VI. Potential and Trends

New technologies and many possibilities of computer based training and realistic simulation of view, movement, acceleration noise and of environmental scenarios are available and will be further improved and with the modern computer-generatied display, a very nearly realistic visual system has already been achieved.

We think that the advantages of the fiber-optic helmet - mounted display in comparison to the dome projection are to be found in a greater brightness and better resolution of that display. Moreover, the infrastructure requirements and procurement costs are lower. Problems causes the relatively heavy helmet and the limited freedom of head movement.

A further attractive application of simulation is offered for the future by the so-called embedded training, a simulation capability integrated in the original equipment, which is being studied at present.

Simulation technology is undergoing a dynamic process and it will be important for the services to follow up closely and actively all technological trends.

VII. Requirements

What are the Air Force requirements derived from the overall training concept?

Requirements

Interactive, Computer-Based Instruction
Improvement of In-Service Simulators
Interlinking
Tactical Simulator Center
Configuration of Future Weapon Systems

1. Interactive, computer-based instruction methodes should be introduced at schools and in units, where they serve to improve training to gain command over complex systems.

   They are available on the market and have been tested in practice with great success.

2. For the in-service fighter simulators, tactical and technical improvements will be necessary which must include the changes out of our combat aircraft performance programs.

   The evaluation results from the upgraded TORNADO simulator will be the basis for further improvement

decisions towards air combat and high speed low level simulation. Our national training concept is not yet completed but for new systems a demand exists for
- a part-task trainer to train specific and limited functions
- operational flight trainer to train general procedures
- full-mission simulator with weapon employment and mission specific threat scenarios.

3. In the long term, the technically feasible linking of flight and tactics simulation systems including command headquarters has to be analysed. Such linking would allow to conduct large scale exercises preplanned on a case-by-case basis.

4. A tactical simulation center offers the best possible conditions for the training of high value missions and missions involving several participants in a tactical scenario. The operational employment of all types of weapon system in air warfare can be trained realistically and it is the only way to permit the training of combined air operations.

   In view of the continuously growing significance of simulation we are just in a process of analysing the possibility of comparing development, evaluation and tactical simulation in such a center.

5. In the planning and configuration phase for new weapon systems, the potential for a weapon system integrated simulation capacity should be assessed and taken into consideration, so that simulation of exercises, partial or full missions would be possible with or including the original system.

Conclusions

Convert the Simulator Experiences
Validate the Evaluation and Flight Test Data
Consider the Possibilities and Limitations
Develop and Oerall Training Concept
Aim for Adequate and Costeffective Solutions

Discussion

QUESTION BY: C.S. Beers, NLR, The Netherlands
Approximates training in peace time the combat situation enough?

AUTHOR'S RESPONSE:
Not our restricted normal peace time flight training. The approximation is somewhat better when flying tactical training missions at Goose Bay. The best trainings are exercises like Red Flag.

AD-P007 514
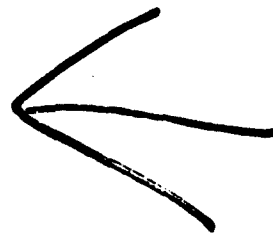
COMBAT AIRCRAFT NOISE - THE OPERATOR'S PERSPECTIVE

Group Captain R Bogg RAF
Deputy Director Navigation Services (RAF)
Ministry of Defence
Whitehall
London SW1A 2HB
United Kingdom

1.   SUMMARY

1.1   Combat aircraft are not subject to the same noise reduction regulations as civil aircraft and are operated closer to their performance limits and at high power settings for extended periods. There is general pressure to reduce noise of all kinds, but particularly that from low flying aircraft. Although there is little that can be done to quieten in-service engines, operational palliatives, such as noise abatement procedures and restrictions on low flying, have been introduced. Moreover, there has been a concerted education and public relations campaign, and numerous airspace management changes have been introduced to reduce the impact of low flying on the population. These subjects were considered during a Pilot Study into aircraft noise under the auspices of the NATO Committee on the Challenges of Modern Society; the findings of the Study are discussed, giving both the international viewpoint and the UK perspective in particular. Some options for the reduction of low flying are also considered, but so long as military aircraft need to fly low to evade enemy air defences, low flying will remain a principal tactic of NATO air forces, and peacetime training will remain an essential military requirement. Thus, noise from low flying combat aircraft will remain a sensitive issue, and ways of reducing it will continue to be of importance for many years to come.

92-17417

2.   INTRODUCTION

2.1   In a world which has become increasingly environmentally aware, noise of all forms has its critics, particularly aircraft noise. As civil aircraft have become quieter, military flying has faced increased criticism. Although many aspects of military aircraft noise from all classes of aircraft and helicopters have come in for criticism, including noise around airfields, it is the combat aircraft, particularly in its low flying role, which has been the centre of most attention, and this paper concentrates on this element of military flying by fixed-wing aircraft.

2.2   Operationally, NATO has concentrated on flying at low level as a key tactic to reduce attrition in the face of sophisticated and increasingly potent air defences. Low level in this context means penetrating enemy airspace at around 100ft, and as fast as possible, typically at 480-600kts. However, air forces have recognised for a long time that a peacetime training balance has to be struck between value of training, acceptable peacetime training risk, and the impact of such training on the population. The easing of East-West tension has led to a call for reductions in low flying, particularly in Germany, and significant airspace restrictions have already been applied in some countries to limit the opportunities for such low flying training.

2.3   For its part, the Military has recognised and fully understands the

desire to minimise the impact of low flying on the general population and which has provoked political interest in several countries. Recently, for example, the UK House of Commons Select Committee on Defence and the Western European Union have both carried out investigations into low flying, the former concluding that 'a requirement for low flying training will remain as long as military aircraft need to fly low to evade air defences' (Reference 1), and the latter recommended, inter alia, that nations 'should take suitable measures in the future to reduce the noise to which the public are exposed' (Reference 2). In parallel, NATO has noted the increasing concern about low flying, commissioning its own study of the problem of aircraft noise through the auspices of its Committee on Challenges of a Modern Society (CCMS), and, in 1991, both AAFCE and AGARD embarked on separate studies which, for the former, re-examined the military requirement for low flying in the light of revised force postures and readiness states, while the latter is examining the requirement for low flying training in an attempt to reduce the environmental impact of such flying. While efforts continue to find solutions, it is a delicate balancing act to reconcile these conflicting considerations.

3.   REGULATION

3.1   Within the civil aviation sector, there has been legislation for many years aimed at controlling engine noise, and manufacturers have been obliged to cater for such legislation in the design of their engines.   However, many military aircraft, including passenger and transport aircraft which operate into civil airfields, are not bound by such regulations, but this immunity may not last and, inevitably, there will be impact on some areas of military operations.   The military position is lessened in this respect through equipment replacement programmes which, for transport and passenger

flying, often make use of aircraft or engines already in commercial use and, therefore, subject to international regulation.   Current legislation excludes combat aircraft, defined as those which fall into the fighter and bomber categories;   these aircraft have been built for performance and survivability and, hitherto, it has not been necessary to devote significant effort to the quietening of these aircraft.

3.2   Parliamentarians and members of the public are aware of the existence of civil legislation and the broad technological measures which have been taken to quieten airliner engines, and they have some difficulty in appreciating why similar measures cannot be taken to reduce noise levels from combat aircraft.   To the layman, the solution is simple;   all that is needed is the modification of engines already in-service.   The reality, of course, is quite different, and while some measures might be possible, there are compelling counter considerations which confront not only the military but their government paymasters also.   With the easing of East-West tension, there has been a concomitant call for an evident peace dividend, not only in a reduction of armed forces but, more importantly, a reduction in the amount of government money required to meet defence needs.   In the specific context of engine noise modifications, the inevitable result is an even greater difficulty to find funds for both the research and for the modifications themselves.   Thus, there is conflict facing governments; they have to decide whether such modification is either necessary or indeed worth the investment.   The other consideration is the timescale for such modification, assuming that the will is there to invest in the work. In-service engines are notoriously difficult to modify in any significant way, and, for most current military aircraft, it is doubtful whether evaluation and development of the appropriate modifications and their subsequent introduction into service

could be achieved in the remaining life of the aircraft. In reality, there is probably little that can be done to significantly quieten in-service combat aircraft and this aspect of the debate is somewhat academic. Significant reductions are likely only from future engines, probably 15-20 years hence, and, in the meantime, it is necessary to consider other alternatives.

4. THE ONUS PLACED ON THE OPERATORS

4.1   Since any measures to quieten engines in combat aircraft are both long term and expensive, aircraft operators have to live with the problem from day to day, for it is they who have to face the political and public criticism of low flying. The most vociferous opponents of low flying suggest that the military has neither concern for the amount of noise they make, nor for the feelings of those who have to listen to military aircraft either on the ground or in the air. Such a view does not reflect the thinking of any military commander or crew, either now or for many years past, and the general swing towards greater environmental awareness has been reflected in military training and operating philosophies. It is important to recognise that low flying military training has been based for many years on a compromise between what the operators would like to do, first to attain, and then to sustain, operational proficiency, balanced against what is a reasonable burden to impose on the general public.

4.2   In operational terms, the principal aim of combat aircraft is to reach their target safely, to release weapons accurately, and to return home, also in one piece, and to repeat the operation if necessary. Combat aircraft need engine power, both for performance and for survival; in the former category, there is an increasing demand for shorter take-off runs and high transit speed, and,

for the latter, power is needed to evade either ground defences or any lurking fighters. Operators recognise that, generally speaking, power equals noise. On the one hand, it does not matter how much noise is made in combat provided it means survival, although acoustic signature in a stealth sense is of concern. However, on the other hand, crews are concerned about noise made in peacetime, but, as long as Governments have defence policies which require an air capability, then an air force's task is to train for war. Nevertheless, normal modus operandi are conditioned by the compromise of realistic training and environmental impact as has already been mentioned. Until recently, 250ft has been the generally accepted minimum height overland for training throughout NATO, although three countries, Canada, UK and US, have allowed some training down to 100ft in specially designated areas. However, environmental pressures have threatened this compromise and, recently, have led to the imposition of additional restrictions on minimum height in some countries with knock-on effects elsewhere which threaten training standards across NATO as a whole.

4.3   Commanders, supervisors, and aircrews all have to be aware of the impact of their peacetime activity on the population, and this awareness and concern starts on the ground. Base Commanders, in particular, are in no doubt about the impact of flying operations on those who live near their airfields, and recognise the need to establish a good rapport with local communities, discussion with whom often includes the vexed question of aircraft noise. However, it is often forgotten that the military and their families, too, are part of the same local community and have to live with the noise also. There is thus some incentive to pay close attention to the reduction of airfield noise wherever it is practicable.

4.4   Good relations start with good housekeeping, and, as a principle,

3-4

tight controls are imposed on the ground running of engines, a regular cause of complaint. At most bases, running is not permitted before 7am or after 11pm unless absolutely necessary, and then only on the express authorisation of senior officers. Most ground running of engines is allied to maintenance and involves high power settings and slam accelerations; inevitably, this is very noisy and often prolonged. To some extent, running in hardened aircraft shelters has helped to attenuate the noise, but greatest reduction has come from the introduction of engine running hush houses. With advances in technology, a long term objective should be the development of engines which do not require extensive ground running; rather, a comprehensive electronic set-up procedure should be evolved, although most combat aircrew would need considerable reassurance of the efficacy of such an approach before feeling comfortable with it.

4.5   In the vicinity of many military airfields in the UK, the Government has provided grants for the installation of acoustic secondary glazing for civilian homes, and this has proved to be very popular with the local population. The noise criterion used has been 70dB(A) - or more properly LA, eq, 12h 70dB and provided homes lie within the measured average 70dB(A) noise contour in the vicinity of the selected military airfield, they qualify.

4.6   Arguably, most noise from combat aircraft is generated on take-off and departure, and noise abatement procedures are generally adopted at military airfields, similar to those used within the civil community for many years. Generally, engines are not run at full reheat prior to take-off; rather, the military tend towards rolling take-offs, with minimum reheat at first, then full reheat once on the move. Where all-up-weight considerations permit, to obviate the need for reheat, and provided overall combat

performance is not compromised, an alternative would be to build bigger and more powerful engines. However, residual thrust represents a higher investment in development and production, but the premium has not been acceptable for many military aircraft engine designs, although governments may have to give greater prominence to this consideration in the future.

4.7   A successful mission in the air is crucially dependent upon thorough mission planning on the ground, and there are many route constraints which are determined by noise considerations. Ideally, aircrew would like to fly as low and as fast as possible to practise for survival at 100ft and 600kts, but, because of the previously mentioned compromise, the military limit their peacetime training to 250ft and around 420kts, except for simulated attack profiles where higher speeds are sometimes used for short periods.

4.8   In terms of the impact of routine flying on the population, every effort is made to avoid overflying centres of population, and power settings are limited, with use of reheat being specifically precluded overland. Nor is supersonic flying permitted at low level overland in most countries; such flying is allowed only in the most remote parts of the world ! Avoidance areas are established around major conurbations, civil and military airfields, some hospitals, nuclear power stations, and so on. In consequence, there is a comprehensive set of restrictions with which the aircrew must be thoroughly familiar. Crews go to great lengths to avoid overflying smaller towns, villages, even isolated communities, manoeuvring around or climbing well above those that are seen. But it is impossible to avoid overflying every single house or person, and this is sometimes difficult for the public to comprehend; inevitably, therefore, the military does cause annoyance to some people, and, despite all of the safeguards, the

operator does get accused from time to time of being irresponsible, of frightening people, and of causing hearing damage.

4.9   While not underestimating the impact of overflight on people on the ground, particularly the startle effect, a comprehensive literature search carried out in the UK has failed to unearth conclusive evidence of permanent hearing loss due to low flying aircraft, and best evidence suggests that the likelihood of permanent hearing damage is infinitesimally small at levels up to 125 dB(A);   at worst, there might be a temporary shift in hearing threshold for a few highly sensitive people, but the risk of permanent damage is negligible (Reference 3). Nevertheless, following flight trials in the UK (Reference 4), steps have been taken as a precaution to control low flying so that not more than 125dB(A) of noise is received on the ground;   at typical low flying heights and speeds, combat aircraft are considerably quieter than this.

4.10   Significant effort is devoted to explaining the need for low flying and its careful conduct to the general public and on educating aircrew, supervisors and commanders at all levels of the impact of their day-to-day operations.   Experience has shown that such explanation reduces some of the emotive reaction and gives a better understanding of the issues involved, making acceptance of low flying and of its restrictions more palatable.   Briefings to aircrew are given at regular intervals, and questions of low flying are addressed on national and NATO flying supervisors' courses.   In terms of briefing the public, pains are taken, certainly in the UK, to include reference to low flying as part of a nationwide public relations campaign, and the Ministry of Defence has a special briefing team which faces the public at open meetings particularly in areas in which there are perceived to be particular problems with low flying.

5.   AIRSPACE FOR LOW FLYING

5.1   Most NATO nations provide airspace for low flying, and although the definition of low flying differs from nation to nation, for example it is below 2000ft in UK and below 1500ft in Germany, the acknowledged upper limit for useful training is 500ft.   In addition, the amount of airspace open for such flying varies from nation to nation, both in terms of area and altitude limits.   There is a significant difference between that available in, say, Holland, which has two 250ft narrow routes along the length of the country, with a restriction of 1000ft elsewhere; Germany, until 1990, had a system of seven 250ft areas of varying sizes and a 500ft limit elsewhere, but, recently, a 1000ft limit has been imposed everywhere; and the UK has a general 250ft minimum height (except over densely populated areas), with three 100ft areas for restricted training under special conditions.   Clearly, crews plan to fly in the 250ft areas, and the smaller these are, the more concentrated the noise in those areas;   this has been at the heart of the problem in Germany. The principle applied in the UK is to spread the noise burden as widely as practicable by opening as much airspace as possible to 250ft flying.

5.2   Management of low flying needs to be both proactive and reactive to make most efficient use of airspace, restrict flying where safety or other considerations apply, and provide a quick and efficient information dissemination system to inform aircrew of changes, hazards, and navigation data.   In the current debate, a key issue remains the availability of airspace and the need for burden sharing.   Many people argue that, in an Alliance, every nation should provide facilities for low flying, ideally at 250ft. Restrictions placed by one nation are naturally reflected in equivalent restrictions in another, and while NATO co-operation remains crucial, there are understandable political constraints which limit flying by

foreign air forces to conditions no more favourable than made available to Alliance partners in their home country.

5.3   Consideration has been given to the role of computers in the management of low flying, and here too there are differences in approach.   The Germans are examining a system which will collect data retrospectively on patterns of low flying, information from which will allow redistribution of flying to avoid over-saturation of one particular area.   In the UK, a reactive system is being introduced which will allow operators to make their low flying booking and receive both clearance and up-to-the-minute data on other aircraft in the vicinity. local warnings and hazards: in addition, the system will ease the considerable burden of statistical data gathering.

6.   ALTERNATIVES TO CURRENT LOW FLYING PATTERNS

6.1   To ease the impact of low flying, the military have been sought to examine several alternative approaches;   many are not practical, but are discussed nevertheless.   First and foremost, there is the question of The Threat which determines the military need for low flying.   Some people consider that the threat no longer demands either qualification or currency to be able to fly at low level.   It remains a political decision to define the readiness state required for air forces, and, to meet that political directive, air forces must be provided with appropriate flying training.   Some work has been carried out to determine the time required to qualify crews for competency at low level, and while there are many arguments and considerations, the required time is principally a function of warning time and availability of suitably qualified flying instructors. the latter being essential to underpin operational training.   While NATO

can boast an extensive availability, at present, of both experience and instructors, the longer an air force is not exposed to low flying, the longer it will take to regain competency;   in the process of acquiring such competency, there would probably be a higher accident rate during the transition since low flying would represent an unfamiliar training regime and, in war, higher attrition levels would have to be expected.

6.2   Next, some suggest that low flying could be undertaken over the sea where disturbance to the public would not be a factor.   Although many air forces already carry out some training over water, the option has limited utility since the most demanding aspect of low flying is learning to contend with the undulations of the ground and avoidance of obstructions, and, very quickly, the demands of flying over the sea and the tactical value of such flying reaches its peak and there would be very limited equivalence to the perspective of overland flying. Further, performance and use of many avionic systems are severely limited over the water, for example, terrain following radars.

6.3.   Alternatively, the necessity for peacetime training to be carried out at such low altitude is questioned, and some wonder whether the same training could be carried out at a higher level.   However, there are several skills needed to be safe and proficient at low altitude, and these have to be first acquired and then sustained through regular practice. Skill at aircraft handling, navigation, tactics, target acquisition and radar handling, weapon aiming and use of electro-optical devices all need to be developed, and the demands on the aircrew above 500ft, where the flight regime can be considered benign, are quite different and much less demanding than at heights of 100-250ft.   The differences between visual cues and work rate at the various levels are not linear, and, at the lower levels, terrain avoidance assumes greater importance, and low

level navigation becomes more difficult as aspects change from planform to elevation. Thus, flying higher leads to a non-representative training regime, and in terms of noise there is not a significant reduction between 250ft and even 1000ft, and, the higher an aircraft is flown, the longer its noise is heard on the ground and over a wider footprint.

6.4 Finally, many people believe that modern simulators could be used, thereby negating the need for actual flying. While simulators have been used extensively for many years, they have their limitations. Not only are they expensive, but they have been unable to provide realistic tactical low flying; indeed, many do not have visual flight attachments to allow low flying to be replicated. Simulators have an important part to play in conversion and emergency training, and in the teaching of procedures. Nevertheless, recent advances in digital landmass databases and visual scene generation are allowing more extensive use to be made of simulators and this may provide for more representative training than is possible at present, for instrument training, night flying, use of electro-optical devices, and limited tactical flying; however, whatever is said about their advantages and capabilities, simulators cannot replicate the pressure of actual flying and crews will always be aware that they cannot be killed as a result of mistakes they make. There is no substitute for actual flying and, as at present, in the low flying regime, simulators are likely to complement flying training rather than replace it.

7. NATO CCMS STUDY

7.1 Many of the issues discussed so far were considered during the recent NATO CCMS study (Reference 5). The study itself was wide ranging, with detailed consideration of aircraft source noise, methods of mitigating the nuisance on the ground, and operational considerations to reduce the concentration of aircraft in time and space. The latter area has been discussed extensively in this paper and brief reference is made now to the work in the other areas.

7.2 The Source Noise Sub-Group concluded that significant reductions in jet exhaust noise were not possible without major performance penalties; since the majority of our aircraft do not have excessive spare power, reduction in performance is not an acceptable military option. However, the group suggested that improvements in aerodynamics of the aircraft would allow lower power settings to be employed. While this is true, there is only limited scope for such aerodynamic streamlining since many current aircraft need to carry fuel tanks and practice weapons dispensers on many occasions; nevertheless flying supervisors should consider operating their aircraft as aerodynamically clean as possible. Perhaps the design of future fighter-bomber aircraft should include bomb-bays, like some of their predecessors, rather than have to resort to the external carriage of weapons. The group noted that there was a paucity of information on source noise data for aircraft operating at high speed and at low altitude, and collection of such information would allow a better understanding of the mechanics of noise generation to assist future research into quieter aircraft. The CCMS study provided the spur for work to be undertaken in this area in the UK (References 6 and 7).

7.3 A second sub-group concentrated on aspects of receiver technology, concluding that acceptance of noise on the ground through consideration of its effects, abatement, community and land use planning and their interactions would be difficult to achieve. At the time of the study, there was no clear evidence that aircraft could produce noise induced hearing loss on humans and it was not possible to

assess the effects and risks on hearing, communications, sleep, and the associated physiological/ psychological impact. In follow-up work, Canada, UK and US may carry out a collaborative research programme into these subjects. The original work examined abatement techniques and the complicated considerations of community and land use techniques. Modelling was identified as a useful tool, but the study established that there was not a standard set of noise indices recognised internationally and useful work was undertaken to produce conversion factors to transpose data from one nation to the indices adopted in another.

7.4. The work of the CCMS was timely given the sharp public and political interest in environmental matters generally and aircraft noise in particular. The CCMS report has been noted by the NATO Council and the work is being continued through a Follow-on Group which is progressing the recommendations of the original study. Clearly, paper studies have their limitations, and while many of the conclusions and recommendations are important, many would require extensive changes in training patterns or expenditure to overcome the problems addressed. The difficulty is to maintain the international momentum and to put the scale of the noise problem into perspective, particularly now that some nations have placed significant restrictions on the extent and altitude of low flying training.

8. CONCLUSIONS

8.1 It is not always easy to quantify the true extent of the combat aircraft noise problem, for there is much emotion generated which has clouded the issue to some extent. Nevertheless, and rightly, close attention has been paid to the concerns of the public and many measures have been taken to reduce the impact of low flying on the population. Hitherto, it has not been necessary to introduce noise reduction measures on combat aircraft and while marginal noise reductions might be possible, significant reductions could only be made to take-off noise with massive investment, but any measure which reduced available thrust and performance would not meet military requirements. The technical difficulties and timescale for modification of in-service engines is such that this approach is unlikely to prove cost effective, and the only alternative is to await new engines designed with lower noise output and maximum thrust in mind. However, governments must be prepared to pay the price for meeting such conflicting goals.

8.2 In the meantime, aircraft operators will continue to restrict noise nuisance as far as is practicable, through restrictions on their activity both on the ground and in the air. The call for a peace dividend in response to the welcome easing of East-West tension and as a result of CFE Treaty measures, will leave most air forces with fewer aircraft. The total noise on the population will, therefore, reduce over the next few years. However, the world and politics are notoriously fickle, and while everyone would wish to believe the world is a more stable place, nations are a long way from being able to discard defence forces completely. Governments will need to be prepared to counter aggression wherever it may arise and, while air forces require an offensive capability, the low flying tactic will remain an essential element of military strategy. In turn, this will require regular training in peacetime, and thus low flying aircraft noise will remain a topical issue for many years to come.

REFERENCES

1.   House of Commons Defence Committee Fifth Report 'Low Flying', 28 March 1990, para 238

2.   Western European Union Thirty-Sixth Ordinary Session, Document 1222, 'The Future of Low Flying', 24 April 1990, para 188

3.   Lawton, BW and Robinson, DW. "Risk to Hearing from Overflight Noise of Military Aircraft", November 1990

4.   Berry, BF, Payne, RC, and Harris, AL. "Noise Levels of Military Aircraft at Low Altitude", January 1991

5.   CCMS, 'Aircraft Noise in a Modern Society', Final Report of the Pilot Study, Number 185, November 1989

6.   Pinker, RA. "A Brief Review of Source Noise Technology Applicable to Fixed-Wing Military Aircraft", April 1991

7.   Strange, PJR, Bryce, WD, and Pinker, RA. "Identifying the Principle Noise Sources of a Fixed-Wing Combat Aircraft in High-Speed Flight", April 1991

HUMAN NOISE EXPOSURE CRITERIA FOR COMBAT AIRCRAFT TRAINING AREAS

Robert A. Lee
Dr. C. Stanley Harris
Dr. Henning E. von Gierke
Armstrong Laboratory/OEBN
Area B, Bldg 441
Wright-Patterson AFB, Ohio, 45433-6573
United States of America

92-17418

SUMMARY

This paper provides an overview of interpretive criteria for noise exposure conditions associated with low altitude flying operations in the United States. It includes description of single event and cumulative noise characteristics unique to such flying activity and discussion of rationale for using the measure, onset rated adjusted Day-Night Average Sound Level, for predicting population annoyance.

INTRODUCTION

The U.S. Air Force (USAF) currently has about 600 training routes in the continental United States that involve in some cases low altitude overflights of populated civilian areas by military aircraft. Most of the major Air Force commands use the routes regularly for training and proficiency exercises producing relatively high levels of noise for short durations scattered sporadically over time. The USAF flies a wide variety of aircraft over these routes from the high speed F-15 to the slow flying A-10, from the small F-16 to the large B-1. The total impact from all operations in a route must be described by an Environmental Assessment process before they can be used. Evaluation of the effects of the noise produced from these aircraft operations on the exposed populations involves two major dimensions. The first dimension is the definition of the physical parameters of the noise such as level, duration, frequency content, onset rate of the event, and numbers of operations and their location relative to noise sensitive areas. The other dimension is a description of the potential effects this noise has on people such as annoyance, activity interference, and sleep disturbance.

The USAF uses the energy equivalent continuous sound level, Leq(24) and its associate Ldn (24-hour Leq with a 10 dB nighttime penalty) for describing the noise around its air bases. The Percent Highly Annoyed (%HA) is then used to measure the effect on the community. This has been a very effective tool for the USAF and many others for evaluating the effects of aircraft noise around air bases and airports. Indeed in attitude studies, conducted worldwide, the percentage of people who feel highly annoyed when exposed to equal Ldns of aircraft noise is in remarkable agreement. Studies have also shown this same result for military

aircraft flown at USAF bases. But there are several factors that make noise from military aircraft operating on training routes substantially different from aircraft noise around airports or military air bases.

1. NOISE MEASUREMENTS

To define the differences in the acoustic signatures between aircraft operating under Military Training Route (MTR) conditions and typical air base operating conditions, a series of noise measurements were made at Wright-Patterson AFB in Ohio and Edwards AFB in California. These measurements were made on several types of military aircraft at typical MTR speeds (up to 580 Knots), current MTR altitudes (down to 150 m Above Ground Level, AGL), and proposed flight altitudes (down to 30 m AGL). Figure 1 is a comparison of the acoustic signatures for an F-4 aircraft of a typical MTR flight operation versus noise from an operation near an airbase (abbreviated in the following "airbase noise"). The maximum noise level for the MTR operation is considerably higher than for the airfield operation and has a dramatic increase in the onset rate. Not only are these levels higher, but they usually occur in areas where the background noise is less than that in which typical airfield flights operate. Therefore, the aircraft signal to background noise ratio or intrusion level for the MTR noise exposure will be substantially greater and perhaps lead to a greater annoyance response than for conventional airport/airbase noise exposure.

Because of the relatively low altitudes flown along MTRs, the higher level noise may have a major impact on communities. Table 1 is a comparison of measured noise levels from these low altitude-high speed studies that shows the difference between typical airbase and MTR operations. These aircraft noise levels often exceed 100 dB which is sufficient to induce some structural vibrations in residences. Occasionally these can be perceived directly as visual or tactual stimuli, or indirectly as rattling of loose objects. Studies have indicated that noise induced rattles have a significant effect in increasing the annoyance reaction. Also the increased noise levels, rapid onset of the signal and relatively large signal-to-noise ratios can, depending on circumstances, contribute to startle which, in turn, contributes to increased annoyance.

Table 1. MTR vs Airbase Operation Noise Levels*

AIRBASE OPERATION

Aircraft	Power	Altitude (m)	Airspeed (Kts)	Max A-Level (dBA)	SEL (dB)	Onse.. Rate (dBA/sec)
F-4	100 %RPM	500	250	104	112	4
F-16	90 %RPM	500	250	96	104	3
B-1	98 %RPM	500	250	100	108	3
B-52G	1.5 EPR	500	200	109	116	2

MTR OPERATION

Aircraft	Power	Altitude (m)	Airspeed (Kts)	Max A-Level (dBA)	SEL (dB)	Onset Rate (dBA/sec)
F-4	89 %RPM	60	500	120	115	61
F-16	84 %RPM	60	500	112	108	54
B-1	98 %RPM	60	580	121	117	60
B-52G	1.5 EPR	60	340	113	112	29

* Onset Rate computed from the 1/8 sec integration time history
  5 dBA above ambient to 5 dBA from Maximum A-weighted level.
* All values are for exposures directly under the flight track.

2. TRAINING ROUTE USE

The primary users of USAF MTRs are Tactical Air Command (TAC) and Strategic Air Command (SAC). TAC basically utilizes the routes with its high performance aircraft, like the F-15 and F-16 for training in low altitude Terrain Avoidance (TA) and Terrain Following (TF) exercises. SAC uses their routes primarily for low altitude penetration runs with bomber aircraft (B-52 & B-1) to a preselected target. Although TAC and SAC are the primary users, the Military Airlift Command (MAC), Air Force Reserve (AFRES), Air National Guard (ANG), and the Alaskan Air Command (AAC) use the routes developed by TAC and SAC and are beginning to develop routes for their own use.

The USAF under contract to Wyle Laboratories has conducted several studies to better define the type of operations and track dispersions along MTRs (ref 1 & 2). Figure 2 shows a typical SAC low altitude TF operation with a stage length of 240 to 400 kilometers with minimum heights of between 100 and 300 meters above the ground (AGL). SAC has four major routes similar to this that are flown by the B-52 aircraft between 1000 and 1500 times per year. MTRs are about eight kilometers wide for SAC routes and 20 kilometers wide for TAC routes. Aircraft fly these routes in the same direction creating a serial stream of noise exposures. The aircraft will be at the same altitude and airspeed for relatively long periods of time before changing to a new condition at a navigational point. Therefore to evaluate the total impact of a particular route one need only evaluate a cross section of each of these segments. This approach assumes that the aircraft noise is propagated over a relatively flat terrain and shielding effects are not considered.

The SAC pilots and navigators are scored by their ability to fly very precise bombing runs. Therefore they tend to fly very close to the route centerline. Conversely TAC pilots try to avoid detection, consequently they have a more even distribution over the entire route width (Figure 3). Measurements of dispersion from the track centerline were made for approximately one month each at one SAC route and two TAC routes. The measurements on these SAC and TAC routes shows that the lateral dispersion of the aircraft relative to the route centerline is a Gaussian distribution. For the SAC routes the standard deviation is about 800 meters (.5 statute mile). For the TAC routes where the aircraft follow a single dominant track the standard deviation is about 2000 meters (1.25 statute miles). For the TAC routes where the aircraft follow several tracks the distribution is the sum of the dispersion about each of these tracks. If multiple tracks are used but the location of the tracks are not known, the lateral dispersion can be estimated as Gaussian about the route centerline with a standard deviation of slightly over 4000 meters (2.5 statute miles).

Figure 4 is a cross section of an MTR segment showing the average Sound Exposure Level (SEL) values from a typical TAC MTR operation. This figure shows that although directly under the flight track there are very high SEL levels, these drop off rather quickly at ground locations off to the side of the flight track. In 300 - 600 meters (1000 - 2000 ft) offtrack, the noise levels can drop off by 20 to 30 from the maximum noise level for a single flight directly overhead. This rapid drop off is attributable to two factors. First, the slant distance to the aircraft increases rapidly for offtrack ground locations due to the low altitude of the flight. Second, the elevation angle to the flight track from low altitude flights causes a rapid transition from Air-to-Ground propagation to Ground-to-Ground propagation conditions. This attenuates the sound levels more as Excess Sound Attenuation losses in addition to those from spherical spreading and atmospheric absorption effects come into play. Along with the levels dropping off rapidly, the onset rate also falls off

rapidly with increasing lateral distance (Figure 5). This decreases the potential for startle and will cause less annoyance at these offtrack sites.

3. MTR HUMAN RESPONSE STUDIES

The USAF has conducted several experiments inhouse and under contract to examine the response of people to MTR noise exposures (references 4 & 5). One of the most important factors seems to be the onset rate of the flyovers. In a series of in-house studies USAF researchers examined the question of whether high onset flyover noise, typical of MTRs, contributes more annoyance than equal energy low onset rate noise. Forty-nine subjects were tested in four laboratory experiments. The subjects in experiment 1 were volunteers, military and civilian, ranging in age from 22 to 65. The remaining 3 studies were conducted using paid subjects consisting of mainly college students and housewives. Each subject experienced all conditions within a particular study. All experiments were designed to compare 24 hr equal energy exposure of low onset rate flyovers with high onset rate flyovers. In these experiments the subject sat between two banks of speakers and the flyovers seemed to pass over his head in a front to back direction. The noise source consisted of recordings of flyovers measured at Wright-Patterson AFB. A background noise level of 45 dBA was used for all experiments.

The annoyance reported by subjects after each simulated aircraft flyover was the most sensitive measure of low versus high onset rate. The results indicate that onset rate contributes annoyance that adds to the annoyance produced by the acoustic level of the flyover. A serial search task performed during the last three experiments enhanced the annoyance reaction to high onset rate flyovers. The annoyance measures showed a statistically significant difference between high and low onset rate conditions across all experiments. This difference was shown at the highest 76 dB Leq level in experiment 1 and at both the 72 and 66 dB Leq levels of experiment 2. Figure 6 shows the results of these experiments. In experiment 1 the greatest difference between conditions with equal Leqs was obtained for the highest level of 76 dB. In experiment 2 it can be seen that both high onset rate conditions were rated higher than their equivalent energy low onset rate condition. In experiment 3, all four conditions had an Leq of 67 dB and the difference between conditions was onset rate. For the mean annoyance based on exposure to the four flyovers during a 15 minute period, the three highest onset rate conditions were all significantly different from the lowest onset rate. In experiment 4, a paired comparison test was used to compare onset rates within a SEL value. The highest onset rate within a SEL level was rated as more annoying, in most cases it was rated significantly more annoying than at least one of the lower onset rates level. However, no

significant differences in annoyance ratings were obtained for the difference between the two lower onset rate values.

The overall results provided support for an interim metric proposed earlier; that the Sound Exposure Level be corrected by 16.6 log (onset rate/15 dBA per second) for onset rates between 15 and 30 dBA per second. The results of the most recent study suggest that the penalty is needed but it may be necessary to extend the penalty beyond 30 dBA per second. More research is needed to determine exactly how a final metric for high onset rate noise is to be applied.

The USAF under contract to Wyle Laboratories conducted and is currently conducting various Laboratory studies to determine the key psychoacoustic parameters associated with MTR flyover noise exposure. The parameters that are being studied are Onset rate, Decay rate, Duration, Level, Direction of sound source, Expectation, and Indoor/Outdoor exposures. A basic set of twelve stereo sound recordings was prepared, consisting of four types of military aircraft with various onset rates plus one civil aircraft. These aircraft flyby sounds were presented at four sound levels to subjects in an indoor listening facility and at an outdoor facility. Indoor sounds (from 95 to 65 dB SEL) were filtered according to a typical outdoor/indoor residential noise reduction curve. Sounds were presented in random order, at random time intervals, and random approach from either in front of or behind the subjects. Subjects rated each sound on a seven-point word annoyance scale with two out-of-bounds selections available for a total nine-point scale. Two companion experiments were performed at the outdoor facility (from 115 to 85 dB SEL). These experiments used modified military aircraft sounds with particular onset rates from 5 to 100 dBA/second and decay rates from 2 to 30 dBA/second.

Participants in these experiments were drawn from the local area around Langley, Virginia. Thirty-six subjects participated in the Kernel experiment that consisted of 2 sessions each, indoors and outdoors. Twenty-four subjects participated in an onset rate specific study that consisted of 2 sessions outdoors. Another 24 subjects participated in the independent variable experiment that also consisted of 2 outdoor studies. Each session had six participants per session that lasted two hours and had 48 to 60 flyover exposures with a ten minute break between sessions. The participants were instructed to read magazines for their tasking. An analysis was made to see which methodological and psychoacoustic effects showed a significant variance. All tests for significance were at the alpha = 0.05 level. For the methodological effects, no significance was found for repetition 1 vs 2, front vs back approach, or interactions of effects. Significant variance was found

Table 2. MTR annoyance effects

EFFECT	R²	SLOPE
Sound Level (SEL, dB)	.513	.154
Onset Rate (dB/sec)	.079	.009
Decay Rate (dB/sec)	.081	.027
Total Duration (sec)	.023	-.010

Slopes are ANNOYANCE SCORE PER: dB for SEL
Log(rate) for rates
Seconds for duration

All variables are significant at 0.05 level.

for outdoors vs indoors, groups of 8 participants, and for individuals. Significant variance was found for all the psychoacoustic effects of Sound Level, Onset Rate, Decay Rate, Total duration, 10-dB down duration, and interactions. Table 2 shows the preliminary results of the linear regressions for these data. This table shows that sound level accounts for the majority of the annoyance response but onset and decay rates do have a measurable effect. Although in the laboratory studies the onset and decay rates have the same level of effect, in the MTR environment a typical noise signature will always have a steeper onset than decay rate. Although not complete, these studies show that annoyance response to MTR noise is significantly different from response to most airbase type aircraft noise.

4. LDN METRIC

The typical use of MTR routes leads to another important difference from airbase operations. MTR operations have a relatively low occurrence on a daily basis and can have stream missions with serial exposures of five to ten aircraft flyovers with approximately 15-minute spacing between flyovers. Sporadic noise exposure of this type has not been represented in any previous studies conducted on response to aircraft flyover noise. The Ldn - %HA approach assumes at least a certain number of flights on a daily basis. Some suggest that, at a minimum, there must be one to three daily noise events for the Ldn - %HA relationship to be valid. This relationship currently has no provision to cover flights that occur every third day, weekly, monthly, or generally with a sporadic pattern.

In a review (ref 3) of the origin and domain of the Ldn metric, Wyle Labs examined several major socioacoustic studies and found that fundamentally all tended to support a 10 Log₁₀N event factor (a range of 8 to 12 times Log₁₀N could be supported by these studies). In the United Kingdom airports study, this is of significance since it supersedes the earlier studies which had supported the 15 Log₁₀N adjustment. Figure 7 shows the range of number of events and levels that these studies covered. Although no community response studies have been done in the range of typical MTR exposures (upper left of Figure 7), there are credible studies at comparable sound levels and higher numbers, and at comparable numbers and lower levels. Therefore, it seems reasonable to extrapolate into the MTR domain from either sound level or number of events. Because of the sporadic nature of an MTR exposure the USAF has suggested computing the Ldn over the busiest (calendar) month within any given year. This is because training phases or exercises can exist for periods of weeks or months and then quit. This creates a situation where the annual average will underestimate the impact of these operations. These two factors, onset rate and monthly operations, are the only deviation from a pure Ldn that the USAF is using for predicting the community annoyance from MTR operations.

5. HEARING DAMAGE

Aside from annoyance, the other major factor to be considered in evaluating the impact of the noise from combat aircraft training areas is potential hearing damage. The USAF position with regard to assessing the risk of hearing damage is to use the ISO Standard 1999 (1990) (ref 8). This standard provides guidance for the prediction of potential hearing impairment from daily exposure to steady, fluctuating, or impulsive type noise. It was approved by the overwhelming majority of all countries voting on it. The standard allows the calculation of the statistical distribution of the noise-induced permanent hearing loss to be expected in a population experiencing exposure to various sound pressure levels over periods from zero to forty years. The recommendations of this standard are extensions of a very large data base of the effects of noise on human hearing.

Figure 8 shows an eight hour Leq plotted against the log number of events for SELs of 115, 110, 105, and 100 dB. The actual number of events are shown above each data point. Twenty-nine events at a SEL of 115 dB gives an Leq(8h) of 85 dB while 911 events are necessary at a SEL of 100. This 85 dB Leq(8h) level is the level where less than a 10 dB Noise Induced Permanent Threshold Shift (NIPTS) would be expected in the most sensitive 10% of the population for the frequencies of 0.5, 1, 2, 3, 4, and 6 kHz after a 40 year daily exposure according to ISO Standard 1999. Although not included in Figure 8, it can be shown that 3 flights with a SEL of 125 dB would be needed to produce an Leq(8h) of 85 dB. It would take an F-4 flying at 100 ft AGL directly overhead to obtain an SEL of 125 dB which would be an accidental

exposure. It is important to recognize that these values are for levels directly impinging on the human ear. If a person were inside a building these levels would be attenuated by 10 to 30 dB depending on the structure. Also in order to reach these high noise levels all of the overflights would have to fly directly over the individual. Although these higher SEL levels have been recorded for single low level passes, these levels of exposure (to obtain an 85 dB Leq(8)) have never been observed or documented on a continuing basis from any MTR operations. It is also important to realize that according to ISO 1999, this 85 dB Leq(8h) can occur for at least 5 days a week (the work week), every week for 40 years before this rather low level of permanent hearing damage is reached.

To further examine the potential for hearing damage from MTR operations, the USAF is currently conducting an inhouse study to look for Temporary Threshold Shifts (TTS) caused by MTR noise exposures. The same recordings used in the previous studies will be used with programmable attenuators to control the exposure level at the ear. Current plans are for 30 subjects to be exposed to MTR flyover noise signatures at levels up to 128 dBA maximum level. Audiograms for each subject will be collected before and after each of these tests looking for TTS. If no TTS is found in any of the 30 subjects the test will be expanded to include more subjects and multiple exposures. These tests are currently scheduled to be completed in December 1991.

SUMMARY AND CONCLUSION

In conclusion, we believe that MTR type noise exposures are different from typical airbase noise exposures and require a modification of the procedure to relate annoyance to Ldn. This alteration is needed to account for the increased annoyance caused by the rapid onset rate of MTR noise. Although these differences are most pronounced directly under the aircraft, it should be noted that this onset rate decreases very quickly as the lateral offset distance to the flight track is increased. The preliminary findings of our studies show that although a penalty for high onset rates is warranted, it is not clear what the exact level or range of the penalty should be. Due to the sporadic nature of the MTR operations, we believe that the Ldn metric needs to be integrated over a calander month of the MTRs busiest operations. To evaluate any potential hazard to hearing we believe that the recommendations of ISO standard 1999 are the best data available to describe the impact from MTR operations. Even though we do not think, based on this standard, that hearing loss is or will be a problem from present day numbers and levels of overflights, we are conducting studies to further address this question.

REFERENCES

1. Plotkin, K.J., Croughwell, E.P., "Environmental Noise Assessment for Military Aircraft Training Routes Volume 1: SAC Low-Level Routes", AAMRL-TR-87-001, April 1987.

2. Plotkin, K.J., "Environmental Noise Assessment for Military Aircraft Training Routes Volume 3: TAC Low-Level Routes", AAMRL-TR-87-001, January 1988.

3. Plotkin, K.J., Sutherland, L.C., Molino, J.A., "Environmental Noise Assessment for Military Aircraft Training Routes Volume 2: Recommended Noise Metric", AAMRL-TR-87-001, April 1987.

4. Harris, C.S., "Effects of Military Training Route Noise on Human Annoyance", AAMRL-TR-89-041, October 1989.

5. Harris, C.S., "Effects of Military Training Route Noise on Human Annoyance", NOISE-CON 90, Austin TX, 15-17 October 1990.
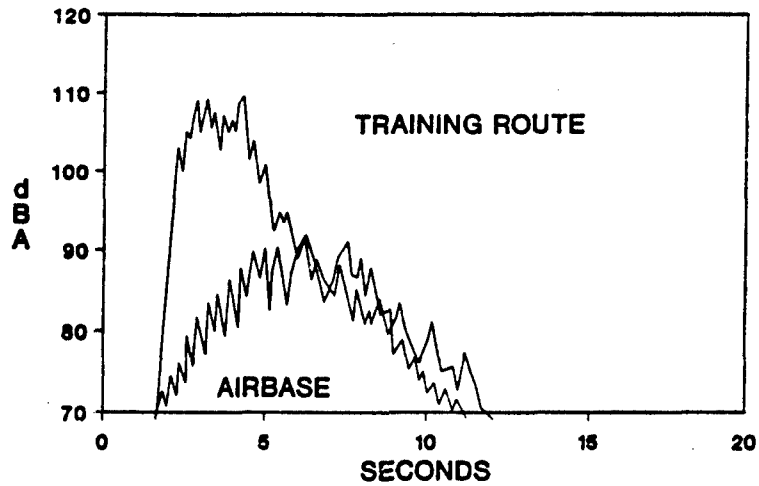
F-4 AIRCRAFT NOISE
(AL/OEBN)

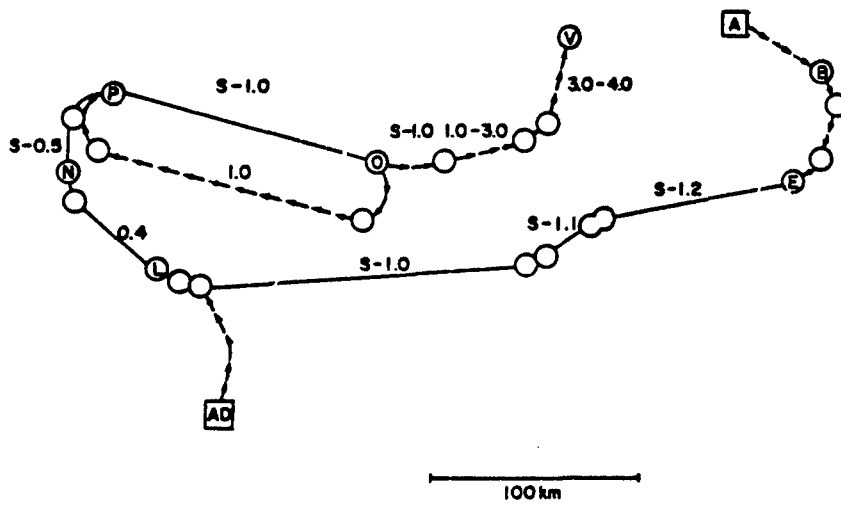
FIGURE 1. MTR VRS AIRBASE NOISE SIGNAL

100 km

FIGURE 2. TYPICAL STRATEGIC TRAINING ROUTE - ALTITUDES ARE
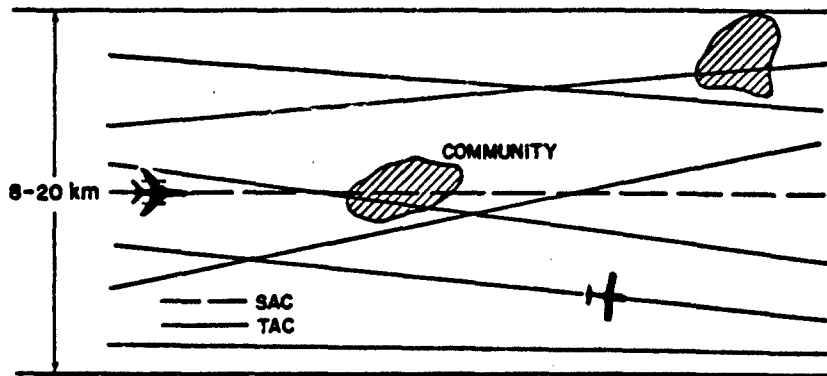SURFACES(S) TO MINIMUM ALTITUDE AGL x 1000 M
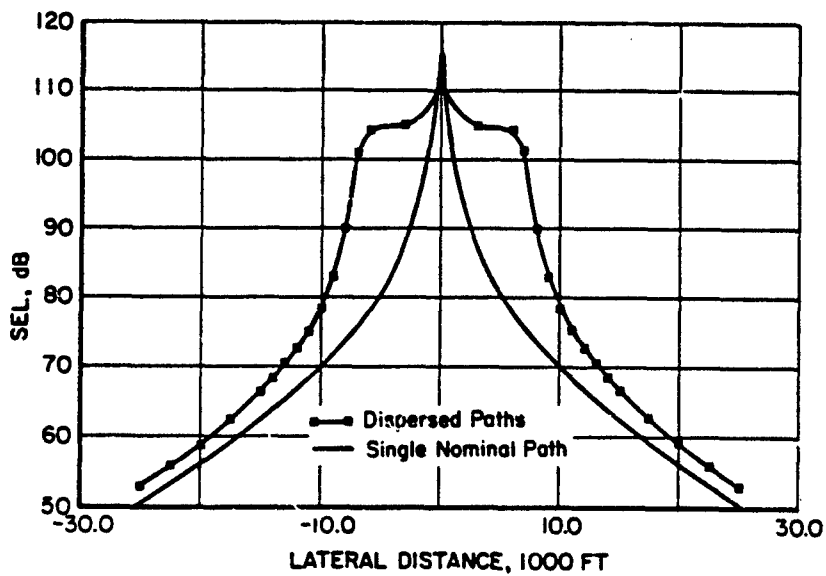
FIGURE 3. TYPICAL FLIGHT TRACKS FOR MTR

FIGURE 4. ESTIMATED AVERAGE SEL VALUES ON A TYPICAL MTR
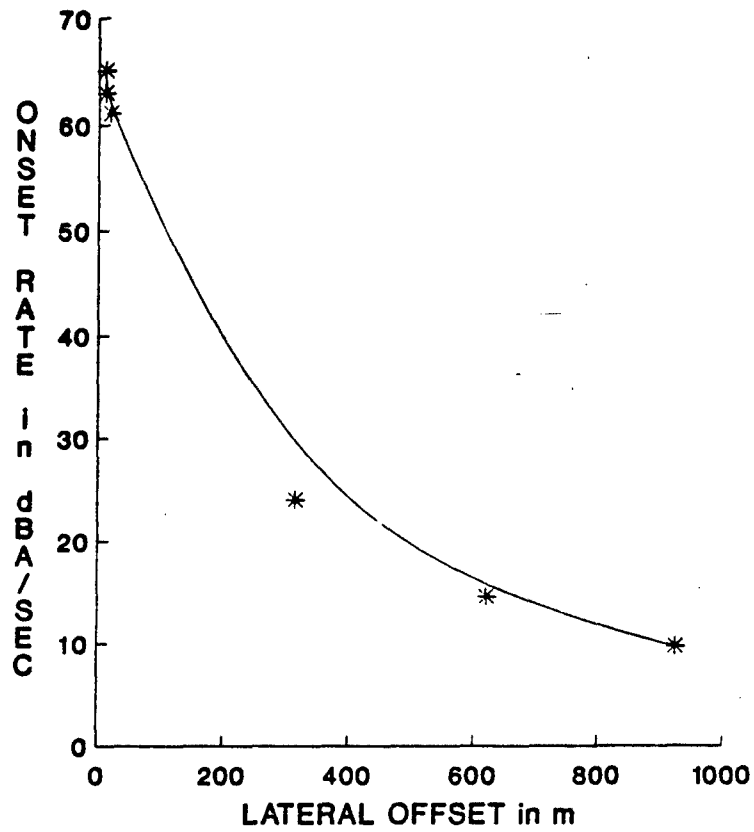(F-15 AT 250 FT AGL)
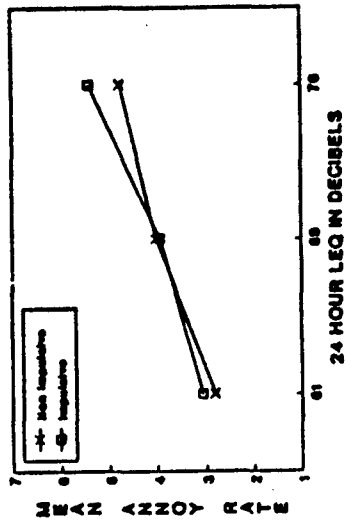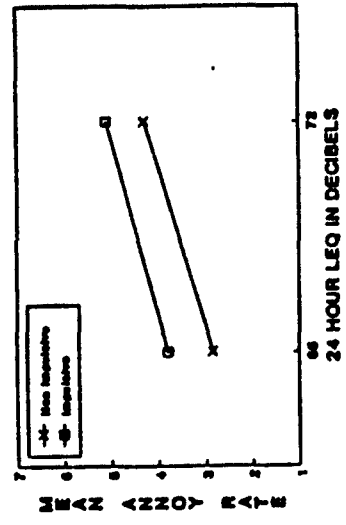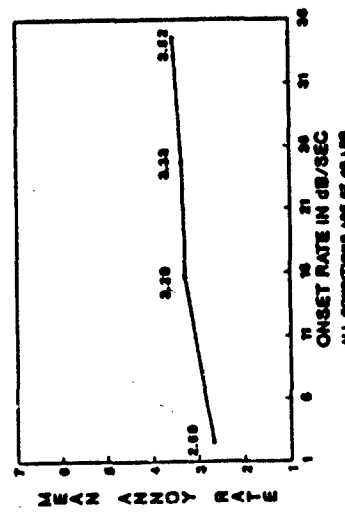
F-4 TRAINING ROUTE (AL/OEBN)
76 METERS AGL (590 kts)

Figure 5. Offtrack Onset Rates

Mean Annoyance for Four Flyovers per Condition
versus Leq for Experiment II.

24 HOUR LEQ IN DECIBELS

Mean Annoy versus SEL and Onset Rate for Exp. 4.

ONSET RATE IN dB/SEC

Mean Annoyance for Four Flyovers per Condition
versus Leq for Experiment I.

24 HOUR LEQ IN DECIBELS

Mean Annoyance for Four Flyovers per Condition
versus Onset Rate for Experiment III.

ONSET RATE IN dB/SEC
ALL CONDITIONS ARE 67 dB LEQ
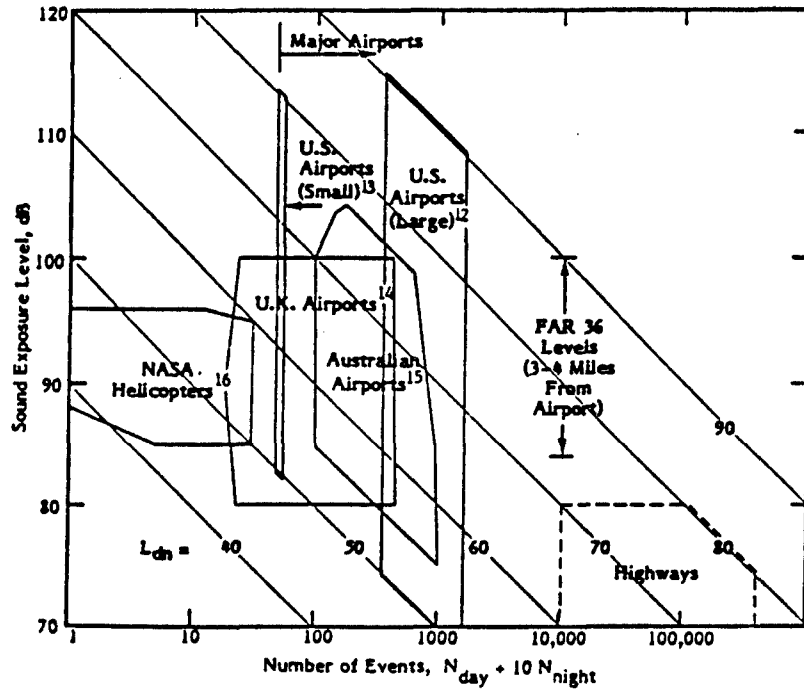
FIGURE 6. IN-HOUSE ANNOYANCE VS ONSET RATE STUDIES

FIGURE 7. SOUND EXPOSURE LEVEL AND NUMBER-OF-EVENTS DOMAIN
OF SOCIOACOUSTIC STUDIES SUPPORTING L_{DN}

(TAKEN FROM WYLE LABORATORIES TECHNICAL REPORT,
AAMRL-TR-87-001, APR 87)

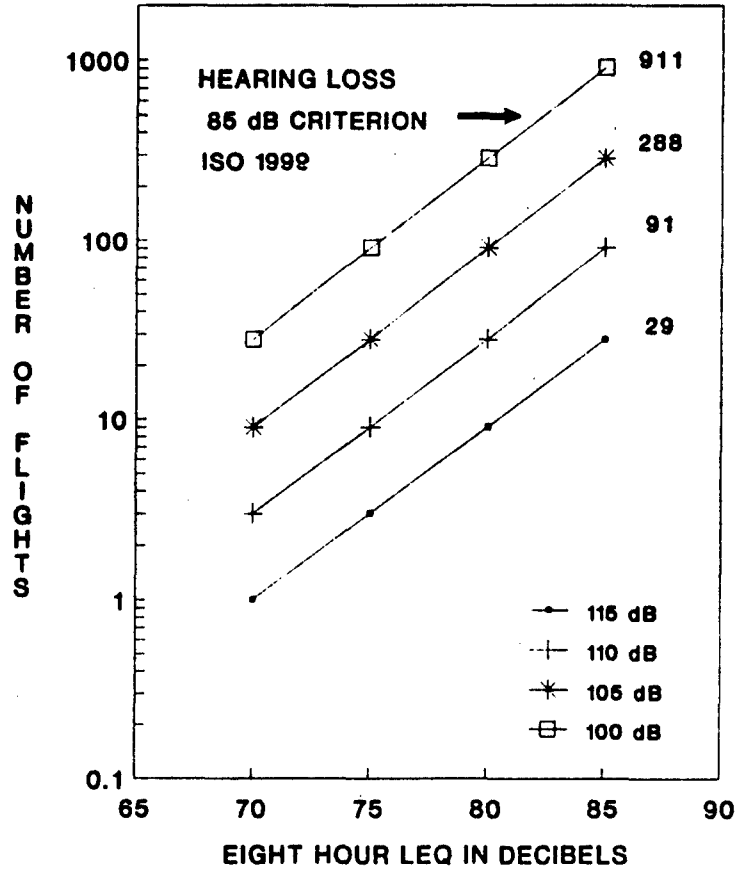Number of Flights allowed per day at 85 dB.

FIGURE 8. Leq vs Number of Flights for various SELs

Discussion

QUESTION BY: R.A. Pinker, RAE Pyestock, UK
Please could you define your metric "onset rate"?

AUTHOR'S RESPONSE:

Onset rate is a measure of the suddenness of the acoustic signal from an approaching aircraft measured in dBA per second. Specifically, we calculate the onset rate from the acoustic time history by measuring the time when the signal is 5dB above the background level to the time of the peak A-level. The difference in these two levels is then divided by this time difference to obtain the slope of the rising signal. This is the onset rate. We only compute an onset rate if the background to peak difference is greater than 15dBA. If the peak is not on the uprising slope then the computation is made from a point 5dBA below the peak.

BRUIT DES AVIONS DE COMBAT A PROXIMITE DES BASES AERIENNES
-Revue des possibilités de réduction du bruit à la source-

par

D.COLLIN,J.JULLIARD et G.RIOU
(SNECMA,Villaroche,77550,France)

RESUME

Les opérations effectuées par les avions de
combat sont source de nuisances pour les
populations situées à proximité des bases
aériennes.Il apparait que le bruit de jet
constitue la source de bruit dominante au
cours de la quasi totalité des opérations
concernées.

Les auteurs proposent d'aborder la question
de la réduction des nuisances sonores
correspondantes en utilisant l'expérience
acquise par la SNECMA au cours de plus de
vingt années de recnerches sur le bruit des
turboréacteurs civils,et notamment du
programme de transport supersonique
Concorde. L'importante base de données
expérimentale résultant de ces études a
permis de développer et d'évaluer méthodes
de prévision et solutions de réduction du
bruit. Les différents mécanismes et sources
de bruit significatifs seront donc passés
en revue ainsi que les possibilités de
réduction et d'amélioration actuelles ou
futures.

1.0 INTRODUCTION

Si on assiste à l'émergence de nouveaux
problèmes,liés au caractère particulier des
opérations propres aux avions de combat
(vol à basse altitude et grande vitesse),
et qui concernent principalement les
populations de zones non urbaines en
général peu habituées aux nuisances
sonores,il n'en reste pas moins que les
contraintes de voisinage associées à une
urbanisation sans cesse grandissante ne
peuvent plus être considérées comme
l'apanage exclusif des aéroports civils.
Dans cette optique,l'examen du bruit généré
par les simples opérations de décollage et
d'atterrissage des avions de combat semble
présenter un intérêt certain.

Si l'on compare,à titre d'exemple,
l'empreinte au sol(Fig.1) d'un avion de
combat au décollage, à celle d'un avion
civil de 150 places ainsi qu'à celle d'un
autre type d'avion militaire (ravitailleur
1ère et 2ème génération),il apparait en
effet que malgré des performances
supérieures entrainant une trajectoire plus
favorable ,la nuisance reste identifiable,
quoique nettement réduite par rapport à
celle d'un quadriréacteur de première
génération.

L'essentiel des recherches acoustiques
effectuées dans l'industrie ayant été
consacré,pour raison de certification des
avions civils,au bruit émis lors des phases
de décollage et d'approche,il convient
d'examiner dans quelle mesure ces
enseignements sont applicables aux avions
de combat.

Après avoir identifié les sources de bruit
dominantes sur deux types de moteur
d'avions de combat,on passera donc en revue
les solutions possibles de reduction du
bruit du point de vue de la technologie des
moteurs civils et principalement du
programme Olympus ainsi que des recherches
associées qui furent menées à la Snecma.

2.0 IDENTIFICATION DES SOURCES DE BRUIT DOMINANTES

Une étude a été conduite sur deux moteurs
équipant respectivement un chasseur
monomoteur(Mirage 2000/M53) et un bimoteur
d'attaque au sol (Alphajet/Larzac).
Elle a consisté en une caractérisation
acoustique détaillée effectuée sur banc
d'essais au sol.

Bien qu'étant de nature et de conception
fort différentes,ces deux moteurs
présentent certaines similitudes dans leur
comportement acoustique (Fig.2).

L'émission du M53,monocorps double flux
avec rechauffe,est dominée par le bruit de
jet dès les conditions d'approche.Le bruit
interne et le bruit de soufflante méritent
cependant une certaine attention à faible
poussée.

L'émission du Larzac,double corps double
flux sans rechauffe,possède en revanche la
caractéristique d'être légèrement dominée
par le bruit interne dans la plage de
poussée correspondant à l'approche avant
que le bruit de jet ne reprenne la
prépondérance.

Si l'on estime que ces observations
s'appliquent vraisemblablement à l'immense
majorité des moteurs actuellement utilisés
sur les avions de combat,il s'agit donc
bien de considérer en priorité le bruit de
jet et ses moyens de réduction.

Il sera toutefois sage de ne pas négliger
pour autant l'importance des sources de
bruit généralement regroupées sous le
qualificatif un peu vague de "bruit
interne".

3.0 SOLUTIONS ELABOREES DANS LE CADRE DES RECHERCHES SUR TURBOREACTEURS CIVILS

On rappellera dans un premier temps que la
prépondérance du bruit des parties
tournantes sur les machines civiles
actuelles a conduit à l'élaboration d'une
technologie de pointe dans le domaine des
structures absorbantes que ce soit sur le
plan des méthodes ou celui de la
fabrication autorisant désormais la
réalisation de structures complexes à
plusieurs degrés de liberté fort efficaces
et de faible poids grâce à l'introduction
de matériaux composites.
Ceci s'accompagne de mesures conservatoires
prises lors des phases de conception du
moteur afin de limiter son émission sonore.

Toutefois,en ce qui concerne les sources de
bruit évoquées plus haut pour les moteurs
militaires,ce sont les études effectuées au
début des années 70 dans le cadre du
programme Concorde ainsi que les recherches
effectuées dans son prolongement qui sont
les plus à mêmes de fournir des éléments de
réponse quant aux possibilités réelles de
réduire le bruit des avions de combat.

3.1 Etudes Sur La Réduction Du Bruit De Jet

La première leçon à tirer des études menées
dans le cadre du programme Concorde est
désormais bien connue.Il s'agit de
l'influence importante des effets de vol
sur le comportement des sources de bruit
(Fig.3).Cette observation a conduit la
Snecma à mener ses études postérieures sur
des moyens d'essais simulant les conditions
d'écoulement du vol,soit dans un premier
temps le véhicule expérimental Aérotrain,
puis actuellement la soufflerie anéchoïque
CEPRA19.D'une manière plus générale, cette
expérience a contribué à forger une
philosophie de prudence vis à vis des
performances de tout système réducteur
démontrées sur le papier ou lors d'un essai
en condition statique,lorsque le bruit de
jet est impliqué.

Pour cette raison ,seules seront présentées
ici les solutions ayant effectivement fait
l'objet d'une démonstration en vol sur
Concorde,trois principales directions ayant
été explorées jusqu'à cette étape décisive.

Soit:

- l'optimisation dynamique de la
  géométrie de la tuyère secondaire
  en fonction des phases de vol

- le fonctionnement du moteur avec des
  sections de tuyères maximales

- l'introduction de dispositifs
  silencieux dans le jet

3.1.1 Effet De La Tuyère A Paupières (dite "2S")

La réduction maximale du bruit au point de
contrôle latéral a été obtenue en
positionnant en phase initiale de montée
les paupières de la tuyère variable à un
angle de 30° avant repositionnement à 10°
lors de la phase de réduction de poussée.

Le braquage de paupières permet en effet de
jouer sur la directivité de l'émission
sonore du jet par pincement de celui-ci
(Fig.4). Schématiquement,on note que le
pincement réduit l'énergie acoustique
rayonnée dans le plan horizontal pour
l'accroître toutefois dans une moindre
mesure dans le plan vertical.

Le gain obtenu par ce dispositif sur le
niveau de bruit au point de controle
latéral a pu être évalué à 2.5 EPNdB.

3.1.2 Effet De La Section De Tuyère Primaire Variable

L'adoption d'une configuration de tuyère
primaire à section variable a permis une
réduction de bruit très significative en
autorisant le fonctionnement du moteur avec
des sections d'éjection agrandies pour
réduire la vitesse du jet à poussée
constante,à l'exception bien sûr de la
phase de montée initiale.

Les mesures effectuées sur banc volant et
plus tard sur Concorde(Fig.5) ont montré
les bénéfices importants à tirer d'un tel
procédé,ceci s'accompagnant évidemment de
modifications également importantes de la
régulation du moteur.

3.1.3 Etudes Sur Les Concepts De Dispositifs Silencieux

Les inconvénients des dispositifs
silencieux surajoutés sont bien connus.
Généralement pesants et volumineux,ils
contribuent à augmenter de façon
significative la consommation.Ils sont en
outre générateurs de pertes de poussée
importantes et la compensation nécessaire
les ampute de tout ou partie de leur
efficacité.

Afin d'éviter toute pénalisation de trainée
supplémentaire en croisière supersonique,on
s'est orienté dès le début du programme
Concorde vers le développement de systèmes
internes escamotables en croisière et le
système retenu après une multitude d'essais
au sol fut le système dit "à pelles"
pouvant fournir un gain estimé alors à 4
EPNdB tout en limitant les pertes de
poussée à environ 5%,ce que l'on pensait
suffisant pour obtenir un gain appréciable
en vol.

Les essais en vol de ce dispositif se sont hélas révélés moins prometteurs.En effet pour les deux gradients de montée envisageables dans la phase de réduction de poussée,aucune amélioration significative n'a pu être observée (Fig.6) et le système fut donc purement et simplement abandonné.

Cependant un vaste programme d'études fut entrepris consécutivement afin d'étudier plus finement le comportement du bruit de jet en vol et d'approfondir d'autre part les connaissances en termes de bruit et poussée sur divers types de silencieux dans l'optique d'un éventuel transport supersonique de deuxième génération.

L'utilisation pour ce faire du véhicule expérimental Aérotrain(Fig.7) a permis de s'affranchir des problèmes causés,lors du programme Concorde,par l'évaluation en condition statique des dispositifs réducteurs de bruit.

L'étude et l'évaluation expérimentale de plusieurs concepts a permis en finale la réalisation d'un silencieux dit "41 Tubes" d'encombrement minimum(rapport de la section du culot sur section efficace d'éjection égal à 2),fournissant un gain égal à 10 EPNdB et pouvant atteindre 15 EPNdB lorsqu'associé à un éjecteur traité (Fig.8).

La perte de poussée associée,estimée à 8%,situe ce type de silencieux dans un rapport de 2dB d'atténuation par % de perte de poussée,ce qui semble être désormais la tendance générale si l'on se réfère aux informations publiées sur le sujet.

Il sera utile de mentionner enfin que, parallèlement,ce programme Aérotrain aura conduit à poser les bases de la quantification de l'effet de la vitesse de vol relative sur le bruit de mélange telle que formulée dans l'ARP 876C,ainsi qu'à établir une base de données expérimentale utilisée postérieurement pour la validation de la soufflerie CEPRA19.

3.2 Etudes Sur La Réduction Du Bruit Interne

Les caractéristiques particulières du moteur Olympus ont également été à l'origine d'enseignements sur la génération de ce que l'on a voulu définir par la notion large de "bruit interne".

En effet si l'on observe le comportement du moteur Olympus à régime partiel(Fig.9),on constate que le bruit interne exerce une influence grandissante jusqu'à devenir prépondérant dans les conditions d'approche.

Le bruit interne fut alors défini comme la différence sur tout le domaine de fréquences entre le bruit total émis par le moteur et le bruit d'un jet pur qui correspondrait aux conditions d'éjection équivalentes,posant par là même le bruit de soufflante ou de compresseur comme négligeable.

Cette définition résultait du fait que les différents mécanismes générateurs et surtout leur interdépendance étaient alors très mal connus.

Un simple exemple illustrera cette notion d'interdépendance des mécanismes générateurs.Il traduit l'effet produit sur l'émission sonore de l'Olympus 593 par la substitution d'une chambre annulaire à la chambre de combustion d'origine(Fig.10). Alors qu'a priori on se serait attendu à des modifications caractéristiques dans la partie basses fréquences du spectre, généralement attribuée au bruit de combustion,on observe également des modifications notables du domaine hautes fréquences.

Une tentative de classification des différents mécanismes fut effectuée à la même époque.Elle mettait en évidence trois familles distinctes(Fig.11):

- les sources internes,c'est à dire toutes les sources naissant à l'intérieur du moteur entre un plan situé au voisinage de la chambre de combustion et une position située approximativement à une longueur d'onde caractéristique en amont du plan d'éjection de la tuyère.

- les sources de tuyères qui résultent des phénomènes d'interaction des hétérogénéités de l'écoulement et des instabilités de la couche de cisaillement initiale du jet avec la tuyère.

- Une amplification paramétrique des sources internes par la couche de cisaillement du jet.

Dans le but d'améliorer la compréhension de certains de ces points et particulièrement des mécanismes à l'origine des sources internes,une série d'expériences complémentaires fut réalisée à l'aide d'un dispositif spécifique élaboré sur la base d'un moteur Larzac,et permettant de s'affranchir de toute source autre que le bruit interne(Fig.12).

Grace à ce dispositif,on a pu dans un premier temps cerner les caractéristiques des différentes composantes des sources internes et distinguer ainsi trois domaines de fréquences distincts(Fig.13):

- Basses fréquences(< 400 Hz) dans lequel apparait une bosse bien marquée aux faibles régimes avec une fréquence de pointe au voisinage de 125-160 Hz. Cette bosse subsiste plus estompée aux régimes plus élevés et à une fréquence supérieure (200 à 250 Hz).Cette émission est directement imputable aux effets de la combustion.

- Moyennes fréquences(entre 500 et 3000 Hz) dont la fréquence de pointe ne varie pratiquement pas avec le régime et dont l'origine est à rechercher au niveau des interactions de l'écoulement

turbulent avec des obstacles fixes
ou mobiles du moteur.

- Hautes fréquences(>3000 Hz) dans
lequel coexistent raies
caractéristiques issues des turbines
et bruit large bande y prenant
naissance tant par des mécanismes
directs que par des phénomènes plus
complexes.

Ces caractéristiques pour spécifiques
qu'elles soient du moteur Larzac utilisé
présentent un fort lien de parenté avec les
observations effectuées sur l'Olympus.

Un deuxième type d'expérience,réalisé à
l'aide du même dispositif, a permis
d'évaluer diverses solutions de réduction
du bruit interne dans sa partie basses et
moyennes fréquences.

Les différentes solutions essayées ont
consisté d'une part en l'insertion d'écran
entre source et observateur et d'autre part
en la mise en oeuvre de structures
absorbantes dans le canal d'éjection
primaire.La conception volontairement
simplifiée de ces structures a permis
d'apprécier aisément l'influence de l'effet
d'épaisseur.

Tenant compte de ces conditions ,les
résultats présentés(Fig.14) pour la
combinaison la plus efficace peuvent être
considérés comme représentatifs de l'ordre
de grandeur de ce qu'il est possible
d'atteindre en matière de réduction du
bruit interne par des dispositifs de ce
genre.

On rappelera pour mémoire que l'application
d'une solution voisine (canal primaire
traité) fut un moment envisagée sur
l'Olympus avant d'être abandonnée en raison
de la persistance d'une résonance
acoustique de l'ensemble secondaire qui en
masquait les effets positifs.

4.0 APPLICABILITE DES SOLUTIONS AUX AVIONS DE COMBAT

L'expérience de Concorde et les études
associées présentées plus haut ont certes
mis en évidence la possibilité de réduire
d'une dizaine de décibels le bruit des
sources prépondérantes à l'aide de
dispositifs réducteurs essentiellement
externes.Mais elles ont également souligné
le caractère rapidement illusoire de telles
mesures lorsqu'elles sont appliquées à des
moteurs dont la conception a été figée
préalablement. Importantes pertes de
performances,excédents de poids plus que
significatifs,sans oublier les problèmes de
maintenance générés par la complexité
mécanique de ces dispositifs,ce sont là des
inconvénients majeurs dont un avion de
combat peut a priori difficilement
s'accomoder.

Il est donc raisonnable de considérer que
seul un objectif de réduction limité
pourrait tirer profit de la technologie
existante.

De fait,l'identification de solutions
adaptées aux nuisances générées par les
avions de combat aux abords des bases
aériennes réside en premier lieu dans un
effort de définition du problème:
la disparité des missions confiées à ces
avions constituant,à cet égard, un élément
important du débat.

Si une telle phase de clarification
s'avérait nécessaire du point de vue de
l'environnement,il serait alors essentiel
de dégager les facteurs spécifiques aux
nuisances acoustiques des avions de combat,
quelle qu'en soit leur nature(opérationels,
technologiques,psycho-acoustiques, socio-
économiques,...), non sans avoir au
préalable déterminé dans quelle mesure la
situation présente des similitudes avec les
contraintes imposées aux avions de
transport civils.

Ainsi seulement pourrait-on parvenir à
définir ce qui est acceptable et ce qui ne
l'est pas.

S'il est en effet difficilement admissible
de se voir confronté sans préavis à une
réglementation dont la sévérité ne repose
sur aucun fondement technologique,il est en
revanche important de pouvoir anticiper sur
des objectifs de réduction de bruit futurs,
de manière à permettre l'identification et
le développement des technologies les mieux
adaptées.

Dans un tel contexte,des solutions
intégrées dès le premier stade de la
conception d'un moteur,ou mieux encore
faisant intégralement partie,tel le cycle
variable,du concept lui-même mériteraient
d'être considérées.

BIBLIOGRAPHIE

J.CALMON/R.HOCH
Performance and noise aspects of supersonic
transport.
Inter Noise 73

P.THOMAS/R.HOCH/E.WEISS
An experimental investigation of the core
engine noise of a turbofan engine.
AIAA 2nd Aeroacoustics conference 1975

JP.DUPONCHEL/P.THOMAS
Impact of flight effects on multitube
suppressor design.
AIAA 6th Aeroacoustics conference 1980

Figure 1

Comparaison De L'Exposition Au Bruit Pour Différents Types D'Avions
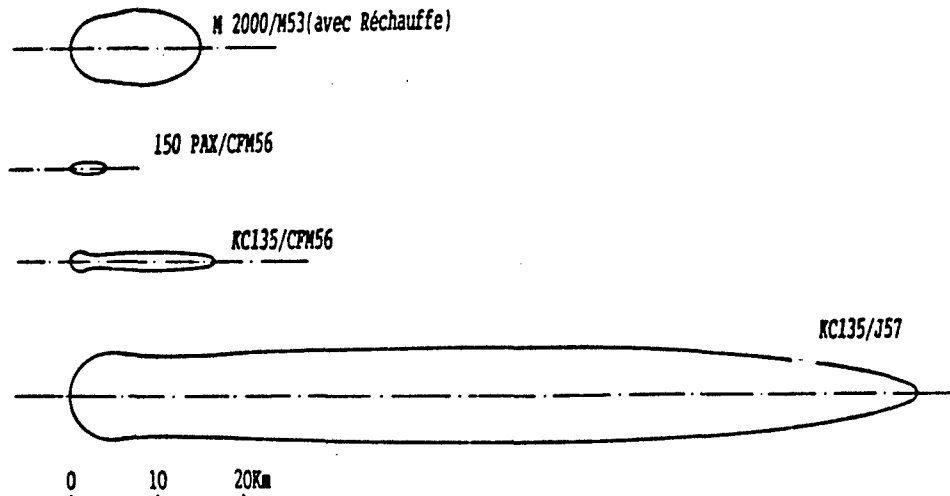
ISO CONTOUR 90 EPNdB - Décollage Sans Réduction

M 2000/M53(avec Réchauffe)

150 PAX/CFM56

KC135/CFM56

KC135/J57

0   10   20Km

Figure 2

Contribution Relative Des Sources De Bruit

OASPL(Valeurs Maximales)   M53-5

APPROCHE   Plein Gaz Sec   Plein Gaz PC

JET

BRUIT INTERNE

SOUFFLANTE

10 dB

POUSSEE STATIQUE

OASPL(Valeurs maximales)   LARZAC 01

Plein Gaz Sec

APPROCHE   JET

BRUIT INTERNE
SOUFFLANTE

10 dB

POUSSE STATIQUE
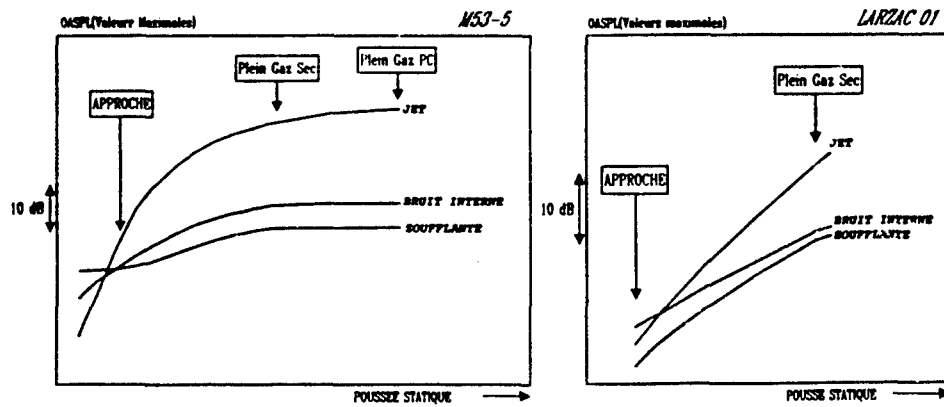
Figure 3

Effets De Vol Sur Le Bruit De Jet
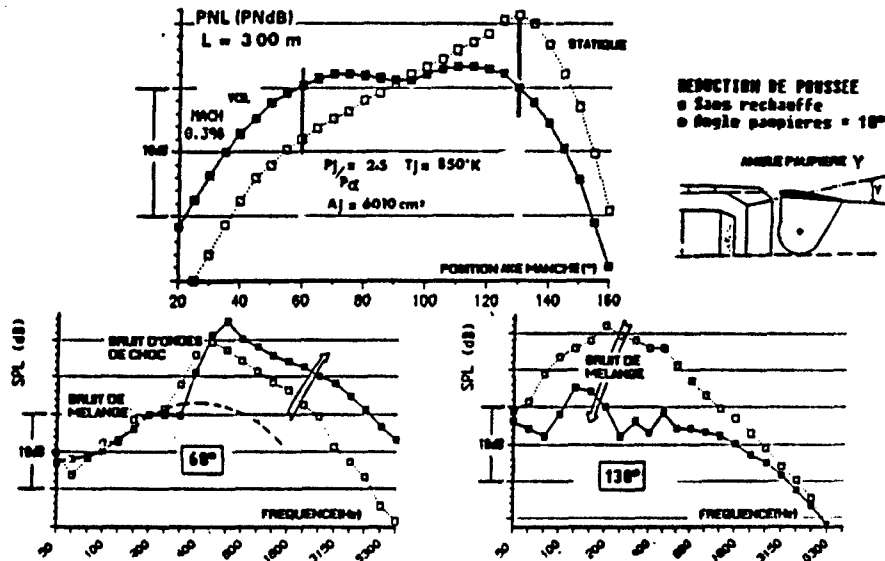
Figure 4

Performances Acoustiques de La Tuyère 28
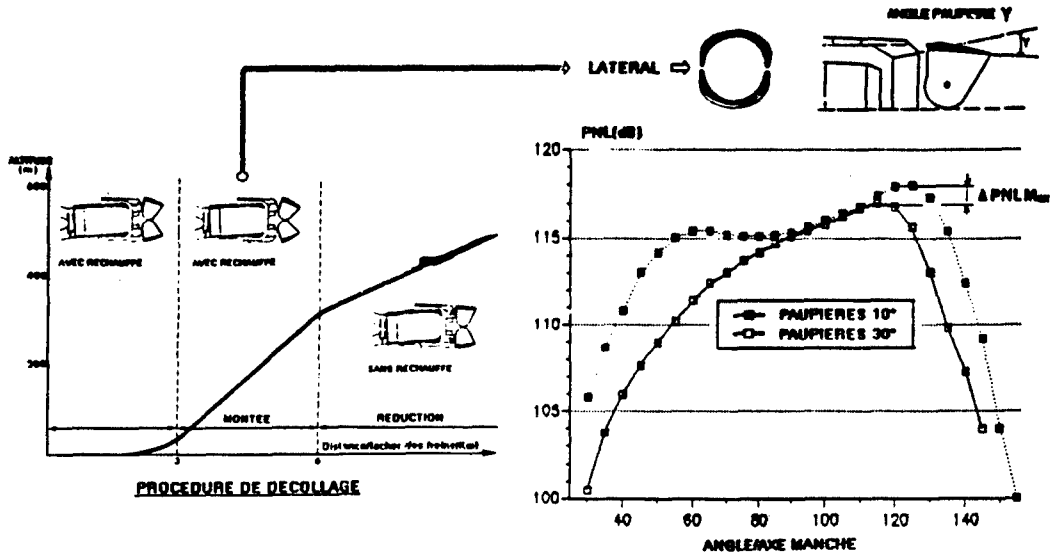
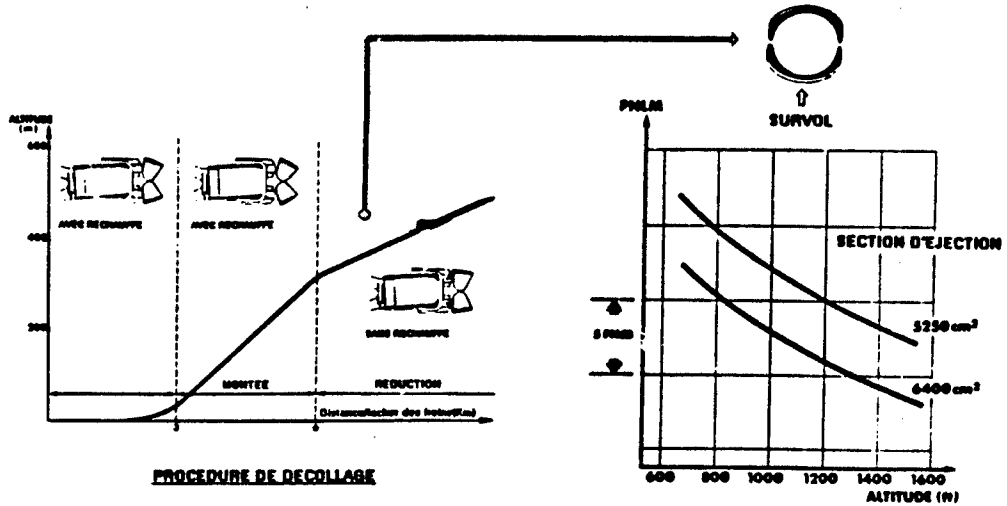**Figure 5**

Influence De L'Ouverture De La Tuyère Primaire

PROCEDURE DE DECOLLAGE

Figure 6

Efficacité Du Silencieux A Pelles

PROCEDURE DE DECOLLAGE
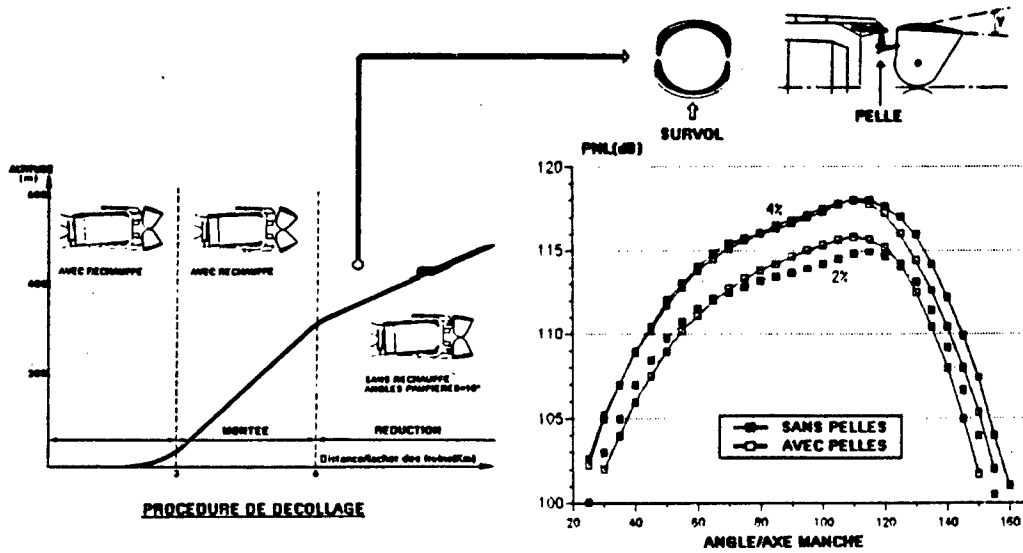
Figure 7

Moyen D'Essai Aerotrain

MOTEUR J85

DISPOSITIFS
REDUCTEURS
DE BRUIT

VITESSE MAXIMALE=90 m/s

MULTITUBE   TUYERE 28   PAMPLEMOUSSE
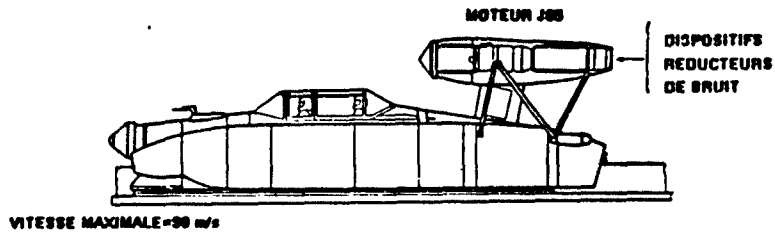
Figure 8

Efficacité De Divers Silencieux Essayés
Sur L'Aerotrain

PNL (PNdB)
L = 61 m

Δ STAT
Δ VOL

10
PNdB

Convergent

41 Tubes avec
Ejecteur traité

STATIQUE
VOL

ANGLE/MANCHE D'ENTREE

30 60 90 120 150

Δ VOL
(PNdB) 61 m

Pamplemousse   Pelles
Marguerite   T28 avec Pelles
Encoche   104 Tubes
Tuyere 28   41 Tubes

10

5

SANS CORRECTION
DES PERTES DE
POUSSEE

Δ STATIQUE

0   5   10
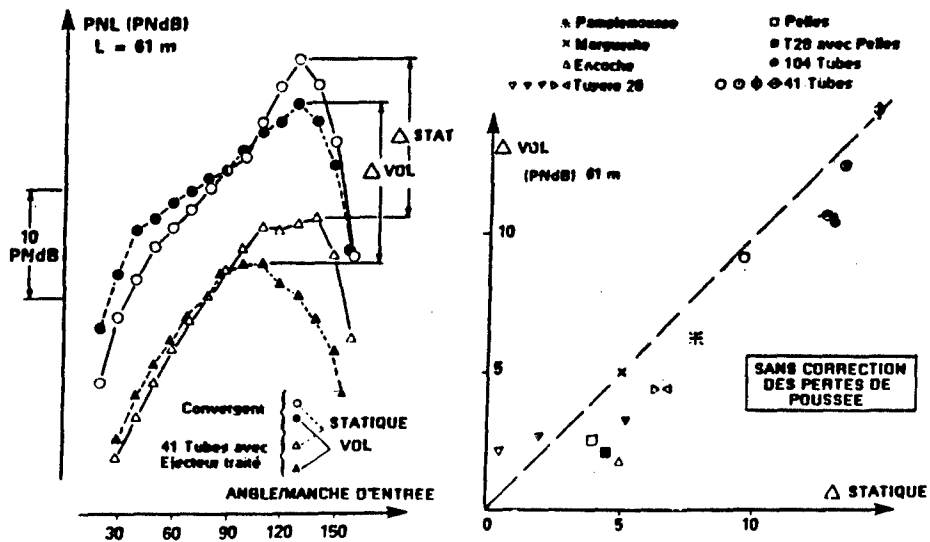
Figure 9

Evolution Des Sources De Bruit Sur
L'Olympus 593

NIVEAU NORMALISE A 70° DE L'AXE DU JET

10 dB

BRUIT GLOBAL DU MOTEUR

BRUIT DE JET PUR

BRUIT INTERNE

VITESSE DU JET log Uj/Co

- 0,3   - 0,2   - 0,1   0   0,1   0,2   0,3
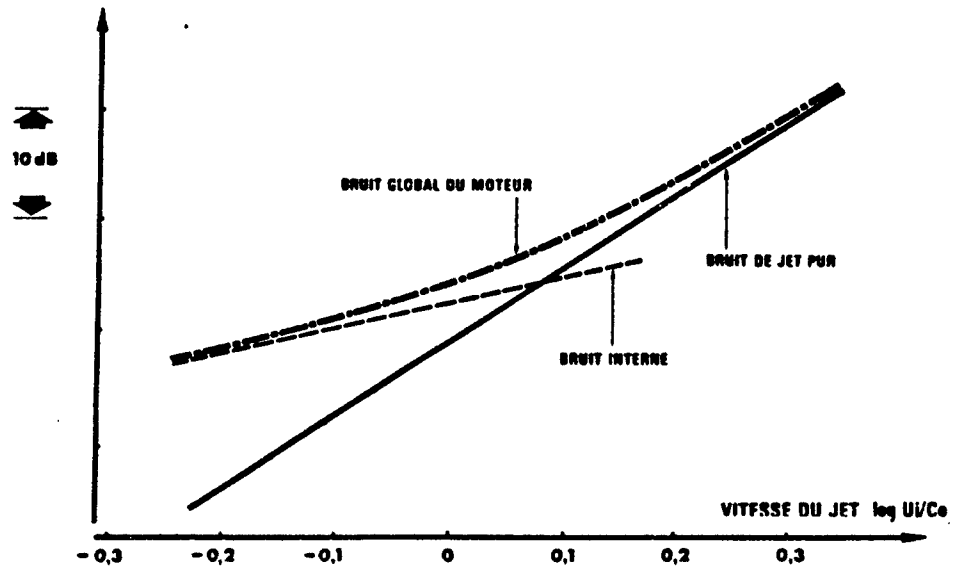
Figure 10

Effet Du Type De Chambre Sur Le Bruit
Interne

—— CHAMBRE CANNULAIRE
—·— CHAMBRE ANNULAIRE

OASPL

5 dB

50   100   150

ANGLE Ψ A L'AXE DU JET (θ)

CHAMP SONORE LINEAIRE

1/3 OCT. SPL

10 dB

F_{LP} F_{HP}

θ=46°

10 dB

F_{LP} F_{HP}

θ=70°

0,1 0,2 0,4 0,8 1,6 3,15 6,3 12,500

FREQUENCE (KHz)

SPECTRES 1/3 D'OCTAVE
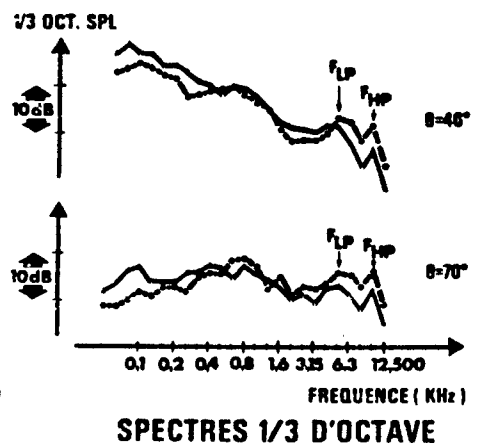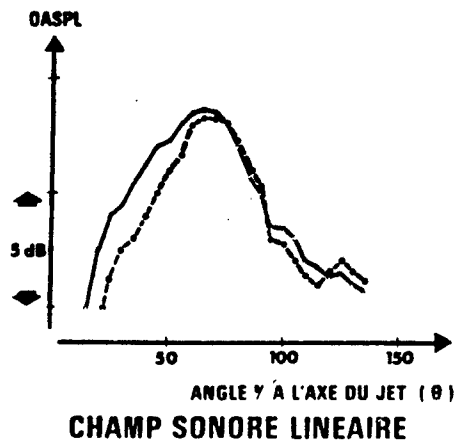
Figure 11

Mécanismes Générateurs Du Bruit Interne

C AMPLIFICATION PARAMETRIQUE DES CHAMPS SONORES PAR LA COUCHE DE CISAILLEMENT

SOURCES DE TUYERE RESULTANT DE L'INTERACTION AVEC LA TUYERE DES FLUCTUATIONS D'ECOULEMENT ET DES INSTABILITES DE LA COUCHE DE CISAILLEMENT

A SOURCES INTERNES CHAMPS CONVECTES PAR L'ECOULEMENT, DIFFRACTES PAR LA TUYERE, REFRACTES ET DIFFUSES PAR LA COUCHE DE CISAILLEMENT
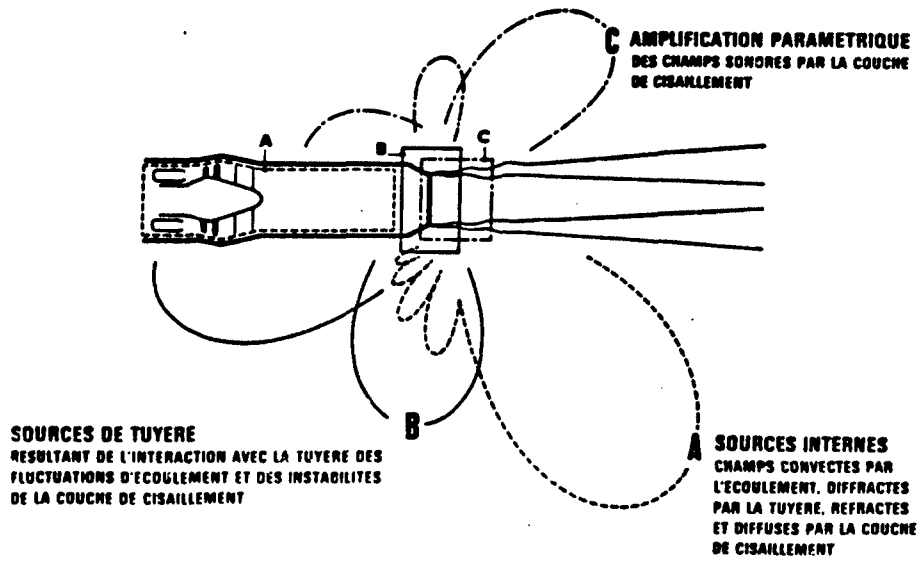
Figure 12

Montage Experimental Larzac
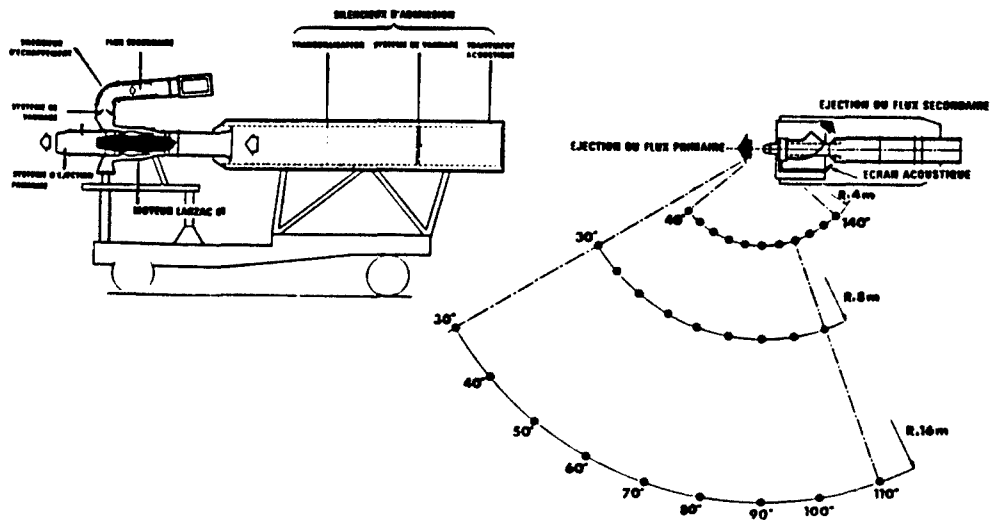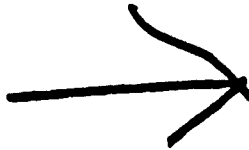
Figure 13

Caracteristiques Du Bruit Interne
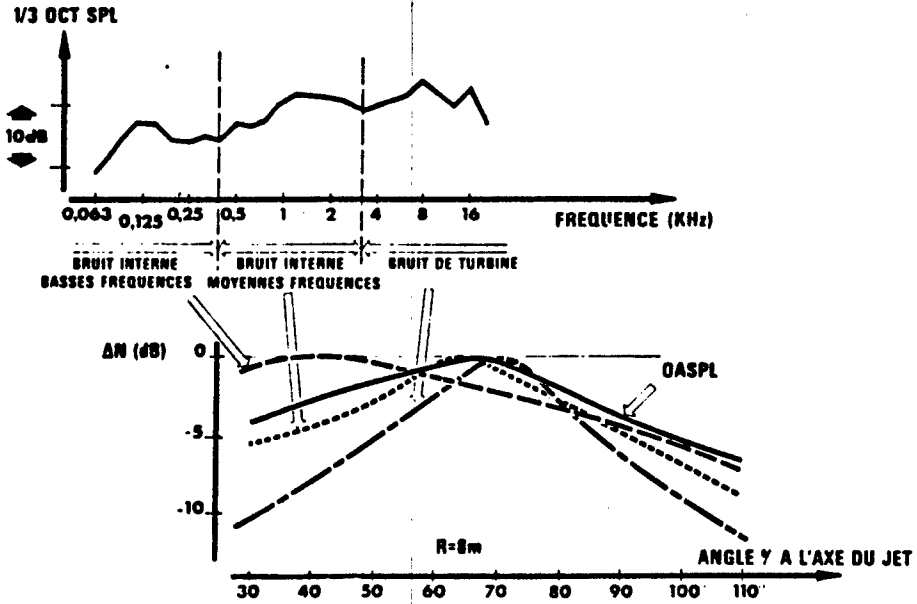
Figure 14

Performances Acoustiques des Dispositifs De Reduction du Bruit Interne

AD-P007 516

||||||||||||||||||||||
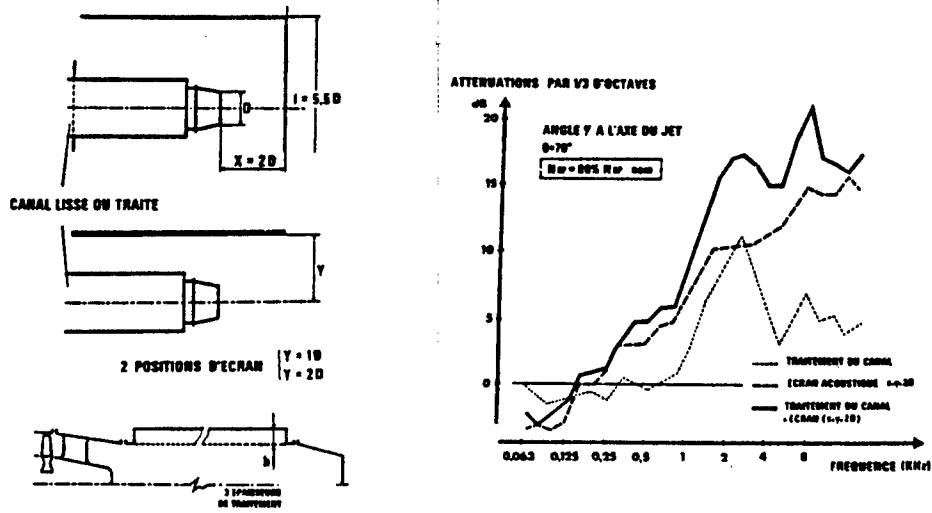
NOISE STUDIES FOR ENVIRONMENTAL IMPACT ASSESSMENT
OF AN OUTDOOR ENGINE TEST FACILITY

G. Krishnappa
Institute for Mechanical Engineering
National Research Council
Ottawa, Ontario, Canada K1A 0R6

92-17419

||||||||||||||||||||||

1. SUMMARY

The potential impact of noise in the community surrounding a proposed outdoor test facility in the Ottawa area was evaluated. The test stand was planned for the testing of high performance gas turbine engines. Theoretical predictions based on the outdoor sound propagation model were made for the noise generated from a General Electric F404 engine. The results were verified by carrying out measurements of noise generated from a single engine of a parked CF-18 aircraft. The measured results qualitatively confirmed the validity of theoretical predictions. However, the tests clearly demonstrated the strong influence of the atmospheric conditions in the observed noise levels in the surrounding community. The usefulness of the theoretical predictions in devising noise control measures in the test area and for the scheduling of tests in favourable weather conditions to minimize noise impact in the surrounding area have been discussed.

2. INTRODUCTION

The Engine Laboratory of the NRCC Institute for Mechanical Engineering has provided unique national facilities for gas turbine engine testing and development for many years. These facilities have been used by the Canadian engine and equipment manufacturers, and Canadian Armed Forces (CAF) and their engine maintenance and overhaul contractors. One of the NRCC test cells is a national calibrated reference cell used by the CAF. All CAF test cells in Canada and abroad, and the cells of their prime contractors can be referenced against the NRC calibrated test cell.

When the test cells were built at the present site on the NRCC Montreal Road Campus, they were situated in a sparsely populated neighbourhood, considerably beyond the densely populated residential area and the Ottawa City limits. No serious consideration was given to the reduction of noise from the test cells. With the gradual development of residential areas around the campus and subsequent noise complaints, some silencing was provided for the cells. Despite substantial investment in improved silencing and increasingly stringent environmental constraints, operational capability became more limited. Large engine operation, particularly military engines with afterburning capability, can cause unacceptable noise levels in residential areas under certain weather conditions. Operation of the NRCC cells is currently restricted to normal working hours. This limits their usefulness, as winter night operation is desirable for testing cold weather performance. In addition, the extensive silencing and restrictions on cell configuration prevent certain kinds of acoustic tests, necessary for the development of more environmentally acceptable commercial engines.

With more emphasis being placed on measuring the absolute performance, the requirement for a free air engine facility has become very important. The increased demand to investigate performance of engines installed in aircraft, and the pressure from environmental agencies to reduce engine noise emissions have made an improved facility a high priority.

Therefore, it was proposed to develop an outdoor test facility in the Ottawa area for the following objectives: to provide a reference standard for all test cells in Canada, to study the performance of engines installed in aircraft, and to perform noise measurements. The new complex was to include an outdoor test stand, and an indoor test cell and support area, for testing high performance and high airflow gas turbine engines.

The site selected for this facility was next to the Ottawa International Airport in the Uplands area. The main considerations in selecting this location was that the surrounding residential area was exposed to the airport noise and that the noise problem would not be as severe as in the other areas in the city. The site was close to runways, facilitating transport of aircraft to the test site. Major fuel handling facilities were also in the immediate vicinity.

The proposed site was evaluated for the potential impact of noise generated by testing high performance engines in the facility. This paper presents the results obtained from theoretical predictions, based on the sound propagation model of the noise generated from a F404 engine, and confirmation of these results by static engine run tests.

The studies were also intended to determine the extent of noise control measures required at the test location and the requirements for scheduling of tests, based on favourable weather conditions to minimize noise impact in the community. The theoretical predictions of noise levels were developed by Davis Engineering Limited (Ref. 1) under contract to NRCC. To confirm the predictions, noise tests using static engine runs were made by the NRCC Engine Laboratory Staff.

3. ENGINE SELECTION - NOISE IMPACT STUDIES

The proposed outdoor facility was intended for testing a wide range of gas turbine engines. These include turboprops such as the Allison T56, high bypass commercial aircraft engines, and fighter aircraft engines like the GE F404-400 engines used in the CF-18 aircraft. It was not possible to study the noise impact of all these engines because of cost restrictions. The worst case among the types of test engines was considered to be the afterburning military engines. In addition, detailed noise data for the F404 engine were readily available to calculate the noise contours surrounding the proposed test site.

The noise spectra for a typical turbofan engine at several ranges from the source are shown in Figure 1. The spectra clearly demonstrate the attenuation of high frequency components at distances greater than 2000 metres. The higher attenuation for these components is mainly due to molecular absorption of sound energy.

4. OUTDOOR SOUND PROPAGATION

Outdoor sound propagation is a complex phenomena because a large number of wave propagation and meteorological factors affect the results. Sound propagation under various ground surface and meteorological conditions are discussed in References 2 to 4.

Sound propagates under free-field conditions, spreading spherically at large propagation distances. Sound levels fall 6 dB each time the range doubles. Additional attenuation occurs because of molecular absorption of sound as it propagates through the air. At normal temperatures, the attenuation is directly proportional to the distance and square of the frequency, and inversely proportional to the relative humidity. At normal temperature and humidity, oxygen relaxation causes strong absorption of sound at frequencies above 2000 Hz.

For a source and receiver near the ground, interference occurs between the direct sound from the source and that reflected at the ground surface. Most ground surfaces, apart from concrete and asphalt, are not acoustically hard. The reflection drastically changes the distribution of sound levels as a function of height and distance from the source and of frequency. Figure 2 shows the interference of direct and reflected waves from the ground surface of impedance Z_n. The sound pressure p at the receiver point is given by the equation[1]:

$$\frac{p}{p_0} = \frac{e^{ikr_1}}{kr_1} + R_p\frac{e^{ikr_2}}{kr_2} + (1 - R_p)\frac{e^{ikr_2}}{kr_2}F, \qquad (1)$$

where r_1 and r_2 are the lengths of direct and ground reflected ray paths respectively, and k is the wave number of the sound in air. R_p is the plane wave reflection coefficient at the appropriate angle of incidence; it can be described by the grazing angle of incidence and the ratio of surface normal impedances. The function F describes interaction of a curved wave front with the surface of finite impedance, and is a function of several variables having complex argument.

The first term on the right hand side of Eq. (1) is the direct wave, showing sound pressure decreasing inversely as the distance r_1 increases. The numerator is merely a phase term. The second and the third terms on the right hand side of the equation together constitute the sound field reflected from the ground. The second term corrects for the reflected sound wave. The third term compensates for the fact that R_p is the plane wave reflection coefficient, and is not independent of the angle of incidence. The sound field is usually incident on different areas of the ground at different angles. The third term is known as the ground wave, and includes the trapped surface wave component which relates to low frequency sound at large distances from the source. This wave propagates in the air, spreading cylindrically over the surface of the ground. Because it decreases less rapidly with distance as the other components of the sound field, the surface wave tends to be more significant at long range. The contribution, apart from the direct wave under finite ground impedance, is known as

excess attenuation. This excess attenuation always exists, but is often partially nullified at various frequencies and distances, or under specific circumstances by various phenomena. The shadow region is penetrated by a ground wave at low frequencies to an extent that depends principally on distance and ground impedance. At high frequencies, it is partially dependant on interference between direct and reflected waves and is determined by the source and receiver heights.

At larger distances meteorological conditions play an important role. The finite impedance of the ground surface can produce a shadow region near the surface in a neutral atmosphere, where sound levels could be as much as 40 dB lower than predicted by geometrical spreading and molecular absorption. Under most weather conditions both wind and temperature vary with height above the ground. These vertical gradients cause the speed of sound to vary with height, forcing the sound waves to travel along curved paths. The speed of sound relative to wind increases with height for downwind propagation, and produces ray paths that are concave downwards. The sound ray path for the upwind propagation is concave upwards, producing a shadow zone near the ground beyond a certain distance from the source. In a temperature inversion, most common at night and early morning hours, the sound speed increases with height up to a few tens or hundreds of metres depending on the temperature gradient, and the ray paths are concave downwards. Under temperature lapse conditions, which are a common daytime occurrence during most of the year, the ray paths curve upwards. This produces a refractive shadow zone near the ground beyond a certain distance, which depends on the height of source above the ground. The ray paths for temperature lapse and inversion conditions are shown in Figure 3.

The sound levels at large distances, normally reduced under neutral weather conditions by distance, molecular absorption, and destructive ground interference, are further reduced by daytime temperature lapse conditions. During the night however, temperature inversion usually prevails and refractive effects allow sound to propagate via paths that are not near the ground. This effectively eliminates sound levels reductions normally provided by ground effects. Sound levels then rise to values determined by distance and molecular absorption, plus one or two decibels if additional refractive paths exist. Upwind and downwind propagation are similar to the temperature lapse and temperature inversion conditions.

Some typical calculations on favourable daytime attenuation and realistic night attenuations made by Davis Engineering Limited[1] are shown in Tables 1 and 2.

5. SOUND LEVEL CONTOURS

The attenuation data summarized in Tables 1 and 2 were combined with typical generic turbofan and turbojet aero-engine spectra for calculating the noise contours. A constant spectrum to a frequency of 500 Hz was assumed for simplicity. Octave band levels range from 100 dB to 140 dB, depending on the engine type. For frequencies higher than 500 Hz, a 3 dB attenuation per octave decay was assumed.

Sound level contours based on F404 data for the mean summer wind and mean winter prevailing wind are shown in Figures 4 and 5. The contours are superimposed on an area map with the centre at the proposed facility site. The sound pressure levels are in dBA and assume no attenuation for ground cover or acoustical treatment at the site. Under favourable

propagation conditions, the 50 dBA contours in both the figures extend to 12 km in the direction of the wind. At the time this report was prepared, the City of Gloucester Noise By-law limited noise levels to 55 dBA during the day and 50 dBA during the night. Noise generated by the engines at the residential site should be 3 dBA (10 dBA desirable) below these levels to prevent test activities from adding significantly to the day/night sound levels.

Noise levels may be reduced by providing a favourable ground cover and inserting an acoustical barrier close to the test area. The barriers should be constructed close to the source to be effective, and must be sufficiently high to prevent any direct transmission from the source to the observer. The barrier height should be of the order of the wavelength of the sound that is to be controlled. A preliminary evaluation of the possible sound level reductions was made incorporating an exhaust silencer as part of the outdoor facility. The silencer was not supposed to physically contact the engine and would facilitate handling and positioning. The numbers circled in the figures are the levels under favourable attenuations from ground cover and exhaust silencer at the site.

6. NOISE PROPAGATION TESTS OF A CF-18 AIR-CRAFT AT OTTAWA INTERNATIONAL AIRPORT

The noise radiation from a CF-18 aircraft during static engine run ups at Ottawa International Airport was measured to asses the noise impact from the proposed outdoor facility. The primary purpose was to confirm the theoretical predictions of the noise levels in the surrounding community made by Davis Engineering Limited. A secondary purpose of the test was to note the community response to the noise of these tests.

The CF-18 aircraft was parked on the taxiway of the Uplands Airport as shown in Figure 6. The nose of the aircraft was pointing to the west wind and the aircraft was aligned within approximately 20 degrees of the taxiway. The tests were designed to measure the noise radiation from a single engine at two power levels: military power and full afterburner. Although operational procedures for the aircraft required that the second engine remain at idle power at all times, the small addition to the total noise from the idling second engine was not considered to be significant.

The far-field noise levels were monitored at eight locations equally spaced around a circle of 2 km radius during the first engine run up sequence. The radius was increased to 4 km for the second sequence. The measurement sites were on flat, open, grass covered terrain with the microphones set at 1.8 metres above the ground. Near-field measurements were made to ensure that the sound power of the engine during the tests was the same as that used in the theoretical predictions. The overall sound pressure levels were measured along a line normal to the jet axis in the plane of the exhaust nozzle, at height of approximately 1.8 metres.

The instrumentation used stored the average sound pressure levels for one minute time intervals. By coordinating the starting time of the data acquisition and engine running times, the noise levels for each of the engine power settings were determined. During the tests the temperature was 23° C with winds from the west at 22 kph, gusting to 44 kph. The humidity varied between 57% and 44%, and the weather office reported a 'normal' temperature profile (adiabatic lapse rate).

7. RESULTS AND DISCUSSIONS

The near-field sound pressure levels of the engine measured close to the aircraft are shown in Figure 7 and are compared with the data supplied by the engine manufacturer. While it is recognized that sound pressure levels change with the measurement angle, the good agreement at this one angle indicates that the sound power of the engines during the tests was close to that stated by the manufacturer.

Table 3 shows the average A-weighted noise levels based on one minute equivalent sound level readings for military and afterburner power settings. The observed levels were as high as 70 dBA at 2 km and 61 dBA at 4 km. Figure 8 shows a sample of the output from noise monitors. Each value is a one minute average of the A-weighted noise at the site. A clear correlation is evident between the engine power setting and the noise level at the site. At some of the locations, the engine noise was inaudible or below the background noise levels. For these sites no estimate of the engine noise was possible.

Table 4 shows a comparison of noise levels observed at the military power setting with the predicted levels, taking into consideration the ground propagation effects. The predicted values include only the effects of geometrical spreading and molecular absorption and do not include the effects of wind, ground impedance, or temperature gradients. These values were interpolated from the noise level contours shown in Figure 4. The far-field levels were generally 15 to 20 dBA below theoretical predictions, considering molecular absorption and geometrical spreading only. This difference is reasonable when allowance is made for the effects of wind and thermal gradients. The normal vertical temperature profile causes the sound rays to be refracted upwards, away from the ground surface. This effect reduces the sound pressure levels observed close to the ground. Similarly, sound rays propagating upwind tend to be refracted upwards and away from the ground by the velocity gradients near the surface. Both of these effects tend to create an acoustic shadow region near the surface of the ground where the sound levels are much lower than that would be expected in calm air with no temperature gradients. The only locations where these differences were not observed are at the sites downwind of the aircraft. At two of these sites, the observed levels were only 1 or 2 dBA below the theoretical predictions. Sound rays propagating downwind tend to be refracted downward toward the ground surface. The downwind effect would negate the favourable effects of a normal temperature profile.

The large differences between the theoretical and experimental values show the importance of atmospheric effects on sound propagation and the difficulty of outdoor predictions. The theoretical predictions were developed for propagation under mean prevailing wind conditions, without any consideration of temperature gradients. Similar effects are encountered under upwind sound propagation and temperature lapse conditions. The theoretically predicted noise contours are helpful in determining the extent of noise impact on the neighbouring residential areas under different weather conditions. Measures can then be taken to minimize this impact by devising noise control methods on site. The studies will also be useful for engine test scheduling under varying weather conditions so as to comply with local noise by-laws.

8. CONCLUSIONS

The tests with the CF-18 aircraft qualitatively confirmed the validity of the theoretical model for the noise predictions at the proposed outdoor test facility. The predictions for noise propagation into the community were valid under the assumed atmospheric conditions. However, the tests clearly showed the strong influence of atmospheric conditions on observed noise levels in the surrounding community. The studies carried out are helpful in determining the extent of on-site noise control measures and in test scheduling based on weather conditions.

The 70 dBA noise levels, observed in the downwind direction at 2 km, are well above the background noise levels. With less favourable atmospheric conditions, the levels observed in other directions could have been as much as 10 to 20 dBA above the measured levels. Outdoor tests with an engine equivalent to the GE F404-400 will generate noise levels in excess of the existing background levels. While no complaints were received from the residential communities at the time of the study, elevated noise levels during prolonged running could easily generate complaints, especially during adverse environmental conditions.

9. REFERENCES

1. Davis Engineering Limited, *Project Definition Documentation for the Outdoor Gas Turbine Test Facility at Ottawa International Airport*, 1987.

2. Embleton, T.F.W., *Sound Propagation Outdoors - Improved Prediction Schemes for the 80's*, Noise Control Engineering, Vol. 18, No. 1, 1982.

3. Embleton, T.F.W., Piercy, J.E., Olsen, N., *Outdoor Sound Propagation over Ground of Finite Impedance*, Journal of the Acoustical Society of America, Vol. 59, No. 2, 1976.

4. Embleton, T.F.W., Thiessen, G.J., and Piercy, T.E., *Propagation in an Inversion and Reflections at the Ground*, Journal of the Acoustical Society of America, Vol. 59, No. 2, 1976.

5. Ball, N.G., *Noise Propagation Tests of a CF-18 Aircraft at Ottawa International Airport*, NRC Controlled Technical Report, CTR-ENG-015, 1987/11.

Table 1. Favourable daytime attenuation.

Distance (m)	Mechanism	Frequency (Hz)							
		31.5	63	125	250	500	1000	2000	4000
150	GS	0	0	0	0	0	0	0	0
	Air	0	0	0	0	0	0	1	4
	Excess	-5	-7	-7	0	15	8	0	-3
	Total	-5	-7	-7	0	15	8	1	1
300	GS	6	6	6	6	6	6	6	6
	Air	0	0	0	0	0	1	3	8
	Excess	-5	-6	-6	3	15	10	3	0
	Total	1	0	0	9	21	17	12	14
600	GS	12	12	12	12	12	12	12	12
	Air	0	0	0	0	1	3	6	17
	Excess	-5	-5	0	13	12	6	3	-3
	Total	7	7	12	25	25	21	21	26
1200	GS	18	18	18	18	18	18	18	18
	Air	0	0	0	1	3	6	12	34
	Excess	-5	-5	7	12	7	0	-3	-3
	Total	13	13	25	31	28	24	27	49
2400	GS	24	24	24	24	24	24	24	24
	Air	0	0	1	3	7	12	24	68
	Excess	-5	-5	7	12	7	0	-3	-3
	Total	19	19	32	39	38	36	45	89
4300	GS	30	30	30	30	30	30	30	30
	Air	0	0	2	6	13	24	44	136
	Excess	-5	-2	13	13	5	0	-3	-3
	Total	25	28	45	49	48	54	71	163
9600	GS	36	36	36	36	36	36	36	36
	Air	0	0	4	12	27	48	92	272
	Excess	0	7	13	10	3	-3	-3	0
	Total	36	43	53	58	66	81	125	308

Table 2. Realistic nighttime attenuation.

Distance (m)	Mechanism	Frequency (Hz)							
		31.5	63	125	250	500	1000	2000	4000
156	GS	0	0	0	0	0	0	0	0
	Air	0	0	0	0	0	0	1	4
	Total	0	0	0	0	0	0	1	4
300	GS	6	'	6	6	6	6	6	6
	Air	0	0	0	0	0	1	3	8
	Total	6	6	6	6	6	7	9	14
600	GS	12	12	12	12	12	12	12	12
	Air	0	0	0	0	1	3	6	17
	Total	12	12	12	12	13	15	18	29
1200	GS	18	18	18	18	18	18	18	18
	Air	0	0	0	1	3	6	12	34
	Total	18	18	18	19	21	24	30	52
2400	GS	24	24	24	24	24	24	24	24
	Air	0	0	1	3	7	12	24	68
	Total	24	24	25	27	31	36	48	92
4000	GS	30	30	30	30	30	30	30	30
	Air	0	0	2	6	13	24	44	136
	Total	30	30	32	36	43	54	74	166
9600	GS	36	36	36	36	36	36	36	36
	Air	0	0	4	12	27	48	92	272
	Total	36	36	40	48	63	84	128	308

Table 3. Far-field A-weighted sound pressure levels (dBA).

2 km Distance	A0	A45	A90	A135	A180	A225	A270	A315
Military Power	-	-	55	66	69	70	68	58
Afterburner	-	57	58	76*	71	70	77	62
4 km Distance	B0	B45	B90	B135	B180	B225	B270	B315
Military Power	-	-	-	55	53	61	55	-
Afterburner	-	-	50	63	55	65	64	-

Table 4. Comparison of theoretical and observed sound pressure levels at military power.

2 km Distance	A0	A45	A90	A135	A180	A225	A270	A315
Observation	-	-	55	66	69	70	68	58
Theory	82	77	81	85	70	80	87	78
Difference	-	-	-16	-19	-1	-10	-19	-20
4 km Distance	B0	B45	B90	B135	B180	B225	B270	B315
Observation	-	-	-	55	53	61	55	-
Theory	64	64	60	73	55	70	72	57
Difference	-	-	-	-18	-2	-9	-17	-
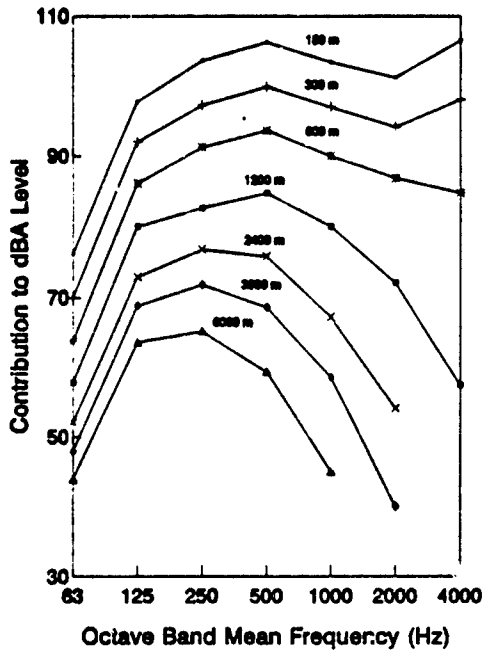
Figure 1. Noise spectra for a typical turbofan engine.
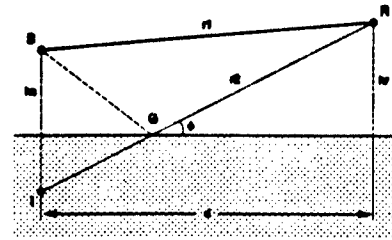
Figure 2. Interference of direct and reflected waves at the ground surface (source S and receiver R).
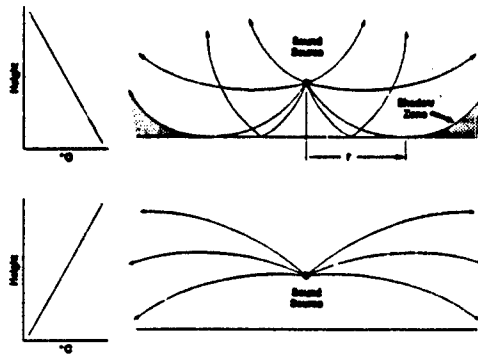
Figure 3. Sound ray paths for temperature lapse and temperature inversion conditions.

Figure 4. Sound level contours for mean summer prevailing wind.
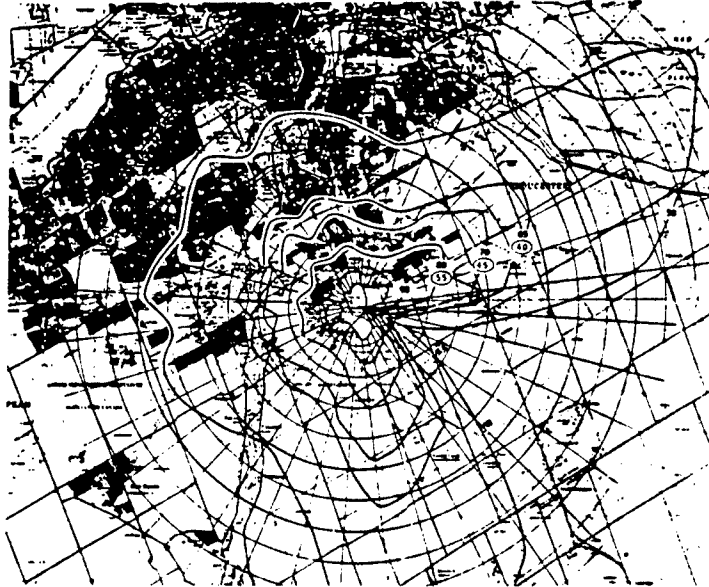
Figure 5. Sound level contours for mean winter prevailing wind.
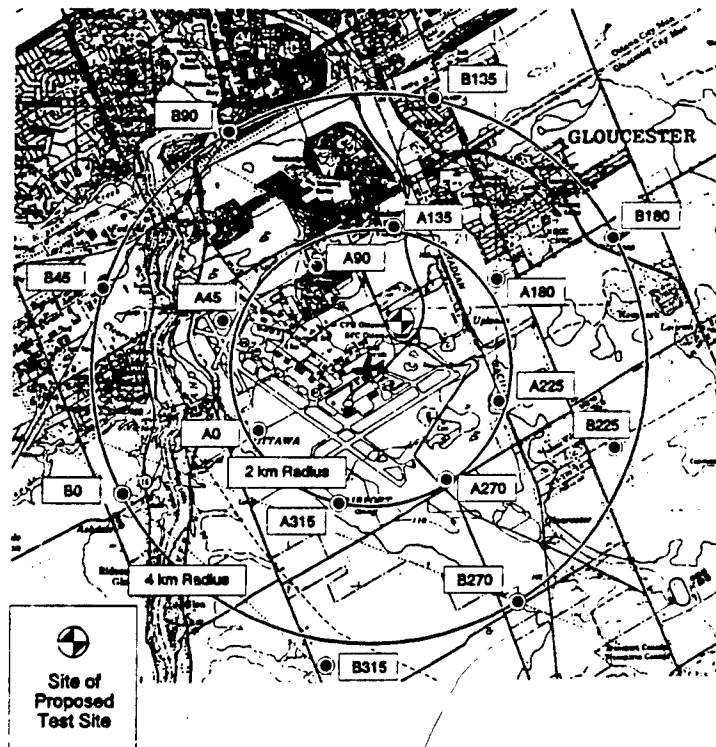
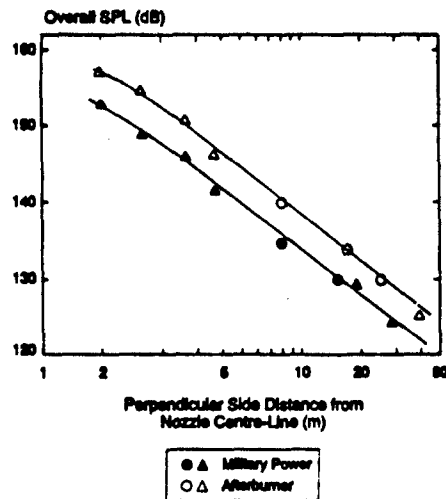Figure 6. Measurement sites and aircraft location.

Overall SPL (dB)

Figure 7. Near-field sound pressure levels adjacent to
aircraft.

Discussion

QUESTION BY: P. Artaz, SNECMA, France
D'après quelles donneés avez vous validé vos modèles
d'attenuation atmospherique et ceux d'impédance de sol?

AUTHOR'S RESPONSE:
The sound level contours presented in the paper are for the
summer and winter average prevailing wind conditions. At wind
flow conditions, the sound waves, due to refraction propagate
in curved paths above the ground after a short distance from
the source. Tables are given for day and night time
propagation when different vertical temperature gradients
exist. The model includes excess attenuation, which is for
grass covered ground.
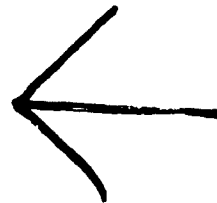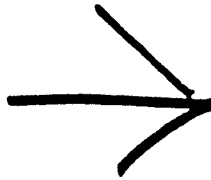
NON-PROPULSIVE AERODYNAMIC NOISE

William L. Willshire, Jr.
Maureen B. Tracy

NASA Langley Research Center
Mail Stop 460
Hampton
Virginia 23665
United States

92-17420

SUMMARY

In the first part of the paper, the contribution of airframe noise to total aircraft noise on approach is assessed for a large current technology transport and for the same airframe powered with bypass ratio 10 engines with an additional 5 dB noise suppression applied to the fan and turbine noise sources. The airframe noise of the envisioned advanced subsonic transport is 2 EPNdB less than the largest contributor to the total aircraft noise, the fan inlet. The noise impact of the airframe noise, as measured by noise contour area, is 1/4 that of fan noise. Further fan noise reduction efforts should not view airframe noise as an absolute noise floor.

In the second part of the paper, the results from one recent cavity noise wind tunnel experiment is reported. A cavity of dimensions 11.25 in. (28.58 cm) long, 2.5 in. (6.35 cm) wide, and variable depth was tested in the Mach number range of .20 through .90. Reynolds number varied from 5 to 100 million per foot (16 to 328 million per meter). The l/d ratio was varied from 4.4 to 20.0. The model was tested at yaw angles from 0 to 15 degrees. In general, the deeper the cavity, the greater the amplitude of the acoustic tones. Reynolds number appeared to have little effect on acoustic tone amplitudes. Tone amplitude and bandwidth changed with Mach number. The effect of yaw on acoustic tones varied with Reynolds number, Mach number, l/h, and mode number. At Mach number 0.90, increased yaw shifted the tone frequencies of the higher modal frequencies to lower frequencies. As cavity depth decreased, the effect of yaw decreased.

LIST OF SYMBOLS

f	frequency, Hz
f_m	acoustical tonal frequencies, Hz
h	cavity depth, inches (cm)
$k(M_\infty)$	empirical ratio of shear layer and free-stream velocities
l	cavity length, inches (cm)
M_∞	free-stream Mach number
m	acoustic tone order number
p	acoustic pressure, psf (N/m^2)
$<p^2>$	mean-square far-field acoustic pressure
q_∞	free-stream dynamic pressure, psf (N/m^2)
R	unit Reynolds number, per foot (per meter)
U_∞	free-stream flow speed, ft/sec (m/sec)
u	typical mean flow velocity
x	distance along cavity floor, in. (cm)
$\alpha(l/d)$	empirical parameter giving the phase lag between instabilities in the shear layer and acoustic waves in the cavity
θ	polar directivity angle, zero in downstream direction
σ	azimuthal directivity angle, zero in downward direction
γ	ratio of specific heats of air at constant pressure and constant volume
ω	frequency, radians/sec

Abbreviations:

BPR	bypass ratio
EPNL	effective perceived noise level, EPNdB
FPL	fluctuating pressure level, db (re q_∞)

1.0 INTRODUCTION

Non-propulsive aerodynamic noise concerns for military aircraft may be divided into the two areas of airframe noise and cavity noise. Airframe noise is important to the operational acceptability of all aircraft, while on armed aircraft, the particular issue of cavity noise-induced vibration is critical to store integrity and separation.

With current engine technology, airframe noise is a contributing source for large commercial aircraft on approach, but not the major contributor. With the promise of much quieter jet engines with the planned new generation of high-by-pass turbofan engines, airframe noise has become a research topic of interest for the next generation of commercial airliners. Questions being raised include: Will airframe noise be the dominant noise source on approach? How well can it be predicted? Is airframe noise an absolute noise floor to which other noise sources should be reduced, or can airframe noise be reduced? The concerns raised in these questions ultimately are connected to the noise acceptability of the aircraft, and are applicable to large military cargo aircraft, as well as commercial aircraft, operating near population centers.

This paper is divided into two parts. The first part of the paper includes a summary of the current airframe noise prediction capability. Total aircraft noise, including airframe noise, is predicted for approach for a current technology transport and for an envisioned advanced technology transport. The relative contribution of airframe noise to each type of transport total noise is assessed. In the second part of this paper, the results from a recent cavity noise experiment is reported.

2.0 AIRFRAME NOISE

2.1 Background

Airframe noise arises from the interactions of unsteady air flow on the aircraft structure exposed to the flow. The unsteadiness of the air flow may be natural or a consequence of flight, for instance the turbulent boundary layer of a wing or the impingent of a turbulent wake of an up-stream aircraft component on a downstream aircraft component. The primary airframe noise sources are usually considered to be trailing edges, landing gear, cavities, flaps, and slats. These sources are not, in general, independent and may interact. The air flow around an aircraft is highly energized and dynamic, making airframe noise a significant and complex aircraft noise source. Airframe noise is expected to contribute the most to overall aircraft noise during approach when the engines are throttled and the aircraft is in a dirty (high lift devices and landing gear deployed) configuration.

Much airframe noise research has been done. Both experimental and theoretical investigations have been extensive, much of the work being performed over a decade ago. Experimental investigations have included full scale flight experiments, complete model and component wind tunnel testing, and free flight glider and model experiments. Theoretical investigations have been concerned with the fundamental physics of individual airframe noise sources. Many excellent summaries of airframe noise research are available (refs. 1-4). The state of airframe noise understanding will be briefly addressed and then applied to the case of the approach noise of an envisioned advanced subsonic aircraft equipped with the next generation of high-by-pass ratio engines. The objective will be to assess the contribution of airframe noise relative to the other aircraft noise sources on approach. These findings will be compared to similar results for a current technology aircraft.

Interest in the area of airframe noise was stimulated in the early 1970s by the desire for an ultra quiet military surveillance aircraft (ref. 5). Interest soon turned to commercial aircraft when it was discovered that airframe noise on approach was approximately 10 EPNdB less than the more dominant aircraft noise sources, typically fan noise. Initially, airframe noise modelling was aimed at whole aircraft Overall Sound Pressure Level (OASPL) prediction which was empirically based with pertinent parameters identified from analytical insight. These methods soon were extended to pre-dict 1/3 octave band spectra. These empirical methods worked reasonably well when applied to the same or similar class of aircraft.

Whole aircraft airframe noise prediction, valid for its intended purpose of first cut airframe noise prediction, was soon surpassed by component noise prediction models in which the airframe noise of particular aircraft components is predicted. Component prediction models followed two different paths. One method of component prediction is very similar to the whole aircraft models in that the individual component prediction models are largely empirical; however, much greater use of analytical insight, where available, was used. The component prediction method of Fink (ref. 6). is an example of this prediction method. The other component prediction method is the drag element method developed by Revell (ref. 7). In the drag element method, airframe noise is viewed as a by-product of mechanical energy dissipated by drag (ref. 2).

Fundamental principle aerodynamic and aeroacoustic models were developed for many airframe noise sources. In particular, models for predicting trailing edge noise are well founded and complete for many flow environments (ref. 4). Trailing edge airframe noise is caused by unsteady flow passing over or near the trailing edge of a wing or flap and is considered the dominant airframe source in the cruise condition. Trailing edge airframe noise models have established that the functional dependence of this noise source is

$$<p^2> \propto u^5 \sin^2 \frac{\theta}{2} \cos \sigma \tag{1}$$

where $<p^2>$ is the mean-square far-field acoustic pressure, u is a typical mean flow velocity, θ is the polar directivity angle, zero in the downstream direction, and σ is the azimuthal directivity angle, zero in the downward direction. The directionality of eq. 1 is not that of a simple dipole and has been referred to as that of a half baffled dipole (ref. 8). Theoretical aspects of trailing edge noise have been extended to include the correlation of trailing edge pressure fluctuations with far field radiated acoustic pressures and the ability to predict the acoustic pressures based on the measured trailing edge surface pressures (refs. 9-10).

Another airframe noise component which in principle is well understood and predictable is that due to landing gear. The airframe noise generated by the components of landing gear, the wheels, struts, and axles, is considered to be caused by bluff bodies and is dipole in nature with the axes of the dipoles parallel to the lift and drag elements. The amplitude, $<p^2>$, dependence of this airframe component is on velocity to the sixth power. Cavities associated with landing gear are sources of low frequency, less than 100 Hz, airframe noise which are excited most easily in depth modes. Evidence indicates that such cavities radiate less intense airframe noise than expected due most probably to their complex internal shapes (ref. 11).

During approach, dominant airframe noise sources other than landing gear are those caused by the deployment of high lift devices, such as flaps and slats. The increase in airframe noise with flap and slat deployment over that of a clean wing is on the order of 10 EPNdB (ref. 1). Flap and slat airframe noise is associated with the physical gaps or slots between slat and wing, or wing and flap, and with the edges of the flaps. These conclusions are based on flight and wind tunnel data where the various stages of flaps and slats were incrementally deployed (refs. 12-13).

Other sources of airframe noise which are not currently in the component prediction models are flap edge, panel vibration, and nacelle. Flap edge has already been mentioned and appears to be an important source of airframe noise (refs. 13-14). Panel vibrations, caused again by the unsteady air flow, have been identified as an important airframe noise source for wing panels on a DC-10 (ref. 15) and for landing gear doors left in the air stream (ref. 16). The nacelles of the advanced engines which are to power the next generation transports are expected to be very large in diameter and need to be investigated as sources of airframe noise. These sources of airframe noise need also to be incorporated into the component airframe noise prediction models.

An advantage of a semi-empirical prediction method based to some extent on full-scale and realistic model data is that noise components that are not explicitly addressed in the method, like flap side edge noise in the Fink method, are to some degree accounted for in the method. If the sources are important, their influence is in the measured data and are reflected in the empirical best fit curves. The other side of this is that errors are generated if the data are forced to be fit by a fundamentally incorrect parameter dependence. This is why analytical insight is so important in empirical modelling.

For example, the azimuthal directivity attributed to trailing edge noise in the Fink method is the dipole directivity or

$$<p^2> \propto \cos^2 \sigma \qquad (2)$$

The correct azimuthal dependence for trailing edge noise, as given previously, is the square root of this dependence. Another example of an incorrectly assumed parameter dependence is the reflection from the underside of aircraft fuselages and wings of vertical dipoles caused by horizontal landing gear elements. The reflection leads to longitudinal quadrupole-like behavior which has a narrower directivity than the assumed dipole directivity in the Fink method. The impact of these discrepancies, noted in reference 1, should be minimum in the downward direction where airframe noise is known to be the greatest.

Continued analytical work is needed so that new airframe noise sources can be incorporated in future component prediction schemes either by parametrically correct empirical methods or by first principle methods. First principle methods are preferred over empirical methods; however, it is often difficult to obtain sufficient input to use the first principle methods. This is the case for both trailing edge and landing gear airframe noise prediction for complete aircraft. The air flow around a complete aircraft is in general not known sufficiently to predict either of these two airframe noise sources from analytical expressions. Parametrically correct empirical prediction methods are then the next best methods to predict airframe noise for complete aircraft.

2.2 Predicted Total Aircraft Noise

The Fink component method is recommended in reference 1 to make whole aircraft airframe noise predictions, and was used to make the airframe noise predictions in this paper. NASA Langley Research Center's Aircraft Noise Prediction Program, ANOPP, (ref. 17) was used to make the total aircraft noise predictions (ref. 18). The Fink airframe noise method is incorporated in ANOPP. The airframe noise prediction method in ANOPP was validated in reference (ref. 19) with a variety of measured data not incorporated into the Fink method. The result of the validation showed that the Fink method agreed within ±2 EPNdB to the measured results.

ANOPP, and programs similar to it, requires detailed information in order to make an aircraft noise prediction. For example, one of the needed categories of information is engine operating parameters, often referred to as the engine operating deck. The engine data are critical to the prediction of the fan, core, turbine, and jet noise. It typically is very difficult to obtain the required engine parameters, particularly for an engine in the current fleet or an engine in development. The required input to make airframe noise predictions is relatively easily obtained from published descriptions (ref. 20). One of the early ANOPP validation studies involved a DC-10 (ref. 21). The ANOPP input parameters listed in reference 21, although somewhat different from the current required input, were used as the basis to make ANOPP predictions for a DC-10 on approach. These predictions were used to verify the numbers being predicted by ANOPP 15 years after the DC-10 validation and to serve as a baseline for comparison to the projected advanced subsonic transport noise predictions. Noise sources included in the total aircraft ANOPP predictions are fan inlet, fan discharge, core, turbine, and jet; along with main landing gear, flap, slat, nose landing gear, wing, horizontal tail, and vertical tail airframe noise sources.

Another important category of input to ANOPP which is difficult to obtain is the amount of suppression to apply to the fan and turbine noise sources. ANOPP does not predict the noise suppression to be applied to the fan and turbine noise sources. Noise suppression is supplied by the user of ANOPP. Noise suppression technology is very competitive sensitive. To make the baseline current technology DC-10 noise predictions with ANOPP, the following values of noise suppression 0, 10, and 10 dB were applied to the fan inlet, fan discharge, and turbine noise sources, respectively.
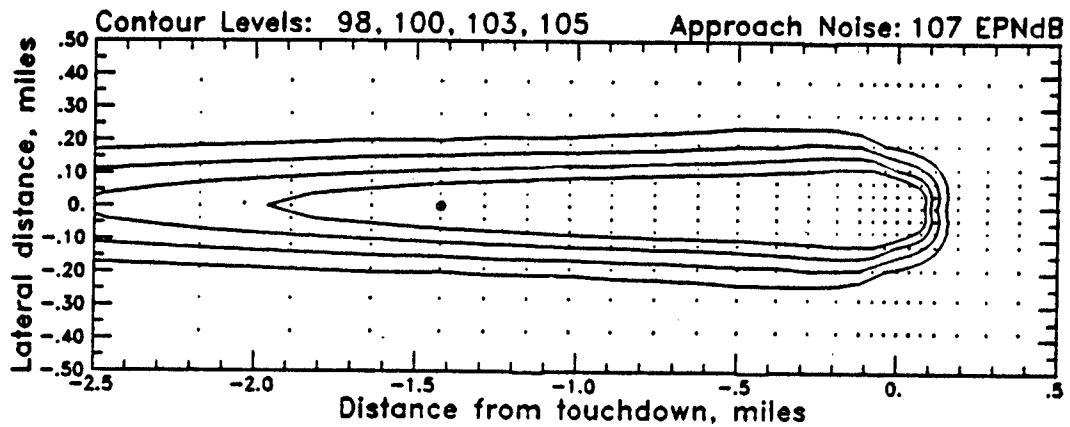
Figure 1. EPNL noise contour for current technology total landing noise.

These values of suppression were selected based on available published information (refs. 24-25), engineering insight into known suppression technology, and known behavior of the noise sources of current technology transports on approach. Suppression of fan and turbine noise is achieved by the placement of absorbing material (liners) in and the design of the fan and turbine ducts. The selection process for the noise suppression amounts to a calibration of ANOPP necessitated by a lack of detailed information for current technology engines.

An example of the result of the noise prediction process is given in figure 1 for the baseline DC-10 in the form of an Effective Perceived Noise Level (EPNL) contour plot of the total aircraft noise. This result and all the results to be given are for an aircraft flying an approach consisting of a 3 degree glideslope. The maximum approach EPNL value is given in the upper right portion of the plot for the approach position. The approach position is the one specified in the FAR 36 (ref. 22) noise certification regulations which is 1.5 miles (2.4 km) from the end of the runway. The 3-degree approach glideslope results in the aircraft passing approximately 120 m above the approach position. In figure 1, the circle symbol underneath the flight track is the location of the approach position. Similar noise contour results were predicted for individual noise sources. All noise predictions were made for a microphone positioned 1.2 m above the ground. The results for the baseline DC-10 ANOPP noise predictions are summarized in Table 1 in the form of approach EPNL values and areas of the 103 EPNL noise contours. In Table 1, results are given for the total aircraft noise, and the noise contributions of fan discharge, fan inlet, turbine, airframe, core, and jet noise sources.

The total aircraft noise approach EPNL value which corresponds to the FAA approach certification position is compatible with published values for a DC-10-40 powered with JT9D-59A engines. The predicted total level of 107 dB is one EPNdB above the largest reported certification level in reference 23 for a DC-10. One decibel is within the accuracy of the predictions which is believed to be on the order of 2 EPNdB. The

contributions of each of the predicted noise sources are presented in Table 1 in increasing order of importance. The largest contributor to the total noise on approach is fan noise with airframe noise, on the basis of approach position EPNL values, the fourth largest contributor, 10 EPNdB less than fan noise.

Table 1. Noise Predictions for Baseline DC-10

Noise Source	EPNL, dB	Contour Area, mi^2 (km^2)
Core	86	—
Jet	91	.003 (.008)
Airframe	92	.003 (.008)
Turbine	100	.064 (.166)
Fan Inlet	101	.134 (.347)
Fan Discharge	102	.108 (.280)
Total	107	.531 (1.375)

The frequency content of the various noise sources is given in figure 2 for the sound emitted when the aircraft was over the approach centerline microphone position. At frequencies less than 300 Hz, airframe and jet noise sources are comparable in level and dominate. Turbine noise dominates in the frequency range of 300 Hz to 1500 Hz. At frequencies greater than 1600 Hz, the turbine and fan discharge noise levels are similar and dominate.

To make total aircraft noise predictions for an advanced subsonic transport, the engines on the baseline DC-10 were replaced with engines having a by-pass-ratio (BPR) of 10 and an additional 5 dB of suppression was applied to both the fan (inlet and discharge) and turbine noise sources. This 'rubber' engine was obtained by using the Navy/NASA Engine Program, NNEP, (ref. 26) to extrapolate the engine deck of a smaller (approximately 40,000 lbs thrust), BPR 6 engine. The resulting engine generated 53,000 lbs of thrust at full (100%) throttle. The same airframe and approach flight profile were used in ANOPP to make the noise predictions. A BPR of 10 and an additional 5 dB suppression represent modest assumptions for an advanced

subsonic transport. BPRs in the range of 20 and additional fan noise suppression in the range of 10 dB have been discussed as goals for advanced subsonic transports. The additional suppression would be obtained through the use of advanced technology liners which might include bulk absorbers, multi-layered honeycomb reactive liners, and possibly, active noise control.
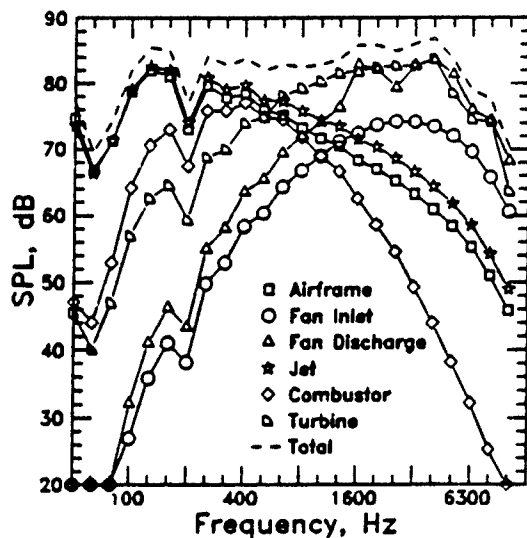

Figure 2. Current technology overhead noise source spectra.

The noise prediction results for the advanced technology transport are summarized in Table 2 in the form of approach EPNL values and areas of the 103 EPNL noise contours. Results are given for the total aircraft noise, the fan inlet, the fan discharge, the airframe, turbine, and core noise sources. The predicted jet noise was so small that it is not presented in Table 2. The higher BPR engines have resulted in less jet noise and the additional noise suppression is evident in the results. For this realization of an advanced technology transport, the airframe noise is the second largest (tied with fan discharge noise) noise contributor on the basis of approach microphone EPNL levels behind fan inlet noise. The airframe noise is 2 EPNdB less than the largest contributor to the total aircraft noise predicted for the advanced technology transport.

Table 2. Noise Predictions for Advanced Technology Transport

Noise Source	EPNL, dB	Contour Area, mi^2 (km^2)
Core	86	—
Turbine	91	.001 (.003)
Airframe	92	.003 (.008)
Fan Discharge	92	.003 (.008)
Fan Inlet	94	.014 (.036)
Total	99	.060 (.155)

For the advanced technology transport, a large reduction in total noise impact is evident when comparing the size of the noise contours for the current technology (Table 1) and the advanced technology (Table 2) transports. An approximate nine-fold reduction is observed in the area of the total aircraft noise 103 EPNdB noise contour area for the two transports.

The spectra of the various noise sources for the advanced technology transport are given in figure 3 for the noise emitted when the aircraft was above the approach centerline microphone. At frequencies less than 200 Hz, airframe noise is the dominant noise source. From approximately 200 Hz to 800 Hz, airframe and combustor noise dominant. From 800 Hz to 4 kHz, fan discharge noise is dominant. Above 4 kHz, turbine noise becomes dominant. Jet noise is seen to be very low and not a contributing noise source.
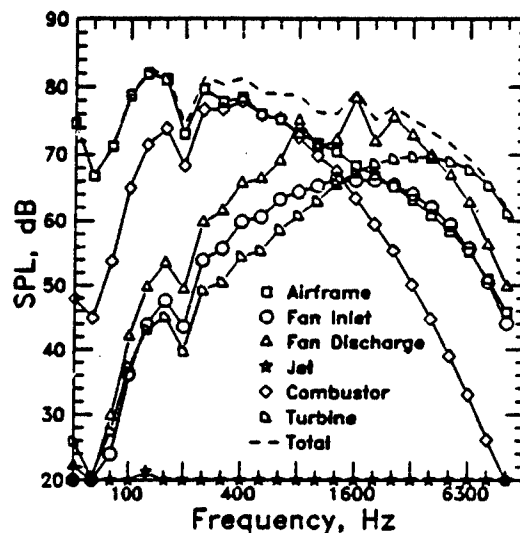
Figure 3. Advanced technology overhead noise source spectra.

Within the accuracy of the noise predictions, on the order of 2 EPNdB, the contribution of airframe noise in terms of EPNL is comparable to the contribution of fan noise to the total noise of this advanced technology transport. Additional reductions in fan noise alone will ultimately result in airframe noise becoming the dominant noise source on approach. From a noise impact point of view, as measured by the area of the 103 EPNL noise contour, fan inlet noise of the advanced technology transport has an impact over four times that of airframe noise. Further reductions in fan noise need to be done with consideration of airframe noise. However, the higher frequency content of fan noise over that of airframe noise and the larger noise impact (larger contour area) make reductions in fan noise more attractive to further increase the noise acceptability of the next generation of transport aircraft.

The airframe noise predictions were the same for both the baseline and the advanced technology transport due to the fact that the same airframe and approach flight path were used to make the noise predictions. The approach noise levels and the area of the 103 EPNL noise contours are given for the major airframe noise sources in Table 3. A finer grid was used to generate the individual airframe noise source contours. The total airframe noise contour area in Table 3 is slightly different and more accurate than the total airframe noise contour area given previously. On the basis of approach EPNL, main landing gear noise is the largest contributor, followed by trailing edge flap noise and slat edge noise. The approach EPNL levels of these three airframe noise sources are comparable, falling in the range of 85 to 87 EPNdB. On the basis of noise impact, as measured by the area of the 103 EPNL noise contour, main landing gear and trailing edge flap noise are comparable, having a little less than twice the noise impact of leading edge slat noise.

Table 3. Airframe Noise Predictions

Noise Source	EPNL, dB	Contour Area, mi^2 (km^2)
Nose Landing Gear	76	—
Leading Edge Slat	85	.00015 (.00039)
Trailing Edge Flap	86	.00024 (.00062)
Main Landing Gear	87	.00024 (.00062)
Total	92	.00195 (.00505)

Airframe noise should not be considered an absolute noise floor. Many ideas to reduce airframe noise have been published (ref. 1). Lower approach speeds would lessen airframe noise, but great reductions in landing speed are not likely. A move toward simpler high lift systems with fewer slat and flap segments with thought given to downstream wake impingement would tend to minimize airframe noise. Porous, serrated, swept, sucking, and blowing leading and trailing edges have been proposed to reduce the intensity of the interaction between the unsteady flow and trailing edges. In the case of flap edge noise, the above listed surface changes or an edge plate might be used to reduce the noise. Interactions between airframe noise components have been shown to be either adverse, causing an increase in airframe noise or favorable, causing a decrease in total airframe noise. In a model experiment involving an Advanced Supersonic Transport (ref. 27), the airframe noise with the flaps and main landing gear deployed was greater than the sum of the noise from each component deployed individually. In another model study (ref. 13) the total noise of a wing with a particular combination of deployed slats and flaps was less than the sum of the noise generated separately by each component. These results indicate that the interactions between airframe noise components are complex but once understood should be able to be exploited to yield lower airframe noise aircraft designs. Poor designs can increase airframe noise; good designs can reduce airframe noise.

Further systematic research is needed to identify ways to reduce airframe noise.

2.3 Summary

Total aircraft noise, including airframe noise, for approach was predicted for a current technology large transport and for an envisioned advanced technology transport. An objective of the research was to assess the relative importance of airframe noise to the other noise sources on approach for the two aircraft types. Airframe noise for the current technology transport was 10 EPNdB less than the more dominant fan and turbine noise sources. The advanced technology transport was modelled as having engines with a BPR of 10 with an additional 5 dB suppression on fan and turbine noise. On approach, the airframe noise for this envisioned aircraft was 2 EPNdB below the largest contributing noise source, the fan inlet. This level difference was within the prediction accuracy; therefore, a conclusion is that airframe noise is comparable in amplitude to fan noise sources on approach for the studied advanced technology transport. The noise impact of fan noise, as measured by noise contour area, was greater by more than a factor of four over airframe noise. Further reduction in fan noise needs to be done with consideration of airframe noise. Airframe noise should not, however, be considered an absolute noise floor. Airframe noise can be reduced by good design practice. Many airframe noise reduction ideas have been identified and need to be validated.

3.0 CAVITY NOISE

3.1 Introduction

The second area of non-propulsive aerodynamic noise that is of concern for military aircraft is cavity noise. This issue arises from the current interest in internal carriage of weapons in high speed aircraft. Although internal carriage provides aerodynamic advantages in flight, flow disturbances can occur when the weapons bay is open to an otherwise undisturbed flow. Suggestions that intense acoustic pressure fluctuations could arise that could cause structural and functional degradation of a store have led to studies of the acoustic characteristics of cavities and documentation of the conditions under which acoustic tones are generated. (refs. 28- 42)

Of the four types of flow field observed for cavities in supersonic flows (refs. 43 and 44), one, open cavity flow, consistently supports the generation of acoustic tones. Open cavity flow, in which the shear layer bridges the cavity, is typically seen for cavities with length-to-depth ratios (l/h) less than 10. The mechanism that produces the acoustic tones is understood to be a reinforcement between instabilities in the shear layer that bridges the cavity and pressure waves generated in the cavity when the shear layer impinges on the aft wall. Acoustic tones occur at discrete frequencies which correspond to characteristic pressure patterns, or modes, in the cavity.

To date, there is no satisfactory method to predict the amplitudes of tones or under what conditions specific tones will occur. A semi-empirical equation was obtained by Rossiter (ref. 28) to predict the frequencies at which tones would occur. Rossiter theorized, based on observations of rectangular cavities in subsonic and transonic flows, that the tones resulted from a coupling between vortex shedding and acoustical waves in the cavity. Heller, Holmes, and Covert in reference 29 made a modification to Rossiter's equation to accommodate supersonic cases in which the difference between the free-stream static and cavity internal temperatures is significant. The fact that cavity internal temperature is approximately equal to the free-stream stagnation temperature rather than the free-stream static temperature has been shown experimentally by Kaufman, Maciulaitis, and Clark (ref. 33). The modified Rossiter equation from reference 29 is:

$$ f_m = \frac{U_\infty [m - \alpha(l/h)]}{l\left[\left(\frac{M_\infty}{\sqrt{1 + \frac{\gamma - 1}{2}M_\infty^2}}\right) + 1./k(M_\infty)\right]} \tag{3}$$

The wind tunnel experiment was performed at NASA Langley Research Center in the 0.3-m Transonic Cryogenic Tunnel (0.3-m TCT) at subsonic and transonic speeds using a cavity model that was 11.25 inches (28.58 cm) long by 2.5 inches (6.35 cm) wide (ref. 45). The objective of this test was to characterize the internal acoustic field generated by cavities in flow and determine its dependence on Reynolds number (at nearly constant boundary layer thickness) and yaw angle.

3.2   Effects of Reynolds Number and Yaw Angle on Cavity Acoustics in Transonic Flow

The experimental study was performed in the 13-in. by 13-in. (33 by 33 cm) test section of the 0.3-m TCT, a continuous, fan-driven, cryogenic pressure tunnel which used nitrogen as a test gas. (References 46-48 describe the facility and operation in detail.)

A rectangular cavity model was mounted on a turntable which was installed in the sidewall of the 0.3-m TCT. The cavity was 11.25 in. (28.58 cm) long by 2.5 in. (6.35 cm) wide and had a depth that could be varied to obtain l/h ratios of 4.40 (h = 2.56 in.) (6.50 cm), 6.70 (h = 1.68 in.) (4.27 cm), 12.67 (h = 0.89 in.) (2.26 cm), and 20.00 (h = 0.56 in.) (1.42 cm). The turntable could be rotated with respect to the flow, to position the cavity with yaw angles of 0 and 15 degrees.

A total pressure rake was used to measure the boundary layer thickness at the leading edge of the cavity with the cavity floor positioned flush with the turntable (h = 0.0). For Mach 0.6, the boundary layer thickness ranged from 0.58 in. (1.47 cm) at a Reynolds number of 5 million per foot (16 million per meter) to 0.47 in. (1.19 cm) at the Reynolds number of 85 million per foot (279 million per meter). For Mach 0.9, it ranged from 0.51 in. (1.30 cm) at a Reynolds number of 13 million per foot (43 million per meter) to 0.49 in. (1.24 cm) at the Reynolds number 100 million per foot (328 million per meter).

The model was instrumented with 18 (16 along the centerline) differential dynamic pressure transducers. The reference pressure was local static and a calibration at 1000 Hz verified that the temperature compensation was within the manufacturer's specifications.

3.2.1 Data acquisition, reduction and analysis

Data were obtained for the Mach number range 0.20 through 0.90, the Reynolds number range 4 through 100 million per foot (328 million per meter) and model yaw angles of 0 and 15 degrees. Data were sampled at 12.5 kHz (with an antialiasing filter applied at 5 kHz), divided into 50 blocks of 4096 points each, Fourier analyzed and the resulting spectra averaged. This produced spectra with a frequency resolution of 3 Hz with a 95 percent confidence that the spectral estimate was within ±1 dB of the true spectra based on a chi-square distribution.

Since the data were obtained for a wide range of temperature and freestream dynamic pressure, the data were nondimensionalized using freestream parameters. The pressure is presented in decibels (dB) with pressure referenced to free-stream dynamic pressure.

$$ FPL = 20.\log \frac{p}{q_\infty} \tag{5}$$

The frequency is nondimensionalized using cavity length, l, and the free-stream flow speed, U_∞.

3.2.2 Results and discussion

An illustration of an acoustic mode shape in the cavity can be obtained by plotting the amplitude of a tone, at a given frequency, measured at positions along the length of the cavity. Figure 4 presents three different mode shapes (corresponding to fl/U_∞ approximately equal to 0.7, 1.1, and 1.5) in a cavity with l/h = 6.7, Mach = 0.80, yaw = 0 degrees, and R = 99 million per foot (325 million per meter). Subsequent data will be presented as acoustic spectra. Data from the transducer that was located furthest upstream will be used in this report because the least amount of broadband noise was measured at that location. Except where indicated, all data are presented for yaw of 0 degrees.

One of the objectives of this study was to determine if acoustic tones are generated by cavities with the same l/h ratios at transonic speeds as they are at supersonic speeds. Figures 5 and 6 present plots comparing FPL spectra for the four l/h configurations at Mach equal to 0.90 and 0.60. Data are presented for the highest Reynolds number obtained (100, and 85 million per

foot (328 and 279 million per meter), respectively). A first observation is that the deeper the cavity (or greater the volume), the greater the acoustic pressures. Tones are observed for cavities with l/n equal to 4.4 and 6.7 and not 20.0 which agrees with data obtained previously under supersonic conditions. An unanticipated result is, while no tones occur at Mach = 0.90 for a cavity with l/h = 12.67, they do occur at Mach = 0.60. Data for M = 0.20 was only available for l/h equal to 4.4 and 6.7. There were no tones apparent and no notable differences between the spectra.
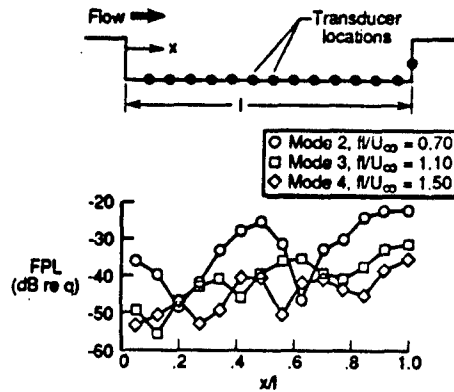
Figure 4. Acoustic mode shape in cavity.
l/h=6.70, M=0.80, R=99 million per foot
(325 million per meter).
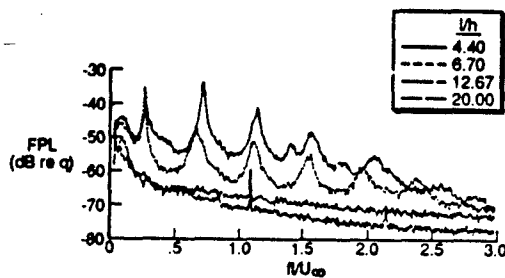
Figure 5. Effect of length-to-depth ratio.
M=0.90, R=100 million per foot
(325 million per meter).
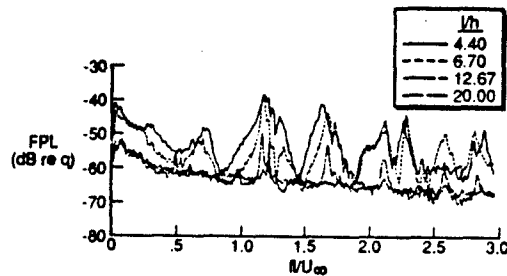
Figure 6. Effect of length-to-depth ratio.
M=0.60, R=85 million per foot
(279 million per meter).

Reynolds number appeared to have little effect on the FPL spectra measured. Figure 7 gives typical results for a cavity with l/h = 6.70 at Mach = 0.80. Returning to figures 5 and 7, it is possible to observe the effects of Mach number variation. Tone amplitude and bandwidth changed with Mach number as well as which tones dominated the spectra. Again it is important to note the change in FPL spectra for l/h = 12.67. It appears that a change in flow field may have occurred as the Mach number decreased from 0.9 to 0.6. Static pressure distributions (see ref. 49) are expected to aid in identifying the flow field type at each Mach number.
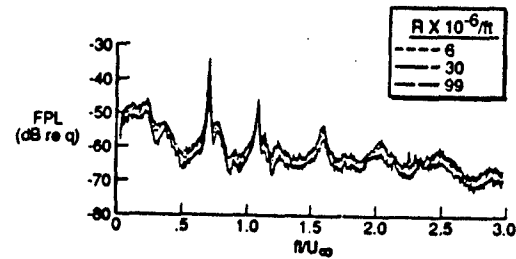
Figure 7. Effect of Reynolds number.
M=0.80, l/h=6.70.
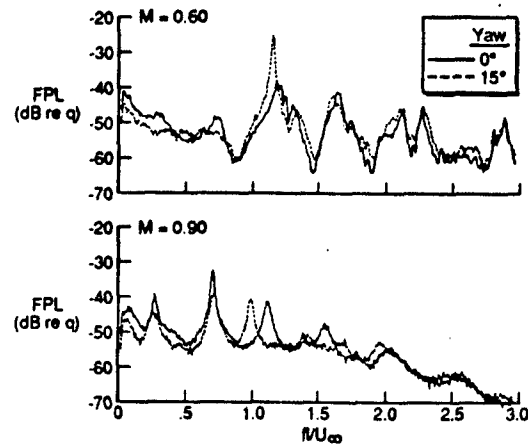
Figure 8. Effect of yaw.
R=90 million per foot (295 million per meter),
l/h=4.40.

Changes in the cavity fluctuating pressures with yaw angle varied with Mach number, Reynolds number, l/h and mode order. There was no case in which the tones were eliminated altogether indicating a change from open to closed cavity type flow. Figure 8 gives spectra comparing data for yaw of 0 degrees with 15 degrees, for l/h = 4.4, R = 90 million per foot (295 million per meter) and Mach = 0.60. Figure 8 gives the corresponding plot for Mach=0.90. It is also apparent that some tones increase in amplitude while others decrease with an increase in yaw. An example of a tone increasing in amplitude is the third mode

(fl / U_∞ approximately equal to 1.1) at Mach = 0.60. The opposite effect is seen for the first, second and

forth modes at Mach = 0.90. An interesting phenomenon is observed at Mach = 0.90. Beginning with the third mode (fl / U_∞ approximately equal to 1.1), there is a shift down in the higher modal frequencies with increased yaw. This may result from the cavity appearing longer to the shorter wavelength modes when it is in the yawed position. As the cavity becomes more shallow, these effects become less dramatic. There was no effect of yaw in the l/h = 20.0 configuration. The effect of yaw at Mach = 0.20 was minimal.

3.2.3 Summary

Reynolds number appears to have little effect on the acoustic spectra generated by rectangular cavities at yaw = 0 degrees for Mach numbers 0.20 though 0.90. Results for cavities with l/h ratios of 4.40 and 6.70 were consistent with supersonic results. For a cavity with l/h equal to 12.67 (transitional at supersonic speeds), there appears to be a change in flow field type as the Mach number decrease to 0.60 and tones appear. Mode amplitude and band width depended on Mach number. There were no tones apparent at Mach = 0.20. The effect of yaw on cavity acoustics varied with Reynolds number, Mach number, l/h, and mode number. Higher order modes shifted down in frequency with yaw at Mach equals 0.90.

4.0 CONCLUSIONS

In the first part of the paper, the contribution of airframe noise to total aircraft noise on approach was accessed for a large current technology transport and for the same airframe powered with BPR 10 engines with an additional 5 dB noise suppression applied to the fan and turbine noise sources. For the current technology transport, airframe noise was found to be 10 EPNdB smaller than the dominant noise source, fan discharge. This result was in agreement with the known behavior of current technology aircraft. The airframe noise of the envisioned advanced subsonic transport was 2 EPN dB less than the largest contributor to the total aircraft noise, the fan inlet. It was concluded that airframe noise is comparable to other noise sources on approach, and further reductions of approach noise would have to be made with consideration of airframe noise. Airframe noise was not viewed as an absolute noise floor. Further research is needed to investigate ways to reduce it.

In the second part of the paper, the results from two recent cavity noise wind tunnel experiments are reported. A cavity of dimensions 11.25 in. (28.58 cm) long, 2.5 in. (6.35 cm) wide, and variable depth was tested in the Mach number range of .20 through .90. Reynolds number varied from 5 to 100 million per foot (16 to 328 million per meter). The l/d ratio was varied from 4.4 to 20.0. The model was tested at yaw angles from 0 to 15 degrees. In general, the deeper the cavity, the greater the amplitude of the acoustic tones. Reynolds number appeared to have little effect on acoustic tone amplitudes when they existed. Tone amplitude and bandwidth changed with Mach number.

The effect of yaw on acoustic tones varied with Reynolds number, Mach number, l/h, and mode number. At Mach number 0.90, increased yaw shifted the tone frequencies of the higher modal frequencies to lower frequencies. As cavity depth decreased, the effect of yaw decreased.

5.0 REFERENCES

1. Crighton, David G.: Airframe Noise. Aeroacoustics of Flight Vehicles: Theory and Practice, Volume 1: Noise Sources, Harvey H. Hubbard, ed., NASA RP-1258, WRDC TR 90-3052, 1991.

2. Heller, H. H.; and Dobrzynski, W. M.: A Comprehensive Review of Airframe Noise Research. ICAS, proceedings,Lisboa, Portugal, 0-16 September 1978.

3. Hardin, J. C.: Airframe Noise/A Design and Operating Problem, NASA SP-416, October 1976.

4. Howe, M. S.: A Review of the Theory of Trailing Edge Noise, Journal of Sound and Vibration, (1978), 61(3), 437-465.

5. Revell, J. D.; Healy, G. J.; and Gibson, J. S.: Methods for the Prediction of Airframe Aerodynamic Noise, AIAA Paper 75-539, AIAA 2nd Aero-Acoustics Conference, Hampton, Va., March 24-26, 1975.

6. Fink, M. R.: Airframe Noise Prediction Method, FAA-RD-77-29, March 1977, (AD-AO39 644).

7. Revell, J. D.: Induced Drag Effect on Airframe Noise, AIAA 75-487, 1975.

8. Hayden, R. E.; Kadman, Y.; Bliss, D.; and Africk, S.: Diagnostic Calculation of Airframe Radiated Noise, AIAA Paper No. 75-485, 1975.

9. Brooks, T. F.; and Hodgson, T. H.: T. E. Noise Prediction from Measured Data, Vol. 78, No. 1, Sept. 8, 1981, pp. 69-117.

10. Brooks, T. F.; Pope, D. S.; and Marcolini, M. A.: Airfoil Self-Noise and Prediction, NASA RP 1218, July 1989.

11. Heller, H. H.; and Dobrzynski, W. M.: Sound Radiation from Aircraft Wheel-Well/Landing-Gear Configurations, J. Aircraft,

12. Kipersztok, O.; and Sengupta, G.: Flight Test of the 747-JT9D for Airframe Noise, J. Aircraft, Vol. 19, No. 12, December 1982.

13. Fink, M. R.; and Schlinker, R. H.: Airframe Noise Component Interaction Studies, AIAA 5th Aeroacoustics Conference, Paper 79-0668, Seattle, Wa., March 12-14, 1979.

14. Hardin, J. C.: Noise Radiation from the Side Edges of Flaps, AIAA Journal, Vol. 18, No. 5, May 1980.

15. Dobrznski, W. M.: Trailing-Edge Airframe Noise Source Studies on Aircraft Wings, J. Aircraft, Vol. 18, No. 5, May, 1981.

16. Fethney, P.: An Experimental Study of Airframe Self-Noise, AIAA Paper 75-511, March 1975.

17. Aircraft Noise Prediction Program Theoretical Manual, NASA TM 83199, Part I, Part II, February 1982.

18. Willshire, W.L., Jr.; and Garber, D. P.: Advanced Subsonic Transport Noise, NASA TM 104112, August 1991.

19. Block, P. J. W.: Assessment of Airframe Noise, J. Aircraft, Vol. 16, No. 12, p. 834-841.

20. DC-10 Design Features, Report DAC 61556E, October 1979.

21. Kapper, C. Y.: Validation of Aircraft Noise Prediction Program, DC 10-Validation, NASA CR 159047, June 1979.

22. Noise Standards: Aircraft Type and Airworthiness Certification. Federal Aviation Regulations, Pt. 36, FAA, June 1974.

23. Noise Levels for U.S. Certificated and Foreign Aircraft ,FAA AC 36-1E, June 30, 1988.

24. Matta, R.K.; Sandusky, G. T.; and Doyle, V.L.: GE Core Engine Noise Investigations- Low Emission Engines. FAA RD-77-4, February 1977.

25. "Aero-Propulsion Technology (APT), Task V- Low Noise ADP Engine Definition Study", Final Contract Report NAS3-25952, March 1991.

26. Fishbach, Laurence H.; and Caddy, Michael J.: NNEP - The Navy NASA Engine Program. NASA TM-X-71857, December 1975.

27. Preisser, J. S.: Airframe Noise Measurements on a Supersonic Transport Small-Scale Model; J. Aircraft, Vol. 17, No. 11, November 1980, pp 795-801.

28. Rossiter, J. E.: Wind-Tunnel Experiments on the Flow over Rectangular Cavities at Subsonic and Transonic Speeds. RAE Report No. 3438, October 1964.

29. Heller, H. H.; Holmes, G.; and Covert, E. E.: Flow-Induced Pressure Oscillations in Shallow Cavities. AFFDL-TR-70-104, December 1970.

30. Heller, Hanno H.; and Bliss, Donald B.: Aerodynamically Induced Pressure Oscillations in Cavities - Physical Mechanisms and Suppression Concepts.AFFDL-TR-74-133, February 1975.

31. Bartel, H. W.; and McAvoy, J. M.: Cavity Oscillation in Cruise Missile Carrier Aircraft. AFWAL-TR-81-3036, June 1981.

32. Clark, Rodney L.: Evaluation of F-111 Weapons Bay Aero-Acoustic and Weapon Separation Improvement Techniques. AFFDL-TR-79-3003, February 1979.

33. Kaufman, Louis G.; Maciulaitis, Algirdas; and Clark, Rodney L.: Mach 0.6 to 3.0 Flows Over Rectangular Cavities. AFWAL-TR-82-3112, May 1983.

34. Shaw, L.; Clark, R.; and Talmadge, D.: F-111 Generic Weapons Bay Acoustic Environment. AIAA-87-0168, January 1987.

35. Gates, Roger S.; Butler, Carroll B.; Shaw, Leonard L.; and Dix, Richard E.: Aeroacoustic Effects of Body Blockage in Cavity Flow. AIAA-87-2667.

36. Shaw, Leonard; and Banaszak, Dave.: Weapons Internal Carriage/Separation-'WICS' Aeroacoustic Research. AFWAL-TM-86-243-FIBG, March 1987.

37. Dix, R.E.: Weapons Internal Carriage and Separation at Transonic Conditions. AEDC-TMR-89-P4, October 1989.

38. Shaw, Leonard L.: Supersonic Flow Induced Cavity Acoustics. Shock and Vibration Bulletin, Bull. 56, Pt. 2, U.S. Dep. of Defense, Aug. 1986, pp. 209-216.

39. Dix, R. E.; and Dobson, T. W., Jr.: Database for Internal Store Carriage and Jettison, Volumes I and II. AEDC-TR-90-23, November 1990.

40. Block, P. J. W.; Stallings, Robert L., Jr.; and Blair, A. B., Jr.: Effect of Doors on Fluctuating Pressure Measurements Inside a Shallow Cavity in Supersonic Flow. NASA TP-2849, 1988.

41. Dix, Richard E.; and Bulter, Carroll: Cavity Acoustics.: Presented at the Store Carriage, Integration, and Release Conference, April 4-6, 1990, Bath, England.

42. Tracy, Maureen B.; and Stallings, Robert L., Jr.: Coupling of Acoustic Environment in Rectangular Cavity with Store Vibration Characteristics During Simulated Separation in Supersonic Flow (Confidential). NASA TP-2986, June 1990.

43. Wilcox, Floyd J., Jr.: Experimental Measurement of Internal Store Separation Characteristics at Supersonic Speeds. Presented at the Store Carriage, Integration, and Release Conference, April 4-6, 1990, Bath, England.

43. Stallings, Robert L., Jr.; and Wilcox, Floyd J., Jr.: Experimental Cavity Pressure Distributions at Supersonic Speeds. NASA TP-2683, 1987.

45. Tracy, M. B.; Plentovich, E. B.; Chu, J.; and Shearin, J. G.: Cavity Acoustics in High Reynolds Number Transonic Flows. Proceedings of the Eighth Joint Ordinance Commanders Group Aircraft/Stores Compatibility Symposium, October 23-25, 1990, Fort Walton Beach, Florida.

46. Ladson, Charles L.; and Ray, Edward J.: Evolution, Calibration, and Operational Characteristics of the Two-Dimensional Test Section of the Langley 0.3-Meter Transonic Cryogenic Tunnel. NASA TP-2749, September 1987.

47. Rallo, Rosemary A.; Dress, David A.; and Siegel, Henry J.A.: Operating Envelope Charts for the Langley 0.3-Meter Transonic Cryogenic Wind Tunnel. NASA TM-89008, August 1986.

48. Mineck, Raymond E.: Hardware and Operating Features of the Adaptive Wall Test Section for the Langley 0.3-Meter Transonic Cryogenic Tunnel. NASA TM-4114, June 1989.

49. Plentovich, E. B.; Chu, Julio; and Tracy, M. B.: Experimental Study of a Rectangular Box Cavity at High Reynolds Numbers. NASA TM-4209, 1990.

Discussion

QUESTION BY: L. Fottner, Universität der Bundeswehr, Germany
Could you please comment on the ratio of airframe/engine noise propagation for _combat_ aircraft?

AUTHOR'S RESPONSE:
It is the co-authors understanding that the predictions made for the DC10 would be identical for the KC10 military transport and that the projected enhancements to the propulser would apply for an advanced military transport. (Since the "advanced technology transport" exists only on paper, it is possible to call it an advanced technology military transport.) The characteristics of the advanced propulser were obtained using the NAVY/NASA Engine Program as described in the paper.

QUESTION BY: H. Körner, DLR Braunschweig, Germany
Engines with large bypass-ratio will be installed very near to the wing. This may result in a high-lift flap configuration, where you have externally blown flaps. Do you have an estimate or results how much this influences the airframe noise level?

AUTHOR'S RESPONSE:
Unfortunately, I can not answer this question. It would be better addressed to the first author.

QUESTION BY: H. Körner, DLR, Germany
You did your investigations in a cryogenic wind tunnel. Did you have difficulties with the pressure transducer working in a cryogenic surrounding?

AUTHOR'S RESPONSE:
The transducers contained a temperature compensation module and we had them calibrated for the test range of temperatures. The calibration indicated that the sensitivity of the transducers did not deviate from reference sensitivity by more than 10 % (manufacturers specifications). The

majority of the data obtained while varying Reynolds number (temperature) did not change in a way that would indicate a change in sensitivity.
(Unfortunately the calibration was done at a single frequency so I can not say definitively that there was no change in sensitivity for the entire frequency range.)

QUESTION BY: H. Körner, DLR, Germany
Your investigations show that there is small influence of Reynolds number. This indicates that viscous effects are not dominating this problem. It should therefore be possible to have an appropriate CFD approach using Euler-equations. Could you comment on this?

AUTHOR'S RESPONSE:
There is ongoing work with both Navier-Stokes codes and Euler codes. Although we do not have direct comparisons with our experimental data we are pleased with what we see from the Euler calculations.

QUESTION BY: P. Artaz, SNECMA, France
Est-il possible, avec votre modele, d'évaleur la calibration parametrique de chacune des regions de la cellule (voilure, volets, trains,....)?
With your model, is it possible to evaluate the respective contribution of each part of the airframe (wings, flaps, gear,...)?

AUTHOR'S RESPONSE:
Yes - Table 3 in the paper gives the results calculated for nose landing gear, leading edge slat, trailing edge flap, main landing gear.

QUESTION BY: R.E. Smith, jr. Consultant, U.S.
What is the state of the boundary layer on the tunnel wall at the leading edge of the cavity? What is the influence of this boundary layer on the cavity results?

AUTHOR'S RESPONSE:
Of course boundary layer thickness/cavity depth has been determined to be an important parameter in the generation of cavity tones. That is why it was important to maintain a boundary layer of (approximately) constant thickness throughout the study. We believe that the boundary layer that had developed on the side wall of the tunnel approaching the cavity did not vary significantly for the Reynolds number range tested. (The paper includes the measured values.)
Also there was fully developed turbulence (a laminar boundary layer approaching the cavity would produce much more intense tones).
Although we had flight Reynolds numbers (based on cavity length) we cannot say that we had boundary layer thickness/cavity depth matching full scale aircraft. We are currently working with a larger model in the Langley 8 foot Transonic Pressure Tunnel.

AD-P007 518
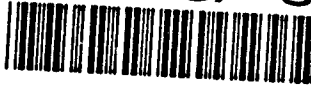
COMPARISON OF FLYOVER NOISE DATA FROM AIRCRAFT
AT HIGH SUBSONIC SPEEDS WITH PREDICTION

J. Böttcher* and U. Michel**

* Institut für Entwurfsaerodynamik, Deutsche Forschungsanstalt
für Luft- und Raumfahrt, DLR, Flughafen, D-3300 Braunschweig,
Germany

** Institut für Experimentelle Strömungsmechanik, Deutsche For-
schungsanstalt für Luft- und Raumfahrt, DLR, Müller-Breslau-
Straße 8, D-1000 Berlin 12, Germany

SUMMARY

Flyover noise measurements are evaluated
for four different military jet aircraft
types flying at low altitudes. Flight Mach
numbers ranged from 0.5 to 0.9. The ana-
lysis shows that noise immission is caused
by jet mixing and broadband shock associ-
ated noise. Based on the experimental re-
sults existing noise prediction schemes
are extended toward higher subsonic flight
Mach numbers. The novel prediction schemes
describe the observed acoustic signatures
quite accurately. This holds for the over-
all sound pressure level in dependence of
the emission angle, for sound-pressure
level time histories and for one-third-
octave spectra.

1. INTRODUCTION

In recent years military jet aircraft
noise became a major community noise prob-
lem. In addition to the sound immission
near airfields caused from starting and
landing airplanes the noise from military
jet aircraft flying with high subsonic
speeds at low altitudes constitutes a par-
ticular problem. The latter one is the
concern of the present investigation.

The in-flight sound emission of a jet air-
craft in general is created in the jet en-
gine itself and in the downstream free
jet. At certain flight conditions, for ex-
ample approach, airframe noise may also
contribute to the total sound emission. In
Figure 1 the jet engine and the jet are
shown schematically. Significant internal
noise sources are the fan and the turbine,
while external sound is generated by the
jet as jet mixing noise and also, under
certain circumstances, as shock noise. Jet
mixing noise is caused by the turbulent
mixing process of the hot core, the cold
by-pass, and the ambient stream. A prereq-
uisite for the occurrence of shock noise
is that the Mach number of the fully ex-
panded jet becomes larger than one and
that the nozzle lip pressure differs from
the ambient pressure. Then the free jet
consists of a supersonic jet plume with a
regular, quasi-stationary shock cell
structure and an outer subsonic region
(see Figure 1). Inside the supersonic core
interaction of convecting disturbances and
the shock cells may lead to broadband
shock associated noise. For more details

concerning development and characteristics
of jet mixing and shock noise the reader
may refer e.g. to Smith [1] and Seiner
[2].
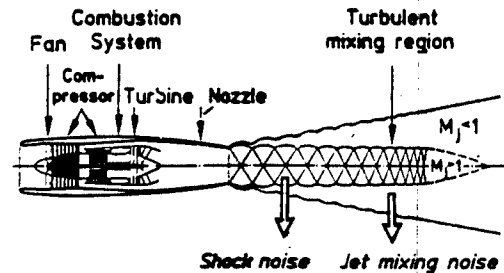
Figure 1.- Schematic illustration of a jet
engine and the jet

An important objective of this study about
noise immission of jet aircraft flying
with high subsonic flight speeds at low
altitudes is the identification of the
dominating noise sources. For that purpose
extended flyover measurements are evalu-
ated (Section 2) and analyzed in detail
(Section 3). Based on these experimental
results, existing noise prediction schemes
will be extended to high subsonic flight
speeds in Section 4. Finally, the flyover
noise data will be compared with predic-
tion in Section 5.

2. EXPERIMENTAL PROCEDURES AND DATA EVALUATION

The DLR was not involved in the flyover
measurements themselves, however, the ex-
perimental data were made available to the
authors as microphone signals stored on
tape. Figure 2 shows the experimental test
set-up. The aircraft's nominal altitude
above ground during the flight tests was
75 m. The flight speed was determined from
the airspeed indicator in the cockpit. The
jet conditions had to be computed from the
aircraft-engine flight data by assuming
the aircraft's drag condition. Sound im-
mission was measured by using an array of
microphones positioned on an axis vertical
to the flight path. The acoustic signals

of three microphones with distances y = 0 m, +100 m, and -100 m to the flight path were utilized. The microphone height was given as 1.5 m above a grass surface. In Figure 2 the emission angle θ is defined as the angle relative to the flight direction.
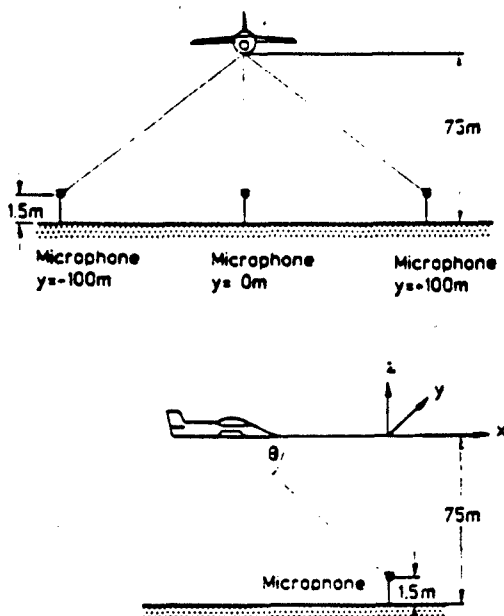
Figure 2.- Flight test set-up

By utilizing two goniometers, the altitude and sideline deviation from the defined flight path were determined for later correction. The goniometer in prolongation of the microphone axis was also used to determine the time when the plane crossed the microphone axis. At that moment a sounding impulse was released by hand. This impulse was recorded on magnetic tape in addition to the microphone signals. This procedure and the knowledge of the aircraft's flight speed permit the correlation of the acoustical data and the position of the aircraft at any time during the flight test.

It should be mentioned here that for the purpose of this study it would have been better to place the microphones on the ground, to determine aircraft position and airspeed more accurately, and to record the jet exhaust conditions with an instrumented aircraft.

Flyover noise data were available for four different military jet aircraft. For every plane noise data were evaluated for 2 or 3 different flight speeds or Mach numbers. Altogether, flight Mach numbers ranged from M_f = 0.5 to 0.9, approximately. In order to obtain more reliable results, between four and eight flight tests for each aircraft and Mach number were included in the data acquisition.

The microphone data were digitized and then evaluated utilizing the Fast Fourier Transformation (FFT) in order to obtain frequency spectra and overall sound pressure levels. The FFT was carried out for "de-Dopplerized" time series. This procedure eliminates the Doppler frequency shift which would otherwise have obscured the frequency spectra and smeared out tonal contributions in the spectra. Using the International Standard ISO 3891 /3/, attenuation due to atmospheric absorption was corrected separately for every microphone. Ground reflection and attenuation effects could only be corrected in a frequency independent manner (see Böttcher and Michel /4/).

Noise signals were evaluated for the emission angle range θ = 30 to 150 degrees. The results for all emission angles were normalized to a wave normal distance of 75 m which leads to the so-called polar presentation. With exception of the sound-pressure level time histories all results will be shown in wind-tunnel coordinates, i.e. in a coordinate system where "de-Dopplerized" data are plotted. By this means the results for different emission angles and different flight Mach numbers can be compared more easily. All sound pressure levels are plotted with no weighting in order to show the physical aspects more clearly. For further description and discussion of the data acquisition and evaluation process one should refer to /4/.

3. DATA ANALYSIS

3.1 Data Accuracy

The objective of this section is to demonstrate the accuracy of the measurements. For that purpose, first results for the three different microphones positioned at y = 0 m, +100 m, and -100 m will be compared. In Figure 3 the overall sound pressure level (OASPL) is plotted in polar presentation for a single flight test for the different microphones versus the emission angle. Flight Mach number is M_f = 0.73. One can observe from the figure that the OASPL for the microphone positioned directly below the flight path (at y = 0 m) is on average slightly above the OASPL for the microphones in the sideline positions.

Figure 4 shows one-third-octave spectra of the three microphones for the same flight test as in Figure 3. The emission angle is 90 degrees. Again the sound pressure level (SPL) for the microphone at y = 0 m is tendentiously above the SPL for the sideline microphones.

The differences between the three microphone positions in Figure 3 and 4 can be explained with ground reflection and ground attenuation effects and in addition, with lateral attenuation effects. These effects could not be corrected in a frequency dependent manner (see /4/). Nevertheless, the sound pressure level differences for microphones placed at different positions can be accepted in this study considering the overall accuracy of

measurements. This holds especially since the averaging of results over three microphone positions and up to eight flights tests leads to a "smoothing" of the observed effects and therefore, to a minimization of the absolute error.
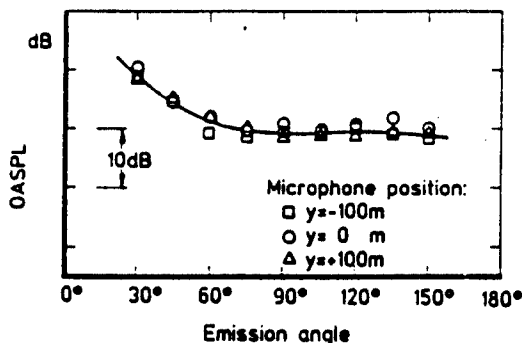
Figure 3.- Measured overall sound pressure level versus emission angle (relative to flight direction) for a single flight test at flight Mach number M_f = 0.73 for three microphones at different positions. The results are plotted in polar presentation
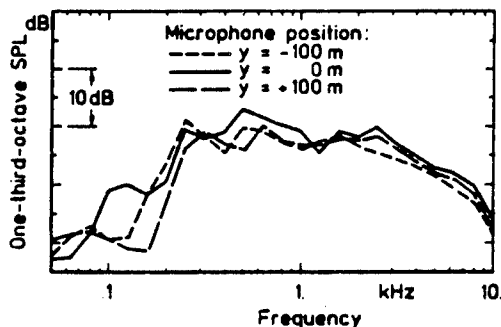

Figure 4.- Measured one-third-octave spectra for a single flight test at flight Mach number M_f = 0.73 for three microphones at different positions. Emission angle is 90 degrees

In order to demonstrate the typical scatter between results for nominally identical test conditions, acoustical signals for different flight tests conducted with the same aircraft type are compared next. Flight Mach number is M_f = 0.73 again. Figure 5 shows the OASPL versus the emission angle in polar presentation. For every flight test, averaging was carried out for the acoustical signals of all three evaluated microphones. With exception of flight test No. 5 one can observe from Figure 5 that the scatter of measured OASPL between the different flyover tests is negligible, i.e. the variation is smal-

ler than ±1.5 dB. For flight test No. 5 the figure indicates an OASPL systematically up to 2 dB below average in the emission angle range 90 to 150 degrees. Nevertheless, again this variation can be accepted, if the study's overall accuracy is taken into consideration, i.e. also the acoustic signals from flight test No. 5 can be included in the averaging process.
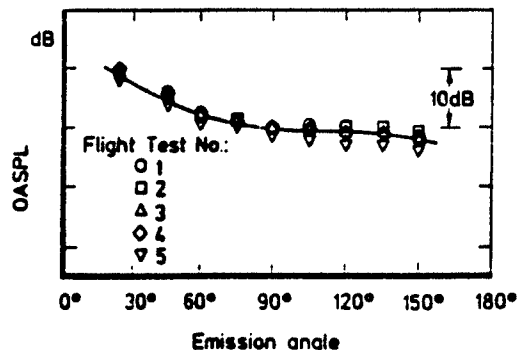
Figure 5.- Measured overall sound pressure level versus emission angle (relative to flight direction) for five flight tests performed with the same aircraft type under nominally identical test condition. Flight Mach number is M_f = 0.73. For every test the acoustic signals of all three microphones are averaged

Figure 6 shows time histories of the sound pressure level for the five flyover tests already utilized in the previous figure. Here only the acoustical signals for the microphone positioned at y = 0 m are utilized. At the x-axis of Figure 6 the time t = 0 s marks the moment the aircraft crossed the microphone axis. One can observe that the noise level time histories for all flight tests are quite similar. Especially, the peak value for all tests appears nearly at the same time. One should note the steep ascent prior to the maximum which will be discussed in Section 5.

Finally, Figure 7 shows one-third-octave spectra for five flight tests at flight Mach number M_f = 0.73. Emission angle is 90 degrees. Here again - as in Figure 5 - the acoustical signals of all three evaluated microphones are averaged for every flight test. Figure 7 again demonstrates that the scatter in general is small between results of different flyover tests at nominally identical test conditions. This holds for both the shape of the spectra and the absolute values of the measured sound pressure levels.

3.2 Source Identification

An important objective of this study is the identification of the dominating noise sources. For that purpose frequency spectra for different flight Mach numbers and
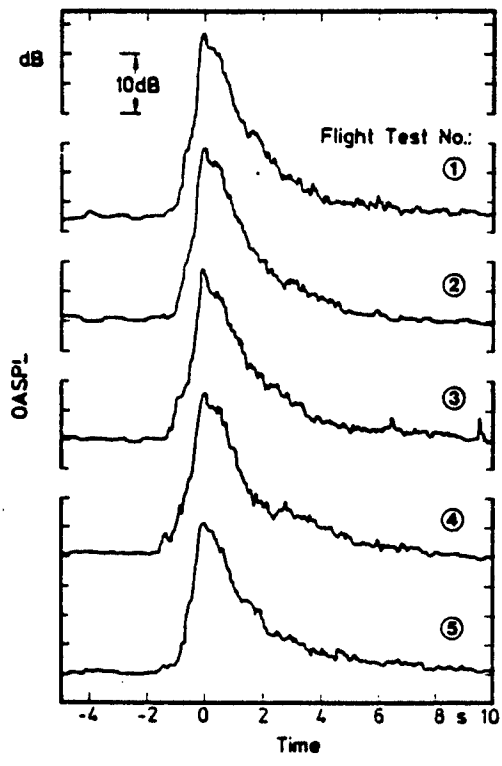
Figure 6.- Measured sound-pressure level time histories for five flight tests performed with the same aircraft type under nominally identical test conditions for the microphone positioned at y = 0 m. Flight Mach number is 0.73. Time t = 0 s denotes the flyover moment
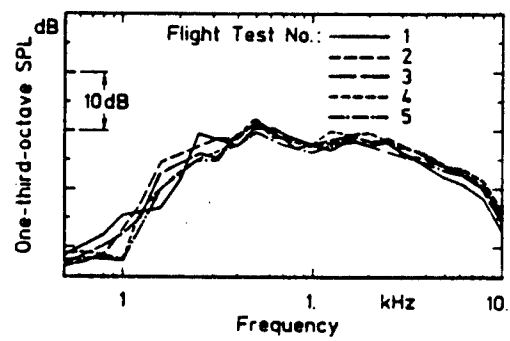
Figure 7.- Measured one-third-octave spectra for five flight tests performed with the same aircraft type under nominally identical test conditions. Flight Mach number is M_f = 0.73, and emission angle is 90 degrees. For every test the acoustic signals of all three microphones are averaged

emission angles will now be analyzed. Figures 8 a-d in each case show nine one-third-octave spectra for emission angles from 30 to 150 degrees in steps of 15 degrees. Results for flight Mach number M_f = 0.64 are plotted in Figure 8 a, for M_f = 0.73, 0.80, and 0.87 in Figures 8 b, c, and d, respectively.

As a first result from the figures it can be stated that no distinct sound pressure level peaks can be identified in the one-third-octave spectra. This finding is confirmed by the corresponding narrowband spectra (bandwidth 25 Hz). On the other hand, internal noise sources such as the fan, the compressor, and the turbine will always contribute tonal components which should appear as distinct peaks in the narrowband spectra. Therefore, it is concluded that internal noise sources of this kind are not important for the sound emission.

On the other hand sound pressure level peaks (marked with an arrow) which mostly cover two one-third-octave bands can be seen in the frequency spectra of Figures 8 a-d. At lower flight Mach numbers the peaks only appear at small emission angles (see Figures 8 a and b). At higher flight Mach numbers or correspondingly higher jet Mach numbers (the latter one is of more importance for the discussion, see below) the peaks also can be observed at higher emission angles (see Figures 8 c and d). At a constant Mach number the peak's frequency increases with increasing emission angle. However, the peaks vanish for angles of about 120 degrees and above, i.e. towards the rear radiation arc.

According e.g. to Seiner /2/ sound pressure level peaks with the stated characteristics are caused most likely by broadband shock associated noise. As mentioned before, shock noise is generated by the interaction of convecting disturbances and the regular shock cell structure. The latter one appears if the supersonic jet Mach number differs from the nozzle design Mach number. In the present examples of Figures 8 a-d the jet Mach number increases from M_j = 1.09 to 1.47 (compare the captions of Figures 8 a-d), while the design Mach number of the nozzle is constant at M_j = 1.0. In these cases the shock cells are still quite weak. Since the distinct characteristics of shock noise are most easily observed at small angles to the flight direction (after /2/), it seems reasonable that they are visible at small emission angles but not at large ones.

Apart from these "broadband" peaks it is very likely that jet mixing noise is responsible for the noise immission at high subsonic flight Mach numbers. This conclusion is based on the characteristic shape of the frequency spectra and their variation with shifting emission angle (e.g. compare the frequency spectra presented by Drevet et al. /5/). Airframe and combustion noise will certainly be a component of the total flyover sound immission. However, from the frequency spectra there is no conclusive indication for the importance of airframe or combustion noise in the high speed cases discussed here.
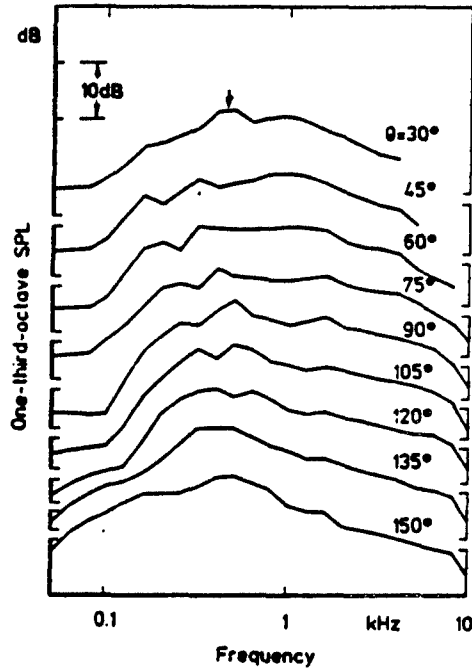
Figure 8a.- Measured one-third-octave spectra for emission angles from .J to 150 degrees at flight Mach number M_f = 0.64 and jet Mach number M_j = 1.09. Individual spectra are separated 7.5 dB in each case in the ordinate scale for clarity
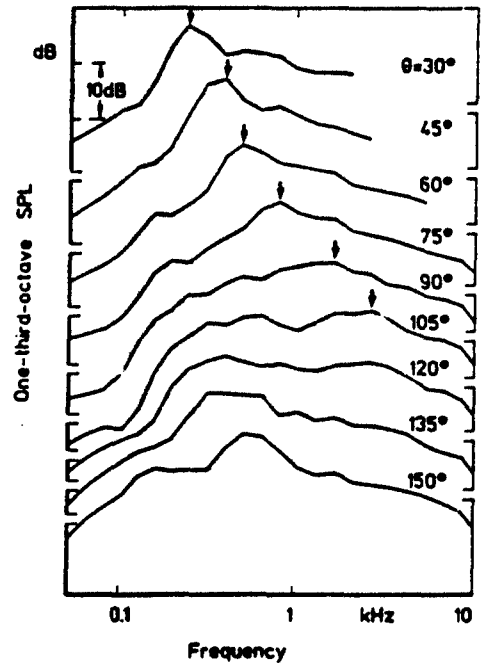
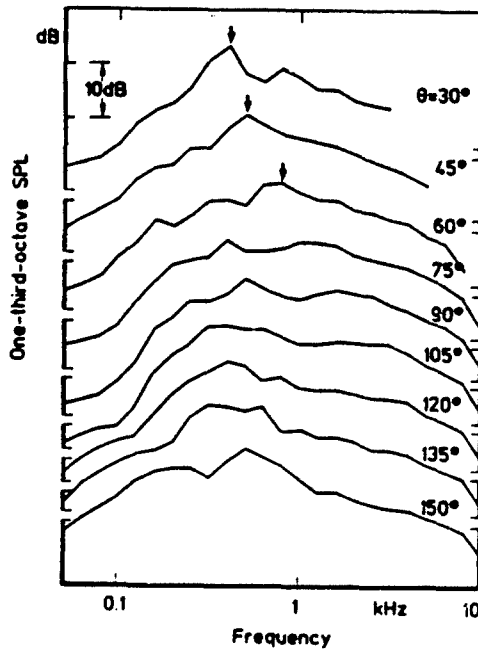Figure 8c.- As Figure 8a, only for flight Mach number M_f = 0.80 and jet Mach number M_j = 1.29

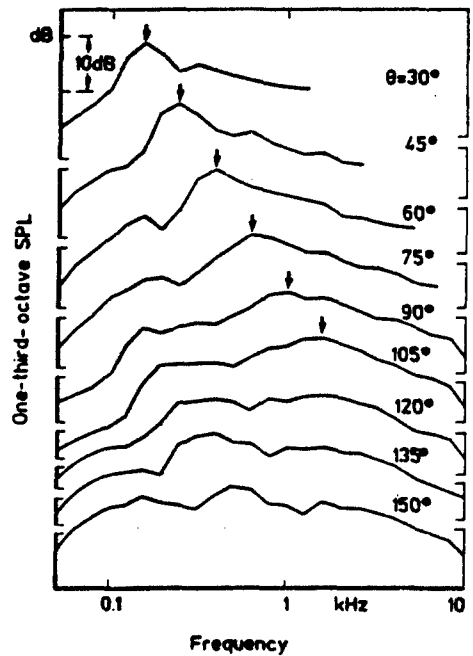Figure 8b.- As Figure 8a, only for flight Mach number M_f = 0.73 and jet Mach number M_j = 1.19

Figure 8d.- As figure 8a, only for flight Mach number M_f = 0.87 and jet Mach number M_j 1.47

4. PREDICTION SCHEMES FOR JET NOISE

To date, prediction schemes are available for jet mixing noise up to a flight Mach number of approximately $M_f = 0.4$ (e.g. SAE /6/ and Michalke and Michel /7/) and for broadband shock associated noise up to approximately $M_f = 0.5$ (e.g. Tam /8/). In order to enable a comparison with the experimental results both schemes had to be extended towards higher subsonic flight Mach numbers up to approximately $M_f = 0.9$ and the thereto attached higher jet temperatures. In this chapter the necessary extensions will be discussed.

4.1 Jet Mixing Noise

The empirical SAE method /6/ is a fairly reliable scheme to predict the jet mixing noise of single stream jets at take-off and approach. The SAE overall sound pressure level in flight is given as

$$(1) \quad OASPL_f = OASPL_{s,iso}$$

$$+ 10 \, \omega \, \log(\rho_j/\rho_o)$$

$$- 10 \, m \, \log[U_j/(U_j-U_f)]$$

$$- 10 \, \log(1-M_f \cos \theta).$$

Here $OASPL_{s,iso}$ designates the overall sound pressure level of the static jet at constant density. U_j and U_f are the jet and the flight speed, respectively, and a_o is the ambient speed of sound. ρ_j and ρ_o denote the jet and the ambient density, respectively. The second line of (1) describes the density influence expressed with the density exponent ω. In the third line the influence of the relative velocity variation is considered in terms of the velocity exponent m. ω and m were determined utilizing experimental results.

For an extension towards higher subsonic flight Mach numbers Michel and Böttcher /9/ suggest the following equation to calculate the overall sound pressure level:

$$(2) \quad OASPL_f = OASPL_{s,iso}$$

$$+ 10\log\left\{ (\rho_j/\rho_o)^2 + \left[\frac{(1-\rho_j/\rho_o)(1-M_f\cos\theta)}{(U_j-U_f)/a_o} \right]^2 \right\}$$

$$- 10 \, m \, \log[U_j/(U_j-U_f)]$$

$$- 30 \, \log(1-M_f\cos\theta)$$

$$+ 20 \, \log \sigma.$$

Here σ denotes the stretching factor which accounts for the stretching of the jet plume in flight. According to /7/

$$(3) \quad \sigma = 1 + 1.4 \, U_f/(U_j-U_f).$$

A detailed discussion of the extended pre-diction scheme for jet mixing noise can be found in /9/. In this paper only the most important aspects will be mentioned:

o The second line of equation (2) replaces the SAE method density term. The density influence now consists of a quadrupole and a dipole term similar to the theory presented in /7/. The first term in braces describes the quadrupole portion, the second term the dipole portion.

o The third line of equation (2) - as in the SAE method - describes the influence of the relative velocity variation to the noise. The exponent m was determined empirically by utilizing the experimental results available for this study.

o The fourth line describes the convective amplification due to the flight speed. In contrast to the SAE method the Doppler factor now is used as third order term to improve the agreement with the measured results.

o The last line of equation (2) describes the amplification due to the stretching of source and coherence volume in flight.

o The relative one-third-octave sound pressure level of the SAE method was calculated utilizing the Strouhal number

$$(4) \quad St = (f \, D_j)/[\xi(U_j-U_f)].$$

Here f is the frequency, D_j the fully expanded jet diameter, and ξ the Strouhal frequency adjustment factor of the SAE method determined as a function of U_j. Including the stretching factor one now obtains

$$(5) \quad St = (f \, D_j)/[\sigma \, \xi(U_j-U_f)]$$

for the Strouhal number in the wind-tunnel coordinate system.

4.2 Broadband Shock Associated Noise

In order to calculate the broadband shock associated noise, a theoretical approach of Tam /8/ was utilized. As mentioned before, Tam's prediction scheme includes the flyover case with flight Mach numbers up to $M_f = 0.5$, whereas several correction factors were determined by comparison with experimental results of Norum and Shearin /10/. For extension towards $M_f = 0.9$ the following modifications are recommended here:

o According to Tam (Equation (3.4) in /8/) the convection speed of the disturbances is

$$(6) \quad U_c = U_f + 0.7 (U_j-U_f)$$

After Tam the broadband shock associated noise is generated far downstream at the end of the potential core. There, a lower convection speed can be

justified which better describes the peak's Doppler shift in the measured frequency spectra. Therefore, here the relationship

$$(7) \quad U_c = U_f + [\rho_j/(\rho_j+\rho_o)] \ (U_j-U_f)$$

is used. This formula also considers an influence of jet density ρ_j and ambient density ρ_o on convection speed.

o The governing parameter influencing the shock noise peak frequency is the Doppler shift. In contrast to Tam's Doppler factor (see the denominator of his equation (3.8)) the interaction between convecting disturbances and the shock cells here leads to the Doppler factor

$$(8) \quad DF = \frac{1}{[1-(M_c-M_f)\cos\theta](1-M_f\cos\theta)}.$$

for the wind-tunnel coordinate system. In this equation $M_c = U_c/a_o$ is the convective Mach number.

o The broadband shock associated noise frequency peaks are also influenced by the wave number of the shock wave modes in flight. Tam uses the following approximation (see equation (3.7) in /8/) for the influence of flight Mach number:

$$(9) \quad k_m(flight) \sim 1/(1 + 0.625 \ M_f).$$

In the present case of higher Mach numbers one gets a better agreement with the measured frequencies by using the approximation

$$(10) \quad k_m(flight) \sim 1 + 0.1 \ M_f.$$

While $k_m(flight)$ is reduced with increasing flight Mach number in Tam's approximation, it now increases with increasing Mach number after equation (10). Higher $k_m(flight)$ corrosponds to shorter longitudinal structures in the supersonic jet plume (see Figure 1).

o Tam's amplitude factor (his equation (3.7)) contains the proportionality

$$(11) \quad F \sim (U_j \ \rho_o)^2/(1-M_f^2 \ \sin^2\theta).$$

In comparison to the theory of Tam a different convective amplification is assumed here for the same reasons which already have led to equation (8). In addition, the influence of speed and density changed because broadband shock associated noise depends on the turbulence intensity. This leads to the following proportionality:

$$(12) \quad F \sim [(U_j-U_.) \ \rho_j]^2/(1-M_f\cos\theta)^2$$

o The factor $U_./U_.$ in Tam's equation (3.7) is eliminated. By this means the spectral width of the sinɑle modes in the frequency spectra is slightly enlarged.

o To further improve the agreement with the measured sound pressure levels the proportionality factor c (see equation

(3.7) in /8/) is altered from

$$c = 2.65 \ 10^{-4} \ S_o \ (S_o = 0.35) \ to$$

$$c = 1.10 \ 10^{-4} \ S_o.$$

5. **COMPARISON OF MEASURED AND CALCULATED RESULTS**

The comparison of experimental and calculated results will be demonstrated for the overall sound pressure level in dependence of the emission angle, for sound-pressure level time histories and for one-third-octave spectra. Altogether, the comparison was carried out for results in the flight Mach number range M_f = 0.54 to 0.87. As in Section 3, all sound pressure levels are plotted with no weighting. With exception of noise level time histories the results will be presented in the wind-tunrel coordinate system.

Figures 9 a,b show the OASPL versus the emission angle in polar presentation for flight Mach numbers M_f = 0.64 (Figure 9 a)and 0.80 (Figure 9 b). Calculated jet mixing and broadband shock associated noise yield the total jet noise. A good agreement between experimental results and
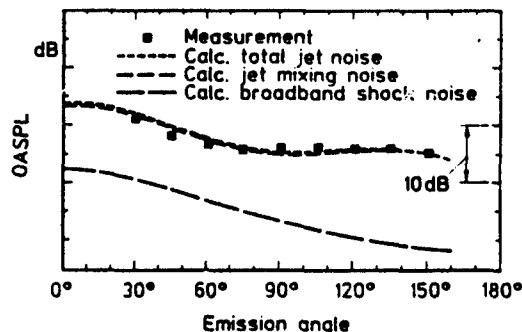
Figure 9a.- Measured and calculated overall sound pressure level versus emission angle (relative to flight direction) in polar presentation at flight Mach number M_f = 0.64
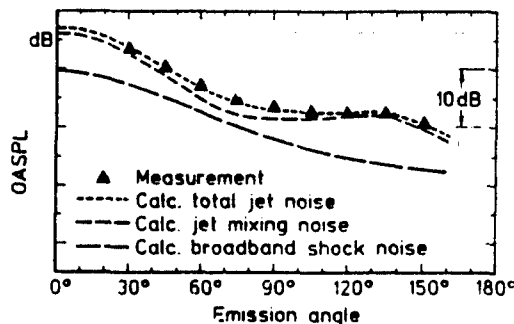
Figure 9b.- As Figure 9a, only for flight Mach number M_f = 0.80

calculated total jet noise with deviations of typically less then or equal to ±1.5 dB at most is observed.

The figures make it clear that the shock noise influence may be neglected at small flight Mach numbers (see Figure 9 a for M_f = 0.64). The reason is a jet Mach number only slightly larger than 1.0 (compare with the discussion in Section 3). At larger flight Mach number (and larger jet Mach number, respectively) the shock noise becomes more important. Nevertheless, it may be concluded from Figure 9 b that the OASPL at M_f = 0.80 is still dominated by jet mixing noise.

One can see from Figure 9 a,b that the OASPL of the calculated jet mixing noise has its maximum at small angles to the flight direction. This result is in contrast both to the stationary case and to the results at low flight Mach numbers where the maximum is observed at high emission angles. However, the present result can be explained with the Doppler amplification of the noise level towards small angles due to the relatively high flight Mach number.

In Figures 10 a,b experimentally obtained time histories of the sound pressure level are compared with the calculated total jet noise. Here only the acoustical signals for the microphone positioned directly below the flight path (position y = 0 m) are plotted. Figure 10 a shows time histories for M_f = 0.64, Figure 10 b results for M_f = 0.80. On the x-axis of the figures, the time t = 0 s marks the moment where the aircraft is in the overhead position.

In the figures, the steep sound pressure level ascent prior to the maximum peak is particularly remarkable. As expected, the ascent rate increases with increasing flight Mach number (at M_f = 0.64 the measured gradient is 19 dB/s; at M_f = 0.80 the gradient is 33 dB/s, approximately). In the present examples the measured ascent rates are slightly steeper than the calculated ones. However, a good agreement between experimental and calculated time histories can be stated. This can also be concluded from the peaks which are predicted with an accuracy of ±1.5 dB.

For comparison of measured and calculated one-third-octave spectra Figures 11 a-d and 12 a-d will be utilized. In Figures 11 a-d frequency spectra for flight Mach number M_f = 0.64 and in Figures 12 a-d spectra for M_f = 0.80 are plotted. In each case results are shown for emission angles 30, 60, 90 and 135 degrees in the wind-tunnel coordinate system.

In correspondence with the preceding results one can again conclude that the sound pressure level at the low flight Mach number M_f = 0.64 is dominated by jet mixing noise. Only at M_f = 0.80 broadband shock associated noise becomes more significant. For a given jet Mach number the influence of shock noise is greatest at small emission angles and continuously decreases with increasing angle (see Figures 12 a-d and compare also with Figures 8 a-d of Section 3).
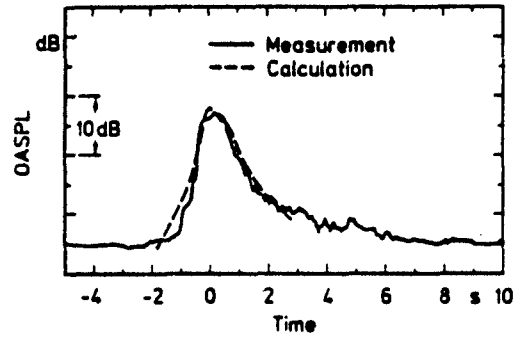
Figure 10a.- Measured sound pressure level and calculated total jet noise time histories for the microphone positioned at y = 0 m. Flight Mach number is M_f = 0.64. Time t = 0 s denotes the flyover moment
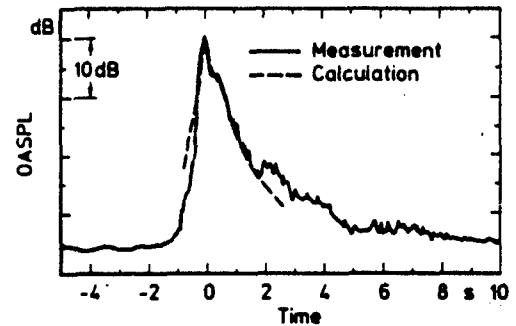
Figure 10b.- As Figure 10a, only for flight Mach number M_f = 0.80

Utilizing the prediction scheme for broadband shock associated noise, the sound pressure level peaks particularly noticeable in the forward arc can now be calculated. In Figure 13 measured and calculated frequencies of the first "broadband" peak, f_{max1}, are compared for three of the four aircraft (aircraft No. 4 shows no shock noise because the jet Mach number is smaller than one). One can observe from Figure 13 that in general good agreement between measured and calculated frequencies is achieved. The corresponding sound pressure level for the first "broadband" peak generally is predicted slightly too low (in the presented examples about 1 dB, see Figures 12 a and b).

6. CONCLUDING REMARKS

The noise immission from miltary jet aircraft flying with high subsonic flight speeds at low altitudes was analyzed and discussed in this paper. Data from four different aircraft types flying with flight Mach numbers in the range of approximately M_f = 0.5 to 0.9 were used to

a) θ = 30°

a) θ = 30°

b) θ = 60°

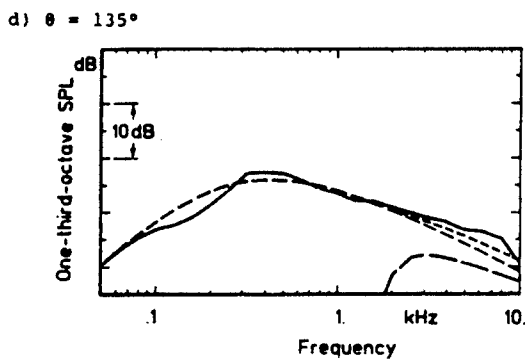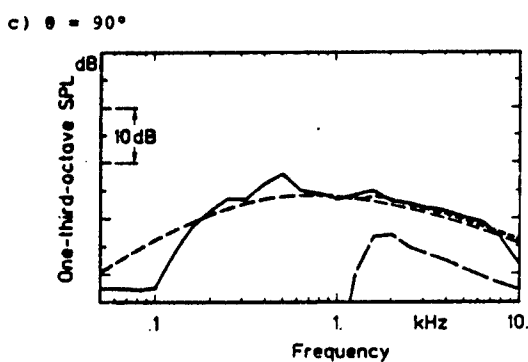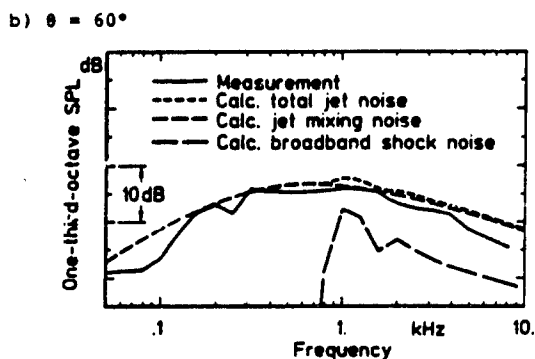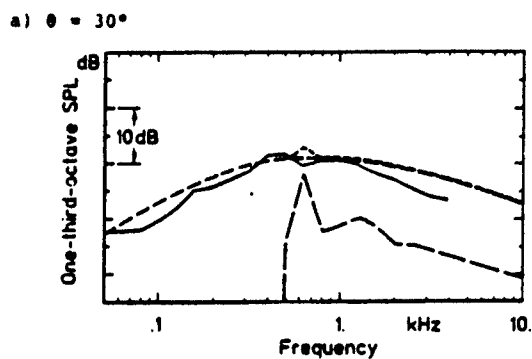b) θ = 60°

c) θ = 90°

c) θ = 90°

d) θ = 135°

d) θ = 135°

Figure 11a-d.- Measured and calculated one-third-octave spectra for flight Mach number M_f = 0.64 and emission angles θ = 30, 60, 90 and 135 degrees
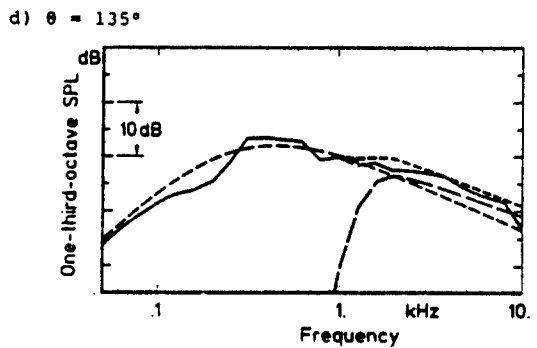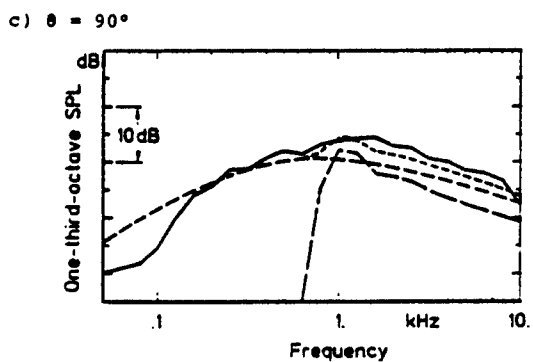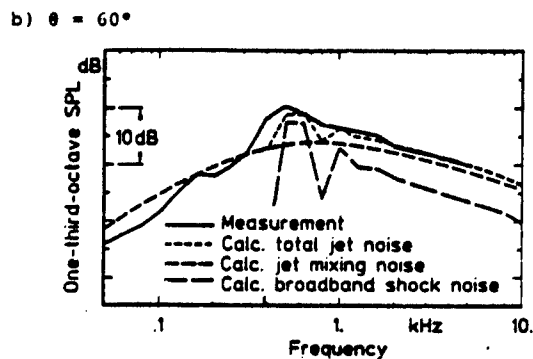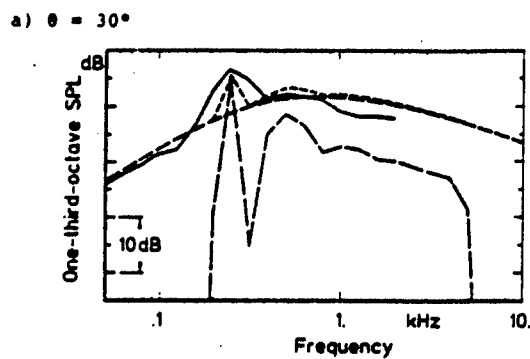
Figure 12a-d.- Measured and calculated one-third-octave spectra for flight Mach number M_f = 0.80 and emission angles θ = 30, 60, 90 and 135 degrees

improve existing schemes for the prediction of jet mixing and of broadband shock associated noise.
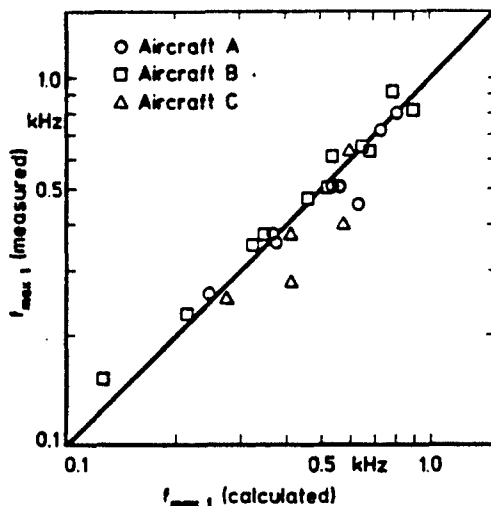
Figure 13.- Comparison of measured and calculated frequencies of the first sound pressure level peak, f_{max1}, for three different aircraft types

Significant tonal contributions to the measured noise were not found in the study. Therefore, it is concluded that fan, compressor, and turbine noise do not play a major role. Broadband shock associated noise was identified especially in the forward arc in all cases in which the jet Mach number was sufficiently different from the design Mach number of the nozzle. It is shown that broadband shock associated noise can be calculated quite accurately with the newly presented scheme which required significant, albeit physically realistic, changes to the scheme of Tam /8/.

After the subtraction of broadband shock noise, the remaining noise can be very well described by the new jet mixing noise scheme /9/ that is based on the SAE method /6/ after incorporating important results of Michalke and Michel /7/. The most important change is a consideration of the increase of the frequency of jet mixing noise proportional to the lengthening of the jet plume. This change results in a very good agreement between measured and calculated frequency spectra. Since the agreement between predictions and measured spectra is so good it is concluded that other noise sources play only a minor role in the total noise immission of the high speed cases discussed here. It seems quite unlikely that airframe or combustion noise would generate the same frequency spectra as jet mixing noise in all the measured cases.

If other noise sources do only play a minor role, it must be concluded that the observed forward arc amplification with increasing flight speed is caused by jet mixing noise. The physical possibility of such an amplification was discussed controversially over a long period and was rejected in earlier jet noise papers. However, the amplification was shown to be theoretically realistic by /7/. The results of this paper are a further support of their result.

The prediction schemes presented in this paper can now be used to demonstrate and quantify the noise reduction potential achievable by varying operational parameters such as flight Mach number, rate-of-climb or -descent or the flight altitude. The new schemes can also be used to study the influence of engine cycle design on the flyover noise.

The prediction schemes are applicable to single stream or "almost single" stream jets exhausting from a circular nozzle. No consideration was given to the effects of non-circular nozzles. The noise reduction potential of such nozzles is sometimes assumed to be considerable, opening a much needed noise attenuation concept for future supersonic transport aircraft.

REFERENCES

/1/ Smith, M.J.T.: "Aircraft Noise". Cambridge Aerospace Series, Cambridge University Press, 1989.

/2/ Seiner, J.M.: "Advances in High Speed Jet Aeroacoustics". AIAA-84-2275, 1984.

/3/ International Organisation for Standardization: "International Standard ISO 3891, Acoustics-Procedure for Describing Aircraft Noise Heard on the Ground", 1978.

/4/ Böttcher, J.; Michel, U: "Der Lärm von Strahlflugzeugen bei hohen Unterschall-Flugmachzahlen". To be published as DLR-FB in 1991.

/5/ Drevet, P.; Duponchel, J.P.; Jacques, J.R.: "The Effect of Flight on Jet Noise as Observed on the Bertin Aérotrain". J. of Sound and Vibration, Vol. 54, No. 2, 173-201, 1977.

/6/ Society of Automotive Engineers, Inc.: "Gas Turbine Jet Exhaust Noise Prediction". Aerospace Recommended Practice SAE ARP 876 C, 1985.

/7/ Michalke, A.; Michel, U.: "Prediction of Flyover Jet Noise Spectra from Static Tests". NASA Technical Memorandum 83219, 1981.

/8/ Tam, C.: "Forward Flight Effects on Broadband Shock Associated Noise of Supersonic Jets". AIAA-89-1088, 1989.

/9/ Michel, U.; Böttcher, J.: "Prediction of Jet Mixing Noise for High Subsonic Flight Speeds". Proceedings of the AGARD Propulsion and Energetics Panel

Specialists' Meeting on Combat Air-
craft Noise, Bonn, 23 - 25 October
1991.

/10/ Norum, T.D.; Shearin, J.G.: "Shock
Noise from Supersonic Jets in Simu-
lated Flight to Mach 0.4". AIAA-
86-1945, 1986.

Discussion

QUESTION BY: Berry, B.F., National Physical Lab, U.K.
Those of us involved in considering environmental impact of
low-altitude noise are primarily interested in A-weighted
levels and not in overall, linear levels. For the purposes of
inter-comparison with similar measurements such as ours at
NPL and American data, do you plan to publish any A-weighted
data?

AUTHOR'S RESPONSE:
Since it was our goal to investigate the basic physical
phenomena, it was more reasonable not to include any
weighting during the data analysis. Therefore, we did not
plan to publish any A-weighted data. On the other hand,
utilizing our computer program it is not a great problem to
introduce any weighting.

QUESTION BY: W.D. Bryce, W.D., RAE Pyestock, UK
Our research in this area, which I will describe in a paper
tomorrow, leads us to a very different conclusion to yours.
We find that airframe noise makes an important contribution
to the overall aircraft noise and that jet mixing noise does
not play the dominant role that you describe. We two have had
several discussions on this issue recently, and I hope that
they will continue, but perhaps you would respond here to the
criticism that you have not actually shown that airframe
noise is not important but that you have simply obtained a
plausible fit to the measured aircraft noise by adjusting the
constants in your jet mixed noise equations?

AUTHOR'S RESPONSE:
With our measurements (flight tests at a constant altitude,
no glide data with low power setting) we were not able to
investigate the influence of airframe noise. Similarity to
some extent in the frequency spectra of jet mixing and
airframe noise increases the difficulty to distinguish
between both noise sources. However, from the general
experience on aircraft noise it is known that jet mixing
noise is very important for low bypass ratio engines with
high jet speeds and temperatures. Airframe noise, on the
other hand, plays only a major role during landing (low power
setting, low jet speed). If we proceed from this general

knowledge it can be concluded that in the present case (high power setting, high jet speed) jet mixing noise (and in addition shock noise) is responsible for the sound emission and that airframe noise is of no importance.

Now familiar with your results, we can not totally exclude that one portion of our "jet mixing noise" is airframe noise. However, section 9.2 of your paper No. 22 shows that you also have some doubts whether the noise measured from the aircraft glides is all generated by the airframe. In addition it should be mentioned that the aircraft configuration during your flight condition was different from our configuration. Therefore, results can probably not be compared directly. We hope that further discussions and data analysis will lead to a clear result concerning the noise source identification.

QUESTION BY: F.R. Grosche, DLR Göttingen, Germany
Referring to Fig. 3 and Fig. 5 of the written version: Why do the curves showing OASPL as function of emission angle, end before reaching their maximum (at $\theta < 30°$), although the scatter at the last given point is still quite small?

AUTHOR'S RESPONSE:
We also evaluated results for the emission angle $\theta = 15$ degrees. In that case the distance between the aircraft and the microphone position is 290 m and larger. The correction of the atmospheric absorption then leads to an over-amplification in the higher frequency range. Also background noise becomes very important. Therefore, it seemed not reasonable to include results for $\theta < 30°$ in the data analysis.

QUESTION BY: J.M. Seiner, NASA Langley, USA
Many F-15 aircraft missions involve engagement at $M_f = 0.4$ and disengagement with afterburner. On this case, jet noise would be dominant, not shock noise. You did not mention what power settings were used in your study. Could you comment on this, and how different power settings may change your conclusions regarding the importance of jet, shock, airframe, and internal noise source?

AUTHOR'S RESPONSE:
The power setting in each case was adjusted just to reach the wanted flight Mach number during the level flight. Specifying the power settings together with the flight Mach numbers in our opinion would mean to publish restricted data.

In the present study all tested aircraft flew in a typical training configuration with no additional weapons. That means that the measurements were carried out with a "standard" configuration with a "standard" power setting at a certain Mach number.

Different power settings due to different drag coefficients at the same flight Mach number may indeed change the importance of the different noise sources to some extent. However, with our present knowledge it is not reasonable to speculate on these changes.

AD-P007 519

92-17422

NOISE EMISSION OF LOW FLYING MILITARY AIRPLANES

H.-D. Marohn
Federal Environmental Agency
Bismarckplatz 1
D - 1000 Berlin 33
Federal Republic of Germany

Umweltbundesamt

SUMMARY

Until the end of 1990 a great amount of low altitude flying of military airplanes was done in the Federal Republic of Germany. Up to then approximately 80 000 low altitude flights were performed annually. Many of these flights took place at a height from 500 ft to 1500 ft. Nearly 2/3 of the whole area of the Federal Republic of Germany was used for low altitude flights between 500 ft and 1500 ft. In seven distinct low flying areas flights even down to a height of 250 ft above ground were allowed. In a relative densely populated country these low altitude flights caused a great amount of disturbance and annoyance.

In order to have some information on noise emission of military airplanes flying at subsonic speeds at low altitude a measurement campaign was done in the vicinity of the shooting range in Meppen. A special aim of the campaign was to obtain insight into the influence of operational parameters on the noise emission during low altitude flights. The results of these measurements, for instance noise emission as a function of speed and height above ground, will be presented.

In general, people affected by low altitude flights would not often receive extremely high noise levels because only a part of the population was exposed to direct overflights. It was therefore of interest to determine the number of occurrence and the statistical distribution of noise levels experienced by people living in low flying areas of Germany. For this purpose a research activity was performed in Germany in the years 1986 and 1990. During six weeks at 16 locations within four low flying areas continous noise measurements were made. The results, for instance relative frequency of noise levels and noise duration, are to be presented.

1   INTRODUCTION

In the Federal Republic of Germany approximately 80 000 low altitude[1] flights with military jet aircraft were performed annually. A great deal of these flights are taking place at a

height ranging from 500 ft to 1500 ft. Nearly 2/3 of the whole area of the Federal Republic of Germany can be used for low altitude flights between 500 ft and 1500 ft.

In seven distinct "low-level areas"[2] flights even down to a height of 250 ft above ground were allowed. These "low-level areas" are shown in figure 1. In our relatively densely populated country - the Federal Republic of Germany as other European countries is approximately 10 times as densely populated as for instance the United States of America - these low altitude flights were causing a great amount of disturbances and annoyance.

In order to find out methods for the possible reduction of noise emission during low altitude aircraft missions the Federal Minister of Environment, Nature Conservation and Nuclear Safety and the Federal Minister of Defence performed noise measurements. A special aim of the campaign was to obtain insight into the influence of operational parameters on the noise emission during low altitude flights. The measurements were conducted in autumn 1984 in Meppen by the Bundeswehr Test Station 91. During the measurements it was requested that all military aircraft types which will conduct low altitude flights over the territory of Germany should participate. To reach this goal the full cooperation of the Allied Air Forces was grateful acknowledged.

---

[1] In this paper the term "low altitude flight" is used instead of the common term "low-level flight" mostly used by airmen. This is done in order to avoid confusion between "low noise level" and "low flight level".

[2] Throughout this paper these areas are called "low-level areas" in accordance with aeronautical charts

2 MEASUREMENT OF NOISE EMISSIONS

Figure 2 shows the lay-out of the flight track and the five microphones and two theodolites for these measurements. The theodolites were used to measure the exact altitude above the microphones and the deviation of the flight track. The track itself was made visible for the pilots by huge markers plate. In some cases the help of a forward air controller was necessary to aligne the aircraft to the centerline. Flights were performed at altitudes of 250 ft and 500 ft, respectively.

During the measurements two aircraft of each type used a "race track" traffic pattern (approximately 6 NM in length and 4 NM wide). In order to keep the noise level contribution from the other aircraft on the microphones at a minimum the two aircraft were flown with a half cycle difference, i.e., on opposite parts of the "race track".

For each aircraft type noise measurents were performed at speeds typical for low altitude flights. The F-4 Phantom, for instance, was flown at 420 kts, 450 kts, 480 kts, 575 kts and 0.8 M. This includes all speeds from low altitude cruise to IP-to-target speed which is normally used only during a very short period of the flight.

As an example figure 3 shows the noise emissions of all fighter aircraft used by the German Air Force as a function of speed. (By the way the famous F-104 Starfighter is no longer in use in the German Air Force). Figure 4 shows the influence of height on noise level received on the ground for an F-4 aircraft. Doubling the height above ground decreases the noise level by approximately 5.2 dB at a speed of 420 kts, and by 6.6 dB at a speed of 0.8 M. The next figure 5 shows the influence of aircraft speed on noise emission for a F-4 Phantom flying at 250 ft. In Figure 6, a summary of all measured noise emission levels is shown for all aircraft types measured in the campaign. For comparison in the diagram, the aircraft speeds in each case are the lowest operating speeds for low altitude flights.

3 MEASUREMENT OF NOISE IMMISSION LEVELS

The above mentioned measurements indicate the maximum noise levels which occure during a direct low altitude overflight with military aircraft. But in general, people affected by low altitude flights would not receive such high noise levels very often because only a part of the population is exposed to direct overflights. It is, therefore, of interest to determine the number of occurrence and the statistical distribution of noise levels experienced by people living in low altitude flying areas. For this purpose, a research activity was started with the German company Messerschmitt-Bölkow-Blohm

(MBB) as a contractor. During this research program MBB developed and constructed a low-cost automatic noise measurement unit especially used for the detection of low-flying military aircraft. This unit uses a small pocket calculator with enough internal storage capacity to store the time-history of the noise events above a certain threshold during a whole day Each day the content of the memory was transfered and stored on a transportable floppy disk unit.

During the years 1986 and 1990 four measurement campaigns were conducted. One around a miltary airfield with low altitude training activities mostly with Alpha Jets, two campaigns within "low-level areas" and one outside the "low-level areas" but with military flights between 500 ft and 1500 ft.

Figure 7 to 10 show measured noise levels versus time duration (10 dB-down-time) for all four measurement campaigns and all microphons during the whole campaign.

Figure 11 to 14 give the relative distribution of noise levels for one measurement position for each measurement campaign.

Figure 15 gives an impression of the distribution of aircraft noise as a function of time of day measured within "Area 5".

Figure 16 and 17 show the noise events per month at the microphon positions in "Area 7" and outside the "low-level areas". In this picture it is distinguished between aircraft noise and noise from other sources.

Finally figure 18 and 19 give the time between two aircraft noise events as a function of noise level for "Area 7" and outside the "low-level areas" based on statistical considerations.
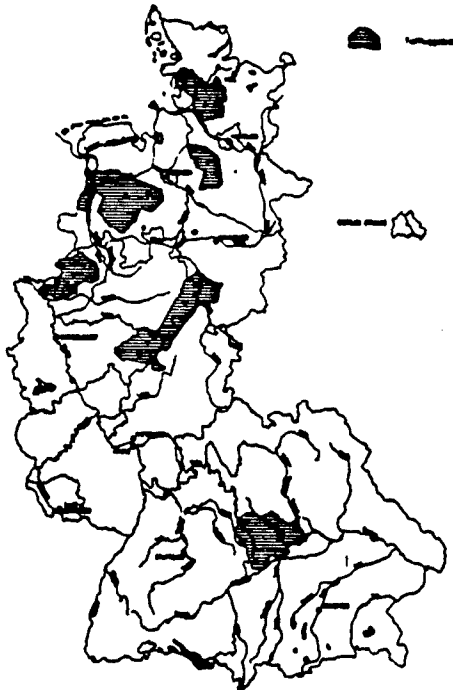
Figure 1: "Low-level areas" in the Federal
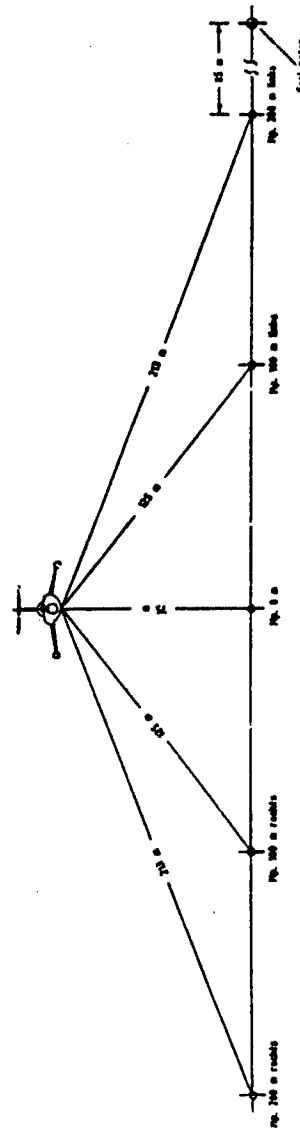
Republic of Germany

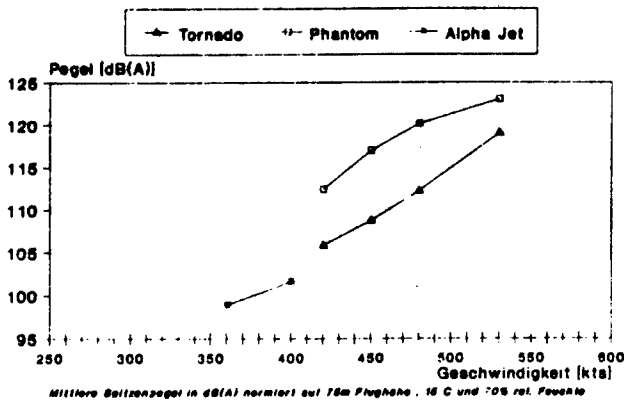

Figure 2: Low altitude noise measurement site

Figure 3: Noise levels of German Air Force fighter aircraft as a
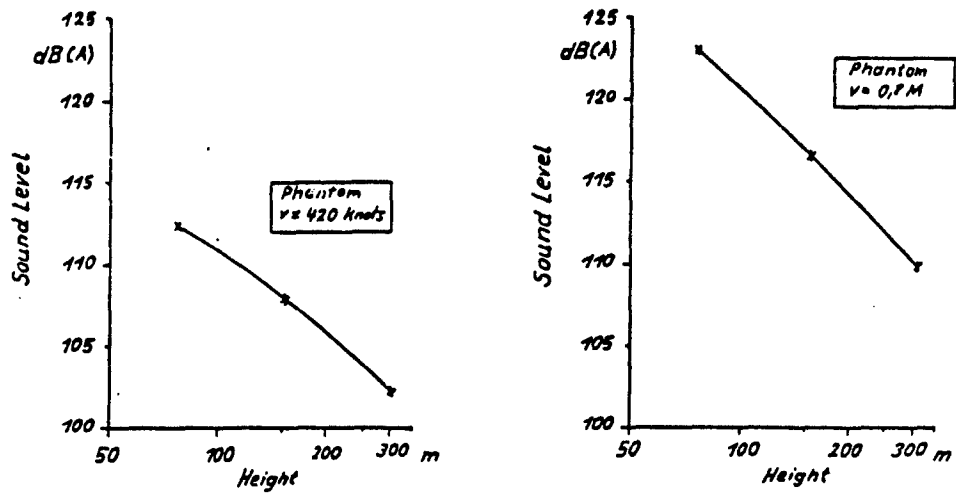function of speed

Figure 4: Noise level versus flight level height for a F-4
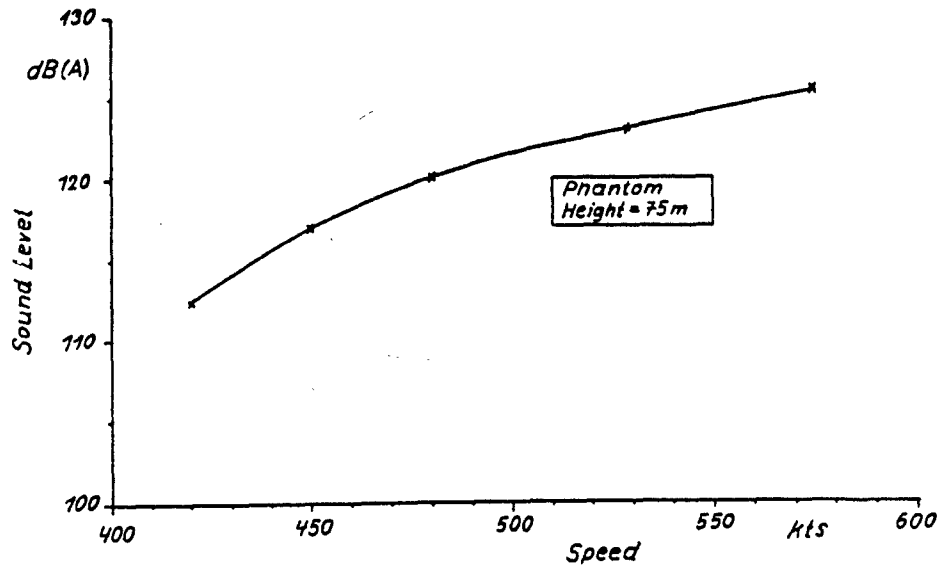Phantom overflight (speed 420 kts and 0.8 M, center
microphone)

Figure 5: Noise level versus speed for a F-4 Phantom overflight
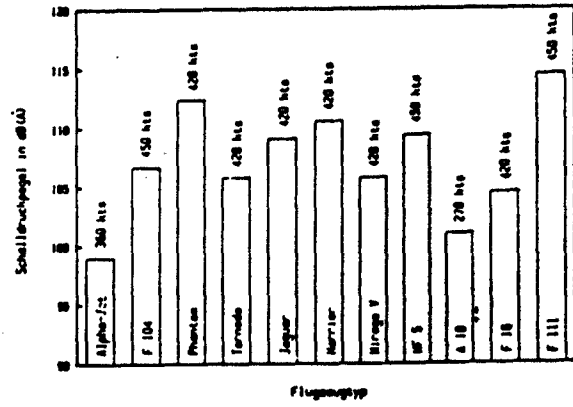(height 75 m, center microphone)

Figure 6: Noise levels for all measured aircraft types (height
75 m, speed as indicated, center microphone)
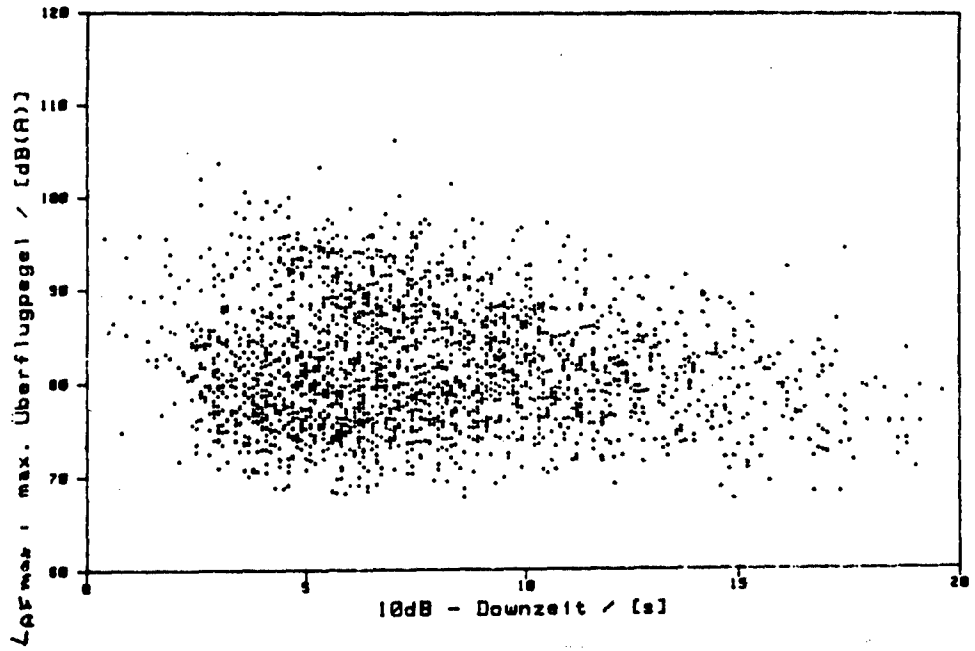
Figure 7: Noise level versus time duration (10 dB-down-time)
measured near Fürstenfeldbruck Airfield
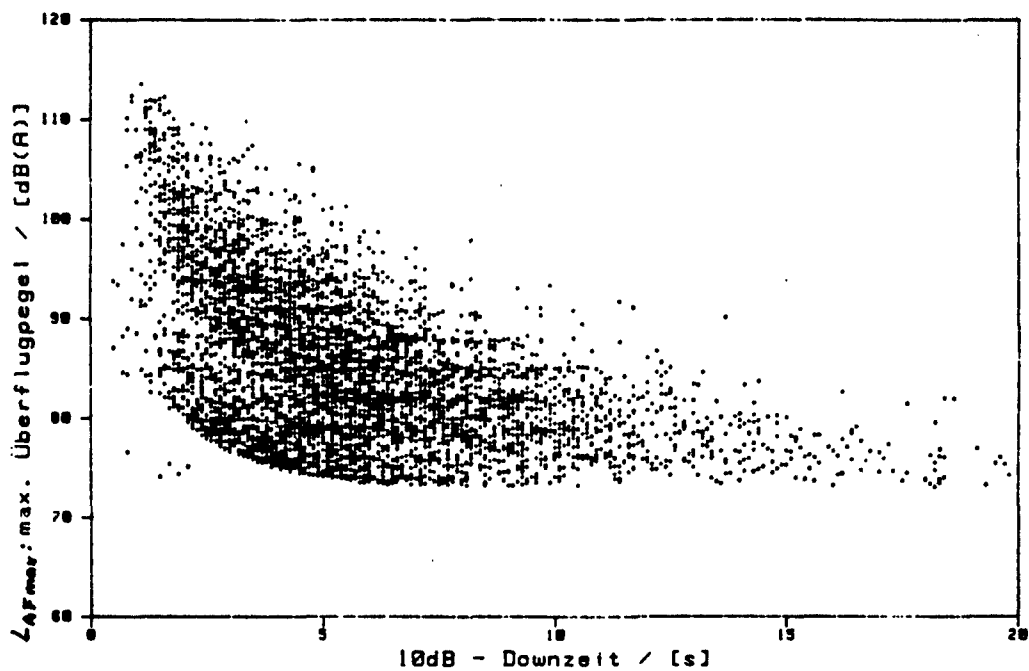
Figure 8: Noise level versus time duration (10 dB-down-time)
measured in "Area 5"
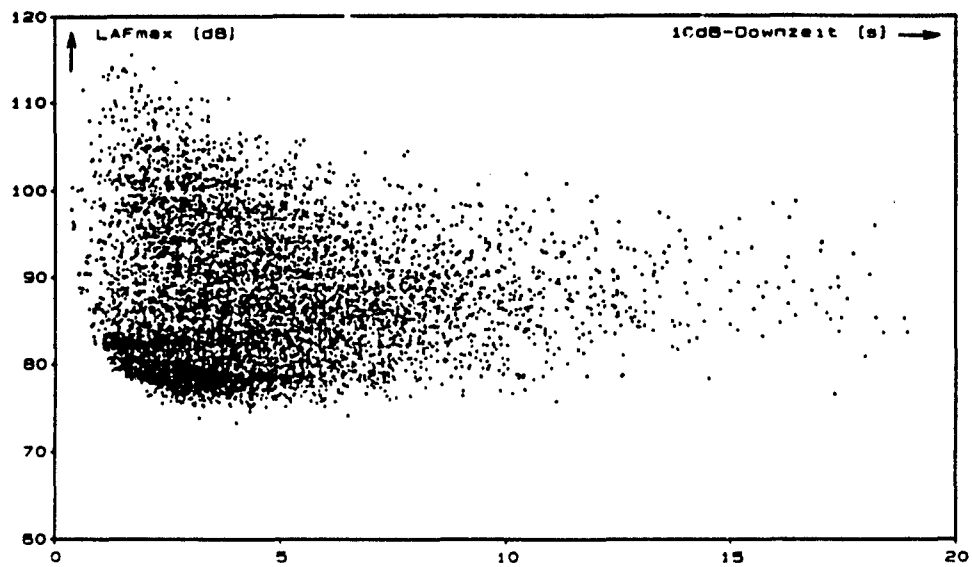
Figure 9: Noise level versus time duration (10 dB-down-time)
measured in "Area 7"
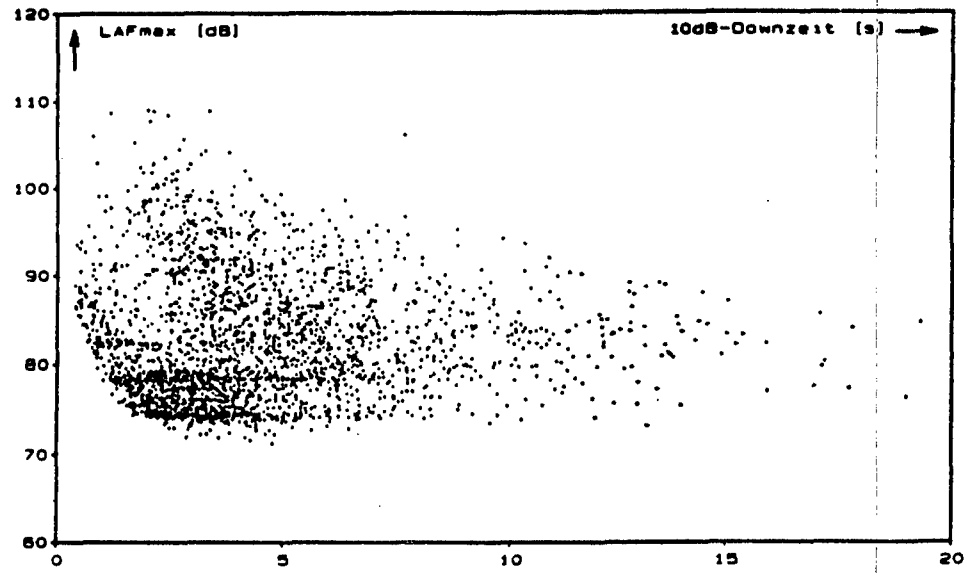
Figure 10: Noise level versus time duration (10 dB-down-time) measured near Gundelsheim
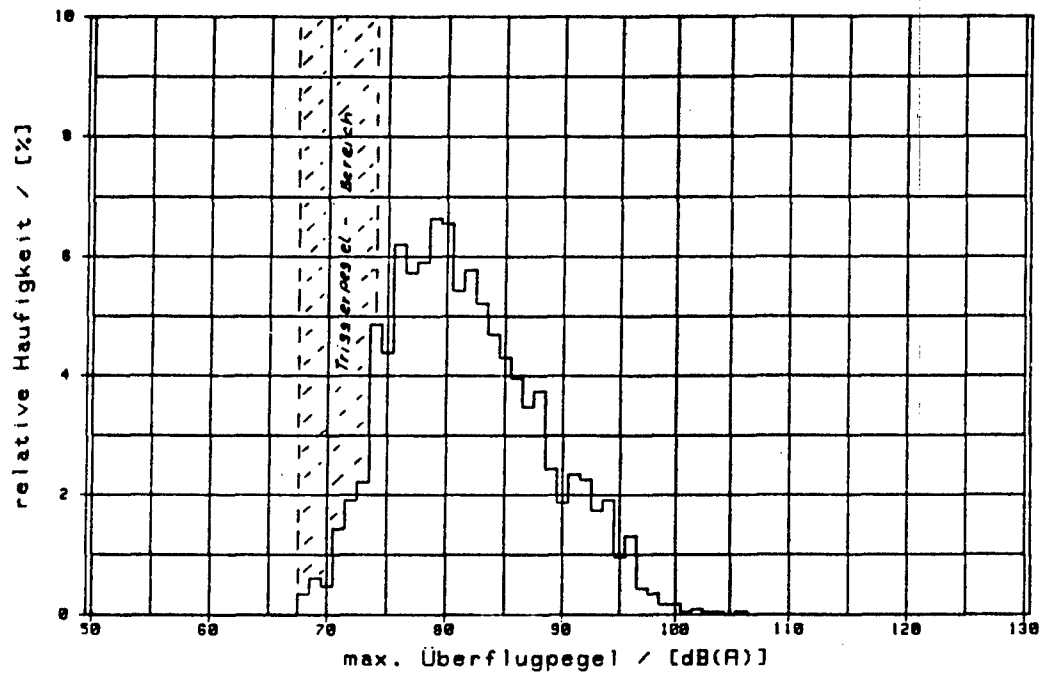
Figure 11: Relative distribution of noise levels measured near Fürstenfeldbruck Airfield

relative Häufigkeit / [%]

max. Überflugpegel / [dB(A)]
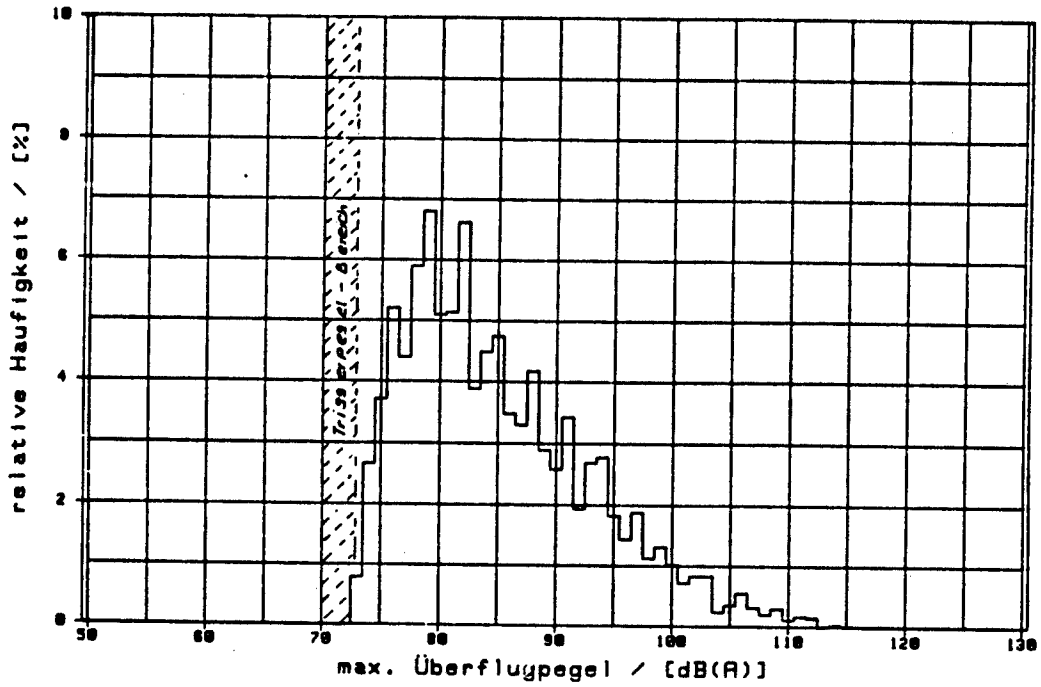
Figure 12: Relative distribution of noise levels measured in
"Area 5"

max. Überflugpegel / [dB(A)]
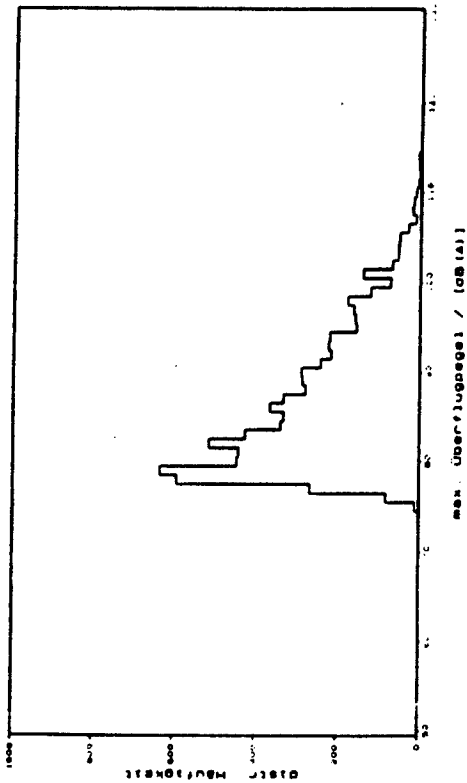
Figure 13: Relative distribution of noise levels measured in
"Area 7"

max. Überflugpegel / [dB(A)]
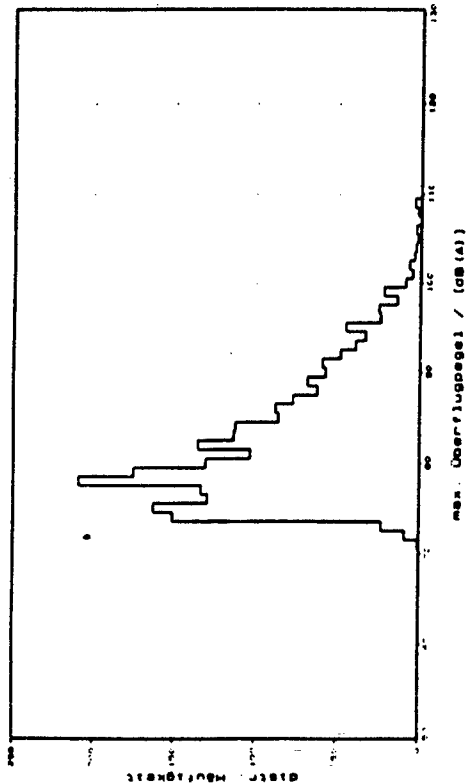
Figure 14: Relative distribution of noise levels measured near
Gundelsheim

Ueberflugereignisse / Woche

Zeit / h
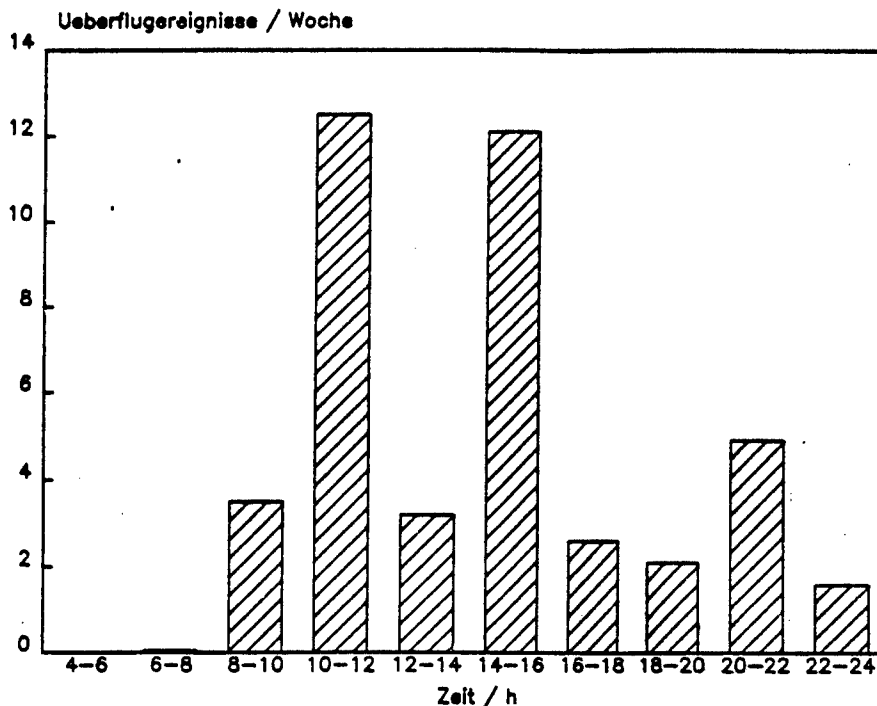
Figure 15: Distribution of aircraft noise as a function of time
of day measured in "Area 5"

monatl. Lärmereignisse pro 5 dB(A) Intervall

Maximalpegel / [dB(A)]

Fluglärmereignisse
Gesamtereignisse
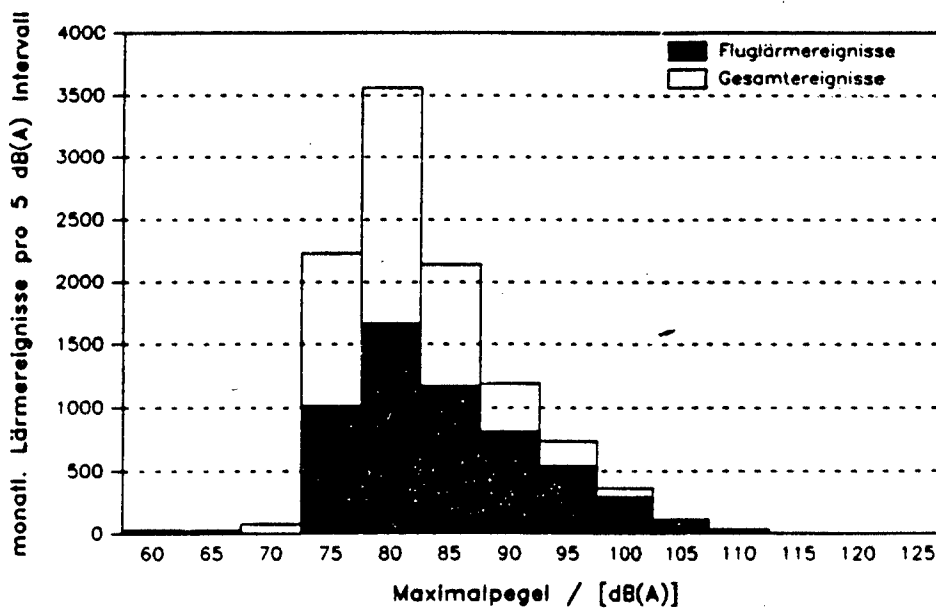
Figure 16: Noise events per month measured in "Area 7"
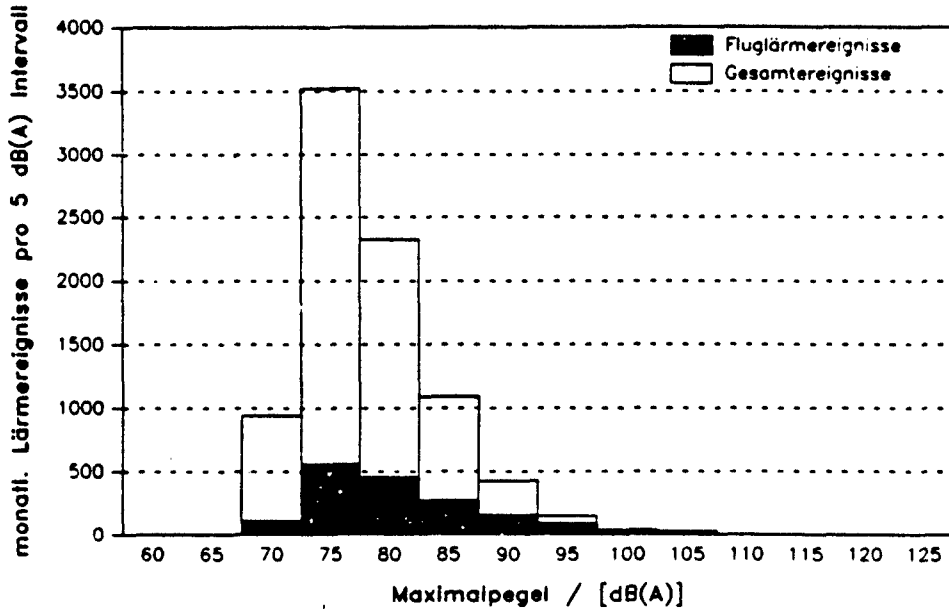
Figure 17: Noise events per month measured near Gundelsheim
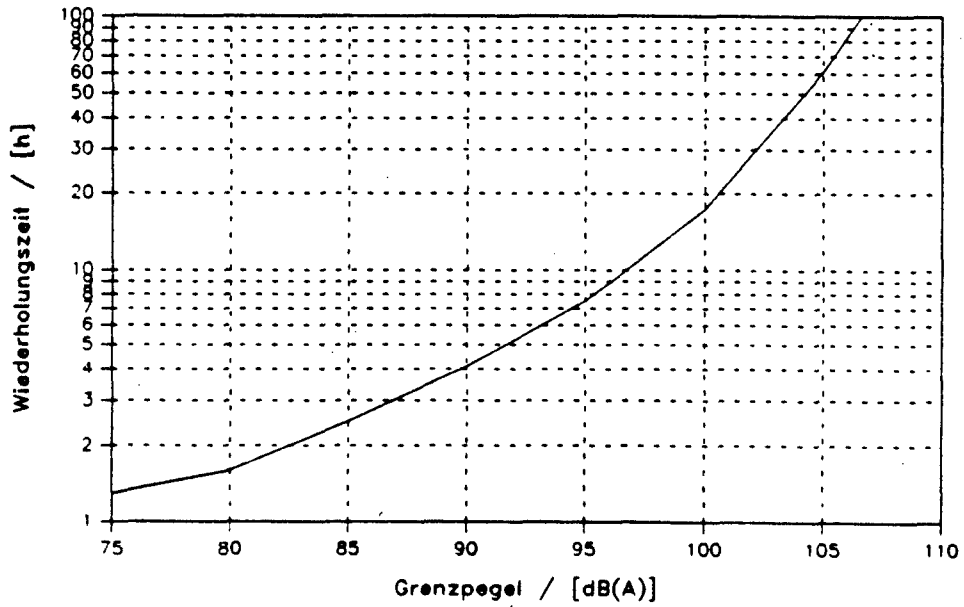
Figure 18: Time between two aircraft noise events as a function
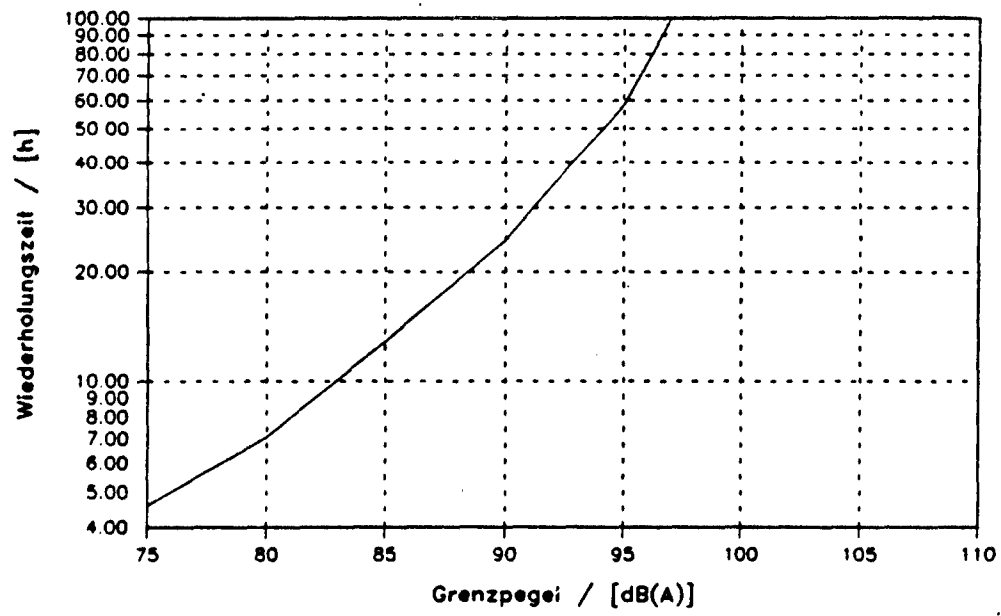of noise level calculated for "Area 7"

Figure 19: Time between two aircraft noise events as a function of noise level calculated for "Gundelsheim"

BRUIT DES AVIONS DE COMBAT

M. SGARBOZZA
DASSAULT AVIATION
DIRECTION GENERALE TECHNIQUE
DIVISION ACOUSTIQUE
78, QUAI MARCEL DASSAULT 92214 - ST CLOUD - FRANCE

et

A. DEPITRE
DIRECTION GENERALE DE L'AVIATION CIVILE
SERVICE TECHNIQUE DE LA NAVIGATION AERIENNE
CHEF DE LA DIVISION NUISANCE
245, RUE LECOURBE - 75732 PARIS - FRANCE

RESUME

Après un exposé des caractéristiques et des niveaux de bruit des principaux avions de combat et d'un avion d'entraînement français au décollage et à l'atterrissage, on présentera quelques moyens de réduction du bruit :
- différentes procédures opérationnelles anti-bruit,
- conception des futurs moteurs (post-combustion silencieuse ? cycle variable, etc...).

On examinera également quelques résultats de mesure concernant le bruit généré en vol à grande vitesse et à basse altitude.

Enfin, la protection contre le bruit de l'environnement des bases aériennes françaises sera décrite et les possibilités de réglementation examinées.

1 - INTRODUCTION

Le bruit des avions militaires n'est devenu une gène pour la population que depuis quelques années avec la prise de conscience écologique des années 70.

Pendant longtemps le bruit a été considéré comme un facteur psychologique important qui à même conduit dans le passé à installer des dispositifs spéciaux à bord des avions de combat pour l'augmenter pendant la phase d'attaque. D'autre part les missions dévolues aux avions modernes ayant conduit à augmenter régulièrement les poussées des réacteurs (les premiers ATAR avaient une poussée d'environ 3000 daN et le M53-P2 9500 daN), cette augmentation a conduit en contre partie à un acroissement progressif et sensible des niveaux de bruit.

Dans la conjoncture actuelle les avions de combat sont, en Europe, utilisés principalement pour des vols d'entraînement ou de surveillance et la gène ressentie au sol est d'autant plus mal supportée.

D'autre part le concept actuel de furtivité appliqué en électromagnétisme et en infra- rouge devrait pouvoir s'appliquer aussi au bruit émis.

On peut ainsi distinguer deux phases bruyantes perçues au sol lors de ces vols : les phases de décollage et d'atterrissage d'une part et de survol à basse altitude d'autre part.

II - LE BRUIT AU DECOLLAGE ET A L'ATTERRISSAGE

Les avions considérés peuvent se répartir en 2 catégories : les avions légers d'entraînement ou d'appui rapproché, et les avions de combat. Leurs caractéristiques sont assez différentes ainsi que les niveaux de bruit qu'ils engendrent.

Prenons l'Alphajet pour exemple d'avion d'entraînement/appui sol. Sur la base de mesures en vol, des courbes du niveau de bruit en EPNdB, (Effective Perceived Noise Level in Decibel, unité utilisée pour la certification acoustique des avions civils) en fonction de la poussée du moteur et paramétrées en fonction de la distance microphone-avion ont pu être établies. (cf figure 1)

Le tableau de la figure 1 donne les niveaux de bruit calculés dans les conditions du Règlement de Certification Acoustique International (Annexe 16 de l'OACI). Le Chapitre 3 de ce Règlement qui est aujourd'hui le plus sévère, est respecté par l'Alphajet , il est vrai en utilisant la compensation légale pour le bruit en latéral. Mais ce bruit se produisant à l'altitude de 300 m, est perçu principalement à l'intérieur de la base militaire, et ne devrait pas constituer une gène importante pour les riverains.

Les niveaux de bruit des avions d'entrainement ou des avions légers d'appui sol peuvent donc satisfaire les exigences du Chapitre 3 de l'OACI ; en outre ils peuvent encore être sensiblement réduits en adaptant leurs procédures opérationnelles au tissu urbain environnant.

Quant aux avions de combat, ils sont équipés de réacteurs simple flux ou de réacteurs double flux à faible taux de dilution correspondant aux exigences de leur mission. En particulier pour conserver suffisamment de poussée à grande vitesse. le jet doit être fortement accéléré, ce qui explique le choix du moteur (simple flux ou double flux à faible taux de dilution) à vitesse de jet élevée et donc produisant un bruit important.

L'exemple relatif à la deuxième catégorie d'appareils le Mirage 2000, avion de combat moderne monoréacteur, est équipé du réacteur SNECMA M53. Les niveaux de bruit générés ont été mesurés en vol (cf figure 2).

Malgré les niveaux élevés, des procédures opérationnelles spécialement adaptées peuvent limiter sensiblement la gène des riverains des bases aériennes. Le décollage s'effectuant avec la réchauffe, la montée doit être effectuée sous la pente la plus grande possible pour monter le plus haut possible avant de sortir des limites de la base. Et avant et pendant le survol des zones sensibles, la poussée doit être réduite et la poussée max ensuite réaffichée dès que l'éloignement des agglomérations est suffisant.

La figure 3 montre l'évolution du niveau de bruit au décollage pour 2 configurations du Mirage 2000, en un point situé à 6 500 m du lacher des freins. (point de référence pour la mesure en survol de l'Annexe 16 de l'OACI). Les niveaux obtenus sont nettement supérieurs aux limites de l'Annexe 16.

Cependant l'application de procédures opérationnelles simples permettent une réduction des nuisances perçues au sol dans les zones sensibles. Par rapport à un décollage avec réchauffe, il est possible d'obtenir sans l'utilisation de la réchauffe une diminution du niveau de bruit de 4 à 5 dB.

Le STNA a conduit une campagne de mesures en 1974 pour vérifier, sur un trafic opérationnel de décollage, la faisabilité et l'influence de procédures à moindre bruit. Les avions impliqués étaient les Mirage III B, Mirage III C et Mirage F1.

La zone sensible aux nuisances sonores, où étaient disposés les microphones, était située entre 3050 m et 3500 m du lâcher de freins.

Les procédures étudiées pour divers chargements (lisse ou bidons) pour les

Mirages III B et III C et en lisse pour le
Mirage F1 furent :

- des décollages avec PC maximale, montée à pente
  maximale
- des décollages avec PC maximale, montée à pente
  normale
- des décollages avec PC minimale, montée à pente
  maximale
- des décollages avec PC minimale, montée à pente
  normale
- des décollages plein gaz sec, montée à pente
  maximale
- des décollages plein gaz sec, montée à pente
  normale
- des décollages avec PC maximale, montée à
  l'assiette de 22°.

Chaque exercice fut répété au moins 2 fois.

A titre d'exemple, la figure 4 montre le
niveau de bruit obtenu en PNdB et la hauteur de
passage de l'avion en un point situé à 3050 m du
lâcher des freins pour un avion de type
Mirage F1.

On voit donc que les procédures de décollage
avec une montée à pente maximale sont bénéfiques
pour l'environnement sonore. Il est préférable
d'utiliser la post-combustion plutôt que le plein
gaz sec au décollage, la différence de hauteur de
survol et donc l'atténuation géométrique et
atmosphérique sur le bruit étant prépondérante
par rapport à l'augmentation de bruit à la
source.

Les résultats obtenus avec les Mirages III B
et III C conduisent aux mêmes conclusions.

On peut donc optimiser les procédures anti-
bruit en fonction de l'urbanisation autour de
chaque base militaire.

III - DETERMINATION DU BRUIT PRODUIT PAR LES
AVIONS MILITAIRES POUR LE CALCUL DU PLAN
D'EXPOSITION AU BRUIT DES AERODROMES

Le Service Technique de la Navigation
Aérienne (STNA) qui est un service de la
Direction Générale de l'Aviation Civile est
amené à mesurer le bruit produit par les avions
militaires dans le cadre de la caractérisation
de ces avions afin d'en intégrer les paramètres
acoustiques dans le calcul du plan d'exposition
au bruit (zonage) autour des aéroports ou bases
militaires.

Le code de calcul qui permet de déterminer
les différentes zones de bruit autour des
aérodromes français nécessite la connaissance
des niveaux de bruit produits par les avions à
300 m sous trace pour les phases de décollage,
de survol et d'approche. L'unité de mesure est
le PNdB.

Des campagnes d'essais ont été réalisées sur
les avions Mirage III B, Mirage III C,
Mirage III E, Mirage F1, Jaguar, Mirage 2000,
Alpha jet, Etendard, Atlantic, Alizé, Crusader.

Toutes ces campagnes ont été conduites avec
la technique utilisée lors des essais de
certification acoustique des avions civils.
(Annexe 16 de l'OACI)
- technique de vol :
  Quatre procédures de vol ont été testées :
  . le décollage avec Post Combustion
  . le décollage plein gaz sec
  . l'approche
  . le survol palier (conditions break).

Les procédures de décollage et d'approche,
ont été réalisées sous forme de décollages
simulés et d'approches interrompues et répétées
identiquement quatre fois.

Pour toutes ces procédures, l'avion passe à
300 m de hauteur au-dessus du microphone placé
sous trace.

- presentation des résultats :

Les niveaux de bruit exprimés en PNdB pour une hauteur de 300 m et transposés dans les conditions météorologiques : Température 25°C, Humidité Relative 70 % sont consignés dans le tableau 1.

NIVEAUX DE BRUITS EN PNdB A 300 M

AVION	PROCEDURE			
	Décollage avec réchauffe	Décollage Plein Gaz Sec	Approche (-3°)	Palier (break)
MIRAGE III B	120.0	114.5		
MIRAGE III C	120.0	112.0	97.0	99.0
MIRAGE III E	115.5	106.5		
MIRAGE IV	123.0	114.5	103.0	102.5
MIRAGE F1	122.5	117.0	93.0	98.0
JAGUAR	122.0	117.0	97.0	97.0
MIRAGE 2000	126.0	116.5	104.0	101.0
ALPHA JET		105.5	86.0	89.0
ETENDARD		114.5	98.0	96.5
ATLANTIC		98.5	85.5	90.5
ALIZE		97.5	90.0	90.5
CRUSADER	122.5	111.5	96.5	97.0

TABLEAU 1

IV - LE BRUIT A GRANDE VITESSE ET BASSE ALTITUDE

Le STNA a également travaillé dans le passé sur une étude de bruit et vibrations produits sur une maison pour des vols à très basse altitude (de 17 m à 217 m), en collaboration avec le Centre Scientifique et Technique du Batiment et le Centre d'Essais en Vol.

Des mesures de bruit et de vibrations produits sur une maison par des avions militaires la survolant à très basse altitude ont été réalisées sur la base d'Istres en 1976. A cette occasion, le STNA a disposé entre autres un microphone sous trace à 50 mètres de la maison (au dehors de l'influence acoustique de celle-ci) afin de quantifier les niveaux de bruit produits.

Les photographies 1 et 2 montrent cette maison avec les survols d'un Jaguar et d'un Transall.

Tous les vols ont été réalisés en palier pour des régimes différents : régimes de décollages avec post combustion, régimes à puissance adaptée. Ces régimes ont été appliqués juste avant le passage sur la maison de façon à avoir une vitesse significative de la configuration simulée au passage de cette maison.

Les bandes magnétiques bruit ont été réanalysées en 1991 en exprimant un spectre chaque 0,1 seconde car compte tenu de la vitesse angulaire très rapide de déplacement de l'avion le niveau de bruit évolue très rapidement et une analyse chaque 0,5 seconde (comme préconisée dans l'Annexe 16) ne permet pas de déterminer le niveau de bruit maximal.

Dans un but de comparaison des avions entre eux, les niveaux de bruit ont été transposés pour des hauteurs de 100 m et 300 m pour les conditions de référence de température : 25°C et d'humidité : 70 %. Le tableau 2 récapitule ces niveaux de bruit.

RECAPITULATIF DES NIVEAUX DE BRUIT
EXPRIMES EN PNdB (AVIONS EN PALIER)

PNdB MAX.	A 100 M			A 300 M		
AVIONS	AVEC RECHAUFFE	PLEIN GAZ SEC	PUISSANCE ADAPTEE	AVEC RECHAUFFE	PLEIN GAZ SEC	PUISSANCE ADAPTEE
MIRAGE III A	125.0	120.0	111.5	113.0	108.0	99.0
MIRAGE III E	126.5	120.0	115.5	115.0	108.0	102.5
MIRAGE IV A	132.0	127.5	113.0	120.0	115.0	100.5
JAGUAR A1	125.5		113.5	113.5		101.5
ETENDARD IV		119.0	108.5		106.5	95.5
CRUSADER	126.5	120.0	108.5	115.0	108.0	96.0

TABLEAU 2

V - EXAMEN DES RESULTATS :

L'examen de l'ensemble des résultats obtenus dans ces diverses campagnes d'essais permet de voir qu'une dispersion parfois assez forte apparaît pour un même type d'avion, pour des mêmes régimes.

Deux paramètres doivent être considérés :

- dans l'essai à très basse altitude sur la maison la transposition spectrale s'effectue sur des rapports de distances assez grands, d'où une imprécision certaine (transposition souvent d'une vingtaine de décibels).

- dans l'essai à très basse altitude les régimes de décollage ont été appliqués en vol en palier, la directivité de la source diffère donc par rapport au micro et les distances (hauteur de l'avion ou distance de propagation) sont parfois fort différentes.

Pour ces deux raisons il est préférable d'associer les niveaux de bruit aux conditions d'essais. Cependant une première recommandation peut être de déterminer le niveau de bruit des avions militaires par rapport à la distance à l'avion au moment de l'émission du bruit maximal et non par rapport à la hauteur de passage de l'avion au-dessus du point de mesure.

VI - PROTECTION CONTRE LE BRUIT DE L'ENVIRONNEMENT DES BASES AERIENNES FRANCAISES

Outre les procédures à moindre bruit utilisées au décollage et des aménagements des vols à des horaires acceptables notamment pour les vols de nuit, la protection en France contre le bruit dans l'environnement des bases aériennes françaises est réalisée de la même façon que pour les aéroports civils, il s'agit d'agir sur l'urbanisme autour des aérodromes.

L'action sur l'urbanisme se situe à deux niveaux :

- action sur l'urbanisation projetée (permis de construire et plans d'occupation des sols),

- action sur les constructions existantes et soumises au bruit des avions (lorsqu'elle est possible).

Le plan d'exposition au bruit des avions d'un aérodrome donné définit trois zones d'exposition au bruit. Dans ces trois zones, l'urbanisation est interdite ou admise dans certaines conditions.

Elaboration d'un plan d'exposition au bruit:

L'indice psophique Ip est l'indice utilisé en France pour quantifier l'exposition au bruit autour des aéroports. Il est fondé sur l'utilisation du L_{PN} max comme descripteur (niveau de bruit maximal exprimé en PNdB). La base de temps étant la journée, le descripteur L_{PN} max représente l'exposition au bruit résultant d'un trafic journalier.

Le trafic de nuit est considéré comme 10 fois plus gênant que le trafic de jour. Le nombre de mouvements de nuit est donc pondéré par un facteur 10.

La formulation de l'indice psophique Ip est obtenu à partir de la règle de composition des niveaux de bruit instantanés. L'énergie totale est ramenée à sa moyenne par minute en la divisant par 1440 (24 h = 1440 minutes).

$$\text{donc } Ip = 10\log\left[\frac{\sum_{i=1}^{n} 10^{\frac{Li}{10}} + 10\sum_{j=1}^{P} 10^{\frac{Lj}{10}}}{1440}\right]$$

où Li est le niveau maximal de bruit en PNdB du ième avion

n est le nombre de mouvements de jour (6h-22h)

et p est le nombre de mouvements de nuit (22h-6h).

La détermination par le calcul de l'indice psophique en un point au sol nécessite donc la connaissance des données suivantes :
- le trafic en nombre de mouvements et par type d'appareil
- les niveaux de bruit des avions à la source
- les trajectoires
- les lois de propagation du son dans l'air.

. Les plans d'exposition au bruit sont établis à partir d'un trafic prévu à un horizon donné, afin qu'ils soient valables pendant une assez grande période, l'horizon généralement choisi est de 15 ans. Il faut donc prévoir assez longtemps à l'avance les caractéristiques principales des bases aériennes en matière de trafic et de type d'avions utilisés.

. Les niveaux de bruit à la source introduits dans le programme de calcul sont déterminés sous le trajectoire de l'avion à une distance orthogonale de 300 mètres. Si ceci est valable pour les avions civils sans problème, il y a lieu pour les avions militaires de prendre en compte leur spécificité acoustique.

En effet, pour un trafic civil, le niveau de bruit maximal est obtenu sous trace après le bout de piste au décollage.

Pour un trafic militaire on peut obtenir le résultat inverse. A titre d'exemple un résultat d'une campagne de mesures de bruit réalisée autour d'une base militaire française est présenté :

Village A

600 m

QFU1 ⇒ piste ⇐ QFU2

2000 m   2400 m
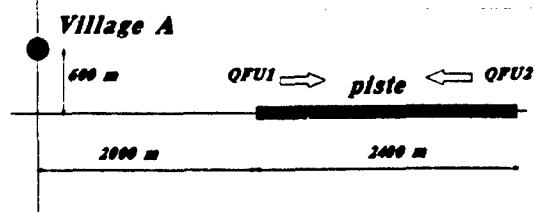
Le bruit produit dans le village A par des Mirage 2000 au décollage est plus important lorsque l'avion décolle au QFU1 par rapport à un décollage au QFU2.

Les niveaux mesurés dans le village A, généré au cours du décollage d'un Mirage 2000 sont :
QFU1 : 87 dB(A) ou 98 PNdB
QFU2 : 86 dB(A) ou 97 PNdB.
(Ces niveaux sont moyennés pour 9 décollages au QFU1 et 3 décollages en QFU2).

Il est donc important dans toute détermination du bruit autour des bases militaires de tenir compte des caractéristiques particulières des avions militaires à réaction en directivité de la source sonore et en trajectoires.

Etablissement   et   contenu   du   plan d'exposition au bruit

L'expression graphique du P.E.B. fait apparaître trois zones limitées par des courbes isopsophiques.

▶ Décollage
▶ Atterrissage
▢ ZONE A : indice > 96
▢ ZONE B : 96 > indice > 89
▢ ZONE C : 89 > indice > 84
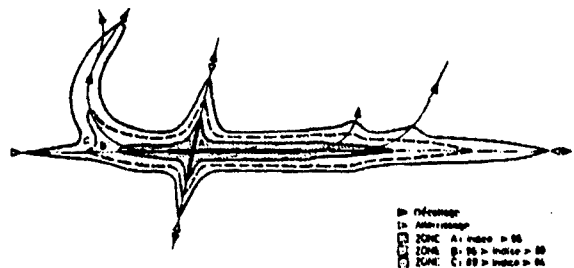
- La zone A, où l'indice psophique est
supérieur à 96 et dans laquelle on considère que
la gène est très forte.

- La zone B, où l'indice est compris entre 96
et 89, dans laquelle la gène peut être considérée
comme forte.

- La zone C, où l'indice est compris entre 89
et une valeur choisie entre 84 et 78, dans
laquelle la gène peut être considérée comme assez
forte.

Le prefet, dans certaines conditions, peut
fixer la limite de la zone C entre 86 et 75.

Dans chacune des zones, les possibilités de
constructions nouvelles sont restreintes, en
particulier la construction d'habitation en zone
A ou B est interdite et les normes minimales
d'isolation acoustiques à respecter sont les
suivantes :

NORMES MINIMALES D'ISOLATION ACOUSTIQUE SUIVANT LES ZONES DE BRUIT			
A	B	C	Extérieur immédiat de la zone C
45 dB (A)	40 dB (A)	35 dB (A)	30 dB (A)

TABLEAU 3

VII - CONCLUSION

L'emploi des procédures opérationnelles, bien
que diminuant de façon sensible les niveaux de
bruit, est cependant limité. La diminution du
bruit à la source est donc hautement souhaitable.

Le masque du fan par une entrée d'air en S
permet de piéger le bruit du fan dans le conduit.
Les diminutions espérées sont cependant faibles
car le bruit dominant provient du jet, les
sources de bruit étant situées en aval de la
sortie.

Les moteurs à cycle variable pourraient
constituer une solution pour diminuer le bruit du
jet l'adaptation de leurs caractéristiques en
fonction de la phase de vol autorise une
optimisation de leurs performances (comme pour

les avions de transport supersoniques futurs).
L'augmentation du taux de dilution aux basses
vitesses résultant du cycle variable a pour
effet de diminuer le bruit tout en permettant de
fournir la poussée requise aux autres régimes de
vol. Des prototypes de ce type de moteur ont été
développés et essayés en vol sur les avions
concurrents du programme ATF (Advanced Tactical
Fighter) mais finalement cette solution n'a pas
été retenue.

La règlementation Française actuelle établit
des règles d'urbanisme autour des aérodromes
militaires en attendant de pouvoir prendre en
compte une avancée technologique importante
permettant une diminution sensible du bruit à la
source, ce qui engendrera nécessairement, une
diminution des nuisances provoquée par les vols
à basse altitude.

ALPHA JET

NIVEAUX DE BRUIT   (VC= 160 Kt)

EPNL transcrit (EPNdB)

Niveaux de bruit EPNdB	limites de l'annexe 16 de l'OACI et de la FAR, Part 36	
	Chapitre 2 EPNdB	Chapitre 3 EPNdB
Décollage avec réduction	84	93	89
Latéral	95.5	102	94
Approche	90	102	98

poussée nette (daN)

figure 1

MIRAGE 2000
NIVEAUX DE BRUIT AU DECOLLAGE
EN FONCTION DE LA DISTANCE PERPENDICULAIRE AU MICRO

EPNL (EPNdB)

Réchauffe max

Plein Gaz Sec

DISTANCE PERPENDICULAIRE (m)

figure 2

MIRAGE 2000
NIVEAUX DE BRUIT AU DECOLLAGE

Configuration	Procedure	altitude à 6500m du lâcher des freins (m)	EPNL (EPNdB)
2 Magic + 2 Super 530	avec réchauffe	2500	98.5
	Décollage avec réchauffe et réduction à la poussée militaire à l'altitude de 300 m	1200	99.0
	Décollage avec réchauffe et réduction à la poussée militaire à l'altitude de 1600 m	2100	94.5
2 Magic + 2 Beluga + 1 bidon 1300 l	avec réchauffe	1850	102.0
	Décollage avec réchauffe et réduction à la poussée militaire à l'altitude de 1000 m	1400	98.0

figure 3

MIRAGE F1
NIVEAUX DE BRUIT A 3050 M DU LACHER DES FREINS
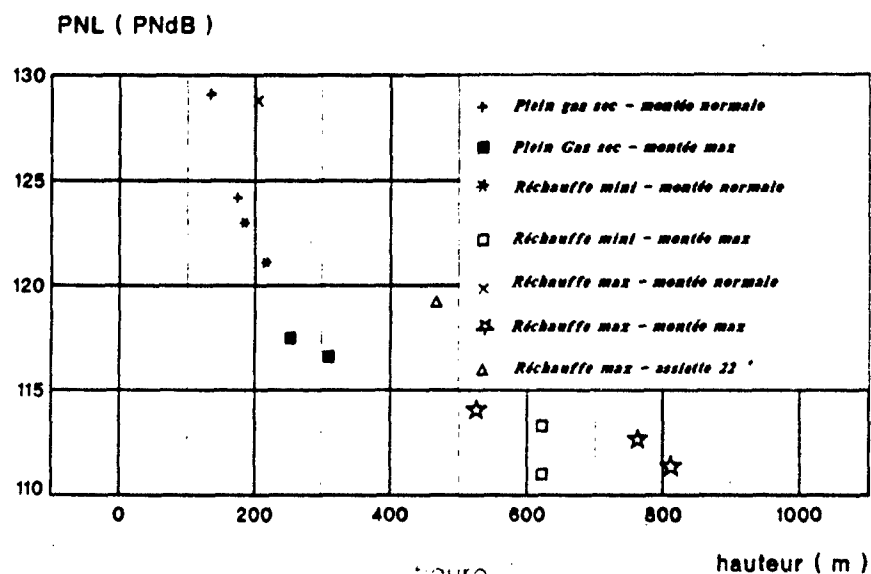
figure -

photo 1

photo 2

Discussion

QUESTION BY: R. Sc..neider, Luftfahrt Bundesamt, Germany
The equation on page 10-6 is different from your viewgraph. What is the right one?

AUTHOR'S RESPONSE:
L'equation publiée dans la conférence, publication d'octobre 1991 "AGARD CONFERENCE PREPRINT 512" est correcte.

QUESTION BY: H. Körner, DLR Braunschweig, Germany
In Germany the complaints on combat aircraft noise have risen considerably in the last years. What is the situation in France?

AUTHOR'S RESPONSE:
Les plaintes contre le bruit des avions autour de aéroports sont liées à deux principaux phénomènes:
- la "densité" de plaintes est en fonction du nombre de personnes habitant autour de l'aérodrome travaillent ou ont un lien avec l'aéroport, il y a donc un phénomène sociologique de rapport avec l'aéroport.
- le taux de plaintes augmente sensiblement à l'approche d'élections politiques importantes, phénomène bien connu dans de nombreux pays, le taux décroissant après les élections.

LE BANG ET LES PROBLEMES LIES AUX VOLS SUPERSONIQUES DES AVIONS MILITAIRES

par
Christian THERY - Claude LECOMTE
ONERA
BP 72
92322 Châtillon-Cedex
France

Résumé :

On rappelle les principaux aspects de la propagation du bang, le principe de son calcul et les enseignements tirés de l'expérience. Les diverses formes que peut revêtir le bang sont décrites (bangs normaux et bangs focalisés). Les effets du bang sur les structures et sur les êtres vivants sont résumés.

On indique enfin les facteurs à prendre en considération lors de la préparation d'un survol supersonique des terres.

Summary :

The main features of the boom propagation, the principle of its calculation and the main experimental results are recalled. The various shapes that booms may present are described (normal boom and focused booms). The effets of booms on structures and living beings are summarized. Guidances are given concerning the preparation of supersonic flights overland.

1. Introduction

Le vol d'un projectile supersonique s'accompagne d'un claquement nommé détonation balistique. De même un avion en vol supersonique crée un bang qui se propage jusqu'au sol. Le bang présente un caractère impulsionnel qui provoque une réaction de sursaut chez les êtres vivants et fait vibrer les structures. En raison de l'altitude de vol élevée des avions, le bang est ressenti le long d'une bande de terrain, située de part et d'autre de la trajectoire de l'avion, large de plusieurs dizaines de kilomètres. L'intensité du bang dépend essentiellement de la taille (volume, poids) de l'avion qui l'engendre, de son altitude de vol et de la manoeuvre qu'il effectue : le bang créé par un chasseur volant à haute altitude à vitesse rectiligne uniforme est d'intensité modérée, il provoque cependant une gêne mais ne peut pas être cause de dommages significatifs ; plus l'avion sera lourd plus le bang sera important et plus l'avion devra par suite voler à altitude élevée ; malheureusement les manoeuvres qu'exécutent les avions militaires provoquent localement des renforcements très importants des bangs, ce sont les focalisations et superfocalisations. Ces phénomènes apparaissent notamment lors de l'accélération transsonique et lors des virages. La gêne résultant de ces bangs focalisés est alors certaine et des dommages intéressant des structures vieillies ou mal conçues peuvent intervenir ; le seul moyen de limiter les nuisances qui en résultent serait de situer ces zones de bangs focalisés sur des régions inhabitées, mais une bonne prévision des zones affectées demande une connaissance précise a priori de la trajectoire réelle de l'avion et des conditions météorologiques ; en pratique donc, les zones susceptibles d'être affectées par ces phénomènes sont assez vastes.

Il ne faut pas toutefois surestimer les effets du bang :

- le bang ne peut pas avoir d'effets lésionnels, les premières atteintes temporaires au système auditif sont observées pour des niveaux d'intensité d'onde très supérieurs aux niveaux des bangs (3000 à 5000 Pa au lieu de 50 ou 70 Pa pour un bang),

- les effets structuraux des bangs normaux sont d'un ordre de grandeur comparable à ceux résultant de sollicitations naturelles (vent) ou liées à la vie moderne (trafic routier), les bangs focalisés ne peuvent avoir d'action sur des structures saines et bien conçues que par effet cumulatif (fatigue).

2. Détonation balistique

Le passage d'un projectile supersonique (balle de fusil par exemple) s'accompagne d'un claquement dû aux ondes de choc qui se forment au nez et au culot du projectile, la distance L séparant les deux ondes étant un peu supérieure à la longueur du projectile (Fig. 1). Les ondes de choc étant de faible intensité peuvent être assimilées à des ondes de Mach et le 1/2 angle au sommet du cône qu'elles forment est donné par

$$\sin \alpha = \lambda/L = {}^{\circ}/_{v} = {}^{1}/_{M} \quad \text{(a vitesse du son)}$$

L'interprétation acoustique du phénomène est simple (Fig. 2) : un projectile émet aux différents instants de son vol des ondes sonores qui sont toutes internes les unes aux autres et un observateur en ce cas n'entend qu'un bruit confus alors qu'un projectile supersonique émet des ondes sonores successives qui admettent une enveloppe conique C le long de laquelle les perturbations arrivent en phase, un observateur placé en P perçoit une détonation qui a été émise antérieurement alors que le projectile était en M_0.
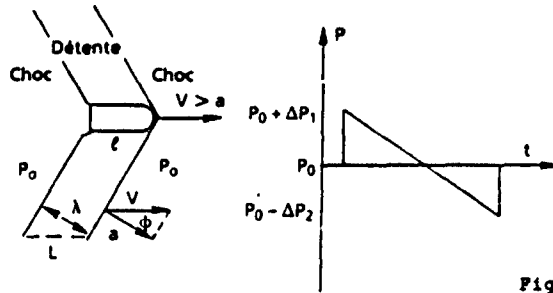
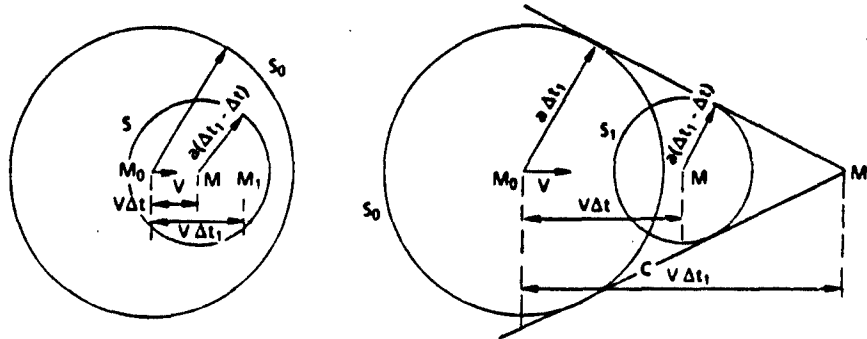Fig. 1 a)b) - Onde balistique d'un projectile.

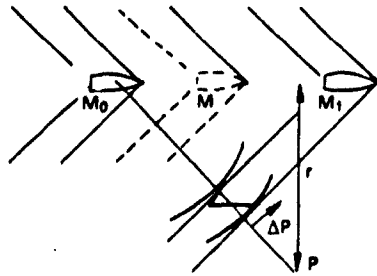Fig. 2 a)b) - Ondes émises par des projectiles subsonique et
supersonique.

Fig. 2 c) - Propagation de l'onde balistique.

L'intensité sonore du phénomène dépend de l'éloignement r du point d'observation à la trajectoire ; l'expansion étant conique, la puissance sonore dans l'onde décroît comme r^{-1} et donc la surpression comme $r^{-1/2}$ si toutefois on néglige les effets non linéaires résultant de l'intensité finie de l'onde. En réalité, ces derniers entraînent une atténuation supplémentaire qui résulte du fait que les perturbations de détente situées entre les fronts de choc avant et arrière rattrapent le front de choc avant ou sont rattrapées par le front de choc arrière qui s'affaiblissent ainsi. Ce phénomène s'accompagne d'un allongement de la longueur d'onde proportionnel à l'intensité relative $\Delta P/P$ du choc et inversement proportionnel à la longueur d'onde dans la mesure où l'intensité du choc peut être considérée comme faible ($\Delta P/P \ll 1$).

3. Le bang des avions supersoniques - vol stabilisé

La description du bang des avions supersoniques est pour l'essentiel la même que celle de la détonation balistique : les différences résultent de la géométrie différente du mobile et de l'inhomogénéité de l'atmosphère dans laquelle se propage le bang.

3.1 Influence de la géométrie de l'avion et de sa portance

En raison de l'incidence de l'avion et de la répartition de portance qui en résulte et de l'irrégularité de sa géométrie (cockpit, voilure, fuseaux moteur, empennage ...), l'intensité de l'onde émise dépend de la direction d'émission (repérée par l'angle β du plan contenant le rayon sonore considéré avec le plan vertical contenant la trajectoire de l'avion ; figure 4). De plus, en champ proche, le signal de pression émis est beaucoup plus complexe, des chocs de recompressions partielles venant se mêler à la détente qui relie les fronts d'onde avant et arrière (figure 3). Ces chocs de recompression tendent, à mesure que l'on s'éloigne de l'avion émetteur, à venir coalescer avec les fronts de choc avant ou arrière, régularisant ainsi progressivement la signature du bang. Cette régularisation de la signature sera en général réalisée avant que le bang n'atteigne le sol pour des avions

de taille modérée ou faible (avions militaires) sauf si certains accidents de signature se situent dans la zone neutre où une perturbation ne tend à rejoindre ni le choc avant, ni le choc arrière.
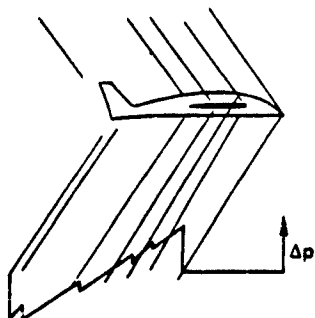

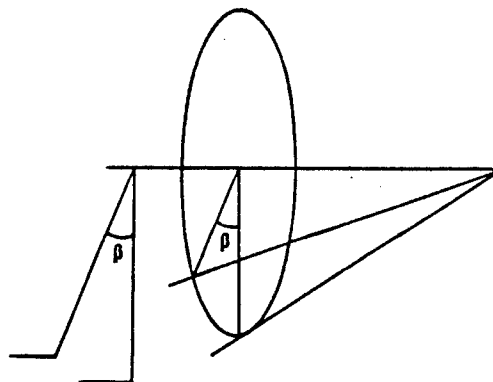Fig. 3 - Système d'ondes en champ proche d'un avion et champ de pression.

Fig. 4 - Repérage du plan d'émission d'un rayon sonore.

3.2 Influence de l'atmosphère - Cas de l'atmosphère standard

L'atmosphère standard est caractérisée par une décroissance régulière de la température jusqu'à 11 000 m (dT/dz = - 6,5 10⁻³ d°/m), la température demeurant constante au-delà (11 000 m <z< 25 000 m), elle est de plus soumise à la pesanteur : la masse volumique et la pression décroissent quand l'altitude croît.

3.2.1 Influence du gradient de pression (cas d'une atmosphère isotherme)

Considérons tout d'abord une atmosphère isotherme : la géométrie des surfaces d'onde n'est pas affectée, le cône de Mach non plus. Par contre l'onde pénètre à mesure qu'elle se rapproche du sol dans des couches atmosphériques de plus en plus denses et l'intensité de l'onde est modifiée. La surpression dans le front de l'onde varie comme la racine carrée de la pression atmosphérique locale P : $\Delta P (h) \sim P (h)^{\frac{1}{2}}$

La variation de la pression atmosphérique a en outre une influence sur l'intensité initiale de l'onde émise en champ proche :

- l'onde de volume (onde qui serait émise par l'avion à portance nulle) n'est liée qu'à la géométrie de l'avion, son intensité relative : ΔP_v (champ proche)/P (hvol) demeurera inchangée lorsque l'altitude de vol varie. Par suite en valeur absolue ΔP_v (champ proche) décroît comme la pression.

- La contribution de portance ΔP_z est liée au poids de l'avion, elle demeure en première approximation inchangée lorsque l'altitude de vol varie, par suite, elle tend à devenir prépondérante pour les vols à altitude élevée.

Ces effets opposés du gradient de la pression atmosphérique joints à ceux de l'expansion quasi cylindrique et de l'atténuation non linéaire ne permettent pas de définir une dépendance analytique entre intensité du bang et altitude de vol, on observe cependant en pratique que celle-ci évolue le plus souvent à peu près comme $h^{-3/4}$.

3.2.2 Influence du gradient de température

Le gradient de température vertical qui caractérise une atmosphère standard provoque une variation de la vitesse du son avec l'altitude : si $T = T_0 (1-kz)$ pour $z < 11 000 m$, $a = a_0 (1-kz)^{1/2}$. Il en résulte une réfraction de la nappe de bang dans l'atmosphère telle qu'on a dans le plan vertical contenant la trajectoire de l'avion (figure 5a).

$$\sin \alpha = a (z)/v = {}^{\infty}/_v \cdot a (z)/a_0 = \sin \alpha_0 \ a(z)/_\infty$$

Examinons la propagation des rayons sonores caractéristiques, lignes suivant lesquelles se propage l'énergie acoustique contenue dans le bang, normales à la surface d'onde en atmosphère sans vent et telles que dM /dt = a $\bar{n}$ (figure 5b).

Considérons un plan d'émission du rayon sonore faisant un angle β avec le plan vertical contenant la trajectoire ; l'angle d'émission ψ_i du rayon sonore contenu dans ce plan est (figure 5c) :

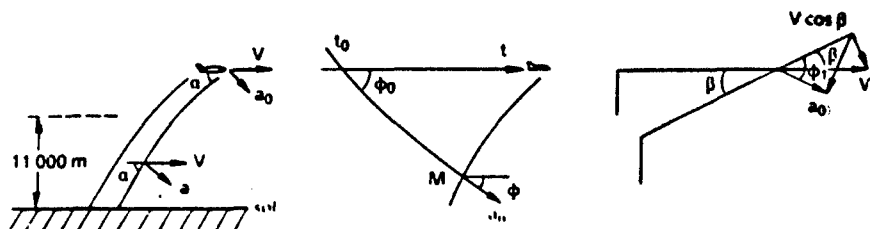$$\cos \psi_i = {}^0/_{vo} \cos \beta \quad \text{et} \quad \cos \psi = {}^0/_\infty \ \cos \psi_i$$

Fig. 5 - Réfraction du bang et des rayons caractéristiques.

Examinons tout d'abord la géométrie des rayons sonores et pour simplifier l'analyse, prolongeons l'atmosphère fictivement, si nécessaire, avec la même loi de température $(T = T_0 (1-kz)$ même pour $z < 0)$ (figure 6) :

- les rayons sonores émis à un instant quelconque se déduisent (pour un vol stationnaire) par simple translation de ceux émis à un instant de référence,

- les rayons sonores émis dans les différentes directions descendantes passent tous par une altitude minimale à partir de laquelle ils sont réfractés vers le haut,

- les rayons sonores admettent une enveloppe cylindrique, nommée caustique, limitant un domaine à l'extérieur duquel le bang n' pénètre pas et à la surface de laquelle il se réfléchit totalement suivant une arête de rebroussement.

Une telle surface est le siège d'une focalisation de l'énergie et l'on doit s'attendre à y observer des intensités de bang particulièrement importantes. Si on applique la théorie acoustique de la propagation de l'énergie à l'intérieur des tubes sonores caractéristiques (figure 7a), on montre que la surpression ΔP dans l'onde devrait au voisinage de la focalisation, évoluer comme

$$\Delta P_{ref} \left(\propto \left(\frac{\sin \ell \varphi_{ref}}{\sin \ell \varphi} \right)^{1/2} \right)$$

avec $\varphi = 0$ à la focalisation, ΔP_{ref} et φ_{ref} étant la surpression et l'incidence du rayon sonore à une distance suffisamment éloignée de la focalisation. Cela conduirait à une intensité infinie de l'onde, la théorie acoustique cesse en ce cas d'être valable ; en calculant de proche en proche la réfraction d'une onde de choc stationnaire, on montre que la surpression à attendre au niveau de la focalisation est, pour les intensités habituelles des bangs, de l'ordre de trois à quatre fois ce qu'elle est loin de la focalisation, ceci compte non tenu de l'onde réfléchie.
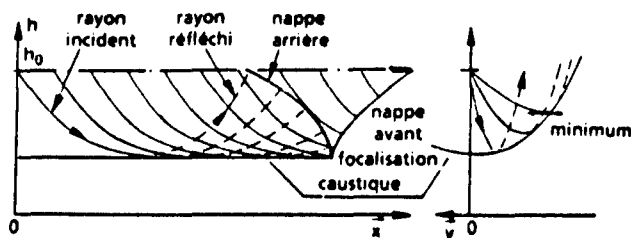
Fig. 6 - Formation d'une caustique en atmosphère stratifiée (vol à vitesse uniforme). (Réf. 1/[3]).
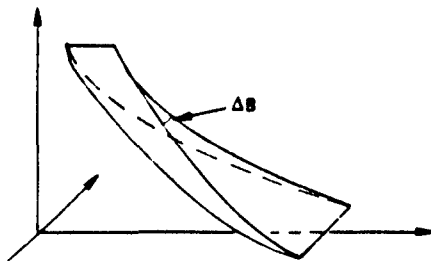

Fig. 7 a) - Allure de la propagation d'un tube sonore en atmosphère stratifiée.
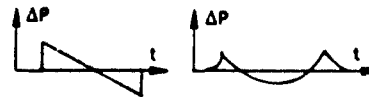

Fig. 7 b) - Allure de la signature du bang avant et après réflexion sur une caustique.

NOTA :

1/ On a observé qu'à l'extérieur du domaine délimité par la caustique, le bang ne pénétrait pas ; cependant (cf. §1) le bang lui-même n'est que la focalisation des ondelettes de perturbation émises par l'avion en ses différentes positions ; dans le domaine voisin de la caustique, mais extérieur à celle-ci, ces ondelettes sont encore presque en phase et on y entendra un grondement violent.

2/ L'analyse de la réflexion du bang sur la caustique (et l'observation expérimentale) montre que la signature du bang change de forme après cette réflexion (figure 7b) : le signal de pression qui a la forme d'un N avant d'avoir atteint la caustique prend ensuite approximativement la forme d'un U.

Si on revient maintenant au cas d'une atmosphère limitée par le sol, les conséquences pratiques sont les suivantes :

- si l'avion vole à Mach trop faible $M = V/a_o < a_{sol}/a$. ($M < 1,156$ en atmosphère standard, si $z > 11\ 000$ m) le bang n'est pas perçu au sol,

- si $M > a_{sol}/a$. le bang n'est perçu que dans un "couloir" de bang dont la largeur est définie par les rayons qui arrivent tangents au sol donc contenus dans les plans $\pm \beta_c$ tels que cos $\beta_a = a_{sol}/v_o$. Ce couloir de bang sera d'autant plus large que l'avion vole plus haut et à Mach plus élevé (figure 8a) :

$$\frac{1}{2}\ \Delta y\ (km) = \left(\frac{a_s}{a_o}\right)^2\ Arc\ cos\ \frac{a_o}{a_s} \times \sqrt{1 + \left(\frac{a_s^2}{a_o^2} - 1\right)^{1/2}}\ h$$

- le trajet acoustique est considérablement plus long pour les rayons latéraux que pour les rayons émis sous-trace et en particulier dans la basse atmosphère : les effets non linéaires seront donc beaucoup plus marqués ainsi que les perturbations apportées par la basse atmosphère. En outre, l'effet de l'expansion tridimensionnelle sera lui aussi plus marqué. On observera donc un bang nettement plus intense sous-trace que latéralement (figure 8).
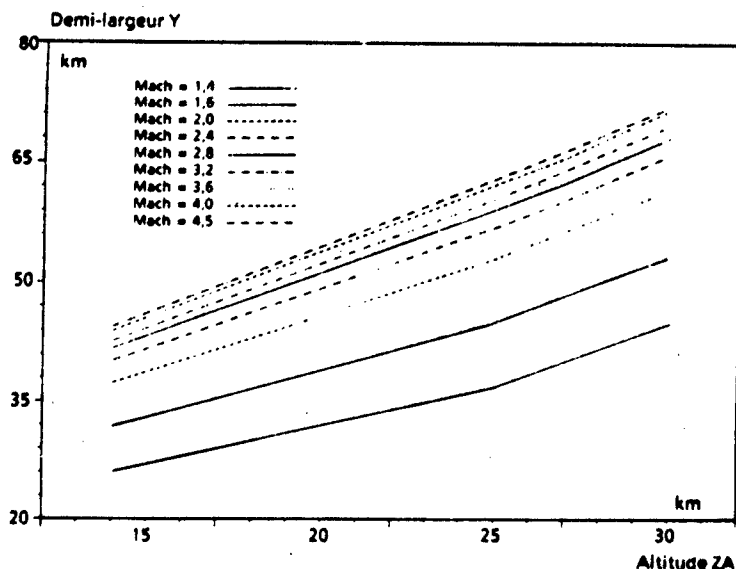

Fig. 8 a) - Evolution de la demi-largeur du tapis de bang en fonction de l'altitude de vol et du Mach (atmosphère standard). (Réf. 1/[22]).
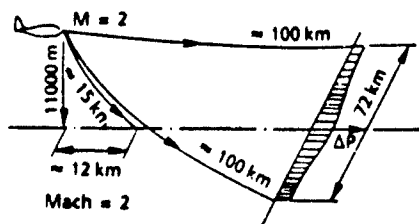

Fig. 8 b) - Trajet des rayons caractéristiques sous trace et dans les plans $\pm \beta = \beta_o$, couloir de bang et répartition des suppressions. (Réf.1/[3]).

- Le phénomène de focalisation tel qu'analysé ci-dessus n'est pas ressenti au sol (cas du vol stabilisé) car ou bien M < 1,156 et la focalisation a lieu en altitude ou bien M > 1,156 et les rayons sonores sont réfléchis par le sol avant d'avoir touché la caustique théorique. L'introduction du phénomène de focalisation faite ci-dessus sera utile lors de l'étude des phénomènes plus complexes présentés au § 4. Une simulation de focalisation en altitude est présentée sur la figure 9 sur laquelle on peut voir la réfraction de l'onde balistique d'une balle de fusil se propageant dans une atmosphère simulée à vitesse du son variable. Les mesures de pression faites lors de cette expérience ont montré un accroissement sensible de la surpression de l'onde au niveau de la focalisation.

Fig. 9 a) - Réfraction et focalisation d'une onde balistique en atmosphère stratifiée horizontalement (mélange air + CO_2). (Réf. 1/[20]).

Fig. 9 b) - L'onde réfractée présente un rebroussement et augmente rapidement d'intensité au voisinage de la focalisation, en dessous de la zone de focalisation une onde acoustique est transmise. (Réf. 1/[20]).
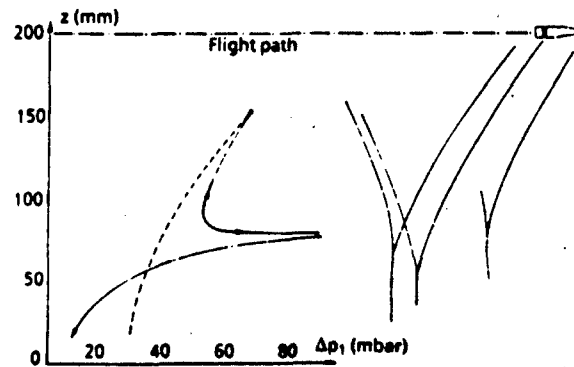
3.3 Propagation atmosphérique : cas de l'atmosphère réelle

L'atmosphère réelle diffère de l'atmosphère standard principalement par :

- une loi d'évolution de la température avec l'altitude plus irrégulière,

- l'existence de vents variables en grandeur et direction avec l'altitude,

- l'hygrométrie,

- l'existence de turbulences, principalement au niveau du sol.

On sait assez bien prendre en compte les deux premiers effets. L'existence d'un gradient de température plus irrégulier ne modifie en rien l'analyse du phénomène de réfraction des rayons sonores présentés précédemment ; il rend leur propagation plus irrégulière en particulier lors d'inversion de température.

L'existence de vents variables avec l'altitude modifie la loi de propagation des rayons caractéristiques qui cessent d'être normaux aux surfaces d'onde :

$$\vec{\omega}/_{\sigma n} = a\vec{n} + \vec{w} \quad (\vec{n} \text{ normale au front d'onde, } \vec{W} \text{ vitesse du vent})$$

ainsi que la valeur de l'invariant caractéristique du débit d'énergie acoustique à travers une section droite :

$$Q = \frac{\Delta p^2}{\rho a^2}(1 + \vec{\omega}.\vec{n})$$

Ces écarts par rapport à l'atmosphère standard ont des conséquences pratiques importantes. En fonction de l'importance du vent en altitude, le Mach de coupure, Mach à partir duquel le bang commence à être perçu au sol, peut varier entre 1,0 et plus de 1,35 au lieu de 1,156 en atmosphère standard, le tapis de bang peut être déplacé de manière importante en fonction des vents latéraux, les trajets sonores et les temps de propagation peuvent être fortement modifiés ainsi que l'intensité du bang. Cette influence des conditions météorologiques est l'une des causes de difficultés dans la préparation des vols supersoniques ainsi que dans leur exploitation ultérieure.

L'hygrométrie de l'air provoque un filtrage des fréquences élevées dans l'onde et devrait avoir pour résultat de donner des temps de montée en pression finis dans les fronts d'onde de compression : toutefois, il n'a jamais été rendu compte de manière satisfaisante de cet effet.

Les turbulences atmosphériques dont la longueur d'onde est comparable à celle des bangs devraient avoir pour conséquence de modifier le spectre de phase de l'onde et donc de déformer la signature de l'onde. Aucune description numérique de cet effet n'est aujourd'hui disponible. On observe en pratique, lorsqu'on mesure la signature des bangs successifs sous la trajectoire de l'avion, une évolution relativement périodique des signaux de pression qui évoluent, sur des distances assez courtesde l'ordre de la centaine de mètre, d'une forme présentant une crête de pression à une forme arrondie (figure 10a).

En extrêmité latérale de tapis de bang, là où les trajets sonores dans la basse atmosphère sont particulièrement importants, on n'observe en pratique que des ondes aux formes arrondies (figure 10b) : ce phénomène, dont le modèle numérique ne rend pas compte, doit résulter de l'effet combiné d'un long trajet des rayons sonores dans les basses couches turbulentes de l'atmosphère et de la proximité de la zone de "silence".
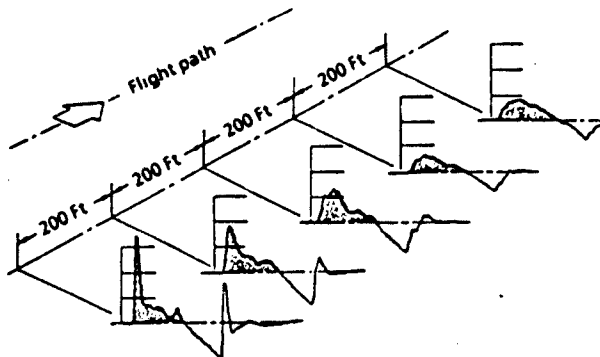
Fig. 10 a) - Exemple d'évolution de la signature du bang en des points de mesure voisins. On observe que l'apparition de pointes de pression localisées est associée à des temps de montée en pression dans l'onde courts. L'existence de telles cretes de pression ne doit pas être oubliée lors de l'étude des réactions de sursaut liées au bang. (Réf. 2/1).
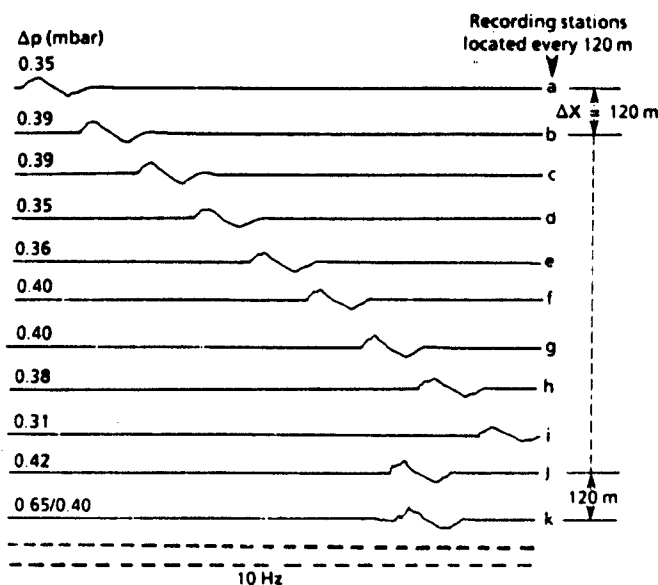

Fig. 10 b) - Signatures de bang successives de Concorde vers l'extrémité latérale du tapis de bang (M = 2, h = 15 600 m, distance de l'axe de mesure à la trace au sol de la trajectoire 30 km). (Réf. 2/7).

3.4 Réflexion au sol - Réflexion sur les constructions

Le bang se présente au sol avec des incidences variables suivant la vitesse de l'avion et l'éloignement latéral : il se présente sous forte incidence (pour M = 2, $\propto$ 35°) sous trace lors du vol de croisière et à incidence quasi rasante au voisinage de l'extinction.

La réflexion d'une onde en N sur un sol plan rigide indéfini provoque la naissance d'une onde symétrique de même intensité ($\propto = \beta$, $\Delta P_1 = \Delta P_2$ ou $k_r = 2$) (figure 11).

Au niveau du sol, la surpression dans l'onde est doublée. Il n'en est plus de même à une certaine altitude puisque l'onde perçue est alors dédoublée (figure 12). l'intervalle de temps séparant le passage des deux fronts de choc successifs au niveau de l'oreille humaine n'est pas négligeable en regard de ses temps de réponse

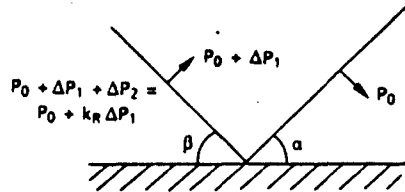(Si : M = 2,3, $\alpha \approx 30°$, pour h = 1,55 m, $\tau = \frac{2 h \sin\alpha}{a_0} \approx 8$ ms).

Fig. 11 - Réflexion sur un sol rigide
($\alpha = \beta$, $k_r = 2$).
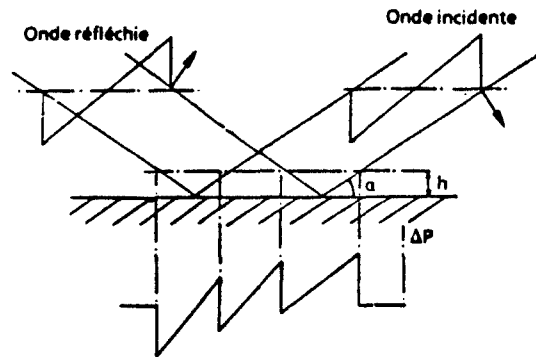
Fig. 12 - Signature de pression à une altitude h après réflexion sur le sol.

Pour les incidences quasi rasantes (extrémité latérale du tapis), les lois de la réflexion sont plus complexes (le coefficient de réflexion évolue rapidement et pour une onde bien formée peut atteindre 3), mais ce phénomène paraît être sans importance pratique, l'onde incidente étant alors fortement déformée.

Les mesures du coefficient de réflexion du bang sont peu nombreuses et d'exploitation difficile, elles conduisent à admettre que le coefficient de réflexion réel est assez voisin de 2 (compris entre 1,8 et 2).

Compte tenu de la faible longueur d'onde du bang et de son incidence, le relief influe peu sur le phénomène de réflexion. La réflexion sur les constructions conduit à des modifications de signature assez importantes sans pour autant changer profondément l'amplitude des surpressions maximales (figure 13), toutefois, cette modification de signature n'est pas sans conséquence lorsqu'on étudie l'effet du bang sur les structures ou le champ sonore induit à l'intérieur des habitations.
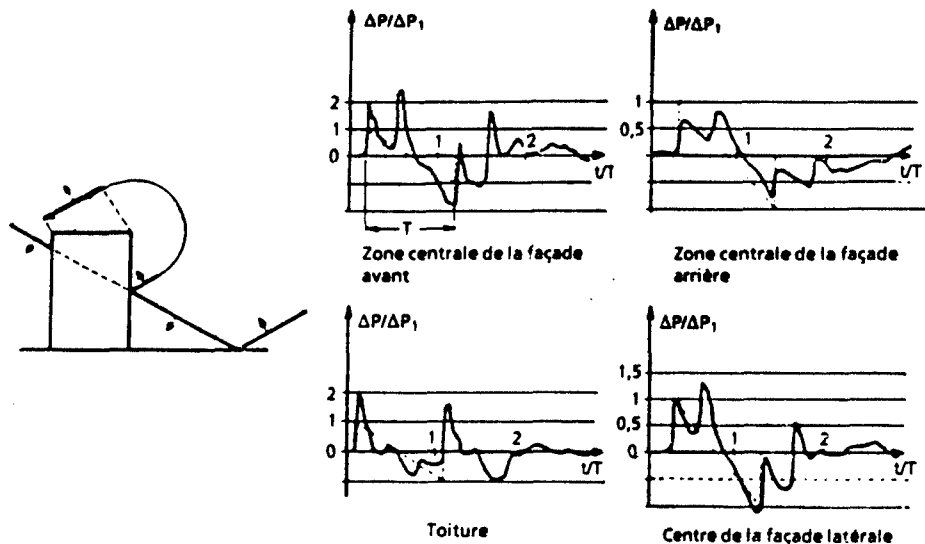

Fig. 13 - Enveloppement d'une construction par un bang : signaux de pression obtenus au centre des diverses façades d'un immeuble de hauteur modérée soumis à l'action d'un bang se présentant frontalement sous incidence de 30° (simulation de laboratoire, en pointillé l'onde incidente). (Réf. 1/[18]).

4. Bang des avions : influence des manoeuvres

4.1 Focalisation en vol rectiligne accéléré

Le bang apparaît lors de la phase de vol transsonique accéléré de l'avion. A partir de Mach 1, l'avion émet des rayons sonores caractéristiques de plus en inclinés par rapport au plan horizontal de la trajectoire (figure 14a).

Ces rayons admettent une enveloppe (caustique) qui constitue une surface d'accumulation d'énergie et la nappe de bang admet une ligne de rebroussement sur cette surface.

En tout point du segment FC compris entre les points de focalisation et d'extinction sous trace, deux rayons sonores différents parviennent au sol l'un n'ayant pas encore touché la caustique et alimentant la nappe de bang incidente, le second ayant déjà touché la caustique et alimentant la nappe arrière ; dans toute cette zone, on percevra donc deux bangs successifs (le second ayant une forme différente du premier : forme en u). Au-delà du point C, les rayons qui alimentent en atmosphère indéfinie la nappe arrière touchent le sol et s'y réfléchissent et ne peuvent plus contribuer à la formation de la nappe arrière : on ne perçoit plus qu'un seul bang.

La ligne de focalisation au sol est limitée à un arc c_1 c_2 (figure 14a) borné par les points c_1 et c_2 d'extinction latérale où les rayons sonores sont à la fois tangents à la caustique et au sol.

Sur la ligne de focalisation, les tubes sonores se referment suivant un segment. L'application de la théorie acoustique conduirait à prévoir une intensité sonore infinie pour le bang le long de cette ligne. Une analyse au second ordre du phénomène de propagation en atmosphère non pesante montre que la surpression à la focalisation ΔP_1 est liée à la surpression loin de la focalisation ΔP (s) par une relation faisant intervenir la courbure relative $1/R$ du rayon sonore et de la caustique :

$$\Delta P_1 / \Delta P_1 \approx \left(\frac{\&s}{\Delta s}\right)^{3/5}\left(\frac{\gamma}{\gamma+1}\right)^{4/5}\left(\frac{\Delta(\cdot\Delta)}{R}\right)^{3/5}\left(\frac{\Delta P_4}{P}\right)^{-1/5}$$

où sf et s sont les abscisses curvilignes des points de focalisation et du point courant sur le rayon sonore. La géométrie de la caustique étant dépendante de l'accélération de l'avion, on voit que celle-ci interviendra dans l'intensité de la focalisation ; cependant en pratique, cette influence est modérée. L'application de la formule ci-dessus fournit des estimations du coefficient de renforcement de l'onde plus faibles (de l'ordre de 3,5) que celles observées expérimentalement (voisine de 5).

Remarque :

Toutefois, en cas d'accélération faible, la caustique et les rayons sonores au voisinage de cette dernière sont peu inclinés par rapport au sol : les trajets sonores près de la focalisation se situent donc dans les basses couches de l'atmosphère ; on s'attend donc en ce cas à une très forte influence de la structure de ces basses couches et de la turbulence qui les affecte et donc à une dispersion importante. C'est bien ce qui est observé expérimentalement.

Les dimensions de la zone affectée par la focalisation sont naturellement dépendantes de l'accélération de l'avion ; pour fixer les idées, on donne figure 14b, quelques éléments dimensionnels. La zone du net renforcement du bang n'a toutefois à partir de l'arc C_1FC_2 qu'une profondeur un peu supérieure à cent mètres.

Rappelons enfin que les conditions météorologiques (vent, répartition de température) affecteront ce phénomène de focalisation.
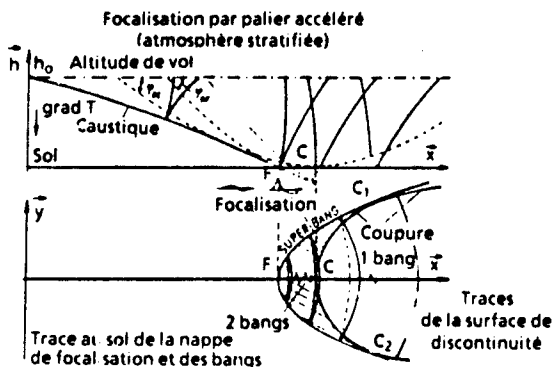

Fig. 14 a) - Focalisation en vol accéléré. Trajet des rayons sonores et intersections au sol. (Réf. 1/[3]).
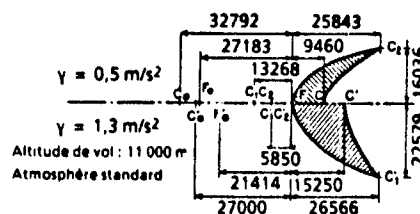

Fig. 14 b) - Traces au sol de la caustique et de la ligne de coupure pour deux niveaux d'accélération. (Réf. 1/[3]).

4.2 Vol décéléré - extrémité longitudinale du tapis du bang

Lors de la décélération qui suit le vol de croisière, les rayons sonores émis divergent, l'intensité du bang est alors affaiblie à condition que l'altitude de vol n'ait pas changé (en général, on observera le phénomène inverse en raison de la diminution de l'altitude de vol) ; l'extrémité longitudinale du tapis de bang sera définie par le point de contact avec le sol du rayon sonore émis au Mach de coupure ($M = 1,156$, en atmosphère standard et pour $z \geq 11\,000$ m, figure 15a). Le Mach d'émission correspondant et la position au sol de la coupure sont fortement dépendants des conditions météorologiques (figure 15b).
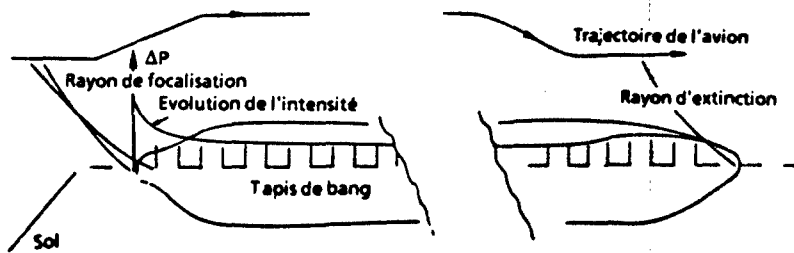
Fig. 15 a) - Allure générale du tapis de bang et de l'évolution de l'intensité sous trace.
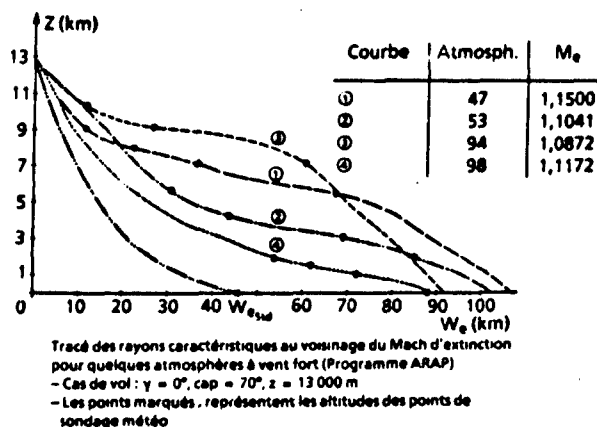

Courbe	Atmosph.	M_e
①	47	1,1500
②	53	1,1041
③	94	1,0872
④	98	1,1172

Tracé des rayons caractéristiques au voisinage du Mach d'extinction pour quelques atmosphères à vent fort (Programme ARAP)
- Cas de vol : γ = 0°, cap = 70°, z = 13 000 m
- Les points marqués, représentent les altitudes des points de sondage météo

Fig. 15 b) - Influence des conditions météorologiques sur la position du point d'extinction longitudinale.
(Réf. 1/[7]).

4.3 Autres manoeuvres de l'avion - Focalisation en virage et superfocalisation

Toute manoeuvre de l'avion (accélération, montée, descente, virage) fait que les rayons sonores émis aux différents instants se présentent les uns par rapport aux autres d'une manière différente de celle examinée dans le cas du vol rectiligne uniforme à vitesse constante.

Il en résultera des augmentations ou des diminutions de l'intensité du bang perçu par rapport à sa valeur nominale. Ces variations resteront en général d'importance modérée, à moins que la manoeuvre soit importante, ou intervienne alors que l'avion vole à un nombre de Mach voisin du Mach critique. A titre d'exemple, on donne (figure 16) les caractéristiques géométriques d'une focalisation au sol due à un virage de l'avion. La caustique peut présenter elle-même, une ligne de rebroussement ; au voisinage de l'intersection de cette ligne avec le sol, des bangs plus intenses que ceux normalement perçus au voisinage d'une focalisation classique sont observés. Des renforcements d'intensité un peu inférieurs à 10 ont été observés en ce cas. En de tels points, en effet les tubes sonores se referment sur un point au lieu de se refermer suivant une arête comme dans le cas de la focalisation classique. Aucune approche théorique ne permet actuellement d'estimer l'intensité de l'onde au voisinage de la superfocalisation, il n'est donc pas possible d'évaluer son évolution en fonction des caractéristiques de la manoeuvre qui la provoque. De plus les mesures expérimentales, très difficiles à réaliser, sont encore très peu nombreuses.
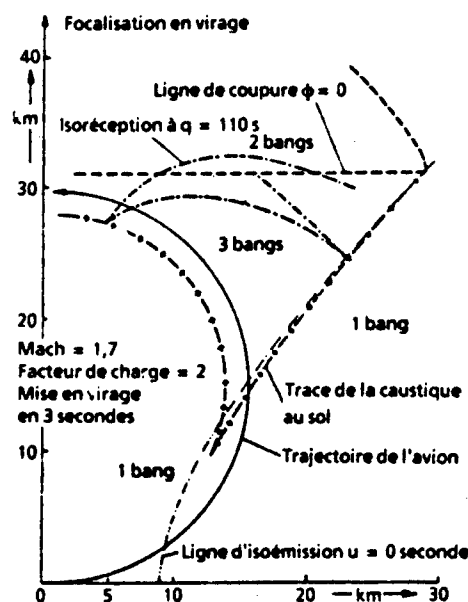
Fig. 16 - Exemple de focalisation due à une manoeuvre de l'avion : trace au sol de la nappe de focalisation due à un virage et position de la nappe de choc (altitude 11 000 mètres, Mach 1,7 facture de charge n = 2, temps de mise en virage : 3 secondes). (Réf. 1/[3]).

5. Prévision pratique des bangs

5.1 Position au sol du tapis de bang

La prévision de la position géométrique des nappes de bang s'effectue très simplement par calcul de la propagation des rayons sonores à partir de la loi du mouvement de l'avion sur sa trajectoire et des conditions météorologiques, on calcule ainsi largeur de tapis de bang, isoémissions, isoréceptions, coupures latérales et longitudinales ; les zones de focalisation se déterminent en tant qu'enveloppes des isoémissions.

5.2 Calcul de l'intensité du bang

Le calcul de l'intensité du bang est un peu plus lourd, il demande en particulier l'introduction d'une fonction des caractéristiques de volume et de portance de l'avion et dépendante des conditions de vol. Un certain nombre de programmes de calcul de cette intensité existe qui dérivent tous de celui établi en 1969 par W.D. Hayes à Princeton.

La donnée d'entrée du programme est le champ de pression aérodynamique proche autour de l'avion obtenu à partir d'une théorie linéarisée qui est caractérisée par la fonction F de Whitham :

$$\Delta P(x - \beta r, \theta) = \gamma \frac{P_0}{(2 \beta r)^{1/2}} F(x - \beta r, \theta)$$

avec P_0 : pression ambiante :

M : mach de vol,

$\beta = (M^2 - 1)^{1/2}$

θ : position angulaire du plan d'émission,

$$F(\xi) = \frac{1}{2\pi} \int_0^\xi \frac{A''(x)}{(\xi - x)^{1/2}} \, dx$$

où A représente l'aire de la section d'un corps de révolution équivalent à l'avion par les plans tangents aux cônes de Mach le long des différentes lignes $x = c^{te}$ (figure 17).

La propagation dans l'atmosphère de cette perturbation acoustique initiale est ensuite étudiée suivant les principes de l'acoustique géométrique décrits dans les paragraphes précédents, c'est-à-dire en utilisant les propriétés des tubes et des rayons sonores et en corrigeant au premier ordre des effets non linéaires résultant de l'interaction permanente des ondes de détente et de compression dues à l'amplitude finie du signal acoustique.

Le code de calcul permet de tenir compte des vents horizontaux et de la stratification en température de l'atmosphère, ainsi que des manoeuvres de l'avion. Il ne permet cependant pas d'étudier l'aspect quantitatif du phénomène de focalisation ni de rendre compte des distorsions du bang résultant de la turbulence régnant dans les basses couches de l'atmosphère.
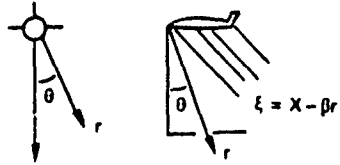
Fig. 17 - Système de coordonnée utilisé pour le calcul de la fonction F.

La figure 18 donne un exemple pratique de l'application de ces programmes. Elle fournit les signatures de bang attendues de Concorde sur une trajectoire type. On observe en particulier le dédoublement du front avant lorsque l'avion vole à altitude modérée et le niveau important du bang en début de montée (altitude modérée, avion lourd) et en fin de descente.

Des formules analytiques approchées, associées à des graphes spécifiques de chaque formule d'avion, ont été également établies ; elles permettent une évaluation rapide de l'ordre de grandeur de l'intensité du bang à attendre d'un avion déterminé ainsi qu'une analyse aisée de l'influence d'un changement des conditions de vol. Leur examen montre en particulier qu'un changement du Mach de vol, pour les Mach sensiblement supérieurs au Mach de coupure, n'affectera que très peu l'intensité du bang et qu'en règle générale le bang s'atténue avec l'altitude de vol un peu moins rapidement $h^{3/4}$. L'utilisation de ces formules s'avère en général suffisante pour la détermination de l'intensité du bang des avions militaires.

	Masse tonnes	Mach	Altitude (m)	Pente degré	Surpression max. Pascal	Durée (s)
① Début de montée	173,35	1,2	10 670	+ 3,0	140,3	0,297
② Début de croisière	147,73	2,0	15 330	0	91,2	0,194
③ Fin de croisière	111,20	2,0	17 050	0	72,2	0,190
④ Fin de descente	110,37	1,2	13 540	- 2,0	106,2	0,288

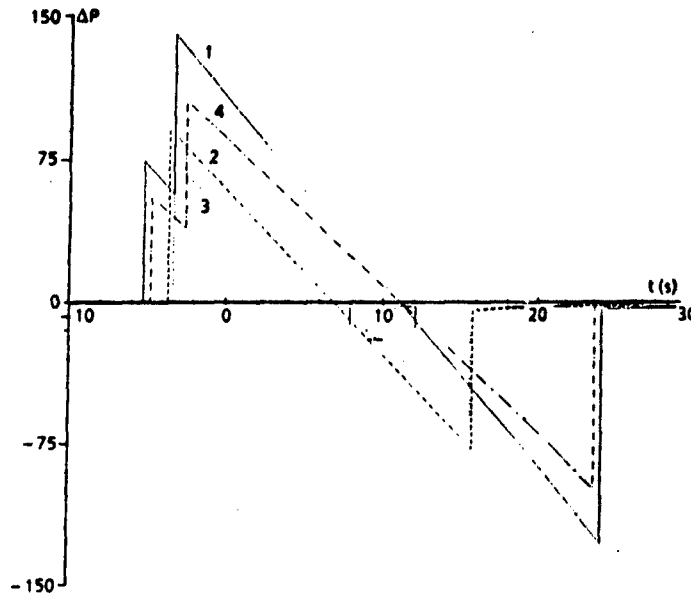Calculs faits pour un avion sans accélération

Fig. 18 - Concorde : évolution de la surpression sous trace le long d'une route type. (Réf. 1/[22]).

6.- Recoupements expérimentaux

De très nombreuses campagnes de mesure du bang ont été menées aux Etats-Unis, en France et dans d'autres pays utilisant les vols supersoniques d'entraînement des avions militaires ou des vols spécialement organisés pour l'étude d'aspects spécifiques du bang (par exemple : la focalisation).

On peut résumer comme suit les principaux enseignements tirés des essais en vol :

- bons recoupements des prévisions du calcul concernant la position du tapis de bang lorsque les conditions météorologiques (vent et température) sont bien connues. En particulier, la position des zones de focalisation peut être ainsi déterminée à environ un kilomètre près,

- recoupement apparemment assez satisfaisant des prévisions intéressant l'intensité du bang sous trace ; toutefois, les comparaisons entre bangs calculés compte tenu des conditions météorologiques et les bangs mesurés sont encore peu nombreuses,

- recoupement statistiquement satisfaisant de l'ensemble des mesures de bangs sous trace et hors trace avec les valeurs prévues par le calcul sans tenir compte des conditions météorologiques : les valeurs moyennes coïncident à 10 % près environ mais la dispersion est alors assez grande (figure 19). Cette remarque est importante, lorsqu'on parle d'une valeur nominale du niveau de bang. Cette dispersion qui, sur la figure 19, concerne des vols différents d'un même avion affecte également de manière importante les bangs émis au cours d'un même vol, et ce en des points de mesures voisins (voir fig. 20 et 21),

- sous trace, dans des conditions atmosphériques calmes, le bang perçu au sol est généralement bien formé (front de compression dans le choc avant étalé sur un temps allant d'une fraction de milliseconde à plusieurs millisecondes). Lorsque l'atmosphère est turbulente, les temps de montée dans les chocs peuvent être souvent plus importants (quelques millisecondes) et la signature varie d'un lieu à un autre de manière assez périodique (fig. 21),

- les signatures de bang tendent à présenter des fronts de montée plus progressifs jusqu'à atteindre des allures le plus souvent presque sinusoïdales vers l'extrémité de tapis. Rappelons en outre que le bang en extrémité latérale de tapis est d'intensité beaucoup plus faible : les bangs d'extrémité de tapis sont transportés suivant des rayons sonores presque horizontaux au voisinage du sol et qui de ce fait se propagent très longtemps dans les couches très turbulentes de la basse atmosphère, ce qui paraît être une des causes de cette distorsion du signal acoustique (figure 22),

- les bangs focalisés mesurés lors des accélérations transsoniques sont 4 à 5 fois plus intenses que ceux émis lors du vol stabilisé, ceci indépendamment du niveau d'accélération de l'avion, la dispersion des mesures étant toutefois plus grande quand l'accélération est faible, ce renforcement est un peu plus important que ne le laissait prévoir la théorie (3,5), ce qui peut s'expliquer par le fait que la théorie ne prend pas en compte l'onde réfléchie au niveau de la caustique. La profondeur sur laquelle cette amplification est observée est de l'ordre de cent à quelques centaines de mètres (figure 23),

- les caractéristiques des bangs focalisés observés lors de virages sont très voisines des précédentes : renforcement voisin de 5 et profondeur sur laquelle le renforcement est sensible de l'ordre de quelques centaines de mètres ; toutefois les conditions expérimentales des essais (Mach 1,7 et 2 ; facteur de charge de 2) ont été peu variées et aucune tentative théorique n'a été faite pour donner à ce résultat un certain caractère de généralité (figure 24),

- les mesures de bangs au voisinage de la superfocalisation, très difficiles à réaliser, sont peu nombreuses : on a observé des renforcements d'intensité du bang dépassant 8. Cette valeur paraît être un minimum compte tenu de la difficulté qu'il y a à placer un capteur de mesure suffisamment proche du point de superfocalisation, la superficie affectée paraît très réduite, de l'ordre de quelques centaines de mètres carrés (figure 25). En ce cas également il est difficile d'évaluer le caractère de généralité du résultat,

- les focalisations et superfocalisations peuvent intervenir pour de très faibles manoeuvres de l'avion quand le Mach de vol est proche du Mach de coupure (figure 26),

- sur la planche 27 figure un récapitulatif des mesures d'intensité de bangs effectuées aux USA. Il donne une vue d'ensemble sur les influences respectives de la taille et de la forme de l'avion, de l'altitude de vol et du Mach sur l'intensité du bang perçu au sol.
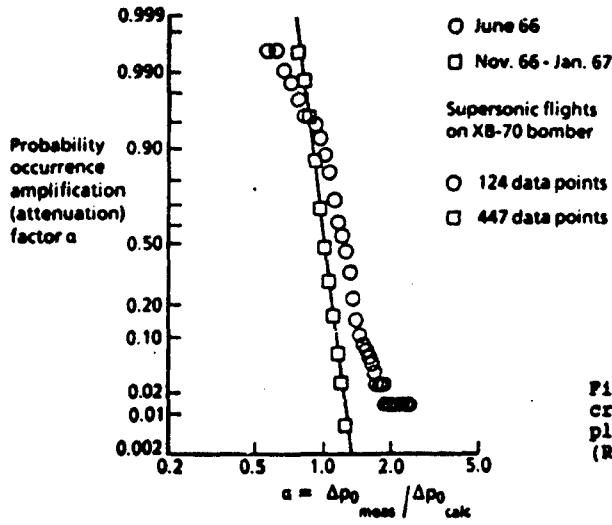
Probability
occurrence
amplification
(attenuation)
factor α

O June 66

□ Nov. 66 - Jan. 67

Supersonic flights
on XB-70 bomber

O 124 data points

□ 447 data points

$\alpha = \Delta p_{0_{mess}} / \Delta p_{0_{calc}}$

Fig. 19 - Dispersion des surpressions de crête dans le bang. La dispersion est plus grande en été qu'en hiver. (Réf. 2/[1]).

Concorde   Z = 17 000 m
Mach = 2

1 mbar

500 ms

Fig. 20 - Bangs de Concorde mesurés en des points voisins. Les fronts de choc sont nets mais des fluctuations sensibles affectent les pressions de crête. (Réf. 1/[7]).

F-104   B-58   XB-70

Peaked

Normal

Rounded
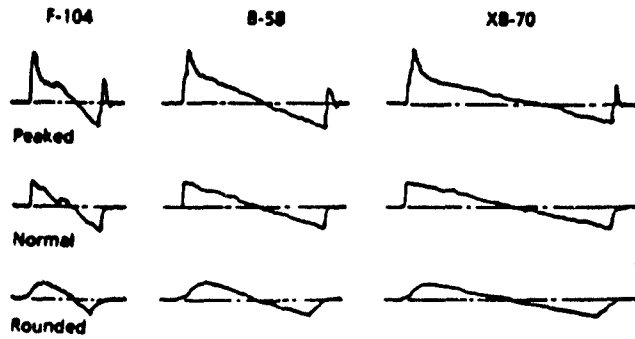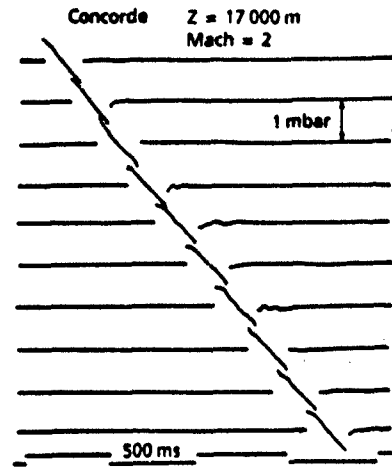
Fig. 21 - Variabilité des signatures de bang perçues au sol. (Réf. 2/[1]).
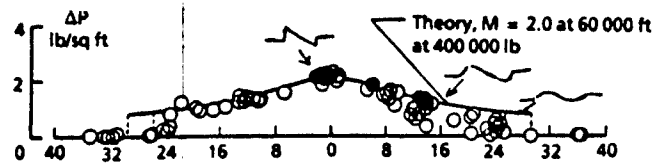
Fig. 22 - Variation de l'intensité et de la borme du bang avec l'éloignement latéral XB-70. (Réf. 2/[1]).
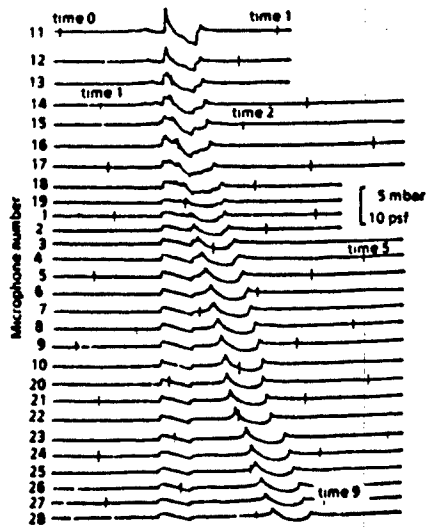
Fig. 23 - Focalisation au cours d'une accélération transsonique. Les microphones situés sur un axe rectiligne sont distants de 100 m les uns des autres. On voit que l'effet de la focalisation est très local. (Opération Jéricho - focalisation). (Réf. 1/[8]).
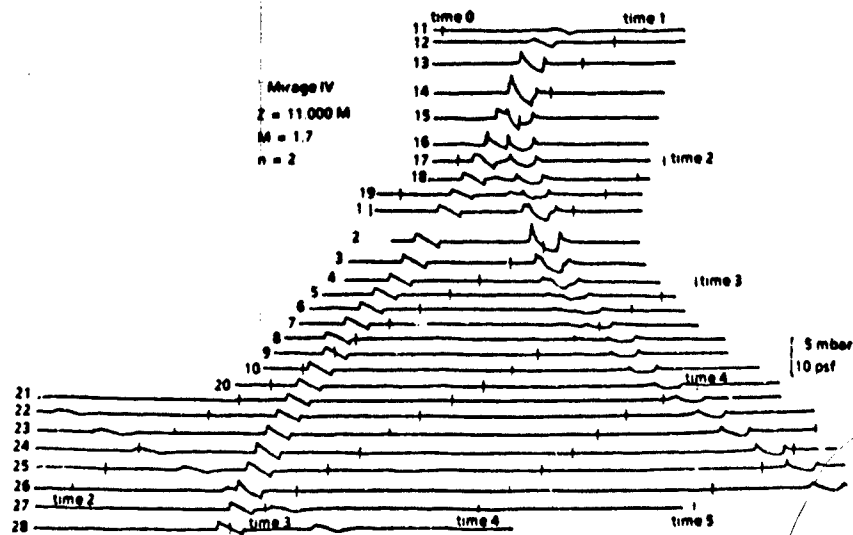

Fig. 24 - Focalisation en virage stabilisé. Les points de mesure sont alignés et distants de 100 m les uns des autres. On distingue les 3 nappes de bangs (Opération Jéricho-Carton). (Réf. 1/[8]).
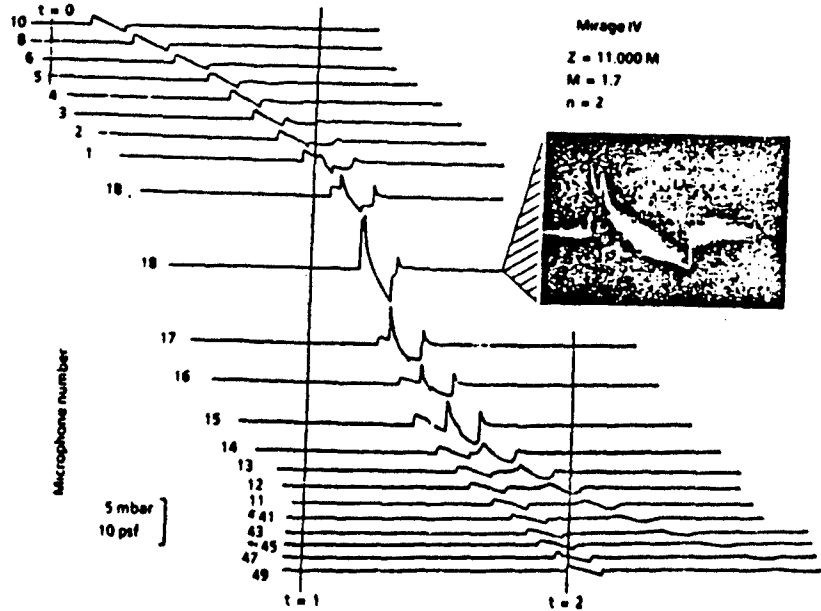
Fig. 25 - Superfocalisation résultant d'une mise en virage. Les points de mesure sont alignés et distants de 100 m les uns des autres. L'axe de mesure passe à environ 200 m du point de superfocalisation présumé (Opération Jéricho-Carton). (Réf. 1/[8]).
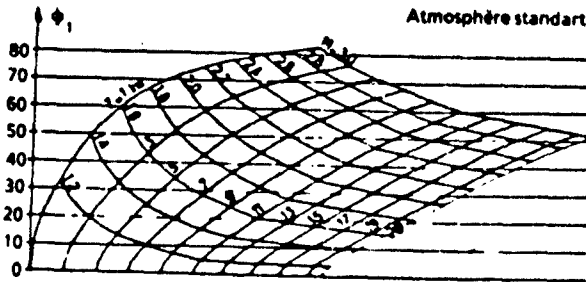

Fig. 26 - Limites de focalisation ; angle d'inclinaison maximum autorisé (tgθ = V²/Rg) pour éviter la focalisation en fonction de M et de l'altitude. (Réf. 1/[8]).
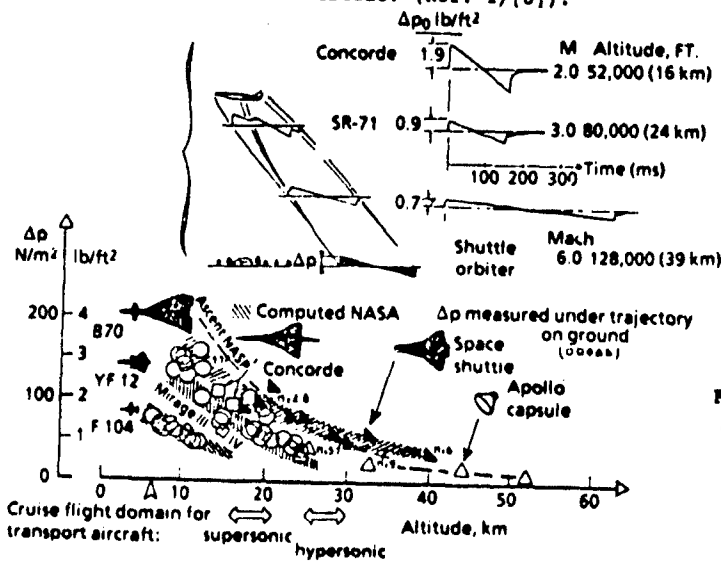

Fig. 27 - Sonic boom signature and intensity. (Réf. 1/[23]).

7. Effets du bang

7.1 Moyens d'études

Pour étudier l'effet des bangs, tant sur les structures que sur les êtres vivants, il est nécessaire de produire un très grand nombre de bangs de manière à pouvoir étudier les effets de fatigue ou d'habituation. Pour cela, on a besoin de moyens d'essais permettant de créer aisément des ondes de pression bien reproductibles présentant les caractéristiques du bang.

Deux grands types de moyens peuvent être utilisés à cette fin :

· soit un tube à choc conique de très grande dimension tel que celui décrit sur la figure 28 : l'éclatement de la membrane qui obture la partie motrice du tube emplie d'air en surpression, donne naissance à une onde en N qui présente toutes les caractéristiques d'intensité et de durée du bang, intensités et durées étant réglables en fonction du choix que l'on fait de la position de la membrane. Dans la vaste chambre de mesure qui est ainsi balayée par l'onde en N, on peut procéder à des études d'effets physiologiques ou structuraux, ou encore étudier les effets induits à l'intérieur d'un local construit en parallèle de cette chambre de mesure,

- soit créer par l'intermédiaire de haut-parleurs dans un local de faible volume (figure 29), ou de pistons dans un local de plus grand volume (figure 30) une évolution de pression reproduisant une onde en N ou l'onde induite à l'intérieur d'un local par un bang externe : un tel moyen sera particulièrement bien adapté aux études des effets sur les structures.

En dehors de ces deux moyens principaux et des mesures que l'on peut faire lors de vols d'essais, beaucoup d'autres moyens peuvent être utilisés tels que la création de deux petites impulsions simulant les fronts avant et arrière du bang et obtenues par l'éclatement successif des membranes de fermeture de deux réservoirs d'air comprimé (figure 31). Un moyen de ce type suffit pour une première approche de l'étude des réactions de sursaut en champ libre.
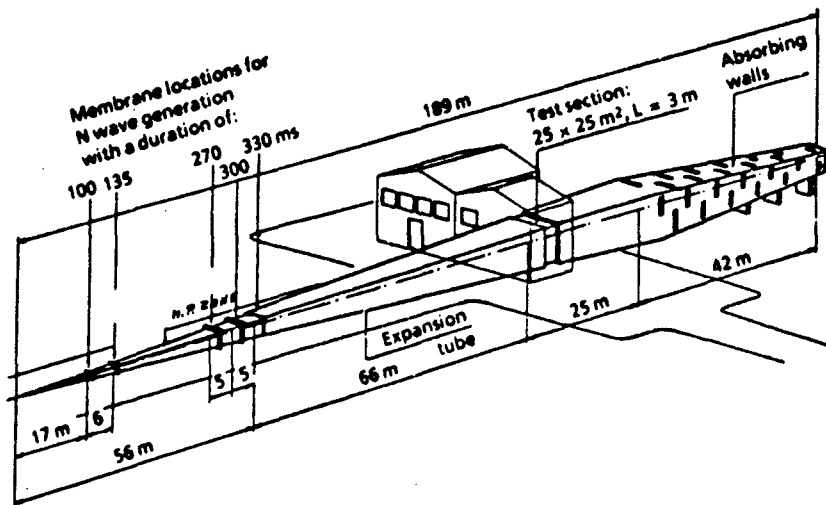

Fig. 28 - Générateur de bang de l'ISL ; tube à choc conique fournissant une onde en N ajustable en intensité et durée au niveau de la chambre d'expérimentation. (Réf. 1/[7]).
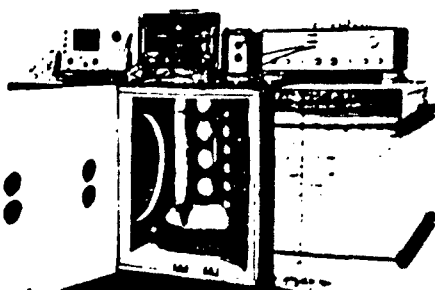

Fig. 29 - Chambre excitée par des hauts-parleurs pour simulation de l'effet du bang sur des structures de petites dimensions ou de petits animaux (Volume 1701). (Réf. 1/[7]).
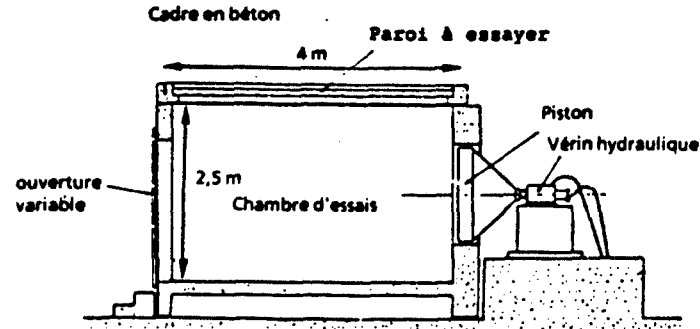
Fig. 30 - Banc de fatigue du CSTB/Grenoble pour étude de la tenue des structures exposées au bang. (Réf. 5).

Fig. 31 - Dispositif fournissant en champ libre deux pics de pression successifs résultant de la vidange de deux réservoirs d'air comprimé et permettant l'étude des réactions de sursaut. (Réf. 1/[7]).

7.2 Effets physiologiques

De très nombreuses études ont été menées tant en laboratoire que sur le terrain pour déterminer les effets physiologiques du bang :

- études intéressant la production animale : effets sur le comportement des chevaux, des porcs, des volailles, des oiseaux sauvages, sur la reproduction des bovins, le taux d'éclosion des couvées d'oeufs de poules ou de faisans, le comportement des poissons ...

- études de l'effet du bang sur les fonctions physiologiques de l'animal pour en évaluer les effets sur l'être vivant en général et plus particulièrement en vue de connaître son action possible sur l'homme : effets sur l'équilibration et l'audition sur les réactions hormonales, cardiovasculaires, électrophysiologiques, comportementales ...

- études directement réalisées chez l'homme : influence sur le sommeil, l'audition, le système cardiovasculaire ...

Cet ensemble d'études a montré que, en plus de la gêne résultant de tout phénomène sonore, seules des réactions directement liées à une réaction de sursaut (ou d'arrêt) des individus pouvaient être mises en évidence.

On peut caractériser les résultats obtenus pour un bang de signature en N classique comme suit :

- la fréquence et l'ampleur de la réaction de sursaut croissent avec l'intensité de crête du bang. La réaction paraît générale pour un bang isolé bien formé d'intensité supérieure ou égale à 100 Pascals,

- elles décroissent quand le temps de montée dans le front de compression avant de l'onde croît,

- il y a habituation, l'amplitude de la réaction moyenne pour un groupe de sujets donné décroît, au fur et à mesure que les sujets expérimentent des bangs successifs, par exemple à raison de dix par jours. On notera toutefois qu'après interruption momentanée de la série expérimentale, une déshabituation partielle intervient et qu'à l'intérieur d'un groupe de sujets habitués subsistent de manière aléatoire et individuelle des réactions de sursaut,

- si les résultats obtenus par les différents expérimentateurs sont très cohérents qualitativement pour ce qui concerne l'influence de la surpression de crête, du temps de montée, et de l'habituation, ils diffèrent quantitativement en fonction des tests appliqués, de l'état de préparation et d'information des sujets, de l'ambiance générale des essais : il semble cependant que pour des bangs d'intensité modérée (<50 Pascals), à front de montée

progressif (quelques millisecondes), les réactions de sursaut après habituation puissent devenir peu nombreuses, tout au moins pour des sujets exposés au bang tel qu'il est ressenti en champ libre (figure 32).
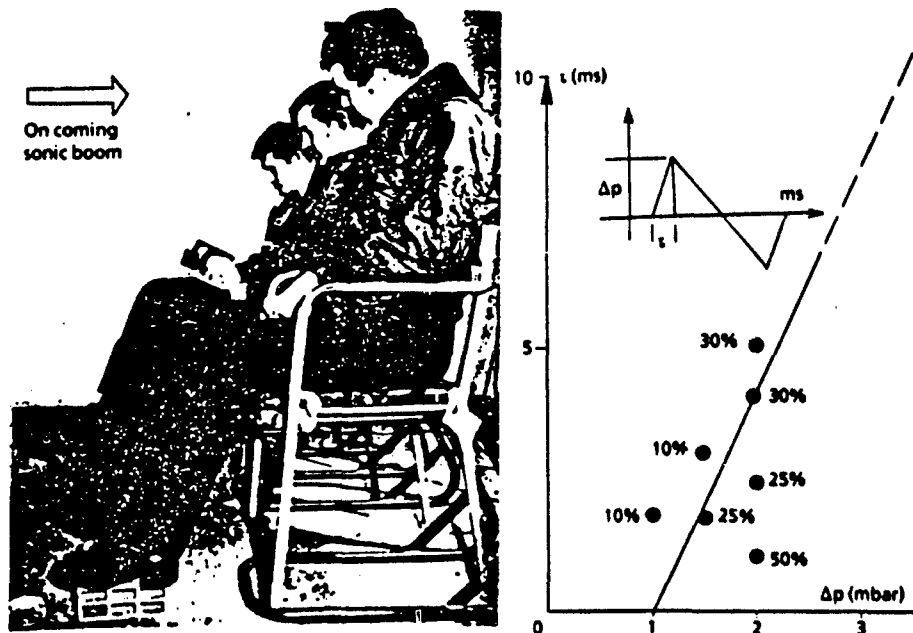

Fig. 32 - Etude de sursaut au générateur de bang, les sujets sont assis sur des sièges équipés de jauges de contrainte et courbe indiquant le taux de sursaut de 30 %. (Réf. 3/[5]).

Parallèlement à ces études de laboratoires, de nombreuses expérimentations ont été menées sur le terrain permettant de connaître la réaction des populations soumises au bang, soit lors de campagnes de survol spécialement destinées à ces études, soit utilisant des bangs simulés, soit en effectuant des enquêtes d'opinion auprès des populations soumises régulièrement aux bangs des vols d'entraînement des avions militaires.

Les résultats des enquêtes d'opinion et l'exploitation des plaintes déposées recoupent bien les résultats de laboratoire, pour ce qui concerne l'effet d'habituation et l'influence de la pression de crête du bang. Ils fournissent cependant quelques informations complémentaires :

- à l'intérieur des habitations, les bangs sont jugés au moins aussi gênants qu'en champ libre,

- l'attitude vis-à-vis du bang ne dépend pas uniquement des caractéristiques physiques de celui-ci mais aussi de nombreux facteurs en particulier psychologiques (campagnes de presse, information, degré de culture des individus, intérêt pour l'aéronautique, âge, sexe),

- l'habituation au bang si tant est qu'elle puisse exister lors d'exposition à des bangs d'avions militaires, très irréguliers dans leur présentation, ne paraît pas impliquer l'acceptation du phénomène : ainsi il est caractéristique d'observer que les populations les moins disposées a considérer comme admissibles les bangs reguliers qui résulteraient des vols supersoniques des avions commerciaux sont celles qui ont été le plus fréquemment soumises au bang des avions militaires.

De cet ensemble il semble que l'on puisse tirer les conclusions suivantes :

- le bang tel qu'il est ressenti sous la trace de l'avion ou à son voisinage, d'intensité moyenne de 50 à 65 Pascals (pour un avion militaire) avec une probabilité importante de crêtes de pression d'intensités supérieures et un temps de montée en pression tantôt important (quelques millisecondes) et tantôt court (de l'ordre de la milliseconde) entraînera une proportion de réactions de sursaut non négligeable,

- les bangs d'extrémité de tapis peu intenses et mal formés ne doivent provoquer que peu (ou pas) de réactions de sursaut,

- les bangs de focalisation très intenses et généralement bien formés seront mal supportés.

7.3 Effets sur les structures et les bâtiments

Les effets du bang sur les structures et les bâtiments ont fait l'objet de très nombreuses études : études en laboratoires pour déterminer les seuils d'endommagement par action d'ondes isolées ou par fatigue d'éléments de construction. études du comportement de bâtiments et de structures lors de campagnes d'essais en vol ou lors du survol par des avions militaires, étude du comportement des monuments historiques, analyse des plaintes émises lors des vols d'entraînement des avions militaires.

Une analyse complète et générale des effets du bang sur les éléments de structure est délicate ; en effet ceux-ci sont soumis à une onde externe déjà rendue complexe en raison des réflexions qu'elle a subies sur le bâtiment considéré et dans son voisinage (figure 33) et qui induit à l'intérieur des locaux un champ de pression fonction des ouvertures (fenêtre, toiture), et des dimensions du local.
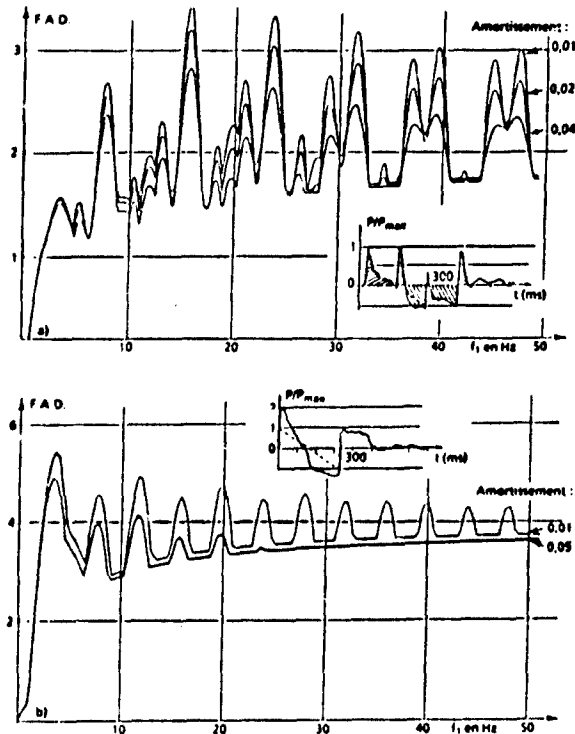

Fig. 33 - Influence de la présentation du bang sur le facteur d'amplification dynamique caractérisant son action. (Réf. 5/1).
a) facteur d'amplification dynamique pour la signature résultant d'une onde en N inclinée réfléchie sur un bâtiment haut ; b) facteur d'amplification dynamique pour la signature résultant d'une onde en N frappant normalement un bâtiment haut.

Les essais de laboratoire montrent que le seuil d'endommagement de structures saines et convenablement montées (plafonds, cloisons légères, vitres) se situe généralement aux environs de 2000 à 3000 Pascals pour des expositions à un bang unique et donc bien au-delà du niveau habituel du bang, même compte tenu de l'amplification qui peut résulter des phénomènes de résonance acoustique internes aux locaux ; toutefois des désordres légers, par effet de fatigue, peuvent apparaître sous l'action de bangs répétés à des niveaux d'intensité moindres (200 ou 300 Pascals). Le bang paraît donc n'avoir d'action que sur des structures vieillies ou soumises à des contraintes anormales ou encore mal conçues, le risque est alors d'autant plus grand que le bang est plus intense (bangs focalisés).

D'une manière générale, l'effet du bang sera d'autant plus sensible que sa fréquence fondamentale sera voisine de la fréquence propre de la structure considérée et de la fréquence de résonance du local ou de l'ensemble de la série de locaux communicants où elle se trouve placée.

Les mesures faites sur le terrain lors du vol d'avions militaires en vol stabilisé montrent que le plus souvent, le bang n'induit pas de sollicitations d'un niveau supérieur à celui induit par d'autres sollicitations (vent, vibrations dues à la circulation routière) ; toutefois son action est assez spécifique et est plus prononcée sur certaines structures telles que certains types de plafonds.

Parallèlement à ces effets sur les structures, il faut également tenir compte des bruits engendrés par les vibrations d'objets (vaisselle par exemple) dont le principal inconvénient est la gène auditive qui en résulte.

Le bang apparaît en définitive comme une agression qui s'ajoute aux autres résultant de l'environnement (vent, tempête, circulation, cycles thermiques, gesticulations diverses tels que sauts, claquements de portes ...), mais qui parfois a un effet assez spécifique. Il ne paraît pas avoir d'action significative, même par fatigue sur les constructions saines mais peut être cause de désordres intéressant des éléments de construction mal entretenus ou mal montés ; de manière exceptionnelle, les désordres peuvent s'étendre à l'ensemble de la construction.

Compte tenu de ce caractère "anormal" des dégâts dus aux bangs, il paraît difficile de fixer un seuil d'admissibilité en la matière. On ne peut que se reporter aux statistiques concernant les plaintes (nombre, gravité) résultant des survols des avions militaires avec la réserve importante qu'il est difficile d'associer à un dommage déterminé un niveau de bang, compte tenu de la précision insuffisante de la connaissance que l'on a alors de la trajectoire précise suivie par l'avion émetteur et de la manoeuvre qu'il a pu exécuter. Il semble que seuls des bangs violents (bangs focalisés ou des bangs émis à trop basse altitude) puissent être causes de désordres significatifs.

8. Conclusion

La connaissance que l'on a du bang et de ses effets paraît suffisante pour les besoins pratiques de la préparation des vols militaires même si certains progrès demeurent souhaitables : on sait calculer la position au sol des zones où seront ressentis des bangs, celle des zones où risquent d'apparaître des focalisations ; on sait prévoir une intensité nominale du bang et sa répartition à l'intérieur du tapis de bang et l'expérience nous donne un ordre de grandeur des dispersions à attendre par rapport à ces valeurs calculées. Le calcul ne permet pas de préciser l'intensité des bangs focalisés mais l'expérience nous renseigne assez bien là-dessus même si les données intéressant la superfocalisation demeurent insuffisantes. Il est difficile de préciser les conséquences pratiques des réactions de sursaut résultant du bang mais on sait que, compte tenu notamment de la dispersion des bangs en niveau de crête et en temps de montée, le bang perçu sous trace de l'avion sera cause d'un certain nombre de telles réactions et de ce fait constituera une gêne d'autant plus grande que l'avion sera plus lourd ou volera plus bas. Ce type de gêne ne devrait plus être ressenti en extrémité latérale de tapis. Bien qu'il soit difficile d'en apprécier l'importance, on sait que les bangs focalisés risquent d'être causes de dommages aux structures vieillies ou mal entretenues.

Le survol supersonique des terres par des avions militaires peut n'être pas toujours évitable : de tels vols doivent alors faire l'objet d'une préparation attentive ; la difficulté de cette préparation provient des incertitudes liées à la connaissance de la météorologie et à celle du détail précis de la trajectoire que suivra l'avion. Les règles qui guident une telle préparation sont évidentes : altitude de vol élevée, positionnement des zones susceptibles d'être affectées par des focalisations en des régions inhabitées, trajectoires rectilignes placées au-dessus de zones aussi peu peuplées que possible, minimisation des portions de trajectoires parcourues à nombre de Mach faiblement supersonique afin d'éviter les risques de focalisations imprévues.

Le plus souvent les vols supersoniques s'effectueront au-dessus de l'océan, en ce cas également des précautions devront être prises pour éviter l'émission de bangs vers la terre en particulier au cours de la phase de décélération finale.

BIBLIOGRAPHIE

1/ ASPECTS THEORIQUES ET NUMERIQUES - ASPECTS GENERAUX

[1]   K.J. PLOTKIN
        Review of sonic boom.
        AIAA 89-1105 (1989).

[2]   J.C. WANNER
        La propagation atmosphérique du bang sonique.
        Revue d'Acoustique n° 40 (1977).

[3]   A. JAUMOTTE
        Chocs et ondes de choc. Tome II : Applications Techniques.
        Chapitre 2 : Le bang des avions supersoniques.
        Masson (1973).

[4]   D.J. MAGLIERI, H.W. CARLSON, H.H. HUBBARD
        Status of knowledge of sonic booms.
        Noise and Control Engineering, vol. 15 (1980).

[5]   W.D. HAYES, R.C. HAEFELI, H.E. KULSRUD
        Sonic boom propagation in a stratified atmosphere with computer programm.
        NASA, CR 1299 (1969).

[6]   A.D. TAYLOR
        The traps sonic boom programm.
        NOAA T.M. ERL ARL-87.

[7]   L. BOBIN, A. DANCER, G. PARMENTIER, M. SCHAFFAR, C. THERY
        Les ondes aériennes et leurs effets : résumé de vingt cinq années d'activité
        (1959-1984).
        Notice bibliographique ISL NB 401/85 (1985).

[8]   J.C. WANNER, J. VALLEE, C. VIVIER, C. THERY
        Theoretical and experimental studies of the focus of sonic booms.
        JASA, vol. 52 (1972).

[9]   C. THERY
        Réfraction atmosphérique et réflexion au sol des bangs.
        AGARD CP 42 (1969).

[10]   C. THERY, M. PORBOSE, P. RIGAUD, G. SCHULTZE
        Ondes de choc faibles : revue des travaux effectués à l'ISL en matière de bang
        (A 61 - 1970).
        Notice ISL NB 1171 (1971).

[11]   C.M. DARDEN
        Charts for determining potential minimum sonic boom over-pressures for supersonic
        cruise aircraft.
        NASA TP 1820 (1981).

[12]   C.M. DARDEN
        Minimization of sonic boom parameters in real and isothermal atmospheres.
        NASA TN D. 7842 (1975).

[13]   H.W. CARLSON
        Simplified sonic boom prediction.
        NASA TP 1122 (1978).

[14]   M. SCHAFFAR, C. THERY, F. SCHLOSSER
        Calcul de la propagation géométrique du bang sous trace dans le cas d'atmosphères
        réelles avec vents.
        Rapport ISL 37/71 (1972).

[15]   M. SCHAFFAR, F. SCHLOSSER
        Influence des conditions météorologiques et de leur précision sur la position au
        sol du tapis de bang (extinction, focalisation sous trace).
        Rapport ISL 19/73 (1973).

[16]   M. SCHAFFAR, M. PFISTER, J.J. BRUNNER
        Etude expérimentale de la réfraction d'une détonation balistique dans une
        atmosphère stratifiée.
        Rapport ISL 18/73 (1973).

[17]   M. SANAI, T.Y. TOONG, A.D. PIERCE
        Ballistic range experiments on superbooms generated by refraction.
        JASA, vol. 59 (1976).

[18]   C. THERY, A. PETER, M. PFISTER
        Interaction entre bangs et obstacles.
        Notes Techniques ISL T2/70 et T9/70 (1970).

[19]   A. PETER, C. THERY, J.C. BRUNNER, F. SCHLOSSER
        Interaction du bang et d'une nappe d'eau.
        Rapport ISL 31/71 (1971).

[20]   C. THERY, C. LECOMTE, P. SMIGIELSKI
        Quelques résultats de calcul et d'expérience concernant les bangs de
        focalisation.
        Note Technique ISL T 28/70 (1970).

[21]   C. THERY, C. LECOMTE, F. REGGIANI
        Remarques concernant les renforcements du bang des avions supersoniques au
        voisinage des zones de focalisation.
        Note Technique ISL T 51/68 (1968).

[22]   A. AURIOL, C. LECOMTE, C. THERY
        Le problème du bang sonique pour de futurs avions de transport à haute vitesse.
        Note Technique ONERA 1990-3.

[23]   C. DRIVER, D.J. MAGLIERI
        The impact of emerging technologies on an advanced supersonic transport.
        Eagle Engineering Corp. (1987).

2/ MESURES

[1] J.O. POWERS, J.M. SANDS, D.J. MAGLIERI
Survey of United States sonic boom overflight experimentation.
AGARD CP 42 (1969).

[2] G.T. HAGLUND, E.J. KANE
Flight test measurements and analysis of sonic boom phenomena near the shockwave extremity.
AIAA Paper 74-62 (1974).

[3] E.G. STANSBERY, J.F. STANLEY
Descent sonic boom measurements for STS 26 including a Mach 23 measurement.
NASA JSC 23-579 (1989).

[4] G.A. HERBERT, W.A. HASS, J.K. ANGEL
A preliminary study of atmospheric effects on the sonic boom.
AGARD CP 42 (1969).

[5] M. FROBOSE, G. PARMENTIER, G. MATHIEU, R. RIGAUD, G. EVRARD
Bang sonique de Concorde 001. Enregistrement des variations de pression au sol.
Rapport Technique ISL RT 3/72 (1972).

[6] G. PARMENTIER, G. MATHIEU, D. SEYDEL, A. PETER
Bangs soniques de Concorde 001 en vols rectilignes à vitesse constante.
Notice ISL SN 11/70 (1970).

[7] G. PARMENTIER, G. MATHIEU, M. SCHAFFAR, C. JOHE
Bangs soniques de Concorde : enregistrement hors trace des variations de pression au sol.
Rapport Technique ISL R 19/73 (1973).

[8] M. SCHAFFAR, F. SCHLOSSER
Calcul de la propagation du bang en atmosphère réelle : position géométrique de la focalisation pour la loi de montée de Concorde, intensité du bang au voisinage des extinctions longitudinales et latérales.
Rapport ISL 11/74 (1974).

[9] M. SCHAFFAR, B. MASURE
Résultats d'intensité du bang sonique au voisinage de l'extinction latérale concernant les deux vols de Concorde dans les Landes.
Rapport ISL 9/74 (1974).

[10] G. PARMENTIER, G. MATHIEU, D. SEYDEL, H. KRANZ
Bangs soniques de Mirage III et Mirage IV en vol rectiligne accéléré ou en virage.
Etude de focalisations - Opération Jéricho Carton.
Rapport ISL 17/70 (1970).

[11] M. FROBOSE, G. MATHIEU, D. SEYDEL
Knalle und geräusche von starfightern und andere Quellen an Bodenpunkten und Hauswänden registriert.
Rapport ISL 1/70 (1970).

[12] P. PERROUD, C. LECOMTE
Opération "Bangavalanches". The sonic boom effect on avalanches.
IAHS Publ. n° 162 (1987).

[13] J. VALLEE
"Opération Jéricho Carton" - Essais de focalisation et de superfocalisation de bangs soniques.
Rapport d'étude CEV n° 291 (1972).

[14] C. LECOMTE, C. MARTIN
Vol d'endurance du Concorde ; comparaison des résultats de mesure d'intensité du bang avec le calcul.
ONERA. Rapport n° 11/7145 CY (1977).

[15] C. LECOMTE, C. MARTIN
Concorde. Campagne de mesure à Aurigny : comparaison des mesures d'intensité du bang avec le calcul.
ONERA. Rapport n° 13/7145 CY (1977).

[16] J.C. WANNER
Essais Mirage IV.
AGARD CP 42, Paper 14 (1969).

(Voir également Références 1/4 et 1/7).

3/ EFFETS PHYSIOLOGIQUES ET PSYCHOLOGIQUES DU BANG

[1]   H. VON GIERKE, C.W. NIXON
      Human response to sonic boom.
      AGARD CP 42 (1969).

[2]   J. BREMOND
      Préjugés envers le bang supersonique et leurs corrélatifs dans la population de
      deux régions de France.
      Compte rendu du Colloque qui s'est tenu à l'ISL du 18 au 20 octobre 1967, portant
      sur les bangs et leurs effets.
      Rapport ISL 11/67 (1967).

[3]   "ANONYME"
      Human response to sonic boom : a research program plan.
      FAA rpt 70-2 (1970).

[4]   R. RYLANDER, A. DANCER
      Startle reactions to simulated sonic booms : influence of habituation, boom level
      and background noise.
      Journal of Sound and Vibrations, 61 (1978).

[5]   K. BUCK, A. DANCER, M. HARTMANN
      Etude du sursaut provoqué chez l'homme par le bang sonique.
      Rapport ISL R 114/77 (1977).

[6]   A. NIEDZWIEKI, H.S. RIBNER
      Subjective loudness of "minimized" sonic boom wave forms.
      JASA, 64 (1978).

[7]   G. JANSEN
      Beeinflussung des Nachtschlafs durch Flugzeug Knall.
      Rapport ISL 2/74 (1974).

[8]   G. JANSEN, B. GRIEFAHN
      Experimentelle Untersuchungen zum Problem der Schlafstörungen durch überschall
      Knall.
      Rapport ISL 21/74 (1974).

4/ SIMULATION DU BANG SONIQUE

[1]   C.H.E. WARREN
      The simulation of sonic bangs.
      AGARD CP 42 (1969).

[2]   I. SCHWARZ
      Sonic boom simulation facility.
      AGARD CP 42 (1969).

[3]   C. THERY, A. PETER, F. SCHLOSSER
      Le générateur de bangs de l'ISL.
      Rapport ISL 15/71 (1971).

[4]   M. FROBOSE, G. MATHIEU
      Générateurs portables d'ondes en N de différentes puissances pour la simulation
      du bang.
      Rapport ISL R 123/75 (1975).

V/ EFFET DU BANG SUR LES STRUCTURES

[1]   D. MULE
      Le bang supersonique : effets sur les structures : synthèse des études effectuées
      par le CSTB.
      Cahiers du Centre Scientifique et Technique du Bâtiment n° 186 (1978).

[2]   G. WEBER
      Probability of aircraft noise and sonic boom induced building dammage.
      AGARD CP 42 (1969).

[3]   C. JOHE
      Détermination du seuil d'endommagement de cloisons légères exposées à des bangs
      unitaires ou répétés.
      Rapport ISL 31/73 (1973).

[4]   C. JOHE, J. ROLLAND, G. PARMENTIER
      Etude expérimentale du comportement d'éléments de vitraux soumis au bang.
      Rapport ISL 34/73 (1973).

Discussion

QUESTION BY: L.W. Illston, BAe, UK
Is there likely to be a level of overpressure which does not cause annoyance, and if so, what level do you think it is?

AUTHOR'S RESPONSE:
L'effet le plus caractéristique du bang réside dans le sursaut qu'il provoque. Ainsi que cela a été exposé, la réaction de sursaut se prête assez bien à une analyse quantitative (amplitude, fréquence) même si les résultats obtenus par les différents expérimentateurs varient en fonction du contexte des essais (nature des tests retenus, degré de préparation des sujets, nature des simulations, ambiance générale des essais). Ainsi on pense généralement qu'une onde qui a une intensité de 30 ou 35 pascal et un temps de compression de quelques millisecondes ne devrait plus provoquer de réactions de sursaut lors qu'elle est perçue en champ libre; supposons, ce qui n'est en rien prouvé actuellement, qu'il en soit de même á l'intérieur des habitations, une telle onde aurait perdu la seule caractéristique réellement néfaste des bangs mais demeurerait bien perceptible et ferait encore vibrer portes et fenêtres: Rien ne permet aujourd'hui d'affirmer qu'une telle onde serait jugée tolérable dans le contexte des vols réguliers des transporteurs supersoniques commerciaux (le cas du bang isolé d'un avion militaire est different). On peut rappeler à ce propos que les trajectoires de Concorde ont été modifées afin de minimiser le perception en Grande Bretagne des bangs secondaires qui sont pourtant d'une intensité bien moindre, de l'ordre de la fraction de pascal.

QUESTION BY: U. Michel, DLR Berlin, Germany
1. You mentioned that the pressure difference depends on the weight of the aircraft. There are papers that express hope that the pressure difference can be reduced by design changes of the aircraft. What is your opinion about this?
2. Would these changes of the waveforms not vanish due to the nonlinear effects in long range propagation?

AUTHOR'S RESPONSE:
En allongeant l'avion et en modifiant la répartition de forces de portance agissant sur l'avion il est possible de modifier la signature du bang de telle sorte que celui-ci parvienne incomplètement formé au sol. L'effect de surprise

: 12 (Continued)

qui dépend de l'intensité du front de choc initial sera alors atténué. Le NASA et Boeing out beaucoup travaillé sur ce sujet. Dans l'état actuel du savoir faire, des avions ainsi optimisés du point de vue du bang qu'ils émettent présentent l'inconvénient de traîner davantage et de poser des problèmes structuraux et par suite pèsent plus lourds à mission donnée (charge utile, rayon d'action); on reperd ainsi partiellement l'avantage d'une signature plus favorable.

Il faut observer aussi que si la gène sous trace et en champ libre peut être ainsi théoriquement être fortement atténué, cela est moins clair à l'intérieur des habitations et latéralement. Des études sur ce thème sont menées en préparation des générations futures de transporteurs supersoniques civils.

Il est clair que les modifications à apporter aux formes aérodynamiques sont d'autant moins importantes que l'altitude de vol est plus faible et certaines études (chez Boeing en particulier) tendent à rechercher le meilleur compromis possible (forme aérodynamique-altitude-Mach de croisière) conduisant à un bang au sol d'intensité et forme données.

Il est trés peu vraisemblable que ces études trouvent pleinement leur application pour la prochaine génération de transporteurs supersoniques d'une part parce que les modifications de formes nécessaires pour atteindre le but visé apparaissent trop profondes et les pénalités correspondantes trop lourdes et d'autre part parce qu'en l'absence d'un consensus sur des formes d'ondes admissibles, qui ne parait pas dépendre uniquement de considérations objectives, le succès d'une telle operation ferait incertain.

QUESTION BY: H. Dean, HQ USAF, USA

Mention was made of habituation to sonic booms. I am not aware of definitive studies on the degree to which people accomodate to sonic booms. What were the overpressure levels that were used in your studies on people and animals and what levels did you require to cause damage in new and old building and new and old glass?

AUTHORS RESPONSE:

Les études concernant l'habituation chez l'homme ont été assez nombreuses: May et Rice (coups de pistolet, Southampton, 1971), Chatelier, Rylander et Dancer (bangs soniques, Ile de Gotland, 1972), Chatelier (Simulation de bang, Mont de Marsan, 1976), Buck et Dancer ainsi que Rylander et Dancer (Simulateur de bang, St. Louis, 1977 et 1978). Les phénomènes observés sont chaque foic semblables.

Les séries expérimentels les plus complètes paraissent être les dernières: elles mettent en oeuvre des bangs simulés d'intensités comprises entre 100 et 200 pascals et de 1 á 5 millisecondes de temps de montée, elles montrent un très net phénomène d'accoutumance atteint en général vers le dixième bang perçu, sans pour autant que les réactions de sursaut disparaissent complètement. Par example pour certains tests le taux de reactions de sursaut tombe 100 % pour le premier bang à 25 % pour le deuxiéme bang et se maintient à cette valeur pour les bangs ultérieurs. Pour d'autres tests c'est sur l'amplitude du mouvement résultant de l'effet de surprise qu'on fera une constation analogue. Des phénomènes assez analogues ont été mis en évidence chez les animaux en particulier pour les élevages de volailles (Pr. Cottereau, Ecole Vétérinaire de Lyon).

PAPER NO. : 12 (Continued)

Concernant les effects sur les constructions, si l'on écarte les études de laboratoires qui sont fort complètes mais qui ne concernent que des élémentes de construction isolés, on ne peut se référer pour des constructions complètes que à deux types d'experimentation: les premiers concernent des constructions neuves, réalisés pour les besoins de l'étude, dotées d'éléments jugés particuliérement sensibles à l'action du bang (plafonds suspendus, cloisons légères...) et de volumes intérieurs en résonnance avec le bang externe qui sont survolées à altitude variable par des avions supersonique (par example Operation Jericho-Casbah, Istres, 1972), les seconds concernent des constructions anciennes situées en dessous des trajectoires d'entrainement des avions militaires (par example: campagne d'analyse du comportement des monuments historiques exposés au bang, faite par le CSTB dans les années 1970): dans le premier cas, on maîtrise le niveau d'intensité des bangs et on observe des dégradations significatives à partir de quelques centaines de pascals dans le second cas les bangs incidents ont toujours des intensités voisines (60 à 65 percels), aucune dégradation n'est observée et on mesure des niveaux de déformation sur les éléments de structure qui, à quelques exceptions près sont comparables à celles dues à l'action d'autres types de sollicitation. Il est alors difficle de déterminer pour quelle intensité de bangs des dégradations apparaitraient.

A BRIEF REVIEW OF THE SOURCE NOISE TECHNOLOGY APPLICABLE TO FIXED-WING MILITARY AIRCRAFT

by

R.A. Pinker

DRA Aerospace Division
RAE
Pyestock, Farnborough
Hampshire GU14 0LS
United Kingdom

1 BACKGROUND

Although the last two decades have seen major reductions in the noise from civil aircraft, that from military operations both around airfields and from low-flying aircraft continues to be a source of irritation and a potential health hazard. As a consequence a pilot study on Aircraft Noise was established in 1985, jointly piloted by Germany and the United States, under the auspices of NATO's Committee on the Challenges of a Modern Society (CCMS). Its brief was to assess the scale of the problem, particularly with respect to military aircraft noise, and to propose remedial measures. Sub-groups, comprising of Government officials from interested member nations, were thus set up to study the areas of

> Source technology - possibilities of reducing noise at source, and
>
> receiver technology - mitigating the nuisance on the ground, and
>
> operations and information.

To assist in the preparation of the reports from the Pilot Study sub-groups, two conferences involving international experts were held. The first, which was broadly based and of interest to all sub-groups, was held at Mittenwald in Germany in September 1986. The second, at Williamsburg in April 1988, was specifically targetted at source noise technology and took the form of briefings by industry representatives on their perspective as to the future of military aircraft noise and the potential for mitigating it. This second conference also provided a venue for detailed discussions between these representatives and the members of the Source noise sub-group.

The reports[1,2] from the Pilot study group were subsequently produced drawing upon the information presented at these conferences, the views expressed during the subsequent discussions, the available literature and the knowledge of the sub-group members.

Because of the continuing concern about the noise levels produced by combat aircraft, the following paper is intended to provide some of the background to the main conclusions and recommendations reached in the final report of the NATO/CCMS Pilot Study on AIRCRAFT NOISE IN A MODERN SOCIETY Number 185[2]. Although biased towards fixed wing combat aircraft noise, the present paper also considers other fixed wing military aircraft but specifically excludes sonic booms and rotary wing aircraft as they both have their own particular noise sources and problems.

2 INTRODUCTION

Historically, civil aircraft have been required to meet ever tightening international standards, namely ICAO Annexe 16[3] in Europe and FAR part 36[4] in the United States and as a result the noise levels for new civil aircraft entering service have dropped by almost 20 dB[5] as shown in Fig 1. This was initially due to the change from turbo-jets (or low-bypass ratio engines) to the modern high-bypass ratio engines[6] such as the RB211,JT9 and CF6. The impetus behind their development was primarily for greater propulsive efficiency but the associated move towards lower specific thrusts, that is thrust provided by greater mass flows and lower exhaust velocities, reduced the dominance of the jet mixing noise and this trend is evident from Fig 2. Further advances in noise reduction technology, driven by tighter legislation, and coupled with the gradual retirement of the older and noisier jets has thus significantly improved the noise climate around civil airfields.

Unfortunately the trend for high-performance combat aircraft is towards engines of high specific thrust to give the aircraft increased agility and to enable them to operate at high flight speeds (exhaust velocity must exceed flight speed). A measure of this growing disparity between civil and military aircraft noise in the airfield environment can be judged from Fig 3 which shows "certified" noise levels for various aircraft[7]. Civil aircraft can be up to 20 dB quieter than a military aircraft of the same weight but they are usually not capable of the same missions.

3 NOISE SOURCES

Although military and civil aircraft engines share many common noise sources, the sources which dominate differ as can be seen from the diagrams in Fig 4. Some of these sources are more amenable to treatment than others and thus depending upon their nature and the engine application, significantly different noise levels are produced. The low-bypass-ratio engine is a high specific-thrust engine and typical of those fitted to most modern combat aircraft.

During take-off its noise is dominated by the jet noise whereas that of the high-bypass-ratio engine with its lower specific-thrust tends to have all the sources roughly of equal magnitude. This is a general feature of civil power plants and arises from the fact that to achieve low noise signatures no one source should be allowed to dominate.

In order to understand the various problems associated with military aircraft noise, it is best to start with a description of the noise sources and effects involved.

3.1 Jet mixing noise

Jet mixing noise is the source synonymous with the public's image of jet aircraft and is generated by the high-velocity exhaust gases from the engine shearing and mixing with the surrounding atmosphere. The sources are external to the engine forming a region approximately 10 nozzle diameters long. The noise is highly sensitive to changes in the exhaust velocity[7] as is evident from Fig 5 showing how the noise from a single-stream jet varies with exhaust velocity.

The reduction in gradient at the very high velocities arises both from changes in the magnitude of the convective amplification of the quadruples and another source, eddy-mach-wave radiation, coming into play[8]. This additional source starts to appear when the convection speeds of the eddies in the mixing region become supersonic relative to the surrounding atmosphere and radiate noise as miniature "sonic booms". It is not easy to distinguish this radiation from jet mixing noise and theory[8] suggests that it can be normalised using the same parameters as the mixing noise. However these conditions are significantly in excess of the generally available data base for jet mixing noise[9] and thus the prediction of existing and future engines at extreme conditions may be subject to error.

The jet mixing noise associated with high-bypass-ratio engines behaves in a similar manner[10] but is complicated by the two concentric exhaust streams which aerodynamically interact to modify the noise source regions. With these engines the noise is generally dominated by the core jet flow even after allowing for the blanketing effect of the lower velocity bypass flow. Quieter exhaust systems have been developed for these high-bypass-ratio engines which forceably mix the two flows inside the engine and if correctly designed, this results in reduced jet noise together with improved performance. A further advantage is that a greater area, in a benign environment, is available for fitting noise absorbent linings to reduce internally generated noise.

Finally, since the jet mixing noise is a function of the shear gradient, its source strength will reduce with increasing flight speed[11] often exposing the other sources.

For single-stream and low-bypass-ratio engines other than by the reduction of velocity, suppression with low thrust losses is generally difficult since the actual source

noise region is external to the engine and extends for many nozzle diameters downstream.

3.2 Shock noise

Shock cells are formed in the engine exhaust when the jet is under-expanded, that is when the exhaust flow becomes supersonic relative to the local conditions. For exhaust systems fitted with convergent nozzles this occurs when the exhaust pressure ratio exceeds the critical pressure ratio of around 1.9. These cells produce two different forms of acoustic radiation, shock cell screech and shock associated noise.

Shock cell screech is generated by the oscillation of the train of shock cells due to positive acoustic feedback around the jet[12]. Although exhibited strongly by model jets as intense tones, especially when cold, this mechanism is not so dominant with the turbulent hot flow from real engines. Up to now, screech has only really been of concern to the structural engineer since the necessary pressure ratios have usually been achieved at high flight Mach numbers. However future combat aircraft will be fitted with engines having exhaust pressure ratios significantly above choking at take-off.

Shock associated noise is the open loop equivalent of screech whereby broadband noise is generated by spatially coherent turbulence in the jet producing pressure pulses as it passes though the quasi-periodic shock cell structure[13]. It is dependent on pressure ratio and not velocity as can be seen from Fig 6 which shows the variation of noise intensity with a Mach number function.

Reductions in both shock noise sources can be best achieved by using a matched convergent-divergent nozzle to correctly expand the exhaust gases and prevent formation of the shock cell train. The level of the jet mixing noise in the figure has been achieved by this means. Complete elimination is unlikely with full-scale engines, even with an active variable nozzle system, since the mechanical difficulties make it virtually impossible to achieve perfectly expanded flow over a wide range of pressure ratios. However useful reductions may be possible and although these nozzles are heavy and complicated by the requirement for area variability for reheat, they offer potential improvements in performance.

Other techniques found useful at model scale to reduce shock cell screech, such as breaking up the structure by the insertion of fingers or negative feedback have not been successfully employed on real engines.

Flight has little direct affect on the source strength[14] although as the flight speed increases, more of the noise radiates forward of the aircraft by a phenomenon known as convective or Doppler amplification. All sources in motion undergo this process but it tends to be more identified with sources, as here, which are directly linked with the motion of the aircraft.

3.3 Turbomachinery noise

This is generated by the rotating and static aerofoils or blades within the engine which form the fan, compressor and turbine[15,16] by three quite separate noise mechanisms.

Dealing first with the random or broadband noise, the individual blades produce this noise through random lift fluctuations on their surfaces caused both by upstream turbulence producing variations in blade incidence and by random vortex shedding at the blade trailing edge. This latter mechanism is less powerful and is observed in fans having no guide vanes or supports upstream of the rotating stage.

Discrete or tone noise is produced by cyclic lift fluctuations on the blades caused by the blades of one row interacting with the wakes and potential flow fields of the adjacent rows. Distortion in the fan inlet flow will also give rise to tone noise. The tone levels can be reduced by increased spacings between the stages, albeit at the expense of increased length and hence engine weight. Also by the judicious choice of blade and vane numbers, it is possible to prevent the propagation of some tone frequencies by a mechanism termed "cutoff".

With fans having supersonic tip speeds an additional source buzz-saw noise is evident[17], arising from differences in the shock waves on the individual blades but by careful matching of blades this source can be reduced.

Thus on civil high-bypass ratio engines turbomachinery sources are of major importance but by good design it is possible to reduce the levels of turbomachinery noise and because all the sources lie within the engine the externally propagating noise can be further reduced by the fitting of acoustic linings. However with combat aircraft the smaller fan size and buried installation means that these sources should not be a major problem.

3.4 Combustion noise

This noise is generated both directly and indirectly by the combustion processes[18], directly as local pressure fluctuations in the burning zone and also indirectly from the downstream turbomachinery as a consequence of fluctuations, both temperature and pressure, incident upon it. These mechanisms should not be a problem with high-specific-thrust engines, even though they are present in the reheat process, as their magnitudes are considerably less than the noise of the jet exhaust. With the larger bypass-ratio civil engines, the noise is detectable under certain conditions but the levels are sufficiently low as not to cause concern.

3.5 Airframe noise

Although airframe noise is not an engine source it is a potentially important mechanism. It is a general term and covers the noise generated by the airframe and deployed structure, such as the landing gear and flaps, which generate extra turbulence[19]. For clean airframes the mechanisms are believed to be principally due to trailing edge noise, that is noise caused by the convection of wing turbulent boundary layers past the wing trailing edge. Although significant reductions can be achieved by cleaning up the airflow around the deployed structures, as can be judged from Fig 7, little can be done about the underlying mechanisms which are a function of the aircraft size. This noise is not likely to be a problem with combat aircraft in airfield operations due to their low speed and small physical size, but it will contribute to their signature in high-speed low-altitude operations especially when fitted with external stores and munitions.

At very low altitudes and high speeds, the noise can also be felt as the lift pressure pulse due to the aircraft presence passes. This results in sub-audible pressure fluctuations[20] as shown in Fig 8.

3.6 Absorptive treatments

The advent of the high-bypass-ratio prompted the widespread use absorptive treatments[21] because of the increased magnitude of noise sources, within the engine and the greater area, available for treatment. Two basic mechanisms are exploited in their use. Reactive effects whereby the incident wave is cancelled locally by the reflected wave and is highly frequency dependent. And resistive effects, which are broader band in their response, caused by the instantaneous motion of the air through the material dissipating the sound energy as heat. In practice combinations of these two approaches are used and are targetted at particular problem sources. By their judicious use reductions of up to 10 dB in the radiated internal noise can be achieved.

3.7 Installation effects

The installation of an engine into an airframe can cause substantial changes in the apparent behaviour of the engine sources[23]. Four fundamentally different types of mechanism can be present. The three that can be observed statically[24], that is without forward motion, are illustrated for an under-wing installation in Fig 9. First an acoustic interaction which in its simplest form is reflection from the adjacent aircraft structure such as the under-surface of a wing but it can also occur as scattering of the acoustic wave by an edge. This is particularly applicable with compact highly directional sources such as internal noise. Secondly noise can be generated by the presence of a surface close to but not actually in the jet flow. This is because the surface in the near-field inhibits the normal cancellation processes that occur when the sound propagates into the far-field. Thirdly, noise will be generated by the jet if it impinges upon a surface such as the wing-flaps.

Finally the noise from a jet will be increased in flight due to flight stream turbulence entering the jet. Fig 10 shows the results from research tests[25] on a model of a military trainer aircraft operated both statically, that is with no forward motion, and at a modest simulated flight speed. Statically the effects for the presence of the model are small but in flight substantial increases are observed at large angles from the jet axis while in the rear arc the full flight reduction for clean jets is almost achieved. This forward arc increment is likely to increase with flight speed and thus become significant with combat aircraft operating at high subsonic flight speeds.

4 PROSPECTS

Since the spectrum of military aircraft types and their associated missions are considerably more diverse than their civil counterparts. It is best to consider the peace-time noise problem under four main headings, first support aircraft, second combat aircraft in the airfield environment, third combat aircraft training at low-level and finally special category aircraft.

4.1 Support aircraft

In general the requirements of support aircraft such as tankers, AWACs, cargo, etc mirror their civil counter-parts. The technology improvements made in the civil sector to reduce fuel consumption, life-cycle costs, emissions (smoke) and improve reliability are all features that are of importance to the military operators. In addition these improvements have gone hand in hand with noise reductions brought about by the legal requirements to meet international noise regulations[3,4]. Thus available in todays market place are engines having all the necessary attributes for military use without the need to provide significant development funding.

Apart from the capital expenditure, which could be offset in some measure by reduced fuel and life-cycle costs, in principle there is no technical reason why the noise of support aircraft should not be significantly reduced. In some notable cases this has already been done and probably the best example is the USAF re-engining of the Boeing KC-135 tankers[26], where the fitting of CFM-56 turbo-fan engines has reduced the noise by 17 EPNdB (a footprint reduction of 98%) and produced an aircraft with increased range and no smoke. Other examples are the use, by the USAF and RAF, of modified civil airliners as tankers and general transports.

A possible cheaper alternative to re-engining, is the fitting of "hush kits" to existing powerplants[27]. The situa-tion is complex with a variety of manufactures making claims for their particular scheme; few have yet been flight tested for noise and performance. The latest designs, which utilise modified intakes, lined bypass ducts and internal mixers (or in some cases variable geometry), are said to offer the ability to achieve the latest certification levels. With civil operators facing even more stringent noise standards in the form of "local airport rules", the ability to just meet the certification levels may not be sufficient. The choice, by both civil and military alike, has then to be made on whether to "hush kit" an old engine or to buy, at greater expense, a more modern engine with all the extra benefits including the flexibility to operate into noise sensitive airports. In the limited military instances to-date, the pressure to reduce life-cycle costs and significantly improve performance has favoured re-engining rather than fitting hush-kits.

Either way the application of readily available civil technology can have a beneficial effect on the noise of support aircraft without any detriment in performance.

4.2 Combat aircraft in airfield environment

Of the various noise sources existing within the engine of a combat aircraft, it is evident that in the airfield environment, jet and shock noise are by far the most dominant sources in terms of level and probably cause the most complaints from the public. Unfortunately they are also the most difficult group of sources to silence even though the problem has been studied for many years.

A closely parallel problem to combat aircraft noise was the Concorde[28] with similar exhaust conditions, where in spite of an extensive research programme no simple universal silencer was found. Spade silencers developed on static ground rigs and engines were found to be ineffective in flight and discarded. The important lesson that was learnt was that silencer development must be carried out under representative conditions, that is, the engine exhaust conditions, flight speeds and geometries must be accurately simulated.

On the production engines squeezing of the jet during take-off gave about 3 dB attenuation for a relatively low thrust loss but this was restricted to a small azimuthal angle to the side of the aircraft. The most successful silencing technique employed during flyover and approach was a modification of the engine control system enabling the final nozzle to be enlarged thus passing more mass flow and reducing the jet velocity for a given thrust. The extent to which this latter technique can be generally applied depends on the characteristics of the particular engine involved but could offer benefits with minimal hardware changes. However none of these techniques enabled Concorde noise to be sufficiently reduced to the subsonic certification levels.

For the next and future generations of super-sonic transports (SSTs) meeting the noise certification targets is one of the most critical questions that must be answered. On-going research has produced several new ideas and developments of existing techniques such as "porous plugs"[29], "inverted profile jets"[30], "thermal acoustic shielding", "multi-tube" and "ejector" silencers.

While with some schemes the principle reductions are in shock noise, other schemes, such as mixers with downstream lined ejectors[31] reduce both jet mixing and shock noise and thus offer significant potential for commercial SSTs applications. A simplified example is illustrated in Fig 11.

An ICAO review[32] carried out in the early 1980s, of the then available noise technology for future supersonic transports, suggested that the latest technology could offer noise reductions of about 15 dB with an exchange rate of 3 dB per 2% of gross thrust but with an increase in all-up weight, see Fig 12. With all such schemes a measure of variable geometry is vital in the design to permit the silencer to be stowed for supersonic cruise and thus minimise cruise thrust losses. However for combat aircraft, the thrust loss, weight and mechanical complexity are likely to be unacceptable.

More recent work[33] is focussing on the use of variable cycle engines which enable gross changes in the engine cycle and geometry to be achieved. This form of engine, with little or no extra silencing, might then meet the diverse targets of low airport noise and good supersonic cruise performance. This approach is equivalent to having the benefits of a high-bypass-ratio engine in the airfield environment and a high-specific thrust mode for supersonic operation.

The use of such engines for commercial SSTs is dictated by the need to meet specific noise levels and as a result compromises in aircraft performance are made. For military applications these compromises may not be acceptable and unless the engines offer significant advantages elsewhere, the massive allocation in both money and manpower is unlikely to be committed on military noise grounds alone.

One option that has been considered is the "bolt on" silencer for peace-time use but like all silencers it must offer a better exchange rate of noise for thrust than the simple expedient of throttling back.

As well as direct reduction in source noise through engine design, improvements in airframe performance through increased lift/drag ratios do offer advantages. During take-off, the extra lift for a given drag and hence engine thrust will result in the aircraft climbing more steeply and hence reducing its noise impact on the ground. An alternative would be to use less thrust reducing the source noise while still maintaining the same flight profile.

Thus, for the near term future, increased specific thrusts mean more source noise with little hope for substantial silencing. However the improved airfield performance with new designs will mean that the noise impact on the community should not increase. Longer term prospects may be more favourable with the possible use of variable cycle engines.

4.3 Combat aircraft operating at low-level

In source noise terms, the noise from combat aircraft operating at low-altitude and at high subsonic speeds is complicated by the high flight speeds. Virtually all the knowledge that has been acquired over the last 30 years has been concerned with civil operations around airports and hence flight speeds have been limited to 0.3 Mach. At higher speeds, around 0.7 Mach, typical of training missions, the sources of noise involved are known but not which ones are dominant. Fig 13 illustrates the scale of the problem and the current state of our understanding based upon the simple extrapolation of existing data. Some of these sources may be amenable to treatment but it critically depends on which are dominant.

Schemes for reducing jet and shock noise such as ejector mixers, which appear attractive at the lower speeds, may not be suitable for these higher speed operations. Indeed from a closer examination of Fig 12, showing the ICAO findings for SSTs, it can be seen that the data for a Mach number of 0.4 suggests substantially poorer performance. It is the available net thrust from the engine that propels the aircraft, thus loses in gross thrust become more critical with increasing aircraft velocity. However other schemes such as increasing nozzle area could be beneficial but only to a limited extent and then depending upon which sources dominate.

Before even a start can be made on assessing what noise reduction methods may be possible, the breakdown of the sources needs to be known and their characteristics understood by means dedicated flight tests. In the past there have been relatively few known flight tests[34-39] investigating military noise and in the main these have been aimed at providing information for noise zoning and community responses. This form of information is inadequate to identify the sources as carefully structured and controlled flight tests are required.

Thus the first priority is for a series of dedicated flight tests to provide the necessary information. Judgements can be then be made as to future research programmes aimed at investigating potential silencing methods and techniques. Within the constraints imposed by lack of data, certain conclusions can be drawn regarding low-altitude training. It is likely that reductions in aircraft drag, brought about by reducing external stores, will enable the engine to operate at a lower power and hence reduce noise, tests are needed to confirm the magnitudes. Operating at higher altitudes reduces the noise on the ground, by about 6 dB per doubling of distance and is also likely to reduce startle. However due to propagation effects the levels to the side of the flight path can increase slightly. With our current state of knowledge it is difficult to forecast trends but it seems that both technological and operational means will need to be found to reduce the noise impact.

4.4 Special category

Within the military inventories are aircraft designed for very specific roles or functions and these have their own unique acoustic characteristics.

One such class of aircraft are those designed for low detectability. The measures employed to reduce observability, that is by employing buried, non-reheated engines with a mixed cool flow exhausting through slot nozzles[40], are all conducive to a low noise signature and hence reduced noise impact on the community. Although they might at first glance seem to have solved the noise problem, the compromise that has had to be made will have reduced their general performance making them suitable only for specialised missions.

Combat aircraft that have the capability of vertical take-off and landing (VTOL) such as the Harrier do have a serious noise problem. This stems from the use of a relatively high specific thrust engine to provide direct lift. Later generations may simply rely on increasing the thrust by reheating thereby exacerbating the problem or adopt alternative more benign concepts such as ejector lift[6]. Studies of these future designs have taken noise as a prime factor because of the problem of structural fatigue and to a lesser extent the ground crew environment. Fortunately, for the community, their ability to take-off and land vertically does mean that the noise can be confined within the airfield/operations boundary. However low-altitude training missions are likely to remain a problem.

5 RECOMMENDATIONS AND COMMENTS

The following recommendations were suggested in the Final Report on Aircraft Noise to the NATO/CCMS[2] for reducing at source the noise caused by fixed wing military aircraft.

(i)   The concept of "design for noise" must be incorporated into the design and development process for all future engine and aircraft types.

Although encompassing all types of aircraft and engine, this recommendation is primarily concerned with combat aircraft and proposes that specific noise requirements should form part of the general specification of any future project.

It is not intended that combat efficiency should be compromised but that noise at the very least should be taken into account. For example, future engine projects could be biassed towards the largest possible bypass ratio that will achieve the required role and not compromise performance. Even the quite small reductions obtained in exhaust conditions can mean significant changes in noise exposure and in the areas affected by a given noise contour.

(ii)   Wherever practical civil noise technology should be applied to fixed wing military aircraft where high speed and/or manoeuvrability is not a critical performance requirement.

It is considered that this should include all support role aircraft, for example transports, trainers, tankers and AWACs. Significant reductions in noise levels and community exposure have and should be achieved together with the potential for improved performance.

(iii)   Expand fundamental noise research for low-altitude/high-speed flight.

Since high exhaust velocities are inherent with high-specific-thrust engines there seems little hope for a satisfactory method of producing substantial noise reductions in the foreseeable future. The exhaust conditions and flight speeds are generally outside the data on which the present understandings are based and further studies may produce new insights enabling potential silencing techniques to be developed.

(iv)   Pursue the acquisition of a comprehensive data base on aircraft noise sources associated with high-subsonic flight speeds and the development of a concomitant prediction methodology.

Accurate prediction and understanding of the noise sources of future engines is limited by the extent of the present data bases. No real research information is available for source identification of aircraft operating at high-subsonic speeds. Until this is available, research cannot be focussed on reducing the dominant mechanisms.

(v)   Undertake investigations to better optimise aircraft design trade-offs, (including variable cycle engine concepts) to reduce noise associated with part-power operation of high-performance aircraft without sacrificing operational capability.

These studies represent a significant commitment in terms of resources and expenditure, thus before they can be realistically started they need the outcome from the research programmes aimed at identifying the dominant sources and their characteristics.

(vi)   Assess the potential of performing quieter training missions, particularly for low-altitude flight conditions, by reducing aircraft weight and drag (and therefore thrust) by eliminating/reducing external stores.

Although this recommendation borders on the operational aspects, it nevertheless represents a potentially simple and effective technique for reducing the source noise while still maintaining the flight envelope. However the removal of stores will invalidate the military's requirement to train with the same aircraft configuration as in a war scenario.

6.0 CONCLUSIONS

A start has been made on the reduction of military aircraft noise with the International recognition that there is a problem. However to reduce the impact on the community needs a positive commitment by the military to consider noise in all aspects of its activities, from the initial design studies for new engines/aircraft right through to their operational use. As can be seen from Fig 14, technology is available and being applied for some classes of aircraft. Unfortunately the performance requirement and mission flexibility of combat aircraft invalidates the application of existing technology and in todays political climate if suitable technology cannot be developed then operational constraints may well be adopted.

ACKNOWLEDGEMENTS

REFERENCES

1   'Interim report of the NATO/CCMS pilot study on Aircraft Noise in a Modern Society'. NATO/CCMS Paper No.163, May 1987

2   'Final report of the NATO/CCMS pilot study on Aircraft Noise in a Modern Society'. NATO/CCMS Paper No.185, November 1989

3   'International standards and recommended practices - Environmental protection' - Annex 16 to the convention on International civil aviation. Vol.1, aircraft noise. Second edition. ICAO Montreal (1988)

4   'Federal Aviation Regulations (FAR), Part 36. Noise standards: Aircraft type and airworthiness certification'. US Department of Transportation; Federal Aviation Administration 1969 onwards

5   Smith, M.J.T.; 'Aircraft noise control - prospects for the 21st century'. 52nd Conference of National Society for clean air, Scarborough, England, October 1985

6   Bushell, K.W.; 'An overview of engine noise technology'. [Rolls-Royce]. CCMS Conference, Williamsburg, USA, April 1988

7   Lee, R.; 'Noise perspectives - Year 2000 military and commercial aircraft'. [General Electric]. CCMS Conference, Williamsburg, USA, April 1988

8   Ffowcs Williams, J.E.; 'The noise from turbulence convected at high speed.' Journal Fluid Mechanics, pp 469-503, Vol 255 A. 1061, April 1963

9   'Gas turbine jet exhaust noise prediction.' SAE ARP 876C, November 1985

10 Cocking, B.J.; 'An experimental study of coaxial jet noise'. NGTE Report R333, May 1976

11 Cocking, B.J.; 'The effect of flight on the noise of subsonic jets'. AIAA Paper 76-555, July 1976 and NGTE Report R343, October 1976

12 Powell, A.; 'On the mechanism of choked jet noise'. Proc. Phy. Soc. B., Vol 66, pp 1039-1056

13 Harper-Bourne, M. and Fisher, M.J.; 'The noise from shock waves in supersonic jets'. AGARD Fluid Dynamics Specialist Meeting on Noise Mechanisms. AGARD CP131-11, Brussels, September 1973

14 Bryce, W.D. and Pinker, R.A.; 'The noise from unheated supersonic jets in simulated flight'. AGARD Paper No.77-1327, Atlanta, October 1977

15 Smith, M.J.T. and House, M.E.; 'Internally generated noise from gas turbine engines. Measurements and prediction'. ASME Paper No.66-GT/N43, Zurich, May 1966

16 Smith, M.J.T. and Bushell, K.W.; 'Turbine noise - its significance in the civil aircraft noise problem'. ASME Paper No.69-WA/GT12, Los Angeles, 1969

17 Stratford, B.S. and Newby, D.R.; 'A new look at the generation of buzz-saw noise'. AIAA Paper No.77-1343, Atlanta, October 1977

18 Hoch, R.G., Thomas, P., Weiss, E.; 'An experimental investigation of the core engine of a turbofan engine'. AIAA Paper No.75-526, Hampton, Va., March 1975

19 Fink, M.R.; 'Noise component method for airframe noise'. AIAA Paper No.77-1271, Atlanta, October 1977

20 Speakman, J.D.; 'Private Communication'. May 1990

21 Vaidya, P.G. and Dean, P.D.; 'The state of the art of duct acoustics'. AIAA Paper No.77-1279, Atlanta, October 1977

22 Rolls-Royce; 'Noise technology'. TS 1448, May 1979

23 Bryce, W.D.; 'Experiments concerning the anomalous behaviour of aero-engine exhaust noise in flight'. AIAA Paper 79-0648, Seattle, March 1979

24 Way, D.J. and Turner, B.A.; 'Model tests demonstrating under-wing installation effects on engine exhaust noise'. AIAA Paper 80-1048, Hartford, June 1980

25 Way, D.J. and Pinker, R.A.; 'Preliminary tests modelling acoustic installation effects on the Jet Provost'. NGTE Internal Report, November 1977

26 Hodge, C.G.; 'Commercial aircraft community noise levels'. [Boeing Commercial Airplane Company]. CCMS Conference, Williamsburg, USA, April 1988

27 Marsh, A.H.; 'Application of noise-reduction techniques to existing transport-category airplanes'. Paper B-35, CCMS Conference, Mittenwald, FRG, September 1986

28 Smith, M.J.T., Lowrie, B.W., Brooks, J.R., Bushell, K.W.; 'Future supersonic transport noise - Lessons from the past. AIAA Paper 88-2989, Boston, USA, July 1988

29 Maestrello, L. 'An experimental study on porous plug jet noise suppressor'. AIAA Paper 79-0673, Seattle, March 1979

30 Crouch, R.W. and Coughlin, C.L.; 'Nozzle flow profile shaping for jet noise reduction'. AIAA Paper 76-511, Palo Alto, July 1976

31 Brooks, J.R., McKinnon, R.A., Johnson, E.S; 'Results from flight noise tests on a Viper turbojet fitted with ejector/suppressor nozzle systems'. AIAA Paper 80-1028, Hartford, June 1980

32 ICAO Circular 157 - Arv101, 1981

33 Stern, A. and Peracchio, A.; 'The challenge of reducing supersonic civil transport noise'. AIAA Paper 89-2363, Monterey, July 1989

34 Burcham, F.W., Lasagna, P.L., Oas, S.C.; 'Measurements and predictions of flyover and static noise of a TF30 afterburning turbofan engine'. NASA TP 1372, December 1978

35 Burcham, F.W.; 'Measurements and predictions of flyover and static noise of an afterburning turbofan engine in an F-111 airplane'. AIAA Paper 79-7018

36 Fethney, P. and Hazell, A.F.; 'The external noise of MOD military aircraft'. RAE Technical Report 83058 (1983)

37 Marohn, H.D.; 'Noise emission of military jet aircraft flying at subsonic speeds'. Paper B-63, CCMS Conference, Mittenwald, FRG, September 1986

38 Marohn, H.D.; 'Influences of aircraft operation parameters on noise emissions during low-level flights'. Paper C-29, CCMS Conference, Mittenwald, FRG, September 1986

39 Speakman, J.D., Powell, R.G., Lee, R.A.; 'Community noise exposure resulting from aircraft operations - acquisition and analysis of aircraft noise and performance data'. AMRL-TR-73-107, February 1978

40 Dornheim, M.A.; 'Aviation week and space technology'. 9 April 1990
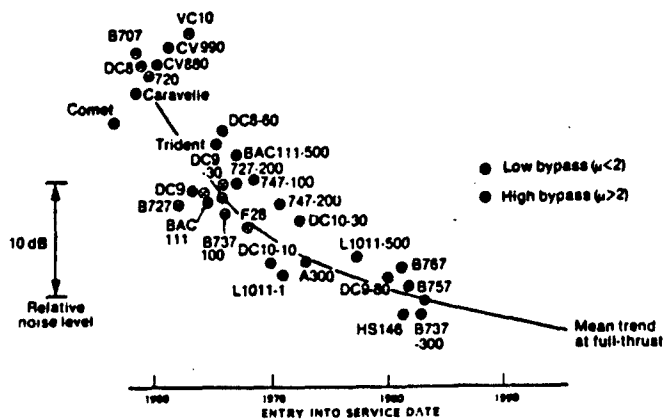
Fig 1 Progress in civil aircraft noise control
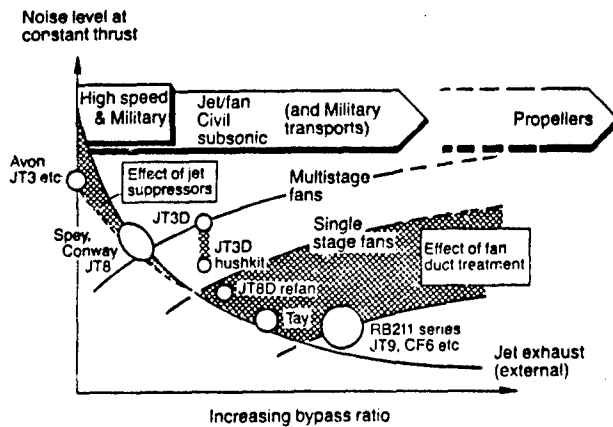
Fig 2 Noise trends with bypass ratio

Effective Perceived Noise Level, EPNdB - 1000 ft, Takeoff power
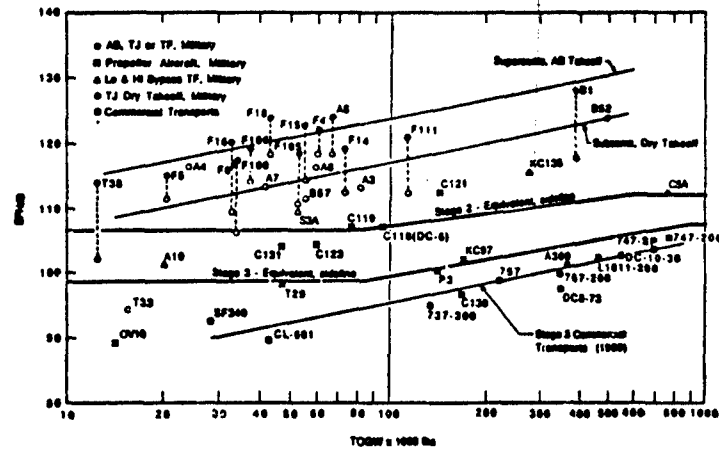
Fig 3   Military and aircraft noise levels

Low bypass ratio   High bypass ratio
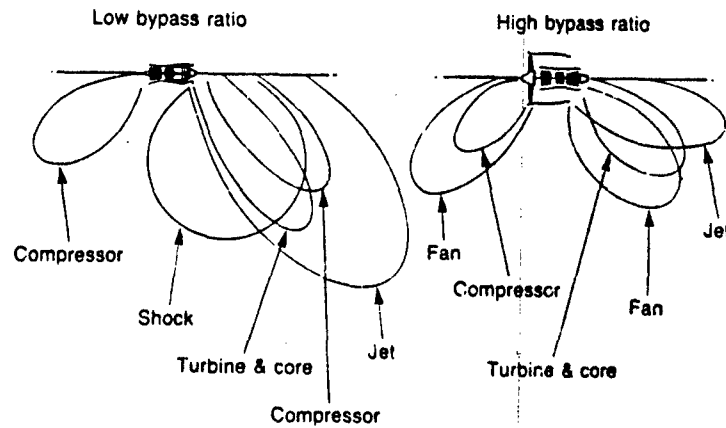
Fig 4   Engine noise sources
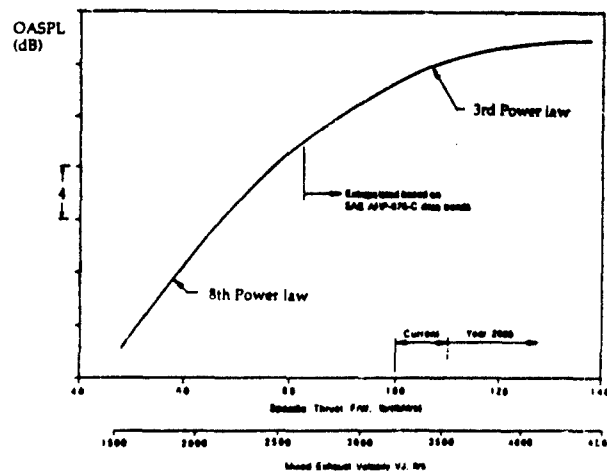
Fig 5   Jet mixing noise trends

INTENSITY
(dB)

10

$\beta = \sqrt{M^2 \cdot 1}$

Fig 6 Shock noise trends

Airframes with extended landing gear.

SYMBOL	AIRCRAFT
	C–5A
	AERO COMMANDER
	JETSTAR
	CESSNA 180
	HS 125
	HP 115
	BAC 1–11
	VC 10

Airframes with retracted gear and flaps.

SYMBOL	AIRCRAFT
	CONVAIR 240
	DC–3
	AERO COMMANDER
	SCHWEIZER 2–32
	C–5A
	LIASON
	HS 125
	VC 10
	JETSTAR

Aerodynamically clean airframes.

SYMBOL	AIRCRAFT
	SCHWEIZER 2–32
	LIBELLE
	PRUE–2
	BAC 1–11
	F–106B
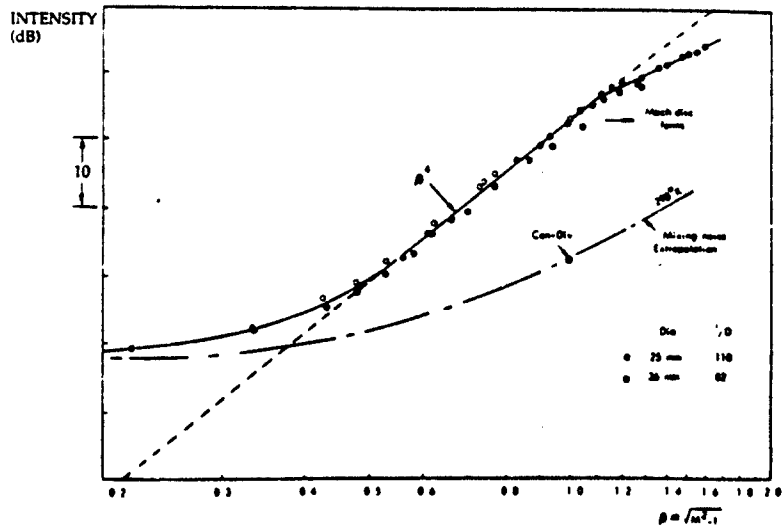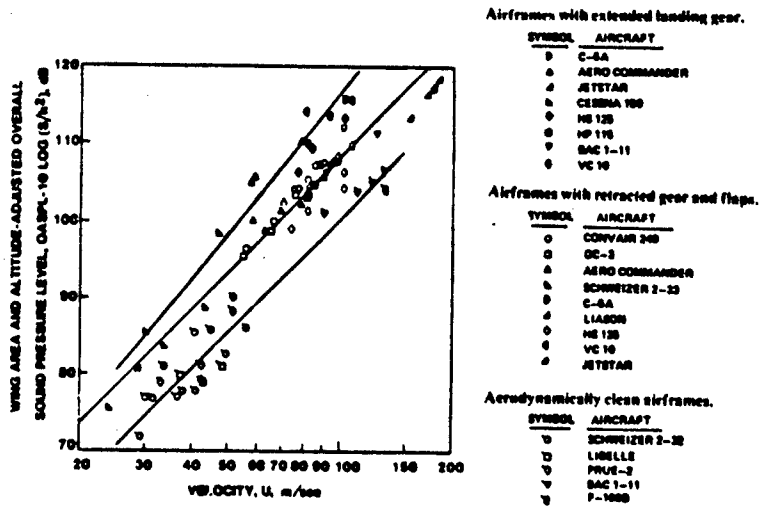
Fig 7 Airframe noise trends

COMPOSITE
MAX SPLs
(dB)

$M_a = 0.8$
50m AGL

10

□ bomber
+ fighter

← AUDIBLE RANGE

ONE THIRD OCTAVE CENTER FREQ in Hz
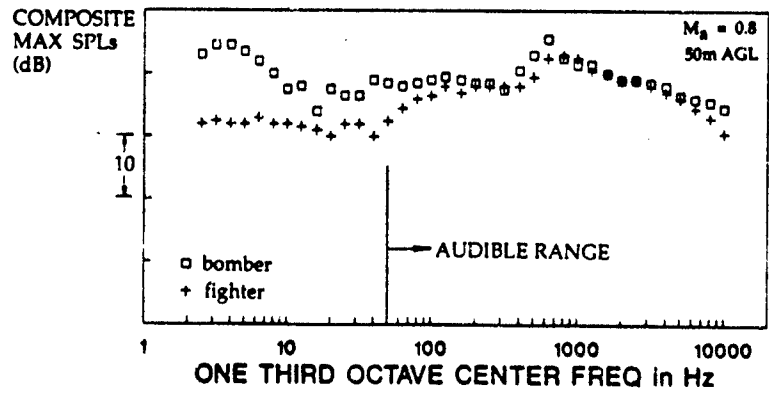
Fig 8 Noise from high-speed flyovers

THIRD OCTAVE
SPL (dB)

10 dB

JET – WING
INTERACTION

JET – FLAP
INTERACTION

JET – WING
REFLECTION

10   20   40   80   160   315   630   1250   2500
ENGINE FREQUENCY
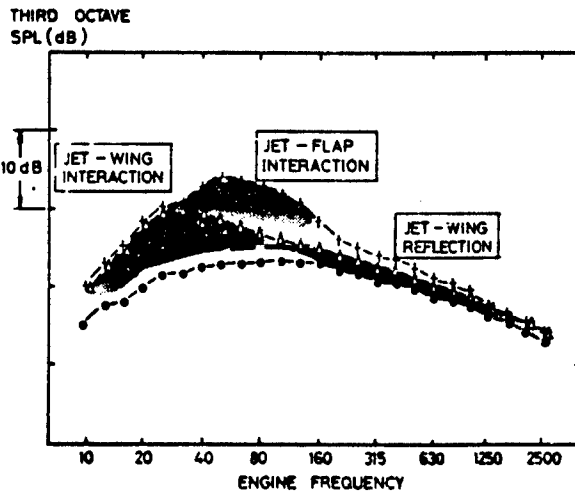
Fig 9   Installation effects of underwing mounted engines

Noise Level

(dB)

Linear field-shape

Model & jet
(static)

Clean jet
(static)

Model & jet
(flight 90 m/s)

Clean jet
(flight 90 m/s)

Exhaust velocity 300 m/s
Exhaust temperature 285K

0   20   40   60   80   100   120   140
Angle from jet axis (deg)
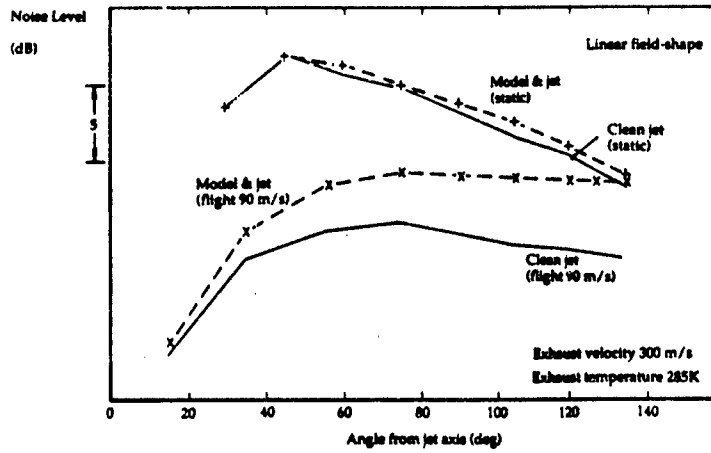
Fig 10   Installation effect on single engine aircraft

SUPPRESSOR MODE

SUPERSONIC CRUISE MODE

SUPPRESSOR   ACOUSTIC LINING   THRUST REVERSER
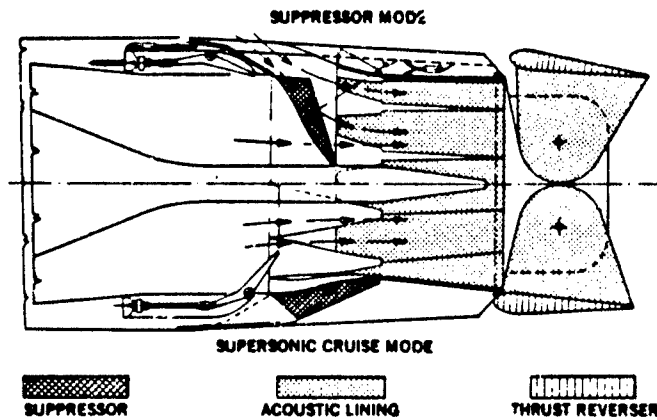
Fig 11   Typical silencer for SST
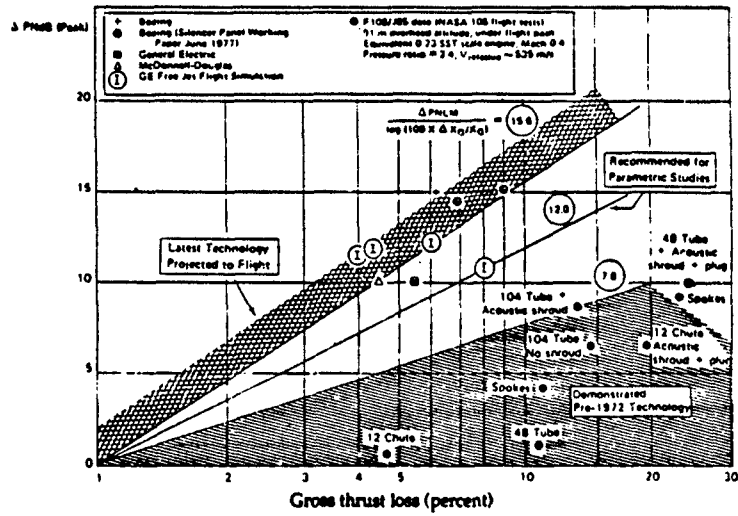
Fig 12   Jet noise suppressor technology
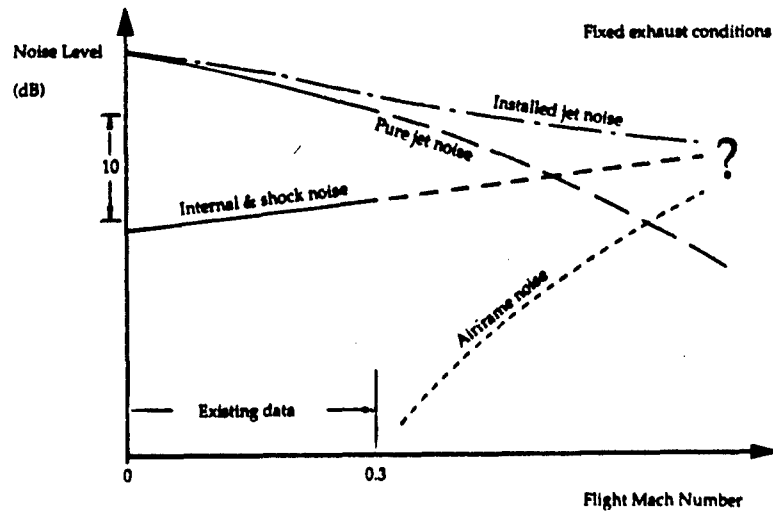
Fig 13   Noise sources at high flight speeds
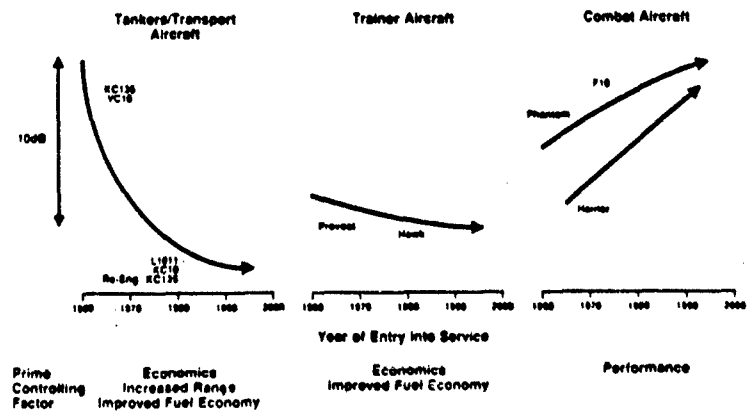
Fig 14   Noise trends for military aircraft

Discussion

QUESTION BY: F.R. Grosche, DLR Göttingen, Germany
You showed an example for increased jet noise radiation due to flow over the tail structure in front of (upstream of) the nozzle exit. Can you give a physical explanation for this installation effect?

AUTHOR'S RESPONSE:
The potential mechanisms have been suggested for this phenomena. First, that the presence of the fuselage/cuff inhibits the flight-effect on the jet by providing a region of low velocity near the initial part of the jet development and secondly, that extra turbulence, shed from the upstream structure, entering the mixing region of the jet causes a general increase in the jet noise.

QUESTION BY: D.J. Way, DRA, Aerospace Division Pyestock, UK
Startle arising from the rapid onset of the noise, appears a major factor of annoyance for low-level training. This would remain a significant problem, even if the peak noise levels are reduced significantly. This makes the job of reducing combat aircraft overall noise subjectively at the source even more difficult. Would the author like to comment?

AUTHOR'S RESPONSE:
I agree the onset rate of the noise will strongly influence the degree of annoyance and to this end we are actively considering ways of modifying the aircraft noise signature to reduce the onset rate as a means of reducing the annoyance. But I believe the whole problem of annoyance is even more complex: first the absolute peak noise level in subjective units such as dBA, second the onset rate perhaps in a manner described in paper 4 and finally "true startle" which can be achieved even silently.

QUESTION BY: H., Tönskötter, IABG, Ottobrunn, Germany
In Fig. 13 jet noise is decreasing with flight velocity. This is probably because of the fixed exhaust conditions. For a real aircraft with increasing flight velocity the required thrust and hence jet noise will increase.

AUTHOR'S RESPONSE:
The figure represents a possible balance in the noise sources at various Mach numbers with fixed exit conditions, that is at a constant gross thrust equal to that required to maintain level flight at around 0.7 Mach. A comparable figure representing the source balance with the aircraft at steady flight speeds could be produced but would have no sources present at M = 0. See paper 22, Fig. 24.

QUESTION BY: L.W. Illston, BAe, UK

In your discussion on jet noise suppressor technology, you described that 3 PNdB for 2 % thrust loss was possible.

Would you agree that such suppressor technology would be very difficult to apply to existing aircraft, and could only be considered for new aircraft, if the thrust loss and weight penalty could be accepted?

AUTHOR'S RESPONSE:

Application of the technology to significantly reduce the take-off noise from aircraft requiring high-specific thrust engines would entail major redesign, manufacture and flight clearance not to mention expense. The same technology might be considered for future aircraft but I believe that the compromises in performance together with the knowledge that there would be no substantial reductions in noise due to high-speed/low-altitude training, make it a non-starter.

This does not mean that some measure of silencing should not feature in future combat aircraft/engine designs but that it should be viewed in context.

ETUDES SUR LE BRUIT DES TURBOREACTEURS APPLICABLES AUX AVIONS DE COMBAT

S. Léwy, G. Fournier
Office National d'Etudes et de Recherches Aérospatiales,
BP 72, 92322 Châtillon Cedex, France

et M. Pianko
ICARE, 91300 Massy, France

RESUME

Les avions de combat à l'entraînement à basse altitude constituent une grave nuisance sonore pour les populations survolées, produite principalement par les turboréacteurs. La présente communication expose les méthodes de prévision et de réduction du bruit, en s'appuyant sur l'expérience acquise dans le domaine civil. Les premiers étages de compression sont une source de bruit, d'autant plus importante par rapport au jet que le taux de dilution est élevé. La prévision du rayonnement et de sa directivité repose sur la mesure des fluctuations de pression sur aubes et sur l'analyse modale du champ sonore se propageant dans l'entrée d'air. Le jet reste cependant la principale cause de bruit des moteurs militaires. Les mécanismes générateurs sont rappelés aussi bien pour les simples flux subsoniques et supersoniques que pour les doubles flux. Les méthodes de prévision, fondées au départ sur l'équation de Lighthill (tenseur lié à la turbulence fine) sont passées en revue, ainsi que les divers moyens de réduire le bruit de jet. Pour terminer, sont décrites les possibilités offertes par la soufflerie anéchoïque CEPRA 19, spécialement conçue pour étudier, avec effet de vol, le bruit de jet rayonné en champ lointain.

SUMMARY

The noise emission from combat aircraft at low level flight training is perceived by the public as a strong nuisance, which is mainly due to the turbojet engines. This paper presents methods of noise prediction and reduction, based on results obtained in civil applications. The first compressor stages are a noise source, all the more important as the bypass ratio is higher. Input data for radiation and directivity predictions are given by measurements of blade and vane pressure fluctuations, and by modal analysis of the spinning waves propagating in the inlet duct. However, the jet remains the main noise source of military turbojet engines. Sound generation mechanisms are described for subsonic and supersonic single jets and for bypass jets. The prediction methods, based on the Lighthill's equation (tensor due to the turbulence) are reviewed, and also the various means of jet noise reduction. The last section describes the CEPRA 19 anechoic wind tunnel, which is primarily designed for studying the jet noise radiated in the far field with flight effects.

INTRODUCTION

Le bruit des avions de combat à l'entraînement constitue une très grave nuisance pour le public ; il en résulte des contraintes sur les missions, par exemple de nuit, qui peuvent être pénalisantes et difficilement acceptables pour les militaires. Cet aspect acoustique a, jusqu'à présent, été négligé (au contraire, un appareil très bruyant peut affoler davantage l'ennemi), à l'opposé de ce qui se passe dans l'aviation civile, surtout depuis l'avènement de la propulsion par turboréacteur.

Il apparaît clairement aujourd'hui qu'un effort doit être mené sur les avions de combat, afin de réduire l'émission sonore à la source. Il est évident que les recherches ne partent pas de rien, puisqu'elles peuvent s'appuyer sur les acquis obtenus dans les avions de transport, même si la transposition n'est pas immédiate car les performances requises sont différentes.
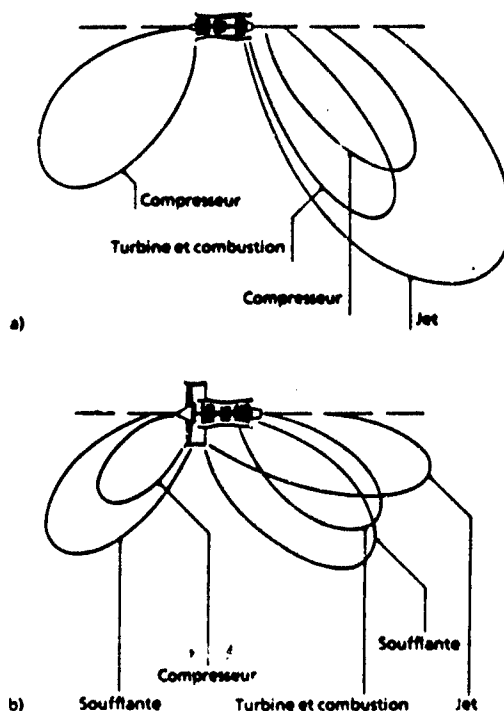
Figure 1 Rayonnement sonore typique des turboréacteurs à faible taux de dilution (a) et à taux de dilution élevé (b). Extrait de [1], d'après Grieb & Heinig, Motoren-und Turbinen-Union.

Dans les deux cas, ce sont bien sûr les moteurs qui constituent la principale source sonore. Une synthèse particulièrement intéressante est exposée dans la référence [1], d'où est extraite la figure 1. Celle-ci montre que l'émission acoustique vers l'amont provient essentiellement des raies engendrées par les premiers étages de compression et que celle vers l'aval est plutôt à large bande, due au jet. Cependant, les deux types principaux de turboréacteurs doivent être distingués :

* ceux à simple flux ou à très faible taux de dilution, qui représentent les moteurs de première génération et sont encore actuellement les mieux adaptés au vol supersonique, où le bruit de jet domine largement ;

* ceux à double flux à grand taux de dilution, qui sont

maintenant généralisés pour le transport subsonique, dans lesquels la diminution des vitesses d'éjection réduit fortement le bruit de jet et où la source prépondérante, même dans l'arc aval, est la soufflante en amont de la séparation des flux primaire et secondaire.

Cette communication expose une sélection de résultats marquants des recherches effectuées dans le domaine civil et pouvant aboutir à des retombées directes pour les avions de combat. Le chapitre 1 porte sur l'acoustique des compresseurs, actuellement secondaire dans les moteurs militaires, mais dont l'importance relative ne fait que croître au fur et à mesure que des progrès sont réalisés sur le bruit de jet, traité au chapitre 2. Le dernier chapitre est consacré à CEPRA 19 qui, avec le DNW (Duits-Nederlandse Windtunnel) aux Pays-Bas, est l'une des seules souffleries anéchoïques au monde, avec une veine ouverte permettant des mesures acoustiques en champ lointain ; la vitesse de l'écoulement couvre les conditions de décollage et d'approche. Cette installation est conçue avant tout pour l'étude du bruit de jet mais des projets en cours visent à l'équiper d'une alimentation pour banc de compresseur ou d'hélice.

1. BRUIT DE COMPRESSEUR AXIAL

1.1. Généralités

Le bruit d'un compresseur subsonique est dominé par les raies aux fréquences $f_n = n.B.N$, harmoniques du passage des aubes (B est le nombre d'aubes du rotor, N son régime de rotation et n un entier positif). Il est engendré essentiellement par les fluctuations de pression sur les aubes fixes et mobiles, dues aux interactions entre rotor et stator et entre rotor et distorsions de l'écoulement incident (figure 2). Il en résulte des ondes acoustiques hélicoïdales dans la manche d'entrée d'air. Un mécanisme physique fondamental est la propriété de coupure du conduit, telle que seules les ondes à structure spatiale suffisamment simple (autrement dit, les modes les plus bas) se propagent dans la manche et rayonnent à l'extérieur, tandis que les autres sont évanescentes. Il est montré au paragraphe 1.2 que le bruit est produit par des harmoniques de charge sur aubes atteignant des rangs élevés, que les calculs aérodynamiques ne sont pas encore capables de prévoir [2]. C'est pourquoi des données expérimentales sur les sources sonores sont nécessaires : ces mesures sont exposées au paragraphe 1.3.
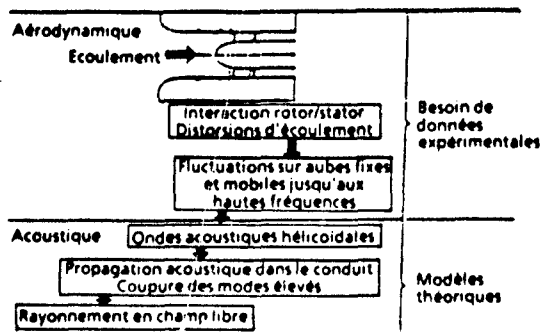
Figure 2 Mécanismes généraux de rayonnement du bruit de raie par un compresseur axial subsonique.

Le rayonnement d'un compresseur transsonique (c'est-à-dire avec des vitesses relatives supersoniques en tête d'aube) est à la fois plus compliqué et plus simple. Les irrégularités de position et de calage des aubes mobiles créent des différentes

d'inclinaison et d'intensité des ondes de choc associées à chaque aube, de sorte que la symétrie angulaire $2\pi/B$ du rotor est rompue et seule subsiste celle en 2π. Toutes les fréquences harmoniques de la rotation $f_l = l.N$ (l entier positif) peuvent être émises, à l'exception des premières : la figure 3 compare les spectres acoustiques mesurés en paroi de la manche d'admission du compresseur transsonique maquette CA6 de la SNECMA (diamètre 47 cm), pour des régimes subsoniques ($M_{rel} < 1$) et transsoniques ($M_{rel} > 1$), où $N_0 = 19310$ tr/min est le régime nominal et M_{rel} le nombre de Mach relatif en bout d'aube. En revanche, il est expliqué au paragraphe 1.2.2 que la charge moyenne du rotor crée alors des ondes propagatives dans la manche et cette source sonore domine largement les autres, liées à des phénomènes d'interaction.

Cette présentation rapide met en relief l'importance de la structure spatiale (modale) du champ sonore engendré à chaque fréquence. Le paragraphe 1.4 indique comment il est possible de la mesurer dans un conduit. L'apport de cette analyse est illustré, au paragraphe 1.5, par la caractérisation de la perte par insertion de traitements absorbants en paroi.

1.2. Rappels théoriques sur la propagation des ondes acoustiques en milieu guidé

Ces rappels sont fondés sur la théorie maintenant classique de Tyler et Sofrin [3]. La pression sonore d'une onde élémentaire dans un conduit cylindrique s'écrit :

$$p(r,\theta,z,t) = A \cdot J_m(k_T \cdot r) \cdot \exp[i(\omega t - m\theta - kz)]. \quad (1)$$

où r, θ et z sont les coordonnées cylindriques (z selon l'axe du conduit, t est le temps, $\omega = 2\pi f$ la pulsation, m le nombre d'ondes (ou mode) angulaire (entier), k le nombre d'ondes axial, k_T le nombre d'ondes transversal, J_m la fonction de Bessel de première espèce d'ordre m et A une amplitude.

1.2.1. Propriétés de coupure d'un conduit

Si $K = \omega/a$ est le nombre d'ondes total, avec a la célérité du son, la relation de dispersion donne :

$$(K - Mk)^2 = k^2 + k_T^2 \quad (2)$$

où M est le nombre de Mach de l'écoulement dans le conduit. L'onde (1) se propage si k est réel, c'est-à-dire si le discriminant de l'équation (2), du second degré en k, est positif, soit :

$$K \geq \sqrt{1 - M^2} \cdot k_T. \quad (3)$$

Dans un conduit de rayon R à paroi rigide :

$$\left(\frac{\partial p}{\partial r}\right)_{r=R} = 0 \quad \text{ou} \quad \left[J_m'(k_T \cdot r)\right]_{r=R} = 0.$$

La plus petite valeur possible de k_T, à m donné, est :

$$k_T = \chi_m/R, \quad (4)$$

où χ_m est l'abcisse du premier extremum de la fonction de Bessel J_m. Les valeurs supérieures de k_T sont repérées par un second indice μ entier positif, le mode radial. Il est cependant inutile de l'introduire explicitement ici car les symétries angulaires des sources sonores créent une sélection seulement sur m et non sur μ (voir paragraphe 1.2.2 ci-dessous).

Compte tenu de (3) et (4), un mode m se propage à une fréquence f si $f \geq f_c(m)$, fréquence de coupure :

$$f_c(m) = \sqrt{1 - M^2} \cdot \frac{a \cdot \chi_m}{2\pi R}, \qquad (5)$$

avec, en pratique, $\sqrt{1-M^2} = 1$. Le conduit agit donc comme un filtre passe-haut en fréquence. Indiquons que : $\chi_0 = 0$, cas d'une onde plane, qui se propage quelle que soit la fréquence, et si $m \neq 0$,

$$\chi_m = |m| + 0.8086 |m|^{1/3} + 0.0725 |m|^{-1/3}$$

$$- 0.051 |m|^{-1} + 0.0094 |m|^{-5/3} + \ldots \qquad (6)$$

Tous les modes m propagatifs à une fréquence f donnée sont tels que :

$$\sqrt{1 - M^2} \cdot \frac{a\chi_m}{2\pi R} \leq f \; ; \quad \text{comme } \chi_m \text{ croît avec } |m|, \text{ cette}$$

inégalité définit un mode maximum, ou de coupure, m_c et elle est satisfaite si :

$$|m| \leq m_c. \qquad (7)$$

Le conduit agit ainsi comme un filtre passe-bas en mode.

1.2.2. Conséquences sur l'émission sonore d'un compresseur

Comme déjà noté, les symétries angulaires du compresseur limitent les valeurs de m possibles : un harmonique de charge

$$f_{j_1} = j_1 \cdot N$$

sur aube mobile (j_1 entier), engendre une onde acoustique à une fréquence $f_l = l.N$, dont le mode angulaire vaut [4] :

$$m = l \cdot j_1. \qquad (8)$$

Le rapport de coupure : $f_c(m)/f_l \leq 1$ s'écrit encore, d'après (5),

$$\chi_m \leq l \frac{M_R}{\sqrt{1 - M^2}}, \qquad (9)$$

où $M_R = 2\pi RN/a$ est le nombre de Mach de rotation périphérique.

Le son de rotor seul, dû à la charge moyenne ($j_1 = 0$), est tel que $m = l$. D'après (6), $|m| < \chi_m$ et (9) devient :

$$1 < \frac{\chi_m}{m} \leq \frac{M_R}{\sqrt{1 - M^2}}, \qquad (10)$$

ce qui entraine :

$$1 < M_R^2 + M^2 \quad \text{et} \quad M_{rel} > 1.$$

où $M_{rel} = \sqrt{M_R^2 + M^2}$ est le nombre de Mach relatif en bout d'aube. Ceci démontre l'affirmation du paragraphe 1.1, selon laquelle la charge moyenne du rotor ne peut constituer une source de bruit que dans un compresseur transsonique. Cette condition est nécessaire mais non suffisante car

$\chi_m / m \leq M_R/\sqrt{1 - M^2}$ dans (10) est plus restrictif, ce qui justifie l'absence des premiers harmoniques de la rotation dans les spectres sonores (cf. figure 3 à $N = 0.8.N_0$).

CA6 $B = 46$ aubes - $N_0 = 19\,310$ tr/min
$z = 155$ mm en amont du rotor. Ras de paroi
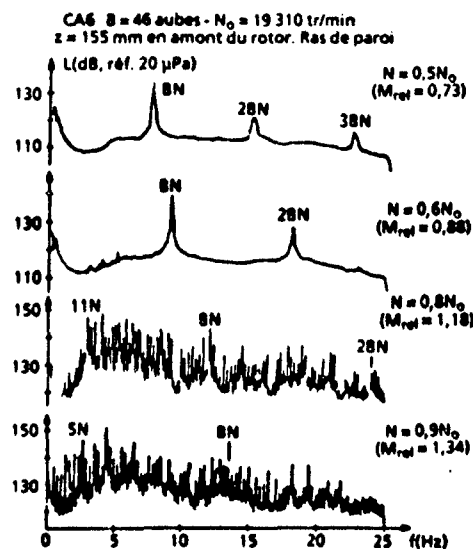
Figure 3 Evolution du spectre acoustique dans la manche d'entrée d'air d'un compresseur transsonique, en fonction du régime de rotation.

Pour un rotor subsonique à B aubes, $M_R/\sqrt{1 - M^2} < 1$ et $l = nB$, donc $\chi_m < nB$ et, a fortiori, $|m| < nB$. Seuls des sons d'interaction peuvent se propager. Si l'interaction se produit avec un stator à V aubes, les harmoniques de charge engendrés sur aubes mobiles sont tels que $j_1 = j.V$ (j entier), $f_l = j.V$ et :

$$m = nB - jV. \qquad (11)$$

La condition nécessaire (mais non suffisante) pour que ces modes m se propagent est qu'ils soient situés dans la plage :

$$-nB < m < nB, \quad \text{soit } 0 < jV < 2nB. \qquad (12)$$

L'accent est mis habituellement sur le fondamental acoustique $f_1 = BN$ car il se situe généralement vers quelques kilohertz, dans la gamme du maximum de sensibilité de l'oreille. Les harmoniques sont, d'une part, moins gênants d'un point de vue physiologique et sont, d'autre part, davantage atténués au cours de leur propagation, par l'absorption atmosphérique. Les inégalités (12) deviennent, pour $n = 1$:

$$0 < jV < 2B. \qquad (13)$$

ce qui est impossible quel que soit j (entier) si $V \geq 2B$. Ceci démontre la règle bien connue adoptée pour les compresseurs de conception silencieuse : rotor subsonique, absence de roue

directrice d'entrée et grande distance entre rotor et redresseur, afin d'éviter des interactions fortes, avec en outre au moins deux fois plus d'aubes fixes que de mobiles.

1.2.3. Rayonnement en champ libre

Pour terminer cet exposé théorique, signalons que le rayonnement en champ libre se calcule [5] :

* soit de manière approchée, en considérant le champ sonore (1) dans le plan de sortie du conduit comme un ensemble de sources monopolaires élémentaires possédant entre elles des relations de phase (modèle du piston) ;

* soit exactement en résolvant l'équation d'onde avec des conditions aux limites imposées à la source réelle et sur les parois du conduit.

La directivité dépend de la fréquence f et du mode m. Le paramètre essentiel est le rapport de coupure $f_c(m)/f$. Le rayonnement est latéral si f est voisine de la coupure et devient de plus en plus axial, avec davantage de lobes secondaires, quand f augmente (mais seul le mode m = 0 rayonne sur l'axe et le maximum se trouve alors sur l'axe). Une bonne indication, particulièrement simple, de l'angle φ_{max} où le niveau sonore est maximum (origine φ = 0 dans l'axe du conduit) est donnée par [6] :

$$\sin\varphi_{max} = k_r/K = f_c(m)/f \qquad (14)$$

1.3. Etude expérimentale des sources sonores dans les compresseurs subsoniques

Comme le nombre d'aubes mobiles B est typiquement de l'ordre de 30 à 50, les relations (12) ou (13) montrent que le rang des harmoniques de charge contribuant à l'émission sonore peut atteindre plusieurs dizaines d'unités. Jusqu'à présent, seules des mesures permettent d'accéder au niveau de ces raies.

1.3.1. Technique de mesure des fluctuations de pression sur aubes

La détermination expérimentale des fluctuations de pression sur aubes reste cependant délicate. Les capteurs ne doivent pas créer de protubérance, afin de ne pas perturber l'écoulement pariétal, mais il est souvent exclu d'usiner les aubes pour ne pas diminuer leur résistance, surtout sur maquette à échelle réduite où les profils sont très minces.

La Division Electronique et Mesures de l'ONERA développe des capteurs pelliculaires depuis plus de dix ans [7]. Ils sont de type capacitif et leur principale caractéristique pour la présente application est que leur épaisseur totale ne dépasse pas 50 µm, de sorte qu'ils peuvent être collés directement sur les aubes. Ils sont constitués de couches de diélectrique (film de polyimide) métallisées (figure 4) ; une microélectronique en bout d'aube assure l'adaptation d'impédance sur la ligne de mesure. La surface sensible vaut typiquement 3 mm selon la corde sur 5 mm en envergure. Dans les modèles actuels, le diélectrique est alvéolé (environ 50 poches d'air dans la zone sensible), ce qui augmente la réponse à la pression car la déformation mécanique est nettement supérieure à la déformation élastique. De la sorte, l'effet des grandeurs d'influence (accélérations, contraintes, température, humidité) est négligeable devant celui de la pression. L'efficacité est de l'ordre de 20 µV/Pa sous une

tension de polarisation E = 100 V, avec une bande passante plate jusqu'à au moins 100 kHz. La tension de sortie vaut :

$$E_s = \frac{\Delta C_p}{C} \cdot E, \qquad (15)$$

où C_p est la capacité polarisée de l'élément sensible et C la capacité totale du capteur, incluant les connexions.

De nombreux essais se sont déroulés au banc anéchoïque 5C2 de la SNECMA-Villaroche, sur la maquette de compresseur aéronautique subsonique (de type soufflante) nommée CA5. Les principales caractéristiques sont données sur la figure 5 (N_0 = 12600 tr/min est le régime de rotation nominal). La figure 5 montre aussi qu'un filtre tranquillisateur hémisphérique peut être monté sur la manche [8]. Il est constitué d'un nid d'abeilles doublé d'un grillage sur la face intérieure ; son diamètre est voisin du triple de celui du compresseur. Le rôle de ce dispositif est de mieux simuler les conditions de vol, en réduisant les distorsions d'écoulement propres aux bancs statiques (par exemple l'aspiration du tourbillon de sol), dont l'interaction avec le rotor augmente l'émission sonore [9].
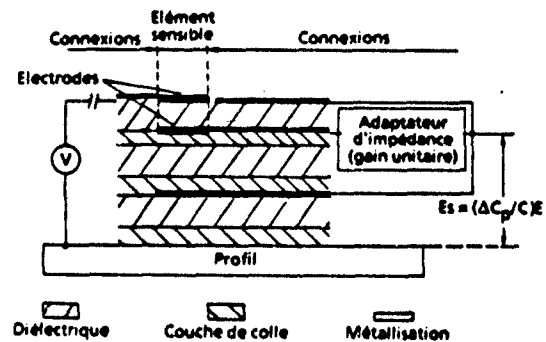

Figure 4 Coupe schématique d'un capteur de pression pelliculaire, conçu à la Division Electronique et Mesures de l'ONERA (épaisseur totale inférieure à 50 µm).

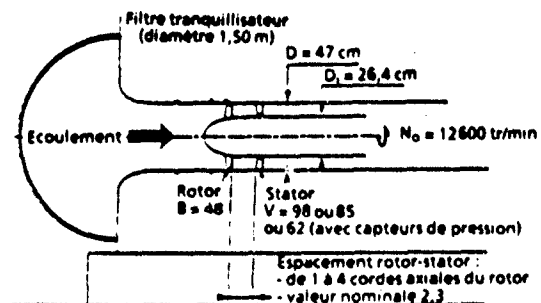Figure 5 Principales données relatives à la maquette de compresseur subsonique CA5 de la SNECMA (débit massique nominal corrigé : 23,4 kg/s).

Certaines expériences ont été effectuées avec six capteurs en tout, sur deux aubes du stator à 62 aubes. D'autres, plus intéressantes, ont été réalisées avec huit capteurs répartis sur trois aubes mobiles ; les signaux sont alors amplifiés par des amplificateurs embarqués dans le moyeu du rotor, puis sont transmis par un collecteur tournant.

1.3.2. Exemples de résultats

Les figures 6 et 7 présentent des mesures sur rotor, à 80 % de l'envergure des aubes, dans le montage avec redresseur à 98 aubes et espacement rotor-redresseur nominal (égal à 2,3 fois la projection axiale de la corde d'une aube mobile). La position radiale retenue est celle où il est couramment admis que l'émission sonore est la plus forte. Les fluctuations de pression sont exprimées en décibels, avec la même référence qu'en acoustique (20 µPa).
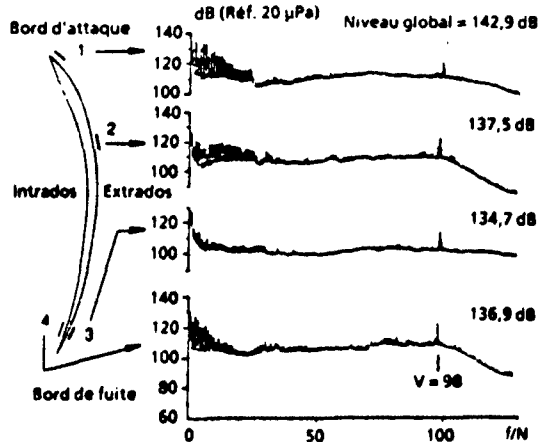

Figure 6 Spectres des fluctuations de pression mesurées sur aube mobile du compresseur CA5, à 80 % de l'envergure : N = 0,6.N$_o$ = 7560 tr/min, fréquence maximum f = 128.N = 16100 Hz.
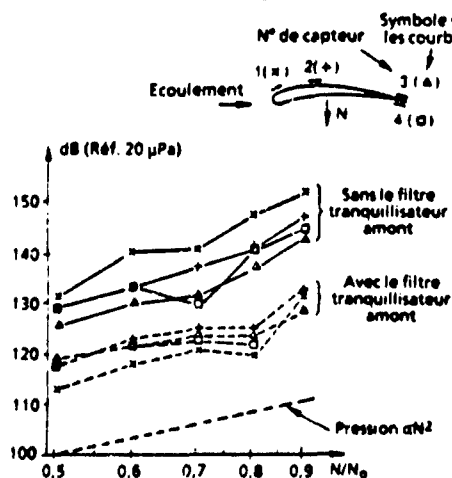
Figure 7 Evolution du niveau total cohérent des fluctuations de pression sur aube mobile du compresseur CA5 à 80 % de l'envergure, en fonction du régime de rotation (abscisse logarithmique).

La figure 6 montre les spectres de pression en quatre positions sur la corde, à 60 % du régime nominal, sans le filtre tranquillisateur. Ils mettent en évidence une trentaine d'harmoniques de la rotation, dus à l'interaction avec les distorsions à basse fréquence de l'écoulement incident, ainsi que la raie à 98.N associée au stator. Malgré l'éloignement de celui-ci, son champ potentiel est nettement perçu sur le rotor, ce qui prouve l'intérêt d'appliquer la règle V ≥ 2B trouvée à

la fin du paragraphe 1.2.2, pour couper le son produit sur le fondamental acoustique. Les autres harmoniques supérieurs à 20.N ou 30.N sont peu visibles à cause de la composante à large bande. Comme il faut connaître leur niveau pour prévoir le bruit émis, une analyse synchronisée sur la rotation, décrite en [10], a été mise au point afin d'éliminer les fluctuations aléatoires et fournir un spectre ne contenant que les raies multiples de N, qui est appelé spectre cohérent.

C'est ce niveau total cohérent qui est porté sur la figure 7, en fonction du régime de rotation (avec une abscisse logarithmique). Les résultats présentés, issus des quatre mêmes capteurs, sont obtenus avec et sans filtre tranquillisateur. Les fluctuations de pression sur chaque courbe évoluent à peu près en N^2, c'est-à-dire selon la loi aérodynamique du carré de la vitesse (la vitesse axiale est pratiquement proportionnelle à celle de la rotation). Le filtre tranquillisateur joue bien le rôle attendu, puisqu'il produit une réduction des fluctuations de l'ordre de 10 dB. Un examen plus approfondi de la figure 7 montre que le niveau sans filtre est plus élevé sur le capteur n° 1 en bord d'attaque, ce qui tend à confirmer l'influence des distorsions de l'écoulement amont. Avec le filtre, au contraire, les quatre courbes sont plus groupées et le capteur n° 1 perçoit les niveaux les plus faibles (le gain atteint 20 dB en cette position), ce qui semble indiquer que les fluctuations de pression seraient alors plutôt engendrées dans la couche limite se développant sur les aubes.

1.4. Analyse modale du champ sonore dans la manche à air

Tous les harmoniques de charge ne constituent pas des sources sonores à cause des propriétés de coupure de la manche, décrites au paragraphe 1.2. Il est donc capital de connaître la structure angulaire (ou modale) du champ sonore se propageant dans le conduit.

1.4.1. Méthode d'analyse modale

La procédure d'analyse modale mise au point à l'ONERA est décrite en [11]. Elle est rappelée sur la figure 8. Un microphone monté sur une virole tournante effectue une révolution en 4 minutes environ (l'angle θ varie linéairement avec le temps t). Un microphone fixe au voisinage de la section étudiée sert de référence de phase.

Le signal fixe $s_F(t)$ et le signal mobile $s_M(t,\theta)$ sont numérisés à une fréquence comprise entre 30 et 50 kHz, grâce à une horloge pilotée par le repère de rotation du rotor (fréquence N). Ils sont stockés sur un disque d'acquisition rapide et découpés en blocs de 1024 points. La moyenne des transformations de Fourier rapides (FFT pour "Fast Fourier Transform") sur 40 blocs successifs fournit $S_F(f,t)$ et $S_M(f,\theta)$, avec une résolution fréquentielle de 30 à 50 Hz et une résolution temporelle de 1 s.

Pour la suite du traitement, plusieurs fréquences f harmoniques de N sont sélectionnées. Pour chacune d'elles, le carré des amplitudes

$$\Gamma_F(t) = s_F \cdot s_F^* \quad \Gamma_N(\theta) = s_N \cdot s_M^*$$

et l'interspectre

$$I_{FN}(\theta) = s_F \cdot s_M^*$$

sont calculés sur environ 240 points (240 s d'enregistrement) en fonction de t (ou θ) ; l'astérisque désigne le complexe conjugué. Le niveau total L_{TOT} de la raie et son niveau cohérent L_{coh}, résultant de la somme de l'intensité de tous les
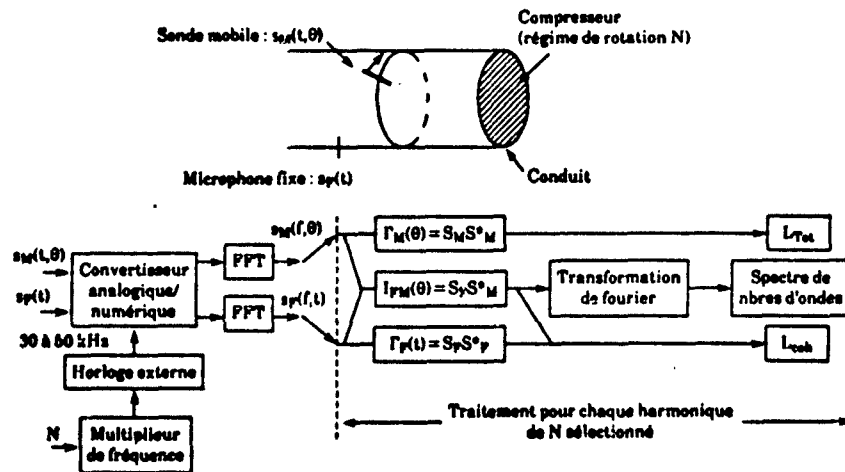
Figure 8 Procédure de mesure et de calcul du spectre de nombres d'onde angulaires
à chaque fréquence sélectionnée.

modes, sont donnés par :

$$L_{Tot} = 10 \cdot \log \ (\overline{\Gamma_p}) \ \ et \ \ L_{Coh} = 10 \cdot \log(|\overline{I_{PM}}|^2/\Gamma_p) \quad (16)$$

où la barre supérieure représente la valeur moyenne sur t (ou θ) pendant l'exploration complète des 360°. Il faut bien noter que le mot "cohérent" n'a pas la même signification qu'au paragraphe précédent : il indique ici la part de bruit spatialement cohérente sur une section droite du conduit, tandis qu'il concernait au paragraphe 1.3 les fluctuations de pression synchronisées temporellement sur la rotation.

La transformation de Fourier en θ de la composante de l'interspectre I_{PM} (θ) à la fréquence considérée fournit le spectre de nombres d'ondes angulaires (ou de modes) L(m) à cette fréquence. Comme I_{PM}(θ) est complexe, les valeurs positives et négatives de m sont séparées, c'est-à-dire les ondes tournant dans le même sens que le rotor ou en sens contraire. Cette distinction est très importante, puisque les modes + |m| et - |m| sont engendrés par des harmoniques de charge différents, compte tenu de (8) ou (11). Comme I_{PM}(θ) est défini en 240 points, le spectre L(m) couvre l'intervalle - 120 < m < + 120. L(m) est tracé sur la plage - 75 ≤ m ≤ + 75 ; L_{Tot} et L_{Coh} sont repérés par deux petits traits horizontaux. Tous les niveaux sonores sont exprimés en décibels, avec la référence de 20 μPa.

1.4.2. Enseignements tirés de l'analyse modale

L'analyse modale permet de vérifier, par exemple, la théorie exposée au paragraphe 1.2.2, selon laquelle le son de rotor seul domine dans les compresseurs transsoniques. Les expériences menées sur la maquette CA6 aux régimes transsoniques (cf. figure 3), décrites en [12], montrent effectivement que m = l est le mode principal à f = l.N.

Les phénomènes sont plus compliqués dans les compresseurs subsoniques. Des mesures ont été effectuées en paroi de la manche d'entrée d'air de la machine CA5, dans le montage avec redresseur à V = 85 aubes et espacement rotor-redresseur minimal (égal à une fois la longueur de la projection axiale de la corde d'une aube mobile). La figure 9 constitue une

synthèse des résultats sur le fondamental acoustique f = BN, en fonction du régime de rotation. Bien que la règle V > 2B ne soit pas rigoureusement respectée (B = 48), le premier son d'interaction rotor-stator à f = B.N, soit m_1 = B - V = - 37 (cf. la relation 11), est coupé jusqu'au régime le plus élevé considéré ici, N = 0,85.N_p. Par conséquent, la raie f = B.N est essentiellement due aux interactions des aubes mobiles avec les distorsions de l'écoulement incident.

La figure 9a fournit les niveaux L_{Tot} et L_{Coh} à f = B.N en fonction de N/N_p, avec une abscisse logarithmique. L_{Coh} reste très peu inférieur à L_{Tot}, ce qui signifie que le champ sonore possède une bonne cohérence spatiale et est bien organisé en modes. Une régression par moindres carrés montre que L_{Tot} varie en 10.log (N/N_0)^{7,4}, ce qui est légèrement plus fort que la loi dipolaire classique, en puissance 6 de la vitesse.

La figure 9b résume les modes trouvés, cette fois-ci avec une abscisse linéaire en N/N_p. Soit L_{max} le niveau du mode le plus intense à chaque régime étudié ; les points noirs repèrent les modes m tels que L_{max} ≥ L(m) > L_{max} - 2 dB et les croix les autres modes m pour lesquels L(m) > L_{max} - 10 dB. Les deux traits continus marquent la coupure théorique ± m_t, déduite de (5). Trois commentaires principaux peuvent être formulés.

* Les modes trouvés sont bien situés dans l'intervalle - m_t ≤ m ≤ + m_t, comme prévu en (7). Le mode m_t + 1 ou - m_t - 1, théoriquement évanescent, est parfois observé. Ceci ne remet nullement en cause le paragraphe 1.2.1 car les variations de température modifient la célérité du son et, par suite, la fréquence de coupure f_c(m) dans (5), ce qui peut changer d'une unité la valeur de m_t calculée. En outre, les modes où f_c(m) n'est que légèrement supérieure à la fréquence f étudiée, décroissent lentement le long du conduit et peuvent conserver un niveau notable dans la section explorée (ici à 285,5 mm en amont du bord d'attaque des aubes mobiles).

* Il existe toujours des modes intenses au voisinage de la coupure ± m_t. Ceci s'explique facilement parce que le profil radial de ces modes, nécessairement associé au mode radial le plus bas (cf. le commentaire après la relation 4), est concentré à la périphérie du conduit, où est effectuée la mesure (une analyse à un rayon plus petit privilégierait d'autres modes).

* En conduit lisse, le mode d'interaction $m_I = -14$ domine largement, comme prévu. Cependant, de nombreux autres modes sont trouvés dans le domaine propagatif calculé ($-m_c \leq m \leq +m_c$, avec ici $m_c = 15$), à cause des distorsions d'écoulement ; ces modes dépassent de plus de 20 dB le bruit de fond du spectre (à $|m| > m_c$).

* Avec le traitement absorbant conventionnel (deuxième courbe), tous les modes propagatifs sont réduits d'une dizaine de décibels, ainsi que les niveaux cohérents L_{coh} et total L_{Tot} de la raie, pratiquement égaux sur les trois graphiques (ils sont repérés sur ceux-ci par le trait en haut à gauche).

* La dernière partie de la figure 10 dégage tout l'apport de l'analyse modale. Le traitement optimisé ne produit qu'un gain supplémentaire de 1,5 dB sur L_{Tot}. Au contraire, le mode $m_I = -14$ subit une diminution excédentaire de 8,6 dB. Le piètre résultat sur L_{Tot} provient de tous les autres modes propagatifs, qui conservent bien sûr à peu près le même niveau avec les deux traitements : ce sont eux qui déterminent L_{Tot} dans ce troisième cas, parce que certains dépassent alors $L(m_I)$.
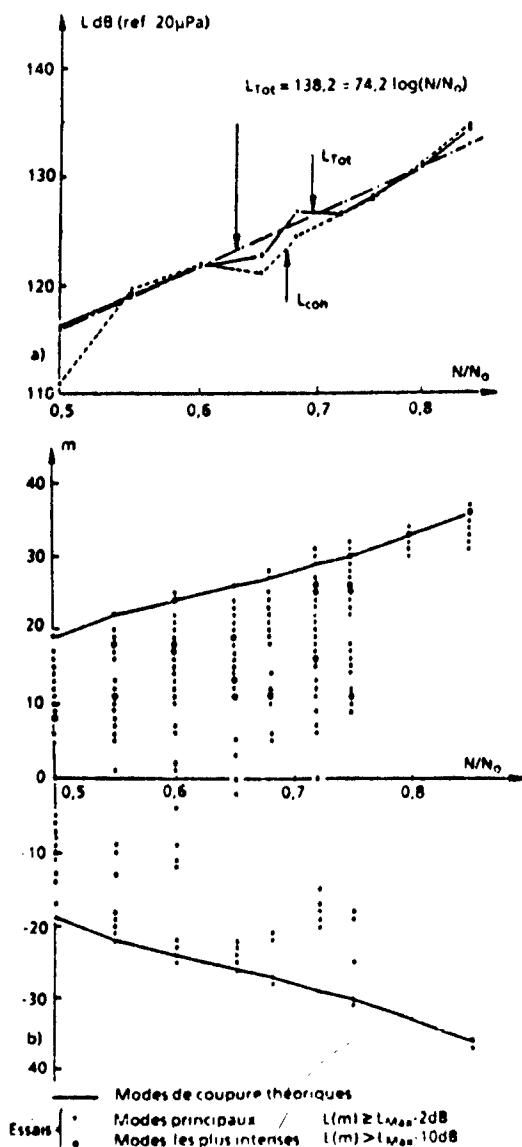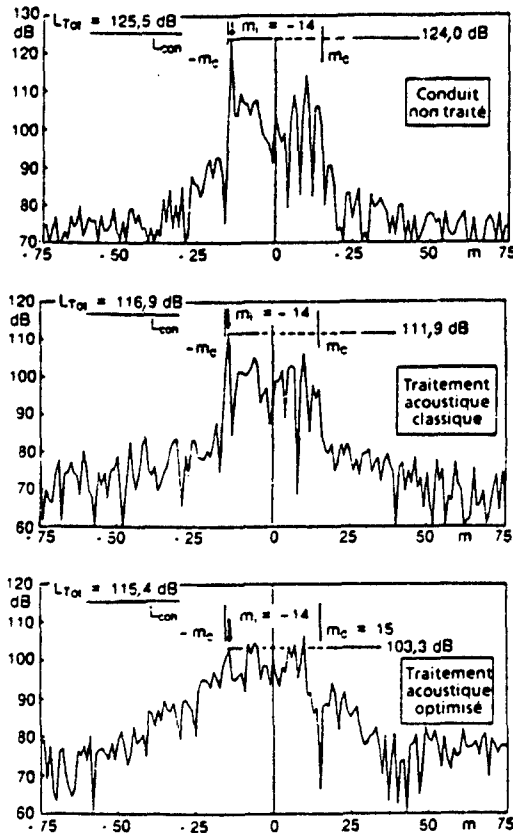

Figure 10 Effet de traitements absorbants sur la manche d'entrée du compresseur CA5 (B = 48, V = 62, espacement minimal), au régime $N = 0,4.N_o \simeq 5040$ tr/min : spectres de nombres d'ondes angulaires à la fréquence de passage des aubes $f = BN$.

En conclusion, la perte par insertion à $f = B.N$ est donnée au banc par :

$$\Delta L_{Stat} = L_{Tot}^R \cdot L_{Tot}^T. \qquad (18)$$

En vol, les modes dus aux distorsions d'écoulement disparaissent pratiquement en totalité, de sorte que la perte par insertion prévisible est certainement plus proche de :

$$\Delta L_{Vol} = L^R(m_I) \cdot L^T(m_I) . \qquad (19)$$

Le tableau suivant résume les valeurs trouvées : alors que les deux traitements produisent une perte par insertion ΔL_{Stat} de l'ordre de 10 dB au banc, celle en vol passerait de 12 dB avec le traitement classique à 21 dB avec celui optimisé par la SNECMA, ce qui prouve son efficacité.

Perte par insertion à $f = B.N$ / Traitement acoustique	Mesure au banc ΔL_{Stat}	Prévision en vol ΔL_{Vol}
Conventionnel	8,6 dB	12,1 dB
Optimisé	10,1 dB	20,7 dB

2. BRUIT DE JET

2.1. Rappels historiques

2.1.1. Généralités

L'intérêt pour le bruit de jet des moteurs d'avions date des années 1950 ; il est lié à la mise en service des avions de transport civils à réaction car ils étaient incomparablement plus bruyants que leur prédécesseurs à hélices. La gêne qu'ils créaient aux riverains des aéroports était très préoccupante et pouvait devenir un obstacle au développement harmonieux du transport aérien. C'est ainsi, à titre d'exemple, que les premiers avions civils à réaction (Caravelle, DC-8, VC-10) produisaient un bruit supérieur de quelque 15 dB au bruit des avions à hélices, qu'ils allaient peu à peu remplacer dans les flottes des compagnies aériennes. La poussée des avions à réaction étant produite par l'éjection d'un jet de grande vitesse (500 à 800 m/s), le bruit de jet est particulièrement pénalisant, non seulement à cause de son intensité mais également par ses autres caractéristiques, comme le diagramme de rayonnement et le spectre, beaucoup plus riche en hautes fréquences que celui engendré par une hélice.

Dans un tel contexte, les pouvoirs publics des pays possédant une industrie aéronautique ont favorisé, incité ou même financé de nombreuses études pour comprendre, connaître et réduire le bruit de jet. Elles ont été entreprises dans plusieurs directions : travaux théoriques, essais et recherches expérimentales en statique et en vol, études psycho-acoustiques, travaux préparatoires de la réglementation.

2.1.2. Travaux théoriques

C'est un fait bien connu que toute la théorie du bruit de jet repose sur les travaux de Lighthill [13, 14, 15]. Cet auteur a

relié les grandeurs acoustiques du jet aux caractéristiques de la turbulence de l'écoulement et a établi une équation (dite équation de Lighthill), dans laquelle il a isolé (mathématiquement parlant) un terme source caractéristique du milieu turbulent émissif. Les travaux de Lighthill ont suscité de très nombreuses et très fructueuses recherches sur les différents aspects du bruit de jet : génération, propriétés, rayonnement, etc. Citons, parmi les résultats les plus représentatifs, ceux de Ribner [16, 17], Ffowcs Williams [18] et Lilley [19]. Ces premiers travaux théoriques étaient tous axés sur la turbulence et, de ce fait, étaient appropriés plus au bruit de mélange qu'au bruit d'onde de choc, dont l'importance s'est manifestée quelques années plus tard. C'est également quelques années plus tard, vers 1970-1975, que les thèmes de "structure cohérente" et "d'instabilité d'onde" ont supplanté auprès des chercheurs celui de la turbulence, vue initialement par les théoriciens sous le seul aspect statistique.

Une retombée importante des premiers travaux théoriques (ceux de Lighthill en particulier) a été le développement des méthodes de prévision du bruit de jet, dont l'un des initiateurs a été Kobrynski [20].

2.1.3. Essais et recherches expérimentales

Les essais sur moteur à l'échelle 1 sont difficiles à mettre en oeuvre pour étudier le bruit de jet. Aux raisons d'ordre économique et de disponibilité des moteurs s'ajoutent des difficultés proprement techniques, comme la contamination du bruit de jet par d'autres sources du moteur (compresseur, turbine, etc.), l'espace nécessaire pour faire des mesures en champ lointain, avec les problèmes météorologiques et métrologiques associés. C'est pourquoi un grand effort a porté sur les moyens et les méthodes d'essais du bruit de jet sur maquettes.

Parmi les moyens d'essai, il faut mentionner les chambres anéchoïques. En France, une telle chambre a été construite au début des années 1960 au CEPr (Centre d'Essais des Propulseurs) et a été utilisée pendant de nombreuses années. Simultanément, on voit apparaître sur le marché des équipements nouveaux d'analyse et de traitement des mesures acoustiques, nécessaires pour manipuler et examiner l'énorme masse de données fournies par les essais.

C'est l'époque où l'on met également au point des procédés d'investigation au sein d'un jet turbulent. L'ONERA, en coopération avec la SNECMA, développe une méthode de caractérisation de la source du bruit dans les jets chauds, fondée sur la mesure de l'émission infrarouge, couplée aux techniques de corrélations de faisceaux croisés [21, 22, 23].

Les premiers essais réalisés dans les chambres anéchoïques avaient lieu en statique. On découvre quelques années plus tard que les propriétés du bruit de jet peuvent être profondément modifiées par le vol. Des moyens de simulation de l'effet de vol sont alors construits : ce sont les souffleries anéchoïques. La conception la plus couramment adoptée est la soufflerie à veine ouverte. C'est le cas en France de CEPRA 19, implantée au CEPr vers 1975-1980 et qui est toujours utilisée sous la responsabilité de l'ONERA (cf. paragraphe 3).

2.1.4. Etudes psycho-acoustiques

C'est également aux caractéristiques spectrales particulières du bruit de jet que l'on doit le lancement des études psycho-acoustiques destinées à trouver une unité acoustique représentative de la gêne créée par le bruit de jet. Ces études,

menées surtout aux Etats-Unis par Kryter [24], vont donner naissance aux PNdB (Perceived Noise Decibels) et aux EPNdB (Effective Perceived Noise Decibels), tenant compte de la durée de passage de l'avion. Ils sont aujourd'hui d'un usage très courant pour la certification aéronautique. L'adoption de ces unités complexes, en rendant nécessaire la connaissance des spectres à tous les azimuts, s'est révélée être un facteur d'approfondissement et de caractérisation fine du bruit de jet.

2.1.5. Réglementation

La certification acoustique des aéronefs promulguée par l'OACI (Organisation de l'Aviation Civile Internationale) en 1969 a été préparée pendant plusieurs années. Les travaux préparatoires et les normes de bruit retenues ont été fortement influencés par les caractéristiques du bruit de jet, source sonore principale dans les premiers types de moteurs d'avions civils et dont la réduction se heurtait à des difficultés techniques et économiques énormes.

2.2. Description du bruit de jet

2.2.1. Caractérisation du bruit de jet

Le bruit de jet est caractérisé en champ lointain (figure 11), pour une distance donnée (r à la tuyère ou d à l'axe du moteur) et un angle de rayonnement α, si la tuyère est de révolution, par :
- un niveau de pression sonore global ou dans une unité de gêne (PNdB par exemple) ;
- le spectre sonore.
L'ensemble de ces grandeurs permet de tracer le diagramme de rayonnement.

Si la tuyère n'est pas de révolution, un deuxième angle ψ (angle de gîte) doit être considéré et l'on obtient un ensemble de diagrammes de rayonnement.
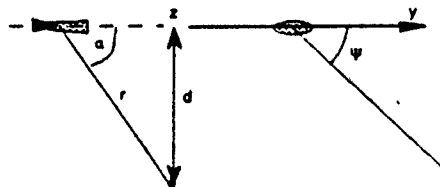

Figure 11 Paramètres géométriques de mesure du bruit de jet en champ lointain.

2.2.2. Simple flux subsonique

Le cas élémentaire le plus simple est un mono-flux subsonique. L'écoulement est éjecté dans l'atmosphère à une vitesse moyenne V_j dans le plan de sortie de la tuyère. En aval de ce plan, on distingue les régions suivantes (figure 12a) :
- le cône potentiel, dans lequel l'écoulement comprend uniquement le fluide provenant de l'intérieur du moteur ;
- l'air ambiant ;
- la zone de mélange alimentée à la fois par le cône potentiel et par l'air ambiant.
Dans la zone de mélange, se développent de fortes turbulences, sources du bruit de jet.

En statique, le bruit engendré par chaque paquet turbulent est soumis aux influences ou modifications suivantes (figure 12b) :
- un effet de convection est dû à la vitesse de l'écoulement ;
- le rayonnement émis par le paquet turbulent subit la

réfraction produite par le profil des températures et des vitesses le long du trajet acoustique ;

- la source turbulente est soumise aux influences provenant de l'intérieur du moteur, qui peuvent être soit d'origine aérodynamique (agissant directement sur les caractéristiques de la turbulence locale), soit d'origine acoustique (bruit créé par d'autres sources internes comme le compresseur, la turbine ou la chambre de combustion), ce qui est susceptible de modifier le bruit de jet proprement dit [25] ;

- enfin, le développement de la zone de mélange turbulente ainsi que les effets de convection et de réfraction dépendent de la géométrie de la tuyère.
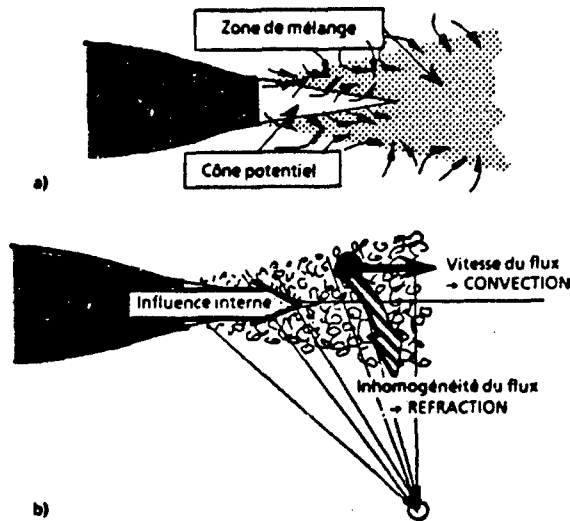

a)

b)

Figure 12 Bruit émis par un jet mono-flux subsonique.
a) Schéma du jet.
b) Modifications du bruit engendré.

Les principaux facteurs déterminant le niveau de puissance acoustique sont, d'abord, la vitesse d'éjection de l'écoulement et, d'autre part, une grandeur caractérisant les dimensions (par exemple, section de tuyère ou débit masse).

En vol, aux phénomènes décrits ci-dessus s'ajoute (outre l'effet Doppler qui déplace les fréquences) une action sur la structure de la région turbulente qui modifie, de ce fait, les caractéristiques du bruit de jet par rapport au cas statique.

Que ce soit en statique ou en vol, le bruit de jet d'un moteur installé sur un avion subit également les effets d'installation, c'est-à-dire les réflexions ou diffractions sur les structures de l'avion.

2.2.3. Double flux

Dans un double flux, les phénomènes sont fondamentalement les mêmes. Les deux flux donnent naissance à deux cônes potentiels ainsi qu'à deux zones de mélange, qui elles-mêmes se mélangent, comme illustré sur la figure 13.

L'utilisation dans les avions de transport civils des turbosoufflantes (turboréacteurs à deux flux), qui sont moins bruyantes que les mono-flux, a donné l'impression que le bruit de jet d'un double flux est inférieur au bruit de jet d'un mono-flux. En fait, le bruit plus faible des doubles flux a pour cause les vitesses d'éjection plus basses. Il a été établi

expérimentalement que, comparé à un flux unique équivalent (égalité de débit masse, égalité d'enthalpie et égalité de poussée), un double flux classique ou à profil des vitesses normal (vitesse extérieure plus faible que la vitesse intérieure) est légèrement plus bruyant. En revanche, un double flux à profil des vitesses inversé (c'est-à-dire dans lequel la vitesse extérieure est plus grande que la vitesse intérieure) est moins bruyant que le flux unique équivalent correspondant.
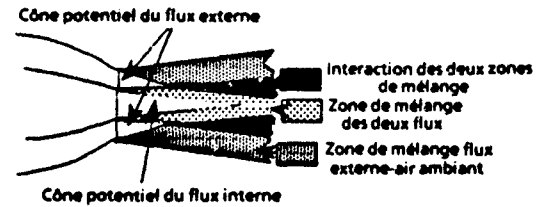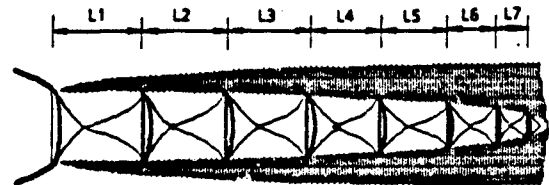

Figure 13 Schéma d'un jet double flux.

2.2.4. Simple flux supersonique

Lorsqu'un écoulement supersonique (rapport de pression supérieur au rapport critique) alimente une tuyère convergente, il se crée en aval de la section d'éjection une série de cellules de chocs (figure 14).

Structure des ondes de chocs
dans un jet supercritique convergent

Figure 14 Structure des ondes de choc dans un jet supercritique convergent.

L'interaction entre le processus de mélange mentionné dans le paragraphe précédent et les cellules de choc produit un bruit supplémentaire au bruit de mélange, appelé bruit d'onde de choc, qui possède, d'une part, une composante à large bande et, d'autre part, des fréquences discrètes appelées "screech".

Le bruit d'onde de choc rayonne essentiellement vers l'amont du moteur. On caractérise simplement ce bruit par le niveau et le spectre du bruit de jet à l'angle d'émission $\alpha = 130°$, où il est sensiblement supérieur au bruit de mélange. Le paramètre fondamental du bruit d'onde de choc est β ($\beta^2 = M_j^2 - 1$, où M_j est le nombre de Mach correspondant à une détente complète du jet).

La figure 15 fournit quelques illustrations des phénomènes qui viennent d'être décrits (dans ce paragraphe, V est une vitesse).

2.3. Méthodes de prévision

Compte tenu de ce qui vient d'être présenté au paragraphe 2.2 sur la génération du bruit de jet, il est clair que les phénomènes sont trop complexes pour envisager une méthode de prévision purement théorique, valable dans tous les cas possibles. De fait, la plupart des méthodes de prévision existantes sont, à la fois, "spécialisées" et semi-empiriques. La spécialisation s'opère selon les caractéristiques suivantes :

- bruit de mélange ou bruit d'onde de choc,

- mono-flux ou double flux,
- dans le cas d'un double flux, profil des vitesses normal ou inversé,
- bruit en statique ou en vol,
- domaine de validité pour les paramètres aérothermodynamiques ou géométriques,
- forme de la tuyère.

Les méthodes de prévision publiées depuis 1979 sont données dans les références 26 à 42. Les plus opérationnelles sont décrites brièvement dans le tableau ci-après. Elles sont toutes relatives à des tuyères sans silencieux. Les moyens de réduire l'émission sonore sont présentés dans le paragraphe suivant.

METHODES DE PREVISION DU BRUIT DE JET								
Référence	Bruit de		Mono-flux	Bi-flux à profil		Effet de vol	Domaine de validité	Commentaires
	mélange	choc		normal	inversé			
26	X	X			X	X	Vs/Vp: 1,03 à 2,8 Ts/Tp: 0,36 à 2,76 Ts: 394 à 1089 K As/Ap: 0,65 à 1,48	
30, 32 et 37	X		X	X		X		Modèle théorique de transposition du statique en vol
31	X	X			X	X		Tuyère à corps central
34	X	X	X			X		
35	X			X		X	Ds/Dp: 4 à 6 Vs/Vp: 0,65 à 0,95 Vs: 120 à 300 m/s Ts/Tp: 0,4 à 0,5 Ts: 300 à 360 K	Méthode dont le domaine de validité est restreint aux turboréacteurs à grand taux de dilution, comprenant une correction due à l'excitation du jet par des sources internes.
36	X	X		X				Version révisée d'une méthode NASA de 1974.
38	X		X	X	X		Ve/s: 0,3 à 2 Ts/Ts: 0,7 à 4,5 Vs/Vp: 0,02 à 2,5 Ts/Tp: 0,2 à 4 As/Ap: 0,5 à 10	
40, méthode 1	X			X				Ex méthode de Rolls-Royce (1975)
40, méthode 2	X			X	X		As/Ap: 1 à 6 Vs/Vp: 0,4 à 2,5 Ts/Tp: 0,33 à 3 Vp: 150 à 600 m/s Ve: 120 à 750 m/s Vs: 120 à 600 m/s	Ex méthode de Boeing (1977)
40, méthode 3	X		X	X	X		Ve/s: 0,3 à 2 Ts/Ts: 0,7 à 4,5 Vs/Vp: 0,02 à 2,5 Ts/Tp: 0,2 à 4 As/Ap: 0,5 à 10	Ex méthode de la NASA-Langley (1983), identique à celle de la référence 38
41	X			X		X	As/Ap: 1,5 à 3,5 Ds/Dp: 2 à 6,5 Vs/Vp: 0,6 à 0,95 Vs: 140 à 330 m/s Ts/Tp: 0,35 à 0,5 Ts: 290 à 360 K	
42		X	X					Modèle théorique

Notations

A	aire		
A	célérité du son	Indice a	atmosphérique
D	débit masse	Indice e	relatif au flux unique équivalent
V	vitesse du jet	Indice p	primaire
Tt	température totale	Indice s	secondaire

Champ sonore d'un jet subsonique

a)

Bruit de jet du Viper 601

b)

Spectres du Viper en vol à V = 172 KTS
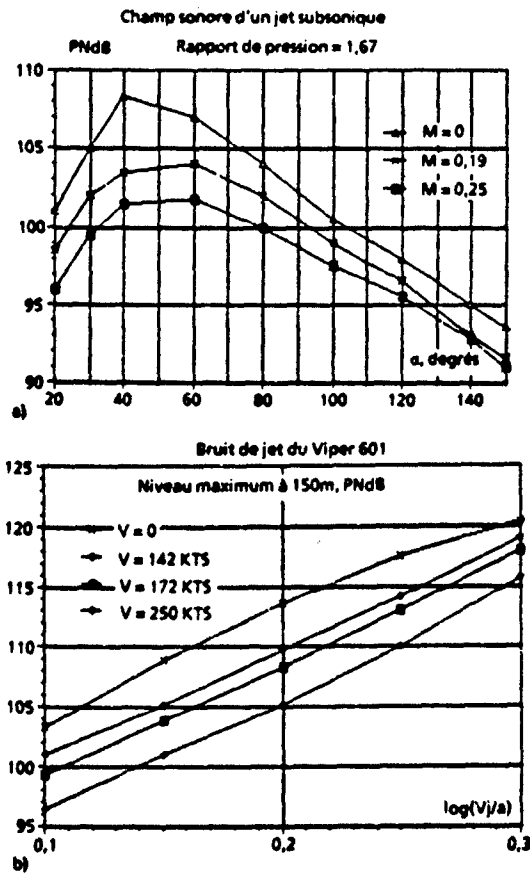

c)

Spectres du Viper en vol à V = 172 KTS

c)

Figure 15 Exemples de mesures de bruit de jet.
Extrait de [45].
a) Champ sonore d'un jet supersonique (M = nombre de Mach d'avancement).
b) Bruit de jet du Viper 601 (V = vitesse d'avancement).
c) Spectres acoustiques rayonnés par le Viper en vol à V = 172 kts, à α = 150° et 30°.

2.4. Moyens de réduction

2.4.1. Réduction du bruit de mélange [43-48]

Si on se limite à une réduction passive, les deux seuls moyens possibles sont :
- d'agir sur la génération de la source ;
- d'agir sur le développement de la région source (zone de mélange).

Le premier procédé se limite à une diminution de la vitesse d'éjection moyenne, ce qui, à poussée constante, nécessite une augmentation des dimensions du moteur. C'est grâce à ce moyen que les doubles flux à grand taux de dilution produisent un bruit de jet relativement faible.
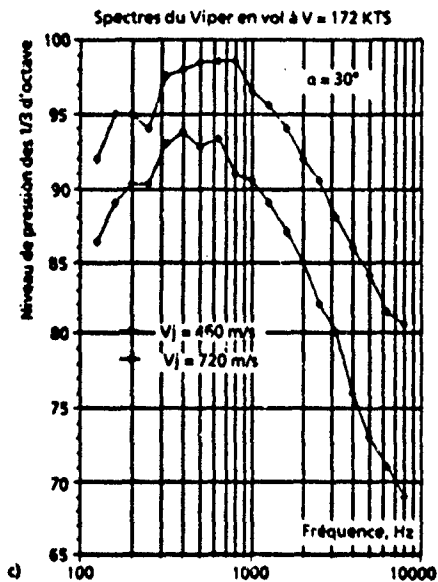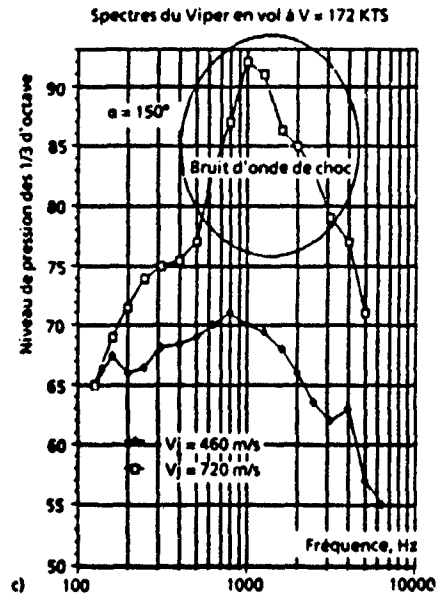
Le deuxième procédé consiste à accélérer le mélange entre le jet et l'air ambiant, de façon à diminuer le volume de la zone de mélange, siège des turbulences qui sont les sources sonores. Une grande variété de techniques, dont les plus connues sont décrites ci-après, peuvent être utilisées pour obtenir l'accélération du mélange.

Augmentation du périmètre de contact entre le jet et l'atmosphère

Cet effet est obtenu simplement avec une tuyère bidimensionnelle (figure 16a). Outre une réduction de la puissance acoustique, une tuyère rectangulaire (hauteur h, largeur L) produit aussi un effet bénéfique grâce au rayonnement dans la direction $\psi = 0$.
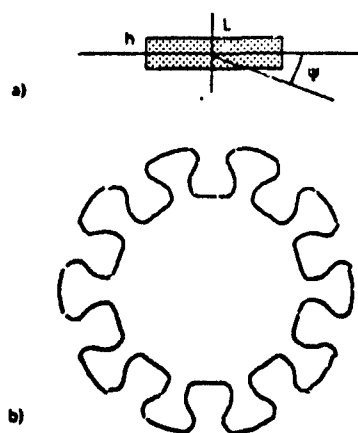
Figure 16 Moyens de réduction du bruit de jet.
a) Tuyère rectangulaire.
b) Mélangeur.

Une tuyère annulaire permet également d'augmenter le périmètre de contact du jet avec l'atmosphère. Des tuyères annulaires de révolution ont fait l'objet de plusieurs études orientées d'ailleurs vers la réduction du bruit d'onde de choc. Peu de données existent sur des tuyères annulaires bidimensionnelles.

Utilisation de mélangeurs

Une autre façon d'augmenter le périmètre de contact du jet avec l'atmosphère est d'utiliser une tuyère avec des ondulations ou corrugations (figure 16b).

Avec une telle géométrie, on se rapproche déjà de techniques propres aux silencieux-mélangeurs. Dans ces dispositifs, dont le but est d'accélérer le mélange, l'air extérieur est conduit vers l'intérieur de l'écoulement ou, à l'inverse, l'air du jet est guidé vers l'extérieur. La fonction de guidage est assurée par des formes diverses. On obtient ainsi des silencieux à "tubes", à "lobes", à "gouttières". Un des silencieux étudiés par la SNECMA pour l'Olympus de Concorde utilisait des palettes qui dirigeaient l'écoulement intérieur vers l'extérieur. A cause de ces palettes ou pelles, le dispositif a été baptisé "silencieux à pelles".

Les problèmes techniques les plus importants posés par les silencieux sont :
- d'obtenir une faible réduction des performances du moteur, surtout en croisière ;
- d'avoir un silencieux qui réduit le bruit de façon significative, non seulement en statique, mais aussi en vol. Le "silencieux à pelles" s'est révélé à cet égard particulièrement décevant puisqu'il a perdu en vol toute son efficacité constatée en statique.

Il a été trouvé expérimentalement qu'une façon de conserver en vol les bonnes performances acoustiques du silencieux est de le compléter par un éjecteur. L'efficacité du système est augmentée si un traitement acoustique est appliqué sur l'éjecteur.

2.4.2. Réduction du bruit d'onde de choc [43, 49-54]

Comme le bruit d'onde de choc provient de l'interaction entre le mélange et les cellules de choc, tout système qui perturbe l'établissement de ces cellules est susceptible d'atténuer le bruit d'onde de choc.
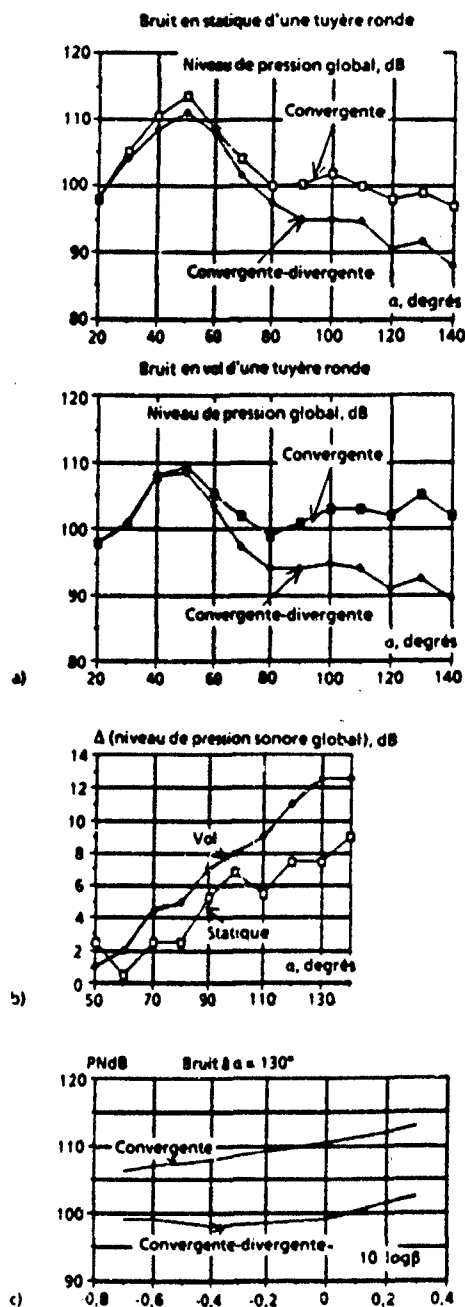

Figure 17 Réduction du bruit d'onde de choc.
Extrait de [43].
a) Bruit en statique et en vol d'une tuyère circulaire.
b) Efficacité du convergent-divergent.
c) Bruit à α = 130°.

Le moyen le plus efficace est, dans ces conditions, l'utilisation d'une tuyère convergente-divergente adaptée, puisqu'une telle tuyère supprime les ondes de choc. Par rapport à une tuyère convergente, une réduction significative du bruit est obtenue dans tout l'arc amont. Un autre grand intérêt d'une tuyère convergente-divergente est qu'elle réduit le bruit d'onde de choc non seulement au point d'adaptation mais pour une large plage du paramètre β (c'est-à-dire du rapport de pression). Il est également intéressant de remarquer que la réduction du bruit d'onde de choc en vol est supérieure à celle en statique. La figure 17, extraite de [43], illustre ces résultats. Le cas de vol correspond à la vitesse de 120 m/s simulée dans une soufflerie anéchoïque.

D'autres procédés ont été essayés pour briser la structure des cellules d'un jet supersonique sous-détendu. Leur efficacité est inférieure à celle du convergent-divergent. Une technique relativement simple consiste à utiliser des parois poreuses pour modifier la structure aérodynamique de l'écoulement supersonique. L'utilisation d'un corps central poreux a fait l'objet de plusieurs études [49, 50, 51].

3. SOUFFLERIE ANECHOIQUE CEPRA 19

3.1. Définition des besoins

Dans le contexte de la perturbation de l'environnement, les mesures acoustiques du bruit d'un avion doivent être faites en conditions de champ lointain, c'est-à-dire que la distance de la source acoustique au point de mesure doit être grande par rapport à l'avion et aux longueurs d'onde examinées. Si l'on veut éviter le coût très élevé des essais en vol, les essais sur maquettes doivent alors être effectués dans une chambre de mesure dont les dimensions sont grandes par rapport à celles de la maquette et dont les parois sont traitées de façon à simuler une propagation en milieu libre infini.

Les similitudes de Mach, de Reynolds et de Strouhal étant incompatibles, la plupart des essais aéroacoustiques sur les rotors et les jets sont faits en similitudes compatibles de Mach et de Strouhal et il est admis que l'écart en nombre de Reynolds a un effet négligeable. Ainsi, entre les conditions réelles et les essais sur maquettes, les vitesses sont conservées et les fréquences sont augmentées dans l'inverse du rapport des longueurs.

Pour les machines tournantes (soufflantes et compresseurs), il faut disposer de maquettes complexes et de leur motorisation. Le point ne sera pas développé ici car l'installation CEPRA 19 n'est pas encore équipée pour entraîner des rotors de grandes dimensions.

Pour les jets, la figure 18 permet de suivre l'enchaînement des implications. Pour simuler le fonctionnement en vol (cf. paragraphe 2.2), le ou les jets de la maquette de moteur doivent se développer dans un écoulement uniforme, c'est-à-dire dans le cône potentiel du jet libre de la soufflerie reproduisant la vitesse de vol. D'autre part, le plan d'éjection des maquettes de tuyères doit se trouver suffisamment loin du brod de la tuyère de la soufflerie pour permettre des mesures acoustiques en zone calme dans l'arc amont des maquettes. L'ensemble de ces exigences n'est pas rempli dans les installations anciennes. La figure 18 montre que l'installation CEPRA 19 :

- permet de faire des mesures jusqu'à près de 160° (comptés à partir de l'axe du jet),
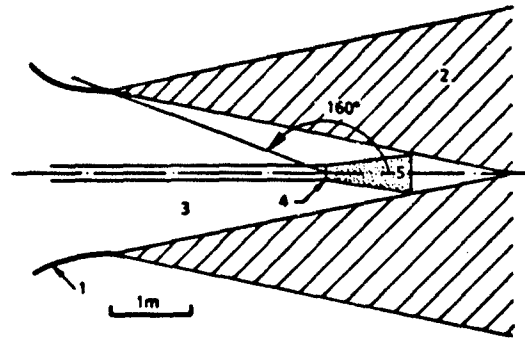- permet aux jets des maquettes de se développer en écoulement homogène sur environ 1 m.

Figure 18 Schéma de principe d'une expérience de bruit de jet à CEPRA 19.
1 - Convergent de la soufflerie.
2 - Zone de mélange de la veine libre de la soufflerie.
3 - Cône potentiel de la veine libre.
4 - Maquette de tuyère.
5 - Région des sources acoustiques des jets de maquettes de tuyères.

Cette dernière distance implique que le diamètre des maquettes de tuyères ne doit pas dépasser 10 cm, s'il est admis que toutes les sources acoustiques importantes sont situées à moins de 10 diamètres.

Pour un réacteur de 1 m de diamètre, l'échelle de réduction est alors de 1/10.

3.2. Possibilités actuelles de l'installation

La vitesse de soufflage reproduisant les conditions de vol est réglable entre 0 et 100 m/s.

Les maquettes de tuyères peuvent recevoir deux flux distincts d'air comprimé :
- le flux central peut avoir un débit de 4 kg/s avec un taux de détente de 3,4 et une température de 300 à 1100 K obtenue par combustion de propane ;
- le flux extérieur peut avoir un débit de 17 kg/s avec un taux de détente de 3,4 et une température de 300 à 400 K.

Ces paramètres correspondent bien au domaine des avions de transports subsoniques ; ils nécessitent des modifications pour les avions de transport supersoniques et pour les avions de combat.

3.3. Modifications prévues pour les avions de transport supersoniques

Une modification importante prévue concerne l'augmentation de la vitesse de vol simulée. Comme il a été expliqué au paragraphe 3.1, il n'est pas souhaitable de changer la configuration géométrique. Si le diamètre de veine libre de soufflerie (2 m) est conservé, une augmentation de vitesse ne peut être obtenue que par une augmentation de débit. Compte tenu de la réserve de puissance sur le moteur de la soufflerie, il est prévu de faire passer prochainement la vitesse maximale à 120 m/s (voire 130 m/s), au prix de travaux qui ne seraient pas trop importants.

Cette nouvelle vitesse correspond bien aux vitesses de décollage ou d'approche d'un avion de transport supersonique

mais elle sera encore insuffisante pour simuler un survol d'avion de combat à basse altitude.

3.4. Perspectives ultérieures

Une vitesse de soufflerie supérieure à 120 m/s pourrait être obtenue, sans toucher au groupe motoventilateur, par réduction de diamètre de la tuyère de veine libre, dans le cadre d'un compromis avec les exigences rappelées au paragraphe 3.1.

Pour un avion de combat, les taux de détente de jet primaire actuellement disponibles peuvent être jugés insuffisants. La possibilité d'augmenter le taux de détente primaire est actuellement examinée. Ce besoin rejoindrait d'éventuelles demandes concernant les lanceurs spatiaux.

Enfin, pour en revenir aux parties tournantes, une étude sur leur motorisation, soit électrique, soit par turbine à air comprimé, va être commencée.

CONCLUSION

Cette communication montre qu'un effort considérable a été consenti au cours de ces quatre dernières décennies, depuis l'avènement des avions à réaction civils, pour prévoir et réduire le bruit des turboréacteurs. Les travaux ont porté essentiellement sur les deux sources sonores prépondérantes, les compresseurs et les jets. Des analyses théoriques approfondies, des méthodes de diagnostic originales et des installations d'essais spéciales ont été développées, de sorte que les mécanismes générateurs de bruit sont maintenant bien compris. Des études intensives continuent toutefois d'être menées, par exemple pour le transport supersonique, car tous les problèmes sont loin d'être résolus, certainement à cause de la complexité des phénomènes physiques en jeu : en particulier, il n'existe toujours pas de méthode de prévision du bruit de jet purement théorique, c'est-à-dire ne recourant pas à des facteurs semi-empiriques déduits de l'expérience.

La nuisance acoustique produite par les avions de combat ne suscite de l'intérêt que depuis quelques années seulement et aucune mesure n'a encore été prise pour réduire l'émission sonore de leurs moteurs. Ceux-ci possèdent certaines caractéristiques spécifiques (citons entre autres la post-combustion) et il serait illusoire d'espérer transposer directement les succès obtenus en aviation commerciale. Cependant, grâce aux acquis qui viennent d'être rappelés, des progrès assez rapides sont envisageables si des programmes de recherche orientés sur le domaine militaire sont mis en place.

REFERENCES BIBLIOGRAPHIQUES

[1] Committee on the Challenges of Modern Society, "Aircraft Noise in a Modern Society", Final Report of the Pilot Study No. 185, North Atlantic Treaty Organization, Nov. 1989.

[2] Fourmaux, A., "Computation of Unsteady Flows in Turbomachine Cascades", 15th Congress of the International Council of the Aeronautical Sciences, London, England, September 7-12, 1986, ICAS Proceedings 1986, Vol. 2, pp. 951-956.

[3] Tyler, J.M., and Sofrin, T.G., "Axial Flow Compressor Noise Studies", SAE Transactions, 70, 1962, pp. 309-332.

[4] Léwy, S., Lambourion, J., Malarmey, C., Pérulli, M., and Rafine, B., "Direct Experimental Verification of the Theoretical Model Predicting Rotor Noise Generation", AIAA 79-0658, March 1979.

[5] Léwy, S., "Exact and Simplified Computation of Noise Radiation by an Annular Duct", Inter-noise 88, Avignon, France, 30 August-1 September 1988, Proceedings, Vol. 3, pp. 1559-1564.

[6] Rice, E.J., "Multimodal Far Field Acoustic Radiation Pattern Using Mode Cutoff Ratio", AIAA J., 16, 9, September 1978, pp. 906-911.

[7] Raffy, P., Léwy, S., Lambourion, J., and Chatanier, M., "Investigation of Subsonic Fan Noise Sources by Fluctuating Pressure Measurements on Rotating Blades", AIAA 77-1321, October 1977, & AIAA J., 16, 8, August 1978, pp. 777-778.

[8] "Methods of Controlling Distortion of Inlet Airflow During Static Acoustical Tests of Turbofan Engines and Fan Rigs", AIR 1935, Society of Automotive Engineers, February 1985.

[9] Hanson, D.B., "Spectrum of Rotor Noise Caused by Atmospheric Turbulence", J. Acoust. Soc. Am., 56, 1, July 1974, pp. 110-126.

[10] Léwy, S., Canard-Caruana, S., and Julliard, J., "Experimental Study of Noise Sources and Acoustic Propagation in a Turbofan Model", AIAA 90-3950, October 1990.

[11] Léwy, S., Canard-Caruana, S., and Kerviel, P., "Study of Propagating Acoustic Sources in a Fan Intake by Modal Analysis of Tone Noise", Inter-noise 88, Avignon, France, 30 August-1 September 1988, Proceedings, Vol. 2, pp. 751-754.

[12] Léwy, S., Lambourion, J., et Raffy, P., "Analyse des sources du bruit de raies en amont de soufflantes", Revue d'Acoustique, 12ème année, No. 48, 1979-1/4, pp. 19-25.

[13] Lighthill, M.J., "On Sound Generated Aerodynamically. I. General Theory", Proc. Roy. Soc., A, 211, March 1952, pp. 564-587.

[14] Lighthill, M.J., "On Sound Generated Aerodynamically. II. Turbulence of a Source of Sound", Proc. Roy. Soc., A, 222, February 1954, pp. 1-32.

[15] Lighthill, M.J., "Sound Generated Aerodynamically", The Bakerian Lecture, 1961. Proc. Roy. Soc., A, 267, May 1962, pp. 147-182.

[16] Ribner, H.S., "On the Strength Distribution of Noise Sources Along a Jet", J. Acoust. Soc. Am., 30, 9, September 1958, p. 876.

[17] Ribner, H.S., "The Generation of Sound by Turbulent Jets", in "Advances in Applied Mechanics", Vol. 8, Academic Press Inc., New York, 1964, pp. 103-182.

[18] Ffowcs Williams, J.E., "The Noise from Turbulence Convected at High-Speed", Phil. Trans. Roy. Soc., A, 255, 1963, pp. 469-503.

[19] Lilley, G.M., "On the Noise from Air Jets", Aero. Res. Counc. Lond., 20, 376-N, 40-F, M-2724, 1958.

[20] Kobrynski, M., "General Method for Calculating the Sound Pressure Field Emitted by Stationary or Moving Jets", in "AFOSR-UTIAS Symposium on Aerodynamic Noise", Toronto, May 1968, pp. 111-130.

[21] De Belleval, J.F., and Maulard, J., "Noise Source Characterization of Hot Jets by the Crossed-Beam Technique", Sixth International Congress on Instrumentation in Aerospace Simulation Facilities, Ottawa, September 1975.

[22] De Belleval, J.F., Maulard, J., et Pérulli, M., "Caractérisation des sources de bruit dans les jets chauds par la technique des faisceaux croisés", AGARD CP-193, Mai 1976.

[23] Dahan, C., Elias, G., Maulard, J., and Pérulli, M., "Coherent Structures in the Mixing Zone of a Subsonic Hot Free Jet", J. of Sound and Vibration, 59, 3, August 1978, pp. 313-333.

[24] Kryter, K.D., "The effects of Noise on Man", Academic Press, 1970, 2nd Edition, July 1985.

[25] Deneuville, P.M., and Jacques, J.R., "Jet Noise Amplification: A Practically Important Problem", AIAA 77-1368, October 1977.

[26] Larson, R.S., "A Jet Exhaust Noise Prediction Procedure for Inverted Velocity Profile Coannular Nozzles", AIAA 79-0633, March 1979.

[27] Stone, J.R., "An Improved Method for Predicting the Effects of Flight on Jet Mixing Noise", NASA TM-79155, 1979.

[28] Dash, R., "Analysis of Flight Effects on Noise Radiation from Dual-Flow Coaxial Jets", AIAA 79-0619, March 1979.

[29] Russell, J.W., "A Method for Predicting the Noise Levels on Coannular Jets with Inverted Velocity Profiles", NASA CR-3176, 1979.

[30] Michalke, A., and Michel, U., "Prediction of Flyover Noise from Plain and Coannular Jets", AIAA 80-1031, June 1980.

[31] Bhutiani, P.K., "A Unique Coannular Plug Nozzle Jet Noise Prediction Procedure", AIAA 80-1007, 1980.

[32] Michel, U., and Michalke, A., "Prediction of Flyover Jet Noise Spectra from Static Tests", NASA TM-83219, 1981.

[33] Obermeier, F., "Some Comments on the Prediction of Forward Flight Effects on Jet Noise", Max Planck Institut 20/1981, 1981.

[34] "Gas Turbine Jet Exhaust Noise Prediction", ARP 876B, 1981, and ARP 876C, Society of Automotive Engineers, 1985.

[35] McDonald, W.B., and Lu, H.Y., "Prediction of High Bypass Ratio Engine Static and Flyover Jet Noise", AIAA 83-0773, 1983.

[36] Stone, J.R., Groesbeck, D.E., and Zola, C.L., "Conventional Profile Coaxial Jet Noise Prediction", AIAA J., 21, 3, March 1983, pp. 336-342.

[37] Rawls, J.W., "Comparison of Forward Flight Effects Theory of A. Michalke and U. Michel with Measured Data", NASA CR-3665, 1983.

[38] Russel, J.W., "An Empirical Method for Predicting the Mixing Noise Levels of Subsonic Circular and Coaxial Jets", NASA CR-3786, 1984.

[39] Knott, P.R., Janardan, B.A., and Majjigi, R.K., "Free Jet Acoustic Investigation of High-Radius Ratio Coannular Plug Nozzle", NASA CR-3818, 1984.

[40] "Gas Turbine Coaxial Exhaust Flow Noise Prediction", AIR 1905, Society of Automotive Engineers, December 1985.

[41] Lu, H.Y., "An Empirical Model for Prediction of Coaxial Jet Noise in Ambient Flow", AIAA 85-1912, July 1986.

[42] Tam, C.K.W., "Broadband Shock-Associated Noise of Moderately Imperfectly Expanded Supersonic Jets", J. of Sound and Vibration, 140, 1, July 1990, pp. 55-71.

[43] Yamamoto, K.J., Brausch, J.F., Balsa, T.F., Janardan, B.A., and Knott, P.R., "Experimental Investigation of Shock Cell Noise Reduction for Single Stream Nozzle in Simulated Flight", NASA CR-3845, 1984.

[44] Gliebe, P.R., "Diagnostic Evaluation of Jet Noise Suppression Mechanisms", AIAA 79-0674, March 1979.

[45] Brooks, J.R., McKinnon, R.A., and Johnson, E.I., "Results from Flight Noise Tests on a Viper Turbojet Fitted with Ejector/Suppressor Nozzle Systems", AIAA 80-1028, June 1980.

[46] Fitzsimmons, R.D., McKinnon, R.A., Johnson, E.S., and Brooks, J.R., "Flight and Wind Tunnel Test Results of a Mechanical Jet Noise Suppressor Nozzle", AIAA 80-0165, 1980.

[47] McKinnon, R.A., Johnson, E.S., and Atencio, A., "Jet Noise Results from Static Wind Tunnel and Flight Tests of Conical and Mechanical Suppressor Nozzles, AIAA 81-1995, 1981.

[48] Brausch, J.F., "Simulated Flight Acoustic Investigation on Mechanical Suppressors for Jet Noise Reduction", NASA CR-4019, 1986.

[49] Maestrello, L.A., "Initial Results of Porous Plug Nozzle for Supersonic Jet Noise Suppression", NASA TM-78802, 1978.

[50] Bauer, A.B., "Jet Noise Suppression by Porous Plug Nozzles", AIAA 81-1993, October 1981.

[51] Das, I., and Dosanjh, D.S., "Noise Suppression of Supersonic Jets by Contoured and Porous Conical Plug-Nozzles", AIAA 84-2363, October 1984.

[52] Janardan, B.A., Yamamoto, K., and Majjigi, R.K., "Experimental Investigation of Shock-Cell Noise Reduction for Dual-Stream Nozzles in Simulated Flight", NASA CR-3846, 1984.

[53] Stone, J.R., "Supersonic Jet Shock Noise Reduction", AIAA 84-2278, October 1984.

[54] Ahuja, K.K., Manes, J., Calloway, A., and Massey, K., "An Evaluation of Various Concepts of Reducing Supersonic Jet Noise", AIAA 90-3982, October 1990.

Discussion

QUESTION BY: W.B. de Wolf, NLR, The Netherlands

To my understanding rotor-stator interaction noise is generated by rotor wake impingement on the downstream stator blades which act as the primary noise sources.

The noise from the stator blades propagates upstream and passes the rotor where it may be measured by microphones on the rotating blades as in your test set-up.

Could you relate the amplitude of the pressure fluctuations on the rotor blades to possibly measured pressures on the stator blades or sound pressure levels in the intake duct or outside the inlet?

AUTHOR'S RESPONSE:

I agree with your model of rotor-stator interaction. However, there is probably also an interaction between the rotor and the stator (outlet guide vanes, OGV) potential field. For instance, the lines $f - VN - 98 N$ in the blade pressure spectra of Fig. 6 may be due both to this potential field and to the acoustic waves generated on the stator vanes. It seems very difficult to separate these two components. It is the reason why we have not attempted to relate the amplitude of the pressure fluctuations on the rotor blades to that on the stator vanes.

Moreover, the rotor under study here (48 blades) has a very high solidity. It is thus assumed that the acoustic waves generated on the OGV mainly radiate downstream, and not upstream through the blade row. This is not shown in the paper, but it may be deduced from OGV pressure measurements presented in Ref. 10. The explanation is the following one. The OGV pressure fluctuations are not modified with or without the inflow control device (ICD, or "Filter tranquillisateur" in Fig. 5). On the contrary the noise levels radiated upstream are reduced by about 10 dB with the ICD.

SUPERSONIC ACOUSTIC SOURCE MECHANISMS FOR FREE JETS OF VARIOUS GEOMETRIES

John M. Seiner
Michael K. Ponton
NASA Langley Research Center
Mail Stop 165
Hampton, VA 23665-5225 USA

SUMMARY

The aeroacoustic performance of several generic nozzle geometries was tested to evaluate the potential benefits of using non-round jet exit geometries to reduce noise from combat military aircraft. Both the aerodynamics and far field acoustics of several $M_d = 1.5$ and 2.0 round, elliptic, and rectangular nozzles, including an ADEN, were studied to assess noise emission. The nozzles were operated to jet total temperatures, $T_o = 1160°R$, and the data scaled to constant thrust. The data were propagated to 1500 ft. and corrected to perceived noise level. The aerodynamic results of the study show that the non-round nozzle geometries mix much faster with the surrounding medium than does an equivalent round nozzle plume. Both the ADEN and elliptic nozzles provide significant reduction of noise, 6 to 7 PNdB, along the major axis direction with little expected impact on nozzle performance. Shock noise processes are eliminated for elliptic nozzles, but are still significant with rectangular nozzles. Comparison of measurements to theoretical predictions of noise using the quasi-linear instability wave model demonstrates good qualitative agreement.

LIST OF SYMBOLS

a_o	ambient sound speed
D_{eq}	area equivalent jet diameter
h	rectangular nozzle exit height
L_c	length of potential core
M_c	turbulence convection Mach number
M_d	nozzle exit design Mach number
M_e	jet exhaust Mach number
M_j	fully expanded jet Mach number
P_a	ambient pressure
P_e	jet static pressure at nozzle exit
P_o	jet total pressure at nozzle entrance
P_s	local jet static pressure
R	radial jet coordinate
T_o	jet total temperature at nozzle entrance
U, U_o	local and centerline jet velocity
U_e	jet exit centerline velocity
V_c	turbulent convection velocity
V_j	fully expanded jet velocity
X, X_j	axial jet coordinate
α	V_c/V_j
β, β_c	$(M^2 - 1)^{1/2}$, $(M_c^2 - 1)^{1/2}$
ε	empirical shock intensity parameter
γ	ratio of specific heats
Θ	Mach wave angle to jet axis
ρ_j, ρ_a	jet and ambient density
ϕ	azimuthal angle around jet
ψ	angle to jet inlet axis

1   INTRODUCTION

This paper evaluates the aeroacoustic performance of simple non-round nozzle exit geometries as a means for reduction of noise emitted by high performance military engines.

Noise reduction associated with combat military aircraft typically has received little attention at the design stage due to concern for unacceptable performance trade-offs that could significantly compromise the aircraft's mission. In the commercial sector, unacceptable noise emission is primarily confined to aircraft operations concerning take-off and landing . Even with this much simpler aircraft mission, there exists no successful supersonic commercial jet noise suppression concept that has ever succeeded in enabling achievement of existing noise regulations without requiring exceptions. The Concorde aircraft contains no suppression concept (Ref 1), simply because it could not afford any performance degradation to achieve its mission goals.

The reduction of noise for combat military aircraft is much more involved, in that many aircraft missions require penetration at low altitude with high engine power settings for disengagement. Few combat aircraft are designed with sufficient margin to permit deployment of engine noise suppressors (Ref 2) during this phase of the mission. Unless stowable, engine noise suppression devices would significantly compromise cruise performance, and therefore, aircraft range.

The relationship between emitted jet noise and aircraft dynamic loads appears to be an area where noise should be accounted for in the aircraft design stage. Twin engine fighters and bombers, such as for example the US F-15 (Ref 3) and B-1B (Ref 4) aircraft, have experienced structural fatigue failures of engine nozzle external flaps. These failures can be associated with noise generated by the high speed jets at low flight Mach numbers (i.e. typically < 0.6). Short Take-Off Vertical Landing Aircraft, such as the McDonnell Douglas AV-8B and the British Harrier aircraft (Ref 5), are subjected to intense structural loads at high temperature due to ground impingement and scrubbing cruise loads.

The majority of noise suppression concepts discussed for commercial applications in reference 2 (see Table I of Ref. 2) are not applicable to combat aircraft. This is due to existence of either a substantial performance penalty or use of an engine afterburner. Thus, while plugs provide noise reduction with performance augmentation, their weight and need for cooling remain unattractive. The inverted velocity profile offers modest noise reductions with low loss of nozzle performance, although efficient utilization requires availability of engine secondary flow, which for most turbojets is severely limited.

In this paper, the use of generic nozzle geometries is evaluated as a means to achieve reduction of jet noise with minimum performance loss. Non-round nozzle exit geometry is thought to provide accelerated mixing of its plume with the surrounding medium. This could produce lower jet plume speeds and consequently lower noise.

In particular, the aeroacoustic characteristics of round, elliptic and rectangular nozzle exit geometries are studied experimentally. These generic geometries are evaluated using both hot and cold jet plumes, with jet total temperatures to 1160°R. Both acoustic far field and aerodynamic flow field measurements were acquired to evaluate the noise reduction mechanism. Comparison of the measured far field sound radiated by the elliptic jet is made to the prediction of Morris and Bhat (Ref 6). A brief summary of the principle sources of supersonic jet noise is included to provide a background for motivation behind methods of jet noise suppression.

2   SUPERSONIC JET NOISE SOURCES

Two fundamental differences exist between low and high speed jet flows that have an important effect on what is observed as the dominant sound production mechanism. These differences, which are discussed below, are present when turbulence is convected at supersonic speed relative to the ambient sound speed and/or shock waves are present in the flow. The second phenomenon requires the flow to be supersonic, but the first phenomenon also occurs with heated subsonic jets (i.e. $M_a = 0.85$; $T_a = 1300°F$). Both mechanisms are known to emit intense noise and attain sufficient energy to be directly visualized by standard optical methods as shown in the spark schlieren photograph of figure 1a.
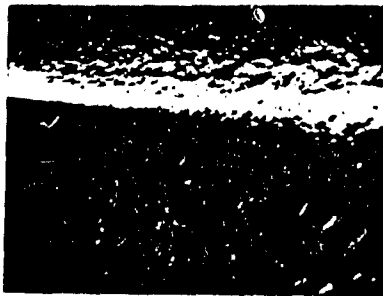
a.   Spark schlieren of underexpanded $M_d = 2$ unheated jet, $P_e = P_a$
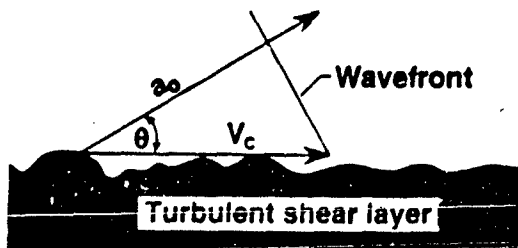
b.   inition of Mach wave angle, θ

Figure 1.   Illustration of Mach wave emission.

2a · Mach Wave Emission

The spark schlieren of Figure 1a, which captures a nearly instantaneous view of both flow and near acoustic fields, was acquired using a horizontal knife edge with spark duration less than 0.1 µ-sec. The pressure waves that appear to emanate from regions along the jet shear layer edge and travel downstream are produced by turbulence convected supersonically relative to the ambient medium. This mechanism was first described analytically by Phillips (Ref 7), who termed the mechanism *eddy mach wave emission*. Physically the model considers the radiation to be generated in the same manner that ballistic waves are created. Thus, as illustrated in figure 1b, Mach waves would be emitted from the shear layer at an angle,

$$\Theta = \cos^{-1}(1 / M_c) = \cos^{-1}(a_o / \alpha V_j)$$

where $\alpha = V_c/V_j = 0.7$. Here V_j, V_c, and M_c are the fully expanded jet and turbulence convection velocities and convective Mach number relative to ambient sound speed. In the schlieren example of figure 1a, the jet flow is produced by a convergent-divergent nozzle with a design Mach number $M_d = 2$. The nozzle is operated fully pressure balanced, so that the exit static pressure is equal to ambient pressure, $P_e = P_a$. The air flow from the nozzle is unheated. With these operational conditions the convection velocity and Mach wave angles are $V_c = 1175$ ft./sec and $\Theta = 16°$. The Mach waves in figure 1 appear inclined 22° to the jet shear layer boundary.

Ffowcs Williams and Maidanik (Ref 8) theoretically predict that acoustic energy emitted by the eddy Mach wave mechanism is proportional to M_c^3. This source strength dependence on convection velocity is indicative of high acoustic source efficiency. In the direction of Mach wave emission, the individual quadrupole sources radiate as individual monopole sources with no net near field cancellation. Because of this high source efficiency, the Mach wave mechanism is capable of converting between 0.1 and 1 % of the jet mechanical energy to noise. This noise is radiated at narrow angles to the jet axis as defined by the Mach angle. At angles beyond this angle, source efficiency drops to that associated with quadrupole emission, which is in the order of 0.01 % of the jet mechanical power.

Noise reduction concepts that would seek to reduce the convection velocity of sources to subsonic should substantially reduce noise in consideration of the change in source efficiency. Typically the jet velocity is lowered by forced mixing with the external stream, as in the application of mixer lobes with ejectors. This paper, as shown below, considers the use of non-round nozzle exit geometry to achieve enhanced mixing and lower jet speeds.

2b · Shock Noise

An equally important noise source for supersonic jets is associated with the convection of turbulence through plume shocks. The schlieren photograph of figure 2 also shows noise radiation from this mechanism. This can be observed as those circular ray centered regions that originate for locations in the shear layer where the oblique shocks terminate. The noise from this mechanism dominates acoustic emission in the jet inlet arc $0 \leq \psi \leq 90°$. A broadband frequency spectrum results from the interaction of turbulence with a shock, with an energy peak that is Doppler dependent. When the shock cell spacing is a near integer multiple of the

Figure 2. Spark schlieren of underexpanded unheated sonic jet illustrating broadband shock noise and eddy Mach wave emission ($M_j = 1.8$).

wavelength associated with the most highly amplified frequency of the shear layer, the shock cells oscillate at that frequency producing what is known as jet screech. This mechanism requires feedback of acoustically generated noise to the nozzle to be maintained. A comprehensive review of the literature on shock noise can be found in Seiner (Ref 9).

Like the Mach wave mechanism, the shock noise source mechanism is extremely efficient. Figure 3 shows the relatively large increase in noise radiated at $\psi = 30°$ that is associated with jets which are operated off-design in either the overexpanded or underexpanded mode. The solid curve is established from data associated with convergent-divergent (C-D) nozzles operating at their design points, so that no shock noise is present. All other data in figure 3 is associated with jet plumes that contain shocks and thus produce shock noise.
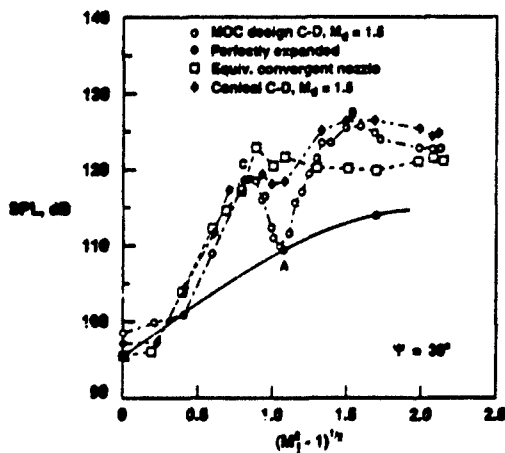
Figure 3. Advantage of shock free nozzle design.

Several combat aircraft, the USAF F-15 being a representative example, have nozzle area ratio schedules that lie near the $M_d = 1.5$ design point. For an ideal laboratory type nozzle designed for $M_d = 1.5$, open circular symbols in figure 3, operation at off-design nozzle pressure ratios leads to a large increase in emitted sound. The data in figure 3 is shown in terms of the fully expanded plume Mach number M_j and the sound pressure level in dB re. 0.00002 N./m². The fully

expanded Mach number is determined from the nozzle pressure ratio through the isentropic relations,

$$M_j = ((2/(\gamma-1))((P_c/P_a)^{(\gamma-1)/\gamma} - 1))^{1/2}$$

where P_c/P_a is the nozzle pressure ratio. Point A in figure 3 is the nozzle design point, point B is in the direction of underexpanded operation and point C in the direction of overexpanded operation. Both points B and C represent those points where Mach discs begin to form in the plume. Between points C and B plume shocks can be considered weak.

The sound pressure level amplitude increase, between shock free and non-shock free nozzle operation, can be seen to be substantial. At points C and B, the noise level increase is between 12 and 13 dB. As a means of comparison, figure 3 shows the degree of shock noise generated by an equivalent thrust C-D nozzle designed using conical segments and a throat with a small constant area section. The nozzle design Mach number is again $M_d = 1.5$. The use of conical segments is typical of all military aircraft engines and helps achieve operation of variable area throat and nozzle area ratio. The nozzle design shape was chosen to emulate the P&W F100 engine nozzle for operation of the F-15 aircraft at cruise power setting.

The data of figure 3 show that a small increase in shock noise occurs at points C and B, but that a significant 9 to 10 dB increase in shock noise occurs even at the conical C-D nozzle design point. Thus, even though there is a modest decrease in shock noise amplitude, the variable area conical nozzle does not represent an adequate method for achieving shock noise control. To evaluate the shock noise reduction associated with the use of the nozzle divergent flap, compare the conical C-D data to that of a convergent nozzle whose thrust is equivalent at the Mach 1.5 design point. Only a 3 dB decrease in noise can be associated with the use of a nozzle divergent flap.

The shock noise amplitude can be related, as expected, to the strength of shocks in the jet plume. As discussed in Ref. 9, the shock noise intensity, I_s, is proportional to the pressure jump across shock waves as expressed by,

$$I_s = \varepsilon\beta^4(1 - \beta^2/\beta^{*2})^2 = \varepsilon(M_j^2 - M_d^2)^2$$

where $\beta = (M_j^2 - 1)^{1/2}$ is a parameter relating the pressure jump across a normal shock to the freestream Mach number M_j. For perfectly balanced jets, where $M_j = M_d$, the above equation would predict $I_s = 0$, as expected. The parameter, ε, is experimentally determined and is found to increase with the nozzle design Mach number. Figure 4 compares prediction of shock noise using the above equation to data measured for three different supersonic nozzles. The jet total temperature for this data is ambient. The data is associated with acoustic measurements at angle $\psi = 90°$. The jet noise is subtracted from the data by computing the jet noise at $\psi = 90°$ using the Stone Module in ANOPP (Ref 10).

For underexpanded nozzle operation, $M_j - M_d > 0$, the data and prediction in figure 4 show reasonable agreement up to those values where strong shocks would be expected in the plume and non-isentropic losses occur. For overexpanded operation, $M_j - M_d < 0$, the comparison appears unsatisfactory even with relatively weak shocks in the jet plume. Figure 4 does
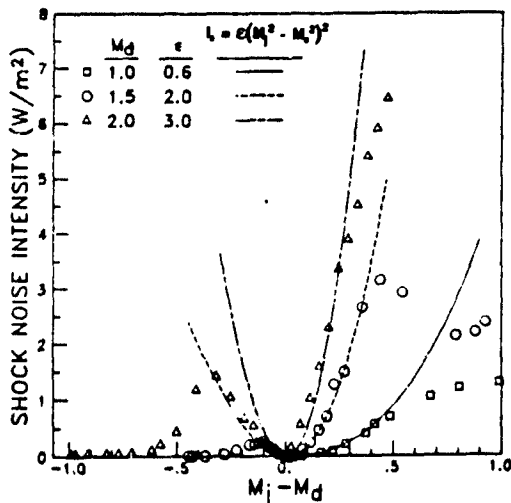
Figure 4. Supersonic exhaust nozzle shock noise intensity I_s at $\psi = 90°$.

show that shock noise amplitude increases rapidly away from the nozzle design point and increases with nozzle design Mach number, as evidenced by the increase in the parameter ε with M_d. The source efficiency of shock noise is competitive with that associated with the eddy Mach wave mechanism. Depending on the strength of the plume shocks and flow Mach number, between 0 and 1% of the jet mechanical energy can be converted to noise by this mechanism.

3   NOISE REDUCTION USING NOZZLE GEOMETRY

In the last section, we have briefly reviewed the two jet noise sources, Mach wave emission and shock noise, that dominate acoustic emission from supersonic jets. Their reduction requires that the plume region for supersonic convection velocities be minimized and the nozzle operated as nearly pressure balanced as possible (exhaust static pressure equal to ambient) to minimize shock strength. To achieve these goals and not compromise aircraft performance represents a significant challenge.

The research of Ho and Gutmark (Ref. 11) shows that an aspect ratio 2 low subsonic elliptic nozzle can entrain three times the jet's own mass flow. Evidently the asymmetric distortions of the mean flow field imposed by the nozzle geometry produce an unequal role-up of vorticity in the initial shear layer. The three dimensional vortex role-up leads to rapid mixing of the plume with external stream air and consequently lower average jet flow field velocities.

Recent research (Ref. 12) has also shown that enhanced mixing can be achieved using supersonic elliptic nozzles. The supersonic nozzle used in this study was designed with an aspect ratio of 2 to produce a shock free plume at $M_d = 1.52$. This prior study demonstrated that, in the principle direction of jet noise emission ($100° \leq \psi \leq 165°$), the elliptic nozzle reduced the OASPL between 6 and 8 dB relative to an equal thrust and mass flow round nozzle in the direction of the nozzle major axis. Larger noise reductions were detected in the direction of peak shock noise emission, since the elliptic nozzle design provided an essentially shock free plume. Along the direction of the nozzle

minor axis, no change in the OASPL was detected. These results were most encouraging, since only small losses in nozzle thrust coefficient could be expected.

The prior supersonic elliptic nozzle results were acquired using unheated supersonic plumes. In an effort to arrive at a more accurate account of the noise reduction potential of such nozzles, a series of tests were conducted with round, elliptic and rectangular nozzles with plumes heated to jet total temperatures $T_o = 1160°R$.

4   EXPERIMENTAL CONFIGURATION

Two round nozzles were used for this study, one was designed for $M_d = 1.5$ and the other for $M_d = 2.0$. Two rectangular nozzles were also studied. One was actually an ADEN (augmented deflector exhaust nozzle) with design Mach number of $M_d = 1.5$ and aspect ratio of 2. The deflector flap extended from the nozzle exit a distance 3.5h, where h is the nozzle exit height. The sidewalls of this nozzle are parallel. The other rectangular nozzle was designed for Mach 2 with an exit aspect ratio 7.6. The sidewalls of this nozzle were also parallel. For this study, a new $M_d = 1.54$ elliptic nozzle with aspect ratio 2 was constructed to withstand the elevated temperature. In addition, a $M_d = 2.0$ elliptic nozzle with aspect ratio 3 was designed and constructed for these studies.

Both the $M_d = 1.5$ round and ADEN nozzles have nearly equivalent exit areas of 2.217 and 2.161 in², respectively. The $M_d = 1.54$ and 2.0 elliptic nozzles have respective exit areas of 1.571 and 1.508 in². The scale size of these nozzles is of concern in scaling acoustic data to full scale PNL values. This scaling is of course necessary to fully evaluate any acoustic reduction. Relative to the F-15 aircraft, the round and ADEN nozzles are 1/15th scale nozzles.
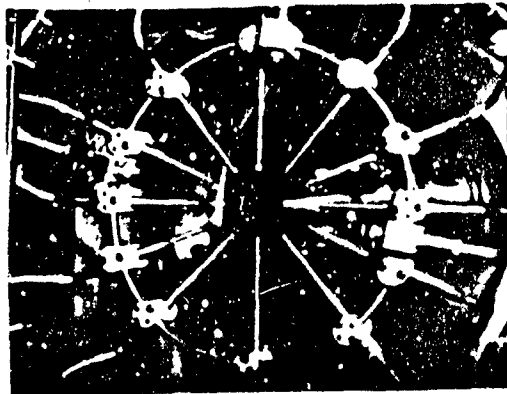

Figure 5. Photograph of $M_d = 1.52$ aspect ratio 2 supersonic elliptic nozzle.

Figure 5 shows a photograph of the $M_d = 1.52$ elliptic nozzle with a surrounding array of near field microphones arranged along a fixed coordinate in an elliptical cylindrical coordinate system. These microphones were used in Ref. 12 and 13 to determine that the axisymmetric mode is the dominant spatial mode of instability for the shock free plume. In the present study, these near field microphones are not used. Instead a 21 element linear array of far field microphones, as shown in figure 6, is used to acquire far field acoustic data. Microphones 22 through 25 were
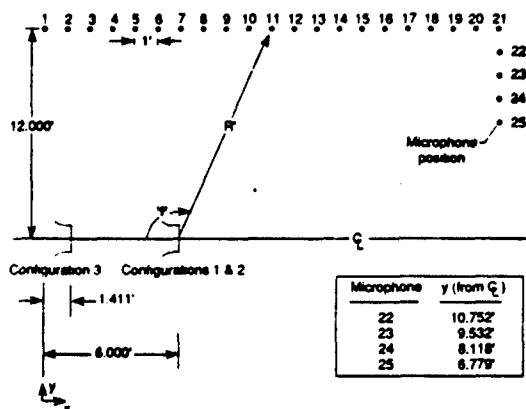
Figure 6. Diagram of microphone array system in JNL

Figure 7. Comparison of M_d = 1.5 elliptic and round nozzle centerline velocities.

added to enable acquisition of data at high angles of ψ. Data from these microphones were scaled to 12 ft. linear array distance. The nozzles were located at different positions in the anechoic room to allow acquisition of data at low angles of ψ. Azimuthal data for non-round nozzles were obtained by rotation of the nozzle.

The microphone data were acquired by a 20 channel simultaneous sample and hold 12 bit A/D converter using a 200 kHz. sample rate. The sample size was 256k per record. A low noise 20 channel amplifier with a 100kHz. low pass filter was used ahead of the A/D converter. The time data was stored on optical disk for later FFT batch processing. All acoustic and aerodynamic data were acquired in the NASA/LaRC Jet Noise Laboratory (JNL).

Aerodynamic data associated with the round and elliptic M_d = 1.5 and 2.0 nozzles were acquired using the JNL digital traverse system with 3-axis positional accuracy of ± 0.001 inch over its entire span. A total pressure probe, designed for supersonic flow, was used to determine the jet velocity. Only aerodynamic measurements at a jet total temperature of 564°R are available. The JNL electric heating system was used to acquire acoustic data to 1160°R.

5   MACH 1.5 ELLIPTIC NOZZLE COMPARISONS

5a - Aerodynamic Data

Only shock free supersonic plume data is reported in this study. Figure 7 compares the centerline velocity between round and elliptic Mach 1.5 nozzles. The data are normalized by the jet exit centerline velocity, U_e. Both jets are operated fully pressure balanced at T_c = 564°R. The axial distance is normalized by an area equivalent jet diameter, D_{eq}. The elliptic nozzle plume clearly decays at a much faster rate than an equivalent round nozzle plume. The centerline velocity of the elliptic nozzle reaches subsonic speed relative to the ambient medium at X/D_{eq} = 10.5. The same point for the round nozzle occurs at X/D_{eq} = 14.5. One explanation for this result is associated with asymmetric distortion of the jet column produced by three dimensional turbulent decay of jet large scale structure.

If one assumes that the axial location where U/U_e ≤ 0.98 defines the end of the potential core, L_c, then the elliptic nozzle's potential core length is 5 D_{eq}. The end of the potential core is also the location where the most
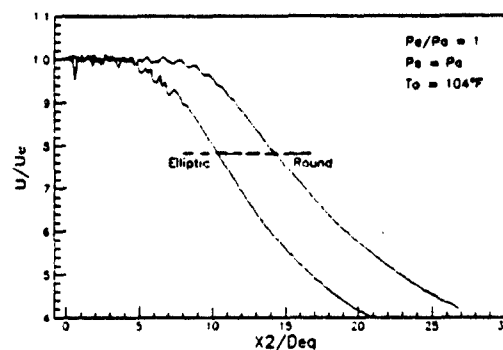
highly amplified wave of the jet shear layer achieves maximum growth. Beyond this point the wave rapidly disintegrates into smaller scale structures. The data of figure 8 show the axial distribution of momentum thickness, defined by,

$$\theta = \int_0^\infty (\rho U/(\rho U)_{cl})(1-(U/U_{cl})dR$$

As can be seen, the initial major and minor axis momentum thicknesses are nearly equal. In the potential core region, the major axis momentum thickness grows at only a slightly lower rate than along the minor axis. Thus no distortion of the jet column can be observed for most of the potential core region.
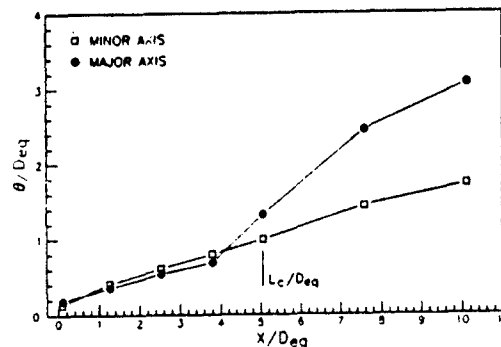

Figure 8. Axial development of major and minor M_d = 1.5 elliptic nozzle momentum thickness.

Near the end of the potential core, the momentum thickness along the major axis grows much faster than along the minor axis. The minor axis growth rate remains unchanged. This rapid growth of the major axis momentum thickness occurs at an axial location close to the vicinity where the dominant spatial mode (See Ref. 13) achieves maximum amplification before undergoing rapid distortion.
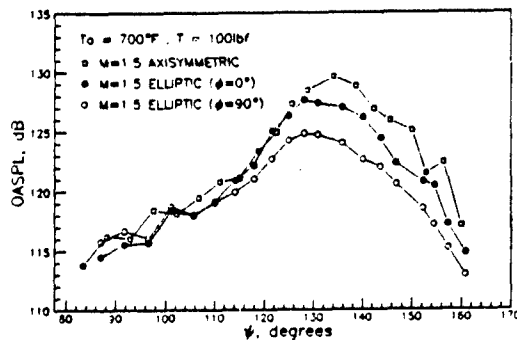
5b - Reduction of Mach Wave Emission

The elliptic nozzle aerodynamic data of the preceding section shows that the axial length for supersonic flow is less than for an equivalent round nozzle. We can directly investigate the reduction of Mach wave emission by comparison of acoustic data for jet total temperatures where the convection Mach number, M_c, is near sonic and where it is much greater

than sonic. Of particular interest are the isothermal case, for which theoretical prediction is available (Ref. 6), and the higher temperature condition, where T_0 = 1160°R. For the isothermal condition the elliptic nozzle conditions are $\rho_j = \rho_a$, T_0 ~ 765°R, Θ = 20°, and M_c = 1.065. Thus in the isothermal M_d = 1.5 jet case, the convection Mach number is barely supersonic. The Mach wave emission will occur at narrow angles to the jet axis. For the higher jet temperature case, the conditions are M_c = 1.312 and Θ = 40°. Strong Mach wave emission should occur at much higher angles to the jet axis.

The acoustic data is acquired using the linear array of microphones shown previously in figure 6. Overall sound pressure levels, for both the round and elliptic M_d = 1.5 nozzles, are presented in dB in figures 9a and 9b as a function of the nozzle inlet angle ψ. Figure 9a shows comparison of round and elliptic data (major and minor axis) for the isothermal condition. Figure 9b shows the corresponding higher temperature case. The elliptic nozzle acoustic data are scaled to the thrust level of the axisymmetric nozzle (i.e. 100ibs.).
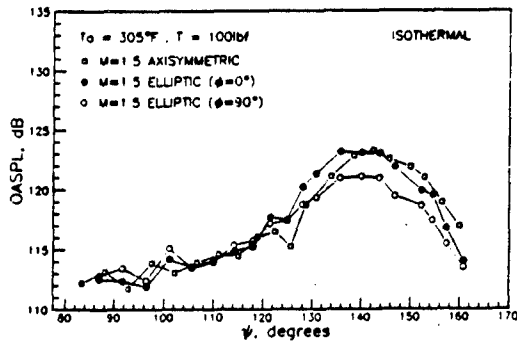
a - T_0 ~ 765°R (Isothermal)

b - T_0 = 1160°R

Figure 9. Reduction of Mach wave emission by elliptic nozzles.

The acoustic data comparisons of figure 9 clearly show that Mach wave emission is substantially reduced by use of the elliptic nozzle. In the isothermal case, only small reductions are evident in the direction of the major axis (ϕ = 90°) in the peak radiation direction ψ > 120°. At the higher temperature, where Mach wave emission is stronger, the acoustic reduction relative to the round nozzle is much larger. The data in figure 9

also show the shift in the direction of radiation with increased M_c. The angles for peak noise emission differ from the predicted Mach wave emission angles because the data is presented in linear microphone array format rather than along a circular arc.

To appropriately determine the benefit of the reduction of noise by non-axisymmetric nozzle geometry requires that the data be scaled to full, propagated, corrected for atmospheric losses, and presented on a weighted noise level basis (PNdB) for human response.
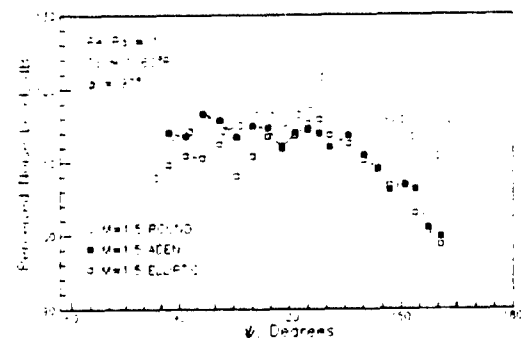
5c - Scaled Acoustic Data

The data was scaled to 50000 lb. of equivalent thrust at a sideline distance of 1500 feet and propagated through a standard atmosphere using appropriate spectral corrections. These conditions are representative of a two engine fighter at maximum after-burner power at a flight Mach number of 0.4.

The acoustic data of figure 10 compare scaled results for the C-D round, rectangular (ADEN), and M_d = 1.54 elliptic nozzle geometries. All plumes have equivalent jet total temperatures T_0 = 1160°R and are operated fully pressure balanced. In the case of the ADEN nozzle, however, plume shock strength is only slightly reduced by the nozzle geometry.

Figure 10a shows that, along the direction of the elliptic nozzle's major axis (i.e. ϕ = 90°) and at angles ψ > 120°, significant noise reduction in the order of 6 to 7 PNdB is obtained relative to the reference round nozzle. At these angles, which represent the peak noise radiation direction, the ADEN performs identically to the elliptic nozzle. At angles ψ < 120°, shock noise processes begin to influence the ADEN nozzle's acoustic field and reduce its effectiveness relative to the round nozzle. The elliptic nozzle appears to provide noise reduction at all angles ψ ≥ 90°.

In the direction of the minor axis (i.e. ϕ = 0°), figure 10b shows that all nozzle geometries produce equivalent noise radiation, except near 90° where the elliptic nozzle produces 2 to 3 PNdB less noise. Figure 10c shows the same data as figure 10b, except that the ADEN divergent flap now lies in the direction of the microphone array. Only a small decrease in noise is observed near an angle ψ = 130°. The ϕ = 180° azimuthal direction

a - ϕ = 90° (major axis direction)
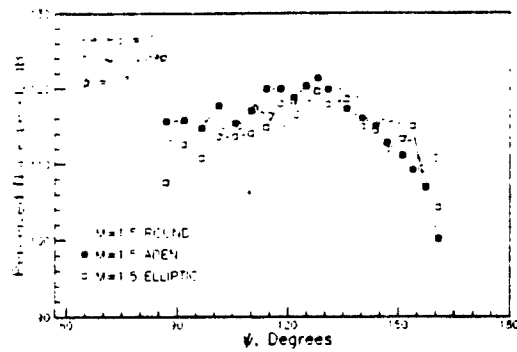
b - φ = 0° (minor axis direction)
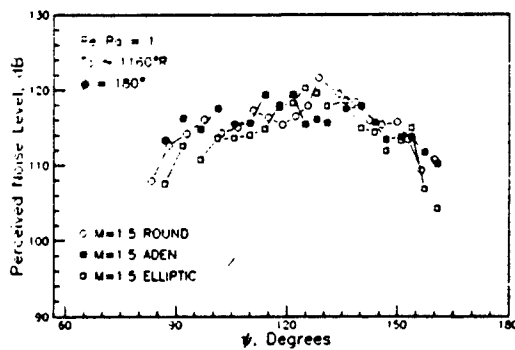
c - φ 180° (minor axis direction - flap location)

Figure 10. Scaled acoustic data for various nozzle geometries.

represents a vector pointed above the aircraft based on the intended design of the ADEN.

The angle ψ = 128° represents the peak noise emission direction for the round nozzle. Figure 11 compares spectra obtained at this angle with the M_d = 1.54 elliptic nozzle at azimuthal directions lying along the minor, φ = 0°, and major axis, φ = 90°, directions. Also included is a spectrum of the M_d = 1.5 round nozzle corrected to the thrust of the elliptic nozzle.
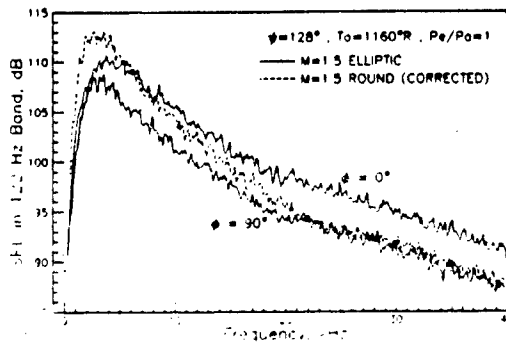

Figure 11. Spectral Comparisons of elliptic and round jet.

Based on this spectral comparison, both major and minor axis directions of the elliptic nozzle show reduced acoustic emission relative to the round nozzle near peak spectral emission. The reduction in acoustic emission in the direction of major axis is spectrally uniform relative to the minor axis direction. In general, the elliptic nozzle reduces peak spectral energy at low frequency, but radiates higher frequency components that can even exceed those associated with round nozzles, as is evident in the minor axis direction. The difference in spectral peak amplitude levels between major and minor axis directions is an indication that the turbulence large scale structure is highly three dimensional at the end of the jet potential core.

6   MACH 2 ELLIPTIC NOZZLE

6a - Aerodynamic Data

Centerline velocity measurements were also acquired for a M_d = 2.0 aspect ratio 3 elliptic jet. These results are shown in figure 12 in comparison to those previously acquired for a round M_o = 2.0 nozzle. The data is normalized by the jet exit centerline velocity and area equivalent diameter. Both nozzles are operated fully pressure balanced, as evidenced by the relative smoothness of the velocity profiles. This data indicates that the M_d = 2 elliptic nozzle mixes faster than the equivalent round nozzle, but does not do as well as the M_d = 1.52 elliptic nozzle. The potential core length of the elliptic nozzle is L_c = 9 D_{eq}, whereas the round nozzle is L_c = 11 D_{eq}. This result may be attributed to the use of a higher nozzle aspect ratio, where from the results of Ref. 14, higher aspect ratio supersonic rectangular nozzles mix slower than lower aspect ratio nozzles.
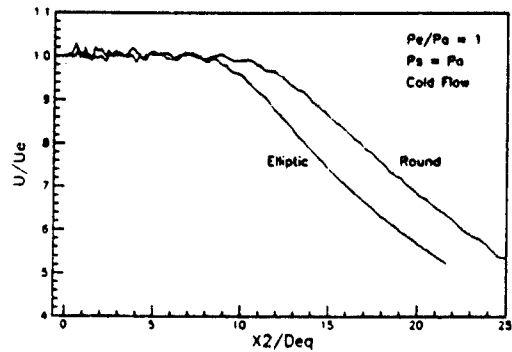

Figure 12. Comparison of M_d = 2 elliptic and round jet centerline velocity.

In figure 13, the axial momentum thickness, θ, along both minor and major axes do not show the same trend as observed with the lower Mach number elliptic nozzle. While both axes start with apparently equal and small θ, the major axis grows much faster throughout the potential core region. In the potential core region, the minor axis momentum thickness has an identical growth rate to the equivalent round nozzle. Beyond the region of the potential core, X/D_{eq} > 9, the minor axis θ begins to grow faster than the round nozzle's and the major axis θ begins to diminish. Both the major and minor θ appear to asymptote to the same value near X/D_{eq} = 30, which is greater than that associated with the round geometry.

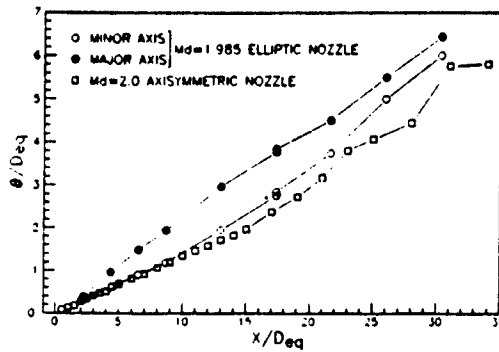

Figure 13. Axial development of major and minor axes M_d = 2.0 elliptic and round nozzle momentum thickness.
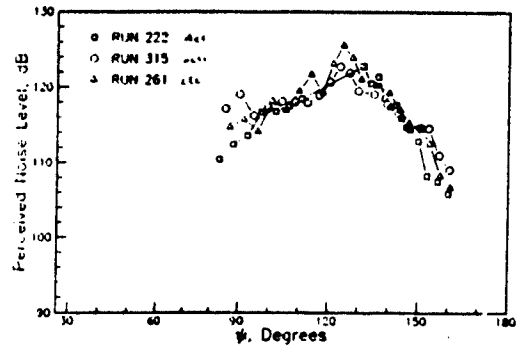
6b - Acoustic Data

The acoustic data for the Mach 2 round, rectangular and elliptic nozzles is shown in figure 14. The data is scaled to the same thrust level as in the Mach 1.5 data of figure 10 and presented in terms of PNdB. Each nozzle is operated pressure balanced with a jet total temperature of T_o = 1160°R.

Figure 14a shows the data in the direction of the major axis, ϕ = 90°, and figure 14b shows data in the direction of the minor axis, ϕ = 0°. Both the elliptic and rectangular geometries show noise reduction in the major axis direction, although the reduction relative to the equivalent round nozzle is not as good as that obtained at the lower Mach number. This could be attributed to the higher nozzle aspect ratio, where it is shown that the mixing is not as effective as the lower aspect ratio nozzle. In the minor axis direction all nozzles appear to emit nearly the same noise level over all angles of ψ.

Figure 15 provides a summary for the azimuthal variation of PNdB for both elliptic M_d = 1.5 and 2.0 elliptic nozzles. It can be observed that the noise level varies nearly linearly with the azimuthal angle ϕ.
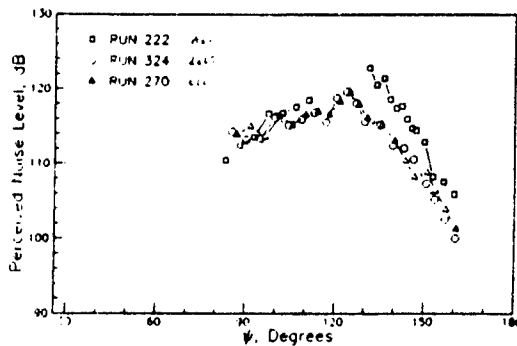
a - ϕ = 90° (major axis direction)

b - ϕ = 0° (minor axis direction)

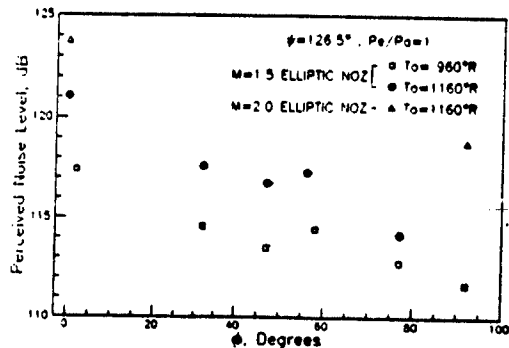Figure 14. Scaled acoustic data for various M_d = 2 nozzle geometries.

Figure 15. Azimuthal variation of PNdB level.

7   COMPARISON TO THEORETICAL PREDICTIONS

Theoretical calculations of the acoustic far field for supersonic elliptic nozzles have been made by Morris and Bhat (Ref. 6). Their spatial stability analysis computes the noise associated with large scale turbulent structures of the free jet shear layer for shock free jets. The characteristics of the large scale structure are described by solution of the linearized compressible Rayleigh equation. The equations are linearized by substituting measured mean velocity data from the M_d = 1.52 elliptic nozzle into the Rayleigh equation in terms of elliptic cylindrical coordinates. The mean density is solved using Crocco's relation. An inner solution is constructed by the method of multiple scales and matched to an outer solution that satisfies the radiation condition by the method of matched asymptotic expansion.

In their paper, calculations for the fixed frequency wave S_t = f_oD_m/U_o = 0.2 are made for several fundamental spatial modes of instability. Figure 16 illustrates several of the fundamental low order spatial modes for the elliptic jet. From previous research with axisymmetric jets, only the varicose (i.e. axisymmetric) and flapping instabilities are found to be important. One jet condition of special interest is that associated with the fully balanced isothermal jet (i.e. ρ_i = ρ_a). This is primarily of interest since elimination of shocks is

Modes of Instability

Varicose instability

Major axis flapping instability

Off axis instability
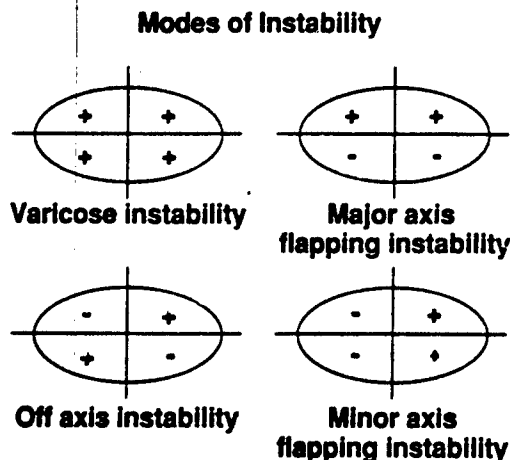
Minor axis flapping instability

Figure 16. Low order spatial modes of instability for elliptic jets.

important for linearization of the governing equations. The calculations of Ref. 6 in fact show that only the varicose spatial mode radiates noise to the far field. The higher order modes do not achieve supersonic phase speed and therefore do not radiate sound to the far field. Measured far field acoustic data from an unforced supersonic jet will contain all radiating spatial modes.

Far field acoustic data was acquired using the elliptic M_d = 1.54 nozzle. The jet was operated fully pressure balanced (P_e/P_a = 3.89) at a jet static temperature equal to the ambient. For this Mach number nozzle, the corresponding jet total temperature to ambient temperature ratio,

$$T_o/T_a = 1 + 0.5(\gamma - 1)M_j^2 = 1.47$$

which corresponds to an average value of T_o = 302°F for the present study. Using the microphone array of figure 6, far field acoustic data was acquired at six azimuthal angles ϕ, over the range 66.5° $\leq \psi \leq$ 160.8°. A comparison between predicted and measured acoustic pressure amplitudes is shown in figure 17 for the Strouhal number S_t = 0.2 component for both minor (ϕ = 0°) and major (ϕ = 90°) directions. The spectral bandwidth associated with measured data corresponds to $\Delta f/f_o$ = .04. Both the measured and predicted

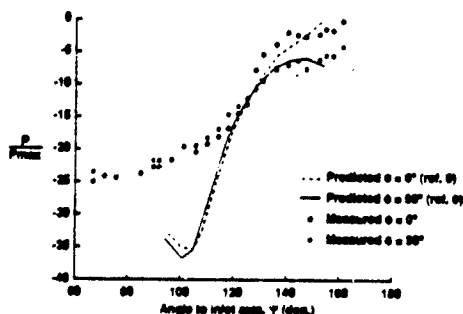AR = 2, Mj = Md = 1.52, St = 0.2, Varicose mode, isothermal

Figure 17. Comparison of measured and predicted acoustic characteristics for elliptic nozzles.

amplitude data in figure 17 are presented in dB relative to the respective peak pressure, P_{max}, which occurs at a different value for ϕ between measured and predicted results.

This comparison shows reasonable agreement between data and theory in peak noise emisson from both major and minor axis planes. The measured and computed difference in radiation between the two axis planes is in excellent agreement. The noise radiated at angles of $\psi \leq 100°$ is due to smaller scale turbulence which radiates less efficiently. The results of figure 17 are very encouraging, since the theory contains the methodology to compute jet flows of arbitrary geometry thus paving the way for treatment of ADEN like nozzles.

8 CONCLUSIONS

In this paper, the principle sources of supersonic jet noise emission have been discussed. For combat military aircraft, these noise sources are associated with shock noise processes and eddy Mach wave emission. Each mechanism, unlike subsonic jet noise sources, is very efficient. Each convert between 0.1 and 1% of the jet mechanical power to noise.

Both the Mach wave and shock noise mechanisms are difficult to suppress without incurring significant compromise of aircraft mission. Reduction of shock noise requires developing new methods for cancellation of internal pressure waves on the interior of the high temperature variable area nozzle. The reduction of Mach wave emission requires lowering jet plume velocities, which can be achieved through accelerated mixing of the shear layer with surrounding medium.

Jet noise suppression concepts proposed for commercial supersonic aircraft appear inappropriate for combat aircraft due to substantial compromise of engine performance. In this paper, the use of simple non-round jet exit geometry is considered as a possible means for reducing noise, while maintaining engine performance.

Several generic non-round jet exit geometries were studied with jet total temperatures, T_o = 1160°R, to determine their aerodynamic and scaled acoustic characteristics. These geometries included round, elliptic, and rectangular nozzles with nominal design Mach numbers of M_d = 1.5 and 2.0. The M_d = 1.5 rectangular nozzle was an ADEN (Augmented Deflector Exhaust Nozzle) configuration. The aspect ratio of the M_d = 1.5 non-round nozzles was 2.0. The M_d = 2 elliptic nozzle had an aspect ratio 3.0. The jet plume total temperatures are within several hundred degrees of those used by current technology fighters at full military power setting.

Aerodynamic measurement of mean flow centerline behavior clearly shows that the non-round nozzle geometry mixes much more effectively with the surrounding medium than a round nozzle. As a result, the axial length of supersonic flow is substantially reduced. Under these circumstances, the Mach wave emission process is expected to play a less substantial role. The aerodynamic data also indicate that higher aspect ratio elliptic nozzles may mix less effectively, but the presents results are inclusive, since the higher aspect ratio nozzle has a higher nozzle design point. The higher flow Mach number may also inhibit mixing.

The acoustic data for both the $M_j = 1.5$ and 2.0 nozzles confirms the above expectations. The acoustic data is scaled to two 25000 lb engines, propagated to 1500 ft., and weighted in perceived noise level. In the direction of peak emission (i.e. $\psi > 120°$) and along the major axis, both elliptic and rectangular nozzle geometries provide between 6 and 7 PNdB noise reduction. Along the minor axis direction, the noise emitted by all nozzles appears equivalent. The importance of these reductions, although modest, is that almost no compromise of performance has been made and the noise reduction occurs over a significant region of azimuthal angles. The data of this study also show that the noise reduction is larger for higher temperature jet plumes (compare figures 9a & 9b). This is consistent with the concept for Mach wave emission reduction.

At angles $\psi < 120°$, shock noise becomes a factor in noise emission. The acoustic data presented all involve nozzles designed using convergent-divergent flow paths. Both the round and elliptic geometries have reduced the strength of plume shocks to the point where shock noise is effectively eliminated. The rectangular, including ADEN, still contain shocks with significant strength. While shock noise is reduced it is still a factor in the acoustic emission.

The ADEN represents a nozzle geometry worthy of further study. The performance of this nozzle is competitive with the round nozzle. It is actually much simpler to design for variable area and is more amendable to stowable nozzle suppressor concepts than round nozzle geometry. Further research on this nozzle is required to cancel internal nozzle shocks.

The prediction of noise from non-round geometry nozzles is shown to compare favorably for peak emission ($\psi > 110°$) along both major and minor axis planes. The theoretical predictions indicate that a non-axisymmetric mean flow field lowers the growth rate of the most highly amplified shear layer mode relative to a round nozzle. The fact that the ADEN produces a similar acoustic field at these angles of ψ suggests that similar aerodynamic processes occur in the rectangular nozzle jet flowfield. These results encourage the further development of the theory to treat high temperature jets and an examination of the analysis to perhaps pace development of a realistic minimum noise mean velocity profile.

9   REFERENCES

1.   Smith, M.J.T., Lowrie, B.W., Brooks, J.R., and Bushell, K.W., "Future Supersonic Transport Noise Lessons from the Past", AIAA Paper No. 88-2989, 1988.

2.   Seiner, J.M. and Kresja, E.A., "Supersonic Jet Noise and the High Speed Civil Transport", AIAA Paper 89-2358, 1989.

3.   Seiner, J.M., Ponton, M.K., Pendergraft, Jr., O.C., Manning, J.M., and Mason, M.L., "External Nozzle Flap Dynamic Load Measurements On F-15 S/MTD Model", AIAA Paper No. 90-1910, 1990.

4.   Seiner, J.M., Manning, J.C., Capone, F.J., and Pendergraft, Jr., O.C., "Study of External Dynamic Flap Loads on a 6 Percent B-1B Model", ASME Paper 91-GT-236, 1991.

5.   Green, D.S., "STOVL Acoustic Fatigue Technologies", Proc. Intl. Powered Lift Conf. P-203, Paper 872360, pp. 553-562, 1987.

6.   Morris, P.J. and Bhat, T.R.S. "The Prediction of Noise Radiated From Supersonic Elliptic Jets", AGARD 78th Specialist Meeting On Combat Aircraft Noise, Bonn, Germany, 1991.

7.   Phillips, O.M., "On the Generation of Sound by Supersonic Turbulent Shear layers", J. Fluid Mech., Vol 9, Pt. 1, pp 1-28, 1960.

8.   Ffowcs Williams, J.E. and Maidanik, G., "The Mach Wave Field Radiated by Supersonic Turbulent Shear Flows", J. Fluid Mech., Vol. 21, Pt. 4, pp. 641-657, 1965.

9.   Seiner, J.M., "Advances in High Speed Jet Aeroacoustics", AIAA Paper No. 84-2275, 1984.

10.   Zorumski, W.E, "Aircraft Noise Prediction Program, Theoretical Manual", NASA TM-83199, 1982.

11.   Ho, C.M. and Gutmark, E., "Vortex Induction and Mass Entrainment in a Small Aspect Ratio Elliptic Jet", J. Fluid Mech., Vol. 179, pp. 383-405, 1987.

12.   Seiner, J.M., "Fluid Dynamics and Noise Emission Associated with Supersonic Jets", The Lumley Symposium: Recent Developments in Turbulence, Nov. 1990, (to appear).

13.   Baty, R.S., Seiner, J.M., and Ponton, M.K., "Instability of a Supersonic Shock-Free Elliptic Jet", AIAA Paper No. 90-3959, 1990.

14.   Seiner, J.M., Ponton, M.K., and Manning, J.C., "Acoustic Properties Associated with Rectangular Geometry Supersonic Nozzles", AIAA Paper No. 86-1867, 1986.

Discussion

QUESTION BY: M.D.Paramour, UK, MOD(PE)
The F-15 "STOL/MTD" technology demonstrator aircraft has variable geometry rectangular nozzles. Has work been done or is work planned to see if such nozzles give a noise reduction compared with the conventional F-15 aircraft?

AUTHOR'S RESPONSE:
I do not know if any full scale acoustic test was ever conducted on the F-15 STOL technoly demonstrator. Model scale work using twin round and rectangular nozzles in the wind tunnel, indicated that noise is reduced with the twin rectangular configuration.

QUESTION BY: U. Michel, DLR Berlin, Germany
You stressed the importance of Mach wave radiation in your experimental and the corresponding theoretical results. Should not this contribution reduce or vanish if the aircraft is in flight?

AUTHOR'S RESPONSE:
Your own prediction of convective source speed, V_c, equation 13 of paper 21, indicates that V_c increases with aircraft forward flight speed V_f for constant jet speed V_j. Since the Mach wave mechanism only requires that $V_c > a_0$, where a_0 is ambient sound speed, you own predictions would suggest that the Mach wave mechanism should still be present at high flight Mach number.

QUESTION BY: W.D. Bryce, RAE Pyestock, UK
While it is interesting to see the noise reductions which can be obtained using non-round nozzles, is it not the case that these jets are extremely noisy and remain so even with the observed noise reductions? While the noise reductions may be of advantage during some short-term periods of aircraft operation, are they of relevance in the context of sustained flight at high subsonic Mach numbers?

AUTHOR'S RESPONSE:
It is true that even after factoring in the noise reductions of these nozzles, the remaining noise still represents a problem. These nozzles, however, like the ADEN, do not compromise on performance and therefore would be beneficial to implement. Sustained flight at high Mach number and low altitudes is associated with bombers and not fighter aircraft. For bombers, the mission profile suggests that these non-round nozzle geometries may produce no noise benefit or detriment. They may, however, provide better performance with regard to other measure of the aircraft mission, such as signature reduction. For fighters the non-round geometries would be of substantial benefit due to the lower Mach number associated with a portion of their mission profile.

QUESTION BY: D.J. Way, DRA, Aerospace Division Pyestock, U.K.
The Concorde experience indicated that noise suppression proposals effective statically did not bring about the predicted noise reductions in flight. What evidence have you that non-round exhaust geometries will maintain their benefits with forward speed?

AUTHOR'S RESPONSE:

First, the suppression concepts for commercial aircraft like the Concorde only must work in the terminal area, up to 400 ft/sec. (M_f - 0.36). The application of non-round nozzle technology requires that the initial growth rate of the shear layer be non-axisymetric, but of the type that will undergo spatial amplification of the shear layer. Based on the success of the "wave model theory" to predict noise from non-round jets, it should be possible to tell if the technique can be applied to a given nozzle/airframe installation and be successful. It may be possible to design an external nozzle cowl that in fact shapes the boundary layer to enable achievement of the noise suppression capability.

NOZZLE INSTALLATION EFFECTS ON THE NOISE FROM SUPERSONIC EXHAUST PLUMES

R.W. Wlezien
Mechanical and Aerospace Engineering Department
Illinois Institute of Technology
10 West 32nd Street
Chicago
Illinois 60616
United States

SUMMARY

The sensitivity of screech coupling in supersonic jets to nozzle installation geometry is explored as a function of nozzle shape, spacing, and orientation. The coupling phenomenon is shown to be a function of geometry for a variety of twin axisymmetric and rectangular nozzle configurations as well as for a single jet in proximity to a solid surface. Rapid plume merging or close proximity to a wall are shown to minimize the noise increment due to coupling. Twin impinging supersonic plumes experience more complex aeroacoustic interactions. The acoustic near field is dominated by screech and impingement tones, but the fuselage undersurface dynamic loads are primarily due to impingement of the unsteady upwash fountain flow on the fuselage undersurface.

1. INTRODUCTION

The ability to predict and control noise from aircraft having supersonic exhausts requires an understanding of the plume dynamic environment for configurations other than an isolated round jet. Noise control is an issue of high priority in populated regions having a high density of low-altitude overflights. The thermal and acoustic loads on aircraft structures in near-proximity to the plumes must also be controlled to maximize the structural fatigue of aircraft components. In practice, many noise prediction codes and approaches to noise reduction are based on data from isolated plume tests. However, the noise field from multiple interacting plumes generally will not combine in a simple additive sense, even when nozzle geometry is taken into consideration.

The deviations from the idealized data sets which occur in real aircraft are typically lumped under the category of installation effects. The simplest installation effect is shielding and scattering by fuselage surfaces. These effects are generally linear and are relatively easy to predict using analytical and computational methods. A somewhat more complicated effect is the shielding which occurs as sound is refracted through velocity and temperature gradients in the flow. This shielding effect is more difficult to predict accurately because a detailed description of the velocity and temperature fields is required. Acoustic shielding by adjacent plumes in multiple nozzle configurations is highly directive and is most beneficial in the aft quadrant due to the high temperature and velocity gradients within the plumes.

A significantly more complex installation effect is acoustic source modification. Source modification is complex and highly nonlinear, and at present cannot be predicted except by empirical methods. The acoustic sources may be indirectly changed through modifications to the mean flow, or directly modified through turbulence-turbulence interactions as in merging jets, or acoustic-flow interaction as in acoustic feedback interactions. While these phenomena are difficult to predict and model, they offer the greatest potential for noise control. The high degree of nonlinearity suggests that small modification to the mean flow or nozzle geometry can produce large changes in the radiated acoustic field.

Many tactical and strategic aircraft use propulsion systems in configurations having two exhaust nozzles in close proximity to each other. These nozzles generally produce supersonic jets with imbedded systems of shock waves. A typical acoustic spectrum of a supersonic jet is illustrated in Figure 1. The acoustic frequency f is normalized with the nozzle diameter, d, and the jet velocity U_j. The three predominant peaks in the spectrum are each tied to specific physical mechanisms. A resonant interaction between shear layer instabilities and the shocks within the plume can produce an intense narrow-band noise component known as screech. Broadband shock-associated noise is produced by the interaction between shear-layer turbulence and the shock waves. The screech peak is almost 20 dB above the broadband shock-associated noise, and extends over a narrow band because of the feedback process characteristic of the screech instability. The third and lowest peak is due to the jet column instability which is responsible for jet noise in subsonic as well as supersonic jets.

In this paper we focus on the screech instability primarily because the noise from screech has the potential to be substantially greater than that from other sources. A schematic of the screech feedback loop is illustrated in Figure 2. A vortical shear-layer disturbance convects downstream and interacts with the shocks because the jet sonic line is within the shear layer. At some point downstream (typically the third or fourth shock cell) the interaction is sufficient to produce an upstream-travelling acoustic wave. This sound wave couples with the flow at the nozzle lip and induces another shear-layer disturbance. Thus the complex combination of the shock cell spacing, the disturbance convection velocity and growth rate and the receptivity to acoustic perturbations at the nozzle lip determines the screech amplitude.

The characteristics of screech in isolated supersonic jets has been studied extensively over the past 30 years, as summarized in the review article by Seiner (Ref. 1). Recent papers on isolated rectangular nozzles (Ref 2), interacting round and rectangular plumes (Refs. 3,4), and round and rectangular nozzles near flat walls (Refs. 5,6) have extended the data available on dynamics of supersonic plumes. At present we know that such configurations can enhance screech, modify acoustic directivity, and even suppress screech resonance. However, present methodology only allows the prediction of screech frequency (Refs. 2,3) and is therefore inadequate to predict screech amplitude, or even screech onset. Because we know that screech is highly sensitive to geometry, we must resort to empirical characterization of the acoustic near-field as a function of geometry. The high sensitivity of supersonic plume acoustics to nozzle configuration also suggests that

optimization for acoustic considerations can be achieved by judicious choice of nozzle shape and location.

In two papers, Seiner, Manning, and Ponton (Refs. 3,4) define the mechanism of twin-plume resonance for both round and rectangular nozzles and show that interacting plumes generate dynamic pressures exceeding the sum of two isolated plumes. Convergent/divergent (C/D) nozzles were investigated at both model and full scale. At model scale, plume coupling produced increased dynamic pressures. Full-scale static tests produced frequencies predicted on the basis of model-scale data, although the amplitudes were lower than those measured in the laboratory.

Seiner et al. (Ref. 2) have also shown that the acoustic characteristics of a single rectangular jet greatly differ from those of a round jet. Low-aspect-ratio nozzles have no detectable screech component, whereas high-aspect-ratio nozzles produce jets with a strong planar flapping component. In Ref. 5 the flapping mode was shown to be dominant for a high-aspect-ratio nozzle in near proximity to a plane wall. Surface-pressure fluctuations greater than 6 kPa were observed, and there was evidence of changes to the plume as a consequence of coupling with the plate.

In this paper we explore the sensitivity of screech coupling in supersonic plumes to nozzle installation geometry. The configurations considered here are typical of advanced tactical aircraft with supersonic exhausts in both cruise and hover. A parametric investigation of round and rectangular twin-plume interaction as a function of nozzle spacing is used to characterize the regimes of high dynamic pressure. Non-standard geometries such as rectangular nozzles and splayed configurations are also considered. Plume resonance in advanced STOVL aircraft in cruise is modelled by a supersonic jet is located adjacent to a plane surface. Finally, the acoustics of aircraft in ground proximity is investigated, and the sensitivity of acoustic amplitude to aircraft and nozzle geometry is explored.

2.   EXPERIMENTS

A model-scale investigations of plume interaction were conducted in the McDonnell Douglas Research Laboratories Aerodynamic Noise Laboratory (ANL) and the McDonnell Aircraft Company Jet Induced Test Apparatus (JITA) in St. Louis, Missouri.

The nozzle sections used in these studies had either constant-area choked-tube or convergent/divergent profiles with nominal throat areas of 487 square mm. All nozzle throat areas were essentially identical to provide equivalent mass flux among all configurations.

Acoustic spectra were obtained for these studies using Bruel and Kjaer microphones directly digitized by a high-speed data acquisition system. An automated processing algorithm was developed to track the magnitude and frequency of the screech peaks. Only those peaks with an amplitude greater than 120 dB were considered. The normalized wavelength λ/d corresponding to these peaks was cast as a function of M_j, the Mach number of a perfectly expanded jet at a given pressure ratio. Previous investigations have shown that the dependence of λ/d on M_j is nearly linear for each screech mode. Linear trends in the data were detected and low amplitude peaks deviating from the trends were eliminated.

2.1   SCREECH INTERACTION BETWEEN ROUND JETS

Two nominally identical convergent/divergent round nozzles were fabricated with a design Mach number of 1.48. The nozzles were connected to a flow system through flexible hoses to determine the effect of nozzle spacing on screech coupling over a range of spacing normalized with diameter, s/d, from 1.8 to 3.2.

Spectra obtained for a microphone located in the nozzle exit plane between the two nozzles is shown in Figure 3 as a function of nozzle spacing at $M_j = 1.56$, or slightly above the design pressure ratio. At s/d = 1.8, there are two relatively small peaks in the spectra near 4 and 4.5 kHz. As the nozzle spacing is increased to s/d = 2.6, the 4 kHz peak dominates the spectrum, but the dominant peak abruptly shifts to the higher frequency when the spacing is increased to s/d = 3.2. These seemingly anomalous changes in screech amplitude and frequency can be better interpreted when the screech modes are tracked as a function of M_j.

Figure 4 is a composite plot of modal wavelength as a function of M_j for both single and dual nozzle configurations. The instability modes for the paired nozzles are essentially the same as those observed for the isolated plumes, and the only discontinuities occur at regions of mode change. Each jet develops axisymmetric A1 and A2 modes at low M_j and helical B and C modes at higher M_j. Although no consistent explanation of mode switching exists at this time, but the phenomena is probably related to changes in shock cell spacing and shear-layer instability growth rates. The modal wavelengths of the two plumes are virtually identical, suggesting similar shock structures in both plumes.

The modal amplitudes for an isolated and interacting jets shown in Figure 5. In the case of the single jet (Figure 5a), the mode switching among the A1, A2, B, and C modes is evident as the Mach number increases. A local minimum of the screech amplitude occurs near M_j the design Mach number and a condition for which the shocks should be weakest. Beyond the design Mach number the plume is underexpanded and the C mode is dominant.Therefore the individual spectrum in Figure 3a has two weak peaks, corresponding to the mode switch near the design Mach number of the nozzles.

Figure 5b through 5d summarizes the changes in modal amplitude as a function of nozzle spacing. Figure 5b shows the characteristic amplitudes for the minimum nozzle spacing, s/d= 1.8. For the toroidal A1 mode, interaction between the plumes produces no net increase in dynamic pressure; the magnitude is approximately the sum of that from the two isolated jets. However, the B mode is significantly enhanced, particularly for $M_j < 1.4$, and the dynamic pressure is as much as 10 dB greater than the sum of that from the two isolated nozzles. For $M_j > 1.4$, the B mode is enhanced relative to the isolated jets, and the C mode is suppressed. However the C mode does not become dominant, and the overall sound pressure level is less than the sum of the isolated jets for $M_j > 1.52$.

A slight increase in nozzle spacing to s/d= 2.2 (Fig. 5c) produces a large increase in the B-mode amplitude at high M_j. Plume interaction produces a noise increment of at least 10 dB for all M_j above B-mode onset. As before, the C-mode interaction is strongly suppressed. The B-mode trends continue through larger values of s/d.

For s/d= 3.2, plume interaction does not occur below M_j = 1.4, and the screech amplitudes are suppressed relative to the isolated jets. A dramatic change occurs in the C mode, with strong coupling occurring for large s/d. For s/d= 3.2 and M_j approximately 1.5, the screech amplitude increment due to plume interaction is approximately 20 dB.

A significant aspect of plume coupling is that screech continues to be supported at the nozzle design Mach number. Only at s/d= 1.8 is there a decrease in amplitude near the design Mach number of 1.48, with no similar decrease for any other nozzle spacing. Although the plume should be nominally shock-free near the design point, screech is supported for the twin-nozzle configuration. It is possible that the plumes are ideally expanded in a mean sense at the design point, but oscillate between under and overexpansion when in the plumes are in screech.

Thus the noise produced by mutual interaction of two supersonic plumes is a strong function of nozzle spacing and jet Mach number, with the design Mach number playing virtually no role. Close spacing supports axisymmetric A and helical B modes, but suppresses the C mode relative to isolated plumes. Wide spacing inverts the modal dominance, and significant C-mode augmentation is observed.

When nozzle spacing is small the plumes merge before the higher modes develop, and screech coupling is suppressed. The fast merging of multiple jets tends to make them act as a single larger jet with no coupling interaction. When the spacing is large, the dominant modes tend to develop farther downstream where shear layers are thick. Therefore a viable strategy for screech reduction in round plumes may be to further reduce nozzle spacing to suppress B-mode interaction.

2.2 SCREECH INTERACTION BETWEEN RECTANGULAR JETS

The models tested in this portion of the study were based on generic 2-D C/D nozzle configurations for low Mach dry power and low Mach afterburning (A/B) engine power settings. The first has an area ratio of 1.05 and a throat aspect ratio (AR) of 2.94 the second has an area ratio of 1.15 and a throat aspect ratio of 1.33.

The screech interaction for the two basic nozzle configurations was investigated as a function of several geometric variables. These variables include throat aspect ratio (width/height), area ratio (exit/throat), nozzle spacing, and inboard splay angle.

When the plumes from two closely spaced nozzles interact, the relative orientation, phase, and acoustic amplitude of the oscillating plumes are determined by the nozzle geometry. Four distinct interaction modes were identified using phase-conditioned schlieren flow visualization, and are summarized schematically in Figure 6. The interaction modes differ from the screech modes described in the previous section in that the interaction modes refer to the phase relation and spatial orientation of two plumes relative to one another.

In the Normal Symmetric (NS) mode both plumes flap in the x-z plane of the nozzles. This mode is denoted as symmetric because both plumes oscillate in phase in the z direction.

The Normal Antisymmetric (NA) mode is characterized by both plumes flapping in the x-z plane, 180 degrees out-of-phase. Thus, in both normal modes the plume is displaced normal to the plane containing the centerlines of both jets.

In the Lateral Symmetric (LS) mode, both plumes flap in the y-direction in the x-y plane of the nozzles. The flapping motion is symmetric with respect to the x-z plane; that is, both jets are either moving toward or away from the x-z plane.

The Lateral Antisymmetric (LA) mode is characterized by both plumes flapping in the x-y plane and moving in the same direction simultaneously. In both lateral modes, the plumes are displaced laterally in the plane containing the centers of the nozzles.

Microphone measurements indicate that each interaction mode exhibits a unique acoustic directivity. All of the configurations investigated in this study exhibited one or more of these four interaction modes when screech was present. The relative orientation and phase relationship between the oscillating plumes controls the acoustic directivity patterns for each interaction mode. These directivity patterns were measured using four near-field microphones as shown in Figure 7.

The NS mode projects the highest acoustic levels toward microphones 1 and 4, located along the x-z plane of symmetry between the nozzles. The directivity pattern for this mode is a consequence of both plumes producing acoustic disturbances in phase above (or below) the x-y plane through the nozzles. The acoustic amplitudes at the other microphones are below those at microphones 1 and 4, which is consistent with the directivity.

The NA mode projects the greatest screech amplitude toward microphone 2, located at 45 degrees to the plane of symmetry between the nozzles. The antiphase relationship between the plume means that the left plume produces an acoustic disturbance above the nozzles when the right plume produces a disturbance below the nozzles. The NA mode produces a dominant wave front which propagates at 45 degrees to the plane of symmetry. Small changes in operating conditions can thus radically change the plume acoustic directivity.

The LS mode projects the highest acoustic amplitude toward microphone 4 (located between the two nozzles) because the in-phase plume oscillation projects strong acoustic waves upstream toward the inter-nozzle region. This interaction mode is not unlike the symmetric interaction mode observed for round nozzles. Microphones 1 and 3 also experience increased acoustic amplitudes, but to a lesser degree than microphone 4.

The antisymmetric LA mode projects the highest amplitudes toward microphone 3, located to the outside of one of the nozzles. Because of phase-cancellation on

the centerline, the microphone 4 amplitude is lower than that observed in the LS mode, and the acoustic amplitudes are greatest at microphone 3.

The near-field acoustic amplitude during jet interaction is strongly dependent upon the particular interaction mode. Furthermore, the dominant interaction mode and its relative strength are dependent on nozzle orientation, aspect ratio, and NPR. The acoustic amplitude measured at the dominant microphone position is used to demonstrate the influence of geometry in Figure 8. The dominant interaction mode is noted for each OASPL to establish the mechanism responsible for the observed trends. The data are segregated by aspect ratio because only the AR 2.94 nozzles produce NS and NA interaction modes and the AR 1.33 nozzles produce only LS and LA interaction modes. In each case, the symmetric modes (i.e. NS or LS) produce greater screech amplitudes than the antisymmetric modes (i.e. NA or LA)

Screech amplitude generally decreases with spacing for the AR 2.94 nozzles. The OASPL trend with spacing ratio is included in Figure 8 for the AR 2.94 nozzles operating at design NPR. Only the NS interaction mode is present at design NPR for all spacing ratios of the AR 2.94 nozzle. This trend of decreasing OASPL with increased spacing indicates that the NS coupling is weakened as the nozzles are moved farther apart.

The AR 1.33 nozzles produce the highest screech amplitude at an intermediate spacing ratio. As shown in Figure 10, the LS mode exhibits maximum coupling at s/w =2.8, where s is the nozzle centerline spacing and w is the nozzle width. Other spacing ratios produce less intense LS coupling or revert to the LA mode. Thus the trends observed as a function of spacing ratio are directly related to the interaction mode. The LA interaction mode produces the lowest OASPL for the AR 1.33 nozzles and occurs at the smallest nozzle spacing (Figure 10). As spacing ratio increases, the interaction mode transitions from antisymmetric to symmetric

The AR 2.94 configuration was evaluated with a maximum inboard splay angle of 8.2 degrees and minimum spacing ratio of 1.25. This configuration produces lower OASPL than the trend established for non-splayed AR 2.94 nozzle configurations (Figure 8) However, as splay angle is reduced to 6.5 degrees, OASPL increases to near that of the non-splayed reference cases. Large as well as moderate splay are effective in reducing acoustic levels for the AR 1.33 configurations. As shown in Figure 10, both splay configurations produce OASPL below the trends established for the non-splayed configurations. The reduction of near-field noise for inboard splay of the AR 1.33 nozzles is attributed to screech suppression for maximum splay and weakening of plume interaction for moderate splay

It should be noted that the twin rectangular nozzle configurations evaluated here produce inter-nozzle acoustic levels 2 to 12 dB lower than similar twin axisymmetric models tested in this same facility. These results are consistent with measurements for isolated plumes

2.3   SCREECH INTERACTION BETWEEN A JET AND A SOLID SURFACE

Advanced STOVL aircraft may be configured with nozzles which rotate to positions parallel to the fuselage during cruise. Screech coupling between a jet and a parallel plane surface was investigated to determine whether coupling mechanisms similar to those experienced in twin plumes exist for these configurations. In principle an infinite flat-plate should appear no different than the plane of symmetry in a twin-nozzle symmetric interaction.

For this investigation a 1200-mm-square flat plate was mounted on a three-dimensional traversing system parallel to the centerline of the jet (Figure 9). The streamwise and transverse coordinates x and y originate from the nozzle exit plane on the axis of the jet. The upstream edge of the plate was aligned with the nozzle exit. The near-field microphone was located at a radial distance r_m = 1.6 d from the jet centerline above the jet, with the flat plate below the jet. The axisymmetric nozzle was the same convergent/divergent nozzle used for the twin plume experiments.

The near-field screech amplitudes for the axisymmetric plume (Fig. 10) are shown for normalized heights h/d = 0.55 through 2.0. In general, the sequence of A1, A2, B, and C modes exists for all h/d, but the relative amplitudes of the modes are strongly modified by wall proximity. The A1-mode amplitude is independent of wall position at low Mach number because the mode does not induce plume motion which tends to be suppressed when the wall is in close proximity. Conversely, the B- and C-mode amplitudes are a strong function of wall position because wall reflections enhance plume oscillation, and wall proximity interferes with screech.

For h/d = 2.0, the B-mode amplitude varies over a wide range with increasing Mach number and the screech is highly intermittent at each NPR. The screech amplitude decreases as expected near the nozzle design point (M_j =1.48), and a strong C mode interaction is engaged at higher pressure ratios. At h/d = 1.0, the B mode is stronger and much less intermittent because of interaction with the wall. There is no decrease in screech amplitude near the nozzle design point, and the B mode dominates at higher NPR than for the free jet. When the wall is at h/d = 0.75, the acoustic amplitudes are similar to those of an isolated jet and decrease at high NPR, but the B mode continues to dominate at high NPR. Near total suppression of the B and C modes occurs over the full Mach-number range at h/d = 0.55. The trends observed here are exactly analogous to those measured for twin interacting plumes; there appears to be little difference between a single plume interacting with its image in a plane surface and the symmetric interaction of plumes from two geometrically similar nozzles

A series of pressure transducers were used to map the unsteady surface pressure below the unsteady jet. Combined contour and carpet plots (Fig. 11) are used to illustrate the range of surface dynamic pressures. Detailed spectra were obtained at all surface transducers, but in most cases the data were screech dominated so that the narrow-band and overall distributions are indistinguishable

Two surface dynamic pressure distributions are shown in Fig. 11. At h/d = 0.55, the greatest unsteady loads are appear in a narrow band along the centerline of the jet where the jet contacts the wall. When the wall is farther

from the jet, high dynamic pressure is observed over a wider segment of the wall. The greatest surface dynamic pressures occur for $h/d = 1.0$, even though the plume is far from the plate surface. The plume is in a strong screech and the prime acoustic sources are at the intersections between the shock diamonds and the shear layer. The multiple source pattern is directly reflected in the OASPL distribution on the surface of the plate. The peak unsteady loads are as much as 10 times greater than those at $h/d = 0.55$, which are barely distinguishable from the background at the screech frequency.

2.4 SCREECH INTERACTION IN IMPINGING JETS

The acoustic environment of a STOVL aircraft in hover is a first-order consideration in terms of structure fatigue life and airframe weight penalties. The hover environment is highly three-dimensional, unsteady, and difficult to model by other than empirical methods (Ref. 7), particularly in the case of supersonic lift jets.

The impingement tones (Refs. 8-10) can often have significantly higher amplitudes than screech when an aircraft is in hover. In multiple jet configurations the upwash fountain (Figure 12) directly impinges on the fuselage undersurface and produces dynamic loading by hydrodynamic rather than by acoustic mechanisms. While the minimization of far-field noise may require that screech and impingement tones be minimized, minimization of undersurface dynamic loads may be more closely tied to the management of the upwash fountain flow.

Four nozzle configurations were investigated with two exit shapes (round and 2:1 rectangular), and two axial variations of cross-sectional area (convergent / divergent designated CD, and constant-area choked-tubes designated CT). The choice of nozzle shape was dictated by two considerations. Round plumes tend to undergo helical oscillation, whereas rectangular plumes have a preferred screech orientation normal to the major axis of the nozzles. The CT nozzles were chosen to produce maximum screech amplitude and the CD nozzles were chosen to minimize screech at the design jet Mach number $M_j = 1.47$.

The distance between the nozzle exit plane and the ground plane, h_n, is typically normalized with the effective nozzle diameter, d_e. The nozzle spacing for this configuration was 4.16 diameters which is significantly larger than that for the previous plume coupling experiments.

The wavelength and amplitude of screech for the impinging twin plumes are plotted in normalized form as a function of distance from the ground plane in Figure 13. The nozzles were operated at NPR=3.5, the design NPR for the CD nozzles. In this case noise observed in the spectra may either be screech or impingement tones. When the normalized wavelength is plotted as a function of height above the ground plane screech is characterized by horizontal lines because the screech frequency is generally insensitive to distance from the ground plane. The impingement tones appear as a series of diagonal lines because the resonant wavelength is linearly related to distance from the nozzles to the ground plane. Changes in the slope of the diagonals are characteristic of impingement tone staging, as

observed by Norum (Ref. 10) for single impinging supersonic plumes.

For the axisymmetric CT nozzles plume screech is the dominant noise source for $h_n / d_e > 3$. Below that point no resonance peaks are observed, probably because the total amplification of the shear-layer instability waves between the nozzle and the plate is insufficient to sustain self-excited oscillation. The other tones present show some evidence of staging, but the impingement tone amplitudes are always lower than those due to screech. Thus the presence of a strong screech resonance appears to interfere with the development of impingement modes.

A discrete screech peak is not present for these CD nozzles at the design NPR=3.5 when $h_n / d_e > 7$, which indicates that screech coupling is weak at this comparatively large nozzle spacing. The screech tone manifests itself only as the distance to the ground plane is decreased, probably because distortion of the entrainment flow due to proximity to the ground plane produces shocks in the plume. There is evidence of strong impingement tones and tone staging at all heights above the ground plane, and the impingement tones have amplitudes greater than the screech amplitude except for locations very close to the ground plane.

A comparison between the CT and CD data for $h_n / d_e < 6$ leads to the rather remarkable conclusion that the CD nozzles operating at their design point produce more intense impingement tones than the underexpanded plumes from the CT nozzles. The interaction between the screech and impingement-tone mechanisms is such that high-amplitude screech resonance tends to suppress the impingement tone feedback loop. Furthermore, when screech is suppressed by using the CD nozzles at their design pressure ratio, the resultant strong impingement tones lead to greater overall acoustic levels for all $h_n / d_e < 6$.

Data for rectangular nozzles exhibit similar trends to those of the axisymmetric nozzles. The rectangular nozzles tend to produce greater acoustic levels than the axisymmetric nozzles for $h_n / d_e < 4$, but the amplitudes decrease rapidly with increasing distance from the ground plane. Suppression of impingement tones is also observed when strong screech is present.

The array of dynamic pressure transducers was used to measure the undersurface dynamic load distributions for a range of operating conditions. The distribution of undersurface dynamic pressure for rectangular CT, axisymmetric CT, and axisymmetric CD nozzles is shown in Figure 14 for $h_n / d_e = 2$ in Figure 14. For all nozzle configurations the region of maximum dynamic loading occurs between the nozzles at $h_n / d_e = 2$. Thus the dominant mechanism is neither screech nor impingement tones, but is instead the unsteady hydrodynamic loading from the upwash fountain flow directly impinging on the fuselage undersurface.

The rectangular nozzles produce significantly greater unsteady loads on the fuselage for small h_n in comparison with the round nozzles. At $h_n / d_e = 2$ the 164-dB contour has a substantially larger footprint and typical wing loads are 4-6 dB greater than those for the round nozzles. At larger h_n the fuselage loads are of the same

order or lower than that for the other nozzles, but the wing loads remain greater. These differences are a consequence of the strong lateral screech coupling observed for the rectangular nozzle configuration. The intense screech and impingement tones tend to increase the fuselage loading in regions away from the fountain impingement zone. The wing loading pattern is consistent with the acoustic directivity of the rectangular plume flapping mode.

The effect of operating the axisymmetric C/D nozzles at their design pressure ratio is also illustrated in Figure 14. At $h_n / d_e = 2$, the peak fuselage loads decrease slightly relative to those of the CT nozzles, but the acoustic loads generally increase over the remainder of the fuselage. This increase is probably a consequence of increased impingement tone amplitude, as observed in the near-field microphone data. For small h_n, the impingement tones tend to be augmented in the CD nozzles because there is no interference from the screech modes. This somewhat surprising result suggests that simple nozzles with slightly reduced performance may minimize the unsteady loading as well as the far-field noise.

3.   ACKNOWLEDGEMENT

4.   REFERENCES

1   Seiner, J. M., "Advances in High-Speed Jet Aeroacoustics," AIAA Paper 04-2215, (1984).

2.   Seiner, J. M., Ponton, M. K. and Manning, J. C., "Acoustic Properties Associated with Rectangular Geometry Supersonic Nozzles," AIAA Paper 86-1867, (1986).

3   Seiner, J. M., Manning, J. C., and Ponton, M. K., "Dynamic Pressure Loads Associated With Twin Supersonic Plume Resonance," AIAA Paper No 86-1539, (1986)

4   Seiner, J. M., Manning, J. C. and Ponton, M. K., "Model and Full Scale Study of Twin Supersonic Plume Resonance," AIAA Paper 87-0144, (1987)

5   Seiner, J. M. Manning, J. C., and Jansen, B., "Supersonic Jet Plume Interaction with a Flat Plate," SAE Paper 872361, (1987)

6   Kibens, V., Saripalli, K. R., Wiezien, R. W. and Kegelman, J. T. "Unsteady Features of Jets in Lift and Cruise Modes for VTOL Aircraft," SAE Paper 872359, (1987)

7   VanOverbeke, T. J. and Holdeman, J. D. "A Numerical Study of the Hot Gas Environment Around a STOVL Aircraft in Ground Proximity," AIAA Paper 99-2882 (1988)

8   Krothapalli, A. "Discrete Tones Generated by an Impinging Underexpanded Rectangular Jet," AIAA J 23 (12), 1910 (1985)

9.   Ahuja, K. K., and Spencer, D. A. "Aeroacoustics of Advanced STOVL Aircraft Plumes," Proceedings of the International Powered Lift Conference, pp. 531-541, Santa Clara, CA (1987).

10.   Norum, T. D., "Supersonic Rectangular Jet Impingement Noise Experiments," AIAA Paper 89-1138 (1989).
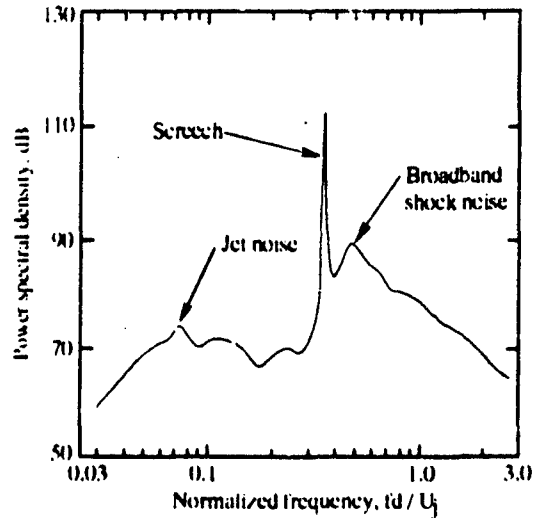

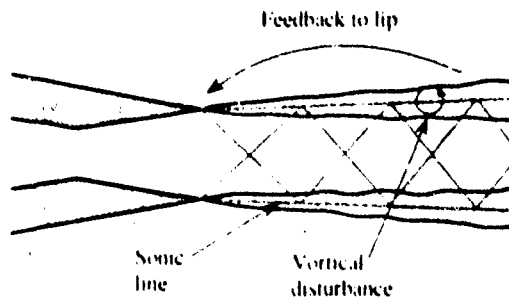Fig.1   Typical supersonic jet acoustic spectrum (from Seiner, Ref. 1)
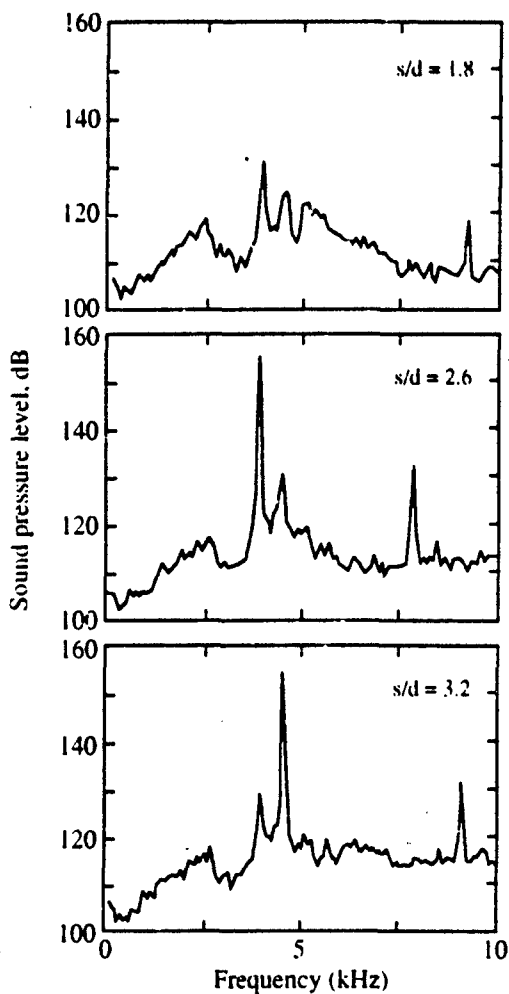

Fig. 2   Schematic of screech instability mechanism

Fig. 3 Twin axisymmetric nozzle acoustic spectra as function of nozzle spacing for M_j = 1.56
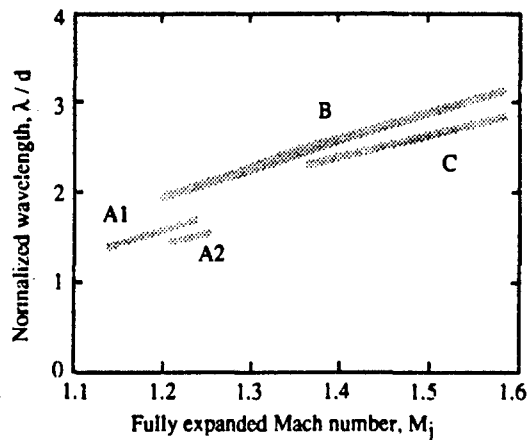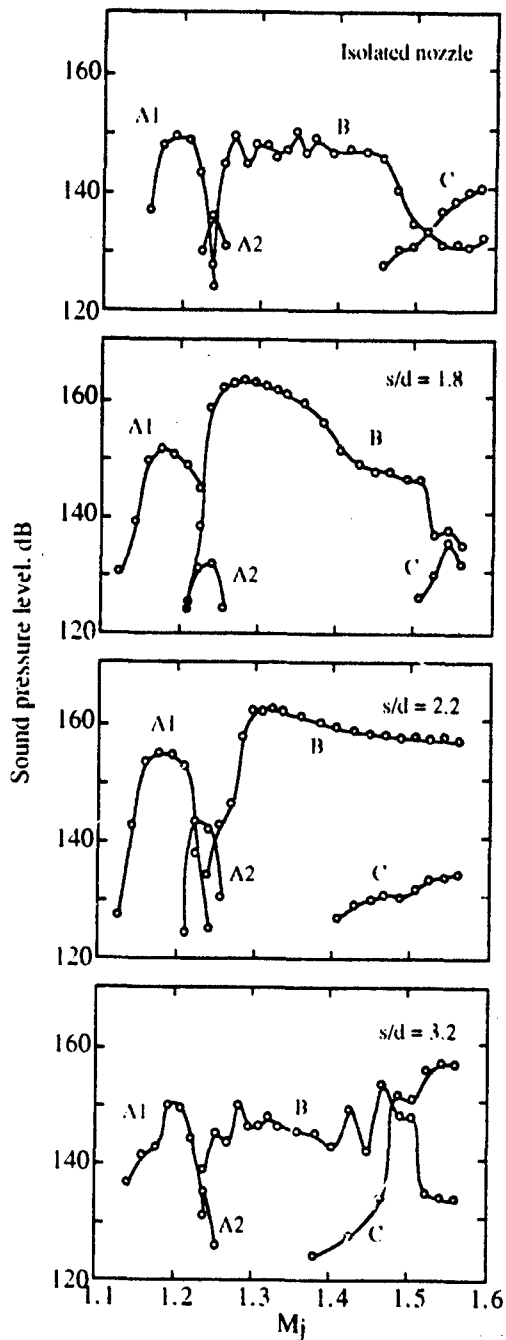
Fig. 4 Twin axisymmetric nozzle screech modes

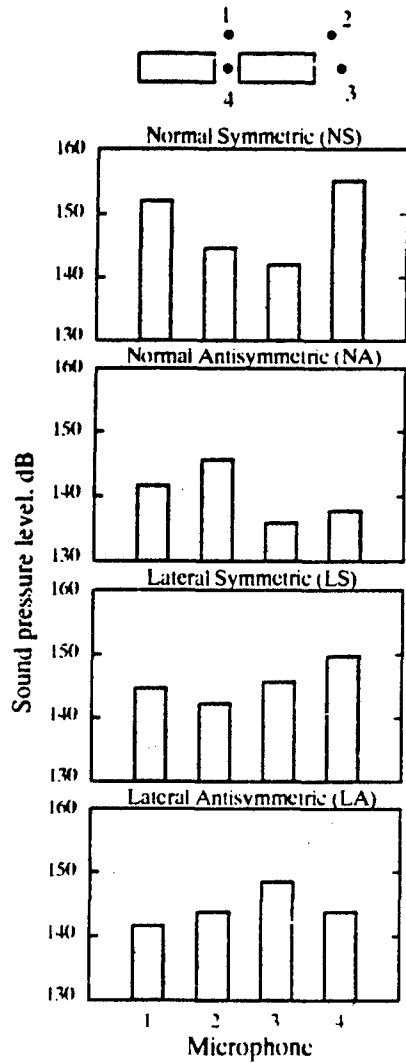Fig. 5 Twin axisymmetric nozzle screech amplitudes

Normal Symmetric (NS)   Normal Antisymmetric (NA)

Lateral Symmetric (LS)   Lateral Antisymmetric (LA)

Fig. 6   Rectangular jet interaction modes

Normal Symmetric (NS)

Normal Antisymmetric (NA)

Lateral Symmetric (LS)

Lateral Antisymmetric (LA)

Sound pressure level, dB

Microphone
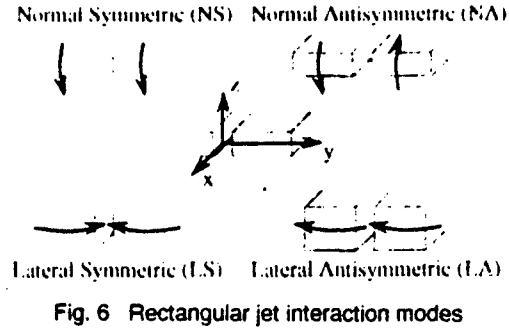
Fig. 7   Typical near-field acoustic directivity for twin rectangular jet interaction

AR = 2.94 nozzles
NPR = 2.63

6.5° inboard splay

8.2° inboard splay

O NS

AR = 1.33 nozzles
NPR = 3.46

6.9° inboard splay

9.2° inboard splay

O LS
□ LA
◇ No screech

Sound pressure level, dB

Spacing ratio, s/w
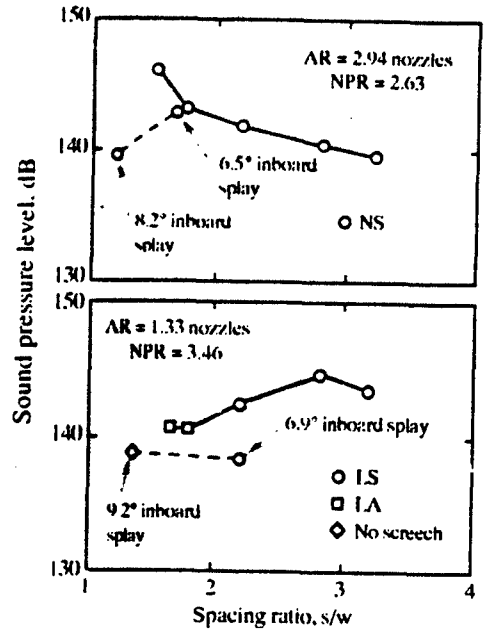
Fig. 8   Influence of rectangular nozzle spacing and splay angle on near field acoustic amplitudes

Microphone

h

y

x

Instrumented flat plate
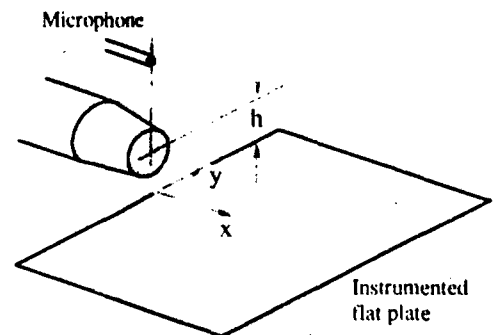
Fig. 9   Nozzle and wall configuration

(a)

(b)

Fig. 11 Wall dynamic pressure distribution at screech frequency for axisymmetric nozzle at nozzle pressure ratio = 3.4; h/d = a) 1.0 and b) 0.55

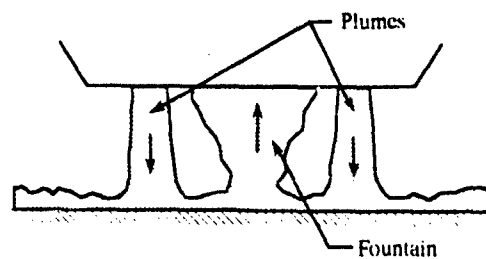Fig. 10 Near-field acoustic amplitudes as function of h/d

Fig. 12 Schematic of twin-plume impingement flowfield with fuselage undersurface
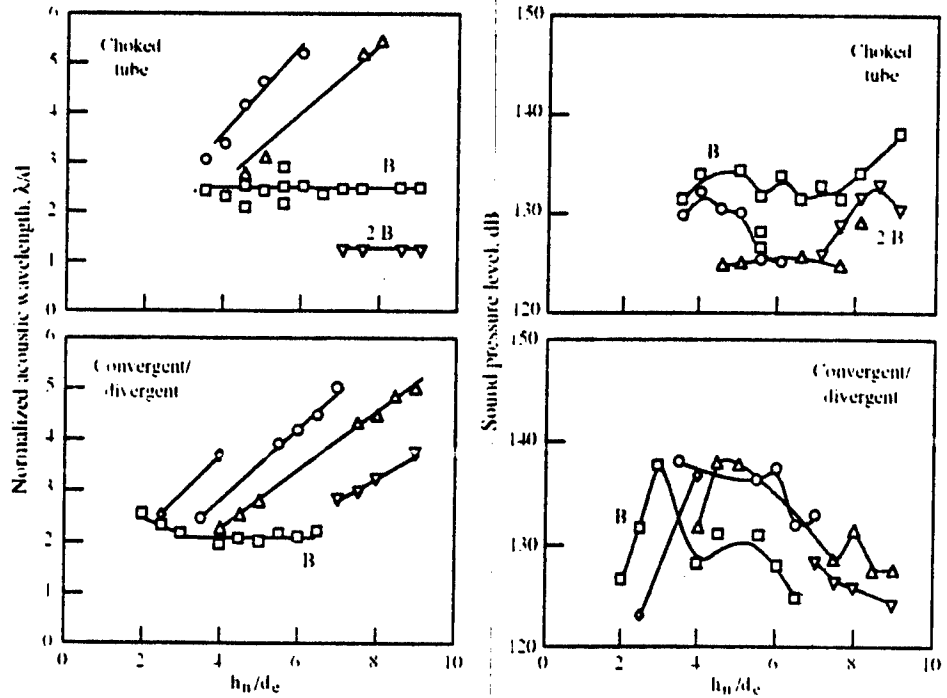
Fig. 13 Height dependence of axisymmetric nozzle
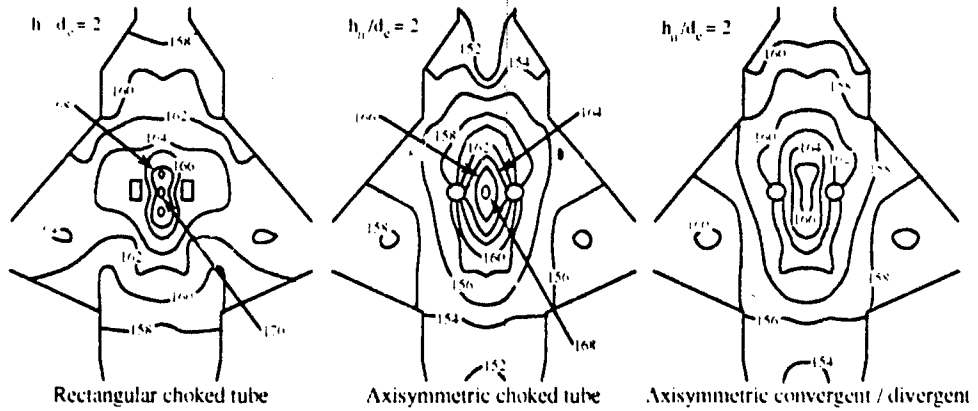modes and acoustic amplitude

Rectangular choked tube   Axisymmetric choked tube   Axisymmetric convergent / divergent

Fig. 14 Advanced STOVL undersurface dynamic
pressure distributions at jet Mach number
$M_j = 1.47$

Discussion

QUESTION BY: W.B. de Wolf, NLR, The Netherlands
To reduce phase locking between screech from twin nozzles, did you consider an axial offset configuration? Or a porous baffle screen between the two jets?

AUTHOR'S RESPONSE:
We considered a large range of geometrical variation, including axial offset, cant angle, inward and outward splay, differential pitch, and nozzle spacing. The only successful approach for reducing plume coupling noise was to cause the plumes to merge rapidly, primarily by inward splay. When the two plumes marge rapidly, they act as a single plume and produce a net lower screech amplitude.

Regarding a porous screen, the screen would have to be sufficiently long to shield the jets from one another, and the drag penalty on an aircraft may be too high for such a device. We have investigated using porous surfaces in contact with the plume (for example, a porous single expansion ramp nozzle) and have been very successful in reducing both screech and shock-associated noise. The porous surface passively reduces stock strength in the plume and produces nearly perfectly expanded jets without movable surfaces.

QUESTIONS BY: F.R. Grosche, DLR Göttingen, Germany
The screech tone of a single jet can be eliminated by destroying the feedback mechanism by disturbing the nozzle symmetry, e.g. by inserting a tab into the nozzle exit. Is this technique or are similar techniques also effective in the case of twin jets as in the case of a jet in the vicinity of a flat surface as discussed in your paper?

AUTHOR'S RESPONSE:
Seiner has shown that an intrusive tab in one of the jets can disrupt screech coupling in twin-plume configurations. The disadvantage of such tabs is the high thrust penalty encounte·ed when the device is located in the high-speed flow. In practical applications, such thrust penalties are unacceptable.
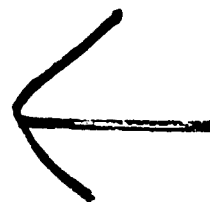
Combustion Noise and Combustion Instabilities in Propulsion Systems

F. E. C. Culick,[†] L. Paparizos,[*] J. Sterling,[†] and V. Burnley[†]

[†]California Institute of Technology
Pasadena, California, U.S.A.

[*]Carnegie-Mellon University
Pittsburgh, Pennsylvania, U.S.A.

92-17426

Abstract

This paper is concerned with some aspects of non-linear behavior of unsteady motions in combustion chambers. The emphasis is on conditions under which organized oscillations having discrete frequencies may exist in the presence of random motions. In order to treat the two types of motions together, and particularly to investigate coupling between noise and combustion instabilities, the unsteady field is represented as a synthesis of acoustic modes having time-varying amplitudes. Each of the amplitudes are written as the sum of two parts, one associated with the random field and the remainder representing the organized oscillations. After spatial averaging, the general problem is reduced to solution of a set of second-order ordinary differential equations whose structure depends on the sorts of nonlinear processes accounted for. This formulation accommodates any physical process; in particular, terms are included to represent noise sources, although only limited modeling is discussed here. Our results suggest that random sources of noise have only small effects on combustion instabilities and seem not to be a cause of unstable motions. However, the coupling between the two sorts of unsteady motions may be important as an essential process in a proposed scheme for noise control.

It is now a familiar observation that many nonlinear deterministic systems are capable of exhibiting apparently random motions called 'chaos.' This is a particularly interesting possibility for systems which also execute non-deterministic random motions. In combustion chambers, a nonlinear deterministic system (acoustical motions) exists in the presence of noise produced by flow separation, turbulent motions, and energy released by combustion processes. The last part of the paper is directed to the matter of discovering whether or not chaotic motions exist in combustion systems. Analysis has not progressed sufficiently far to answer the question. We report here recent results of processing data taken in one combustor to determine the dimensions of any attractors in the motions. No evidence has been found for chaos in the strict sense, but the method seems to be an important means of investigating the nonlinear behavior of combustion systems.

1. Introduction

Jet aircraft in flight carry two types of noise sources: external and internal. External sources include boundary layers, separation regions on the airframe, and especially jet noise associated with the exhaust flow. We are concerned here with some aspects of internal noise generated in combustion chambers.

Following a period of considerable research on the subject of combustion noise during the 1970s, relatively little attention seems to have been directed to theoretical aspects of the subject. A good review of much of the work has been given by Strahle (1978). Both experimental and theoretical results were obtained, but it seems a fair statement that the theory of combustion noise has not progressed as far as the theories of external jet noise. The works by Chiu and Summerfield (1973) and by Chiu, Plett, and Summerfield (1975) seem to be the most complete treatments of combustion noise in chambers or ducts, in which the unsteady motions comprise both random fluctuations and coherent oscillations. More recent experimental work has been reported (Poinsot et al. 1986; Hegde, Reuter, and Zinn 1988) with some analysis of data, but no advances in theory. The general problem of internal noise shares common features with that of external noise, but the differences are sufficiently great that probably a theory of internal noise should take a rather different form.

In the first part of this paper we construct an approximate analysis having such a form as to be applicable only to a restricted class of internal problems. It is important to appreciate, however, that because sources of noise in a flow always are associated with unsteady motions of the fluid

medium, there must be intrinsic similarities between external and internal theories. Hence as a part of the formulation here, we discuss some of those similarities, helping to clarify where the internal and external theories diverge.

The approximate analysis described here is an extension of a formulation used for many years to study combustion instabilities, based on a form of Galerkin's method (Zinn and Powell 1971 and Culick 1971, 1975, 1990 for example). As described in Section 2, the main idea is to represent a general unsteady motion in a chamber as a synthesis of orthogonal acoustic modes of the chamber, computed for the same geometry but with no combustion or mean flow.

Spatial averaging produces a system of ordinary, nonlinear second-order equations in time for time-dependent amplitudes. At this point the chief difference from previous work is that the equations contain random or stochastic sources (unspecified in detail) and correspondingly the amplitudes are sums of deterministic and stochastic parts.

In Section 3 we discuss a procedure for splitting the unsteady field as a superposition of the coherent acoustic and random motions. The results display explicitly coupling between the acoustic motions only, between the acoustic and random motions, and interactions involving only the random motions. In this formulation, the last appear as external stochastic excitation of the acoustical motions.

Following well-established methods (e.g. Krylov and Bogoliubov 1947 for deterministic systems and Stratonovich 1963 for stochastic systems) we then average the equations in time to produce a set of first-order equations used as the basis for the calculations discussed in Section 4. Time-averaging brings errors which can be assessed only by comparison of numerical results with solutions to the second-order equations. Recent work by Jahnke and Culick (1991) has done much to clarify the matter for deterministic systems but we have no corresponding results for systems containing stochastic sources. The results given in Section 4 are preliminary, illustrating possible effects of stochastic sources on stable deterministic motions and on stable limit cycles.

That the unsteady motions in a combustion chamber are intrinsically nonlinear (although the nonlinear effects may often be small in some sense) and that nonlinear deterministic systems are capable of executing apparently random behavior, called 'chaos,' suggests that we should seek the possible existence of chaotic behavior in combustion chambers. The question seems first to have been raised by Kantor (1984) in respect to the processes in a reciprocating engine and later investigated by Keanini, Yu, and Daily (1989) for a dump combustor. The case of a reciprocating engine is different because of the presence of the ignition spark. In any event, those results seem not to have established unambiguously that chaos has been identified in those systems. Difficulties accompanying the methods of processing time-series data tend to obstruct definite conclusions.

In Section 5 we investigate the possibility of chaotic behavior with analysis of data taken at Caltech in the past few years with a dump combustor. Although the results show the existence of an attractor, it has integral dimension 2, i.e. it is a toroidal attractor incapable of chaotic motions. The behavior can be represented by simple models of nonlinear behavior but satisfactory connection with the analysis described in the earlier sections of the paper has not been completed. Our results have been attained only for one combustion system and no generalization can be attributed to our conclusions.

Recent works demonstrating 'control of chaos' both theoretically and experimentally (see Ott *et al.* 1990; Ditto, Rauseo, and Spano 1990) suggest investigating the possibility of exerting corresponding control of a combustion system. At this time, the possibility is thinly founded and speculative. The idea is the following. Chaotic behavior, motion on a strange attractor, consists of motions in many orbits (modes) simultaneously. Controlling chaos consists in exerting an external influence forcing the system to execute chiefly a low-amplitude stable motion. The 'orbits' in a combustion system are the acoustic modes.

If then the true random behavior (the noise so annoying in practice) is coupled (nonlinearly) to the acoustic modes — i.e. the orbits comprising the attractor — then it may be possible to control the noise field by controlling the components (modes or orbits) of the chaotic motion. Of course it is unnecessary to obscure the basic notion with the language of the theory of chaos and dynamical systems theory. However, it is important to understand the connection in order to make use of theoretical methods and results available from recent work in that field. It is also possible that in the case at hand, nonlinear coupling, and hence energy flow, between the noise and acoustic fields may offer the possibility of control even though the acoustical motions do not occur in chaotic form.

Essentially what we suggest is the possibility of reducing the noise field — or perhaps affecting the spectral distribution — by suitable control of the

acoustic modes of the chamber. Nonlinear coupling of the deterministic and random motions is clearly necessary for this scheme to work. We are far from being able to check the validity of this idea in respect to combustion systems. Uncertainty is associated with this particular application, not the general idea, which has been confirmed by results obtained with other systems. Whatever the mechanism, some experimental results (Wilson *et al.* 1991; Gulati and Mani 1990; and Poinsot *et al.* 1989) suggest that control of acoustic oscillations can be used to control the random fluctuations as well. Figure 1, taken from Poinsot *et al.* 1989 shows an example. Reduction of the amplitude of an acoustic mode was accompanied by a reduction in the broadband background. This probably shows in the first instance that the presence of organized oscillations increased the noise level. However, the results also confirm a phenomena already established in experiments with open flames (e.g., Rapp and Schneider 1972; Beckert and Pfizennaies 1972) that the processes generating noise are measurably influenced by an acoustic field. Partly because the more recent works were intended to control the acoustic oscillations only, the matter of controlling noise in this fashion has not been explored either analytically or experimentally.
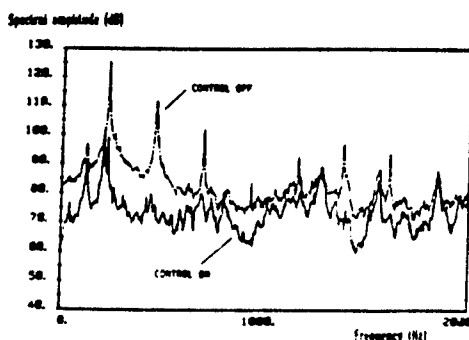

Figure 1.

We must emphasize also that even should control of noise be established as a possibility in principle, the great problem remains of practical implementation. Active control of combustion instabilities, without regard for noise in the system, is a subject of current research (McManus, Poinsot, and Candel 1991 have given a recent review of the subject). Promising results have been obtained in laboratory devices using gaseous fuels and oxidizers. Feedback control of an acoustic generator (loudspeaker) or of a secondary supply of fuel has been used successfully to reduce the levels of unstable oscillations. So far as we know, correspondingly successful results have not been reported for liquid-fueled systems.

2. Formulation of an Approximate Analysis

The sort of analysis described here has been used for many years to investigate combustion instabilities in solid propellant rockets and liquid-fueled systems, mainly ramjet engines. Hence we need only summarize the formulation here with a view partly to comparing this analysis and the theory of combustion instabilities to the well-known theory of aerodynamic noise initiated by Lighthill (1952, 1953).

In order to accommodate the processes occurring in a combustion chamber, we begin with the complete conservation equations for the gas phase with sources of mass, momentum, and energy:

$$Mass$$
$$\frac{\partial \rho}{\partial t} + \nabla \cdot (\rho \vec{u}) = W \tag{2.1}$$

$$Momentum$$
$$\frac{\partial (\rho \vec{u})}{\partial t} + \nabla \cdot (\rho \vec{u}\,\vec{u}) = \nabla \cdot \vec{\tau} + \vec{F} \tag{2.2}$$

$$Energy$$
$$\frac{\partial (\rho e_0)}{\partial t} + \nabla \cdot (\rho \vec{u} e_0) = \nabla \cdot (\vec{\tau} \cdot \vec{u}) - \nabla \cdot \vec{q} + Q \tag{2.3}$$

The heat-flux vector is $\vec{q}$ and the stress tensor is the sum of the isotopic pressure and the viscous stress tensor $\vec{\sigma}$:

$$\vec{\tau} = -p\vec{I} + \vec{\sigma} \tag{2.4}$$

It is necessary to specify the forms of the sources W, $\vec{F}$, and Q which, for example, may contain the influences of condensed phases and chemical reactions. Owing to uncertainties in the properties of actual systems, it is entirely satisfactory to represent the medium as a single mass-averaged perfect gas having the equation of state

$$p = R\rho T \tag{2.5}$$

and internal energy e, such that

$$de = C_v dT \tag{2.6}$$

Subtraction of the scalar product of the velocity and (2.2) from (2.3) leads to the equation for the temperature

$$\rho C_v \left(\frac{\partial T}{\partial t} + \vec{u} \cdot \nabla T \right) = -p\nabla \cdot \vec{u} + \Phi - \nabla \cdot \vec{q} + Q$$
$$-(e_0 - u^2)W - \vec{u} \cdot \vec{F} \tag{2.7}$$

where the dissipation function is

$$\Phi = \bar{\sigma} \cdot \nabla \cdot \vec{u} \qquad (2.8)$$

Because the primary source of data for motions in a combustion chamber is measurement of the time-dependent pressure, there has long been strong motivation to build theoretical frameworks around the pressure as the leading dependent variable. Combination of (2.1), (2.5), and (2.8) gives the energy equation written for the pressure

$$\frac{\partial p}{\partial t} + \vec{u} \cdot \nabla p$$
$$= -\gamma p \nabla \cdot \vec{u} + \frac{R}{C_v} \left[\Phi - \nabla \cdot \vec{q} + Q + \frac{u^2}{2} W - \vec{u} \cdot \vec{F} \right] \qquad (2.9)$$

Finally, the equation for the entropy of the gases follows from its definition

$$T \, ds = de + pd \left(\frac{1}{\rho} \right) = C_v dT - \left(\frac{p}{\rho} \right) d\rho \qquad (2.10)$$

Substitution of (2.7) and (2.1) leads to

$$\rho T \left(\frac{\partial s}{\partial t} + \vec{u} \cdot \nabla s \right) = \Phi - \nabla \cdot \vec{q} + Q - (\gamma e - u^2) W - \vec{u} \cdot \vec{F} \qquad (2.11)$$

As a matter of convenience to simplify writing, we re-write the basic equations (2.1), (2.2), (2.7), (2.9), and (2.11) in the forms

$$\frac{D\rho}{Dt} = \mathcal{W} \qquad (2.12)$$

$$\rho \frac{D\vec{u}}{Dt} = -\nabla p + \vec{\mathcal{F}} \qquad (2.13)$$

$$\rho C_v \frac{DT}{Dt} = -p \nabla \cdot \vec{u} + \mathcal{Q} \qquad (2.14)$$

$$\frac{Dp}{Dt} = -\gamma p \nabla \cdot \vec{u} + \mathcal{P} \qquad (2.15)$$

$$\rho \frac{Ds}{Dt} = \frac{1}{T} \mathcal{S} \qquad (2.16)$$

where $D/Dt = \partial/\partial t + \vec{u} \cdot \nabla$ is the usual convective derivative, and

$$\mathcal{W} = -\rho \nabla \cdot \vec{u} + W$$
$$\vec{\mathcal{F}} = \vec{F} + \nabla \cdot \bar{\sigma} - \vec{u} W$$
$$\mathcal{Q} = \Phi - \nabla \cdot \vec{q} + Q - (e_0 - u^2) W - \vec{u} \cdot \vec{F}$$
$$\mathcal{P} = \frac{R}{C_v} \mathcal{Q} + e W$$
$$\mathcal{S} = \mathcal{Q} - (\gamma - 1) e W = \frac{C_v}{R} \left[\mathcal{P} - a^2 W \right]$$
$$(2.17) a - e$$

These equations. (2.12) – (2.16), are the basis for the theories of both combustion instabilities and noise in combustion systems, but in this form they are much too general. No purpose is served here by tracing detailed construction of the simplified equations actually used in existing works, but it is important to appreciate the gist of the matter in order to understand both the differences and similarities of the two kinds of theories now summarized in turn.

2.1 Combustion Instabilities

Extensive observations obtained during several decades for many systems of all types confirm that combustion instabilities are waves in the combustion product gases excited and sustained primarily by the energy released in chemical reactions. The frequencies of oscillations usually are quite close to those estimated with classical results applied to the same geometry, a chamber enclosed by rigid walls, with the speed of sound equal to that for the high temperature products. Hence, it is reasonable to treat all combustion and flow processes as perturbations of the classical problem. Some adjustments must be made in special circumstances but that view is adequate for the purposes here.

Then the dependent variables are written as sums of mean and fluctuating values, $p = \bar{p} + p'$, etc. with the mean values independent of time, usually (but not always) a good assumption. Two alternative strategies can be followed to obtain nonlinear equations for the fluctuations: either a nonlinear equation for the pressure can be formed from the primitive equations (2.12) – (2.16), followed by substitution of the assumed forms for the dependent variables, or those forms can be substituted in (2.12) – (2.16) and then the nonlinear wave equation for the pressure fluctuation is constructed. For comparison with later remarks on the theories of noise, we first form the wave equation.

Write (2.15) in the form

$$\frac{\partial p}{\partial t} + a_r^2 \nabla \cdot (\rho \vec{u})$$
$$= (a_r^2 - a^2) \nabla \cdot (\rho \vec{u}) - (\vec{u} \cdot \nabla p - a^2 \vec{u} \cdot \nabla \rho) + \mathcal{P}$$

where $a_r^2 = \gamma p_r / \rho_r$ is a reference speed of sound, properly taken as the average value in the chamber, and $a^2 = \gamma p / \rho$ is the local value. Then differentiate with respect to time and substitute (2.1) for $\nabla \cdot (\rho \vec{u})$; some rearrangement leads to

$$\frac{\partial^2 p}{\partial t^2} - a_r^2 \nabla^2 p = a_r^2 \nabla \cdot (\nabla \cdot \bar{T} - \vec{F})$$
$$+ \frac{\partial}{\partial t} \left[(a_r^2 - a^2) \nabla \cdot (\rho \vec{u}) - (\vec{u} \cdot \nabla p - a^2 \vec{u} \cdot \nabla \rho) + \mathcal{P} \right] \qquad (2.18)$$

where

$$\bar{T} = \rho \vec{u}\,\vec{u} - \bar{\sigma} \qquad (2.19)$$

We note for later discussion that equation (2.18) contains the substance of the principles of conservation of mass, momentum, and energy as well as the equation of state for a perfect gas. The boundary condition for the pressure is formed by taking the scalar product of the outward normal vector $\hat{n}$ at the boundary surface with the momentum equation (2.13):

$$\hat{n} \cdot \nabla p = -\rho \frac{\partial \vec{u}}{\partial t} \cdot \hat{n} - (\rho \vec{u} \cdot \nabla \vec{u}) \cdot \hat{n} + \vec{\mathcal{F}} \cdot \hat{n} \quad (2.20)$$

Rather than use (2.18) to construct the wave equation for the pressure fluctuation, we now follow the second strategy noted above, beginning with the equations obtained from (2.1) – (2.3) written to second order in the fluctuations:

$$\frac{\partial \rho'}{\partial t} + \bar{\rho}\nabla \cdot \vec{u}'$$
$$= \rho'\nabla \cdot \vec{u} - \vec{u} \cdot \nabla \rho' - \nabla \cdot (\rho'\vec{u}') + W' \quad (2.21)$$

$$\bar{\rho}\frac{\partial \vec{u}'}{\partial t} + \nabla p'$$
$$= -\bar{\rho}(\vec{u} \cdot \nabla \vec{u}' + \vec{u}' \cdot \nabla \vec{u})$$
$$-\bar{\rho}\vec{u}' \cdot \nabla \vec{u}' - \rho'\frac{\partial \vec{u}'}{\partial t} + \vec{\mathcal{F}}' \quad (2.22)$$

$$\frac{\partial p'}{\partial t} + \gamma \bar{p}\nabla \cdot \vec{u}'$$
$$= -\vec{u} \cdot \nabla p' - \gamma p'\nabla \cdot \vec{u}$$
$$-(\vec{u}' \cdot \nabla p' + \gamma p'\nabla \cdot \vec{u}') + \mathcal{P}' \quad (2.23)$$

These equations have formed the basis for investigating nonlinear combustion instabilities to second order in the gasdynamic fluctuations and first order in the mean flow field. Thus the fluctuations are assumed to represent *only* the acoustic disturbances. The justification for this assumption is the principle most thoroughly discussed by Chu and Kovasznay (1958). In the limit of small amplitude fluctuations, any disturbance can be treated as a synthesis of three independent modes of propagation: acoustic, vortical, and entropic. Hence in the limit of linear behavior, we can study acoustical problems (in particular the stability of waves in a combustion chamber) without regard for other unsteady motions, including turbulent fluctuations. Finite amplitude motions involve nonlinear interactions that mix the modes and the principle of superposition naturally fails.

Chu and Kovasznay estimated the relative magnitude of the various nonlinear interactions coupling the three modes of propagation. A result particularly relevant here is that of the possible sources

of acoustic waves, they found that nonlinear interactions among vorticity disturbances constitute a dominant source of acoustic waves. That conclusion had been reached several years earlier by Lighthill (1952) in his theory of the generation of aerodynamic noise. In combustion chambers, generation of pressure waves by unsteady burning seems to be the dominant source.

Differentiation of (2.23) with respect to time and substitution of (2.22) for $\nabla \cdot (\partial \vec{u}/\partial t)$ leads to the wave equation used in the remainder of this discussion:

$$\nabla^2 p' - \frac{1}{\bar{a}^2}\frac{\partial^2 p'}{\partial t^2} = h \qquad (2.24)$$

where $\bar{a}^2 = \gamma \bar{p}/\bar{\rho}$ is the average speed of sound assumed to be uniform in the chamber, and the right-hand side is

$$h = -\bar{\rho}\nabla \cdot \left(\vec{u} \cdot \nabla \vec{u}' + \vec{u}' \cdot \nabla \vec{u}\right)$$
$$+ \frac{1}{\bar{a}^2}\frac{\partial}{\partial t}\left(\vec{u} \cdot \nabla p' + \gamma p'\nabla \cdot \vec{u}\right)$$
$$- \bar{\rho}\nabla \cdot \left(\vec{u}' \cdot \nabla \vec{u}' + \frac{\rho'}{\bar{\rho}}\frac{\partial \vec{u}'}{\partial t}\right)$$
$$+ \frac{1}{\bar{a}^2}\frac{\partial}{\partial t}\left(\vec{u}' \cdot \nabla p' + \gamma p'\nabla \cdot \vec{u}'\right)$$
$$+ \nabla \cdot \vec{\mathcal{F}}' - \frac{1}{\bar{a}^2}\frac{\partial \mathcal{P}'}{\partial t} \qquad (2.25)$$

The associated boundary condition, formed as the scalar product of $\hat{n}$ and (2.22) is

$$\hat{n} \cdot \nabla p' = -f \qquad (2.26)$$

with

$$f = \bar{\rho}\frac{\partial \vec{u}'}{\partial t} \cdot \hat{n} + \bar{\rho}(\vec{u} \cdot \nabla \vec{u}' + \vec{u}' \cdot \nabla \vec{u}) \cdot \hat{n}$$
$$+ \bar{\rho}(\vec{u}' \cdot \nabla \vec{u}') \cdot \hat{n} + \rho'\frac{\partial \vec{u}'}{\partial t} \cdot \hat{n} - \vec{\mathcal{F}}' \cdot \hat{n} \quad (2.27)$$

In accord with earlier remarks, we have in mind problems in which the primed quantities represent the sum of acoustic and non-acoustic fluctuations, the latter taken here to be 'noise' associated chiefly with vortical fluctuations. We simply ignore the existence of entropic disturbances (or 'hot spots' moving with the local velocity of the medium) justified partly by the estimate provided by Chu and Kovasznay that interactions between the acoustic and vortical fields with entropic disturbances are relatively weak within the volume of the chamber. Interactions of entropic waves with a boundary — particularly a choked nozzle — can produce sound waves, although this seems also a lesser effect (Menon and Jou 1990). Hence whereas in previous analyses of combustion instabilities the fluctuations represented the acoustic field, now we must treat the acoustic and vortical fields

together. All fluctuating quantities will therefore be written as sums of acoustic properties, denoted ( )^a and properties associated mainly with the vortical motions, identified by superscript ($^-$), for example

$$p' = p^a + \tilde{p}, \quad \vec{u}' = \vec{u}^a + \vec{n}, \quad \rho' = \rho^a + \tilde{\rho}, \ldots \text{etc.} \tag{2.28}$$

In this way we shall be able to accommodate combustion instabilities and combustion noise in the same framework, founded on applying a method of spatial averaging to the system of equations derived above.

The idea is that any unsteady motion in the chamber can be synthesized of an appropriate set of modes $\psi_j(\vec{r})$ of the chamber with time-varying amplitudes $\eta_j(t)$; the amplitudes are defined by expressing the pressure fluctuation in the form

$$p'(\vec{r}, t) = \bar{p} \sum_{j=1}^{\infty} \eta_j(t)\psi_j(\vec{r}) \tag{2.29}$$

Thus when we write the variables in the form (2.28), it is the amplitudes that will be split into the acoustic and vortical (more generally, 'non-acoustic') parts. The mode shapes $\psi_j(\vec{r})$ depend on the geometry of the chamber and on the boundary conditions; if the exhaust nozzle is choked, and the Mach number at the entrance is not too large, it is often a good approximation to set the normal gradient of ψ_j equal to zero. Whatever the case, we assume that an orthogonal set of modes is available and here we assume that the ψ_n satisfy

$$\begin{aligned} \nabla^2\psi_n + k_n^2\psi_n &= 0 \\ \hat{n}\cdot\nabla\psi_n &= 0 \end{aligned} \tag{2.30}a,b$$

where k_n is the wavenumber of the nth mode. Then straightforward computations (Culick 1975, 1988; Culick and Yang 1989) lead to the equations for the amplitudes

$$\frac{d^2\eta_n}{dt^2} + \omega_n^2\eta_n = F_n \tag{2.31}$$

where ω_n is the frequency of the nth mode, $\omega_n = \bar{a}k_n$, and

$$F_n = -\frac{\bar{a}^2}{\bar{p}E_n^2}\left\{\int h\psi_n dV + \oiint f\psi_n dS\right\} \tag{2.32}$$

$$E_n^2 = \int \psi_n^2 dV \tag{2.33}$$

Equation (2.31) represents a set of coupled nonlinear equations, one associated with each of the modes ψ_n. For analysis of combustion instabilities, satisfactory results are often obtained by retaining only a small number of modes (Paparizos and Culick 1989a, Jahnke and Culick 1991), but representation

of a noise field requires that the series (2.29) contain high-order modes as well.

The set (2.31) has been the basis for routine analysis of combustion instabilities in solid propellant rockets. Good results have been obtained for linear stability and nonlinear behavior; some important unresolved questions remain, notably satisfactory explanation of nonlinear stability or 'triggering' (Paparizos and Culick 1991). This formalism has also been used to study ramjet engines; with suitable modeling of the special physical processes involved. the approach is applicable to afterburners and liquid rockets.

Before analyzing interactions between a noise field and combustion instabilities, we discuss briefly the relation of this formulation to previous analyses of combustion noise.

2.2 Combustion Noise

Much of the theoretical work on combustion noise has been founded on Lighthill's theory of aerodynamic noise, so it is appropriate to begin with a few remarks on that theory. The chief purposes here are to make connections with the formulation described here and to emphasize certain items that arise in our treatment of noise and combustion instabilities within a chamber. Hence the following is but a brief and incomplete summary of a few general aspects of the theory. In particular, we do not deal with the details of the most important part of the subject — the source of noise. Moreover, this is not a critical survey of previous works: ample coverage of the approximations involved in theory, and the extent to which they may be valid, has been given in several review papers cited later.

Lighthill's theory (1952) begins with rearrangement of the conservation equations to give a wave equation for the density. The corresponding equation for the pressure was subsequently used by several writers (Lilley 1973; Doak 1973; Howe 1975). As noted earlier, we prefer pressure as the primary variable for investigating unsteady motions in combustion chambers. The crucial idea introduced by Lighthill that made possible substantial progress has been given the name "acoustic analogy." Instead of treating the nonlinear wave equation, he formed the difference between the equations for the density fluctuations in the actual flow field and those in a gas at rest.

The acoustic analogy for the pressure is expressed formally by combining the equations for conservation of mass and momentum in the following way. Differentiate (2.1) with respect to time, substitute

(2.2) for $\partial(\rho\vec{u})/\partial t$, and subtract $a_r^2\nabla^2\rho$ from both sides to find

$$\frac{\partial^2\rho}{\partial t^2} - a_r^2\nabla^2\rho$$
$$= \nabla\cdot\left[\nabla\cdot(\rho\vec{u}\vec{u} - \vec{\sigma}) + \nabla\cdot(p - a_r^2\rho)\,\vec{I}\right]$$
$$- \left(\nabla\cdot\vec{F} - \frac{\partial W}{\partial t}\right) \qquad (2.34)$$

With no sources of mass and momentum (W and $\vec{F}$ set equal to 0) this becomes Lighthill's basic equation. To find the corresponding equations for pressure (Lilley 1973), remove the terms $a_r^2\nabla^2\rho$ from both sides of (2.34), multiply the equation by a_r^2, and add $\partial^2\rho/\partial t^2$, giving

$$\frac{\partial^2 p}{\partial t^2} - a_r^2\nabla^2 p$$
$$= a_r^2\nabla\cdot[\nabla\cdot(\rho\vec{u}\vec{u} - \vec{\sigma})]$$
$$+ \frac{\partial}{\partial t}\left[\frac{\partial}{\partial t}(p - a_r^2\rho) + a_r^2 W\right] - a_r^2\nabla\vec{\mathcal{F}} \qquad (2.35)$$

Note that neither (2.34) nor (2.35) involve the energy equation. But the second must be consistent with equation (2.18); the right-hand sides are identical only if the following condition is imposed:

$$\frac{\partial}{\partial t}(p - a_r^2\rho) + a_r^2 W$$
$$= (a_r^2 - a^2)\,\nabla\cdot(\rho\vec{u}) - (\vec{u}\cdot\nabla p - a^2\vec{u}\cdot\nabla\rho) + \mathcal{P}$$
$$= (a_r^2 - a^2)\,\rho\nabla\cdot\vec{u} - \vec{u}\cdot\nabla(p - a_r^2\rho) + \mathcal{P}$$

This can be written in the appealing form

$$\frac{D}{Dt}(p - a_r^2\rho) = (a_r^2 - a^2)\,\rho\nabla\cdot\vec{u} + \mathcal{P} - a_0^2 W \qquad (2.36)$$

which is actually an identity following from the equations for conservation of mass (2.12) and energy (2.15). Upon substituting (2.17)d and (2.16) for $\mathcal{P}$, we have

$$\frac{D}{Dt}(p - a_r^2\rho) = \frac{R}{C_v}\rho T\frac{Ds}{Dt} + (a^2 - a_r^2)\frac{D\rho}{Dt} \qquad (2.37)$$

Thus if the speed of sound is constant, taken to be the reference value, the combination $p - a_r^2\rho$ for a fluid element changes only if the entropy varies.

Following Lighthill's original works in 1952 and 1953, many calculations exist for aerodynamic sound fields, based on the acoustic analogy expressed by equation (2.34). The idea is that the right-hand side is somehow specified so the equation is an inhomogeneous linear wave equation readily solved by well-known methods. The most common problem treated is the sound field emitted by a jet, motivated especially by the practical need to reduce

the noise produced by jet aircraft. Thus the sound field must be computed in the atmosphere outside the region where the sources reside. The problem comes down entirely to specifying the distribution of sources, the right-hand side of (2.33). In fact, it would be enough to be able to specify the source distribution (of monopoles and dipoles) on a surface enclosing the region containing the true sources, a point of view discussed by Ffowcs-Williams (1974). That property implies an intrinsic ambiguity in the problem: two source distributions that differ by a non-radiating distribution produce the same distribution field outside the region in question. Consequently, measurement of the radiated field cannot be interpreted to give a unique source distribution.

Hence a complete solution to the problem of sound produced, for example, by a jet, can be had only by addressing the very difficult theoretical and experimental matters associated with the source distribution in the volume containing the responsible fluctuations. To make connection with combustion instabilities and combustion noise we need to discuss briefly some aspects of the theoretical work, keeping in mind the noise produced by an exhaust jet as the canonical example.

For isothermal flows, Lighthill showed that the dominant term in the right-hand side of (2.34), or equivalently (2.35) is that involving the velocities; the density can be approximately constant, $\rho = \bar{\rho}$ and with $a_r = \bar{a}$, the governing equation (2.35) for the pressure field is

$$\frac{\partial^2 p}{\partial t^2} - \bar{a}^2\nabla^2 p = \bar{a}^2\nabla\cdot[\nabla\cdot(\bar{\rho}\vec{u}\vec{u})] \qquad (2.38)$$

The great difficulty in solving (2.38) arises from the fact that within the source region, where the right-hand side is non-zero, the motions comprise both those causing the acoustic field (in particular, turbulent fluctuations) and the acoustic field itself. But to obtain solutions easily, one needs to know the source terms independently of the acoustic pressure (and hence velocity). Moreover, the mean flow field exerts at least two important influences: the sources are carried with the flow, and a non-uniform flow causes refraction of the acoustic field.

To obtain solutions to (2.35), Lighthill's idea was to replace the true sources by an equivalent source distribution stationary with respect to the ambient field outside their region of activity. ('Solving' equation (2.38) means in this context finding a formula with which one may compute the sound field outside the region containing the sources; see, for example, equation 2.42.) In this first instance, it is clearly convenient simply to ignore convection

and refraction. In principle, as Lighthill noted, if one could specify the equivalent source field accurately, both convection and refraction could be accounted for. In the interests of obtaining results with some ease most investigators have constructed equivalent source distributions without trying to model the effects of convection and refraction: the assumption is not so serious as one might expect. Nevertheless, the problem of accounting for convection and refraction within the acoustic analogy seems not to have been satisfactorily solved.

Perhaps the best known attempts to account for some of the influences of the mean flow are Phillips' (1960) derivation of a convective wave equations (his work was followed by others — see Doak 1973 and Ribner 1981 for summaries) and the work by Mani (1972, 1973), who treated relatively simple cases to display possible effects of convection. Schubert (1972) has examined the problem of refraction using numerical solutions with some success.

It seems fair to conclude that the influences of convection and refraction, while not always small (particularly in supersonic jets), are nonetheless secondary. Hence in low-speed flows, one might suspect that, using Lighthill's acoustic analogy with an equivalent stationary source distribution, the results obtained should be a reasonably good first approximation. That has essentially been the view of those working in the field of combustion noise.

Essentially two theoretical treatments of combustion noise survived the efforts of the 1970s, those of Strahle (1971, 1978, 1985) and of Chiu and Summerfield (1973). The first follows Lighthill's acoustic analogy and the second is based on Phillips' form of the analogy using the convective wave equation. In each case, the transition to a treatment of combustion noise is effected by adding to the equations terms representing heat addition, internal heat transfer, and chemical reactions. Roughly that means in the present context that the starting point is equation (2.18) with no mass and momentum sources $\vec{\mathcal{F}}$ and W being dropped, giving first the equation Strahle chose as his starting point

$$\frac{\partial^2 p}{\partial t^2} - a_r^2 \nabla^2 p$$
$$= a_r^2 \nabla \cdot \nabla \cdot (\rho \vec{u}\vec{u} - \bar{\sigma})$$
$$+ \frac{\partial}{\partial t} \left[(a_r^2 - a^2) \nabla \cdot (\rho \vec{u}) - (\vec{u} \cdot \nabla p - a^2 \vec{u} \cdot \nabla \rho) \right]$$
$$+ (\gamma - 1) \frac{\partial}{\partial t} (\Phi - \nabla \cdot \vec{q} + Q) \qquad (2.39)$$

Chiu and Summerfield (1973) and Chiu, Plett, and Summerfield (1975) based their analysis on an equation in which, following Phillips (1960), time derivatives are replaced by convective derivatives.

We shall only quote the result written in a form consistent with the notation used here:

$$\frac{D^2}{Dt^2} (\ln p) - \nabla \cdot (a^2 \nabla \ln p)$$
$$= \gamma (\nabla \vec{u}) : (\nabla \vec{u}) + (\gamma - 1) \frac{D}{Dt} \left(\frac{Q}{p} \right) \qquad (2.40)$$

where now

$$Q = Q + \Phi - \nabla \cdot \vec{q} \qquad (2.41)$$

For simplicity we shall not display the detailed form of Q which in the work cited includes diffusion. The point is that the convective derivative is used, and the dependent variable is $\ln p$. Those are the main differences between the two formulations.

Once the general problem has been cast in the framework of the acoustics analogy, two tasks remain: modeling the sources and finding approximate solutions for the particular problems at hand. Finding accurate representations for the sources is much the more difficult matter. Computations from first principles are out of the question and the limited experimental results for details of the flow in combustion zones implies that one must resort to assumptions and approximations that cannot always be finally justified.

It appears that all who have studied combustion noise agree that the dominant sources are associated with time-dependent heat release. Large changes in the rate of energy supplied by combustion changes cause substantial fluctuations of the gas density in both time and space. A combustion zone therefore presents a distribution of monopole sources, markedly more effective radiators than the quadrupoles $\nabla \cdot \nabla \cdot (\rho \vec{u}\vec{u})$ dominant in non-reacting turbulent flows. Hence Chiu and Summerfield retain only the term $Q = Q$, equation (2.41), on the right-hand side of (2.40); similarly, Strahle considers only the term $\partial Q/\partial t$ on the right-hand side of (2.39).

In both approaches, the equations are linearized and the results obtained differ, apart from some details of the modeling, only because of the presence of the convective derivatives in (2.40). Strahle (1978) has given formulas for the pressure fluctuations in the sound field far from a compact open flame. 'Compact' means that the flame is small compared with the dominant wavelengths of sound. His results, equations (32) and (33) of that paper, are

$$p' \sim \frac{1}{|\vec{r}|} \int \frac{1}{a^2} \frac{\partial Q}{\partial t} dV \qquad (2.42)$$

$$p' \sim$$
$$\frac{1}{|\vec{r}|} \int \frac{1}{a^2} \left[\frac{\partial Q}{\partial t} + \vec{u} \cdot \nabla Q' + \left(\vec{u} - \frac{T'}{\overline{T}} \vec{u} \right) \cdot \nabla \overline{Q} \right] dV \qquad (2.43)$$

The sources in the integrand are evaluated at the retard time $t - |\vec{r}|/\bar{a}$ where $\vec{r}$ is the position of the observation. Strahle (1985) has since argued that better agreement with observation is obtained with his formula (2.41) not containing the influences of convection. The problem of accounting correctly for the influences of the mean flow, specifically as it introduces convective and refractive effects is a deep theoretical matter intimately connected with the formulation of the acoustic analogy. It seems not to have been satisfactorily solved for non-reacting flows and has received little attention in the context of combustion noise. We shall not pursue the issue here.

Much of the previous work in combustion noise has been devoted to problems associated with open flames on hot jets. The situation is therefore quite similar to that for jet noise: the radiating sources are unconfined. In this paper we are concerned only with problems of noise in combustion chambers. Thus the active regions of the flow are located within confining walls. Consequently, the noise field we wish to analyze is also contained by essentially rigid boundaries. Fluctuations at the exit plane constitute sources for noise radiated through the exhaust nozzle and ultimately to the outside world. We shall not treat the problem of emission.
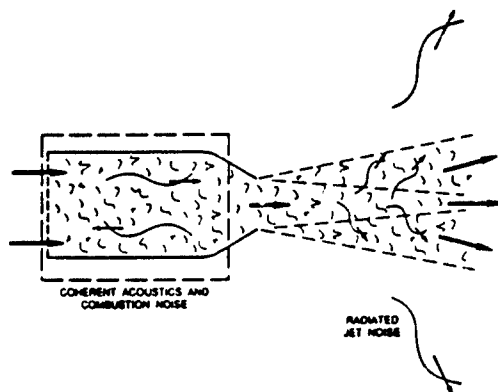
Figure 2.

Figure 2 is a schematic illustration of the matter. The fundamental difference between the problems of confined sources on the one hand and sources freely radiating to an ambient atmosphere on the other has substantial influence on the development of the theory. We shall be able to express the noise field, as well as the acoustic field associated with combustion instabilities, as expansions in natural modes of the chamber. That is why the two classes of phenomena can be treated to good approximation within the same general framework.

Chiu, Plett, and Summerfield (1975) carried out the

first analysis of combustion noise in ducts, including the presence of resonances. Their intent was to explain the spectra of noise emitted when a flame, or more extended combustion processes, are enclosed by confining walls, chiefly for application to gas turbines. The linearized form of (2.39), with only fluctuations of energy release included as sources, becomes

$$\frac{D^2 p'}{Dt^2} - \bar{a}^2 \nabla^2 p' = (\gamma - 1)\frac{DQ'}{Dt} \qquad (2.44)$$

Calculations were carried out by expanding the pressure in eigenfunctions of uniform duct with uniform mean flow. The spectral distribution of the heat release was specified, either uniform or as one half of a sinusoid in the frequency range 0 - 1,000 Hz. Then the spatial and time dependence of Q' were found as an inversion transform in frequency and expansion of the spatial dependence in eigenfunctions of the duct. Equation (2.44) was solved by taking the transform in time, with expansion in eigenfunctions for the spatial dependence of the pressure. Results were then found for the spectral distribution of the pressure.

Figures 3 and 4 show an example of results obtained for the velocity fluctuation at the exit of the duct and its frequency spectrum for a case length/diameter = 8.5. As one should expect, resonance peaks are evident in both figures.
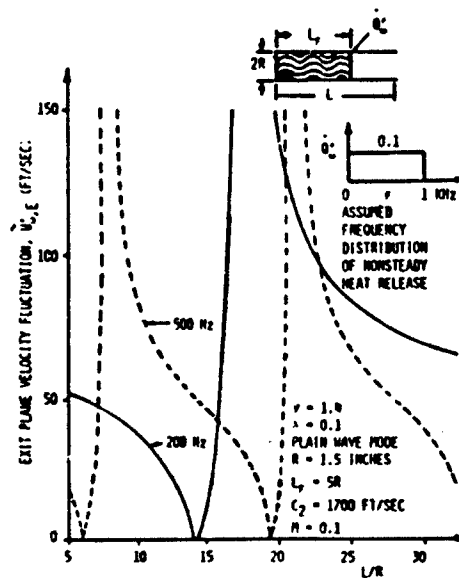

Figure 3.

This method is a straightforward approach to the problem, amounting to computation of the

response of a linear system, the acoustic field in the duct, to a forcing function, the unsteady heat release, consisting of a continuous distribution of sinusoids having spatial dependencies set by the eigenfunctions of the duct. It suffers from at least three serious flaws: the noise sources are independent of the acoustic field, the stochastic nature of the noise field is totally absent, and no nonlinear processes are accounted for. Part of the purpose of the work discussed here is to indicate how these omissions may be corrected.
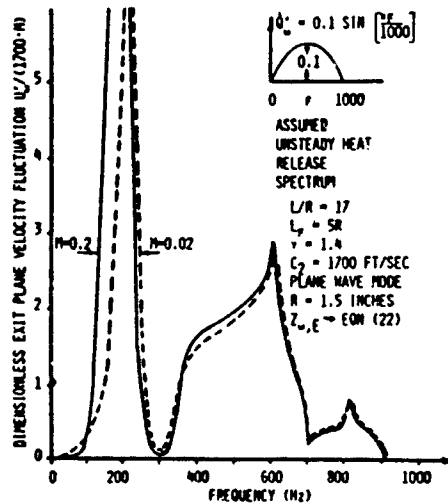
Figure 4.

During the 1980s, interest in combustion noise again grew in connection with work related to oscillators in solid propellant rockets and ramjet engines. Hegde and Strahle (1985) reported their results for the generation of acoustic modes by turbulence in cavities, but no combustion. Their analysis is somewhat closer to actual physical problems for two reasons: they recognize explicitly the different character of irrotational (acoustic) and rotational (vortical) fluctuations; and they account for the spectral content of the vortical or turbulent fluctuations. The analysis naturally contains many approximations; because it is based on a different method of handling the equations of motion, involving definition of the 'Bernoulli enthalpy' (Yates and Sandri 1976), we shall not discuss the calculations. They solve a linear problem of nonreacting flow through a porous lateral boundary and exhausting through a choked exhaust nozzle. Their results show the presence of resonances in satisfactory agreement with observed behavior. The levels of oscillations do not agree well and there is very poor agreement between the measured and computed spectra for the broadband noise.

Closer to the actual problem of combustion noise is the analysis reported by Hegde, Reuter, and Zinn (1988). For the special problem of a compact flame stabilized on a rod in a duct, they solve the linear problem for the pressure fluctuations, essentially using the linearized form of equation (2.39) with only the term $(\gamma - 1)\partial Q/\partial t$ on the right-hand side. The principal difference is that they correctly account for the different speeds of sound up- and downstream of the flame. Their most important contribution is their treatment of the statistical properties of the background noise, based on the observed spectrum of the radiation field in turn related to the energy release according to a known method. Their results show quite good agreement between predictions and measurements of the pressure spectrum. That work seems to be the best confirmation of the internal consistency of the formulation described earlier and expressed by equation (2.39), although only linear behavior was treated.

Poinsot et al. 1986 have reported experimental work with a dump combustor operated over a sufficiently broad range of conditions that measurements could be taken of the noise field with and without substantial acoustic oscillations. As seems often to be the case for such configurations, the noise level is higher over the entire frequency range when an acoustic oscillation is present. A particularly interesting aspect of that work was the use of optical measurements taken simultaneously to form spatial maps of coherence functions strongly suggestive of the regions in which the sources of noise are located. Information of this sort is clearly useful in modeling sources required for analysis of the phenomena.

These brief remarks are intended only to provide relevant background for the sorts of problems considered in the remainder of the paper. There is much data in the works cited, and others, that we shall not review here. Moreover, we shall not be concerned with the important problem of core noise, under some conditions a strong source of emissions from gas turbines: see the work by Cumpsty and Marble (1977) for the most comprehensive treatment of the subject.

3. Splitting the Unsteady Field into Acoustic and Non-Acoustic Fluctuations

The basis for the analysis developed here is combination of the ideas discussed by Chu and Kovasznay (1958) with the approximate analysis developed previously for studying combustion instabilities. As we already noted in Section 2, equa-

tion (2.29), we assume that any unsteady field in a combustion chamber can be synthesized of normal modes of the chamber, with time-varying amplitudes, $\eta_n(t)$. After spatial averaging, the problem comes down to solving the system of nonlinear equations (2.30) for the $\eta_n(t)$. The right-hand sides will contain nonlinear terms of three sorts representing interactions among the acoustic modes themselves, among the non-acoustic motions. and coupling between the acoustic and non-acoustic fluctuations. Apart from use of spatial averaging, the analysis here differs from that of Chu and Kovasznay (1958) in the explicit consideration of nonlinear processes. Their treatment rested on a linearization of the equations of motion by successive or iterative approximation. Also, because eventually we divide the analysis into the two separate problems of finding the acoustic and non-acoustic amplitudes, we have the possibility of investigating stochastic processes. Therefore, unlike the case for combustion instabilities, in which only a few modes are normally present, here we must expect that a broad spectrum of modes must be present.

First we need to write the formula (2.32) for the F_n explicitly showing dependence on the fluctuations. We assume that the average thermodynamic properties $(\bar{p}, \bar{\rho}, \bar{\tau})$ are constant in time and uniform in space. The surface integrals arising from the first, second, and last terms of f, equation (2.27), can be combined with corresponding volume integrals of h to give

$$-\frac{\bar{p}\bar{E}_n^2}{\bar{a}^2}F_n =$$

$$\bar{\rho}\int \left(\vec{u}\cdot\nabla\vec{u}' + \vec{u}'\cdot\nabla\vec{u}\right)\cdot\nabla\psi_n dV$$

$$+\frac{1}{\bar{a}^2}\frac{\partial}{\partial t}\int \left(\vec{u}\cdot\nabla p' + \gamma p'\nabla\cdot\vec{u}\right)\psi_n dV$$

$$+\bar{\rho}\int \left(\vec{u}'\cdot\nabla\vec{u}' + \frac{\rho'}{\bar{\rho}}\frac{\partial\vec{u}'}{\partial t}\right)\cdot\nabla\psi_n dV$$

$$+\frac{1}{\bar{a}^2}\frac{\partial}{\partial t}\int \left(\vec{u}'\cdot\nabla p' + \gamma p'\nabla\cdot\vec{u}'\right)\psi_n dV$$

$$+\bar{\rho}\iint \frac{\partial\vec{u}'}{\partial t}\cdot\hat{n}\psi_n dS$$

$$+\int \left(\vec{\mathcal{F}}'\cdot\nabla\psi_n - \frac{\partial\mathcal{P}'}{\partial t}\psi_n\right)dV \qquad (3.1)$$

Now use a vector identity to rewrite the integrand in the first integral

$$\vec{u}\cdot\nabla\vec{u}' + \vec{u}'\cdot\nabla\vec{u}$$
$$= \nabla\left(\vec{u}\cdot\vec{u}'\right) - \vec{u}'\times\nabla\times\vec{u} - \vec{u}\times\nabla\times\vec{u}'$$

A second identity gives

$$\nabla\left(\vec{u}\cdot\vec{u}'\right)\cdot\nabla\psi_n = \nabla\cdot\left(\vec{u}\cdot\vec{u}'\nabla\psi_n\right) - \left(\vec{u}\cdot\vec{u}'\right)\nabla^2\psi_n$$
$$= \nabla\cdot\left(\vec{u}\cdot\vec{u}'\nabla\psi_n\right) + k_n^2\vec{u}\cdot\vec{u}'\psi_n$$

Then because we assume $\hat{n}\cdot\nabla\psi_n = 0$, we find

$$\int \left(\vec{u}\cdot\nabla\vec{u}' + \vec{u}'\cdot\nabla\vec{u}\right)\cdot\nabla\psi_n dV =$$

$$k_n^2\int \left(\vec{u}\cdot\vec{u}'\right)\psi_n dV$$

$$-\int \left(\vec{u}\cdot\nabla\times\vec{u}' + \vec{u}'\times\nabla\times\vec{u}\right)\cdot\nabla\psi_n dV$$

and (3.1) becomes

$$-\frac{\bar{p}}{\bar{a}^2}E_n^2F_n =$$

$$\bar{\rho}\int \left(\vec{u}\cdot\vec{u}'\right)\psi_n dV$$

$$-\bar{\rho}\int \left(\vec{u}\times\nabla\times\vec{u}' + \vec{u}'\times\nabla\times\vec{u}\right)\cdot\nabla\psi_n dV$$

$$+\frac{1}{\bar{a}^2}\frac{\partial}{\partial t}\int \left(\vec{u}\cdot\nabla p' + \gamma p'\nabla\cdot\vec{u}\right)\psi_n dV$$

$$+\bar{\rho}\int \left(\vec{u}'\cdot\nabla\vec{u}' + \frac{\rho'}{\bar{\rho}}\frac{\partial\vec{u}'}{\partial t}\right)\cdot\nabla\psi_n dV$$

$$+\frac{1}{\bar{a}^2}\frac{\partial}{\partial t}\int \left(\vec{u}'\cdot\nabla p' + \gamma p'\nabla\cdot\vec{u}'\right)\psi_n dV$$

$$+\bar{\rho}\iint \frac{\partial\vec{u}'}{\partial t}\cdot\hat{n}\psi_n dS$$

$$+\int \left(\vec{\mathcal{F}}'\cdot\nabla\psi_n - \frac{\partial\mathcal{P}'}{\partial t}\psi_n\right)dV \qquad (3.2)$$

This formula for F_n shows explicitly only those processes associated purely with gasdynamics. In principle, with $\vec{\mathcal{F}}'$ and $\mathcal{P}'$, we can accommodate any physical process. Because the presence of the mean flow field is included to first order — a fundamental matter for problems of linear stability — the effects of convection and refraction are in some sense included here. However, because emphasis has been placed on standing or traveling acoustic waves, these effects have not been a matter of concern for studies of combustion instabilities, in contrast to the case of aerodynamic noise generation. That is, the effects of non-uniform flow to first order have been accounted for in analysis of combustion instabilities, but without attending to the detailed examination required to distinguish the particular consequences of convection and refraction. Some work in this direction has recently been done numerically (e.g. Baum 1986).

Although we shall not discuss extensively the functions $\vec{\mathcal{F}}'$ and $\mathcal{P}'$, they contain significant contributions. As we have discussed in the preceding section, the term $\partial Q'/\partial t$ in $\partial\mathcal{P}'/\partial t$ has been established as the dominant source for noise production in flames. Unsteady heat release is unquestionably the main reason for both acoustic instabilities and noise in combustion chambers.

However, because they contain important sources of attenuation and noise production due to fluctuating flow variables, the remaining terms in (3.2) must be retained. The fluctuations $\tilde{\mathcal{F}}'$ and $\mathcal{P}'$ are essential for analysis of control, for they contain the only means of actuation, through sources of mass, momentum, and energy.

The next step requires expressing the fluctuations p', $\bar{u}'$, and ρ' in terms of the time-dependent amplitudes $\eta_n(t)$. We assume the splitting suggested by equation (2.28) and write the pressure as the expansion (2.29):

$$p' = p^a + \tilde{p} = \bar{p}\sum_{j=1}^{\infty} \eta_j(t)\psi_j(\vec{r})$$

$$= \bar{p}\sum_{j=1}^{\infty} \left(\eta_j^a + \tilde{\eta}_j\right)\psi_j(\vec{r}) \quad (3.3)$$

where the η_j^a are the amplitudes of acoustic oscillations (combustion instabilities). The $\tilde{\eta}_j$ are the amplitudes of the pressure fluctuations associated with the rest of the motions synthesized as a superposition of normal acoustic modes. To compute the amplitudes as solutions to the system (2.31) we need to devise an approximation to F_n, i.e. we must deal with p', ρ', and $\bar{u}'$ in the integrals. Following the tactic successfully used for studying combustion instabilities, we assume that the acoustic part of the motions satisfies the classical acoustic equations,

$$\frac{\partial \bar{u}^a}{\partial t} = -\frac{1}{\bar{\rho}}\nabla p^a$$

$$\frac{\partial p^a}{\partial t} = -\gamma\bar{p}\nabla\cdot\bar{u}^a$$

$$(3.4)a, b$$

Because there is no entropy change associated with acoustic waves, $\bar{p} + p^a \sim (\bar{\rho} + \rho^a)^\gamma$ and we set $\rho^a = p^a/\bar{a}^2$. Hence the expansions of $\bar{u}^a$ and ρ^a are

$$\bar{u}^a = \sum_{j=1}^{\infty}\frac{\dot{\eta}_j^a}{\gamma k_j^2}\nabla\psi_j$$

$$\rho^a = \frac{\bar{p}}{\bar{a}^2}\sum_{j=1}^{\infty}\eta_j^a\psi_j$$

$$(3.5)a, b$$

The formulas (2.29) and (3.5)a satisfy equations (3.4)a, b exactly because the eigenfunctions ψ_j satisfy (2.30)a and in zeroth order $\ddot{\eta}_j + \omega_j^2\eta_j = 0$ with $\omega_j = \bar{a}k_j$.

Thus we approximate the acoustical variables in F_n by their values existing in zeroth order with no mean flow or sources. For the remaining parts. $\tilde{p}$, $\tilde{\rho}$, and $\tilde{n}$, we appeal to results established by Chu and Kovasznay (1958) who showed that the vortical and entropic modes of propagation carry velocity

changes, but no pressure changes. We shall assume also that the density is constant; hence we *assume* in zeroth approximation

$$\tilde{p} = \tilde{\rho} = 0 \quad ; \quad \tilde{u} \neq 0 \quad (3.6)$$

It is not necessary at this stage to take $\tilde{p} = 0$; we do so to eliminate a few terms. However, if $\tilde{p}$ is taken to be non-zero, the problem arises later of relating $\tilde{p}$ to other thermodynamic properties. With these approximations, to second order in the fluctuations (3.2) becomes

$$F_n = F_n^a + \tilde{F}_n + \tilde{F}_n^a \quad (3.7)$$

where

$$F_n^a =$$
$$-\frac{\gamma}{\bar{\rho}E_n^2}\left[\bar{\rho}k_n^2\int(\bar{u}\cdot\bar{u}^a)\,\psi_n dV\right.$$
$$-\bar{\rho}\int(\bar{u}^a\times\nabla\times\bar{u})\cdot\nabla\psi_n dV$$
$$\left.+\frac{1}{\bar{a}^2}\frac{\partial}{\partial t}\int(\bar{u}\cdot\nabla p^a + \gamma p^a\nabla\cdot\bar{u})\,\psi_n dV\right]$$
$$-\frac{\gamma}{\bar{\rho}E_n^2}\left[\bar{\rho}\int\left(\bar{u}^a\cdot\nabla\bar{u}^a + \frac{1}{\bar{a}^2}p^a\frac{\partial\bar{u}^a}{\partial t}\right)\cdot\nabla\psi_n dV\right.$$
$$\left.+\frac{1}{\bar{a}^2}\frac{\partial}{\partial t}\int(\bar{u}^a\cdot\nabla p^a + \gamma p^a\nabla\cdot\bar{u}^a)\,\psi_n dV\right]$$
$$-\frac{\gamma}{E_n^2}\iint\frac{\partial\bar{u}^a}{\partial t}\cdot\hat{n}dS$$
$$-\frac{\gamma}{\bar{\rho}E_n^2}\int\left(\tilde{\mathcal{F}}^a\cdot\nabla\psi_n - \frac{\partial\mathcal{P}^a}{\partial t}\psi_n\right)dV \quad (3.8)$$

$$\tilde{F}_n^a =$$
$$-\frac{\gamma}{\bar{\rho}E_n^2}\left[\bar{\rho}\int\left(\bar{u}^a\cdot\nabla\tilde{u} + \tilde{u}\cdot\nabla\bar{u}^a + \frac{p^a}{\bar{a}^2}\frac{\partial\tilde{u}}{\partial t}\right)\cdot\nabla\psi_n dV\right.$$
$$\left.+\frac{1}{\bar{a}^2}\frac{\partial}{\partial t}\int(\tilde{u}\cdot\nabla p^a + \gamma p^a\nabla\cdot\tilde{u})\,\psi_n dV\right]$$
$$-\frac{\gamma}{\bar{\rho}E_n^2}\int\left(\tilde{\mathcal{F}}^a\cdot\nabla\psi_n - \frac{\partial\tilde{\mathcal{P}}^a}{\partial t}\psi_n\right)dV \quad (3.9)$$

$$\tilde{F}_n =$$
$$-\frac{\gamma}{\bar{\rho}E_n^2}\left[\bar{\rho}k_n^2\int(\tilde{u}\cdot\tilde{u})\,\psi_n dV\right.$$
$$\left.-\bar{\rho}\int(\tilde{u}\times\nabla\times\tilde{u} + \tilde{u}\times\nabla\times\tilde{u})\cdot\nabla\psi_n dV\right]$$
$$-\frac{\gamma}{E_n^2}\int(\tilde{u}\cdot\nabla\tilde{u})\cdot\nabla\psi_n dV$$
$$-\frac{\gamma}{E_n^2}\iint\frac{\partial\tilde{u}}{\partial t}\cdot\hat{n}\psi_n dS$$
$$-\frac{\gamma}{\bar{\rho}E_n^2}\int\left(\tilde{\mathcal{F}}\cdot\nabla\psi_n - \frac{\partial\tilde{\mathcal{P}}}{\partial t}\psi_n\right)dV \quad (3.10)$$

With the preceding definitions, the system (2.31) becomes

$$\frac{d^2\eta_n}{dt^2} + \omega_n^2\eta_n = F_n^a + \tilde{F}_n^a + \tilde{F}_n \qquad (3.11)$$

The forcing functions F_n^a and $\tilde{F}_n$ contain the stochastic properties of the random field.

Previous work (Culick 1975, 1990) has shown that if only the gasdynamic nonlinear processes are accounted for to second order, F_n^a has the general form

$$F_n^a = \sum_{i=1}^{\infty} [D_{ni}\dot{\eta}_i^a + E_{ni}\eta_i^a]$$
$$+ \sum_{i=1}^{\infty}\sum_{j=1}^{\infty} \left[A_{nij}\eta_i^a\eta_j^a + B_{nij}\dot{\eta}_i^a\dot{\eta}_j^a \right] \quad (3.12)$$

where the coefficients $D_{ni},\ldots$ are constants, depending on the linear processes (including those arising from $\tilde{F}^a$ and $\mathcal{P}^a$) and on the geometry of the chamber. If other nonlinear processes are accounted for, accommodated by the source functions $\tilde{F}^a$ and $\mathcal{P}^a$ (e.g. nonlinear interactions between combustion and the acoustic field), additional terms will appear, not necessarily having the form shown in (3.12).

According to its definition (3.9), the force $\tilde{F}^a$ contains terms linear in the acoustic amplitudes and in the random variables $\tilde{u}$ and $\partial\tilde{u}/\partial t$ plus terms arising from $\tilde{F}^a$ and $\tilde{P}^a$. If we ignore the possibility of higher order nonlinearities in those source terms, we may assume that $\tilde{F}_n^a$ has the general form

$$\tilde{F}^a = \sum_{i=1}^{\infty} [\xi_i\eta_i^a + \xi_i^v\dot{\eta}_i^a] \qquad (3.13)$$

where the ξ_i, ξ_i^v represent (stochastic) parametric excitation of the acoustic modes.

Finally, $\tilde{F}_n$ depends only on the stochastic fluctuations, spatially averaged over the node shapes. To make the notation more consistent, we replace $\tilde{F}_n$ by the symbol Ξ_n:

$$\tilde{F}_n \equiv \Xi_n \qquad (3.14)$$

With these definitions, we write system (3.11) showing explicitly the dependence on stochastic processes:

$$\frac{d^2\eta_n}{dt^2} + \omega_n^2\eta_n = F_n^a + \sum_{i=1}^{\infty}[\xi_i\eta_i^a + \xi_i^v\dot{\eta}_i^a] + \Xi_n \quad (3.15)$$

Note that the ξ_i and the ξ_i' depend linearly on the $\tilde{\eta}_i$ and $\dot{\tilde{\eta}}_i$ while Ξ_n is quadratic in those variables.

An important fundamental aspect of the systems treated here is the general problem of distinguishing deterministic and stochastic behavior. The natural splitting of the forces F_n into the components F_n^a, $\tilde{F}_n^a$, and $\tilde{F}_n$ defined by (3.8) – (3.10) is only an initial step. For unsteady motions in combustion chambers, we must pay particular attention to the source functions $\mathcal{P}^a$, $\tilde{\mathcal{P}}^a$, and $\tilde{\mathcal{P}}$, for they contain representations of energy addition. The acoustic field is purely deterministic, so $\mathcal{P}^a$ contains only deterministic energy sources. At the other extreme, $\tilde{\mathcal{P}}$ includes sources of energy addition that are purely stochastic, i.e., depend only on the turbulent motions and are insensitive to the deterministic acoustic field. Interactions between the deterministic and stochastic fields belong to $\tilde{\mathcal{P}}^a$. For example, turbulent fluctuations in a reacting shear layer may be sensitive to the local acoustic field, thereby affecting the energy release. A difficult part of the subject is construction of realistic models of these processes.

We have reduced the problem to finding the response of a system of nonlinear oscillators whose amplitudes $\eta_n = \eta_n^a + \tilde{\eta}_n$ must be determined when the system is subject to stochastic forces. The developments leading to the definitions of ξ_i, ξ_i^v, and Ξ_n have produced formulas (not given here) showing their explicit dependence on the random fluctuations of the velocity field. Before solutions can be found for the time-dependent amplitudes, those functions should evidently be expressed in terms of the $\tilde{\eta}_i$ and $\dot{\tilde{\eta}}_i$, analogous to the way in which the acoustic contributions in F_n were treated by using the approximations (3.4)a, b.

That is a large and difficult problem. There are at least four approaches to its solution: (1) construct an approximate representation of the flow variables $\tilde{u}$, $\tilde{p}$, $\tilde{\rho}$ and the combustion processes, based on observations and guided by theoretical considerations, in the same spirit as we have treated the acoustic field; (2) extract a representation from numerical simulations using methods of computational fluid dynamics; (3) extract a representation by analysis of experimental data; and (4), the crudest approach, assume forms for the various contributions to $\tilde{F}_n^a$ and $\tilde{F}_n$ and determine the consequences by solving the system (3.11). None of the first three approaches have been investigated extensively for the class of problems considered here. The works by Chiu, Plett, and Summerfield (1975) and by Hegde, Reuter, and Zinn (1988) fall in the first category, but treat only linear behavior. A few elementary results have been reported by Menon and Jou (1990) following the second approach.

Methods of analyzing experimental data or the results of numerical simulations have become active

subjects of research in the past few years. There is a growing body of literature dealing mainly with non-reacting flows. For example, the method called 'proper orthogonal decomposition,' originated in probability theory, has been applied to turbulent flows (Lumley 1967, Aubrey et al. 1988) and other problems of fluid mechanics (Sirovich 1987). That and related methods applied to a wide range of problems were central issues in a recent IUTAM/NATO Workshop (1991). Although those ideas are clearly applicable to the unsteady motions in combustion chambers, no results have been reported.

In order to gain some idea of the possible influences of stochastic sources on the behavior of acoustic modes, we have followed the last of the approaches listed above. We simply assume forms for the random functions of time, ξ_i, ξ_i^v, and Ξ_n, and treat the system of stochastic differential equations

$$\frac{d^2\eta_n}{dt^2} + \omega_n^2\eta_n = F_n^a + \sum_{i=1}^{\infty}[\xi_i\eta_i + \xi_i^v\dot{\eta}_i] + \Xi_n \quad (3.16)$$

This was the approach taken by Paparizos and Culick (1989)a for the simplest case of two longitudinal modes. We discuss that method in Section 4. Note that η_i^a, $\dot{\eta}_i^a$ have been replaced by $\eta_i = \eta_i^a + \tilde{\eta}_i$ and $\dot{\eta}_i = \dot{\eta}_i^a + \dot{\tilde{\eta}}_i$ on the right-hand side, implying the assumption that the random part of the amplitudes is relatively small.

In fact it appears that we may quite realistically assume that the ξ_i, ξ_i^v, and Ξ_i do not depend on the amplitudes η_n of the pressure fluctuations. This assumption has been made in all treatments of the aerodynamic noise problem. In other words, we assume that the random sources of noise do not themselves depend on the noise they generate. That does not exclude dependence of the noise field on the presence of coherent acoustic oscillations, nor does it imply that control of the noise field is impossible. The reason is that the acoustic and random pressure fluctuations are coupled by nonlinear processes, producing energy transfer between the two forms of motion. Practical matters of achieving successful control will rest partly on the strength of the energy exchange and on the possibility of discovering an effective means of control or 'actuation.' However, it may also be the case that if the random sources of noise are affected by the pressure fluctuations, then more effective means of control might be found.

Part of our justification for taking the stochastic sources independent of the pressure field rests on the results discussed by Chu and Kovasznay (1958) who established the independence of the three modes of propagation (acoustic, vortical, and entropic). The argument, however, is weak, ignoring some basic properties of processes present in combustion systems. For example, heat released in flames is indeed sensitive to pressure. Our assumption here is really made in the interests of obtaining some initial results.

4. Combustion Instabilities with Stochastic Sources

The formulation developed in the preceding section accommodates a wide range of problems. Here we shall describe a few results for what is possibly the simplest case: the influence of stochastic sources on a combustion instability. Observations of instabilities in both laboratory and full-scale combustors normally show the presence of a small number of acoustic modes: the data cannot reveal how many modes must be accounted for in an analysis to explain satisfactorily the nonlinear behavior. In the theory used here, a minimum of two modes are required to produce a limit cycle. Energy is supplied to the acoustical system because one mode is unstable; the motions may then reach a steady state only if a stable second mode is available to dissipate energy, thereby providing the possibility for constant total energy in the acoustical motions. Nonlinear gasdynamical processes cause the flow of energy from the unstable mode to the stable mode.

Pressure records of instabilities rarely show purely harmonic motions. The amplitudes for unfiltered data usually fluctuate about some apparent average value. Those fluctuations are erased if the data are filtered. Otherwise, they will cause broadening of peaks in the spectra and as part of the broadband spectral background. The analysis described in this section is an initial effort to explain this behavior. Only limited results have been obtained.

4.1 The Two-Mode Approximation

For the acoustic system described by (3.16) with the stochastic sources equal to zero, and only gasdynamical nonlinear processes accounted for, exact solutions can be found for the time-averaged equations for two (and in some cases three) modes. Most of the known results have been reviewed by Culick (1990). In particular, the conditions for existence and stability of limit cycles can be written explicitly. Although the restriction to two modes carries limitations, serious under some conditions (Jahnke and Culick 1991), this representation is surprisingly accurate under wide realistic circumstances. To maintain simplicity, we therefore consider here only the two-mode approximation.

Moreover, we treat the case of longitudinal modes for which the frequencies are integral multiples of

the fundamental, $\omega_n = n\omega_1$. With all linear processes and only the gasdynamic nonlinearities included, the first two of equations (3.16) are

$$\ddot{\eta}_1 + \omega_1^2\eta_1 = 2(\alpha_1\dot{\eta}_1 + \theta_1\omega_1\eta_1)$$
$$-(F_{11}\dot{\eta}_1\dot{\eta}_2 + F_{12}\eta_1\eta_2) + (\xi_1\eta_1^a + \xi_1^v\dot{\eta}_1^a + \Xi_1)$$
$$\ddot{\eta}_2 + \omega_2^2\eta_2 = 2(\alpha_2\dot{\eta}_2 + \theta_2\omega_2\eta_2)$$
$$-(F_{21}\eta_1^2 + F_{22}\eta_1^2) + (\xi_2\eta_2^a + \xi_2^v\dot{\eta}_2^a + \Xi_2)$$

$$(4.1)a,b$$

where $\omega_2 = 2\omega_1$ and

$$F_{11} = \frac{3-2\gamma}{2\gamma} \qquad F_{12} = \frac{5(\gamma-1)}{2\gamma}\omega_1^2$$
$$F_{21} = -\frac{\gamma+3}{2\gamma} \qquad F_{22} = \frac{\gamma-1}{2\gamma}\omega_1^2 \qquad (4.2)$$

There are six stochastic functions in equation (4.1), in general mutually independent, to be specified. The functions bring with them a large number of parameters, too many at this stage for a sensible treatment of the problem. We shall therefore analyze a much simpler problem, motivated by the following reasoning based on previous results (Paparizos and Culick 1989b) obtained for the deterministic problem with no stochastic sources.

Combustion instabilities in practice commonly appear as oscillations having slowly varying maximum amplitudes and phases; the amplitudes η_i may then be assumed to have the form

$$\eta_i(t) = r_i(t)\cos(\omega_i t - \phi_i(t))$$
$$= A_i(t)\cos\omega_i t + B_n(t)\sin\omega_i t \qquad (4.3)$$

where $\delta r_i/r_i$ and $\delta\phi_i/2\pi$, the changes over one cycle, are assumed small. The method of time-averaging is effective under these conditions, reducing the two second order equations for η_1 and η_2 to four first order equations for the $(r_1, r_2, \phi_1, \phi_2)$.

For technical reasons not covered here, the following transformation is an effective choice to simplify the structure of the first order equations:

$$y_1 = r_1$$
$$y_2 = r_2\sin(\phi_2 - 2\phi_1) \qquad (4.4)a,b,c$$
$$y_3 = r_2\cos(\phi_2 - 2\phi_1)$$

The deterministic equations for the y_i are:

$$\frac{dy_1}{dt} = (\alpha_1 + \beta y_2)y_1$$
$$\frac{dy_2}{dt} = \alpha_2 y_2 + \theta^* y_3 + 2\beta y_3^2 - \beta y_1^2 \qquad (4.5)a,b,c$$
$$\frac{dy_3}{dt} = -\theta^* y_2 + \alpha_2 y_3 - 2\beta y_2 y_3$$

where

$$\beta = \frac{\gamma+1}{8\gamma}\omega_1$$
$$\theta^* = \theta_2 - 2\theta_1 \qquad (4.6)a,b$$

Equations (4.5) are unchanged if y_3 is replaced by $y_3|\theta_2 - 2\theta_1|/(\theta_2 - 2\theta_1)$, showing that no generality is lost by taking θ^* positive. Note that the original set of four equations (not given here) are reduced to three, essentially because there is an arbitrary phase available, the reason that the two phase angles appear only in the combination $\phi_2 - 2\phi_1$ in (4.4)a,b,c.

Fixed points of the system (4.5), defined by $\dot{y}_i = 0$, are the state of rest ($y_i = 0$) or limit cycles. It can be shown (Paparizos and Culick 1989b) that a unique limit cycle, whose properties are independent of initial conditions, exists if $\alpha_1\alpha_2 < 0$. As remarked above, if one mode (say the fundamental) is unstable, $\alpha_1 > 0$, the other must be stable, $\alpha_2 < 0$. In this case, the limit cycle itself is stable if $2\alpha_1 + \alpha_2 < 0$. Hence for existence and stability of the limit cycle, the conditions must be satisfied when $\alpha_1 > 0$ are

$$\alpha_2 < 0$$
$$2\alpha_1 + \alpha_2 < 0 \qquad (4.7)a,b$$

The remainder of this section is concerned with the influences of stochastic sources on the characteristics of this limit cycle.

4.2 Stochastic Averaging

Stratonovich (1963, Vol. II, Chapter 4) introduced the method of stochastic averaging, an extension of the method of averaging outlined above for a deterministic system. See also Roberts and Spanos (1986) and Gardiner (1985) for reviews of the method. Here we simply quote the results of applying the method.

With stochastic sources in the second order equations (4.1)a,b, the averaging proceeds in two steps. First the equations are averaged over the period of the acoustic oscillations (τ_n for the nth mode) to give, eventually, equations (4.5)a,b,c in the variables y_i; that is, the oscillatory motions have been removed from the problem which has been reduced to one of finding the slowly varying amplitudes and phases (equivalent to the $y_i(t)$).

The second step is the 'stochastic averaging,' required to give the fluctuating (stochastic) sources in correct form for the averaged (i.e. first order) equations. We assume that the stochastic sources $\xi_i(t)$, $\xi_i^v(t)$, and $\Xi_i(t)$ have zero mean (eventually we assume that they have the form of white noise). However, the terms $\xi_i\eta_i$ and $\xi_i^v\dot{\eta}_i$, representing parametric excitations, have non-zero mean values.

It is convenient to remove the mean values from the stochastic sources and place them with the deterministic part, accounting for the terms m_i appearing below. By definition, m_i is the average over one period of the oscillation of the expected value of the term in question.

It is also assumed that the auto-correlation times of the random processes are much smaller than the bandwidths (not the periods) of the oscillations. That means that the oscillations have non-zero decay (or growth) coefficients such that

$$\tau_{\text{corr}} \ll |\alpha_i| \tag{4.8}$$

a condition satisfied by the broad-band processes and acoustical motions expected in practice. In the limit considered here, we approximate the random processes by equivalent white noise.

Finally, in order to reduce the difficulty and complexity of finding solutions to equations $(4.1)a, b$ we make two assumptions based partly on physical grounds:

(i) We replace η_i^a and $\dot{\eta}_i^a$ in the terms representing parametric excitation by η_i and $\dot{\eta}_i$. This implies that the stochastic perturbations of the acoustic modes should be small: $|\tilde{\eta}_i|/|\eta_i^a| \ll 1$. That happens to be true in the examples treated here, but not in general.

(ii) We ignore all stochastic sources in the equation $(4.1)b$ for the amplitude of the second mode. This assumption produces considerable simplification, but is also motivated by the expectation that if the fundamental mode has a growth rate much larger than the decay rate of the second mode, then the first-order effects of stochastic sources will be primarily on the fundamental mode. Owing to nonlinear coupling between the modes, there will of course be a secondary random excitation of the second mode.

Omitting the lengthy details of stochastic averaging (which in fact begins with the second order equations) we eventually find the equations for the variables y_i:

$$dy_1 = \left(\alpha_1^* y_1 + \beta y_1 y_2 + \frac{\pi}{2y_1\omega_1^2} S_3(\omega_1)\right) dt + \sqrt{Q_{11}}\, dw_1$$

$$dy_2 = (\alpha_2^* y_2 + \theta^* y_3 + 2\beta y_3^2 - \beta y_1^2) dt - 2y_3\sqrt{Q_0}\, dw_2$$

$$dy_3 = (\alpha_2^* y_3 - \theta^* y_2 - 2\beta y_2 y_3) dt + 2y_2\sqrt{Q_0}\, dw_3 \tag{4.9}a,b,c$$

The $w_i(t)$ are Gaussian (white noise) processes, the dw_i being defined in terms of the stochastic integral of a function $G(t)$ (see Gardiner 1985, p. 83),

$$\int_{t_0}^{t} G(t')\, dw_i(t')$$

The $S_i(\omega)$ are the spectral density functions of the w_i and the Q_{ij} are cross-variances of the stochastic sources, computed in the averaging process

$$Q_{11} = \frac{\pi y_1^2}{4}\left(2S_1(0) + S_1(2\omega_1) + \frac{1}{\omega_1^2}S_2(2\omega_1)\right) + \frac{\pi}{\omega_1^2}S_3(\omega_1)$$

$$Q_0 = \frac{\pi}{4}\left(\frac{2}{\omega_1^2}S_2(0) + S_1(2\omega_1) + \frac{1}{\omega_1^2}S_2(2\omega_1) + \frac{4}{y_1^2\omega_1^2}S_3(\omega_1)\right)$$

$$Q_{22} = 4y_3^2 Q_0$$
$$Q_{23} = -4y_2 y_3 Q_0$$
$$Q_{33} = 4y_2^2 Q_0$$
$$Q_{12} = Q_{13} = 0$$

$$(4.10)a - f$$

The mean values of the sources are

$$m_1 = \frac{\pi}{4}\left[y_1 S_1(0) + \frac{3}{2}y_1\left(S_1(2\omega_1) + \frac{1}{\omega_1^2}S_2(2\omega_1)\right) + \frac{2}{\omega_1^2 y_1}S_3(\omega_1)\right]$$

$$m_2 = 2y_2 Q_0$$

$$m_3 = -2y_3 Q_0$$

$$(4.11)a,b,c$$

Finally, the growth and decay rates of the two modes are now

$$\alpha_1^* = \alpha_1 + \frac{\pi}{4}\left(S_1(0) + \frac{3}{2}S_1(2\omega_1) + \frac{3}{2\omega_1^2}S_2(2\omega_1)\right)$$

$$\alpha_2^* = \alpha_2 - \pi\left(\frac{1}{\omega_1^2}S_2(0) + \frac{1}{2}S_1(2\omega_1) + \frac{1}{2\omega_1^2}S_2(2\omega_1) + \frac{2}{\omega_1^2 y_1}S_3(\omega_1)\right)$$

$$(4.12)a,b$$

4.3 The Center Manifold for Equations (4.9)

Although equations (4.9)a, b, c can be solved numerically in their present form, it is useful to simplify the matter further by taking advantage of some results obtained by Paparizos and Culick (1989b). It is relatively straightforward to find the equation for the center manifold, an approximation to the one-dimensional manifold (or locus) of limit cycles extending from the origin $y_1 = y_2 = 0$. We expect that a similar result should be a good approximation here when stochastic sources are present.

Again omitting details of the argument, the result is that in limit cycles of the deterministic part of the motions — i.e. $\dot{y}_1 = \dot{y}_2 = \dot{y}_3 = 0$ and dw_1, dw_2, dw_3 ignored in equations (4.9)a, b, c — the variable y_2 can be expressed as a function of y_1 only:

$$y_2(y_1) = \begin{cases} \dfrac{\alpha_2^* \beta}{(\alpha_2^*)^2 + (\theta^*)^2} & (y_1 < y_1^*) \\ y_2^* & (y_1 > y_1^*) \end{cases} \quad (4.13)$$

where

$$y_2^* = \frac{\alpha_2^* - \alpha_1^* + 0.5\delta_1}{3\beta} \quad (4.14)$$

$$\delta_1 = \frac{\pi}{4}\left(S_1(0) + S_1(2\omega_1) + \frac{1}{\omega_1^2}S_2(2\omega_1)\right) \quad (4.15)$$

and y_1^* is the smallest positive root of

$$y_1^2 \frac{\alpha_2^* \beta}{(\alpha_2^*)^2 + (\theta^*)^2} = y_2^* \quad (4.16)$$

Note that α_2^*, equation (4.12)b, is a function of y_1.

Equation (4.13) is the equation of the center manifold, essentially a relation between the amplitudes in the limit cycle; substitution of (4.13) in (4.9)c, with $\dot{y}_3 = 0$ and dw_3 dropped gives the values of y_3 in the center manifold.

4.4 The Fokker-Planck-Kolmogorov Equation for Equations (4.9)

We now confine attention to the behavior in the limit cycle executed in the presence of stochastic sources. Assuming that the variable y_2 is sufficiently well-approximated by its dependence on the center manifold, equation (4.9)a is now a stochastic differential equation for y_1 only:

$$dy_1 = \left(\alpha_1^* y_1 + \beta y_1 y_2(y_1) + \frac{\pi}{2y_1\omega_1^2}S_3(\omega_1)\right)dt + \sqrt{Q_{11}}\,dw_1 \quad (4.17)$$

where $y_2(y_1)$ is given by (4.13).

The amplitude y_1 is now a random variable characterized by a probability density $p(y_1, t)$. With

known methods (e.g. Gardiner 1985, Chapter 5) we can construct the Fokker-Planck-Kolmogorov equation for p:

$$\frac{\partial p}{\partial t} = -\frac{\partial}{\partial y_1}\left[\left(\alpha_1^* y_1 + \beta y_1 y_2(y_1) + \frac{\pi}{2y_1\omega_1^2}S_3(\omega_1)\right)p\right] + \frac{1}{2}\frac{\partial^2}{\partial y_1^2}[Q_{11}p] \quad (4.18)$$

This equation possesses a stationary solution independent of time,

$$p'(y_1) = Cy_1 \exp\left\{\int_0^{y_1} \frac{x(\delta_2 + 2\beta y_2(x))}{Q_{11}(x)}dx\right\} \quad (4.19)$$

where

$$\delta_2 = 2\alpha_1^* - 3\delta_1 \quad (4.20)$$

and C is a constant fixed by requiring that $p'(y_1)$ be normalized:

$$\int_0^\infty p'(x)dx = 1 \quad (4.21)$$

The solution (4.19) is an approximation to the distribution of amplitude r_1, in the limit cycle when stochastic sources are assumed to affect directly only the fundamental mode. Just as for the deterministic behavior, the parameters arising in the problem must satisfy a stability condition in order that a stationary solution exist ("existence in mean square value"). Here, the deterministic conditions (4.7)b becomes

$$\alpha_2 + 2\alpha_1 + \pi\left[\frac{3}{4}S_1(0) - \frac{1}{\omega_1^2}S_2(0)\right.$$
$$\left. + \frac{3}{8}S_1(2\omega_1) + \frac{3}{8\omega_1^2}S_2(2\omega_1)\right] < 0 \quad (4.22)$$

Because the noise field is coupled to the acoustic field, producing both parametric and 'external' excitation according to the general equations (3.16), a reasonable question is: can the presence of stochastic sources be responsible for observed combustion instabilities? That is, are the noise sources sufficiently strong to cause excitation and sustenance of acoustic modes that are deterministically stable ($\alpha_n < 0$)?

To obtain meaningful results, we must ensure that a stationary probability distribution exists. The conditions to be satisfied are

$$\alpha_n + \frac{\pi}{4}\left[S_1^{(n)}(2\omega_n) + \frac{1}{\omega_n^2}S_2^{(n)}(2\omega_n)\right] < 0 \quad (4.23)$$

where $S_1^{(n)}$ and $S_2^{(n)}$ are the power spectral density fluctuations of the parameter excitations ξ_n and ξ_n^v in the nth acoustic mode. For technical reasons of analysis, we are ignoring the 'external' excitations Ξ_n which cannot cause modes to be excited under the conditions treated here.

4.5 Some Numerical Results

Because we have not attempted to work out physically realistic models of the non-acoustic fluctuations ($\check{u}, \check{p}, \check{\rho}$) we cannot claim or anticipate that the results faithfully represent observed behavior. The initial results discussed here indicate that the approach taken here, based on time and stochastic averaging, is an effective method for treating problems in which both instabilities and noise are present.

The analysis described above can be used to carry out three independent sorts of computations: Monte Carlo simulations with the second-order equations (4.1)a, b; Monte Carlo simulations with the first-order stochastic equations (4.9)a, b, c; and the probability distribution can be found directly as the solution to the Fokker-Planck-Kolmogorov equation (4.18).

Monte Carlo simulations with the second-order equations are very lengthy, requiring an estimated 100 CPU hours on a VAX 8800 for a simulation consisting of 100 samples, each covering 3,000 periods of the fundamental oscillation. Here we give some results of simulations with the first-order equations, requiring approximately 5 hours each. This work is continuing with other machines, but no results are available.
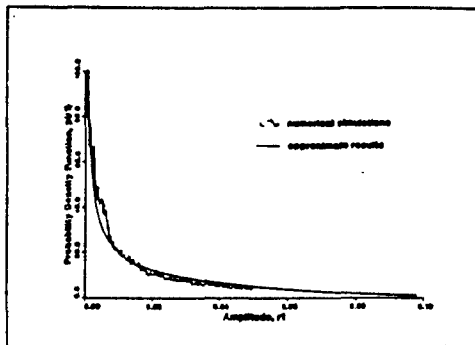
Figure 5.

Attention here is confined to conditions under which stationary probability distributions should exist, with linear parameters ($\alpha_1 \ldots$) assigned realistic values. Figure 5 is a comparison of the distribution given by equation (4.19) with a Monte Carlo simulation. The frequency of the fundamental mode is 800 hertz, $\alpha_1 = 8 \text{ s}^{-1}$, and $\alpha_2 = -125 \text{ s}^{-1}$; both modes are damped. There is no external excitation ($\Xi_1 = 0$) and only the parametric excitation $\xi_1(t)$ is present. Good agreement is apparent. Figure 6 shows the time history of the amplitude of the first mode, computed for two samples chosen from the Monte Carlo simulations. Note that one is 'stable,' decaying within about 20 cycles, while the other exhibits 'asymptotic stability,' associated with the rather long tail of the distribution that is shown in Figure 1.
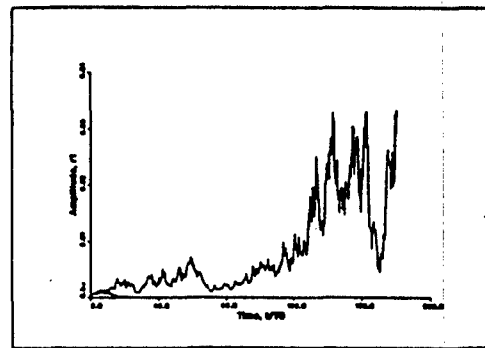
Figure 6.

Figure 7 is a comparison of the distribution computed with equation (4.19) with a Monte Carlo simulation when both parametric and external excitations are present ($\xi_1(t)$, $\xi_2(t)$, and $\Xi_1(t)$ all non-zero). The parameters α_1, α_2 have the same values used to produce Figure 5. Again the approximation (4.19) for the probability distribution is satisfactory. Note that the external excitation is capable of causing the fundamental modes to be excited to an amplitude somewhat larger than that occasionally caused by parametric excitation alone: the most probable and average values of r_1 are larger than those predicted with the distribution given in Figure 1.

Figures 8 and 9 show cases in which the fundamental mode is unstable and the second is stable. The results therefore show the influence of stochastic sources on the amplitude of the first mode in a limit cycle. Now the most probable value of the amplitude naturally obtains a higher value, larger in Figure 9 for which α_1 has greater magnitude: in Figure 8, $\alpha_1 = 8 \text{ s}^{-1}$ and in Figure 9, $\alpha_1 = -25 \text{ s}^{-1}$.
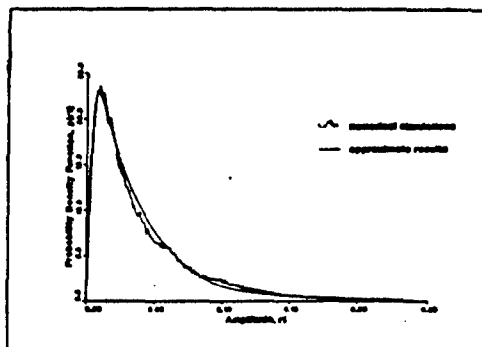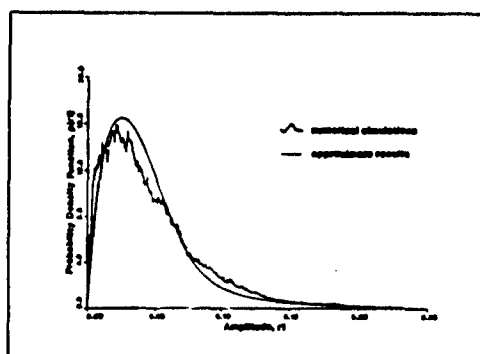
Figure 7.
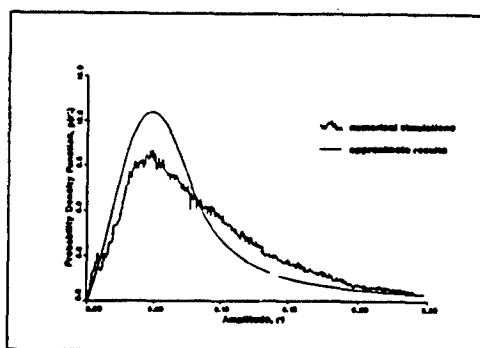

Figure 8.

Figure 9.

5. Determining the Dimensions of Attractors Observed in Combustion Chambers

The noise field treated in the preceding section is produced by stochastic sources. Hence the unsteady motions generated and propagating in the chamber have the characteristics of random processes. In contrast, the motions identified as combustion instabilities constitute a deterministic

system. However, pressure records taken with operating systems often appear also to have a random character, raising the question of possible chaotic motions. It's an important question, not simply because this might be another example of deterministic chaos, but because the search for the answer should provide further information about unsteady nonlinear behavior in combustion chambers.

In the past decade much has been accomplished in developing methods of analyzing experimental data to find evidence of chaos. A central issue is determining the dimensions of attractors, objects in phase space to which the motions of a nonlinear system tend after long times, the subject of this section. A point in phase space uniquely defines the instantaneous state of a dynamical system. For the acoustic field defined by the system of equations (2.31), appropriate coordinates of phase space are the displacements and velocities (η_n, $\dot{\eta}_n$) of the oscillators corresponding to the acoustic modes. In principle, the phase space may be infinite dimensional, but since we can treat only a finite number of modes (a minimum of two), the phase space will always have a finite number of dimensions, at least four.

A path or trajectory in phase space represents the evolution of motion of the dynamical system in time. An attractor is a point or a collection of points in phase space to which the motion tends after a long time. Thus if all modes are stable, the pressure fluctuations ultimately vanish and the origin ($\eta_1 = \dot{\eta}_1 = \ldots = \eta_n = \dot{\eta}_n = 0$) is an attractor, in this case having dimension 0. It is common in combustion systems exhibiting instabilities that the motions settle down to a limit cycle in which many modes may participate, but the motion is periodic. A limit cycle is represented by a closed (non-intersecting) path in phase space, so the attractor in this case has dimension one. Periodic limit cycles have been long known from theoretical work (e.g. Sirigano and Crocco 1964. Zinn 1968. Zinn and Powell 1971, Culick 1975. 1990, Culick and Yang 1989). It is important to note that in a limit cycle, the frequencies of all participating modes must be such that ω_m/ω_n is a rational number for all m, n. That means, as found, for example, in application of (2.31), that the frequencies of the linear acoustic modes for an arbitrary geometry must in general be shifted by nonlinear effects so that all ratios are indeed rational. For the results reported by Zinn and Powell (1971), Culick (1975, 1990), and Culick and Yang (1989), the frequencies in the limit cycle are integral multiples of the fundamental. That relation arose both for longitudinal modes, when $\omega_n = n\omega_1$, for the unperturbed (classical) modes.

and for modes of a cylindrical chamber when the classical frequencies are not in simple ratios.

If there are two or more fundamental frequencies in the limit cycle such that $\omega_n^{(1)} = n\omega_1$ and $\omega_m^{(2)} = m\omega_2$, or if the frequencies of the participating modes form irrational ratios in ultimate steady motion, the corresponding attractor in phase space is a torus having integral dimension, 2, 3, 4, ... or greater, corresponding to 2, 3, 4, ... fundamental frequencies. Those two classes of possible motions are called periodic and quasi-periodic. Even though the phase space may have large dimension, just as limit cycles of dimension 1 may exist, so also may tori of, say, dimension 2 exist. It is possible, as a result of 'frequency-locking,' that a quasi-periodic motion may become periodic. Tori of dimension greater than 3 may be unstable (technically, 'structurally unstable'), and, if so, would not be observable. That is a matter of continuing research; consult Bergé, Pomeau, and Vidal (1984) for a good readable introduction to the subject.

It is now a familiar result that deterministic dynamical systems may exhibit apparently random behaviors called chaos, fundamentally different from true random or stochastic behavior, conveniently called simple noise. Although not theoretically necessary, it appears that for a real system to exhibit chaotic behavior, its phase space must contain an attractor having non-integral dimension, a strange attractor. The question addressed in this section is: can combustion chambers showing instabilities also develop chaotic motions?

To date it appears that no chaotic motions have been definitely identified in analytic or numerical results for the sorts of acoustical systems we are concerned with here, although some examples may have been found in results reported by Paparizos and Culick (1991). Recent work by Jahnke and Culick (1991) has suggested that toroidal attractors may exist, but the results are preliminary and the implications are unknown. It is therefore particularly important to investigate the possibility by examining experimental results. All recordings of pressure in combustion chambers show random fluctuations traditionally assumed to be noise. The problem, a common one, is to discover whether one can distinguish chaos in the noise.

The nonlinear acoustical system itself is of course not the only possible source of chaotic behavior in a combustion chamber. Indeed, much effort has been expended in the recent past on identifying chaotic behavior in many problems of fluid mechanics, with particular emphasis on the development of turbulence. Turbulent fluid flow is typically characterized statistically even though it is governed by deterministic partial differential equations. The stochastic representation is useful because the number of degrees of freedom present in the fluid is very large (it can be approximated by dividing a characteristic volume by the cube of the Kolmogorov scale). However, in many systems, much simpler large-scale dynamics may emerge due to fluid mechanical feedback mechanisms that result in coherent oscillatory flows. The vortex dynamics of jets, wakes, and other separated flows are often modeled as having only a few degrees of freedom even though turbulence is present. Similarly, in combustion chambers, the presence of acoustic modes (given by equations 2.30a, b) often results in coherent oscillations that can be modeled effectively with only a few ordinary differential equations.

However, acoustic oscillations are present because some mechanism exists for transfer of energy from combustion processes or the flow itself (e.g. large-scale vortices) to the coherent motions. The behavior of the organized motions could therefore conceivably serve as a marker of chaotic behavior actually originating somewhere within the system. We are far from understanding the dynamics of the processes in combustion chambers theoretically, but in any event, progress with the theory depends heavily on experimental results. We report here some results obtained with analysis of pressure records taken in a laboratory dump combustor fueled with pre-mixed gases (Sterling and Zukoski 1987, 1991).

Recently developed data analysis techniques may be used to determine the minimum number of degrees of freedom responsible for the generation of a particular time-series signal. The techniques, developed as an outgrowth of modern nonlinear dynamical systems theory during the past decade, make use of a signal processing technique known as the 'time-delay embedding method.' This method allows an experimentalist to embed the data in a phase-space representation. If start-up transients have ceased, the phase-space trajectory traces out a set of points that comprise an attractor. The dimension of this attractor provides a lower limit on the number of degrees of freedom of the system active in the observed nonlinear behavior. Details on both the embedding method and the dimension-finding algorithms can be found in an introductory article by Gershenfeld (1988).

The method, proposed first by Packard et al. (1980), rests on the idea that some properties of a multi-dimensional nonlinear system may be determined from the time-series measurements of a single variable. In particular, under quite broad circumstances often prevailing in actual situations,

a reconstruction of the attractor according to the following procedure will have (almost always) the same dimension as the true attractor. In the present case, we have a recording of the pressure as a function of time, such as that reproduced in Figure 10. Choose a fixed time t when the pressure is $p(t)$ and construct the n-dimensional vector $P(t)$ having components equal to $p(t)$ and the values of the pressure at the delayed times $t + \tau$, $t + 2\tau$, ..., $t + (n - 1)\tau$:

$$P(t) = \{p(t), \ p(t+\tau), \ p(t+2\tau), \ ..., \ p(t+(n-1)\tau)\} \tag{5.1}$$

This representation contains two parameters: the delay time τ and the embedding dimension n. Both must be varied with care as noted below.
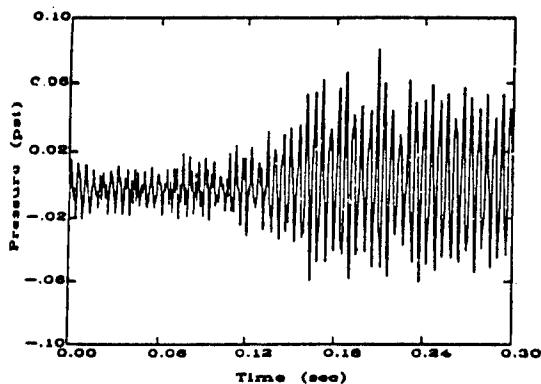
Figure 10.

After τ and n have been chosen, t is assigned discrete values t_1, t_2 ..., (i.e. the pressure record is digitized); the vectors $P(t_i)$ then trace a trajectory in the n-dimensional embedding space. That trajectory is the reconstruction of the attractor. Theoretical results have shown that if the attractor associated with the motion of the system has dimension D, then the dimension of its reconstruction will also be D if $n > 2D+1$ (see, e.g., reviews by Parker and Chua 1987 and by Theiler 1990). The choice of τ is rather delicate: it is sufficient here to remark that it must be neither too small nor too large or too close to the period of a motion in the system. Thus τ is varied in the data processing to produce best results.

The problem now is to estimate the dimension of the object obtained with the procedure just described. Consider a point on the reconstructed attractor and imagine a ball or hypersphere of radius r centered on the point. The number of points within the ball depends on the size of the ball, varying as r^ν where ν is the dimension of the attractor (see Bergé, Pomeau, and Vidal 1984, p. 149 for a supporting

argument); thus if $N(r)$ is the number of points on that portion of the attractor on the ball,

$$N(r) = Ar^\nu \tag{5.2}$$

where A is a constant and ν is the dimension of the attractor. Hence

$$\nu = \frac{\log N(r) + \text{constant}}{\log r} \tag{5.3}$$

and a plot of $\log N(r)$ versus $\log r$ will have slope equal to the dimension.

That idea has been extended by Grassberger and Procaccia (1983) to define a 'correlation dimension.' Consider pairs of points located at the tips of pairs of vectors $P(t_i)$, $P(t_j)$, defined by (5.1). The distance between a pair, $|P(t_i) - P(t_j)|$, can be computed and the spatial correlation $C(r)$ is formed:

$$C(r) = \lim_{N \to \infty} \frac{1}{N^2} \left\{ \begin{array}{l} \text{number of pairs of points for} \\ \text{which } |P(t_i) - P(t_j)| < r \end{array} \right\} \tag{5.4}$$

where N is the total number of pairs considered. The correlation dimension ν is defined in analogy with (5.2), writing

$$C(r) = Ar^\nu \tag{5.5}$$

Hence

$$\nu = \frac{\log C(r) + \text{constant}}{\log r} \tag{5.6}$$

If a plot of $\log C(r)$ versus $\log r$ shows a linear variation, the slope is identified as the dimension of the attractor.

The number of points $P(t_i)$ used depends in the first instance on the length of the pressure record available and on the interval of digitizing, both of which can be varied, of course. We assume that a sufficiently large number is used, so the chief remaining parameter is the embedding dimension n which yields important information when it is varied. Suppose first that the attractor is a limit cycle, a curve of dimension one. If the chosen points $P(t_i)$ are distributed uniformly (for example) on the curve, then for sufficiently small r, it seems reasonable to expect $N(r) \sim r$ so $\nu = 1$ as required. This result doesn't change if the embedding dimension is varied because the points must always lie on the curve.

The case is different if noise is present. As discussed in Section 2, we may view the noise field as the superposed motions of a large number of modes or oscillators (an infinite number for ideal white noise). Hence the trajectories of the system lie in a phase space of large (infinite) dimension and densely cover any embedding space of finite (small) dimension.

Hence the criterion $n \geq 2d + 1$ cannot be satisfied for small n. As a result (Bergé, Pomeau, Vidal 1984, pp. 152) the dimension ν computed according to (5.6) approaches the embedding dimension as r is decreased. In other words, if the procedure based on the idea of correlation dimension is applied to a stochastic or random process, a dimension ν cannot be found independently of the embedding dimension.

In this work we used a version of the algorithm of Grassberger and Procaccia (1983) written by Schneider (1990). Figure 11 shows results obtained for a random signal (the 'data points' were computed with a random number generator). For the two choices of embedding dimension $n = 5, 9$, the slope of $\log C(r)$ versus $\log r$ does not approach a constant value as r (the size of the ball) is reduced. As expected by construction of the data, there is no evidence of a low-dimensional attractor, in confirmation of the remarks in the preceding paragraph.

Spectrum of Pressure Oscillations

Figure 12.

Figure 13 shows the dimension of the signal that was used to generate the spectrum of Figure 12. The points on the attractor, which numbered 8150, were embedded in a 9-D phase space using a 400 microsecond (5 points) time delay. This particular case reveals significant scale separation between noise and deterministic dynamics. A two-dimensional attractor (a 2-torus) is observed over approximately an order of magnitude of scales. A value of two is a result of the excitation of the two acoustic modes. Since the other peaks in the spectrum are subharmonics of these fundamental modes, they are not associated with additional degrees of freedom but are a result of the nonlinear nature of the oscillations, as described in the remarks at the beginning of this section. This dimension determination provides a lower bound on the number of modes that participate in the large-amplitude oscillations. However, the dimension increases abruptly at the smaller scales, suggesting that additional degrees of freedom are present, either due to the presence of additional acoustic modes or as a result of the turbulent combustion.

Figure 11.

Data from the combustor at the Caltech Jet Propulsion Center (Sterling and Zukoski 1987) has been obtained when a premixed methane/air flame was stabilized behind a rearward-facing step. The power was around 45 kW based on the higher heating value of the fuel. A pressure transducer located above the flameholder was used to monitor the oscillatory pressure and data was collected at 80 microsecond intervals. The frequency spectrum of the pressure signal is shown in Figure 12. The prominent peaks correspond to a longitudinal acoustic mode near 460 hertz, a mode near 530 hertz, and the 1/2 and 4/5 subharmonics of the latter mode that are present near 265 and 424 hertz.

Figure 13.

With the limited results obtained to date we have found no evidence for an attractor having fractional dimension, and hence no suggestion of chaotic behavior. The two oscillations defining the toroidal attractor at 460 Hz and 530 Hz correspond to linear acoustic modes of the system (Sterling and Zukoski 1991), but the results of the data analysis do not establish the precise mechanism causing those modes to be excited, or the processes responsible for the existence of the attractor. Nor do we yet have any understanding of possible interactions between the attractor and the noise in the system. Observations reported in earlier publications have shown that the excitation and sustenance of the steady large-amplitude acoustical motions are associated with the shedding of large vortical structures from the rearward-facing step, combustion within the vortices, and interactions with the lateral boundaries of the duct. No analysis has been done for the complete problem.

We believe that the method used here (only one of several known approaches) to extract information about the nonlinear behavior from pressure records can provide important contributions to understanding unsteady motions in combustion chambers. Results obtained in this fashion cannot alone explain observations, or serve as a basis for possible means of active control. Meaningful progress will require collaboration with other methods of the sort described earlier in this paper.

6. Concluding Remarks

The approximate analysis discussed in the first part of this paper has been used successfully for many years to investigate problems of stabilities in combustion chambers. Extension to accommodate stochastic sources representing possible effects of combustion noise is new and only a few results have been obtained. Although the approach taken here seems to produce results consistent with observed behavior, we cannot draw definite conclusions.

In particular, we have not yet carried out sufficient calculations to determine the influences of deterministic motions on noise levels. Therefore, we cannot assess the proposal to control noise levels by controlling the acoustic field. It may not be possible to make such an assessment without incorporating realistic models of the noise sources. We have avoided that issue by assuming that the non-acoustic fluctuations are simply Gaussian noise. That cannot be an accurate assumption even though the sources will in any case enter the analysis as parametric and external excitations of the form appearing in the system equations (3.16). Modeling the non-acoustical motions will likely be the most difficult and important part of the problem: we

have no reason to change the general structure of the analytical framework.

Analysis of experimental data with the methods suggested in Section 5 clearly merits continued effort. The information obtained is likely to provide important contributions to understanding the nonlinear behavior. The same methods can of course be applied to numerical data obtained with the analysis described earlier. Thus one is able to work simultaneously with modeling physical processes, results of the approximate analysis, and experimental data, a necessary strategy for dealing with problems that cannot be solved entirely theoretically from first principles.

References

Aubrey, N., Holmes, P., Lumley, J. L., and Stone E. (1988) "The Dynamics of Coherent Structures in the Wall Region of Turbulent Boundary Layers," *J. Fl. Mech.*, Vol. 192, pp. 115-173.

Baum, J. (1988) "Numerical Investigation of Acoustic Refraction Phenomenon in Solid Propellant Motions," in *Computational Fluid Dynamics*, G. de Vahl and C. Fletcher, eds., Elsevier Science Publisher, pp. 249-265.

Beckert, D. and Pfizennaies, E. (1972) "Über die Verstärkung von Brietband-Strahllärm durch eine Einzeltonanregung," *DLR - Forschungsbericht*, 75-72 (cited by Müller 1976).

Bergé, P., Pomeau, Y., and Vidal, C. (1984) *From Order to Chaos*, John Wiley & Sons, New York.

Breeden, J. L., Dinkelacher, F., and Hübler, A. (1990) "Noise in the Modeling and Control of Dynamical Systems," *Phys. Rev. A*, Vol. 42, pp. 5827-5836.

Chu, B.-T. and Kovasznay, L. S. G. (1958) "Nonlinear Interactions in a Viscous Heat-conducting Compressible Gas," *J. Fl. Mech.*, Vol. 3, No. 5, pp. 494-514.

Chiu, H. H. and Summerfield, M. (1973) "Theory of Combustion Noise," *Acta Astronautica*, Vol. 1, pp. 967-984.

Chiu, H. H., Plett, E., and Summerfield, M. (1975) "Noise Generated by Ducted Combustion," in *Aeroacoustics: Jet Combustion and Noise*, Vol. 37 of *Progress in Astronautics and Aeronautics*, AIAA, New York, pp. 249-276.

Crighton, D. G. (1975) "Basic Principles of Aerodynamic Noise Production," *Progress in Aerospace Science*, Vol. 16, No. 1, pp. 31-96.

Culick, F. E. C. (1971) "Nonlinear Growth and Limiting Amplitude of Acoustic Oscillations in Combustion Chambers," *Comb. Sci. and Tech.*, Vol. 3, No. 1, pp. 1-16.

Culick, F. E. C. (1975) "Nonlinear Behavior of Acoustic Waves in Combustion Chambers — Parts I and II," *Astronautica Acta*, Vol. 3, pp. 715-766.

Culick, F. E. C. (1988) "Combustion Instabilities in Liquid-Fueled Propulsion Systems," AGARD 72B, PEP Meeting, Bath, England.

Culick, F. E. C. (1990) "Recent Results in Nonlinear Acoustics in Combustion Chambers," AIAA 13th Aerospace Conference, AIAA Paper No. 3927.

Culick, F. E. C. and Yang, V. (1989) "Prediction of Linear Stability in Solid Propellant Rockets," to appear in AIAA Progress Series Volume *Unsteady Burning and Combustion Instability of Solid Propellants*.

Cumpsty, N. A. and Marble, F. E. (1977) "Core Noise from Jet Engine Exhausts," *J. Sound and Vib.*, Vol. 54, No. 2, pp. 297-309.

Ditto, W. L., Rauseo. S. N., and Spano, M. L. (1990) "Experimental Control of Chaos," *Phys. Rev. Lett.*, Vol. 65, No. 20, pp. 3211-3214.

Doak, P. E. (1973) "Fundamentals of Aerodynamic Sound Theory and Flow Duct Acoustics," *J. Sound and Vib.*, Vol. 28, No. 3, pp. 527-561.

Ffowcs-Williams, J E. (1969) "Hydrodynamic Noise," *Annual Reviews of Fluid Mechanics*, Vol. 1, pp. 197-222.

Ffowcs-Williams, J. E. (1974) "Sources of Sound," *Proceedings 8th Congress on Acoustics*, London, pp. 1-10.

Gardiner, C.W. (1985) *Handbook of Stochastic Methods*, Springer-Verlag, Berlin.

Gershenfeld, N. (1988) "An Experimentalist's Introduction to the Observation of Dynamical Systems," chapter in *Directions in Chaos*, Vol.

2, Hao Bai-lin (Ed.), World Scientific Press, Singapore.

Grassberger, P. and Procaccia, I. (1983) "Measuring the Strangeness of Strange Attractors," *Physica 9D*, pp. 189-208.

Gulati, A. and Mani, R. (1990) "Active Control of Unsteady Combustion-Induced Oscillations," 28th Aerospace Sciences Meeting, Paper No. AIAA 90-0270.

Hegde, V. G., Rueter, D., and Zinn, B. T. (1988) "Sound Generation by Ducted Flames," *AIAA J.*, Vol. 26, No. 5, pp. 532-537.

Hegde, V. G. and Strahle, W. C. (1985) "Sound Generation by Turbulence in Simulated Rocket Motor Cavities," *AIAA J.*, Vol. 23, No. 1, pp. 71-77.

Howe, M. S. (1975) "Contributions to the Theory of Aerodynamic Sound With Application to Excess Jet Noise and the Theory of the Flute," *J. Fluid Mech.*, Vol. 71, pp. 625-673.

IUTAM & NATO Advanced Research Workshop (1991) "Interpretation of Time Series From Nonlinear Mechanical Systems," 19-23 August, University of Warwick, England.

Jahnke, C. C. and Culick, F. E. C. (1991) "Application of Bifurcation Theory to Nonlinear Acoustics in Combustion Chambers," in preparation.

Keanini, R., Yu, K., and Daily, J. (1989) "Evidence of a Strange Attractor in Ramjet Combustion," 27th Aerospace Sciences Meeting, Paper No. AIAA 89-0624.

Kantor, J. G. (1984) "A Dynamical Instability of Spark Ignition Engines," *Science*, Vol. 224, pp. 1233-1234.

Krylov, N. and Bogoliubov, N. (1947) *Introduction to Nonlinear Mechanics*, Princeton University Press, Princeton, New Jersey.

Lighthill, M. J. (1952) "On Sound Generated Aerodynamically, Part I. General Theory," *Proc. Roy. Soc.*, A211, pp. 504-587.

Lighthill, M. J. (1953) "On Sound Generated Aerodynamically, Part II. Turbulence as a Source of Sound," *Proc. Roy. Soc.*, A2, pp. 1-32.

Lilley, G. M. (1973) "On the Noise From Jets," *Proceedings of AGARD Conference, Noise Mechanisms*, Paper No. 13, AGARD-CP-131.

Lumley, J. L. (1967) "The Structure of Turbulent Flows," in *Atmospheric Turbulence and Radio Wave Propagation*, A. M. Yaglom and V. I. Tatarski, eds., Moscow: Nauka, pp. 166–178.

Mani, R. (1972) "A Moving Source Problem Relevant to Jet Noise," *J. Sound and Vib.*, Vol. 25, pp. 337–347.

Mani, R. (1973) "The Issue of Convective Amplification in Jet Noise," *Proceedings of AGARD Conference, Noise Mechanisms*, Paper No. 10, AGARD-CP-131.

Mani, R. (1976) "The Influence of Jet Flow in Jet Noise. Part 1, The Noise of Unheated Jets; Part 2, The Noise of Heated Jets," *J. Fl. Mech.*, Vol. 73, Part 4, pp. 753–793.

McManus, K. R., Poinsot, T., and Cardel, S. H. (1991) "A Review of Active Control of Combustion Instabilities," *24th Symposium on Combustion, Proceedings.*

Menon, S. and Jou, W.-H. (1990) "Modes of Oscillation in a Nonreacting Ramjet Combustor Flow," *J. Prop. and Power*, Vol. 6, No. 5, pp. 535–543.

Müller, E.-A. (1976) "Flow Acoustics," in *Theoretical and Applied Mechanics*, W. T. Korter (Ed.), North-Holland Publishing Co.

Ott, E., Grebogi, C., and Yorke, I. A. (1990) "Controlling Chaos," *Phys. Rev. Lett.*, Vol. 64, No. 11, pp. 1196–1199.

Packard, N. H., Crutchfield, J. P., Farmer, J. P., and Shaw, R. S. (1980) "Geometry From a Time Series," *Phys. Rev. Lett.*, Vol. 45, No. 9, pp. 712–714.

Paparizos, L. and Culick, F. E. C. (1989a) "The Two-Mode Approximation to Nonlinear Acoustic in Combustion Chambers I. Exact Solution for Second-Order Acoustics," *Comb. Sci. Tech.*, Vol. 65, No. 1–3, pp. 39–65.

Paparizos, L. and Culick, F. E. C. (1989b) "The Two-Mode Approximation to Nonlinear Acoustic Waves in Combustion Chambers with Stochastic Sources," (unpublished).

Paparizos, L. and Culick, F. E. C. (1991) "The Two-Mode Approximation to Nonlinear Acoustic in Combustion Chambers II. Possible Influences of Third-Order Acoustics and Mean Flow in Triggering," submitted for publication.

Parker, T. S. and Chua, L. O. (1987) "Chaos: A Tutorial for Engineers," *Proceedings of the IEEE*, Vol. 75, No. 8, pp. 982–1008.

Phillips, O. M. (1960) "On the Generation of Sound by Supersonic Turbulent Shear Layers," *J. Fluid Mech.*, Vol. 9. pp. 1–28.

Poinsot, T., Hossein, K., Le Chatlier, C., Candel, S. H., and Esposito, E. (1986) "An Experimental Analysis of Noise Sources in a Dump Combustor," in *Dynamics of Reactive Systems Part I: Flames and Configurations*, ed. J. R. Brown, J.C. Leyer, and R. I. Soloukhin, Vol. 45, Part 1 of *Progress in Astronautics and Aeronautics*, AIAA, New York, pp. 333–345.

Poinsot, T., Bourienne, F., Candel, S. H., and Esposito, E. (1989) "Suppression of Combustion Instabilities by Active Control," *J. Propulsion*, Vol. 5, No. 1, pp. 14–20.

Rapp, D. and Schneider, P. E. M. (1972) "Schallverstärkung und Geräuschmindesung bei schallbeeinfluster Flammen," Max Planck Institut für Strömungsforschung, Bericht 8 (cited by Müller 1976).

Ribner, H. S. (1981) "Perspectives in Jet Noise," *AIAA J.*, Vol. 19, No. 12, pp. 1513–1526.

Roberts, J. B. and Spanos, P. D. (1986) "Stochastic Averaging: An Approximate Method of Solving Random Vibration Problems," *Int. J. Non-Linear Mech.*, Vol. 21, No. 2, pp. 111–134.

Schneider, S. P. (1990) "Free-Stream Turbulence: A Limitation on Fractal Descriptions of Open-Flow Systems," *Phys. Fluids*, A2, No. 5, pp. 869–872.

Schubert, L. K. (1972) "Numerical Study of Sound Refraction by a Jet Flow. Part I: Ray Acoustics; Part II: Wave Acoustics," *J. Acoustic Soc. Am.*, Vol. 51, pp. 439–463.

Sirignano, W. and Crocco, L. (1964) "A Shock Wave Model of Unstable Rocket Combustors," *AIAA J.*, Vol. 2, No. 7, pp. 1285–1296.

Sirovich, L. (1987) "Turbulence and the Dynamics of Coherent Structures," *Q. Appl. Math.*, Vol. 45, pp. 561–590.

Sterling, J. D. (1990) "Characterization of the Nonlinear Dynamics of Experimental Signals: Distinguishing Between Noise and Chaos," Caltech Series on Active Control of Combustion Instabilities, Document CI90-2.

Sterling, J. D. (1991) "Characterization and Modeling of Aperiodic Pressure Oscillations

in Combustion Chambers." AIAA/SAE/ASME 27th Joint Propulsion Meeting, Paper No. AIAA 91-2082.

Sterling, J. D. and Zukoski, E. E. (1987) "Longitudinal Mode Combustion Instabilities in a Dump Combustor," AIAA 25th Aerospace Sciences Meeting, AIAA Paper No. 87-0220.

Sterling, J. D. and Zukoski, E. E. (1991) "Nonlinear Dynamics of Laboratory Combustion Pressure Oscillations," *Combustion Science and Technology*, Vol. 77, Nos. 4-6, pp. 225-238.

Strahle, W. C. (1971) "On Combustion Generated Noise," *J. Fluid Mech.*, Vol. 49, pp. 399-414.

Strahle, W. C. (1978) "Combustion Noise," *Progress in Energy and Combustion Science*, Vol. 4, pp. 157-176.

Strahle, W. C. (1985) "A More Modern Theory of Combustion Noise," in *Recent Advances in the Aerospace Sciences*, Plenum Press, pp. 103-114.

Stratonovich, R. L. (1963) *Topics in the Theory of Random Noise* Vols. I and II, Gordon and Breach, New York.

Stratonovich, R. L. (1966) "A New Representation for Stochastic Integrals and Equations," *SIAM*

J. Control, Vol. 4, pp. 362-371.

Theiler, J. (1990) "Estimating Fractal Dimension," *J. Opt. Soc. Am. A*, Vol. 7, No. 6, pp. 1055-1073.

Wilson, K. J., Gutmark, E., Schadow, K. C., and Smith, R. A. (1991) "Active Control of a Dump Combustor with Fuel Modulation," 29th Aerospace Sciences Meeting, Paper No. AIAA 91-0368.

Yang, V. and Culick, F. E. C. (1987) "Stochastic Excitation of Acoustic Waves in a Combustion Chamber," JANNAF Combustion Meeting.

Yates, J. E. and Sandri, G. (1976) "Bernoulli Enthalpy: A Fundamental Concept in the Theory of Sound," in *Aeroacoustics: Jet Noise, Combustion, and Core Engine Noise*, (I.R. Schwarz, Ed.), M.I.T. Press.

Zinn, B. T. (1968) "A Theoretical Study of Nonlinear Combustion Instabilities in Liquid-Propellant Rocket Engines," *AIAA J.*, Vol. 6, No. 10, pp. 1966-1972.

Zinn, B. T. and Powell, E. A. (1971) "Nonlinear Instability in Liquid-Propellant Rocket Engines," *Thirteenth Symposium (International) on Combustion, Proceedings*, pp. 491-503.

Discussion

QUESTION BY: R. Artaz. SNECMA, France
1. You are introducing a parallel between the wave equation of your model and the one of Lilley. As the latter holds in a free environment, how can you justify the comparison for an application to combustion noise in a confined environment?
2. To that effect, how do you treat the limited aspect conditions of the environment?

AUTHOR'S RESPONSE:
1. My purpose has not been to suggest that the same problems have been solved, but only to indicate that the basic assumptions are almost identical in the two subjects of combustion instabilities and aerodynamic noise. It is not an extremely important point nor does it have practical consequences (I think). I make it only to clarify the sort of unity that does exist.
2. If I understand your term correctly, you refer to the presence of the bounding walls and the exhaust nozzle. Their influences appear mainly in the forms chosen for the basis functions (mode shapes) used in the expansion of the pressure field, and partly in the boundary conditions applied to the solution of the problem accounting for perturbations of the classical acoustics for a chamber.

QUESTION BY: J.M. Seiner, NASA Langley, USA
Have you considered application of bi-spectral methods to determine non-linear relationships of your observed fundamental combustion modes?

AUTHOR'S RESPONSE:
We have not. Although bi-spectral methods might provide some interesting information, I do not believe that they will give the sort of results we have sought in this work. We shall investigate your suggestion.

Audibility-Based Annoyance Prediction Modeling

Sanford Fidell
BBN Systems and Technologies
21120 Vanowen Street
Canoga Park, CA 91303, USA

and

Lawrence S. Finegold
AL/OEBN (NSBIT)
Air Force Systems Command
U. S. Air Force
Wright-Patterson AFB, OH 45433 USA

Abstract

The effects of rapid onset times and high absolute sound pressures near military training routes (MTRs), including possible startle effects and increased annoyance due to the unpredictable nature of these flights, have been of longstanding concern. A more recent concern is the possibility of increased annoyance due to low ambient noise levels near military flight training operations and differences in expectations about noise exposure in high and low population density areas. This paper describes progress in developing audibility-based methods for predicting the annoyance of noise produced at some distance from aircraft flight tracks. Audibility-based models which take into account near-ground acoustic propagation and ambient noise levels may be useful in assessing environmental impacts of MTRs and Military Operating Areas (MOAs) under some conditions. A prototype Single Event Annoyance Prediction Model (SEAPM) has been developed under USAF sponsorship as an initial effort to address these issues, and work has progressed on a geographic information system (GIS) to produce cartographically referenced representations of aircraft audibility.

Noise exposure contouring software was developed under U.S. Air Force sponsorship in the early 1970s (cf. Galloway and Bishop, 1970; Galloway, 1974; Reddingius, 1974) as a means of representing and assessing impacts of aircraft operations on communities near airbases. Standard interpretations of such contours are made in terms of long term residential habitability of neighborhoods relatively close to runways, and of the compatibility of other land uses with airbase operations. It was recognized early in the development of these contour models that their construction and interpretation required adoption of simplifying assumptions (e.g., no ground propagation effects for differing terrain, no barriers, and standard weather conditions) for the sake of manageable calculations. The U.S. Air Force is now pursuing research on new modeling approaches to produce accurate noise contours for aircraft flying training operations in areas remote from airbases, especially for low-altitude, high speed operations.

Although aircraft noise contours can in principle be constructed in a variety of ways, assumptions underlying their use in settings of military interest have been tailored to the orderly and predictable circumstances of airbase noise exposure. These circumstances

92-17427

||||||||||||||||||||||||||||

airbase noise exposure. These circumstances include:

1) relatively large and stable numbers of approach and departure operations by a specifiable fleet mix;

2) minor long term variation in numbers and types of operations; and

3) a small number of well defined, fixed flight patterns for airbases.

It is altogether reasonable to draw contours of long term exposure centered on aircraft flight tracks under these circumstances of exposure, as the U.S. Air Force has been doing successfully for two decades. Since flight tracks and profiles can be specified with good precision near runways, and since airbases are generally built on flat terrain, it is also reasonable to assume that lines of sight exist between aircraft and nearby residential neighborhoods; that for most practical modeling purposes the world is flat; and that long range refractive and diffractive acoustic propagation phenomena may be safely ignored. Since noise levels produced during approaches and departures commonly exceed ambient levels in nearby neighborhoods by at least 20 dB, it is also reasonable to ignore ambient levels of neighborhood noise around airbases. The assumptions used in constructing conventional (source-based) noise emission contours guarantee that the resulting exposure contours decrease monotonically in level with distance from airbases.

In fact, these standard assumptions produce such well behaved contours in airport neighborhoods that they are often regarded as essential for representations of environmental impacts of aircraft noise. Furthermore, the assumptions and contours which they produce have become intertwined with land use planning policies and widely accepted interpretations of exposure values in terms of residential habitability. It is only when needs

arise to graphically represent aircraft noise impacts of en route operations (by definition, those occurring in areas remote from airbases) that the utility of assumptions tailored to airbases merit re-examination.

The circumstances of en route noise exposure, particularly that produced along MTRs and within MOAs, differ markedly from those in the vicinity of airbases. In contrast to the regularity, stability and overall predictability of flight operations near airbases, aircraft operations in MTR and MOA environments are often sparse in number and quite variable in altitude, flight speed, aircraft type, power settings, and spatial and temporal distributions. Noise produced in two flight regimes (supersonic, high altitude flight and high subsonic speed, low altitude flight), although absent from airbase environs, is common within MOAs and along MTRs.

Furthermore, in rural and remote areas underlying many MTRs and MOAs, low ambient noise levels permit aircraft noise to be heard at great slant ranges by people engaged in other than residential activities. Additionally, terrain may occlude lines of sight between aircraft flying low altitude missions and observers both near and some distance from flight tracks. Populations affected by en route noise are not necessarily residential ones, may not be familiar with the noise, and are not necessarily exposed indoors.

The net effect of these differences in circumstances of noise exposure is to diminish the applicability of standard assumptions to modeling of aircraft noise exposure in the en route case. Three aspects of conventional aircraft noise exposure prediction in particular merit re-examination of their applicability to the en route case:

1) reliance on long term cumulative exposure metrics (such as DNL) to predict the prevalence of annoyance near MTRs and MOAs;

2) various approximations and simplifications made in estimating short range acoustic propagation for low altitude flights; and

3) consideration of the annoyance of relatively low level aircraft noise in environments with even lower level ambient noise.

The appropriateness of integrated energy metrics of noise exposure as predictors of annoyance is debatable on the grounds that there is little evidence to support application of the "equal energy hypothesis"[1] to conditions of exposure as sporadic as those experienced near some MTRs and MOAs (Fidell, Sneddon and Green, 1990). Likewise, noise level predictions produced by standard contouring software, developed mainly for use over short slant ranges in flat terrain, are not sufficiently accurate for the case of low altitude, high speed operations, because the software is not optimized for the case of near-ground (grazing incidence) propagation over long distances in terrain with topographic relief.

Several efforts to adapt standard approaches and assumptions of the airbase case to the en route case have been made. In general, software models such as ROUTEMAP (developed at the U.S. Air Force Armstrong Aerospace Medical Laboratory), and AIRNOISE (Berry and Harris, 1990) (developed at the National Physical Laboratory) retain a number of assumptions and limitations similar to those of software intended for airbase use (e.g., NOISEMAP and INM). For example, current en route models generally

1) predict exposure in units of long term cumulative exposure which have not yet been validated in field studies as especially appropriate for circumstances of exposure prevailing near MTRs and MOAs;

2) require detailed knowledge of flight tracks and profiles;

3) produce estimates of integrated noise levels over relatively short ranges;

4) are insensitive to terrain shielding of low altitude flight noise; and

5) do not consider the potential influences of ambient noise on annoyance.

Alternative views of the origins and predictability of annoyance associated with MTR and MOA operations can lead to alternative approaches to modeling MTR and MOA noise. For example, there are reasons (such as U.S. Public Law 100-91) to consider expanding the focus of concern from prediction of long term effects of regular exposure on habituated residential populations to include concern for shorter term effects on sporadically exposed populations. If pursued, analyses of shorter term impacts will, of course, require calculation of metrics in addition to long term integrated noise exposure.

Likewise, existing short range air-to-ground noise propagation models may not always suffice in predicting noise exposure at all points because they rely on two dimensional models. Prediction of noise levels in communities some distance from MTRs or MOAs, for example, may require more sophisticated models to produce credible estimates of exposure levels of aircraft operations typical for these types of operations. By the same token, observer-based rather than source-based contours may be more appropriate in cases in which uncertainty about flight track dispersal is too great to be usefully represented in probabilistic terms. For example, Plotkin and co-workers (e.g., Plotkin, Sutherland and Molino, 1987) have documented standard

deviations of flight track dispersal on MTRs as great as half a mile. This degree of uncertainty about aircraft location compromises the interpretability of conventional aircraft noise contours.

If there is sufficient concern about effects of aircraft noise at low sound pressure levels (as, for example, in overflights of some parks and wildernesses, as well as for low-ambient noise rural residences), the effects of the ambient noise environment may be explicitly considered by predicting aircraft audibility exposure rather than integrated sound levels alone.

The remainder of this presentation concentrates on the first of these alternatives - prediction of reactions to individual overflights at points other than those directly underneath flight paths. In a preliminary effort to address the different modeling approaches that may be appropriate to MTR and MOA environments, the U.S. Air Force Noise and Sonic Boom Impact Technology program is sponsoring development of a Single Event Annoyance Prediction Model (SEAPM) for assessment of the annoyance of low altitude, high speed en route flight on MTRs as heard some distance to the side of the flight track. The model first estimates the audibility of an aircraft noise intrusion by calculating its bandwidth-adjusted signal to noise ratio at the observer's location, and then generates a prediction of annoyance via a single event dosage-effect relationship between audibility and annoyance. Derivation of this dosage-effect relationship through a meta-analysis of laboratory data is described by Fidell, Hutchings, Helweg-Larsen, and Silvati (1990).

Estimation of the audibility of aircraft noise intrusions is accomplished through acoustic propagation and detection algorithms developed over the last two decades by the U.S. Army Tank-Automotive Command. The algorithms contained in Version 7 of the Army's Acoustic Detection Range Prediction

Model (ADRPM) account analytically for geometric spreading of acoustic energy, atmospheric absorption, barriers, and a variety of refractive and diffractive propagation effects. The algorithms estimate audibility of acoustic signals with reference to an ideal energy detector operating within human frequency analysis bandwidths. Users of the software may either specify values of two dozen propagation and detection parameters or accept general default values. Details of the model are described by Hutchings and Fidell (1990).

Although prototype SEAPM software represents an advance in the ability to model single noise events and predictions of associated human annoyance, its present limitations include the following:

1) it is based on the ADRPM model, which continues to be refined and improved;

2) it currently treats only ground-to-ground and near-ground propagation effects; and

3) the single event dosage-response relationship requires additional confirmation from further psychoacoustic studies.

Further research and development efforts are being contemplated for improving the SEAPM model, It is not yet certain that the approach adopted in SEAPM will ultimately provide sufficient analytic and predictive modeling capabilities.

Computer-based geoinformation systems provide a convenient means for graphically and analytically representing audibility-based predictions of en route aircraft noise impacts (such as observer-based audibility modeling permitted by SEAPM). In fact, the inherent cartographic orientation of geoinformation systems is well suited to several forms of advanced modeling of near-ground aircraft noise impacts.

Consider, for example, the representation of aircraft noise levels shown in Figure 1, produced under a BBN Independent Research and Development project. The figure is an 30 km² orthographic projection. The flight track shown is that of an air tour operation. Colors encode 10 dB intervals of (bandwidth adjusted) signal to noise ratio for an individual overflight. The information shown was developed over a regular grid of 100 X 100 points separated by 300 m. A simulated aircraft was "flown" over its flight track in 300 m increments. For each 300 m increment, one-third octave band noise levels at each point of the entire grid of 10,000 points were recalculated. Signal-to noise-ratios were calculated at each point in the grid and manipulated to estimate the integrated and maximum audibility of the aircraft and time above criterion levels for a complete mission. Two effects account for the structure apparent in the figure: diffraction of sound over terrain features which obstruct lines of sight, and the local ambient noise at each point.

One of the advantages of performing these calculations in a geoinformation system is the ability to manipulate the resulting map topologically. For example, the various panels of Figure 2 show several projections of this map layer of calculated audibility values onto terrain contours. The layer of audibility information is first draped over the terrain, and then viewed from various perspectives. The resulting map is an obvious and immediately understandable representation of where aircraft can be heard to varying degrees over very wide areas. Because of the ability to display this information topographically, its great detail does not interfere with its intuitive understanding.

Figure 3 shows another example of this approach to modeling near-ground aircraft noise exposure. The terrain in this case is a mountain. A helicopter flight track is shown as a closed ellipse beginning and ending at a heliport. As the helicopter flies through the crater of the volcano, its noise emissions spill out of the jagged rim along the same drainages through which lava flows.

The ability to represent aircraft audibility as shown in these illustrations permits efficient conduct of fine grained assessments of environmental impacts produced over wide areas by MTR and MOA operations. Such analyses can be of considerable interest to both military route planners and environmental analysts.

References

Berry, B.F., and Harris, A.L. (1990). Military Aircraft Noise Prediction and Measurement. International Conference on Military Aircraft Noise. Institute of Acoustics. London.

Fidell, S., Hutchings, L., Helweg-Larsen, M., and Silvati, L. (1990). Audibility and Annoyance of En Route Noise of Unducted Fan Engines. FAA Report 90-03. Washington, D.C.

Fidell, S., Sneddon, M., and Green, D. (1990) Relationship between Short and Long Term Annoyance of Noise Exposure. NSBIT Technical Operating Report 22. Wright-Patterson Air Force Base, OH.

Galloway, W. (1974). Community Noise Exposure Resulting from Aircraft Operations: Technical Review. AMRL-TR-73-106. Wright-Patterson Air Force Base, OH.

Galloway, W., and Bishop, D. (1970). Noise Exposure Forecasts: Evolution, Evaluation, Extensions, and Land Use Interpretations. FAA Report NO-70-9. Washington, D.C.

Hutchings, L., and Fidell, S. (1990). Development of a Single Event Annoyance Prediction Model (SEAPM). NSBIT TOR No. 16. Noise and Sonic Boom Impact Technology Program, Wright-Patterson Air

Force Base, OH.

Plotkin, K., Sutherland, S., and Molino, J. (1987) Environmental Noise Assessment for Military Aircraft Training Routes. AMRL-TR-87-001. Wright-Patterson Air Force Base, OH.

Reddingius, N. (1974). Community Noise Exposure Resulting from Aircraft Operations: Computer Program Operator's Manual. AMRL-TR-73-108. Wright-Patterson Air Force Base, OH.

1. The equal energy hypothesis holds that annoyance is caused by the total energy of noise exposure. The hypothesis predicts, for example, that people are indifferent between the annoyance of short term exposure to small numbers of high level noise intrusions and long term exposure to compensatingly smaller numbers of low level noise intrusions.
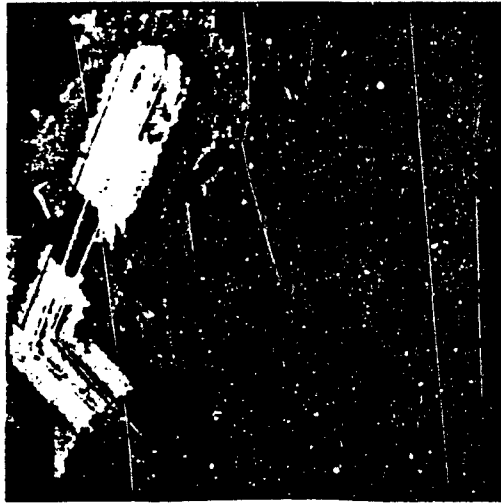
Figure 1 - Orthographic Projection of Aircraft Acoustical
Detectability Sheet
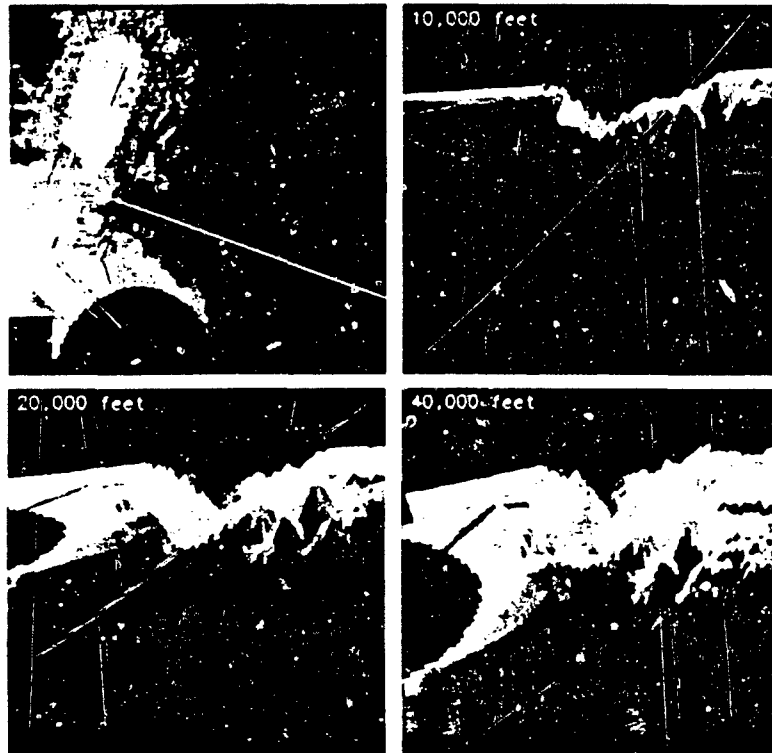
Figure 2 - Detectability Sheet Draped Over Terrain Contours
Viewed from Several Perspectives
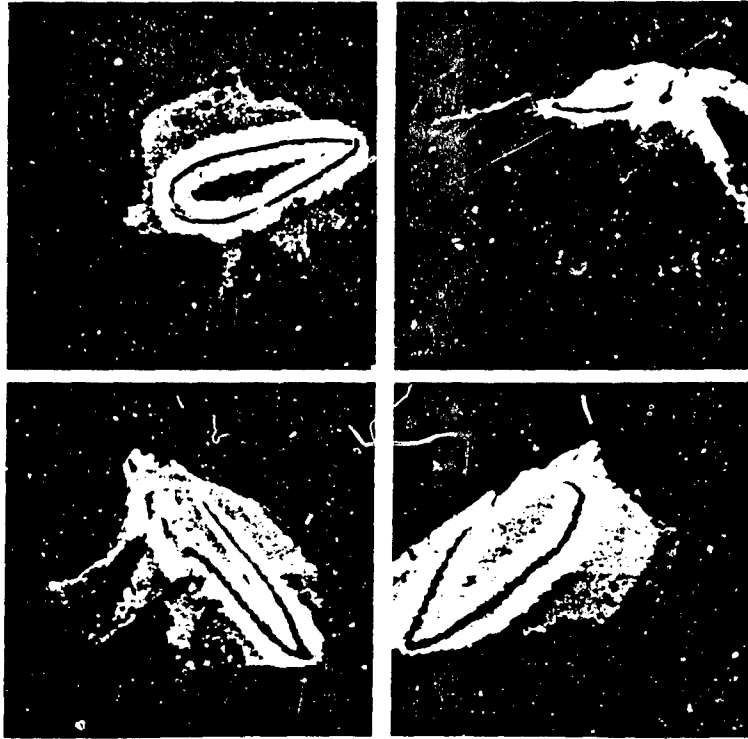
Figure 3 - Projection of Detectability Sheet for Hypothetical
Helicopter Operation on Mountainous Terrain

Discussion

QUESTION BY: J..W. Illston, BAe, UK

It is difficult to make good predictions over relatively flat terrains, but it is even more difficult to make predictions around mountains and in valleys. Have you, or are you, attempting to verify the accuracy of your model? Also, does the model include a correction for the onset rate?

AUTHOR'S RESPONSE:

An initial model validation effort was conducted at the Grand Canyon National Park, where noise measurements were obtained. However, considerable additional validation will be required before new models are approved for use by the US Air Force.
At the present time, no noise rise time corrections are included. The US Air Force is still pursuing research on this issue. The results of that research will be included in future versions of models being developed.

QUESTION BY: R.J. Weston, Royal Air Force, UK

Please will you comment on the concept of audibility as a criterion for annoyance?

AUTHOR'S RESPONSE:

Audibility is being pursued as a possible alternative to the percent of persons "highly annoyed" (i.e., the well-known Schultz Curve") for predicting community response to special military training flight operations. At the present time, however, no exposure criterion exists for the level of audibility which would be considered acceptable versus unacceptable. This issue is planned as a future research topic.
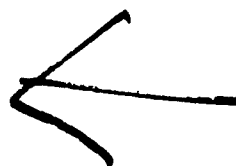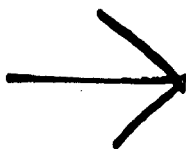
THE PREDICTION OF NOISE RADIATION FROM SUPERSONIC ELLIPTIC JETS

Philip J. Morris
Thomas R. S. Bhat
Department of Aerospace Engineering
The Pennsylvania State University
University Park, PA 16802, USA

SUMMARY

This paper describes the prediction of noise radiation from supersonic elliptic jets. The noise is associated with the large scale structures in the jet mixing layer. These structures are described as instability waves. The local characteristics of the instability waves are determined from a compressible, linear, analysis. The jet mean velocity and density are described in elliptic cylindrical coordinates. The local eigensolution for the instability waves is determined from a finite difference solution of the non-separable boundary value problem. This inner solution which is formulated in terms of the method of multiple scales is matched with the radiated field using the method of matched asymptotic expansions. The form of the far-field directivity is derived. Predictions are presented for the noise radiation by the several modes of instability in the elliptic jet. The radiated field is not axisymmetric and certain modes radiate strongly in the directions of the major and minor axes of the jet. The extension of the present work to other geometries and flow fields is discussed.

1 INTRODUCTION

It is now generally accepted that the mixing process in free shear layers, including jets and wakes, is controlled by large scale structures. These structures engulf fluid from one side of the mixing region and transport this unmixed fluid to the other side of the shear layer. This accounts for the enhanced transport properties of turbulent shear flows. Observations of large scale structures have been made by Brown and Roshko (Ref. 1) and Winant and Browand (Ref 2), in low speed flows, Lepicovsky et al(Ref. 3), in moderately supersonic jets, and Papamoschou and Roshko (Ref. 4), in highly supersonic shear layers. Many other investigations have also observed large scale coherent structures for a variety of free shear layer geometries and operating conditions.

If the speed of the jet or shear layer is sufficiently high the convection velocity of the large scale structures may approach or exceed the speed of sound in the ambient medium. Under these circumstances, there is a direct coupling between the flow field characteristics of the large structures and the radiated acoustic field. This results in intense noise radiation in the downstream arc and has been referred to as "eddy Mach wave noise."

In the present paper the large scale structures are modeled as instability waves. Measurements of the local characteristics of large scale structures in excited shear layers, Gaster et al(Ref. 5), and jets, Petersen and Samet (Ref. 6), have shown that the local variation in amplitude and phase of the large scale structures across the shear layer are predicted remarkably well by a linear, inviscid, analysis. It is perhaps not surprising that flows that are dynamically strongly unstable should be dominated by their primary instabilities. Further evidence of the importance of the linear terms in the "vortex forces" of a turbulent flow is given in the appendix to Morris et al(Ref. 7). To account for the effects of flow divergence on the evolution of the instability waves a multiple scales analysis may be used.

Tam and Morris (Ref. 8) showed that the multiple scales expansion breaks down at large distances from the edge of the jet or shear layer. They showed how the solution could be continued into the far field using the method of matched asymptotic expansions. This enabled them to calculate the noise radiated by the instability waves or large scale structures. Morris and Tam (Ref. 9) extended this work to include the noise radiation by instability waves in supersonic jets. Later, Tam and Burton (Refs 10, 11) extended the technique to higher Mach numbers for shear layers and jets respectively. They showed how difficulties associated with the calculation of damped supersonic instability waves could be overcome.

When the jet is operating off-design the interactions between the instability waves and the nearly periodic shock cell structure of the jet results in broadband shock associated noise and, when a feedback loop is established, screech. The prediction of these noise components requires the calculation

of both the instability waves and the shock cell structure. Tam and Tanna (Ref. 12) showed how a simple model may be developed for the shock cell structure. Tam (Ref. 13) used this model in his theory of shock associated noise.

All the preceding calculations have considered circular jets only. Few calculations have been performed for non-circular jets. This is due to the difficulties in the solution of the non- separable boundary value problem for the local characteristics of the instability waves. Morris *et al*(Ref. 14) used the boundary element technique to predict the shock cell structure in non-circular jets. Bhat *et al*(Ref. 15) extended this analysis to include the effects of finite shear layer thickness and the dissipative effects of the mixing layer turbulence. The characteristics of instability waves in elliptic and rectangular jets were calculated by Baty (Ref. 16) and Baty and Morris (Ref. 17), through the use of a hybrid finite difference/pseudospectral technique.

In the present paper the noise radiation from the instability waves of a supersonic elliptic jet is predicted. In the next section the model equations are developed and the numerical methods are described. Results for the instability wave development and their radiated noise are then presented. Finally, the extension of the present work to jets with other geometries and operating conditions is described.

2 ANALYSIS AND COMPUTATIONS

In this section the equations describing the development of the instability waves in an elliptic jet are given. The form of the outer solution for the radiated noise is also developed. The matching between these two solutions is then described. This leads to an expression for the far-field directivity. Finally, the numerical solution techniques for the inner solution is given.

2.1 The Inner Solution

Consider the development of an instability wave of fixed real frequency ω in a jet issuing from an elliptic nozzle. The jet is assumed to be operating at its design condition and the mean static pressure is assumed to be constant. The instability wave is described by the compressible, inviscid, linearised equations of motion. These equations are non-dimensionalised with respect to the jet exit radius, velocity, density, and temperature. The linearised equations of continuity, momentum, energy, and state, written in Cartesian tensor form, may be

rearranged to give,

$$\left\{\frac{\partial}{\partial t} + \bar{u}_j\frac{\partial}{\partial x_j} + \frac{\partial \bar{u}_j}{\partial x_j}\right\}\rho' + \bar{\rho}\frac{\partial u'_j}{\partial x_j} + \frac{\partial \bar{\rho}}{\partial x_j}u'_j = 0, \quad (2.1)$$

$$\bar{\rho}\left\{\frac{\partial u'_i}{\partial t} + \bar{u}_j\frac{\partial u'_i}{\partial x_j} + u'_j\frac{\partial \bar{u}_i}{\partial x_j}\right\} + \left\{\bar{u}_j\frac{\partial \bar{u}_i}{\partial x_j}\right\}\rho' = -\frac{\partial p'}{\partial x_i}, \quad (2.2)$$

$$\left\{\frac{\partial}{\partial t} + \bar{u}_j\frac{\partial}{\partial x_j}\right\}p' + \frac{1}{M_j^2}\frac{\partial u'_i}{\partial x_i} + \gamma\frac{\partial \bar{u}_i}{\partial x_i}p' = 0, \quad (2.3)$$

where, the overbar denotes a time-averaged quantity and a prime denotes a fluctuation about the mean. M_j is the jet exit Mach number.

Now we seek a solution for a flow in which the mean axial velocity varies slowly with downstream distance. The mean velocity components are then written as,

$$\bar{u} = [\epsilon U(x, y, s) , \epsilon V(x, y, s) , W(x, y, s)], \quad (2.4)$$

where,

$$s = \epsilon x, \quad (2.5)$$

and ϵ is a measure of the rate of spread of the jet mixing layer. The s axis coincides with the jet centerline.

The method of multiple scales may be used to extend a simple series approximation for the fluctuating components in the axial direction. In this paper we outline this procedure but the algebraic details are not provided. This is for two reasons. Firstly, the algebraic details are extremely lengthy. Secondly, the technique is only used to derive the correct matching between the inner flow solution and the outer acoustic solution. In the present calculations, the inner solution has been obtained assuming that the flow divergence corrections are small. This should be a reasonable approximation for high speed jets in which the jet spreading rate is very small.

We seek solutions of the form,

$$\begin{pmatrix} u' \\ v' \\ w' \\ p' \\ \rho' \end{pmatrix} = \sum_{n=0}^{\infty} \epsilon^n \begin{pmatrix} u_n(x, y, s) \\ v_n(x, y, s) \\ w_n(x, y, s) \\ p_n(x, y, s) \\ \rho_n(x, y, s) \end{pmatrix} \exp[i(\theta(s)/\epsilon - \omega t)]. \quad (2.6)$$

$\theta(s)$ is a phase function such that,

$$\frac{d\theta(s)}{ds} = \alpha(s), \quad (2.7)$$

where, $\alpha(s)$ is the slowly varying axial wavenumber.

If solutions of the form (2.6) are substituted into eqns. (2.1-2.3), and the resulting equations are grouped by powers of ϵ, the zeroth-order equation is found to take the form,

$$\nabla_\perp^2 p_0 + \bar{\rho}\Omega^2[\nabla_\perp(1/\bar{\rho}\Omega^2)] \cdot [\nabla_\perp p_0] - [\alpha^2 - \bar{\rho}\Omega^2 M_j^2]p_0 = 0,$$ (2.8)

where,

$$\nabla_\perp \equiv \mathbf{i}\frac{\partial}{\partial x} + \mathbf{j}\frac{\partial}{\partial y},$$ (2.9)

and,

$$\Omega = \omega - \alpha W.$$ (2.10)

This form of the compressible Rayleigh equation is readily transformed into any appropriate coordinate system in the normal plane.

In the present case it is convenient to introduce elliptic, cylindrical coordinates with,

$$x = a\cosh u\cos v, \quad y = a\sinh u\sin v, \quad z = z. \quad (2.11)$$

Then, in elliptic, cylindrical coordinates, eqn. (2.8) may be written,

$$\mathcal{L}(p_0) = \frac{\partial^2 p_0}{\partial u^2} + \frac{\partial^2 p_0}{\partial v^2} + \bar{\rho}\Omega^2\frac{\partial}{\partial u}\left\{\frac{1}{\bar{\rho}\Omega^2}\right\}\frac{\partial p_0}{\partial u} +$$

$$\bar{\rho}\Omega^2\frac{\partial}{\partial v}\left\{\frac{1}{\bar{\rho}\Omega^2}\right\}\frac{\partial p_0}{\partial v} -$$

$$\frac{a^2}{2}[\cosh(2u) - \cos(2v)][\alpha^2 - \bar{\rho}\Omega^2 M_j^2]p_0 = 0.$$ (2.12)

To order ϵ a set of inhomogeneous equations for the fluctuations u_1, v_1, w_1, ρ_1, and p_1 may be obtained. The right-hand sides of these equations are functions of the zeroth-order solutions. These equations may be reduced to a single inhomogeneous equation for p_1 in the form,

$$\mathcal{L}(p_1) = \chi_1,$$ (2.13)

where χ_1 contains derivatives of p_0 with respect to z, u, and v, as well as terms involving $d\alpha/dz$. It may be shown that the form of the higher order equations may be reduced to,

$$\mathcal{L}(p_n) = \chi_n(u, v, z), \quad n = 1, 2, 3\ldots$$ (2.14)

The form of the zeroth-order solution is taken to be,

$$p_0(u, v, z) = A_0(z)\varsigma(u, v, z).$$ (2.15)

Then, from eqn. (2.12), $\varsigma(u, v, z)$ satisfies,

$$\mathcal{L}(\varsigma) = 0,$$ (2.16)

with boundary conditions,

$$\varsigma \text{ is bounded as } u \to 0 \text{ and } \infty.$$ (2.17)

Just outside the jet flow, for $u > u_m$, the coefficients of eqn. (2.16) are constant and a separable solution may be obtained. If a solution is sought of the form,

$$\varsigma = R(u)T(v),$$ (2.18)

it is readily shown that,

$$\frac{d^2T}{dv^2} + [\lambda - 2q\cos(2v)]T = 0,$$ (2.19)

and

$$\frac{d^2R}{du^2} - [\lambda - 2q\cosh(2u)]R = 0,$$ (2.20)

where,

$$q = -\frac{a^2}{4}[\alpha^2 - \rho_\infty M_j^2\omega^2].$$ (2.21)

ρ_∞ is the mean density outside the jet flow. Equations (2.19) and (2.20) are the Mathieu equation and modified Mathieu equation respectively. λ is the separation constant. Thus the general forms of solution outside the jet may be written,

$$\varsigma(u, v, z) = \sum_{m=0}^{\infty} A_{2m+p}\mathrm{ce}_{2m+p}(v, q)\mathrm{Mc}_{2m+p}^{(3)}(u, q),$$

$$p = 0, 1,$$ (2.22)

and,

$$\varsigma(u, v, z) = \sum_{m=0}^{\infty} B_{2m+p}\mathrm{se}_{2m+p}(v, q)\mathrm{Ms}_{2m+p}^{(3)}(u, q),$$

$$p = 0, 1.$$ (2.23)

If $p = 0$ the solutions have period π and if $p = 1$ the solutions have period 2π. Solutions of the form (2.22) are even about $v = 0$ and solutions of the form (2.23) are odd about $v = 0$. $\mathrm{ce}_{2m+p}(v, q)$ and $\mathrm{se}_{2m+p}(v, q)$ are the even and odd Mathieu functions respectively. $\mathrm{Mc}_{2m+p}^{(3)}(u, q)$ and $\mathrm{Ms}_{2m+p}^{(3)}(u, q)$ are the even and odd modified Mathieu-Hankel functions respectively. The notation of Abramowitz and Stegun (Ref. 18) has been used. Additional information about the definitions and evaluation of these functions is given by McLachlan (Ref. 19).

Since the value of q varies with downstream distance it is convenient to express the Mathieu functions in eqns. (2.22) and (2.23) by their series expansions,

$$\mathrm{ce}_{2m+p}(v, q) = \sum_{n=0}^{\infty} C_{(2m+p)}^{2n+p}\cos[(2n+p)v], \quad p = 0, 1,$$ (2.24)

and

$$se_{2m+p}(v,q) = \sum_{n=0}^{\infty} D_{(2m+p)}^{2n+p} \sin[(2n+p)v], \quad p = 0, 1.$$

(2.25)

Thus, the normal modes of solution $\varsigma_{nm}(u,v,s)$ may be written, for example,

$$\varsigma_{nm}(u,v,s) \sim \cos[(2n+p)v] Mc_{2m+p}^{(3)}(u,q), \quad (2.26)$$

with,

$$\varsigma(u,v,s) = \sum_{n=0}^{\infty}\sum_{m=0}^{\infty} A_{2m+p}^{2n+p}\varsigma_{nm}, \quad p = 0, 1. \quad (2.27)$$

As a normalisation condition that must be specified for the local linear solutions the largest coefficient of A_{2m+p}^{2n+p} is set equal to unity.

A similar solution may be obtained for $\varsigma(u,v,s)$ close to the jet centerline. These solutions serve as the boundary conditions for a numerical solution of eqn. (2.12) in the jet shear layer. Eigensolutions may be obtained to this problem. The numerical procedure is described in section 2.4 below.

In order for a solution to exist to eqn. (2.13) it must satisfy a solvability condition; that is, the inhomogeneous terms are orthogonal to every solution of the adjoint problem. This requires that,

$$\int_0^{\infty}\int_0^{2\pi} \psi\chi_1\, dvdu = 0, \quad (2.28)$$

where, $\psi(s,u,v)$ is a solution of the adjoint homogeneous equation. It is readily shown that,

$$\psi(u,v,s) = \varsigma(u,v,s)/\bar{\rho}\Omega^2. \quad (2.29)$$

Equation (2.28), the solvability condition, then leads to an ordinary differential equation for $A_0(s)$ in the form,

$$I_1\frac{dA_0}{ds} + I_2 A_0 = 0, \quad (2.30)$$

where I_1 and I_2 are integrals with respect to u and v. All the terms in the integrand are known as functions of ς except for $\partial\varsigma/\partial s$ and $d\alpha/ds$. These terms may be obtained by differentiation of eqn. (2.16) with respect to s. This leads to,

$$\mathcal{L}(\partial\varsigma/\partial s) = h_1(d\alpha/ds) + h_2, \quad (2.31)$$

where h_1 and h_2 are functions of ς. Application of the solvability condition to this equation, equivalent to eqn. (2.28), leads to an ordinary differential equation for $d\alpha/ds$. The inhomogeneous eqn. (2.31) may then be solved directly for $\partial\varsigma/\partial s$.

These calculations determine completely the inner solution to order zero. A similar procedure may be used to find the higher order terms in the series for the pressure fluctuation. However, Tam and Morris (Ref.. 8) showed that this expansion fails far from the region of mean shear. This constitutes a singular perturbation problem that may be solved using the method of matched asymptotic expansions. This enables the inner solution to be matched with the outer "acoustic" solution. This outer solution is determined in the next section.

2.2 The Outer Solution

In the region $u >> u_m$ the mean velocity components are zero and the pressure fluctuation satisfies the wave equation in elliptic cylindrical coordinates. If a time dependent behavior of the form $\exp(-i\omega t)$ is assumed the pressure perturbation $\bar{p}(z,u,v)$ may be shown to satisfy the equation,

$$\frac{\partial^2\bar{p}}{\partial z^2} + \frac{2}{a^2[\cosh(2u) - \cos(2v)]} \times$$
$$\left\{\frac{\partial^2\bar{p}}{\partial u^2} + \frac{\partial^2\bar{p}}{\partial v^2}\right\} - \rho_\infty M_j^2\omega^2\bar{p} = 0.$$

(2.32)

Define the Fourier transform pair,

$$P(k) = \frac{1}{2\pi}\int_{-\infty}^{\infty} \bar{p}(z)e^{-ikz}dz, \quad (2.33)$$

$$\bar{p}(z) = \int_{-\infty}^{\infty} P(k)e^{ikz}dk. \quad (2.34)$$

Then the equation for $P(k)$ is found to be,

$$\frac{\partial^2 P}{\partial u^2} + \frac{\partial^2 P}{\partial v^2} -$$
$$\frac{a^2}{2}[\cosh(2u) - \cos(2v)][k^2 - \rho_\infty M_j^2\omega^2]P = 0.$$

(2.35)

This is identical to eqn. (2.12) for zero mean velocity and with α replaced by k. Thus the general forms of solution are identical to eqns. (2.22) and (2.23). The unknown coefficients may be obtained by matching this outer solution with the inner solution. Thus the outer solution may be written, for even modes only,

$$P(u,v;k) = \sum_{n=0}^{\infty}\sum_{m=0}^{\infty} G_{2m+p}^{2n+p}(k)\cos[(2n+p)v]\times$$
$$Mc_{2m+p}^{(3)}(u,q), \quad p = 0, 1,$$

(2.36)

where,

$$q = -\frac{a^2}{4}[k^2 - \rho_\infty M_j^2 \omega^2]. \quad (2.37)$$

Finally, the pressure outside the jet flow may be written,

$$p(u, v, z, t) = \int_{-\infty}^{\infty} P(u, v; k)e^{ikz}e^{-i\omega t}dk. \quad (2.38)$$

2.3 Asymptotic Matching and the Far Field Solution

Tam and Morris (Ref.. 8) and Tam and Burton (Refs. 10, 11) showed, for a two-dimensional shear layer and a circular jet, that the lowest order approximation in powers of ϵ to $G_{2m+p}^{2n+p}(k)$ is related to the Fourier transform of the streamwise variation in amplitude and phase of the zeroth-order inner solution. That is,

$$G_{2m+p}^{2n+p}(k) = \frac{1}{2\pi}\int_{-\infty}^{\infty} A_0(\epsilon z)e^{i\theta(\epsilon z)/\epsilon - ikz}dz. \quad (2.39)$$

For cases in which the neutral solutions for the instability waves have a subsonic phase velocity the method of Tam and Morris (Ref.. 8) may be used. The more general analysis, that is valid at higher jet Mach numbers and temperatures is given by Tam and Burton (Ref.s. 10, 11). In the latter case the inner and outer solutions must be matched through an intermediate expansion. The extension of the details of this analysis for a circular jet to the present case of an elliptic jet is beyond the scope of the present paper. However, it should be noted that the outer solutions in the present case could be represented in terms of Hankel functions and the matching procedure would then follow their analysis exactly.

The evaluation of the pressure field outside the jet may now be accomplished using eqns. (2.38) and (2.36). Fast Fourier transforms may be used to determine $G_{2m+p}^{2n+p}(k)$ from eqn. (2.39) and in the evaluation of eqn. (2.38). This provides the full three-dimensional pressure field. However, it is convenient and useful to examine the far field sound pressures. First we introduce spherical polar coordinates with,

$$x = R\sin\chi\cos\phi, \quad y = R\sin\chi\sin\phi, \quad z = R\cos\chi. \quad (2.40)$$

Now, as $u \to \infty$,

$$ae^u \to R\sin\chi \text{ and } v \to \phi. \quad (2.41)$$

Also, (Ref. 19), if

$$w = \sqrt{q}e^u \to \infty, \quad (2.42)$$

$$Mc_{2m+p}^{(3)}(u, q) \approx p_{2m+p}(q)\sqrt{\frac{2}{\pi w}}e^{i(w-\pi/4)}, \quad (2.43)$$

where,

$$p_{2m+p}(q) = [ce_{2m+p}(0, q)ce_{2m+p}(\pi/2, q)]/C_{(2m+p)}^p. \quad (2.44)$$

Here, $C_{(2m+p)}^p$ is the leading coefficient in the series representation of the Mathieu function given by eqn. (2.24). From eqns. (2.37), (2.41), and (2.42) it can be seen that,

$$w = i\lambda(k)R\sin\chi, \quad (2.45)$$

where,

$$\lambda(k) = \sqrt{k^2 - \rho_\infty M_j^2 \omega^2}. \quad (2.46)$$

Thus, for $w \to \infty$,

$$p(R, \chi, \phi, t) \approx \sum_{n=0}^{\infty}\sum_{m=0}^{\infty}\cos[(2n+p)\phi]e^{-i\omega t - i\pi/4}\times$$
$$\int_{-\infty}^{\infty}\left\{G_{2m+p}^{2n+p}(k)p_{2m+p}(q)\sqrt{\frac{2}{i\pi\lambda R\sin\chi}}\times\right.$$
$$\left.\exp[i(i\lambda R\sin\chi + kR\cos\chi)]\right\}dk. \quad (2.47)$$

Now the integral in eqn. (2.47) may be evaluated using the method of stationary phase. The stationary point is found to be,

$$k_s = \rho_\infty^{1/2}M_j\omega\cos\chi, \quad (2.48)$$

and the far field pressure is given by,

$$p(R, \chi, \phi, t) \approx \frac{2}{R}\sum_{n=0}^{\infty}\sum_{m=0}^{\infty}\cos[(2n+p)\phi]\times$$
$$G_{2m+p}^{2n+p}(k_s)p_{2m+p}(q_s)\times$$
$$\exp[i\rho_\infty^{1/2}M_j\omega R - i\omega t + i\pi/2], \quad (2.49)$$

where,

$$q_s = q(k_s) = \frac{a^2}{4}\rho_\infty M_j^2\omega^2\sin^2\chi. \quad (2.50)$$

It should be noted that for $\chi \approx 0$ or π, $q_s \to 0$ so that $w \not> 1$ and the asymptotic form of the modified Mathieu-Hankel functions, eqn. (2.43), are not valid.

Equations (2.48) and (2.49) show that the far field sound radiation at a given frequency is associated with the component of the near field wavenumber spectrum that gives a phase velocity in a direction χ equal to the ambient speed of sound.

Following Tam and Burton (Ref. 11) we may define a far field directivity function as the sound power radiated per unit solid angle. This may be written,

$$D(\chi,\phi)/2\rho_\infty^{1/2}M_j = \frac{R^2}{4}<p>^2$$

$$= |\sum_{n=0}^{\infty}\sum_{m=0}^{\infty} G_{2m+p}^{2n+p}(k_o)p_{2m+p}(q_o)\cos[(2n+p)\phi]|^2.$$

(2.51)

Similar expressions may be derived for the odd solutions.

2.4 Numerical Solution

The compressible Rayleigh equation in elliptic cylindrical coordinates, eqn. (2.12), must be solved numerically in the shear layer to obtain the axial evolution of the pressure fluctuation. In order to obtain the numerical solution, the solution of the governing equation in the regions of constant mean flow properties at the inner and outer edges of the jet shear layer must be obtained. As described in section 2.1, in these regions, a separable solution may be obtained. If a solution is sought of the form given by equation (2.18), the equations for $T(v)$ and $R(u)$ reduces to the form given by equations (2.19) and (2.20) respectively. However, in the potential core of the jet,

$$q = -\frac{a^2}{4}[\alpha^2 - \rho_\infty M_j^2(\omega - \alpha)^2].$$

(2.52)

Thus the general forms of the even and the odd solutions in the potential core may be written,

$$\varsigma(u,v,s) = \sum_{n=0}^{\infty}\sum_{m=0}^{\infty} E_{2m+p}^{2n+p}\cos[(2n+p)v]\times$$

$$Ce_{2m+p}(u,q), \quad p = 0,1,$$

(2.53)

and,

$$\varsigma(u,v,s) = \sum_{n=0}^{\infty}\sum_{m=0}^{\infty} F_{2m+p}^{2n+p}\sin[(2n+p)v]\times$$

$$Se_{2m+p}(u,q), \quad p = 0,1.$$

(2.54)

Once again, if $p = 0$ the solutions have period π and if $p = 1$ the solutions have period 2π. $Ce_{2m+p}(u,q)$ and $Se_{2m+p}(u,q)$ are the even and odd modified Mathieu functions respectively. These

solutions satisfy the boundedness condition as $u \to 0$. Similar solutions valid in the region outside the jet were derived in section 2.1 and are given by eqns. (2.22) and (2.23).

If the mean flow possesses symmetry about any lines in the cross-sectional plane, then the solution need only be obtained in a limited sector. In the present case, the mean flow is assumed to be symmetric about both the major and minor axes and the computation is restricted to one quadrant only. This necessitates the specification of the boundary conditions along the two bounding lines of the shear layer. Along these two lines, the conditions that $\varsigma = 0$ if the fluctuation is odd about an axis and that $\partial\varsigma/\partial v = 0$ if the fluctuation is even about an axis are used.

In order to compute the axial evolution of the pressure fluctuation associated with an instability wave of a fixed frequency or Strouhal number and mode type, the first step is to calculate the local eigenvalue; the complex wavenumber α. In the shear layer, the eigenvalues are obtained numerically using a variable step-size Runge-Kutta scheme. The shear layer is divided into M lines of constant v. The derivatives with respect to v in eqn. (2.16) are approximated by a three-point central difference formula. The governing equation may then be written as an ordinary differential equation in u. The forms of solutions given by eqns. (2.42)-(2.43) and (2.22)-(2.23) provide the starting conditions for the numerical integration. For a given value of frequency and a guessed value for the wavenumber, the numerical solution is started at the inner boundary with one term from the finite series. The integration is repeated using each term in the series as the starting solution and is carried out to some intermediate location in the jet shear layer. A corresponding term from the series for the outer solution is then used to integrate the differential equation inward to the same location. The total number of terms in the series solutions is from $m = 0$ to M and, $n = 0$ to N. In the present calculations the maximum values of M and N were 6 and 10 respectively. The integrated solutions are matched at the intermediate location. This leads to system of homogeneous equations for the unknown coefficients. For this system of equations to have nontrivial solution, the determinant of the coefficient matrix should be zero. The axial wavenumbers, α, that are the eigenvalues of the problem, are then obtained in an iterative fashion by finding the zeroes of the determinant of the matrix using a Newton-Raphson scheme.

The technique described above is used to determine the axial wavenumber as a function of downstream distance. In regions sufficiently far downstream from the jet exit, the instability wave is no longer growing and is damped. For damped waves, the numerical integration scheme has to be modified. The integration contour must be deformed around the critical point $u = u_c$, where $\omega - \alpha W(u_c) = 0$, see Tam and Morris (Ref. 8), so as to obtain the correct solution for inviscid damped waves.

The eigenfunctions or the coefficients of the starting solutions are determined next. The integration procedure is repeated using the computed eigenvalue. Once again, the variable step-size integration scheme with the contour deformation (for damped waves) is used. The eigenvector of the set of homogeneous simultaneous equations is then obtained with an inverse iteration technique. The coefficients A_{2m+p}^{2n+p} may then be evaluated at each axial location. These coefficients are then used in conjunction with the axial variation of the wavenumber to determine the axial variation in amplitude and phase of the instability wave.

In the present calculations, as indicated above, we have not performed a complete multiple scales analysis for the inner solution. At high Mach numbers the rate of spread of the jet is very slow. Thus it is assumed here that the locally-parallel flow solution will give a reasonable approximation to the full diverging flow solution. Thus, in eqn. (2.39), we set,

$$A_0(\epsilon z) = A_{2m+p}^{2n+p}, \qquad (2.55)$$

and,

$$\theta(\epsilon z)/\epsilon = \int_{z_0}^{z} \alpha(z)\,dz. \qquad (2.56)$$

The far-field directivity associated with an instability wave is calculated by first computing the complex wavenumber spectrum of the pressure fluctuation. The wavenumber spectrum is given by the eqn. (2.39) and is calculated with a fast Fourier transform. In the present calculations 1024 points were used in the range $-51.2 \leq z \leq 51.2$. This gives a step size of 0.061 in the wavenumber space. The far field directivity is then obtained from eqn. (2.49). Calculations of the wavenumber spectrum and the far field associated with different instability waves of the elliptic jet are given in the next section.

3 CALCULATIONS

In this section we first define the mean velocity and density profiles in the jet. The local instability characteristics of the elliptic jet instability waves are then presented. The wavenumber spectra associated with the axial evolution of these waves is then described. Finally, the three-dimensional far field directivity for each mode is given.

3.1 Definition of the mean flow profiles

In the present calculations a simple representation of the mean velocity profiles has been chosen such that the axial velocity is a function of u only. It takes the form,

$$W(u) = \begin{cases} 1, & \text{if } u < u_p; \\ \exp\left[-\ln(2)\eta^2\right], & \text{otherwise}, \end{cases} \qquad (3.1)$$

where,

$$\eta = \frac{\sinh(u) - \sinh(u_p)}{\sinh(u_h) - \sinh(u_p)}. \qquad (3.2)$$

Here, u_p and u_h are the values of u at the edge of the potential core and the half velocity point respectively. Their values were obtained from the experimental data obtained at NASA Langley Research Center by J. M. Seiner and M. K. Ponton for an elliptic jet with aspect ratio 2 and a design Mach number of 1.5. The values were selected such that u_p and u_h matched the experimental values on the jet minor axis. Their values are given in Table I. The outer edge of the jet shear layer U_m was chosen such that $W(u_m) = 0.0001$. Figure 1 shows two sections through the jet at different axial locations showing the u_p, u_h and u_m contours. In Table I z_c is the length of the potential core with a measured value of $10.1r_j$. Here, r_j is the equivalent radius of the elliptic jet based on its exit area. W_c is the jet centerline velocity. From the Table it should be noted that downstream of the end of the potential core the mean velocity is assumed to be constant for very small values of u. This assumption allows the asymptotic solutions (2.53) and (2.52) to be used near the centerline of the jet. A series solution could be performed to allow a more realistic description of the mean velocity profile downstream of the end of the potential core.

z/z_c	u_p	u_h	W_c
0.25	0.418	0.637	1.0
0.50	0.300	0.677	1.0
0.75	0.203	0.699	1.0
1.00	0.117	0.737	1.0
1.50	0.050	0.805	0.929
2.00	0.050	0.939	0.836

Table 1   Parameters defining mean velocity profile
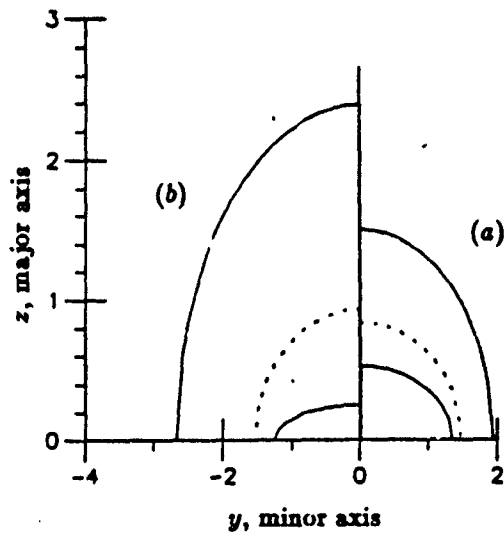
Fig. 1   Mean velocity in elliptic jet at (a) $z/z_e = 0.25$ and (b) $z/z_e = 0.75$

Fig. 2   Variation of axial growth rate with axial distance. Varicose mode. ——, $St = 0.2$, – – –, $St = 0.4$. $M_j = 1.5$, $\rho_\infty = 1$.

In the present calculations the jet is assumed to be isothermal and the jet mean density is constant. This constraint may be relaxed and the Crocco-Busemann formula may be used to determine the relationship between the mean density and the jet axial velocity.

8.2 Instability wave calculations

Calculations have been performed for two types of instability wave. The first is even about both the major and minor axes and will be referred to as the "varicose" mode. This mode is equivalent to the axisymmetric mode in the circular jet case. It is characterised by a $\cos(2mv)$ variation. The second instability wave is odd about the major axis and even about the minor axis. This will be referred to as the "flapping" mode. It is characterised by a $\sin[(2m+1)v]$ variation. Most of the calculations are for a Strouhal number St of 0.2 though calculations have been performed for the varicose mode at $St = 0.4$. We have performed only a few calculations. Further calculations will be performed when experimental data becomes available to verify the calculations.

Figures 2 and 3 show the axial variation in the axial growth rate $-\alpha_i$ and the phase velocity $c = \omega/\alpha_r$ for the varicose mode. The lower frequency wave grows for most of the potential core length and then decays rapidly downstream of the end of the potential core. The higher frequency

Fig. 3   Variation of phase velocity with axial distance. Varicose mode. ——, $St = 0.2$, – – –, $St = 0.4$. $M_j = 1.5$, $\rho_\infty = 1$.

wave is initially faster growing but reaches its neutral point closer to the jet exit. In the potential core region both modes have an average phase velocity of approximately 0.8. Downstream of the

end of the potential core the $St = 0.2$ wave exhibits a rapid decrease in its phase velocity. This is far greater than the rate of decay of the centerline velocity. It is possible that this may not be a physically correct result due to the rather crude description being used for the mean velocity profile. The corresponding results for the flapping mode are shown in fig. 4 for $St = 0.2$. This mode is initially more unstable than the varicose mode but starts to decay much closer to the jet exit. Thus it never achieves the same amplitudes as the varicose mode. We had expected that this mode might be dominant at these operating conditions as flow visualization studies at NASA Langley Research Center had shown that the jet did exhibit a flapping behavior. However, this was most evident when the jet was operating off design. However, the near field microphone measurements by Baty et al(Ref. 20) showed that for a jet operating on design the varicose mode was dominant. This is consistent with the present calculations.
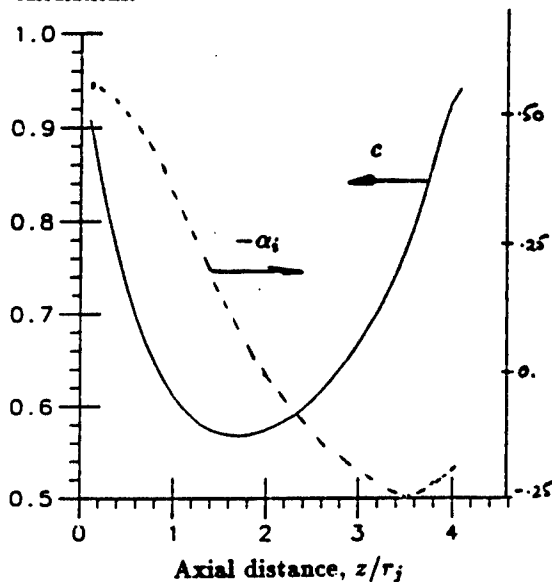
Fig. 4 Variation of axial growth rate and phase velocity with axial distance. Flapping mode. $St = 0.2$, $M_j = 1.5$, $\rho_\infty = 1$.

The amplitude of the wavenumber spectrum G_0^0 for the varicose mode and $St = 0.2$ is shown in fig. 5. It is found that the amplitude of this component of the series representation of the eigensolution is dominant. The peak in the spectrum occurs at $k = 0.95$. THis corresponds to a phase velocity of $c = 2\pi St/k = 0.66$. And the ratio

of this velocity to the ambient speed of sound is $cW_j/a_\infty = cM_j\rho_\infty = 0.99$. Thus only those components of the wavenumber spectrum with wavenumbers less than that at the peak will radiate to the far field. This also indicates that the direction of peak noise radiation by this mode would be directly downstream.
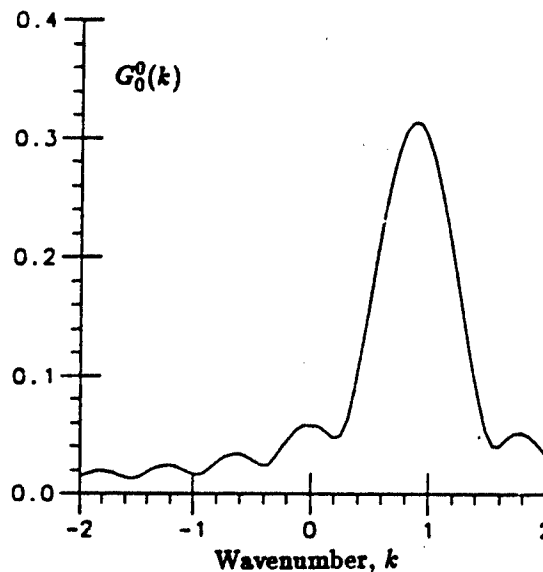
Fig. 5 Wavenumber spectrum for varicose mode. $n = 0$, $m = 0$, $St = 0.2$, $M_j = 1.5$, $\rho_\infty = 1$.

3.3 Far field directivities

Figure 6 shows the calculated far field directivity for the varicose mode as a function of polar angle in the major $\phi = 0$ and minor $\phi = \pi/2$ axis planes. In this calculation, 7 terms in the modified Mathieu function series and 11 terms in the cosine series have been used. The directivity is seen to peak towards the downstream axis in the major axis plane but peaks between 30 and 40 degrees in the minor axis plane. This is consistent with the minor axis plane near field data measured by Baty et al(Ref. 20) who observed a peak radiation angle of 30 degrees. Also, the difference between the levels in the two planes is as much as 7dB for small angles. This is due to the azimuthal variation in the Mathieu functions.

It should be noted that calculations have not been performed for small angles, $\chi < 20$ degrees. This is for two reasons. Firstly, for small values of χ, q_o given by eqn. (2.50), and hence w, given by eqn. (2.42), are very small. Thus the asymptotic
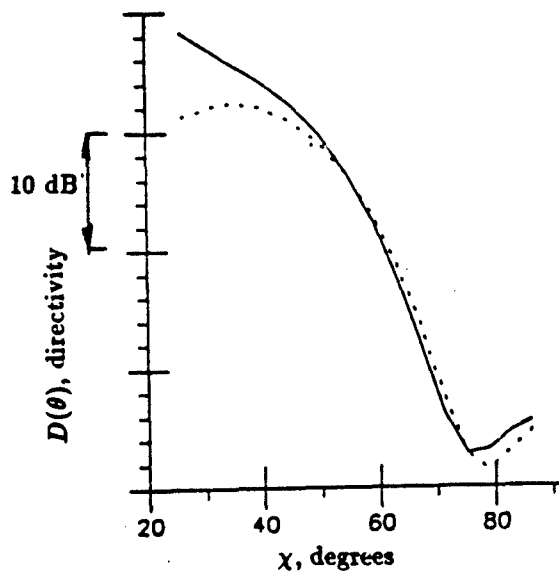
Fig. 6   Far field directivity for varicose mode. $n =$ 0, 6, $m = 0, 10$, $St = 0.2$, $M_j = 1.5$, $\rho_\infty = 1..$ ——, $\phi = 0$, - - -, $\phi = \pi/2$.

form of of the modified Mathieu-Hankel function, eqn. (2.43), is no longer valid. Secondly, unlike the Hankel functions whose magnitude for large arguements is independent of their order, the modified Mathieu- Hankel functions increase in magnitude with increasing order. This is due principally to the normalisation factor p_{2m+p}, eqn. (2.44). We encountered numerical problems in the inclusion of the higher order terms in the series representation of the far field as this involved taking the product of a very small number, the coefficient of a high order term, with a very large number, the corresponding value of p_{2m+p}.

4   DISCUSSION

Predictions ahve been performed for the noise radiation by the instability waves of an elliptic supersonic jet. For the operating conditions considered the varicose mode was predicted to dominate the radiated field. The directivity pattern of this mode was predicted to peak in the axial direction on the major axis and between 30 and 40 degrees on the minor axis. Though the latter result is in agreement with experimental observations further experimental studies are required to give further verification.

At the operating conditions considered it is possible that the proposed noise radiation mechanism by large scale structures is not dominant. The phase

velocity of the characteristic structures in the flow field is only marginally supersonic with respect to the external speed of sound. This suggests that calculations and experiments should be performed at higher jet Mach numbers and tempertures. Such studies are underway.

The present paper has provided the methodology for the prediction of noise from a noncircular jet. The present calculations have been for an elliptic jet but, as long as the mean flow field is known, any jet exit geometry, including a rectangular nossle, could be considered. At present, the authors are continuing their calculations for the elliptic jet with a more general and realistic description cf the mean velocity profile.

5   ACKNOWLEDGEMENTS

6   REFERENCES

1.   Brown, G.L. and Roshko, A., "On Density Effects and Large Structures in Turbulent Mixing Layers", J. Fluid Mech., 64, 1974, pp 775-816.

2.   Winant, C. D. and Browand, F. K., "Vortex Pairing: the Mechanism of Turbulent Mixing Layer Growth at Moderate Reynolds Number", J. Fluid Mech., 63, 1974, pp 237-255.

3.   Lepicovsky, J., Ahuja, K. K., Brown, W. H. and Morris, P. J., "Acoustic Control of Free Jet Mixing", J. Propulsion Power, 2, 1986, pp 323-330.

4.   Papamoschou, D. and Roshko, A., "The Compressible Turbulent Shear Layer: An Experimental Study", J. Fluid Mech., 197, 1989, pp 453-477.

5.   Gaster. M., Kit, E. and Wygnanski, I., "Large Scale Structures in a Forced Turbulent Mixing Layer", J. Fluid Mech., 150, 1985, pp 23-39.

6.   Petersan, R. A. and Samet, M. M., "On the Preferred Mode of Jet Instability", J. Fluid Mech., 194, 1988, pp 153-173.

7.   Morris, P. J., Giridharan, M. G. and Lilley, G. M., "On the Turbulent Mixing of Compressible Free Shear Layers", Proc. Roy. Soc. Lond. A, 431, 1990, pp 219-243.

8.   Tam, C. K. W. and Morris, P. J., "The Radiation of Sound by the Instability Waves of a Compressible Plane Turbulent Shear Layer", J. Fluid Mech., 98, 1980, pp 349-381.

9.   Morris, P. J. and Tam, C. K. W., "On the Radiation of Sound by the Instability Waves of a Compressible Axisymmetric Jet", in "Mecha-

nisms of Sound Generation in Flows", ed. E.-A. Muller, Springer-Verlag, 1979.

10. Tam, C. K. W. and Burton, D. E., "Sound Generated by Instability Waves of Supersonic Flows. Part 1. Two–Dimensional Mixing Layers", J. Fluid Mech., 138, 1984, pp. 249-271.

11. Tam, C. K. W. and Burton, D. E., "Sound Generated by Instability Waves of Supersonic Flows. Part 2. Axisymmetric Jets", J. Fluid Mech., 138, 1984, pp. 273-295.

12. Tam, C. K. W. and Tanna, H. K., "Shock Associated Noise of Supersonic Jets from Convergent-Divergent Nozzles", J. Sound Vib., 81, 3, 1982, pp 337-358.

13. Tam, C. K. W., "Stochastic Model Theory of Broadband Shock Associated Noise from Supersonic Jets", J. Sound Vib., 116, 1987, pp. 265-302.

14. Morris, P. J., Bhat, T. R. B. and Chen, G., "A Linear Shock Cell Model fo Jets of Arbitrary Exit Geometry", J. Sound Vib., 132, 2, 1989, pp 199-211.

15. Bhat, T. R. B., Morris, P. J., and Baty, R. S., "A Linear Shock Cell Model of Non- Circular Jets using Conformal Mapping with a Pseudospectral Hybrid Scheme", AIAA Paper 90-3960, October 1990.

16. Baty, R. S., "Reynolds Stress Closure in Jet Flows using Instability Wave Modeling", Ph.D. Dissertation, The Pennsylvania State University, 1990.

17. Baty, R. S. and Morris, P. J., "Instability of Jets of Arbitrary Geometry", AIAA Paper 89-1796, June 1989.

18. Abramowitz, M. and Stegun, I. A., "Handbook of Mathematical Functions", New York, Dover, 1965.

19. McLachlan, N. W., "Theory and Application of Mathieu Functions", London, Oxford University Press, 1947.

20. Baty, R. S., Seiner, J. M., Ponton, M. K., "Instability of a Supersonic Shock-Free Elliptic Jet", AIAA Paper 90-3959, October 1990.

Discussion

QUESTION BY: H. Körner, DLR Braunschweig, Germany
You have solved the Euler-equation, is'nt it. There is no viscosity in your approach!?

AUTHOR'S RESPONSE:
Yes, the Euler-equations are used. The large scale structures are described by an inviscid analysis. As described in the paper, there is considerable experimental evidence that this assumption is valid when free shear flows are considered. This is because the structures are driven by a dynamic instability and their properties are nearly Reynolds number independent.

QUESTION BY: G. Winterfeld, DLR, Germany
The analysis shown has to rely strongly on information on the spreading rate of the jet, which is a function of the convective Mach number, besides other influences. Where do you take this information from? Do you rely entirely on experimental results?

AUTHOR'S RESPONSE:
For the calculations presented in this paper we have taken the spreading rate of the jet from an empirical curve. However, in a closely-related study by Morris, Giridharan and Lilley (1990) I have used the instability wave model to predict the development of the mean flow and, hence, its spreading rate. The results give very favourable agreement with experiments for a wide range of operating conditions. The calculations presented in Morris et al (1990) consider only subsonic convective Mach number conditions. Additional calculations by Viswanathan and Morris (1992) have included supersonic convective Mach number conditions.

References: Morris, P.J., Giridharan, M.G. and Lilley, G.M., "On the turbulent mixing in compressible free shear layers", Proc. Roy. Soc. London A, 431, 1990, pp. 219-243.

Viswanathan, K. and Morris, P.J., "Turbulent mixing in supersonic axisymmetric jets", accepted for publication, AIAA Journal, 1992.

QUESTION BY: Ph. Ramette, Dassault Aviation, France
Could you comment further on the fact that your model for the turbulence is inviscid?

AUTHOR'S RESPONSE:
As I answered in response to a previous question, the equations describing the evolution of the large scale structures are inviscid. However, the mean flow development in the jet must include viscous dissipation, as it is a turbulent flow. In our calculations for the mean flow development that I mentioned before [Morris et al (1990)] we have shown that the details of the process of energy transfer from the large to the small scales, and its eventual viscous dissipation, are unimportant to the evolution of the flow at the large scale. Thus, in the present calculations, the viscous effects are included implicity in the specification of the development of the mean flow.
For reference: see previous response

QUESTION BY: U. Michel, DLR Berlin, Germany
I should not be difficult to include flight speed in your analysis. This would be interesting. Do you have plans to include the flight effects?

AUTHOR'S RESPONSE:
At present, we are not planning to include the effects of forward flight. However, the extension of the present analysis to include these effects would be relatively straightforward. The outer solution would come from a convected wave equation and the inner solution would include appropriate outer boundary conditions. If necessary, it would be possible to include the effect of the initial wake region in the calculations. This would introduce additional instabilities. However, as long as these instabilities were convective in nature, and not absolute instabilities, the effects of the initial wake should be confined to the higher frequencies.
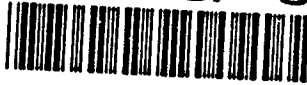
PREDICTION OF JET MIXING NOISE FOR HIGH SUBSONIC FLIGHT SPEEDS

Ulf Michel* and Jan Böttcher**

* Deutsche Forschungsanstalt für Luft- und Raumfahrt, e.V., DLR,
Institut für Experimentelle Strömungsmechanik, Abt. Turbulenzforschung,
Müller-Breslau-Str. 8, 1000 Berlin 12, Germany

** Deutsche Forschungsanstalt für Luft- und Raumfahrt, e.V., DLR,
Institut für Entwurfsaerodynamik, Abt. Technische Akustik,
Flughafen, 3300 Braunschweig, Germany

SUMMARY

A method for the prediction of single stream jet mixing noise in flight is presented that can be used for flight Mach numbers up to 0.9. The method is similar to the empirical SAE method. However, two important results of the theoretical scaling law of Michalke and Michel are incorporated: (i) the total noise of heated jets is separated into quadrupole and dipole noise components because they are influenced differently by the flight Mach number and, (ii) the influence of the stretching of the jet plume in flight on the overall sound pressure and the frequency of the emitted sound is considered. A relative velocity exponent law is used to correlate experimental flyover data. The correlation is based on all available data for combat aircraft with fuselage mounted engines and flight Mach numbers between 0.5 and 0.9. The difference between predictions with this new method and measured overall flyover levels is generally less than two decibels. The spectra are also well predicted.

LIST OF SYMBOLS

a_0	sound speed of the ambient air
D_j	fully expanded jet diameter
D_n	nozzle diameter
f	one-third octave center frequency
f_f	frequency of one-third octave spectrum in flight
f_s	frequency of one-third octave spectrum, static jet
F_d	density factor
M_f	flight Mach number, U_f/a_0
$OASPL_f$	overall sound pressure level for P_f
$OASPL_{iso}$	overall sound pressure level for P_{iso}
p_0	pressure of the ambient air
P_f	mean square sound pressure in far field of jet in flight
P_{f3}	P_f in a one-third octave band
P_s	mean square sound pressure in far field of static jet
P_{s3}	P_s in a one-third octave band
P_{iso}	P_s for jet with constant density
P_{ref}	P_{iso} for reference conditions.
p_{std}	standard pressure of ambient air, 101.3 kPa
P_{qq}	quadrupole contribution to mean square sound pressure
P_{qd}	quadrup.-dipole contrib. to mean square sound pressure
P_{dd}	dipole contribution to mean square sound pressure
r_0	wave normal distance from source
St	Strouhal number, $f D_j/(U_j-U_f)$
St_e	Strouhal number of equivalent static jet, (eq. 11)
St_x	adjusted Strouhal number, (eqs. 23, 24)
T_0	static temperature in the ambient air
T_{jt}	jet total temperature
U_c	convection speed of turbulent disturbances
U_e	jet speed of equivalent static jet
U_f	flight speed
U_j	jet speed
U_s	jet speed of static jet
γ	ratio of specific heats in air
ΔL_p	increase of overall sound pressure level due to σ
θ_0	emission angle relative to the negative jet axis
μ	normalized convection speed, $U_c/(U_j-U_f)$
ρ_j	jet density
ρ_0	density of ambient air
σ	jet stretching factor due to flight speed
σ_1	turbulence amplification factor due to flight speed
ξ	frequency adjustment factor of SAE method
ω	variable density index of SAE method

1. INTRODUCTION

Jet noise has been drastically reduced in modern transport aircraft through engines with low jet speeds. Unfortunately, jet speeds and jet temperatures of modern high performance military aircraft are very high and it may be concluded that jet noise is an important contribution to their noise emission. When these aircraft fly training missions at low altitudes, they create a severe community noise problem. Reliable prediction methods for jet noise in high-speed flight are necessary to study the influence of operational or design parameter changes on the noise emission. These methods would also help to assess the noise of currently considered new supersonic transport designs.

The noise emitted by jet aircraft consists of internal engine noise, airframe noise, and jet noise. Major internal engine noise sources are, e.g., fan, compressor, turbine, and the combustion process. Airframe noise is generated, e.g., by the aircraft's boundary layer and by protruding structures like stores and landing gears. Jet noise consists of jet mixing noise and shock-associated noise. Jet mixing noise is caused by the turbulent mixing process between the jet and its ambience. Shock-associated noise is additional jet noise that is generated when the jet is supersonic but the flow is not fully expanded in the engine's exhaust nozzle.

Jet mixing noise was first discussed theoretically by Lighthill [1]. He already discussed the influence of flight on radiated jet noise. Ffowcs Williams [2] and Ribner [3] took retarded time differences into account. The effects of flight were first discussed in a coordinate system fixed to the nozzle by Michalke and Michel [4]. This and assumptions about the influence of flight speed on the turbulent source field enabled the derivation of a scaling law for the influence of flight Mach number on the radiated jet noise for small flight Mach numbers. The density terms which are important for hot jets were also accounted for in ref. 4. According to this theory, an amplification of jet mixing noise due to flight speed for emission angles in the flight direction is compatible with jet noise. The scaling law was extended to the case of frequency spectra in ref. 5. Experimental evidence was presented in ref. 6 that the assumptions about the influence of flight speed on the turbulent source field were justified.

The prediction of jet mixing noise is usually carried out with the industry standard SAE method [7] or slight variations to better correlate with certain engine data. This empirical method was developed for jet conditions and flight speeds that are common during takeoff and landing of aircraft. However, the predictions with this method for high-speed flight yield too small levels and too small frequencies if compared to experimental data. It is sometimes concluded that jet noise is masked by other noise sources in high-speed flight.

The new method developed in this paper is based on the SAE method. However, two important improvements are introduced. The first relates to the influence of jet density on the overall sound pressure level which is considered empirically in the SAE method by a density correction term. It will be shown in section 2 that the density influence can alternatively be considered by separating the total noise into a quadrupole and a dipole component which eliminates the empirical variable density index ω of the SAE method. This separation is important because the flight effects are different for quadrupole and dipole terms [4,5,6].

The second improvement is the consideration of the jet stretching due to flight speed. This is discussed in section 3 in order to derive the important stretching factor σ which determines the increase of the length of the source region as well as the increase of the equally important coherence length scale. This factor also describes the frequency increase of jet mixing noise in flight.

The new prediction method is then presented in section 4. The idea of a relative velocity exponent of the SAE method is combined with the stretching factor σ. The relative velocity exponent is determined as a best fit to the experimental results that are discussed in more detail in the accompanying paper [8].

2. QUADRUPOLE AND DIPOLE CONTRIBUTION

The mean square sound pressure P_s in the far field of a jet without external flow can be derived from Michalke and Michel [4]:

$$P_s = (\gamma p_o)^2 \frac{(U_j/a_o)^4}{4\pi r_o^2/D_j^2} \times \quad (1)$$

$$\left\{ \left(\frac{\rho_i}{\rho_o}\frac{U_j}{a_o}\right)^2 P_{qq} + \frac{U_j}{a_o}\left|1 - \frac{\rho_i}{\rho_o}\right| P_{qd} + \left(1 - \frac{\rho_i}{\rho_o}\right)^2 P_{dd} \right\}$$

where U_j is the jet speed, a_o the ambient sound speed. ρ_i and ρ_o are the densities of the jet and the ambience, respectively. r_o is the (wave normal) distance from the source region, D_j is the fully expanded jet diameter. In addition to the parameters on the right hand side of eq. (1), P_s is also a function of the emission angle θ_o which is defined here relative to the negative jet axis. P_{qq}, P_{qd}, and P_{dd} are derived from the cross-correlations between the quadrupole source terms, the quadrupole and dipole source terms, and the dipole source terms, respectively. The three terms are functions of θ_o, T_j/T_o, and U_j/a_o. For $\rho_i/\rho_o = 1$, all but the first term in the braces vanish.

The corresponding formulation of the SAE method is

$$P_s = \frac{\pi D_j^2}{4r_o^2}\left[\frac{p_o}{p_{std}}\right]^2 P_{ref}(\frac{U_j}{a_o}, \theta_o)\left[\frac{\rho_i}{\rho_o}\right]^\omega. \quad (2)$$

where it is assumed that the density influence on the mean square sound pressure is fully contained in the last term of the equation with the variable density index ω. According to the SAE method, only the distribution of the mean square pressure in the frequency spectra is influenced by the ratio between the jet's total temperature T_{jt} and the ambient temperature T_o.

In order to compare eq. (1) with the SAE method, eq. (2), we write eq. (1) in a short form as follows

$$P_s(\theta_o) = P_{sq}(\theta_o) \left\{ \left[\frac{\rho_i}{\rho_o}\right]^2 + \frac{\left|1 - \frac{\rho_i}{\rho_o}\right|}{(U_j/a_o)}\frac{P_{qd}}{P_{qq}} + \frac{\left(1 - \frac{\rho_i}{\rho_o}\right)^2}{(U_j/a_o)^2}\frac{P_{dd}}{P_{qq}} \right\}. \quad (3)$$

The expression in braces would be equivalent to the density term of eq. (2) and P_{sq} would correspond to the remaining part of eq. (2). If we assume for simplicity, that quadrupole and dipole source terms are not correlated, $P_{qd}/P_{qq} = 0$, and that $P_{dd}/P_{qq} = 1$ (this value gives a good agreement to the density term of eq. (2) for heated jets), we can reformulate eq. (3) as follows:

$$P_s = \frac{\pi D_j^2}{4r_o^2}\left[\frac{p_o}{p_{std}}\right]^2 P_{ref}(\frac{U_j}{a_o}, \theta_o) F_d. \quad (4)$$

where the density factor F_d is given by

$$F_d = \left[\frac{\rho_i}{\rho_o}\right]^2 + \frac{\left[1 - \frac{\rho_i}{\rho_o}\right]^2}{(U_j/a_o)^2}. \quad (5)$$

This formulation eliminates the empirical variable density index ω. The first term on the right hand side of eq. (5) describes how the quadrupole contribution is reduced with decreasing jet density, the second term describes the corresponding increase of the dipole contribution. Note that the relative dipole contribution may become large for jet speeds small compared to the ambient sound speed. Small differences between ρ_i and ρ_o may be an explanation for the large scatter of jet noise test data for low jet speeds.

A comparison between the density term in eq. (2) and eq. (5) yields for the variable density index of the SAE method

$$\omega = 2 + \frac{\ln\left\{\frac{\left[1 - \frac{\rho_i}{\rho_o}\right]^2}{\left[\frac{\rho_i}{\rho_o}\frac{U_j}{a_o}\right]^2} + 1\right\}}{\ln\left[\frac{\rho_i}{\rho_o}\right]}. \quad (6)$$

It can be seen from this equation that ω is not only a function of U_j/a_o as it is assumed in the SAE method but also a function of the density ratio ρ_i/ρ_o. Results of eq. (6) are compared in figure 1 with the SAE values. It can be seen that the curves are similar only for density ratios ρ_i/ρ_o between 0.25 and 0.5. However, the results of eq. (6) are totally different for cold jets with $\rho_i/\rho_o > 1$. The reason is the different behavior of the two terms in eq. (5) for $\rho_i/\rho_o < 1$ and $\rho_i/\rho_o > 1$. For $\rho_i/\rho_o < 1$ an increase of the second term is accompanied by a decrease of the first term if $|\rho_i/\rho_o - 1|$ is increased. Contrary, for $\rho_i/\rho_o > 1$ both terms grow for increasing $|\rho_i/\rho_o - 1|$.
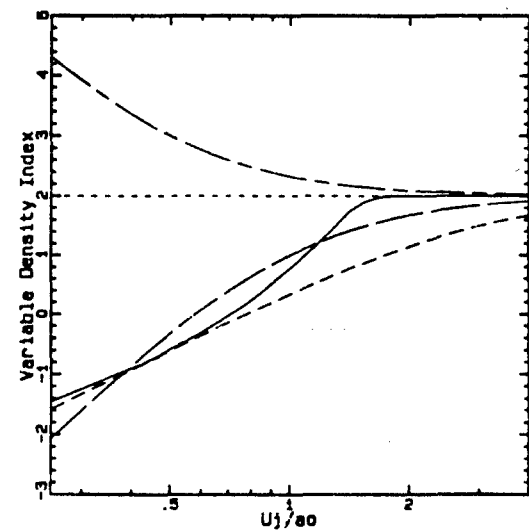
Figure 1: Influence of U_j/a_o and ρ_i/ρ_o on the variable density index ω according to eq. (6). (————) SAE: (— — — —) $\rho_i/\rho_o = 0.25$; (— — — —) $\rho_i/\rho_o = 0.5$; (- - - - -) $\rho_i/\rho_o = 1$; (— — — —) $\rho_i/\rho_o = 2$.

The overall sound pressure level of jet mixing noise according to eq. (2) (SAE) and eq. (4) (new method) is plotted in figure 2 for $\theta_o = 90$ degrees, $r_o = 100$ m, and a diameter of $D_n = 0.5$ m for a conical nozzle as a function of U_j/a_o for two different jet total temperature ratios $T_{jt}/T_o = 1$ and 2. The difference between eqs. (2) and (4) is seen to be small for typical conditions of a jet engine. The two thin straight lines indicate an U_j/a_o to the sixth and to the eighth power law, respectively. It can be seen that the gradient of the low speed part of the two curves for $T_{jt}/T_o = 1$ corresponds to an eighth power law which is the well known result for quadrupole noise whereas the gradient of the corresponding part of the curves for the heated jet is close to a sixth power law which indicates the dominance of the dipole terms.
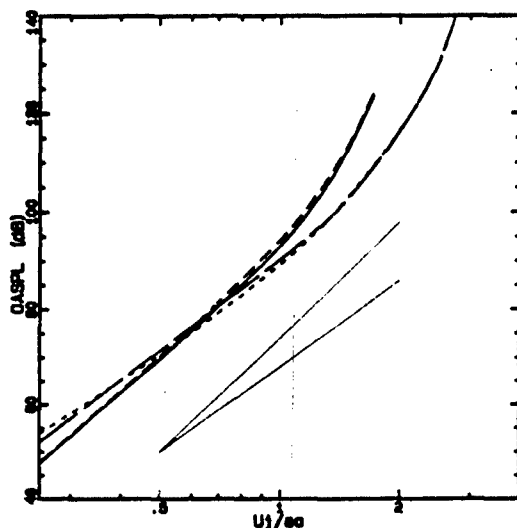
Figure 2: Influence of U_j/a_o and T_{jt}/T_o on the overall sound pressure level for an emission angle $\theta_o = 90$ deg. (————) eq. (2) (SAE), $T_{jt}/T_o = 1$; (— — — —) eq. (4), $T_{jt}/T_o = 1$; (—— —— ——) eq. (2) (SAE), $T_{jt}/T_o = 2$; (- - - - -) eq. (4) $T_{jt}/T_o = 2$;

It is known that the Doppler amplification due to flight speed is different for quadrupole and dipole sources [1,4]. It can be concluded from ref. 4 that the density factor of eq. (5) has to be evaluated in flight for a jet speed

$$U_e = (U_j - U_f)/(1 - M_f \cos \theta_o) \qquad (7)$$

which yields

$$F_d = \left[\frac{\rho_i}{\rho_o}\right]^2 + \left[\frac{\left[1 - \frac{\rho_i}{\rho_o}\right](1 - M_f \cos \theta_o)}{\frac{(U_j - U_f)}{a_o}}\right]^2 . \qquad (8)$$

This equation is evaluated in figure 3 for a jet with $U_j/a_o = 1.5$. The static case $M_f = 0$ and the flight case $M_f = 0.8$ are shown for the two density ratios $\rho_j/\rho_o = 0.5$ and 0.7. It can be seen that the relative dipole contribution is independent of flight Mach number in the studied cases for an angle of about $\theta_n = 50$ deg. The relative dipole contribution is reduced for smaller angles in the forward arc and considerably increased for larger angles in the rear arc. We conclude that the forward arc of an engine jet in high-speed flight is dominated by quadrupole noise terms even if dipole noise plays a role there in the static case and that it is likely be dominated by dipole noise in the rear arc.

The separation of the source terms of jet mixing noise into quadrupole and dipole terms was already proposed in the

scaling laws of Morfey et al. [10]. They assume that the two source terms have different basic spectra and directivities which explains a change of the frequency spectra of jet noise when the jet is heated.
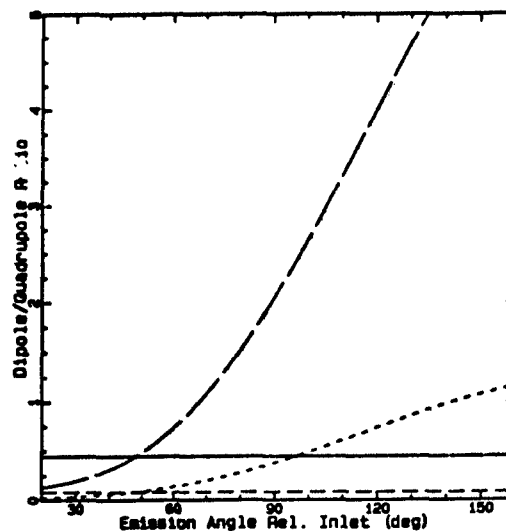
Figure 3: Influence of M_f and ρ_j/ρ_o on the ratio between dipole and quadrupole contribution to jet mixing noise versus emission angle θ_o for $U_j/a_o = 1.5$. (————) $M_f = 0$, $\rho_j/\rho_o = 0.5$; (— — — —) $M_f = 0$, $\rho_j/\rho_o = 0.7$; (—— —— ——) $M_f = 0.8$, $\rho_j/\rho_o = 0.5$; (- - - - -) $M_f = 0.8$, $\rho_j/\rho_o = 0.7$.

3. STRETCHING OF JET IN FLIGHT

Starting from the convective Lighthill equation, the mean square pressure fluctuations P_{f3} in a one-third octave band in the far field of a jet subjected to a flight Mach number M_f was found to be related to the corresponding value P_{s3} in a one-third octave band of an equivalent static jet [6],

$$P_{f3}(St, \frac{U_j}{a_o}, M_f) = \sigma_1 \sigma^2 (1 - M_f \cos \theta_o)^2 P_{s3}(St_e, \frac{U_s}{a_o}), \qquad (9)$$

where U_e is the jet speed of the equivalent static jet which is defined by eq. (7). St is the Strouhal number of the normalized center frequency f of the one-third octave band and is defined with the relative velocity $U_j - U_f$.

$$St = f D_j /(U_j - U_f) \qquad (10)$$

The Strouhal number St_e for which the equivalent static jet has to be evaluated is defined in refs. 5 and 6 by

$$St_e = \begin{cases} St/\sigma & \text{(WT)} \qquad (11a) \\ \dfrac{St(1 - M_f \cos \theta_o)}{\sigma} & \text{(FO)} \qquad (11b) \end{cases}$$

where WT indicates wind tunnel coordinates and FO flyover coordinates. The jet density ratio ρ_j/ρ_o, the normalized wave normal distance r_o/D_j, and the emission angle θ_o are identical for both sides of eq. (9). σ is a jet stretching factor which can be derived from theory. σ_1 is the only empirical factor which describes the increase of the normalized turbulence intensity in flight. A value of

$$\sigma_1 = \sqrt{\sigma} \qquad (12)$$

was proposed in ref. 6 as a result of pressure fluctuation measurements inside the jet's shear layer.

The stretching factor σ of refs. 5 and 6 is used here for the new prediction method. σ describes the stretching of the jet plume due to flight speed. This stretching also results in a reduced spread rate of the jet's shear layer. The situation is illustrated in figure 4. The static jet in the upper part of the figure has a jet speed U_j. The jet in the lower part is immersed in a flow with flight speed U_f and the relative jet speed is U_j-U_f. The external flight speed reduces the shear between the two streams and increases the convection speed U_c of the disturbances in the shear layer.

Static condition

Flight condition
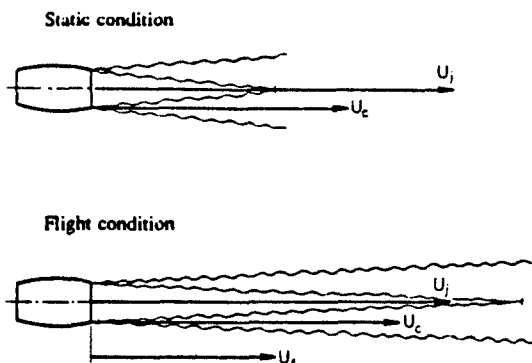
Figure 4: Illustration of the jet stretching due to flight speed.

The stretching factor is determined by the convection speed of the disturbances in the jet's shear layer. The normalized convection speed $\mu = U_c/(U_j$-$U_f)$ for the flight case of a circular jet with constant density is given by

$$\mu = \frac{U_c}{U_j - U_f} = \frac{U_f + 0.7 \, (U_j-U_f)}{U_j - U_f}. \tag{13}$$

The corresponding equation for a plane shear layer has the factor 0.7 replaced by 0.5 which means that in this case the convection speed is equal to the arithmetic mean of the speeds on the two sides of the shear layer. In a round jet, the convection speed is larger due to the self induction of the vorticity distribution in the circular shear layer.

The convection speed also depends on the jet's density. This is not yet considered here. However, it turned out that this influence had to be included in the prediction method for broadband shock noise of ref. 8, because the convection speed has an important influence on the frequency of broadband shock noise.

The stretching factor σ for a jet with constant density is given by the ratios of the relative convection speeds of the jet in flight to the static jet according to eq. (13). This ratio is given by

$$\sigma = \frac{\mu(U_f)}{\mu(0)} = \frac{[U_f + 0.7 \, (U_j-U_f)] \, / \, (U_j-U_f)}{0.7}$$

or

$$\sigma = 1 + 1.4 \, \frac{U_f}{U_j - U_f}. \tag{14}$$

The stretching factor σ is plotted as a function of flight Mach number for four different normalized jet speeds U_j/a_o in figure 5. The vertical axis on the right hand side is labeled with the influence of σ on the sound pressure level of jet mixing noise according to eq. (6). This influence can be described by

$$\Delta L_p = 25 \text{ dB } {}^{10}\!\log \sigma. \tag{15}$$

if eqs. (14) and (12) are inserted in eq. (9).

The influence of σ on the overall sound pressure level can be quite large. For $U_j/a_o = 1.5$ and $M_f = 0.8$ we have $\sigma = 2.6$ and $\Delta L_p = 10.4$ dB. Eq. (15) explains why a reduction of jet speed has a much larger influence on static jet mixing noise than on the noise in flight. In a take-off situation we have a flight Mach number $M_f = 0.25$. If jet speed is reduced from $U_j/a_o = 1.5$ to $U_j/a_o = 1.25$ the stretching factor σ increases from $\sigma = 1.28$ to $\sigma = 1.35$ and its influence according to eq. (15) increases from 2.7 dB to 3.3 dB by 0.6 dB which offsets part of the noise reduction gained by the smaller jet speed. This effect is much more dramatic during approaches with small engine power. A reduction of jet speed from $U_j/a_o = 1.0$ to $U_j/a_o = 0.6$ during an approach with $M_f = 0.25$ increases the stretching factor from $\sigma = 1.47$ to $\sigma = 2$ and ΔL_p is increased from $\Delta L_p = 4.2$ dB to $\Delta L_p = 7.5$ dB. The stretching factor becomes especially large for "engine idle" conditions. As a consequence, the measured noise of clean (no flaps, no gear) transport aircraft may still be dominated by jet mixing noise in these cases despite the low engine power (see e.g. the RB 211 data in Rawls [11]).
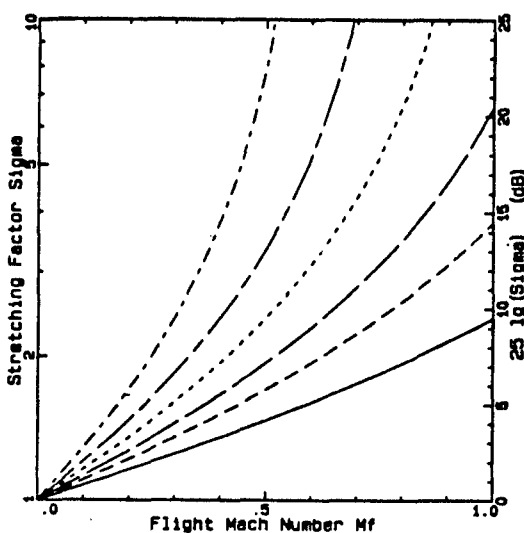
Figure 5: Influence of flight Mach number on the jet stretching factor σ and the increase ΔL_p of the overall sound pressure level according to ref. 6. (————) $U_j/a_o = 2$; (— — — —) $U_j/a_o = 1.5$; (— —— ——) $U_j/a_o = 1.25$; (- - - - -) $U_j/a_o = 1$; (——— —— ———) $U_j/a_o = 0.8$; (— — — —) $U_j/a_o = 0.6$.

Equally important as the effect of the stretching factor on the overall sound pressure level is its effect on an increase of the frequency of jet mixing noise. According to eq. (10) the frequency should become smaller in flight proportional to the reduction of relative jet speed U_j-U_f for constant Strouhal number St. This is assumed by the SAE method. However, the Strouhal number is increased in flight proportional to the stretching factor σ according to eq. (11). The ratio between the frequency f_f in flight to the frequency f_s of the static jet is then given for wind tunnel (WT) and flyover coordinates (FO) by the relation

$$f_f/f_s = \begin{cases} \sigma \, (U_j\text{-}U_f)/U_j & \text{(WT)} \quad (16a) \\ \sigma \, (U_j\text{-}U_f)/[\, U_j(1 - M_f \cos \theta_o)] & \text{(FO)} \quad (16b) \end{cases}$$

This equation is evaluated in figure 6 for six values of U_j/a_o yielding the six lines that indicate a slight increase of the frequency with increasing flight Mach number. The lines

that express a reduction of the frequency in flight are calculated with $\sigma = 1$ which is equivalent to the assumptions made in the SAE method.

The increase of frequency in flight shown in figure 6 is a consequence of the stretching factor σ in eq. (16). For a high performance aircraft with an assumed normalized jet speed of $U_j/a_o = 1.5$ and a flight Mach number $M_f = 0.8$ the frequency is increased by a factor of 1.21 rather than being reduced by a factor of 0.47 according to the SAE method. The effect is even larger for a civil transport aircraft cruising with $U_j/a_o = 1.1$ and a typical cruise Mach number $M_f = 0.84$. In this case the frequency is increased by a factor of 1.3 rather than being reduced by a factor of 0.24. This explains the surprisingly high frequencies observed in these cases and no recourse to nonlinear effects in long range sound transmission needs to be made.
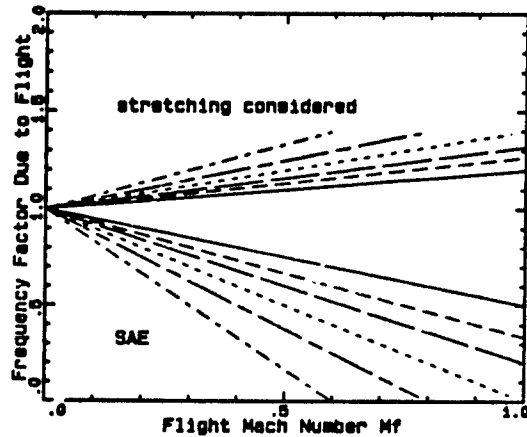
Figure 6: Influence of flight Mach number on the ratio f_f/f_s of the frequencies in flight and in the static case. (windtunnel coordinates or $\theta_o = 90$ deg for flyover coordinates).
(————) $U_j/a_o = 2$; (— — —) $U_j/a_o = 1.5$;
(— — —) $U_j/a_o = 1.25$; (· · · ·) $U_j/a_o = 1$;
(— — — —) $U_j/a_o = 0.8$; (— — —) $U_j/a_o = 0.6$. For the falling curves it is assumed that the frequency is reduced proportional to the relative jet speed U_j-U_f, the rising curves include the effect of the jet stretching factor.

4. PREDICTION METHOD FOR JET MIXING NOISE

A new prediction method for jet mixing noise can be derived if the theoretical results of the two previous sections are introduced into the SAE method [7]. Experimental data from high speed flyover tests with four different aircraft [8] are used to determine a best fit for a new distribution of the relative velocity exponent of this method.

The mean square sound pressure P_f of jet mixing noise in flight is described by

$$P_f(\frac{U_j}{a_o},M_f) = \frac{\pi D_j^2}{4r_o^2}\left[\frac{\rho_o}{p_{std}}\right]^2 P_{ref}(\frac{U_s}{a_o})$$
$$\sigma_1 \sigma^2 (1 - M_f \cos \theta_o)^2 F_d(U_e,\rho_j/\rho_o). \qquad (17)$$

where eq. (9) was utilized for the whole frequency band and P_s expressed by eq. (4). U_e is defined by eq. (7). F_d is defined by eq. (5) and has to be evaluated for a jet speed U_e which leads to eq. (8). To enable a correlation with experimental data an empirical relative velocity exponent law is used to express

$$P_{ref}(\frac{U_s}{a_o},\theta_o) = P_{ref}(\frac{U_j}{a_o},\theta_o) \left[\frac{U_j - U_f}{U_j}\right]^m \left[\frac{1}{(1 - M_f \cos \theta_o)}\right]^n \quad (18)$$

where n and m have to be determined empirically. n could be chosen identical to m but we arbitrarily used n = 5 here, a value that made certain that the relative velocity exponent m satisfied the physical condition to be positive for all emission angles θ_o. The resulting Doppler factor exponent of eqs. (17) and (18) is n - 2 = 3. The turbulence intensity factor was set $\sigma_1 = 1$ which means that the effect of rising normalized turbulence intensity in flight has to be included in m. This yields the final prediction formula

$$P_f(\frac{U_j}{a_o},M_f) = P_{ref}(\frac{U_j}{a_o})$$
$$\left\{\left[\frac{\rho_j}{\rho_o}\right]^2 + \left[\frac{1 - \frac{\rho_j}{\rho_o}}{\frac{(U_j - U_f)}{a_o}}(1 - M_f \cos \theta_o)\right]^2\right\}$$
$$\left[\frac{U_j - U_f}{U_j}\right]^m (1 - M_f \cos \theta_o)^{-3} \sigma^2. \qquad (19)$$

The mean square pressure of jet mixing noise of a jet with constant density is given by

$$P_{ref}(\frac{U_j}{a_o}) = \frac{\pi D_j^2}{4r_o^2}\left[\frac{r_o}{p_{std}}\right]^2 P_{ref}(\frac{U_j}{a_o}) \qquad (20)$$

and can be calculated with the SAE method. The relative velocity exponent m in eq. (19) is determined as a function of U_j/a_o and θ_o from the experimental data that are reported in ref. 8. Data from four different aircraft with flight Mach numbers between $M_f = 0.5$ and 0.9 were utilized. The engines of these aircraft were fuselage mounted. Contributions of broadband shock-associated noise have been eliminated from the data by using a method that is based on Tam [9] but contains some physically justified modifications. All required formulas are presented in the appendix.

The difference between the overall sound pressure levels computed with these formulas and the underlying data is generally smaller than 2 dB.

The ratio between the mean square pressure in a one-third octave band to the overall mean square pressure is defined according to refs. 5 and 6 by

$$P_{f3}(St,\frac{U_j}{a_o},M_f)/P_f(\frac{U_j}{a_o},M_f) = P_{s3}(St_s,\frac{U_s}{a_o})/P_s(\frac{U_s}{a_o}) \qquad (21)$$

where St_s is given by eq. (11) and U_e by eq. (7). The corresponding relation used by the SAE method is

$$P_{f3}(St,\frac{U_j}{a_o},M_f)/P_f(\frac{U_j}{a_o},M_f) = P_{s3}(St_x,\frac{U_j}{a_o})/P_s(\frac{U_j}{a_o}), \qquad (22)$$

where the adjusted Strouhal number St_x is defined by

$$St_x = \begin{cases} \frac{f D_j}{\xi (U_j - U_f)} & (WT) \quad (23a) \\ \frac{f D_j (1 - M_f \cos \theta_o)}{\xi (U_j - U_f)} & (FO) \quad (23b) \end{cases}$$

ξ is called the Strouhal frequency adjustment factor in the SAE method and is a function of U_j/a_o and θ_o. It has to be calculated for U_j/a_o (and not for $U_j/a_o \cdot M_f$) in the flight case.

Eq. (22) is used in the new prediction method. However, the adjusted Strouhal number is determined by the equation

$$St_x = \begin{cases} \frac{f D_j}{\sigma \xi (U_j - U_f)} & (WT) \quad (24a) \\ \frac{f D_j (1 - M_f \cos \theta_o)}{\sigma \xi (U_j - U_f)} & (FO) \quad (24b) \end{cases}$$

which differs from eq. (23) by the stretching factor σ.

The shape of the frequency spectra and their maxima are predicted very well with this formula for all emission angles θ_o that were available for comparison with data (see ref. 8).

Figure 7 demonstrates how poorly the SAE method compares with the results of the new method. The overall sound pressure level of jet mixing noise is plotted for a hypothetical aircraft as a function of emission angle θ_o relative to the negative jet axis on a sideline. Normalized jet speed is $U_j/a_o = 1.5$, jet total temperature ratio is $T_{jt}/T_o = 2$, and flight Mach number $M_f = 0.8$ in an ambient condition $p_0 = 101.3$ kPa, $T_0 = 288.15$ K. The fully expanded jet diameter is $D_j = 0.5$ m and the sideline distance 100 m. Atmospheric absorption and ground interference are not considered. The directivity of the static jet ($M_f = 0$, calculated with the SAE method) exhibits the typical peak of jet mixing noise in the rear arc. The other two directivities are computed for $M_f = 0.8$. The curve for the new method exhibits a strong amplification in the forward arc. The predicted levels of the SAE method are lower.
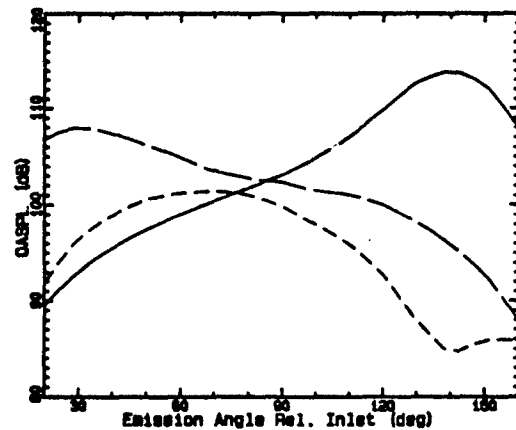
Figure 7: Overall sound pressure levels of a jet for a sideline distance 100 m as a function of emission angle θ_o relative to the negative jet axis. $U_j/a_o = 1.5$, $T_{jt}/T_o = 2$, $D_j = 0.5$ m. (———) $M_f = 0$, SAE method; (— — —) $M_f = 0.8$, SAE method; (—— ——) $M_f = 0.8$, new method.

The most important result of the new method is the considerable amplification due to flight in the forward arc which amounts to 15 dB relative to the static condition for an emission angle of 30 degrees in the studied case. Flight speed has no influence on the overall sound pressure level at 85 degrees. The reduction in the rear arc at 150 degrees is 20 dB. The sound levels predicted with the widely used empirical SAE method are much lower. The SAE prediction comes closest for emission angles between 70 at 90 degrees with a difference of only about 2 dB in this special case. However, the differences rise to values of 11 dB at 140 degrees in the rear arc and to 15 dB at 20 degrees in the forward arc.

Figure 8 presents the corresponding one-third octave spectra for an emission angle of 90 degrees. The peak frequency of the static jet noise spectrum according to the SAE method is about 580 Hz. The SAE method predicts for the flight condition a reduction of the peak frequency to about 270 Hz which is a result of the assumption that the frequency is proportional to the relative speed between the jet and its ambience. The peak frequency of the new method is 2.6 times larger close to 700 Hz. This increase of emitted frequency in flight is related to the corresponding increase of source frequency due to the stretching of the jet plume in flight. The good agreement between the flyover spectra predicted with the new method for $\theta_o = 90$ degrees and the measured spectra for all cases is evidence for the validity of this assumption since no empirical adjustment had to be used.
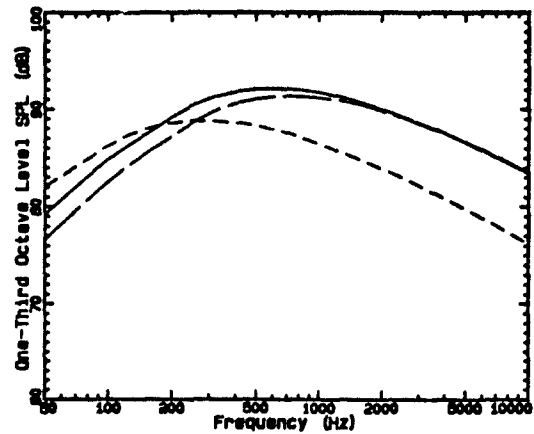
Figure 8: One-third octave spectra of a jet for an emission angle $\theta_o = 90$ deg and a sideline distance of 100 m in flyover coordinates. $U_j/a_o = 1.5$, $T_{jt}/T_o = 2$, $D_j = 0.5$ m. (———) $M_f = 0$, SAE method; (— — —) $M_f = 0.8$, SAE method; (—— ——) $M_f = 0.8$, new method.

Figure 9 displays the corresponding one-third octave spectra for an emission angle of 30 degrees in the forward arc. The peak frequency of the static jet noise spectrum does not change between $\theta_o = 90$ degrees and $\theta_o = 30$ degrees according to the SAE method. The SAE method predicts for the flight condition a slight increase of the peak frequency to about 880 Hz which is a result of the Doppler frequency shift in flight. The peak frequency of the new method is 2.6 times larger close to 2300 Hz. The good agreement with the flyover data for all emission angles indicates that the Doppler frequency shift is correctly described by eq. (24b).
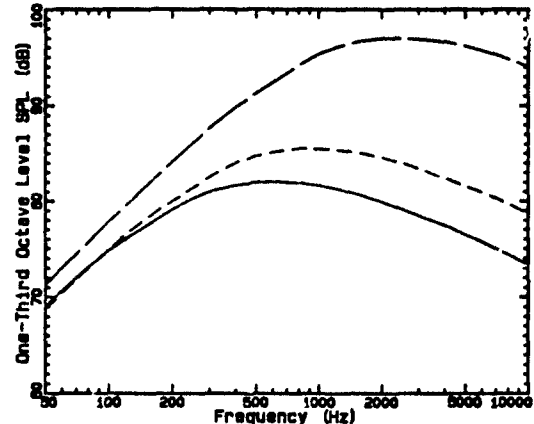
Figure 9: One-third octave spectra of a jet for an emission angle $\theta_o = 30$ deg and a sideline distance of 100 m in flyover coordinates. $U_j/a_o = 1.5$, $T_{jt}/T_o = 2$, $D_j = 0.5$ m. (———) $M_f = 0$, SAE method; (— — —) $M_f = 0.8$, SAE method; (—— ——) $M_f = 0.8$, new method.

The situation during takeoff and landing may be described by a typical flight Mach number $M_f = 0.25$. This case is studied in the following figures. The overall sound pressure level for a sideline distance of 100 m is plotted in figure 10 as a function of emission angle θ_o. The directivity for the static jet is identical to the one in figure 7. The SAE method predicts slightly lower levels than the new prediction method.
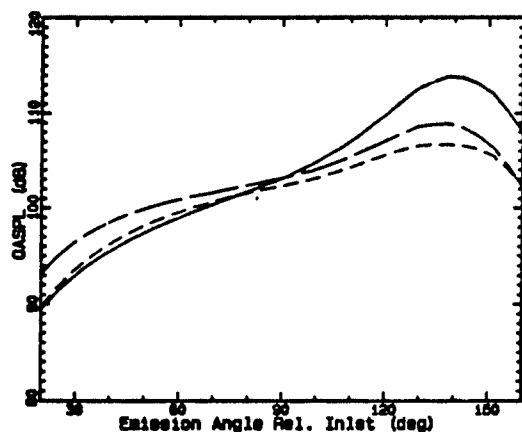
Figure 10: Overall sound pressure levels of a jet for a sideline distance 100 m as a function of emission angle θ_o relative to the negative jet axis. $U_j/a_o = 1.5$, $T_{ji}/T_o = 2$, $D_j = 0.5$ m. (———) $M_f = 0$, SAE method; (— — —) $M_f = 0.25$, SAE method; (— — — —) $M_f = 0.25$, new method.

This agrees with the experience that the SAE method produces an average underprediction of one to two dB [7].

The corresponding spectra are plotted in the next figures. Figure 11 shows for $\theta_o = 90$ degrees that the frequencies predicted by the SAE method are reduced if compared to the static spectrum while they are slightly increased with the new method due to the influence of the stretching factor $\sigma = 1.28$. Figure 12 is the corresponding plot for $\theta_o = 30$.
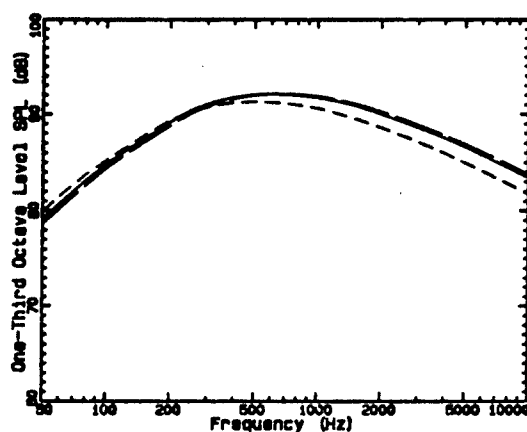
Figure 11: One-third octave spectra of a jet for an emission angle $\theta_o = 90$ deg and a sideline distance of 100 m in flyover coordinates. $U_j/a_o = 1.5$, $T_{ji}/T_o = 2$, $D_j = 0.5$ m. (———) $M_f = 0$, SAE method; (— — —) $M_f = 0.25$, SAE method; (— — — —) $M_f = 0.25$, new method.

CONCLUSIONS

The good agreement between the measured sound pressure levels (see ref. 8) and predictions with the new method can be regarded as a proof for the validity of the aerodynamic source model of Michalke and Michel [4,5,6] which considers quadrupole and dipole noise sources and a stretching of the source region in flight. No "excess noise" is required to explain the differences between measurements and
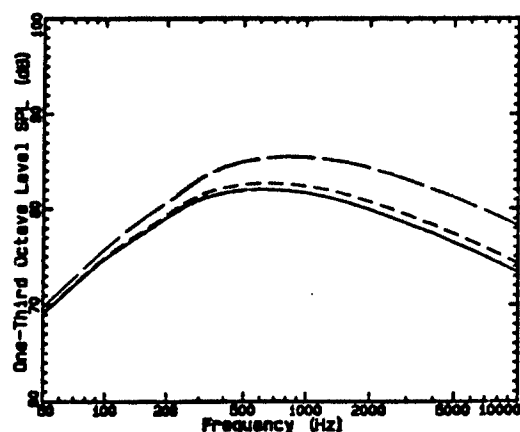
Figure 12: One-third octave spectra of a jet for an emission angle $\theta_o = 30$ deg and a sideline distance of 100 m in flyover coordinates. $U_j/a_o = 1.5$, $T_{ji}/T_o = 2$, $D_j = 0.5$ m. (———) $M_f = 0$, SAE method; (— — —) $M_f = 0.25$, SAE method; (— — — —) $M_f = 0.25$, new method.

predictions. The scaling law of Michalke and Michel for the effect of flight speed on jet mixing noise was derived by considering a source distribution in a frame of reference that was fixed to the nozzle. Nevertheless, the motion of the aeroacoustic sources was considered in the retarded time differences by assuming a constant convection speed U_c. The following two conclusions can be drawn from this source model.

(i) The source frequency is increased proportional to the stretching factor σ and reduced proportional to the relative jet speed U_j-U_f.

(ii) The stretching factor σ plays a role for the increase of the source volume and the coherence length scale resulting in the sound power being proportional to σ^2.

The observed changes of the measured frequencies due to flight agree with conclusion (i). The observed increase of sound power is even higher than that described by conclusion (ii). The remaining difference was described by Michalke and Michel through a turbulence intensity factor σ_1.

In contrast, scaling methods that discuss source frequency in a frame of reference fixed to the observer [2,7] result in the following conclusions.

(i) The source frequency is only a function of relative jet speed U_j-U_f and is not increased proportional to the stretching factor.

(ii) The stretching factor plays a role only for the increase of the source volume and not for the coherence length scale resulting in the sound power being proportional to σ rather than σ^2.

None of these results have been found in the experimental data.

The new method is easy to implement. The modeling may still be improved with the availability of more flyover data. The following improvements may be possible.

(i) The inclusion of the turbulence intensity factor σ_1 which could even be defined to include the influence of installation effects on the normalized turbulence intensity in the jet. E.g., the turbulence intensity inside a jet that is surrounded by a thick boundary layer at the end of an aircraft's fuselage is likely larger than if the same jet

emanates from a nozzle in an engine pod mounted under a wing.

(ii) The choice of n = m in eq. (18) which would be more consistent with ref. 4.

(iii) The consideration of the influence of jet density on convection speed and stretching factor σ.

(iv) The use of the relative jet speed U_j-U_f rather than U_j for the calculation of ξ in eq. (24) if the SAE method is used as a static method.

(v) The use of the static temperature in the jet rather than the total temperature to describe the influence of jet speed and temperature on the frequency spectra if the SAE method is used as a static method.

REFERENCES

1. Lighthill, M.J., "On Sound Generated Aerodynamically", Proceedings of the Royal Society London A211, 1952, 564-587.

2. Ffowcs Williams, J.E., "The Noise from Turbulence Convected at High Speeds", Philosophical Transactions of the Royal Society A225, 1963, 469-503.

3. Ribner, H.S., "The Generation of sound by Turbulent Jets", Advances in Applied Mechanics 8, 1964, 103-182.

4. Michalke, A. and Michel, U., "Prediction of Jet-Noise in Flight from Static Tests", Journal of Sound and Vibration 67, 1979, 341-367.

5. Michel, U. and Michalke, A. "Prediction of Flyover Jet Noise Spectra From Static Tests", NASA Technical Memorandum 83219, December 1981.

6. Michel, U. and Michalke, A. "Prediction of Flyover Jet Noise Spectra", AIAA 7th Aeroacoustics Conference, October 1981, AIAA-81-2025.

7. Anon. "Gas Turbine Jet Exhaust Noise Prediction", Society of Automotive Engineers, Aerospace Recommended Practice, SAE ARP 867C, 1985.

8. Böttcher, J. and Michel, U., "Comparison of Flyover Noise Data from Aircraft at High Subsonic flight speeds with Prediction", Proceedings of the AGARD 78th-B Specialists' Meeting of the Propulsion and Energetics Panel on Combat Aircraft Noise, Bonn, 23-25 October 1991.

9. Tam, C., "Forward Flight Effects on Broadband Shock Associated Noise of Supersonic Jets", AIAA-89-1088, 1989.

10. Morfey, C.L., Szewczyk, V.M., and Tester, B.J., "New Scaling Laws for Hot and Cold Mixing Noise Based on a Geometric Acoustics Model", J. of Sound and Vibration, 61, 1978, 255-292.

11. Rawls, J.W., "Comparison of Forward Flight Effects Theory of A. Michalke and U. Michel with Measured Data", NASA Contractor Report 3665, 1983.

APPENDIX: PREDICTION FORMULAS

The following input parameters are required: U_j, U_f, T_{jt}, p_o, T_o, r_o, D_j.

Step 1: Compute overall sound pressure level $OASPL_{iso}$ for a static jet with constant density for the jet speed U_j and the fully expanded jet diameter D_j with the SAE method (appendix A of ref. 7).

Step 2: Determine relative velocity exponent m as a function of U_j/a_o and θ_o through interpolation of the following values. Each vector of the following table contains values for m for $\theta_o = 20$ degrees to $\theta_o = 160$ degrees in steps of 10 degrees.

$U_j/a_o = 1.1$:
m = 2.0, 2.1, 2.2, 2.3, 2.4, 2.5, 2.6, 2.9, 3.3, 4.0, 4.7, 5.7, 6.3, 7.0, 7.0

$U_j/a_o = 1.18$:
m = 2.1, 2.2, 2.3, 2.4, 2.5, 2.6, 2.7, 2.9, 3.4, 4.1, 5.0, 6.0, 7.0, 7.5, 7.4

$U_j/a_o = 1.33$:
m = 2.7, 2.7, 2.8, 2.8, 2.8, 2.8, 3.1, 3.4, 3.6, 4.1, 4.8, 5.9, 7.0, 7.7, 7.7

$U_j/a_o = 1.47$:
m = 2.7, 2.6, 2.7, 2.8, 2.9, 3.1, 3.2, 3.3, 3.8, 4.2, 5.2, 6.4, 7.3, 7.7, 7.7

$U_j/a_o = 1.62$:
m = 2.8, 2.7, 2.7, 2.8, 3.1, 3.3, 3.3, 3.4, 3.5, 4.2, 4.9, 6.4, 7.5, 7.8, 7.9

$U_j/a_o = 1.77$:
m = 3.0, 2.8, 2.8, 2.8, 3.2, 3.4, 3.6, 3.6, 4.0, 4.6, 6.0, 7.0, 7.6, 8.1, 8.1

$U_j/a_o = 1.95$:
m = 3.7, 3.4, 3.2, 3.4, 3.6, 3.7, 4.0, 4.4, 4.6, 5.5, 7.2, 8.8, 9.8, 9.7, 9.3

$U_j/a_o = 2.20$:
m = 5.1, 4.6, 4.3, 4.1, 4.0, 4.1, 4.5, 4.8, 5.5, 6.8, 8.9, 10.9, 11.7, 11.5, 11.0

Step 3: Determine stretching factor σ

$$\sigma = 1 + 1.4\, U_f/(U_j - U_f)$$

Step 4: Compute overall sound pressure level $OASPL_f$ in dB by using the following relation:

$$OASPL_f = OASPL_{iso}$$

$$+ 10\,{}^{10}\!\log\left\{\left[\left(\frac{\rho_i}{\rho_o}\right)^2 + \left(\left|1 - \frac{\rho_i}{\rho_o}\right| \frac{(1 - M_f \cos\theta_o)}{\frac{(U_j - U_f)}{a_o}}\right)^2\right]\right\}$$

$$- 10\, m\, {}^{10}\!\log\left[\frac{U_j}{U_j - U_f}\right]$$

$$- 30\, {}^{10}\!\log\,(1 - M_f \cos\theta_o)$$

$$+ 20\, {}^{10}\!\log\,\sigma$$

Step 5: Determine the Strouhal frequency adjustment factor ξ for a normalized jet speed U_j/a_o and θ_o with the SAE method.

Step 6: Evaluate the relative sound pressure level SPL - $OASPL_f$ in a one-third octave band with the SAE method for a static jet with normalized jet speed U_j/a_o, jet total temperature ratio T_{jt}/T_o for an adjusted Strouhal number

$$St_a = \begin{cases} \dfrac{f\, D_j}{\sigma\, \xi\, (U_j - U_f)} & \text{(WT)} \\[2mm] \dfrac{f\, D_j\, (1 - M_f \cos\theta_o)}{\sigma\, \xi\, (U_j - U_f)} & \text{(FO)} \end{cases}$$

where WT is valid for the wind tunnel situation and FO for the flyover situation.

Discussion

QUESTION BY: L.W. Illston, BAe, UK
                      Are there any other limitations in terms of jet speed or jet Mach number, to the use of the prediction formulae?

AUTHOR'S RESPONSE:
                      The scaling law by Michalke and Michel (which is the basis of our prediction scheme) enables the scaling of a jet in flight to other jets in flight with different flight speeds or to an equivalent static jet. There is no limit in this theory concerning the jet speed or jet Mach number but the scaling law is limited to small variations of flight Mach numbers between the jets to be scaled. There is a rising source interference error if this condition is not met, which means that a jet with a high flight Mach number cannot be scaled precisely to a static jet. The empirical m-factor was introduced in our paper to overcome this problem. The m-factor was empirically found to be a function of jet speed but it may also be a function of jet temperature. The m-factors reported in this paper are valid for the range of jet speeds, jet temperatures, and flight speeds covered in the low-level flights. They are likely to change for exotic cases with very high jet speeds or very high jet temperatures.

QUESTION BY: W.D. Bryce, RAE, UK

1. The theory that you have described is for pure jet mixing noise in flight. But all the comparisons that I have seen between your theory and experimental measurements use **engine** noise data which can easily be contaminated with other noise sources and with installation effects. Have you compared theoretical results with jet noise measurements obtained from 'clean' model-scale jets?

2. You have previously applied this theory to civil engine noise at flight Mach numbers up 0.3. What changes have you made to your theory to enable it to be used at higher Mach numbers?

AUTHOR'S RESPONSE:

1. Unfortunately I have not yet compared the theory with laboratory data, e.g. those you gave me. You are right. The comparisons made so far are for published engine data. In these cases, the scaling was done between different flight cases which presumably are subject to the same installation effects.

2. In the previous studies, we used the scaling law (e.g. eq. 17) and looked up the static jet data for the correct effective jet speed Ue. The changes made now are, that we use eq. (19) with an empirical exponent m to be able to use a static jet with jet speed Uj rather than Ue. In addition, we used the separation into quadrupole and dipole noise (braces in eq. (19)) to be able to refer to an isothermal static jet.

IDENTIFYING THE PRINCIPAL NOISE SOURCES OF FIXED-WING COMBAT AIRCRAFT IN HIGH-SPEED FLIGHT

by

W.D. Bryce and R.A. Pinker
DRA Aerospace Division
RAE
Pyestock, Farnborough
Hampshire GU14 0LS
United Kingdom

P.J.R. Strange
Rolls-Royce plc
Derby
United Kingdom

92-17430

ABSTRACT

Before considering means for alleviating the noise from modern military combat aircraft operating in high-speed low-level flight, it is important to identify the principal noise sources. To this end, a carefully-controlled flight test programme has been carried out using a Tornado aircraft (in standard training configuration) operating at flight speeds from 0.5M to 0.8M. The major sources of the aircraft noise, airframe noise, installed jet mixing noise and jet shock noise, have been successfully identified, quantified and correlated.

Although the jet mixing noise tends to be the major source at low flight speeds, and the shock noise at high flight speeds, all three sources are comparable in magnitude during the rapid rise-time of the noise signal and at its peak. Indeed, were it possible to reduce greatly both the jet mixing and shock noise, the peak noise levels would only reduce by about 5 dBA.

1 INTRODUCTION

During training, the noise from military combat aircraft flying at high subsonic speed close to the ground can be a considerable nuisance to the people near the flight path. As a first step towards considering what might be done to quieten such aircraft, it is necessary to know the sources of the noise which are contributing to the problem. That is, we require to be able to identify and quantify the principal noise sources of the aircraft. For this purpose, a carefully-controlled flight programme has been carried out on a Tornado aircraft, measuring its noise over a range of engine conditions and flight speeds. The purpose of this paper is to analyse and correlate this data so as to be able to quantify the levels of the various aircraft noise sources which appear - initially in terms of overall sound pressure level (OASPL) and then, having correlated the spectra, in subjective noise units (dBA). It is intended that the source modelling should be sufficiently general to enable the individual noise sources of the Tornado aircraft (in the one configuration tested) to be predicted over a wide range of operating conditions.

While a knowledge of the aircraft noise sources will inevitably lead to considering the effect of their reduction, it should be made clear that it is not possible to describe, in a justifiable manner, the likely social impact of any possible noise changes, because of the lack of a suitable subjective noise unit to express the disturbance caused by the type of noise under study here. For aircraft flying at high speed at low level, the noise experienced on the ground close to the aircraft track is not like that of a civil aircraft (which can be assessed using established subjective noise units such as the dBA unit used here), but sounds explosive in its initial impact. This leads to a "startle" effect which would be expected to be related not only to the peak noise level but also to the suddenness of its imposition. There is, as yet, no means for quantifying human reactions to such noise.

2 NOMENCLATURE

A_j	nozzle area
c	ambient speed of sound
D	directivity function
f	frequency
H	minimum distance during linear flyover
M	Mach number
m, n	exponents
$OASPL_{norm}$	normalised overall sound pressured level (dB)
$OASPL_{meas}$	measured overall sound pressure level (dB)
PR	nozzle pressure ratio
V	velocity
β	shock noise parameter $\left(M_j^2 - 1\right)^{\frac{1}{2}}$
$\varphi_c, \varphi_p, \varphi_e$	aircraft climb, pitch and engine angles
λ	ratio of flight to jet velocity
θ	noise emission angle (deg)
θ_e	wind-corrected noise emission angle (deg)

Suffices

a	airframe
g	ground
j	jet
o	ambient or reference
w	wind

3 THE FLIGHT TEST PROGRAMME

Similar flight tests were actually carried out for two aircraft, a Tornado and a Hawk, but it is only the data from the former aircraft which is being studied here.

The noise measurements were made with the aircraft flying over an array of ground microphones at a nominal overhead height of 450 m. Although it is the noise from low-level flights that pose the main environmental problem, taking the noise measurements under such conditions would pose several technical difficulties for little technical advantage. Accurate tracking of the aircraft would be difficult, the noise signals would have to be analysed at high sampling rates, and the engine conditions would have to be kept close to those required for level flight. On the other hand, noise data taken at a greater height can easily be converted to that at any other height by calculation. The only penalty which is known to be incurred arises from the proportionately greater effects of atmospheric propagation on the noise signal. Height effects are examined further in the next section.

The structure of the test programme was designed to be able to quantify the expected noise sources as follows. The noise from the aircraft airframe was to be determined from aircraft glide data, with the engines at flight idle. Then, from flyover data with the engines operating at high subcritical jet conditions, it should be possible to quantify the jet mixing noise from the engines after making appropriate allowances for the known airframe noise. Then, finally, knowing these two sources, the shock noise from the jet exhaust could be obtained from flyovers with the engines operating at high super-critical jet conditions.

Hence, the aircraft was flown over a matrix of test conditions, covering flight Mach numbers from 0.5 to 0.8, and engine powers from idle to maximum dry. The aircraft was maintained in a stable condition during the noise measurements by allowing it to ascend or descend through the 450 m overhead position as required. Some flight data was recorded at 75 m altitude for reference.

The RAE(B) Tornado aircraft was flown in only one configuration with a standard training fit (two inboard tanks, two outboard pods and two loaded practise bomb carriers on shoulder pylons) with the wing swept 45°, zero flaps and under-carriage up.

The flight programme was carried out during October and November 1989 at RAE Bedford. The noise measurements were made using an array of ground microphones, each installation consisting of a half-inch Bruel & Kjaer type 4134 microphone inverted 7 mm above a point at three-quarters of the radius of a 40 cm diameter steel disc set flush with the surrounding grassland. The noise data was acquired from the ground-level microphone array using the Rolls-Royce 'Kabmobile' mobile laboratory which is equipped with a 32-channel data acquisition system, weather monitoring equipment and RF communications equipment. The wind speed and direction were measured at 10 m above ground level while temperature and dewpoint measurements were measured at 2 m height. After conditioning, the noise signals were recorded on a SE8000A tape recorder configured for 15ips WB1 FM operation. The aircraft tracking was carried out using the Rolls-Royce electro-optical photographic tracking system Mk II. A time-base for both the tracking and the noise data was provided from MSF Rugby standard time. This reference was also used in the Tornado MODAS on-board recording system which, after analysis at RAE Bedford, was used to provide aircraft attitude and engine data. RB199 engine performance syntheses, to provide the engine jet conditions, were carried out by Rolls-Royce (Bristol) based on the flight-recorder information.

4 COMPARISON OF HIGH AND LOW-LEVEL DATA

Carrying out a test programme on low-level flying at a height of 450 m is a feature in the design of the present programme which is often queried. There was, however, no known reason to doubt the validity of the arguments given earlier for preferring this action. Nevertheless, it was considered prudent to take and analyse noise measurements from some flights at 75 m to expose the issue further.

From the flights at 75 m which were successfully tracked, Figs 1 and 2 show noise time histories corrected to reference atmospheric conditions compared with data scaled from 450 m flights. The noise signal sampling times were 0.2 and 0.5 s respectively. These are the only comparisons for which the flight speeds, engine conditions and wind speeds are similar. The high-altitude data shows greater short-term variations, particularly at the extremities of the time histories, as would be expected from greater atmospheric propagation distances and a proportionately shorter sampling time. (Such fluctuations are removed in the subsequent analyses by smoothing the field-shape data from several microphones.) In Fig 1, there is some evidence of a slight timing error, but since the timing is much more difficult with the low-level data, it is probable that the 450 m data is the more correct. At the higher flight speed in Fig 2, the 75 m time history is slightly wider and less peaky. Qualitatively, such effects would be expected from the proportionately longer sampling time. It is therefore concluded that the comparisons do not reveal any reason to question the data from the chosen test height.

5 THE DATABASE AND ITS USE

A complete list of the test point conditions is given in Table 1, although only a subset of this database, reflecting the essential structure of the test programme and the planned analysis, has been used for the source studies.

The two engines of the Tornado aircraft are not in general operating at identical conditions and the jet

properties used in the analyses are simply arithmetic averages of the values for each engine.

Note that the measured noise levels quoted here include the 6 dB increase above the free-field levels arising from the use of ground microphones.

The noise signals measured as a function of time have been combined with the aircraft tracking data (that is, the aircraft position as a function of time) so as to yield the noise levels as a function of the sound emission angles relative to the aircraft track. The noise levels have then been corrected to lossless conditions by allowing for atmospheric absorption over the sound propagation distance (using absorption coefficients, here and elsewhere in this paper, from Ref 1). Inverse-square-law corrections then enable the overall sound pressure levels (OASPLs) and spectra to be presented at a nominal fixed distance (450 m). Mean lines have been drawn through these field shapes, overlaid for the various microphones, and it is these mean curves, read off at 15°, 20° and then every 10° in emission angle, which have been used to assess the noise source strengths. The corresponding spectra, that is for a lossless atmosphere, are used to define the source spectral characteristics. The use of a pistonphone to calibrate the microphones during the testing means that the noise levels are corrected intrinsically to ISA pressure at ground level.

Because of background noise interference (including the electronic noise of the measuring system), particularly with the low noise levels which occur at the extremities of the flyover, spectral levels are only available up to a frequency between 1.5 kHz and 4 kHz. The computed OASPLs have, of course, used only valid spectral data.

6 SOURCE STRENGTH CORRELATIONS

For all of the sources to be examined, the approach taken is to correlate first the source strengths as represented by the polar lossless OASPL field shapes, and then to complete the source modelling by correlating the noise spectra relative to the OASPL at each angle.

The measured data does not take any account of the effects of wind. The component of the wind velocity along the aircraft track V_w alters the sound emission angles θ to corrected values θ_e as illustrated in Fig 3a. For the present test series in which the aircraft ground speed V_g varies from 150 to 275 m/s with wind speeds up to 6 m/s, the corrections to the emission angles (15° to 160°) are less than 2°. There is also a corresponding change to the OASPLs amounting, at extreme angles, to around 1 db. All of the data used in correlating the source strengths have been corrected to wind-less conditions and the corrections have been applied in reverse when the correlated levels are compared with the as-measured data.

This wind-corrected radiation angle θ_e needs to be modified when it is used to express the directivity of the various sources. Airframe noise is defined relative to the aircraft axis, which means that, referring to Fig 3b, corrections for the aircraft pitch and climb angles need to be applied, viz.

$$\theta_a = \theta_e + \varphi_p - \varphi_c .$$

Jet and shock noise are defined relative to the jet axis, which is taken to be the same as the engine axis, so that

$$\theta_j = \theta_e + \varphi_p - \varphi_c + \varphi_e .$$

For the Tornado aircraft, the engine-to-aircraft angle θ_e is -3°. Note that θ_j is defined relative to the jet axis extending upstream of the nozzle, that is, what is normally called the intake axis.

In the subsequent analyses of the aircraft noise, the sound emission angle θ_e relative to the aircraft track is used in the calculation of source Doppler effects in the form

$$(1 - M_a \cos \theta_e)^{-1} .$$

The relevant flight speed of the aircraft is taken to be its airspeed V_a (and Mach number M_a) rather than its ground speed V_g, these airspeed values having been obtained by subtracting the component of the wind velocity measured in the direction of flight from the tracked ground speed. This expression is an approximation. A strict analysis shows that with a wind of Mach number M_w the source Doppler effect is

$$\left(\frac{1 - M_a \cos \theta_e}{1 + M_w \cos \theta_e} \right)^{-1} .$$

At low flight Mach numbers, this relation can be approximated by

$$(1 - M_g \cos \theta_e)^{-1}$$

which expresses the well-known result that wind does not change the Doppler effect derived from the motion of the source relative to the observer. But, at flight Mach numbers above about 0.5, the airspeed-based approximation used here is more, and acceptably, accurate.

Where comparisons are made in the following sections between the measured data and that computed using existing methods, the noise levels from the latter have been increased by 6 dB to allow for the use of ground microphones and have been increased by a further 3 dB when jet and shock noise methods are used to predict the noise of the twin-engined Tornado.

6.1 Airframe noise

The aircraft glide data from test points 33, 16 and 25 were examined to define the airframe noise. With the engines at flight idle, the jet velocities are only about 35 m/s higher than the aircraft flight speeds. Although this does not guarantee that engine-generated nois. negligible, there is, at least, no evidence of engine tones in the glide spectra. Further support for the absence of engine noise is given later by the dominance of airframe noise for test point 73 when the jet is operating at a high subsonic velocity.

The airframe noise would be expected to depend on a function of the type

$$M_a^n (1 - M_a \cos \theta_e)^{-4} \cdot D_a(\theta_a)$$

that is, on a source strength term M_a^n, where $n = 5$ for a "clean" airframe or $n = 6$ for a "dirty" airframe, modified to a source convective amplification corresponding to four Doppler factors, and a source directivity function $D_a(\theta_a)$.

In Fig 4, the measured polar OASPLs (including data from test point 73) have been normalised to

$$OASPL_{norm} = OASPL_{meas} \cdot 50 \log M_a$$
$$+ 40 \log (1 - M_a \cos \theta_e)$$

while in Fig 5 a similar normalisation, but using a sixth-power exponent, is shown. It can be seen that the data collapses quite well in both cases - the range of aircraft flight speeds is not sufficient to determine the appropriate exponent. It would have been of help in resolving this issue if the test programme could have included aircraft glides at a lower Mach number, say 0.3.

An estimate of the noise of the clean Tornado airframe has been made using Ref 2. This noise arises from the wing and the tailplane and, when normalised for M_a^5 and convective effects, is compared with the measurements in Fig 4. Not surprisingly, the measured airframe noise is generally higher than this estimate. The cause of the fall-off in the measured levels in the extreme forward arc (ie at low angles) is not known, but possible mechanisms are discussed in section 9. The noise levels from bluff parts of the aircraft cannot be estimated with any accuracy, but Ref 2 indicates the shape of the noise field from such sources and this, when normalised appropriately, is shown plotted in Fig 5 at an arbitrary level. These calculations suggest that the measured airframe noise is consistent with a combination of components; the extreme forward arc being dominated by the "clean" aircraft sources, while bluff sources dominate in the rear arc. Indeed, the measured forward-arc levels up to about 60° do collapse better using a fifth power. Since, as will be seen later, it is the airframe noise levels in the extreme forward arc that are of importance during a flyover, an exponent equal to 5 is chosen for

correlating the data. This is a rather surprising conclusion bearing in mind the particular aircraft configuration, with under-wing stores, used here.

Hence, the result in Fig 4 defines the polar source directivity $D_a(\theta_a)$ of the airframe noise and by fitting a curve to this data, the OASPL of the airframe noise can be quantified.

6.2 Installed jet noise

From an examination of the spectra, it is evident that, after allowing for the airframe and shock noise character-istics, the remaining noise is essentially broadband. There is no clear evidence of tones which might arise from the engine compressors or turbines and the remaining noise is, therefore, attributed to jet noise. This is consistent with previous practice, such as Ref 3, although because of the possible contribution from other broadband sources, the remaining noise is often described as exhaust noise.

It is known[3] that the presence of aircraft structure in the neighbourhood of a jet can change the jet mixing noise. In the case of a rear-fuselage engine installation such as the Tornado, it can be expected that the turbulence and vortices shed into the jet mixing region from the upstream airframe will give rise to levels of jet noise higher than would be expected for a jet operating in a clean flight stream. There is, however, no available means for predicting such effects quantitatively. Hence, the approach taken here to correlate the so-called "jet" noise is necessarily somewhat arbitrary.

Whereas it is test points 79, 66 and 73, at high sub-sonic jet velocities, which were intended to be used to quantify the jet noise , it has been found that all but the first of these points contain substantial, if not dominant, amounts of airframe noise. For test point 79, the subtraction of the calculated airframe noise from the polar lossless OASPLs as shown in Fig 6 yields an estimate of the jet noise.

This jet noise estimate is compared in Fig 7 with levels of "pure" jet noise calculated for the jet conditions of test point 79 using Ref 4 to obtain the levels that would pertain statically and using Ref 5 to compute the static-to-flight noise reductions. It can be seen that the noise levels of the Tornado suggest a partial reduction of the rear-arc jet noise in flight while there is no reduction, indeed a small increase, in the forward-arc levels. This result is qualitat-ively consistent with the behaviour of a rear-fuselage engine installation (Jet Provost) as described in Ref 3, but the magnitude of the effects is larger than has hitherto been observed. The installation effects, defined as the increase of the measured levels above those for a pure jet, can be seen to be around 10 dB. The twin-jet configuration of the Tornado aircraft is likely to be significant in this context since the region between the jets is bound to be poorly ventilated in flight. While it is possible that the large

installation effects could arise solely as a consequence of the interaction between the mixing regions of the two jets, it is more likely that the lack of a smooth flight stream between the jets is also important.

This single test point is insufficient to enable the jet noise to be correlated and other data need to be sought. Now it can be seen that the field shape of the total noise in Fig 6 has a "double hump"; the airframe noise, as a consequence of its relatively flat source strength increased in the forward arc by convective amplification, causes the forward "hump", while it is the jet noise that peaks in the rear arc. The same type of behaviour can be seen for test conditions with supercritical jets at the lower pressure ratios, after the subtraction of the calculated airframe noise, as shown in Fig 8. This is because the shock noise would be expected, coincidentally, to behave similarly to airframe noise. Hence, it can be concluded that the rear-arc peak levels in Fig 8 are dominated by jet noise.

A more extensive database for assessing the jet noise can, therefore, be constructed by subtracting the calculated airframe noise and shock noise from these test points. However, it will be seen in the next section that the determination of the shock noise requires a knowledge of the jet noise. The process of quantifying both the jet and the shock noise is thus an iterative one. It is the observation that the two sources peak in different regions of the field that enables iteration to provide a reasonably accurate source breakdown. The iteration process will not influence the analysis presented here - the shock noise is simply taken as that to be described in the next section.

The subtraction of the calculated airframe and shock noise from the extended jet noise database yields the jet noise levels given in Fig 9. In order to improve the confidence in this data, values for the jet noise have only been calculated where the total measured noise exceeds the sum of the airframe and the shock noise by at least 3 dB.

The jet noise would be expected to depend on a function of the type

$$ A_j \left(\frac{V_j}{c} \right)^n (1 - \lambda)^m \ , $$

where $\lambda = \dfrac{V_a}{V_j}$

the second term reflecting the increase in jet noise with jet velocity under static conditions and the third term reflecting the reduction of the jet noise in flight. Using a manual form of multi-variable linear regression, a fit of the envisaged function to this data yields $n = 6.7$ and a linear dependence of the exponent m on angle, viz

$$ m = 0.07(\theta_j - 75) \ . $$

This latter function gives rise to noise increases in the forward arc in flight, a noise-reducing exponent of unity at 90°, and greater noise reductions in the rear arc. This behaviour is broadly similar to the qualitative assessment already made in Fig 7. If all of the extended jet noise database shown in Fig 9 is normalised according to

$$ OASPL_{norm} = OASPL_{meas} - 67 \log \left(\frac{V_j}{c} \right) - 10 \ m \log (1 - \lambda) $$

the result shown in Fig 10 is obtained. The collapse of the jet noise data can be seen to be remarkably good. Thus the jet noise is taken to depend on

$$ A_j \left(\frac{V_j}{c} \right)^{6.7} (1 - \lambda)^m D_j(\theta_j) $$

the last function being defined by a curve fitted to the jet noise directivity in Fig 10.

6.3 Shock noise

The shock-associated noise of an under-expanded supercritical jet, or two, would be expected to depend on

$$ A_j \beta^4 (1 - M_a \cos \theta_e)^{-4} $$

where $\beta = \left(M_j^2 - 1 \right)^{\frac{1}{2}}$

and thus, as a consequence of the lack of any distinct directivity coupled with strong convective amplification, shock noise bears some similarity to airframe noise in its radiation pattern.

The spectra show that the characteristic shock noise spectrum shape dominates the noise levels of the test data up to angles of at least 60°. Since, like airframe noise, it is the shock noise levels at low forward-arc angles that are of most importance in high-speed flyovers, this will help with the quantification of the shock noise. Nevertheless, there is a contribution from jet noise in the supercritical jet data and hence this data has had the calculated sum of the airframe and the jet noise subtracted from it (with a minimum subtraction margin of 2 dB) before being normalised by

$$ OASPL_{norm} = OASPL_{meas} - 20 \log (M_j^2 - 1) + 40 \log (1 - M_a \cos \theta_e) $$

to give the correlation shown in Fig 11. There is a reasonable collapse of the forward-arc levels, but there is also a substantial falling-off of the levels towards low angles, similar to that obtained for airframe noise.

Using the approximate relationship for predicting the shock noise from stationary circular nozzles given in Ref 6, the normalised shock noise would be expected to have a uniform polar directivity at a level about 4 dB higher than the level obtained from Fig 11. However, Ref 7 shows that the source strength of shock noise (from unheated jets) can reduce in flight, especially when the jet is operating at the relatively low pressure ratios experienced here.

Hence, there is no reason to suspect that the normalised shock noise cannot be described adequately by a mean curve of the type shown in Fig11.

6.4 Correlation quality

The goodness-of-fit of the noise correlations can best be assessed by comparing measured and predicted time histories for flight at 75 m above the ground since it is in such circumstances that the noise source breakdowns are intended to be used. Because, in general, the aircraft test conditions are such that it cannot actually operate in level flight at the selected conditions, the time histories are computed for a linear flyover at a 75 m minimum distance.

Such "measured" time histories can be computed from the averaged lossless OASPL field shapes. It is only necessary to convert back to time from angle and to add to the noise levels the appropriate inverse-square-law correction

$$20 \log \left(\frac{450}{75} \sin \theta \right) .$$

The individual source OASPLs computed from the normalised source characteristics as a function of the emission angle θ_e can be expressed on a time axis. Since the measured time histories contain the effects of the wind at the time of the test, the inverse-square-law corrections to the computed OASPLs need to include the addition of the wind-effect term.

Figs 12, 13 and 14 present sample comparisons of the measured and computed time histories. The airframe noise, in Fig 12, agrees well with the measured data, although for some other points, in Fig 13 for example, it seems to be high in the extreme forward arc. This is considered to be a significant observation and will be discussed further in section 9. The jet and shock noise levels generally agree remarkably well with the measured data, especially in the parts of the time histories where they dominate. It can be seen that the initial rapid rise in the flyover noise is determined by the airframe and shock noise radiated forwards at low angles, less than 40°, to the aircraft and that the jet noise only dominates once the aircraft has passed overhead.

It is concluded that the analytical models chosen to describe the strengths of the individual sources represent the noise characteristics of the aircraft satisfactorily.

7   SPECTRAL CHARACTERISTICS

The purpose of undertaking a quantitative examination of the noise spectra is two-fold. Firstly, the understanding of the aircraft noise sources can be extended and, secondly, by correlating the spectral characteristics, the aircraft noise levels can be predicted in subjective units.

7.1 Airframe noise

Some of the spectra from the aircraft glides show clear evidence of tonal "spikes"; such observations are a common occurrence with airframe noise measurements on real aircraft and do not prevent the airframe noise being treated, adequately for present purposes, as broadband in nature.

Since the aircraft configuration remains constant, its noise spectra would be expected to correlate with a source Strouhal number modified by a Doppler frequency shift, that is, by

$$St = \frac{f \ell}{v_a} (1 - M_a \cos \theta_e) ,$$

where ℓ is a characteristic dimension of the aircraft. Together with the earlier assumption that the strength of each component of the airframe noise varies according to a similar exponent of the flight Mach number, it follows that although the shapes of the airframe noise spectra can vary with angle as a consequence of differing source directivities, they should remain similar at a given angle as the flight speed is changed. The spectra do indeed seem to exhibit this trend. However, the spectra in the rear arc show a "double-hump", indicating distinct low and high-frequency noise sources, and it is evident on closer examination that the frequency relationship between these two sources does not remain constant. For test point 16, for example, the spectra at 45° and 139° should shift by

$$\frac{1 - 0.63 \cos 139°}{1 - 0.63 \cos 45°}$$

that is, by a factor of 2.7 (equivalent to 4.3 third-octaves). From the spectral comparisons in Fig 15, it can be seen that while the low-frequency source behaves in a manner consistent with such a frequency shift, the high-frequency source does not, indeed it seems to remain constant in frequency - a conclusion which also holds at other flight speeds. The reason for this peculiar behaviour of the high-frequency source is not known but is discussed later in section 9. The amplitude of each of the sources remains roughly constant relative to the OASPL at each angle.

Hence the spectra have been correlated as a combination of two sources, a low-frequency source which behaves in a plausible manner in both amplitude and frequency, and a high-frequency source which although varying in strength according to a fixed exponent, remains constant in frequency. Average spectral shapes for each of the sources have been produced by overlaying several of the measured spectra. Comparisons between measured and predicted spectra show that although the agreement cannot be described as precise, it should be sufficiently good to enable a reasonable modelling of the effects of atmospheric absorption.

7.2 Installed jet noise

The spectra for test point 79, the only one dominated by jet noise at most angles, do not show any consistent variation in shape with angle. For example, the spectra do not become obviously peakier at high angles as would be expected for pure jet noise. Indeed, defining the spectra relative to the OASPL at each angle, it has been found that, with a suitable shift in frequency, the spectra at other angles can be overlaid on the 90° spectrum as illustrated in Fig16a. The pure jet noise spectrum (at 90°) shown on this diagram has been plotted relative to the OASPL of the aircraft noise and shows that the jet noise installation effects are least at low frequencies as would be expected.

This spectral collapse was used as the basis for correlating the jet noise spectra. A mean curve was drawn through the overlaid spectra and the frequency shifts required to obtain the collapse were plotted as shown in Fig 16b. In order to predict the jet noise at other conditions, the assumption was made that the jet noise frequencies will depend on a Strouhal number based on the absolute jet velocity. This is consistent with the behaviour of pure hot jets[5] and is considered to be a plausible supposition for the present type of installed jet noise. On this basis, rear-arc jet noise spectra at other (supercritical jet) conditions can be related in frequency to the 90° spectrum for test point 79, yielding the additional points in Fig 16b. Curve-fitting the resulting trend completes the correlation.

7.3 Shock noise

In Ref 7 it is suggested that the spectrum of shock-associated noise can be approximated, particularly in the forward arc, by a triangular shape which rises at 20 dB/octave to a peak at frequency f_o and then reduces in the high frequencies at between about 2 and 4 dB/octave. A value of 3.6 has been chosen as being broadly suitable for the Tornado data.

Ref 7 gives a formula for the frequency f_o and this is compared with samples of the present data in Fig 17. In Fig 17a, the dependence of the shock frequency on its emission angle is compared for the data at the highest available pressure ratio, test point 27. Bearing in mind that it is difficult to determine the measured frequency to better

than half a third-octave, the agreement between the measured and calculated values is remarkably good. In Fig 17b, the effect of pressure ratio on the shock frequency is examined at a particular emission angle, the nearest to 40° for each test point. This plot does not produce a unique curve because of the varying flight Mach numbers. The agreement is again very good.

The shock noise spectrum is therefore defined according to the equations from Ref 7, the spectral levels being set by the need to match the required OASPL.

7.4 Correlation quality

Proceeding in a similar manner to that described in section 6.4, measured and computed time histories for linear flyovers at a 75 m minimum distance can be compared. In this instance, however, the comparisons are made not at lossless atmospheric conditions but for a standard atmosphere (ISA pressure and temperature, and 70% relative humidity). In addition, the noise levels can now be compared in dBA units.

The source strength and spectral correlations enable absolute spectral levels to be calculated which, after applying atmospheric absorption corrections over a propagation distance of 75/sin θ m and the appropriate subjective weighting, can be summed to yield the dBA noise levels. Similar calculations are performed on the measured data, that is, to convert the data corrected to lossless conditions to dBA levels in a standard atmosphere.

Sample results are presented in Figs 18, 19 and 20. Comparing these results with those for the source strength terms alone given in Figs 12, 13 and 14 shows that there is only a slight deterioration in the quality of the modelling.

The general observation can be made that an important effect of the real atmosphere is to steepen the rise time of the noise, and hence exacerbate the startle effect. This arises because the aircraft noise at shallow angles propagates over a long distance and is reduced by atmospheric attenuation, particularly in the high frequencies to which the human ear is more sensitive - thus, as the aircraft approaches, its level is rising not only because it is getting closer and because its inherent source strength is increasing, but also because the absorption of the atmosphere is reducing.

There is remarkably little change in the relative levels of the sources. The spectra of all three sources tend to peak at frequencies around 1 kHz and, as a consequence, the effects of atmospheric absorption and subjective weighting are similar.

8 SOURCE BALANCE IN LEVEL FLIGHT

The source modelling which has been established can be used to determine the aircraft noise, and particularly the

relative importance of the individual noise sources, when it is flying at a constant height at various speeds. First, however, it is necessary to find the jet conditions (velocity and Mach number) required to maintain level flight.

The level-flight jet conditions have been obtained from an interpolation of the aircraft flight data acquired in the present programme. In steady-state conditions, the climb angle of an aircraft is related to the balance between its drag and its net thrust. The aircraft drag will vary with the airspeed dynamic head which is a function of the square of the flight Mach number M_a. Without reheat, the Tornado engine operates at a fixed nozzle area so that the net engine thrust can be expressed as a function of the jet Mach number. This latter function contains a temperature ratio term but this changes little over the level-flight operating conditions of the aircraft. It is thus possible to plot all of the test points flown against these thrust and drag parameters, to annotate each point according to the aircraft climb rate (which is chosen in preference to climb angle because of wind effects) and then to interpolate this data visually to obtain a line corresponding to zero climb rate. An engine performance synthesis was used both to obtain the jet velocities from the jet Mach numbers and, in conjunction with aircraft performance data, to provide an independent cross-check of the results.

The jet conditions at flight Mach numbers of 0.5, 0.65 and 0.8 have been used to compute dBA time histories for 75 m flyovers in a standard atmosphere. Such computations carried out hitherto in this paper express the noise levels as they were measured, that is, with ground-level microphones which cause a uniform increase of 6 dB in the free-field noise levels. While this is one of the best ways to measure aircraft noise from a technical point of view, it does not give noise levels which are representative of what a listener would actually hear. The ground reflection effects which occur with a person standing in the open are complex[8] but here, where the source noise is mainly of high frequency, they can be approximated by adding 3 dB to the free-field noise levels. Hence, the results shown in Figs 21 to 24 have had 3 dB subtracted from the calculated spectral levels.

At the lowest speed, the jets are subcritical, there is no shock noise and the installed jet noise is the principal source. At 0.65M, a typical condition for low-level Tornado operations, all three sources are comparable in magnitude in what are judged to be the subjectively important parts of the time history, the rising and peak regions. Note the substantial increase in the noise rise-rate which increases further at the highest flight Mach number. At this latter condition, the jet shock noise is the most important source, but the other noise components are not negligible. In the context of the startle effect of the flyover noise, it may be significant to observe that it is shock noise that causes the steepest signal rise-times.

Fig 24 shows how the peak noise level of each source, and the peak of the total noise, varies with Mach number. Because these peaks occur at different times during the flyover, the individual noise levels cannot simply be added to give the total noise. It can be seen that although it is the installed jet noise and then the shock noise that dominate the aircraft noise as its speed is increased, the airframe noise is not a negligible component and its contribution would soon become important if means were found to reduce the jet or the shock noise.

The rise time of the noise signals is not a feature which has been addressed so far. It is difficult to make accurate measurements from single time histories. However, the source modelling enables this issue to be examined with a reasonable precision and the time histories in Figs 21 to 23 form a useful basis. There is, as yet, no agreed means for expressing the rise time of a flyover noise signal. While, for subjective applications, it may be desirable to define the rise time as that taken to rise from a specified noise level to the peak of the time history, this type of definition makes any analytical formulations very difficult. Thus, the approach taken here is to use the maximum rate of rise of the signal. From Figs 21 to 23, the maximum slopes of the approach noise signals have been measured as 25, 47 and 83 dB/s for flight Mach numbers of 0.5, 0.65 and 0.8 respectively.

The rapid increase in these rates with increasing speed is expected on theoretical grounds. From an analysis of this issue based on the directivity and convective amplification terms of the airframe and shock noise, it can be shown that the maximum rise-rate is estimated to vary as

$$7 \frac{c}{H} \frac{M_a}{(1 - 0.87 M_a)} \text{ dB/s} .$$

The constant of proportionality in this expression has been determined from the experimental data. The formula is only valid for the Tornado at high subsonic flight speeds.

9 DISCUSSION

9.1 Forward-arc source directivities

The field shapes of the airframe and shock noise, as expressed by Figs 4 and 11, show a substantial falling-off of the levels towards low forward-arc angles. At 20°, the reduction seems to be around 10 dB for the airframe noise and 15 dB for the shock noise. The jet noise in Fig 6 shows little sign of the effect although there is only one test point.

The observations seems to be genuine insofar as an assessment of possible timing errors or sampling time effects has not revealed a likely explanation.

The occurrence of the effect on test points taken on different days and with different wind velocities eliminates wind or temperature gradients in the atmosphere as the cause.

The possibility of the effects arising from shallow-angle propagation over the ground, the so-called "extra ground correction", has been discounted because this effect is only significant for angles of a few degrees[9].

The similarity of the high and low-level time histories in Figs 1 and 2 indicates that the phenomenon is not strongly dependent on propagation distance. This leads to the consideration of aircraft flow-field effects as an explanation, that is, that the forward-propagating sound field is being distorted by the airflow over the aircraft. The airframe noise directivity in Fig 4 does suggest that the effect may not exist for rearwards-propagating noise. This is obviously a more likely explanation for shock noise, located at the rear of the aircraft, than it is for airframe noise. But it has been suggested that the forward-arc airframe noise is generated by the wing and the effective source position of wing noise would be expected to be near the wing trailing edge. Perhaps jet noise does not show the effect because of the distributed nature of its source.

The distortion of engine noise radiation by the aircraft flow-field is known to occur in some special circumstances (noise refraction by wing-tip vortices, for example) and is believed to contribute to observed differences between aircraft flyover and sideline noise measurements. Although the data given in Ref 10 on the latter issue is not directly applicable here, the broad similarity of the observed effects does confirm a possible cause.

It is difficult to see how this explanation might be validated. Ideally, tests would be carried out with a stable noise source fixed to the front, and then to the rear, of the aircraft. Such tests, even at model scale in a wind tunnel, would not be easy. It would be a simpler proposition to consider testing with and without the undercarriage lowered in aircraft glides, which might at least demonstrate that a source in such a position does not exhibit the phenomenon.

9.2 Interpreting the glide data

Two observations made in the course of the analysis raise doubts as to whether the noise measured from the aircraft glides is, in fact, all generated by the airframe.

Firstly, the high-frequency component evident in the airframe noise spectra does not seem to exhibit a Doppler frequency shift (section 7.1 refers). Taken at face value, this implies that the noise source is essentially stationary in space. Such a source could exist in the turbulent wake shed from the aircraft, but it seems unlikely that its strength could be significant and, being quadrupole in nature, its relative strength would vary markedly over the range of flight speeds tested. There is, however, a more likely explanation. In the glide tests, the jet velocity is

similar to the aircraft speed. At a flight speed of 210 m/s, for example, the jet velocity is 250 m/s. With ideal aerodynamic flows, this would mean that the jet noise levels would be negligible. But, with a turbulent jet flow and with the non-uniform flow surrounding the jet, arising from the boundary layers and vortices shed from the upstream aircraft structure, it may be that there will be substantial turbulence in the mixing layer between the jet and the ambient air, and this turbulence will have low mean velocity relative to the ground. While this argument is relevant to the whole of the jet mixing layers, it is likely to be most strongly applicable to the interface region between the twin jets. The argument is, therefore, simply an extension of the discussion already made in section 6.2 concerning the large jet installation effects observed at a higher jet velocity. To the authors' knowledge, there is no (model-scale) test data on installed turbulent jets operating at high flight/jet speed ratios which could be used to substantiate this proposition.

This mechanism would, however, seem to explain a second observation - that made in section 6.4 concerning the apparent over-estimation of the airframe noise in Fig 13, for example. The mechanism described is, in essence, a jet noise source and it is, therefore, strictly incorrect to include this source when the jet is operating "normally". The jet noise has been correlated in a form which causes its strength to become negligible as the flight speed approaches the jet speed. The proposed mechanism is suggesting that this formulation is incorrect and that the jet noise is "bottoming out" at a level set by the high-frequency component of the so-called airframe noise.

However, this interpretation does not fundamentally alter the relevance of the type of jet noise correlation which has been established. Indeed, it is important to appreciate that the airframe or "glide" noise, as defined in this paper, still represents the noise "floor" that would be reached if the jet and shock noise were able to be reduced.

9.3 The results and their implications

In essence, the results of the programme are represented by the source breakdowns for level flight illustrated in Figs 21 to 24. The most relevant result is that shown in Fig 22 for a typical operational flight Mach number of 0.65. In interpreting these results, the conclusion of the previous section should be borne in mind, that is, that the true level of the airframe noise may be a few decibels lower than that shown which is nevertheless the minimum noise for the aircraft configuration under study. Broadly, the flyover noise characteristics evident from the results are as follows.

As the flight speed is increased, the peak noise level increases as does the rate of rise of the flyover noise. Shock noise from the jet has the most rapid rate of rise.

Although the jet noise tends to be the principal source at low flight speeds, and the shock noise at high flight

speeds, all three sources are comparable in magnitude during the rise-time of the noise signal and at its peak.

Were it possible to greatly reduce both the jet mixing and shock noise, the peak noise levels would only reduce by about 5 dBA. Reducing either the jet noise or the shock noise alone, would have little effect at 0.65M.

The value of any possible noise change is difficult to assess because of the lack of a subjective noise unit which not only reflects the peak noise level, but also the suddenness of its occurrence. On the basis of their personal experience, the authors are inclined to the view that, for flights at 0.65M at least, it is the startle effect that causes the most disturbance and that any means to alleviate it, even without altering the peak noise, would be helpful. Thus, on the basis that lower rise times and/or noise levels are desirable, some practical implications are drawn from the results.

There would seem to be little scope for reducing startle by controlling the rise time of the aircraft noise. The rise time is dependent, firstly, on operational factors, the aircraft speed and height. The startle effect could be reduced simply by flying slower and/or higher, but this would not only obviate the operational training objective of the low-level flying, but would also increase the aircraft noise levels experienced further from the track. Secondly, the rise time is thought to be exacerbated by the aircraft flow-field as discussed above, but this is not a mechanism amenable to control. Thirdly, the rise time depends on the atmospheric conditions as a consequence of the reducing absorption of the approach noise - again not a controllable parameter. And, finally, the rise time depends on the dominant source insofar as shock noise is observed to rise most steeply. At a Mach number of 0.65, the strength of the shock noise is such that it is doubtful whether its elimination would be of great benefit, but it would be a move in the right direction.

The lack of ability to control the rise time of the aircraft noise leads to the idea of attaching a forward-radiating noise source to the aircraft with the sole objective of providing a warning of its approach. Because of the required directionality, such a source would not need to have a high acoustic power and it might even be driven by the flight airstream. It is interesting to note that the present understanding of aircraft flow-field effects would suggest that a forward-mounted source might easily dominate the forward-radiating noise from the whole aircraft.

Reducing both jet and shock noise is estimated to give a maximum reduction of 5 dBA in the peak noise. A reduction of this magnitude in the flyover noise from a civil aircraft would be clearly audible and would be expected to result in a useful reduction in the number of complaints. But it is questionable whether a similar outcome can be expected in the present situation, at least, under the flight-path. Such benefits would, of course, accrue to the side of the aircraft track where the startle effects are reduced.

A means for achieving some reduction in both the jet mixing noise and the shock noise, which proved of some value for Concorde, is to open up the engine final nozzles to the maximum area that can be tolerated. The engine thrust is maintained by increasing the fuel flow, with the result that the engine mass flow is maximised and the nozzle pressure ratio and the jet velocity are lowered. Because the RB199 already has a variable-area nozzle for reheat matching, this would seem to be a feasible proposition. Using an engine performance synthesis to determine the jet conditions at the maximum allowable area, and then using the noise prediction model established here to estimate the potential noise benefits, the worthwhileness of this approach could be appraised.

10 CONCLUSIONS

(1) The Tornado flight trial has enabled the principal sources of the aircraft noise to be identified and quantified.

(2) Although the jet mixing noise tends to be the principal source at low flight speeds, and the shock noise from the jet at high flight speeds, these sources and the airframe noise are comparable in magnitude during the rise time of the noise signal and at its peak.

(3) As the flight speed is increased, the peak noise level increases as does the rate of rise of the flyover noise. Shock noise has a more rapid rate of rise than jet or airframe noise.

(4) Were it possible to greatly reduce both the jet mixing and shock noise, the peak noise levels would only reduce by about 5 dBA. Reducing either the jet noise or the shock noise alone, would have little effect at a typical flight speed of 0.65M.

(5) The most significant components of the airframe noise, as measured from aircraft glides, are believed to be from the wing and from aircraft/jet interactions.

(6) As expected, the levels of the jet mixing noise are substantially (about 10 dB) higher than those predicted for a "clean" jet in flight as a consequence of the poor aero-dynamic quality of the jet environment and the twin-jet configuration.

(7) The shock noise from the jet behaves much as would be expected, but the forward radiation patterns of both shock and airframe noise seem to be reduced significantly by aircraft flow-field effects.

Acknowledgment

REFERENCES

1 'Standard values of atmospheric absorption as a function of temperature and humidity'. SAE ARP 866A, March 1975

2 'Airframe noise prediction'. ESDU Data Item 90023, November 1990

3 Bryce, W.D.; 'Experiments concerning the anomalous behaviour of aero-engine exhaust noise in flight'. AIAA Paper 79-0648, March 1979

4 'Computer-based estimation procedure for single-stream jet noise'. ESDU Data Item 85018, December 1987

5 Bryce, W.D.; 'The prediction of static-to-flight changes in jet noise'. AIAA Paper 84-2358, October 1984

6 'Gas turbine jet exhaust noise prediction'. SAE ARP 876C, November 1985

7 Bryce, W.D. and Pinker, R.A.; 'The noise from unheated supersonic jets in simulated flight'. AIAA Paper 77-1327, October 1977

8 'The correction of measured noise spectra for the effects of ground reflection'. ESDU Data Item 80038, November 1984

9 'Estimation of extra ground correction for ground-to-ground noise propagation in one-third octave bands'. ESDU Data Item 84024, October 1984

10 'Estimation of lateral attenuation of air-to-ground jet or turbofan aircraft noise in one-third octave bands'. ESDU Data Item 82027, April 1983

TABLE 1   THE AVAILABLE DATABASE

		AIRCRAFT PERFORMANCE						AMBIENT CONDITIONS AT ALTITUDE	
RR RUN NO.	ENGINE CONDITION (pressure ratio)	TRACKED FLIGHT SPEED m/s	TRACKED FLIGHT MACH NO. (DOPPLER)	TRUE AIR SPEED m/s	TRUE FLIGHT MACH NO. (SOURCE)	CLIMB ANGLE	A/C PITCH	PRESSURE kPa	TEMP R
12	SUPERCRITICAL	220.1	.66	220.9	.66	4.9	9.3	95.2	278
13	SUPERCRITICAL	235.9	.71	234.7	.71	-2.1	1.6	94.8	277.4
15	IDLE	211.6	.63	210.6	.63	-5.5	.8	95.5	278.6
16	IDLE	209.7	.63	210.4	.63	-4.2	.5	95.6	278.8
17	SUPERCRITICAL	234.9	.7	233.9	.7	5.5	9.5	94.1	277.8
19	SUPERCRITICAL	270.8	.81	269.8	.81	-3.9	-1.5	95.0	277.9
21	SUPERCRITICAL	265.2	.79	263.4	.78	-4.8	-1.6	94.8	277.8
23	IDLE	254.9	.76	253.4	.76	-10.1	-7.3	95.2	278.3
25	IDLE	250.2	.75	248.8	.75	-11.7	-6.7	95.3	278.1
26	SUPERCRITICAL	261.2	.78	263.0	.79	4	7	94.4	278.3
27	SUPERCRITICAL	264.4	.79	262.7	.78	4.8	8.5	93.8	278
28	SUPERCRITICAL	179.1	.54	180.0	.54	7.3	12.6	94.1	278
31	SUPERCRITICAL	178.7	.53	177.0	.52	6	11.4	94.0	277.8
33	IDLE	184.3	.55	183.4	.55	-6.1	-.8	94.9	278.1
34	IDLE	171.4	.51	170.0	.51	-7.5	-2.4	94.5	277.8
36	SUPERCRITICAL	177.4	.53	175.8	.53	10.3	16	93.7	277.4
40	SUPERCRITICAL	206.3	.61	212.2	.63	.3	4.3	99.8	280.8
58	SUPERCRITICAL	211.4	.63	215.2	.64	0	3.3	95.1	279.6
59	SUBCRITICAL	240.2	.72	234.7	.7	-4.8	-1.6	95.2	279.6
61	SUPERCRITICAL	239.7	.72	234.8	.71	0	4	95.1	279.6
63	SUPERCRITICAL	234.5	.7	229.3	.68	-.4	3.8	96.3	279
65	SUPERCRITICAL	228.1	.68	223.3	.67	1	4.6	96.4	279.3
66	SUBCRITICAL	212.4	.63	217.9	.65	-4.5	0	96.4	278.8
68	SUPERCRITICAL	210.9	.63	216.7	.65	4.1	10.2	96.9	279.9
70	SUPERCRITICAL	247.0	.74	251.6	.75	-5.5	-1.7	97.0	279.9
72	SUBCRITICAL	257.3	.77	262.6	.79	-8.1	-4.3	96.8	279.8
73	SUBCRITICAL	274.6	.82	269.7	.81	-7.9	-6.1	96.5	279.2
74	SUPERCRITICAL	258.1	.77	263.0	.78	-3.5	-.2	96.9	279.7
76	SUPERCRITICAL	164.4	.49	169.7	.51	3.7	9	96.0	279.3
77	SUPERCRITICAL	178.1	.53	172.6	.51	5.5	12.6	96.8	280.7
79	SUBCRITICAL	175.9	.53	170.2	.51	1.4	7.6	95.7	278.9
80	SUPERCRITICAL	164.0	.49	169.5	.51	7.4	13.2	95.3	278.8
81	SUPERCRITICAL	179.9	.54	174.5	.52	7.7	15.4	97.1	280.2
86	SUPERCRITICAL	237.3	.7	243.4	.72	-.1	3	101.2	282.7
87	SUPERCRITICAL	167.4	.5	161.5	.48	1.9	7.5	100.9	283.1

Flight Mach number=0.72 : Supercritical PR

dBA: IAS+10C: 70% RH

Fig 2 A comparison of 250ft and 1500ft flyover data

Tornado : Airframe Derivation

Normalised OASPL : 450m polar lossless n=5

Fig 4 Glide data normalised by fifth-power exponent

Flight Mach number=0.62 : Supercritical PR

dBA: ISA+10C: 70% RH
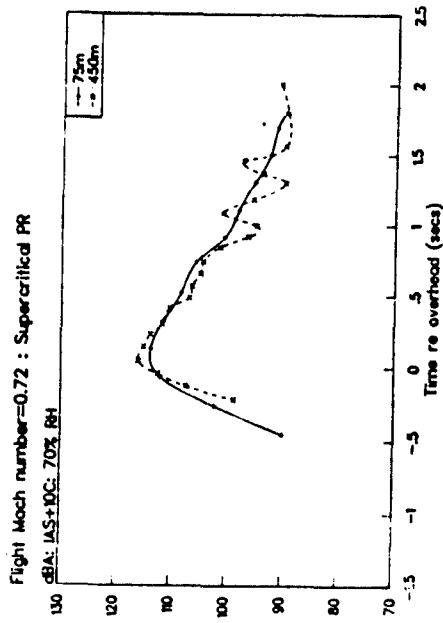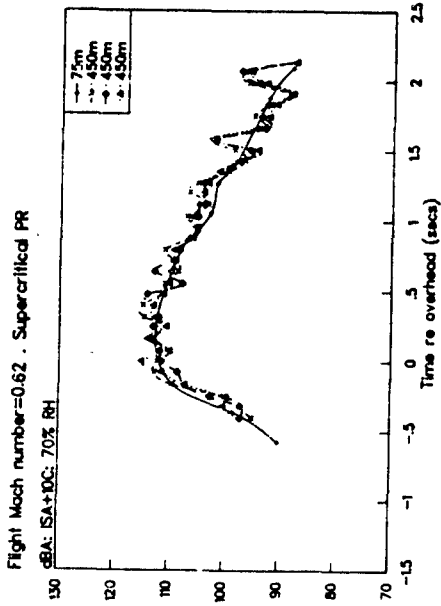
Fig 1 A comparison of 250ft and 1500ft flyover data
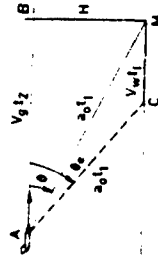
Fig 3a Sound propagation geometry

Fig 3b Aircraft axes

Tornado : Jet Derivation TP 79
Normalised OASPL : 450m polar lossless
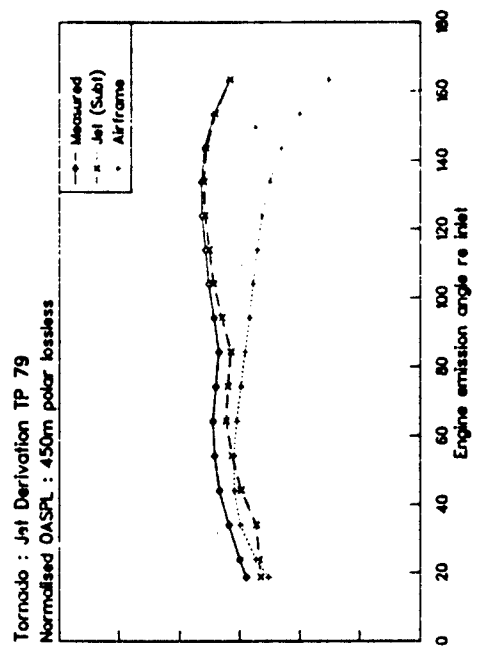
Fig 6   Installed jet noise at subcritical conditions

Tornado : Jet Derivation
Normalised OASPL : 450m polar lossless
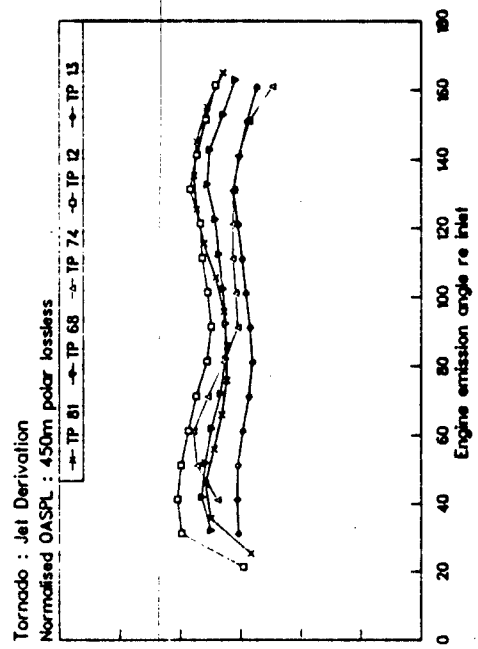
Fig 8   Supercritical jet data with airframe noise removed

Tornado : Airframe Derivation
Normalised OASPL : 450m polar lossless n=6
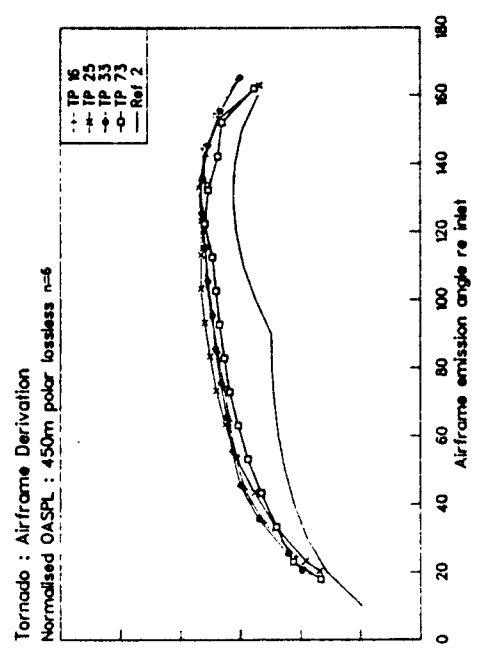
Fig 5   Glide data normalised by sixth-power exponent

Tornado : Jet Derivation TP 79
Normalised OASPL : 450m polar lossless
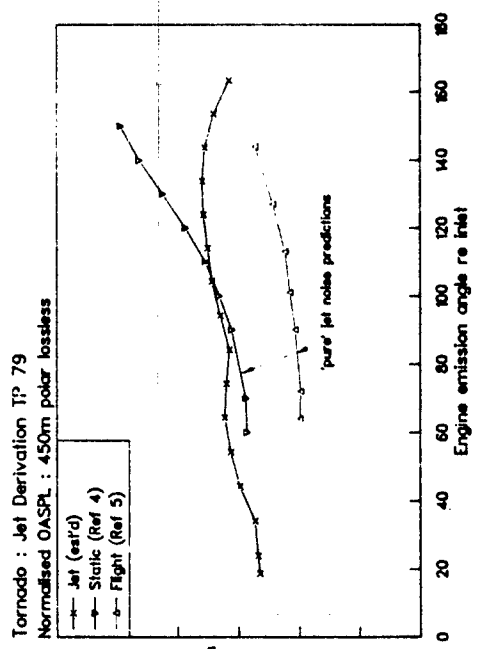
Fig 7   Installed jet noise compared with 'clean' jet data

Tornado : Jet Derivation
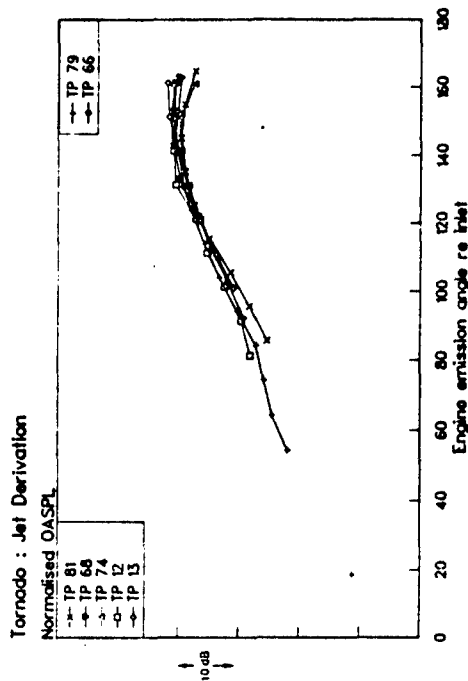
Normalised OASPL

Fig 10 Normalised jet mixing noise
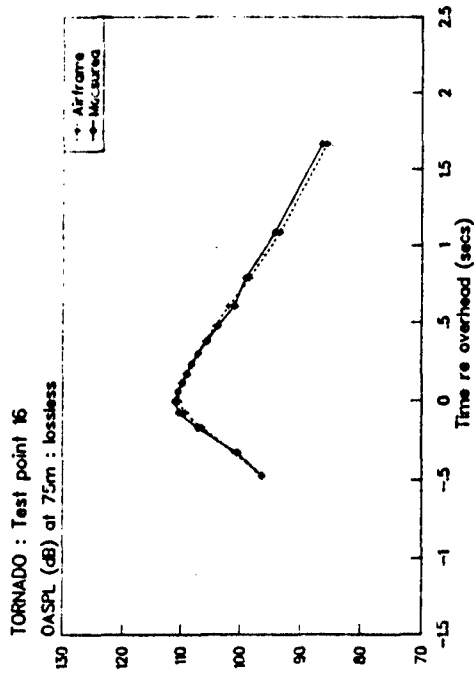
TORNADO : Test point 16

OASPL (dB) at 75m : lossless

Fig 12 Measured and predicted OASPL time histories for an aircraft glide

Tornado : Jet Derivation
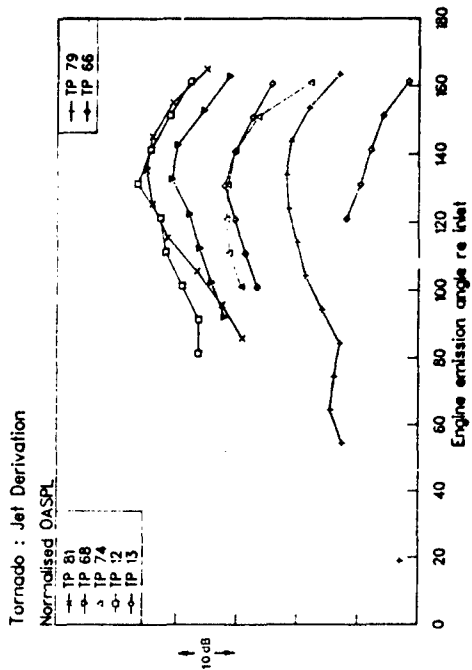
Normalised OASPL

Fig 9 Jet mixing noise database

Tornado : Shock correction
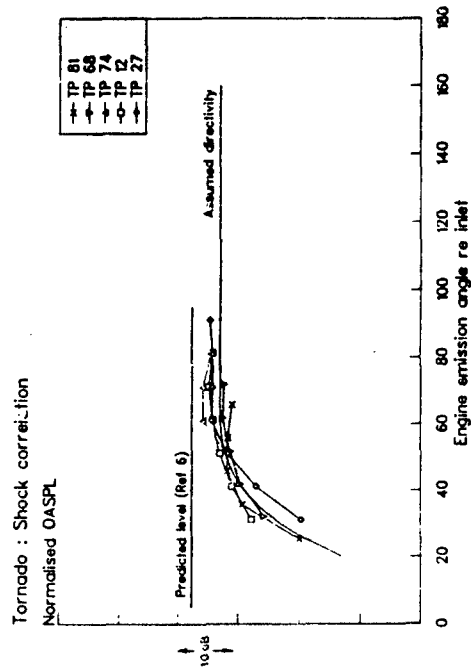
Normalised OASPL

Fig 11 Normalised shock noise

TORNADO : Test point 12
OASPL (dB) at 75m : lossless

Airframe
Jet
Shock
Total
Measured

Time re overhead (secs)

Fig 14 Measured and predicted OASPL time histories at a supercritical jet condition

TORNADO : Test point 66
OASPL (dB) at 75m : lossless

Airframe
Jet
Total
Measured

Time re overhead (secs)
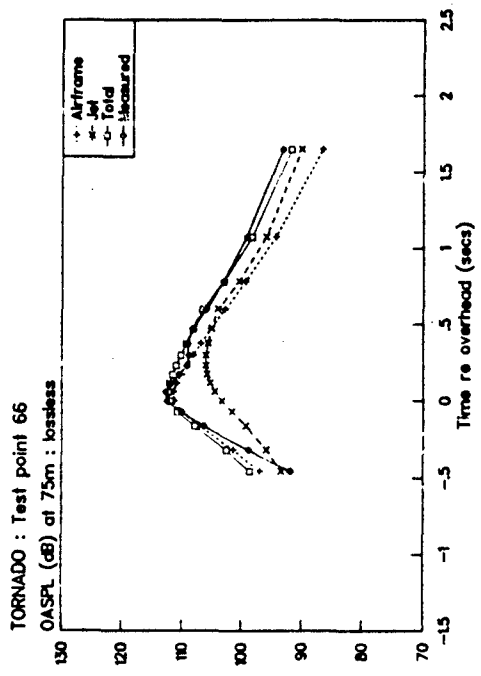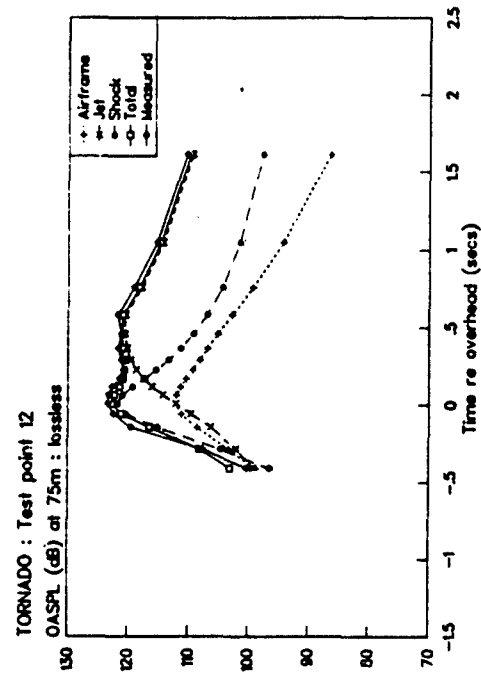
Fig 13 Measured and predicted OASPL time histories at a subcritical jet condition

$\theta = 139°$
$\theta = 45°$

SPL re OASPL (dB)

$\frac{1}{3}$-octave frequency

(b) COMPARING 45° and 139° SPECTRA WITH FREQUENCY FACTOR OF 2.7

Test point 16

$\theta = 139°$
$\theta = 45°$

SPL re OASPL (dB)

$\frac{1}{3}$-octave frequency
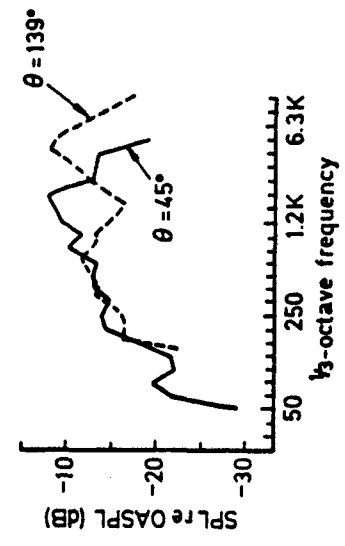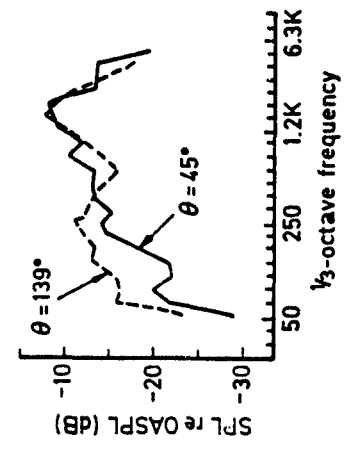
(a) COMPARING 45° and 139° SPECTRA AT CONSTANT FREQUENCY

Fig 15 Spectral characteristics of airframe noise

Test point

● 79
▲ 13
× 68
□ 81

10 log (1+0.7cos θ_j)

Emission angle (degrees)

Frequency shift re 90° (1/3-octaves)
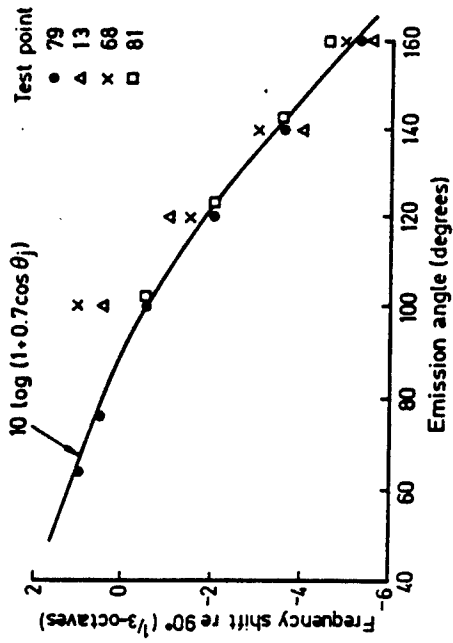
Fig 16b   Angular dependence of jet noise frequency

(b) PRESSURE–RATIO DEPENDENCE   θ ~ 40°

10*Log (f_0) : (1/3 - octaves)

Nozzle pressure ratio

+ Predicted (ref(7))
□ Measured
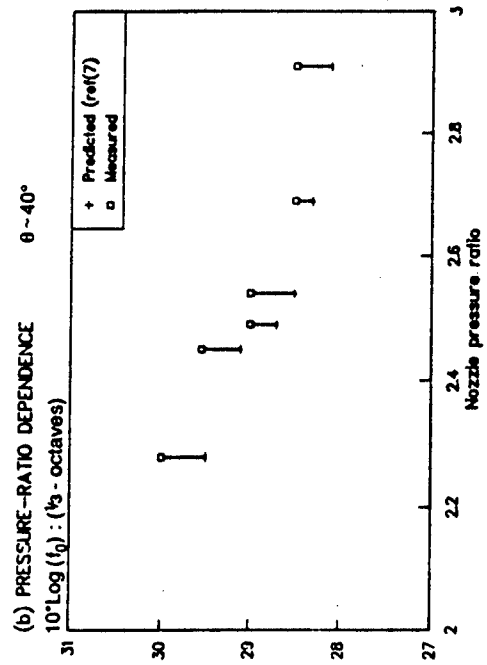
Fig 17   Measured and predicted shock frequencies
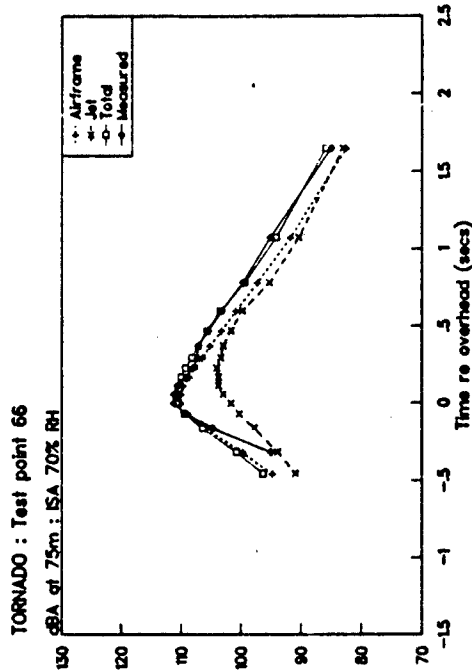
Test point 79

Pure jet noise

1/3-octave frequency

SPL re OASPL (dB)

Fig 16a   Spectral collapse of jet noise

(a) ANGULAR DEPENDENCE   Test point 27

10*Log(f) : (1/3-octaves)

Engine emission angle (deg)

□ Measured   —— Predicted (Ref 7)

TORNADO : Test point 66

dBA at 75m : ISA 70% RH

Fig 19   Measured and predicted dBA time histories at a subcritical jet condition

Tornado : level flight 0.5 Ma

dBA at 75m : ISA 70% RH
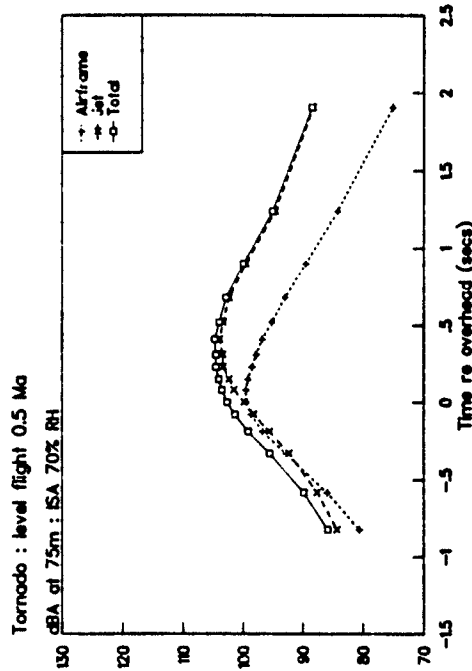
Fig 21   Source breakdown in level flight at 0.5M

TORNADO : Test point 16

dBA at 75m : ISA 70% RH

Fig 18   Measured and predicted dBA time histories for an aircraft glide

TORNADO : Test point 12

dBA at 75m : ISA 70% RH
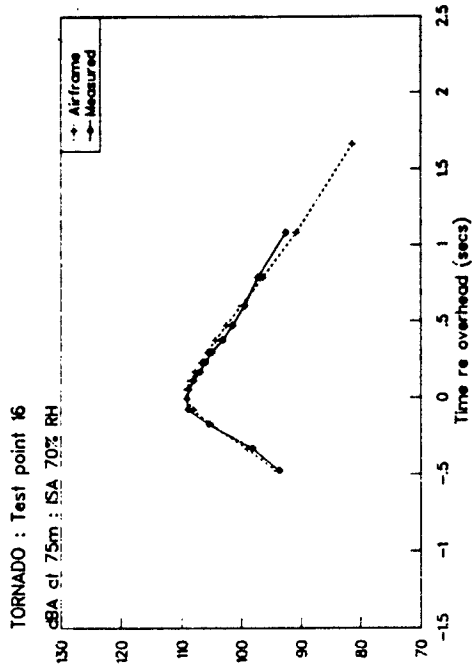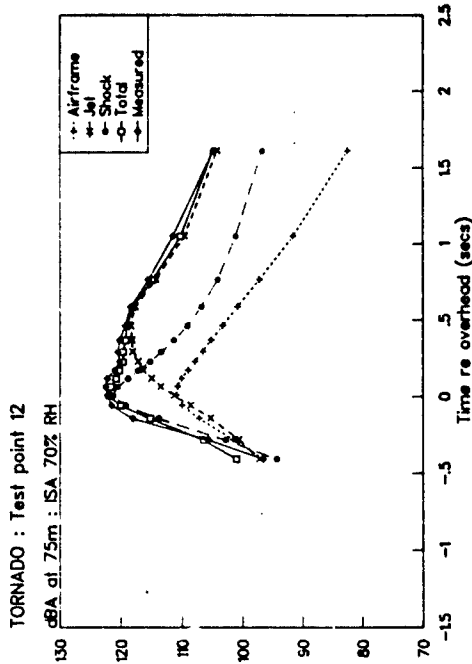
Fig 20   Measured and predicted dBA time histories at a supercritical jet condition

Tornado : Level flight 0.8 Ma

dBA at 75m : ISA 70% RH

Fig 23   Source breakdown in level flight at 0.8M

Tornado : Level flight 0.65 Ma

dBA at 75m : ISA 70% RH
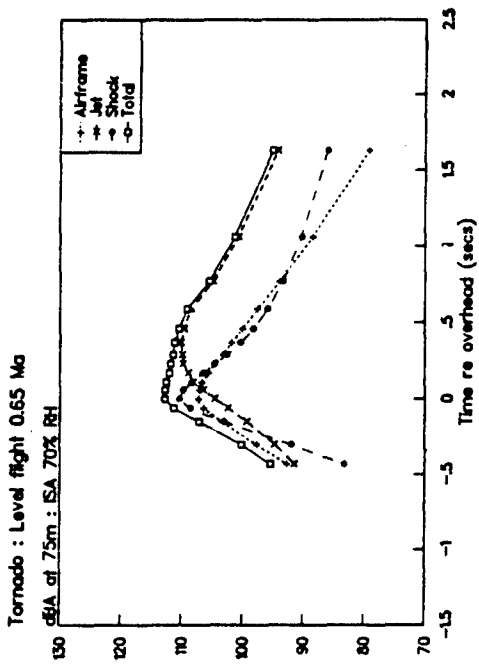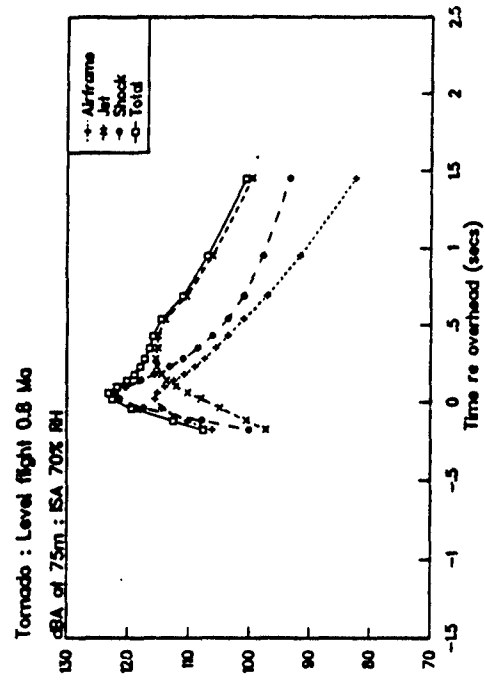
Fig 22   Source breakdown in level flight at 0.65M

Tornado : Level flight at 75m altitude

Peak dBA : ISA 70% RH
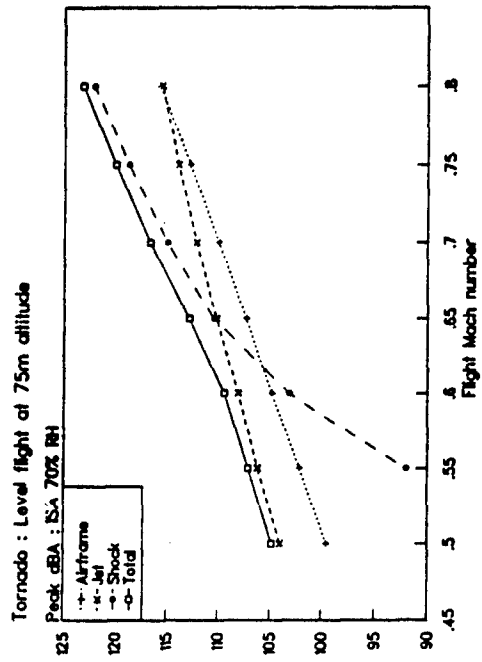
Fig 24   Variation in peak dBA levels with flight speed

Discussion

QUESTION BY: D..Hunt, US Air Force

Could you comment on the possibilities of determining airframe noise using a full scale mock-up in a wind tunnel with the engine-generated noise sources absent?

AUTHOR'S RESPONSE:

Such measurements would indeed be very helpful but I am aware that wind-tunnel noise measurements at high flight speeds suffer from several practical difficulties. I am not expert in this field but I believe that an acoustically-treated transonic wind-tunnel would be necessary and those that I know, the Boeing 12'x8' and the ARA 8'x7', could only accommodate model-scale aircraft. Recent calculations indicate that the background noise levels of these tunnels would dominate the airframe noise of suitable-sized aircraft models, which would make meaningful measurements extremely difficult. However, such tests might be able to be carried out at lower flight speeds (around 0.3M) in a larger low-speed tunnel of better acoustic quality and the comparison of such measurements with aircraft glide data at the same flight speed could still constitute a definitive programme.

QUESTION BY: J.M. Seiner, NASA/LARC, USA

From Table 1 of your paper one cannot tell what the jet noise might actually be expected to be since you do not provide details of your engine conditions. Since you have many negative climb angles, one might suspect that for a resulting jet speed reduced engine power settings would be involved. Thus one expects jet noise to be low, perhaps emphasizing the importance of airframe noise. We do not know from your Table 1 if other constant aircraft velocities were then also conducted with higher power settings. One can only presume that this was done, based on your present comments concerning the relative amplitude of airframe noise.

AUTHOR'S RESPONSE:

The tests with large negative climb angles were conducted solely as a means to try to quantify the airframe noise from the aircraft. They were not intended to be representative of any operational condition of a combat aircraft. By measuring the noise in such tests with the engines operating at flight idle, levels of airframe noise can be obtained which, when compared with the noise levels measured from the aircraft in _level_ flight at the same speed, indicate the contribution that airframe noise makes to the total aircraft noise signature.

QUESTION BY: F. Kennepohl, MTU, Germany
Would you think further research work is necessary on your findings about the contribution of airframe noise to combat aircraft flyover noise, and if yes, what would you propose?

AUTHOR'S RESPONSE:
In the oral presentation of our paper I was able to describe a more recent interpretation of the Tornado data which, to my mind, demonstrates convincingly the importance of airframe noise. However because of the considerable practical significance of the result, I would not rule out a confirmatory test using an alternative technique if this could be done at an acceptable cost and effort. Since I do not know of any such alternative, it would seem to me to be a better approach to carry out further tests of the present type with the aircraft, so that additional information of practical use can be obtained at the same time as research data to help our understanding.

COMMENT BY: U. Michel, DLR Berlin, Germany
I think, everyone in the audience expects a comment from my side since your conclusions differ completely from ours. The design of your study enabled you to operate the aircraft at the same flight speed with different power settings, and you conclude quite convincingly, by comparing a powered and a flight idle case at $M_f < 0,8$ that jet noise is negligible in these cases. This is based on the assumption that there is no jet noise in flight idle. However, the jet is still powerful in flight idle since it is separated from the ambient flow by a wake. I have calculated the instability of such a jet and found that it should be capable of a self sustained, purely natural oscillation. The frequency of this oscillation depends on the width of the wake and could well be 1,5 kHz as reported in your figure 25. Therefore, I feel that further research is needed to resolve this issue.

AUTHOR'S RESPONSE:
We do not make the assumption that the (installed) jet noise is negligible when the engine is operating at flight idle. We agree that would be an unsustainable assertion. Rather, we assume that the engine jet noise will change to an observable extent when, at a given flight speed, the engine operating condition is changed from flight idle to that giving a high sub-critical nozzle pressure ratio. Since this latter change will result in a substantial change in the jet wake conditions, it is our view that the absence of any significant change in the flyover noise levels demonstrates that jet noise is negligible.

MEASUREMENT AND PREDICTION OF NOISE FROM LOW-ALTITUDE MILITARY AIRCRAFT OPERATIONS

Bernard F Berry, Richard C Payne and Anthony L Harris
National Physical Laboratory
Teddington, Middlesex TW11 0LW, U K

and

Ralph J Weston
RAF Institute of Community and Occupational Medicine
RAF Halton
Aylesbury
Bucks,HP22 5PG

SUMMARY

In response to the rapid growth in demand for information on noise levels around military airfields in the UK, NPL developed AIRNOISE, a mathematical model for computing aircraft noise contours. Since its first applications in 1981, the model has been used to determine zones of eligibility within the MoD compensation scheme. The model has been subject to continuous development, e.g. the incorporation of Harrier V/STOL operations. We have now extended the model to include noise from high-speed, low-level operations. The model predicts not only maximum levels but the complete time-history, so that the rapid onset rate can be estimated. To aid refinement and validation of the model, a special exercise has been conducted in which Tornado, Harrier, Jaguar, Hawk, F-15 and F-16 aircraft have flown straight and level at heights between about 100 ana 400 feet, at various speeds and engine power settings over an array of microphones. This paper describes the trial and the results obtained. The prediction model is outlined and comparisons made between predictions and measurements.

1. INTRODUCTION

In the UK as in other NATO countries, there is growing public concern about the noise from high-speed, low-altitude operations of military jet aircraft. The House of Commons Defence Committee recently reported on noise and other aspects of such operations (1). At the Fifth International Conference on Noise as a Public Health Problem, Galloway referred to "of the order of 150,000 sorties" expected in the UK during 1986 (2). For a number of years the National Physical Laboratory, supported by the Ministry of Defence, has been developing AIRNOISE, a mathematical model for computing aircraft noise contours (3). As part of the continuous programme of development of the model we were asked by the Royal Air Force Institute of Community and Occupational Medicine to extend it to include low-altitude military operations. The objective is to predict not only maximum levels but also the onset rate of the noise of these very rapid events. To provide data with which to validate and refine the prediction model a special joint NPL/RAF ICOM

trial - "Exercise Luce Belle" - has been conducted at RAE West Freugh, Stranraer, in which a number of different aircraft types have been flown straight and level at heights between about 100 and 400 feet above ground level, at various speeds and engine power settings. This paper describes the trial and presents the results obtained. The prediction model for noise from low-flying and the comparison of predictions with measurements are also described.

2. FLIGHT TEST PROGRAMME

The tests took place at RAE West Freugh in June 1990. Figure 1 shows an overall view of Luce Bay, the airfield and the "Hard and Soft target" areas. All aircraft followed the track shown at a bearing of 310 degrees. Figure 2 shows the target areas in detail with the measurement sites.

The aircraft types used in the trial were:-

Tornado GR1
Jaguar
Harrier GR5
Hawk T1A
F-15
F-16

Each aircraft was required to carry external stores as normally used in low-flying training.

For each aircraft a number of conditions were selected typical of those encountered in low-altitude flying. For the purposes of the trial these included conditions which might only occur in exceptional circumstances e.g. 550 knots. Pilots were instructed to adjust engine power at the start of the run to achieve the target speed over the primary site. Each aircraft flew one or two sorties during which the selected conditions were replicated over a number of runs across the target area. For each run the Range Controller directed the aircraft on to the correct line from the SE end of Luce Bay. The pilot then used the three lights marked on Figure 1 to line up over the final stage of the run-in. The pilot was required to stabilise the aircraft at the correct conditions at the "Run start" point and maintain steady flight until the radio call "End of run". At this point he was to throttle back, pull up and turn to avoid overflying populated areas.

3. NOISE MEASUREMENTS

The primary site was directly under the flight track on the edge of the hard target area. The deployment of the various microphones, some at 1.2 m high and some in the ground plane, is shown in Figure 3. Each microphone signal was recorded digitally on a Sony PCM 2000 DAT recorder together with IRIG B time-code signals. At the secondary site 1000 m perpendicular to the flight track, a pair of 1.2 m high and ground plane microphones were used. Each of the signals from these was recorded on a Sony PCM 701 system along with a time-code signal. Data from the ground plane microphones are not included in this paper but are being analysed as part of the programme of work on this topic reported on previously by Payne (4). At the third site directly under the flight track a limit-

ed number of direct measurements were made using a Cirrus 2.36 data acquisition integrating sound level meter. This stores successive values of the equivalent continuous A-weighted sound pressure level, $L_{Aeq,125\ ms}$ during an event for later transfer to a portable computer.

4. AIRCRAFT TRACKING

For a noise measurement exercise of this kind it is vital that information be obtained on the aircraft's actual height, speed and ground track, since a small deviation could have a large influence on the results. Optical kine-theodolites and tracking radar data were obtained by staff of RAE West Freugh. In addition video cameras and recorders with associated time-code clocks were used at all noise measurement sites. These were intended to supplement the RAE data particularly in cases where the kine-theodolites could not operate due to wet weather.

5. DATA ANALYSIS AND RESULTS

Each recorded signal was replayed in the laboratory through a Bruel and Kjaer Type 2131 analyser controlled by a Tektronix 4052A computer. The analyser was set to an integration time of 125 ms and 1/3-octave spectra were sampled at a rate of 10 per second and stored on disk. For each event, values of L_{Amax} and sound exposure level L_{AE}, were calculated. The resulting values for each of the 1.2 m microphones at the primary and secondary sites, for each event (run) of each aircraft, are given in the

detailed reports of the trial (5,6). Tracking data for each run, referred to the primary site, are also tabulated in these reports.

Taking the data for the 1.2 m microphone on concrete - set 4 - the values of L_{Amax} have been plotted against actual height for the various groups of speed/engine power conditions for each aircraft. The results for each aircraft are given in the detailed reports, but as an example the results for the Tornado are shown in Figure 4. In each case regression lines were also calculated. Using the regression equations it is possible to calculate the values of L_{Amax} corresponding to heights of exactly 100 and 250 feet in the case of Tornado, Harrier and Jaguar, and 150 and 250 feet for the Hawk. These values are given in Table 1. The values of L_{Amax} for the various conditions in the case of Tornado are shown graphically in Figure 5. Such data can be used to estimate the effects of changes in speed at a given height etc. We can also use this data to compare different aircraft types for the same conditions. Thus Figure 6 compares all four RAF aircraft at 480 knots and 250 ft.

Similar noise trials in the USA have shown a rapid decrease in noise levels as one moves away from the flight track. To illustrate this, levels measured at set 4 under the flight track have been compared to those at 100 m to the sideline - set 1 - and to those measured at the secondary site at 1000 m. Typical results are

given in Figure 7. Thus for Tornado, levels fall by 10 dB over the first 100 m and by 20 dB over 250 m.

Data at the third site were obtained for the Harrier and Tornado sorties. Complete time-histories of $L_{Aeq,125\ ms}$ for a ten-second time period during each event are reproduced in Ref.6. Examples for two runs of Tornado are shown in Figure 8, which also gives the onset rate in decibels per second.

It is interesting to compare the results of the present trial with those published for similar trials in the USA(7). For the F-16, data on over-flights at around 500 knots with an engine power setting of 84% "Intermediate military", and at heights between 166 and 351 feet have been analysed and in Figure 9 the regression line obtained for this US data is overlaid on our data from Exercise "Luce Belle". The slopes of the regression lines are virtually identical. Allowing for differences in power settings and speeds, the two sets of results are reasonably comparable.

6. THE FLYPAST NOISE PREDICTION MODEL

This model is related to the AIRNOISE model but separate from it. The software is designed to calculate a time-history of the A-weighted sound pressure level , at a single point on the ground for a flypast of an aircraft operating under defined conditions. The sound exposure level, L_{AE}, the maximum level L_{Amax}, and

the rise-time over the top 30 dB are also calculated. The calculations make use of the noise-distance-power database of AIRNOISE acquired during Exercise Bedlam (8).

The sequence of stages of the software is as follows.
The required aircraft type is selected from a list of eleven and an appropriate directivity correction file selected. A typical pattern for the Tornado is shown in Figure 10. Corrections are read from the file at ten degree intervals. A power setting is selected and the associated coefficients of the noise distance equation are read from the aircraft data file. The aircraft height, speed and the lateral distance from the observation point to the flight track are entered. From this the minimum slant distance is calculated. Then at one-tenth second intervals throughout the event the slant distance and the angle between the line from aircraft to observation point and the flight path are calculated. Using this angle the directivity correction is interpolated from the table. A level is calculated at the observation point from the noise-distance equation. Corrections are then made for engine power, directivity and lateral attenuation using the SAE procedure (9). From the series of levels throughout the event the other quantities are calculated.

7. COMPARISON WITH MEASUREMENTS

Figure 11 shows an example of the output of the model for a set of conditions actually used

in Exercise "Luce Belle", compared with the measured time-history for this event. Figure 12 compares measured and predicted values of L_{Amax}. On average the model under-predicts by about 1 dB. Further work is in hand to improve the model using source data obtained in an independent noise trial on Tornado (10).

8. CONCLUSIONS

A successful trial has been conducted, giving a unique set of data on noise from military aircraft operating at low-altitude. The data allow the effects on noise levels of changes in airspeed and height to be estimated, and can be used to compare aircraft types in similar conditions.
A prediction model has been developed and shown to give good agreement with measured data.

9. ACKNOWLEDGEMENTS

10. REFERENCES

1. Anon, 1990. Low flying. Defence Committee of the House of Commons. HMSO. May 1990.

2. W J Galloway, 1988. Critical issue - military aircraft. Proc. 5th International Conference on noise as a public health problem, Vol. 5, 137-148. ISBN 91-540-5115-0.

3. R J Weston and B F Berry, 1990. Noise from military airfields in the United Kingdom. Proc. InterNoise '90, 413-416.

4. R C Payne, 1985. An experimental appraisal of the use of ground plane microphones for aircraft noise measurement. NPL Acoustics Report Ac 104.

5. B F Berry, R C Payne and A L Harris, 1991. Noise levels of military aircraft at low-altitude: Exercise "Luce Belle". NPL Report RSA(EXT)14.

6. B F Berry, R C Payne and A L Harris, 1991. Noise levels of USAF aircraft in Exercise "Luce Belle". NPL Report RSA(EXT)16.

7. J D Speakman, 1989. Lateral attenuation of military aircraft flight noise. AAMRL-TR-89-034.

8. P Fethney and A Hazell, 1983. External noise of MoD military aircraft. RAE Technical Report 83058.

9. Society of Automotive Engineers, 1982. Prediction method for lateral attenuation of airplane noise during takeoff and landing. Aerospace Information Report AIR 1751.

10. W D Bryce, P J R Strange and R A Pinker, 1991. Identifying the principal noise sources of a fixed-wing combat aircraft in high-speed flight. These Proceedings.

Table 1.   Estimated values of L_{Amax} from regression lines.

	Height (ft)	Speed (kts)		
		550	480	420
Tornado	100	127.8	123.5	116.4
	250	121.6	117.3	110.0
Harrier	100		127.1	124.2
	250		119.0	115.4
Jaguar	100	126.5	121.5	117.2
	250	119.7	114.0	108.6
Hawk	150		121.9	104.7
	250		119.2	98.2
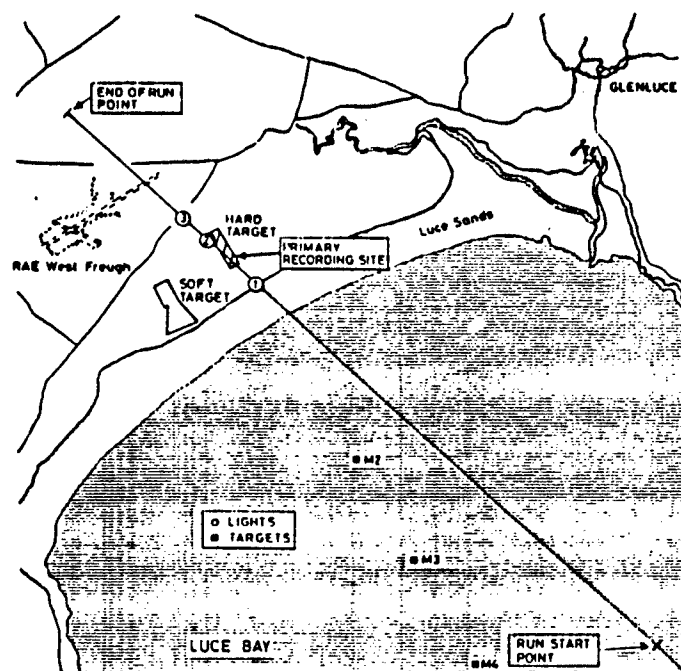
Figure 1. Overall view of Luce Bay.
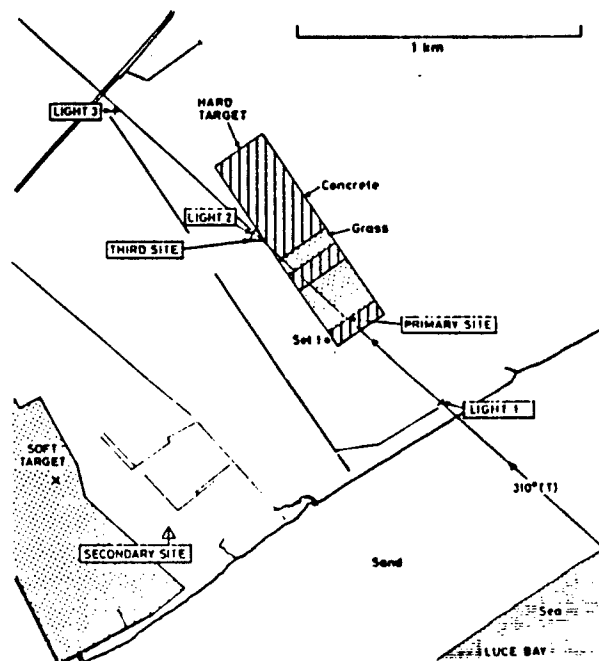
Figure 2. Detail of the Hard Target area and primary site.

o   Ground-plane microphone
●   1.2m-high microphone
□   Tracking camera
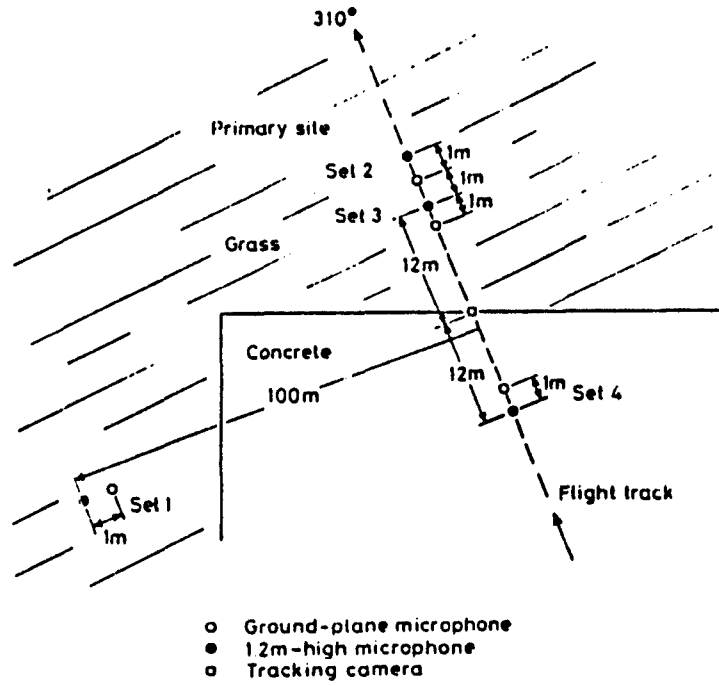
Figure3. Deployment of microphones at primary site.
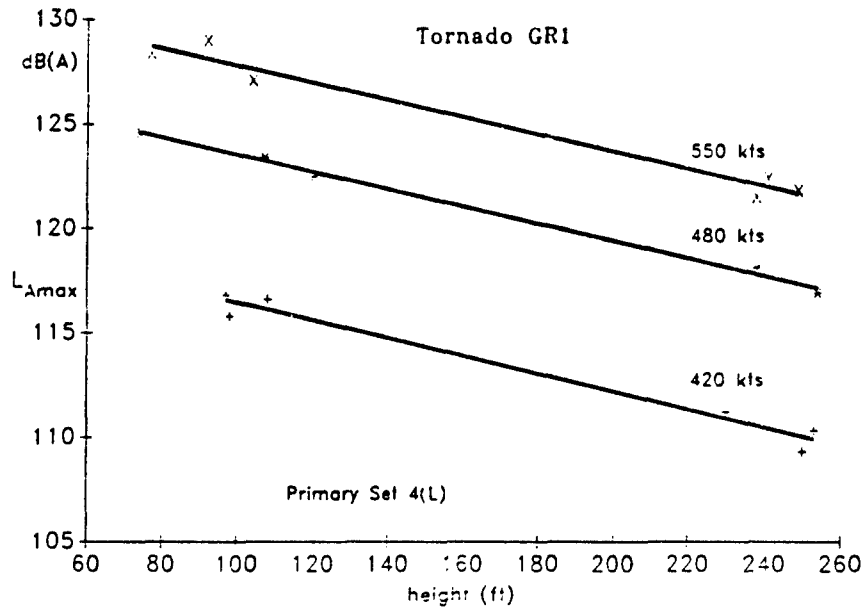
Figure 4. Maximum noise levels at primary site : Tornado.
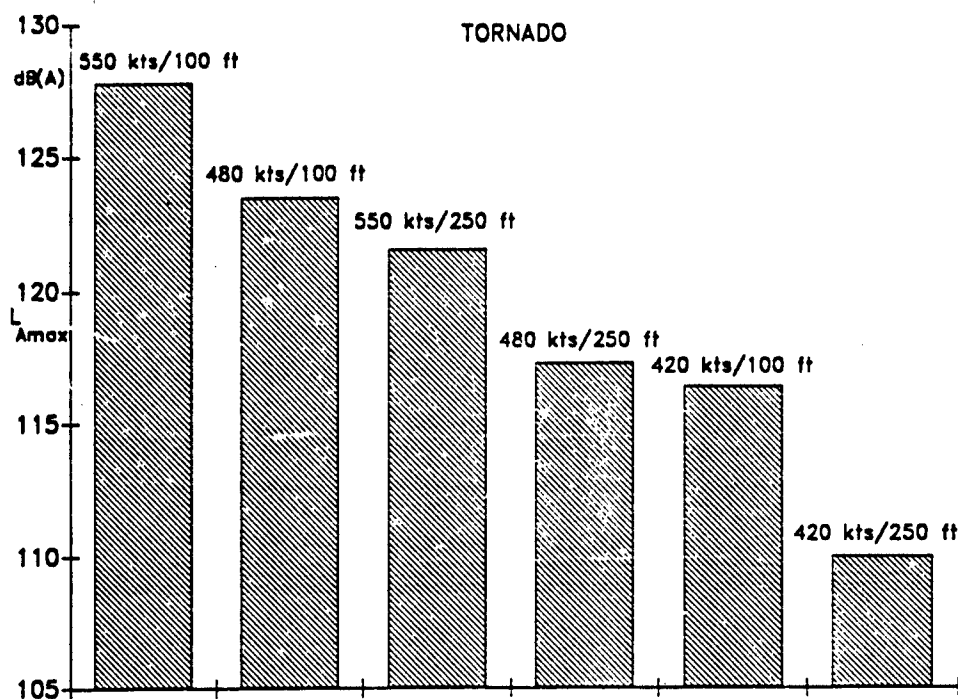
Figure 5. Maximum noise levels for various conditions : Tornado.
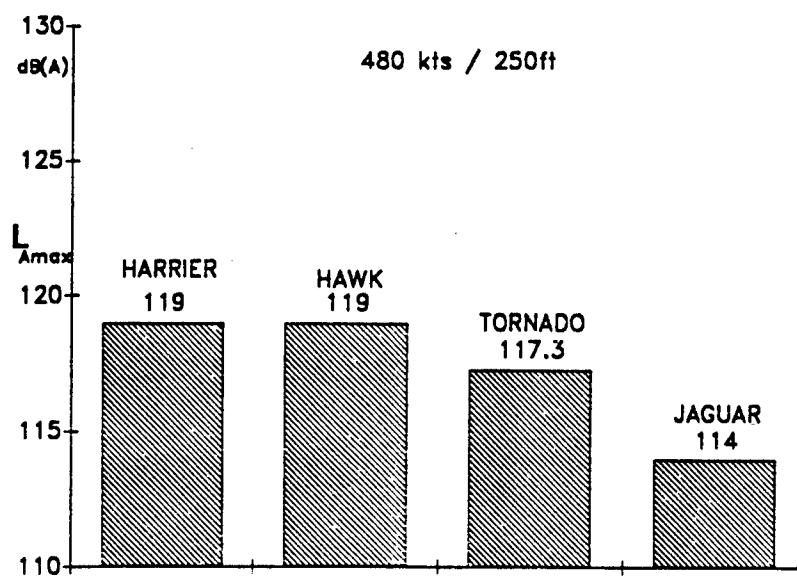
Figure 6. Maximum levels for different aircraft, 480 knots/250 feet.
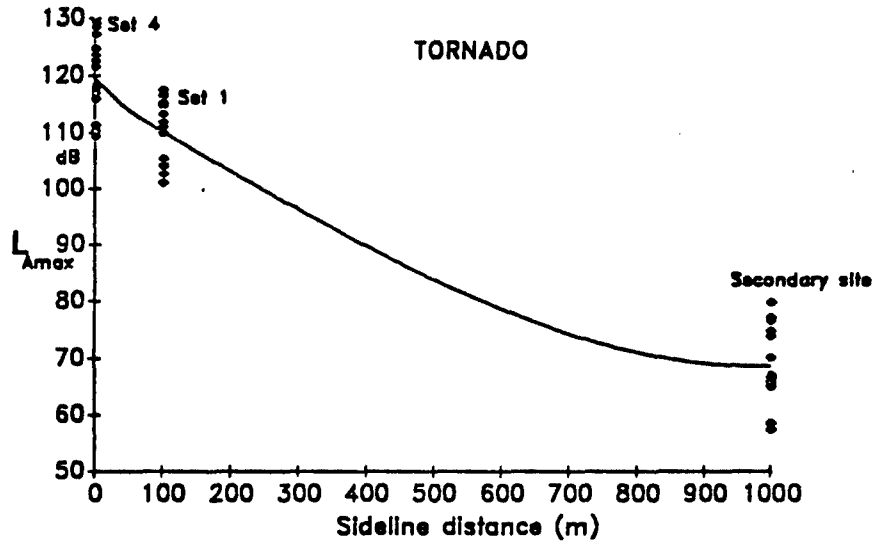
Figure 7. Comparison of overhead and sideline noise levels : Tornado
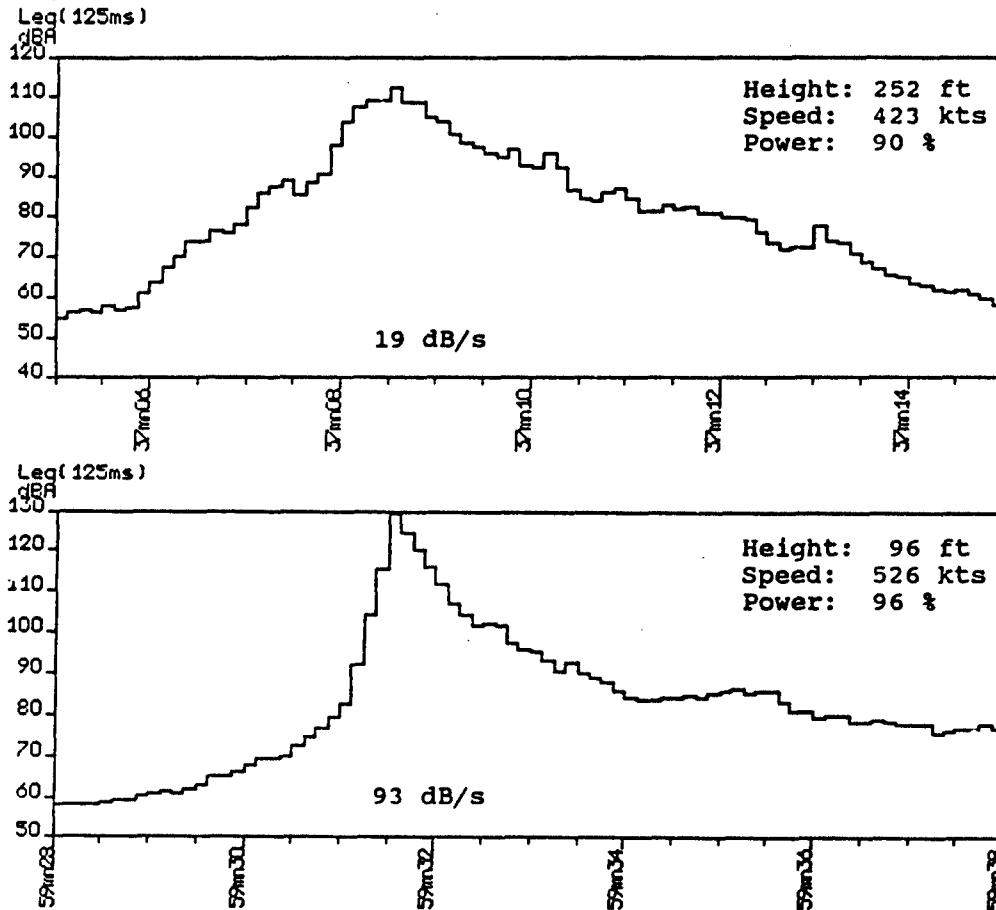
Figure 8. Time-histories at third site : Tornado.

F - 16
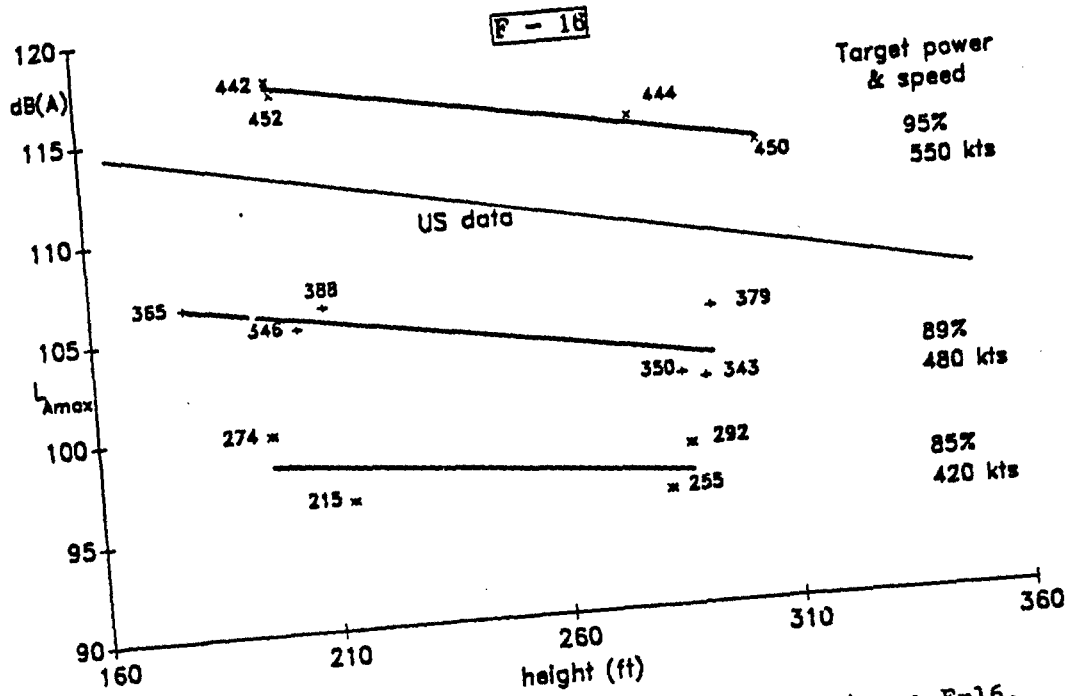
Figure 9. Comparison of US data with this exercise : F-16.

DIRECTIVITY CORRECTION
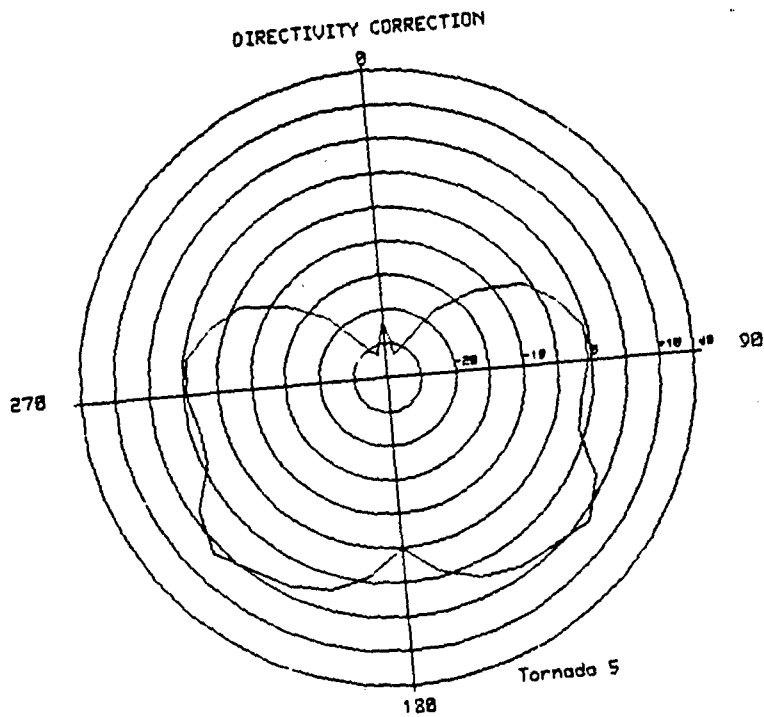
Figure 10. Directivity pattern used for Tornado in flypast model.
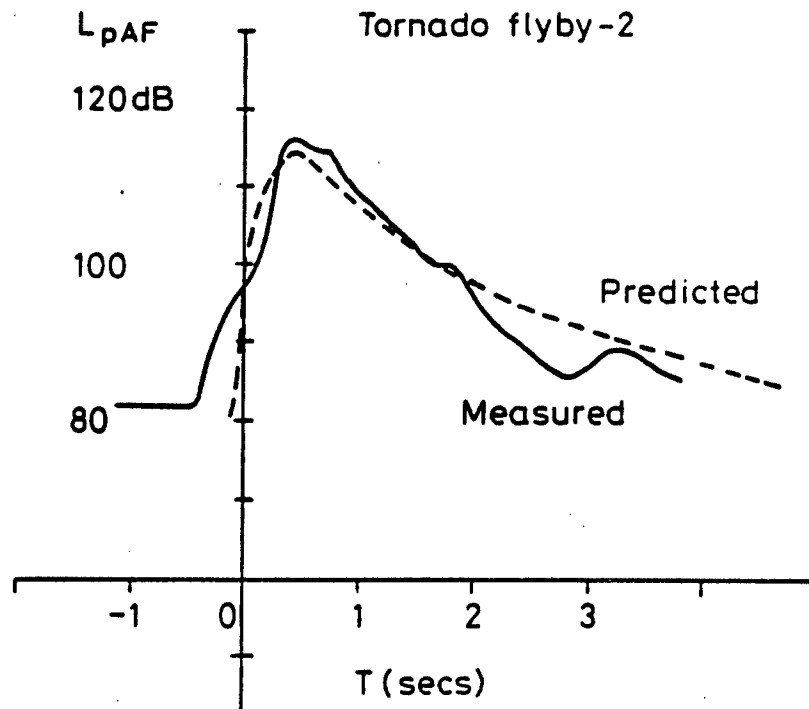
Figure 11. Comparison of measured and predicted time-histories.
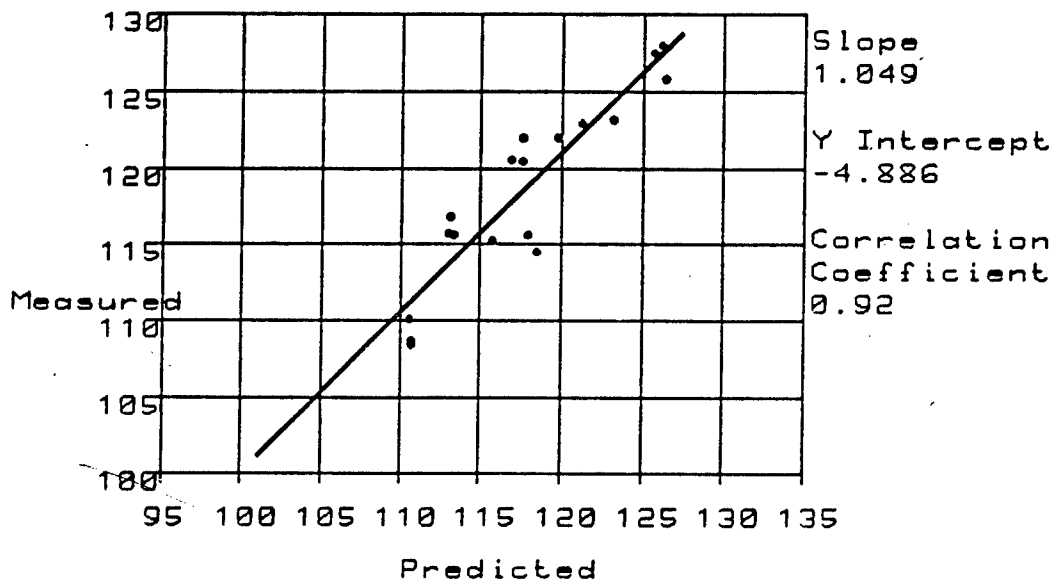
Figure 12. Measured and predicted values of L_Amax

AD-P007 529

|||||||||||||||||||||||||||||||||||

MECHANISMS OF SOUND GENERATION IN SUBSONIC JETS

by

E. Campos and **F. Mallen**
Instituto Nacional de Técnica Aeroespacial
Carretera Torrejon a Ajalvir s/n
28850 Torrejon Ardoz
Madrid
Spain

92-17432

|||||||||||||||||||||||||||||

SUMMARY

This paper gives an overview of some important features of the process of sound generation in subsonic jets. The outstanding aeroacoustic theories are briefly reviewed and some distinguished phenomena relevant to jet noise, like both the effects of source convection and temperature are explained. Finally some mechanisms of sound generation by turbulent jets reported in the literature on the topic are examined.

1. INTRODUCTION

The most fundamental component of the noise issuing from a turbojet exhaust is that due to the turbulent mixing of the jet exhaust with the surrounding fluid, which is termed "jet mixing noise". There is a further important source, restricted to supersonic jets, known as "shock associated noise", which has deserved less attention from the scientific community than the former one, and it will not be treated herein. Additional sources of noise named "excess noise", "tailpipe noise" ... have emerged with the development of low jet efflux velocity engines such as the high bypass ratio ones. However, since it is difficult to distinguish these sources in the modern pure jet or low by-pass ratio used in combat aircraft, because they are masked by the dominant jet mixing noise, then these sources will not be considered in this paper. Therefore attention will be only focused on jet mixing noise.

Lighthill's masterpiece,"the acoustic analogy" [1]-[4], has been the foundation for the study of jet-mixing noise, in particular his result of the fluctuating Reynolds shear stresses as the source for the noise generated by a jet flow, and the subsequent prediction that the jet noise should vary as the eigth power of the jet velocity. This theory was in first instance developed for subsonic flow, but has been extended to the Mach number range of engineering interest. Although the Lighthill theory is exact it is complicated to handle it, because it is almost impossible to evaluate a priori the source function. In fact, the source term includes the actual turbulent sources and, implicitly, the effects of source convection and those of difraction,

absorption, refraction and scattering of sound. To bring these effects explicitly in the theory, and in an attempt to explain discrepancies between the results of various experiments and some predictions of the theory, other researchers developed reformulations of the acoustic analogy [5]-[9], but with the more general view of explaining the topic of aerodynamic sound generation.

The mechanisms from sound generation from turbulent jet is caused by turbulence related phenomena not yet well understood. In the following sections, after an overview of the referred to theories in relation to the jet noise issue, a brief description of the jet noise generation mechanisms devised so far is shown.

2. LIGHTHILL'S ACOUSTIC ANALOGY

Aeroacoustic theory is aimed to give an accurate prediction of the sound generated by turbulent flow from the specification of that flow. The cornerstone of this theory is Lighthill's model [1],[2], which formulates an analogy between the non-linear flow problem and the linear theory of classical acoustics.

Considering a non-steady fluctuating flow in a finite region surrounded by fluid, which far from that region is supossed at rest and uniform, with density ρ_0 and sound speed c_0. The exact equations of conservation of mass and momentum in the fluid, provided there are neither external sources of mass nor external forces acting on the fluid, are

$$\frac{\partial}{\partial t}\rho + \frac{\partial}{\partial x_i}\rho u_i = 0 \qquad (2.1)$$

$$\frac{\partial}{\partial t}\rho u_i + \frac{\partial}{\partial x_i}(\rho u_i u_j + p_{ij}) = 0 \quad (2.2)$$

These equations were arranged by Lighthill [1] to arrive to an equation for the density

$$[\frac{\partial^2}{\partial t^2} - c_0^2 \nabla^2]\rho = \Box \rho = \frac{\partial^2 T_{ij}}{\partial x_i \partial x_j} \qquad (2.3)$$

where T_{ij} is the so-called Lighthill stress tensor

$$T_{ij} = \rho u_i u_j + p_{ij} - c_0^2 \rho \delta_{ij} \qquad (2.4)$$

This is exactly the equation of sound propagation in a uniform medium at rest, acted upon by external fluctuating stresses, represented by the right hand side. Therefore the fluid can be seen as an acoustic field whose source is a quadrupole distribution, the quadrupole stress density being Lighthill's stress tensor T_{ij}. This tensor is zero in the sound field outside the flow region and Lighthill's theory reduces to the ordinary acoustic theory at the points outside the region of unsteady flow. Usually the viscous contributions to T_{ij} are small. On the other hand pressure and density are related by $dp = c^2 d\rho$ or $c_0^2 \rho'$ if the temperatures in the flow are similar to those existing in the surrounding region. Moreover in low Mach number flow ρ may be aproximated by ρ_0. Under all these conditions, which met for subsonic cold jets, Lighthill's tensor can be

expressed as

$$T_{ij} = \rho_o u_i u_j$$

The general solution to the Lighthill equation is the result of applying the differential operator of the right-hand side to the convolution product of T_{ij} by the Green's function of the wave operator. The solution of this latter problem

$$\Box G(\vec{x}, t) = \delta(\vec{x})\delta(t)$$

is

$$G(\vec{x}, t) = \frac{\delta(|\vec{x}|)\delta(t)}{4\pi c_o |\vec{x}|}$$

therefore

$$\rho'(\vec{x}, t) = \rho(\vec{x}, t) - \rho_o =$$

$$= \frac{\partial^2}{\partial x_i \partial x_j} \int_V T_{ij}(\vec{y}, z) \frac{\delta(|\vec{x}-\vec{y}|-c_o(t-\tau))}{4\pi c_o^2 |\vec{x}-\vec{y}|} d^3\vec{y} d\tau$$

(2.5)

Finally integrating over τ gives

$$\rho'(\vec{x}, t) = \frac{1}{4\pi c_o^2} \frac{\partial^2}{\partial x_i \partial x_j} \int_V \frac{T_{ij}(\vec{y}, t-\frac{|\vec{x}-\vec{y}|}{c_o})}{|\vec{x}-\vec{y}|} d^3\vec{y}$$

(2.6)

Each quadrupole element at y generates a field that travels out at the speed of sound c_o to reach the observer at x at a retarded time $|x-y|/c_o$ later.
Since the main interest is the far field solution of the turbulence generated sound one can obtain the following equation

$$\rho'(\vec{x}, t) =$$

$$= \frac{1}{4\pi c_o^2} \int_V \frac{\partial^2 r}{\partial x_i \partial x_j} \left(\frac{1}{c_o^2 r} \frac{\partial^2 T_{ij}}{\partial t^2} + \frac{2}{c_o r^2} \frac{\partial T_{ij}}{\partial t} + \frac{2}{r} T_{ij} \right) d^3\vec{y}$$

(2.7)

where

$$|\vec{x}-\vec{y}| = r$$

and use has been made of

$$\frac{\partial}{\partial x_i} = \frac{\partial r}{\partial x_i} \frac{\partial}{\partial r}$$

If λ is the characteristic wavelength of the sound, the acoustic condition of far field is

$$\lambda/|\vec{x}-\vec{y}| = \lambda/r \ll 1$$

One then arrives to the following expresion for ρ'.

$$\rho'(\vec{x}, t) = \frac{1}{4\pi c_o^4} \frac{(x_i-y_i)(x_j-y_j)}{|\vec{x}-\vec{y}|^3} \int_V \frac{\partial^2 T_{ij}}{\partial t^2} d^3\vec{y}$$

(2.8)

If l is a characteristic length of the source, the geometric condition of far field is

$$l/|\vec{x}-\vec{y}| \ll 1$$

Moreover if the origin of coordinates is taken at the interior of the source then

$$x_i - y_i \approx x_i \qquad x_j - y_j \approx x_j$$

Finally one arrives to the expression for the far field approximation

$$\rho'(\vec{x}, t) = \frac{1}{4\pi c_o^4} \frac{x_i x_j}{|\vec{x}|^3} \int_V \frac{\partial^2 T_{ij}(\vec{y}, t-\frac{|\vec{x}-\vec{y}|}{c_o})}{\partial t^2} d^3\vec{y}$$

(2.9)

Let us consider now in the

light of this theory, the topic of jet noise, that is to say sound radiation from a turbulent flow (i.e. a meanflow upon which is superimposed a distribution of eddies). In fact Lighthill [4] suggested to split the turbulence flow into independent quadrupole distributions, the extent of each one being roughly the size of a typical energy bearing eddy. The internal motion of the eddies can be decoupled of the convection by mean flow, so the effects of these motions can be studied independently. The first thing to do is to choose adequate scales. The velocity fluctuations are characterized by the rms velocity while the width of the mixing layer at any axial station supplies the length scale (typical size of eddies). Both magnitudes define the time scale $1/u$. On the other hand, the sound is radiated from the points inside one eddy at different times, the maximum difference in emission times over a volume 1^3 being of order $1/c_o$. If this time is small compared to the characteristic time $1/u$, which implies that the Mach number of the turbulent eddies is small ($m=u/c_o<<1$), then the differences in emission times are negligible. The typical frequency of the time variations in the eddy is $u/1$, so the wavelength of the radiated sound is c_o $1/1 = 1/m$. Therefore the condition $m << 1$ means that the length of the eddy is much smaller than the wavelength of the sound. In that case the source is compact relative to the

wavelength. Because of the fluctuation velocities are well below the sound speed in jets, the turbulent eddies are compact.

Looking to the internal dynamics of the eddies, some facts have been experimentally determined, namely the correlation of the motion inside any eddy, while this motion is quite uncorrelated with the motion inside any other one. According to a general principle of wave theory, as pointed out by Lighthill [4], with well correlated sources amplitudes combine linearly, but with uncorrelated sources intensities combine linearly. This fact allows to deal with the problem of jet noise by applying Lighthill wave equation, since it is a linear one (with a non-linear source term), and thus we may add the density fields generated by points inside a single eddy, to get the field due to that eddy. Once this process has been performed, we can square the density to obtain the intensity from the eddy. The total intensity is just the sum of the intensities of the eddies. So it is clear that the first and main issue is to get the density field radiated by an eddy in nearly incompressible turbulent flow.

Going back to (2.9), which gives the distant density field, one can obtain that generated by a single eddy by introducing the fact of compactness. Thus, retarded time differences are neglected, so the expression for density is

$$\rho'(\vec{x},t)=\frac{1}{4\pi c_o^4}\frac{x_i x_j}{|\vec{x}|^3}\int\frac{\partial^2 T_{ij}(\vec{y},t-\frac{|\vec{x}|}{c_o})}{\partial t^2}d^3\vec{y}$$

(2.10)

Now, the estimation for $\rho'(x,t)$ is

$$\rho'(\vec{x},t)\sim c_o^{-4}x^{-1}(1/u)^{-2}\rho_o u^2 l^3\sim$$

$$\sim\rho_o(1/x)m^4$$

(2.11)

Since the sound power is

$$P=\int_o I d\sigma$$

where

$$I=\langle p'^2\rangle/\rho_o c_o \qquad p'=c_o^2\rho'$$

One obtains the following estimate for the acoustic power of an eddy

$$P\sim\rho_o u^3 l^2 m^5$$

(2.12)

Therefore the sound power radiated by a distribution of eddies, each being of volume l^3, occupying a volume V is given by

$$P_T\sim\rho_o u^3 l^2 m^5(V/l^3)$$

(2.13)

expression that is equivalent to the famous U^8-law for the variation of acoustic power with jet speed U. This law is deduced by applying Lighthill's theory directly to the jet flow. The fluctuations in $\partial^2 T_{11}/\partial t^2$ will be mainly dominated by $\rho_o U^2(U/l)^2$ where U is the mean exit velocity and l a typical length in the flow (e.g. the nozzle diameter). Therefore the density variations, as provided by Lighthill formula, are roughly

$$\rho'\sim\rho_o(u/C_o)^4(1/x)$$

Then, after estimate the sound intensity, one can get the sound power output P as follows

$$P\sim\rho_o u^8 l C_o^{-5}$$

(2.14)

This prediction agrees very well with experimental results over a range of Mach number values between 0.3 and 2 roughly. It should be noted, however, that for values of M lower than about 0.6 noise sources other than the jet mixing process can contribute, thus giving rise to deviations from the U^8 law. By controlling the experiment, assuming a clean flow upstream of the nozzle, it has been observed that U^8 law continues to hold down to M = 0.3.

3. EFFECTS OF SOURCE CONVECTION

Now, the effect of convection of the quadrupole distribution on the jet noise will be considered. According to Lighthill [1], the time rate of change must be taken in a frame of reference moving with the convection velocity U_c. Only intrinsic rates must be considered, and those must not be inflated by adding convective derivatives. Anyway, these convective derivatives do not contribute to the acoustic radiation, they constitute an octupole field, whose radiation is small compared with the quadrupole field, due to time variations.

The stress tensor T_{ij} which appear in the general expression (2.6), can be rewritten as

$$T_{ij}(\vec{\eta}, t-\frac{|\vec{x}-\vec{\eta}|}{c_o}) \tag{3.1}$$

where

$$\vec{\eta} = \vec{y} + \vec{M}_c |\vec{x}-\vec{y}| = \vec{y} + \vec{M}_c r \tag{3.2}$$

$$\vec{M}_c = c_o \vec{u}_c \tag{3.3}$$

U_c being the convection velocity of the eddies (a static jet is considered). After some manipulation, one arrives to the following expression for the far field solution, θ being the angle between the directions of motion and emission.

$$\rho'(\vec{x}, t) =$$

$$= \frac{1}{4\pi c_o^4} \frac{(x_i x_j)}{|\vec{x}|^o (1-M_c \cos\theta)^o} \int_V \frac{\partial^2 T_{ij}(\eta, t-\frac{r}{c_o})}{\partial t^2} d^3\eta \tag{3.4}$$

Consequently the intensities include an aditional factor $(1-M_c \cos\theta)^{-6}$, but as it was shown by Ffowcs Williams [10], the number of quadrupoles whose radiation arrives simultaneously is the total number affected by the term $(1-M_c \cos\theta)$, therefore the directional distribution of intensity must carry a factor $(1-M_c \cos\theta)^{-5}$.

Let us consider now, according to Crighton [11], the effect of convection on the turbulets eddies. The general formula for a single eddy (2.11) is expressed in the form

$$\rho'(\vec{x}, t) \sim \rho_o (1/x) m^4 \sim$$

$$\sim \rho_o (l_c/x) m^2 (1/\lambda)^2$$

l_c being the eddy size in the convection direction and l the size in direction normal to that one.

The term $(1/\lambda)$ that arises from the far-field nature of the quadrupole can be referred as the compactness ratio. Since the Doppler change in frequency and wavelength is an important convective effect, which modifies the walength λ at rest to $\lambda(1-M_c \cos\theta)$, source convection increases the compactness ratio as well as the radiation ahead of the source and the contrary holds behind the source for $M_c < 1$. Convection also increases the effective quadrupole length scale in the convection direction by the inverse of the Doppler factor, as follows.

$$l_c = l(1-M_c \cos\theta)^{-1} \tag{3.5}$$

Both effects, the wavelength contraction and the change of effective source scale modify Lighthill's result (2.11), which for a convected eddy takes the form

$$\rho \sim \rho_o (1/x) m^4 (1-M_c \cos\theta)^{-3} \tag{3.6}$$

For a distribution of eddies, while the eddy volume increases because of convection, the actual flow volume does not, therefore the number of eddies must decrease correspondingly and the intensity per unit volume is of order

$$I \sim \rho_o u^8 (l_c/x)^2 m^5 (1-M_c \cos\theta)^{-6} (l_c l^2)^{-1} \tag{3.7}$$

And for a fixed volume V .

$$I \sim \rho_o u^8 (\frac{V}{l^o}) m^5 (1-M_c \cos\theta)^{-5} \tag{3.8}$$

Summarizing, convection makes eddies less compact since the wavelength is reduced and the

effective source scale in the convection direction increased by the effect of the inverse of the Doppler factor $(1-M_c \cos\theta)$. To avoid the singularity at $M_c \cos\theta = 1$ a modified Doppler factor C has been derived

$$C=[(1-M_c\cos\theta)^2+\alpha^2]^{-\frac{1}{2}} \quad (3.9)$$

According to Crighton [11] the coefficient α is the compactness ratio, m, of the turbulent eddy, while Ffowcs Williams [12] gives the following expression for α

$$\alpha^2=(\alpha_o^2\sin^2\theta+\beta_o^2\cos^2\theta)M_o^2 \quad (3.10)$$

The parameters α_c and β_c being a measure of non-compactness of the source.

4. EFFECTS OF TEMPERATURE

It was early suggested that the main effect of the elevated temperature of a jet would be a reduction in the noise level, since the effective source density must decrease, so reducing the contribution $\rho u_i u_j$ of T_{ij}, which is the dominant source. But some experiments, especially those carried out by Hoch et al [13], showed that noise reduction is observed only at high exhaust speeds, while at lower velocities high jet temperature increases the noise emission. To explain this discrepancy it is believed that there is an additional source in hot jets depending on the temperature, but it seems that the jet efflux velocity should not be forgotten. This dependence is in such a way that at low

speeds this new source is dominant, while at higher speeds the classical U^8 law holds, but with a lower effective density than in the cold jet, that is to say that the primary effect of increasing the temperature (decreasing of density) is only apparent at high speeds.

The first attempt to explain these facts was that of Lush and Fisher [14], who pointed out that the second term (i.e. $p-c_o^2\rho$) of the Lighthill source could not be avoided because of the speed of sound in the source differs considerably from that in the sound field. They developed scaling laws for the additional source referred to (entropy fluctuations source, according to Ribner [15]). A perfect gas is assumed and let S be the entropy and $\gamma = c_p/c_v$ the specific heat ratio. Then

$$S=C_v\ln(p/\rho^\gamma)+const$$

whence

$$\frac{\partial\rho}{\partial t}=\frac{1}{c^2}\frac{\partial p}{\partial t}-\frac{\rho}{c_v}\frac{\partial S}{\partial t} \quad (4.1)$$

So one obtains for the term $p-c_o^2\rho$ of the stress tensor the expression

$$\frac{\partial}{\partial t}(p-c_o^2\rho)=(1-\frac{c_o^2}{c^2})\frac{\partial p}{\partial t}+\frac{\rho c_o^2}{c_p}\frac{\partial S}{\partial t}$$

$$(4.2)$$

where c is the local sound speed.

The contributions to the density from the Reynolds stresses and from the entropy fluctuations are then estimated and assumed that they are uncorrelated. It is assumed too that the mix density is the arithmetic

mean of the exit density ρ_1 and the ambient one ρ_O as well as that the entropy fluctuations are proportional to the diference between the entropies of the jet exit and the ambient, $S=S_1-S_O$. In this way the following expression for the intensity at 90° to the jet axis was derived by Lush and Fisher.

$$I=A\left(\frac{v_o}{c_o}\right)^8+B\left(\frac{v_o}{c_o}\right)^4 \qquad (4.3)$$

where

$$A\propto\left(\frac{\rho_o-\rho_1}{2\rho_o}\right)^2$$

$$B\propto\left(\frac{\rho_o-\rho_1}{\rho_o}\right)^2$$

This equation predicts the dominance of the U_O^4 term at low speeds and that of the U_O^8 term at high speeds, in this latter case at a lower level than in a cold jet. Fitting of this equation to experimental data is good over a wide range of temperature ratios as well as of velocities. But this theory has a weak point, that is the lack of the assumption that $DS/Dt = 0$. In fact Morfey [16] pointed out that if molecular diffusion effects are neglected the entropy of the fluid particles is constant.
Morfey carried out an analysis expanding the term $\rho-p/c_o^2$. Part of the expansion cancels the Reynolds stress term, replacing it with a similar term with ρ_o instead of ρ. He finally found two source terms relevant to heated jets at low Mach number, namely a quadrupole

$$\frac{\partial^2}{\partial x_i \partial x_j}(\rho_o u_i u_j)$$

and a dipole

$$-\frac{\partial}{\partial x_i}\left[\frac{\rho-\rho_o}{\rho}\frac{\partial p}{\partial x_i}\right]$$

The contributions of these sources to the intensity in the far field are then scaled as follows

$$I_q \sim \rho_o(U^8/C_o^5)(D/r)^2 \qquad (4.4)$$

$$I_d \sim (\rho_s^2/\rho_o)(U^6/c_o^3)(D/r)^2(\Delta T/T_o)^2 \qquad (4.5)$$

Where ΔT is the difference between jet and ambient (T_O) temperatures, ρ_s is the density at the source and r the distance to the source. Pressure fluctuations in the source have been assumed to scale as $\rho_s U_O^2$. These formulae agree with the behaviour at low speed, because the dipole contribution is being more dominant as the speed is reduced. The behaviour at high Mach numbers is explained by Morfey as due to the fact that at such values the wavelength becomes comparable to the local shear layer thickness. Then the equivalent sources are regarded as radiating in a medium whose properties are close to those of the source region, so c_o and ρ_o are taken as c_s and ρ_s. The effect of taking these values in the acoustic analogy is to reduce the intensity. This reduction, for high subsonic Mach numbers and at 90° to the jet axis, is given by a factor $(T_O/T_s)^3$ for the quadrupole and by $(T_O/T_s)^2$ for the dipole.

5. FURTHER DEVELOPMENTS IN THE AEROACOUSTIC THEORY

The acoustic analogy delivered by Lighthill appears as the major contribution to aeroacoustics devised so far. Nevertheless can not provide solution to every model problem in aeroacoustics because there is a lack of knowledge necessary to describe the source term. In fact an acoustic analogy for a problem like that of jet noise (i.e. sound radiation from a bounded unsteady turbulent flow) consists of a forced wave equation

$$\left(\frac{\partial^2}{\partial t^2} - c_o^2 \nabla^2\right)\rho' = q \qquad (5.1)$$

where q is the source term to be estimated from the specifications of the flow. In the analogy of Lighthill

$$q = \frac{\partial^2 T_{ij}}{\partial x_i \partial x_j}$$

and the main difficulty with this formulation is that effects such as refraction of sound by mean flow gradients and scattering of the sound waves by eddies should be displayed rather than embodied in the stress tensor T_{ij}. On the other hand this analogy ceases to adjust to experimental data at flow Mach number ≈ 2. To avoid these problems Phillips [5] derived a convected wave equation for pressure p in which the source term, which does not contain the density, consists of three terms, namely one of velocities and the other two reflecting effects of viscosity and heat conduction. Omitting these two last ones the equation

takes the form

$$\left(\frac{D^2}{Dt^2} - \frac{\partial}{\partial x_i}\left(c^2\frac{\partial}{\partial x_i}\right)\right)\ln(p/p_o) = \gamma\frac{\partial u_i}{\partial x_j}\frac{\partial u_j}{\partial x_i}$$

$$(5.2)$$

where γ is the specific heat ratio and c the local sound speed.

This equation was objected by Lilley [6] who pointed out that as fluctuations amplitudes become small, the source terms should vanish at least quadratically, the equation then describing propagation of small disturbances through a medium of variable mean properties. Since this property is not a feature of the Phillip's equation, Lilley proposed another one, which follows.

$$\frac{D}{Dt}\left\{\frac{D^2}{Dt^2} - \frac{\partial}{\partial x_i}\left(c^2\frac{\partial}{\partial x_i}\right)\right\}\ln(p/p_o) +$$

$$+2\frac{\partial \bar{U}_i}{\partial x_j}\frac{\partial}{\partial x_i}\left(\bar{c}^2\frac{\partial}{\partial x_j}\right)\ln(p/p_o) =$$

= terms at least quadratic in fluctuations.

$$(5.3)$$

The bar indicates that mean velocity and temperature are considered. These two equations are very difficult to solve in analytical form and in fact they have not yet rendered, to our knowledge, widely accepted results.

Coming back to low Mach number turbulent flows, Powell [7] proposed a theory of vortex sound in which the vorticity within a compact eddy in a slightly compressible isentropic flow is the basic source element, that is to say that induce the whole flow, both the

hydrodynamic turbulent field and the acoustic far field. Then the sound sources can be identified with those regions of the flow with non-vanishing vorticity. He derived an equation for the far-field density perturbations which is an acoustic analogy, the source term being related to vorticity

$$\Box \rho' = \rho_o \nabla(\vec{\omega} \wedge \vec{U}) + \nabla^2(\tfrac{1}{2}\rho_o U^2)$$

(5.4)

the effect of the second source term is much smaller than the first if entropy gradients are negligibly. Then the source term can be taken as

$$q = \rho_o \nabla \cdot \vec{L}$$

where $\vec{\omega} = \nabla \wedge \vec{u}$ denotes the vorticity vector, and $\vec{L} = \vec{\omega} \wedge \vec{u}$ is the expression of the isentropic Lamb vector. In fact Powell proved the acoustic equivalence of the source distributions $\rho \, u_i \, u_j$ and $\rho_o \, y_i \, (\vec{\omega} \wedge \vec{u})_j$. The expression (5.4) shows the generated sound in terms of dipole sources, but since Lamb vector can be regarded as a lift force, and due to momentum conservation these lift forces must be arranged in cancelling pairs, it would not be irrealistic to consider a quadrupole-like structure of the Powell vortex dipole.

A generalization of Powell's approach was derived by Howe [8]. He introduced the stagnation entalphy rather than the density as the acoustic variable. Howe showed first that an analogy could be established in a similar way to that of Lighthill, but replacing the quiescent acoustic medium of this latter one by a steady irrotacional mean flow. Howe first studied the problem of determining the equation satisfied by the perturbation potential due to an irrotational disturbance introduced into a compressible irrotational mean flow. Let $\phi_0 (\vec{x})$ and $\phi_1 (\vec{x}, t)$ be the potential of the unperturbed flow and that of the perturbation respectively and $\phi(\vec{x}, t) = \phi_0 + \phi_1$.

Considering the equations of continuity of mass and that of Bernoulli (isentropic irrotational flow), after some manipulation he derived an equation which describes the propagation of the perturbations through the compressible medium, provided that the steady mean flow is known. This equation can be further linearized with respect to the perturbation potential giving rise to a convected wave equation satisfied by the rate of change of the perturbation potential in the case of low Mach number mean flow. Because of this equation, this potential appears as the natural variable for writing the wave equation for acoustic perturbations. But for an arbitrary mean flow (i.e. there can be vorticity and entropy gradients) a scalar potential is not sufficient to describe the perturbations in the flow, so a new variable must be chosen. This variable is easily selected because the Bernoulli integral may be expressed in the following form

$$\frac{\partial \phi}{\partial t} + B = Constant \qquad (5.5)$$

where B is the stagnation enthalpy per unit mass of an isentropic fluid

$$B = \int \frac{dp}{\rho} + \frac{1}{2} \left(\frac{\partial \phi}{\partial x_i} \right)^2 \qquad (5.6)$$

That is to say that adopting either B or $\partial \phi / \partial t$ is equivalent. Howe generalizes further B, to avoid the difficulties of expressing $\rho = f(p)$ in an arbitrary mean flow, by introducing the specific heat function h, which obbeys the differential equation

$$dh = \rho^{-1} dp + Tds \qquad (5.7)$$

Finally the specific stagnation enthalpy
B = h + ½u² is obtained and used as the variable for the analysis. This is carried out by using the fundamental equations of motion (that of momentum is written in Crocco's form) and after some manipulation, including the assumption of ideal gas to express the source term, the following equation is deduced

$$\left(\frac{D}{Dt} \left(\frac{1}{c^2} \frac{D}{Dt} \right) + \frac{1}{c^2} \frac{D\phi}{Dt} \nabla - \nabla^2 \right) B =$$

$$= \nabla \cdot (\vec{\omega} \wedge \vec{u} - T \nabla s) - \frac{1}{c^2} \frac{D\phi}{Dt} \cdot (\vec{\omega} \wedge \vec{u} - T \nabla s) +$$

$$+ \frac{D}{Dt} \left(\frac{T}{c^2} \frac{D\phi}{Dt} + \frac{\partial}{\partial t} \left(\frac{1}{c_p} \frac{D\phi}{Dt} \right) \right.$$

$$(5.8)$$

where the last two terms of the source term represent the effect of heat conduction.

At points of the flow without vorticity or entropy inhomogenities the source terms vanish and the irrotational perturbation equation emerges. The terms of the right hand side of the equation are considered the acoustic sources, but are confined only to the regions of the flow where the vorticity and entropy gradient vectors are non vanishing. For low enough Mach number and isentropic flow as well as no mean flow, Howe's equation reduces to Powell's result.

One further step in dealing with the vorticity was the formulation of Möhring [9], relating the sound field linearly to vorticity, which it is not the case, to our knowledge, in any other theory devised so far. Möhring argued that Powell's result does not represent the sound only in terms of the vorticity but also includes the flow velocity, which implies difficulties in solving some model problems of vortex distributions. He also noted that Powell's equation as well as Lighthill's are local relations, because the derivatives of, for instance, p at a given position are related to derivatives of the flow velocity at that position. Möhring's approach starts by considering the Green's function solution to the Powell's equation. This solution is integrated by parts, giving the expression

$$p(\vec{x}, t) = -\rho_o \int_v \nabla_y G(\vec{x}, t; \vec{y}, \tau) \cdot \vec{L}(\vec{y}, \tau) d^3\vec{y} d\tau$$

$$(5.9)$$

Then a vector Green function G is defined by

$$\nabla_y G = \nabla_y \wedge \vec{G}$$

Once $\nabla_y G$ is substituted in (5.9), a new integration by

parts is performed and Helmholtz vortex equation

$$\frac{\partial \vec{\omega}}{\partial t} + \nabla \wedge \vec{L} = 0 \qquad (5.10)$$

which is valid for incompressible flow, is applied, and a further integration by parts is undertaken, one obtains the result

$$p = \rho_o \frac{\partial}{\partial t} \int_V \vec{G}(\vec{x}, t; \vec{y}, \tau) \cdot \vec{\omega} \, d^3\vec{y} \, d\tau$$

$$(5.11)$$

where V is the region of non-vanishing vorticity. From this result, the pressure can be calculated from the vorticiy alone. Moreover the pressure depends linearly on the vorticity and therefore too on the velocity, so contributions of the vortices to the sound add linearly. However, there exist a main difficulty in this method, namely that in general the vector $\vec{G}$ does not exist, because the integrability condition for (5.9), which is $\nabla \cdot G = 0$, is not usually satisfied. But Möhring argues that in cases where G is symmetric in its arguments, then satisfies

$$\nabla^2_y G = \frac{1}{c_o^2} \frac{\partial^2 G}{\partial t^2} - \delta(\vec{x} - \vec{y}) \delta(t - \tau)$$

$$(5.12)$$

Therefore $\vec{G}$ exists when the right-hand side of (5.12) vanishes, which meets when $\vec{x}$ is in the far field and $\vec{y}$ in the source and at low enough Mach numbers.

Finally it should be stressed that these approaches to the aeroacoustic theory focused on vorticity are specially suited to deal with flows with concentrated vorticity known in analytical form, while if there is only a rough specification of the flow, Lighthill's analogy should be employed.

6. MECHANISMS OF SOUND GENERATION

In the preceeding sections we have seen how the identification of sources of sound in aeroacoustics has been progressively refined, starting from Lighthill's quadrupole convected eddies and then focusing more and more explicitly in vorticity, until arriving to the linearly vorticity-related source due to Möhring. This is reflected in the attempts to find a convincent mechanism for the process of noise generation in jets. One of the first models suggested was that of Laufer et al. [17] who indicated that pairing of vortex rings is the primary mechanism responsible for most of the noise generated by a subsonic jet. The discovery of large scale coherent structures in turbulent flows gave rise to increasing expectations on the role which such structures might play in the process of noise generation. On the other hand, some experimental works (e.g. Moore [18]) showed that this role is in fact important, though he considered the large scale structures in the form of instability waves. But Moore did not recognize a direct role of these structures in the generation of noise in subsonic jets but a mediate one, governing the production of the turbulent fluctuations which radiate broadband noise. Anyway, the

most important result of the experiments of Moore was the significant increase in jet noise produced by exciting the shear layer with a fluctuating pressure at the nozzle of only 0.08% of the jet dynamic head but with the correct Strouhal number. He also found that forcing the jet at high frequencies can reduce the broadband noise of the jet when the boundary layer inside the nozzle is thick, which opens the door to the possibility of active noise control. By using specially developed flash schlieren techniques to visualize the coherent jet structures, he found that these started as an instability wave on the shear layer, were then amplified and finally rolled up into vortices which moved along the shear layer, entraining ambient air and providing large scale mixing. In Fig.1 an schematic diagram of the development of a jet shear layer is shown, featuring discrete concentrations of vorticity which deform and coalesce.

In relation with the coherent structures and particularly with the vortex pairing, Ffowcs Williams and Kempton [19] proposed two models of acoustic sources in a turbulent jet, in order to assess the role of the large scale structures in the noise generation process. In the first model a structure similar to instability waves which initially grow and then saturate and eventually decay is assumed. The second model is devoted to vortex pairing. These models describe much better the characteristics of excited jets than that of

unexcited ones, because forcing a jet modifies its structure inducing unstable waves at the forcing frequency to form the dominant eddies, the whole process of large structures being enhanced. In this respect, Ffowcs Williams and Kempton [19] suggested, according to Moore's results, that the extra broadband noise due to forcing was mainly due to the large structure and not to an increase in the background turbulence. Nevertheless agreement of the referred to models with experimental data is not so good.

Some other researchers have carried out experimental investigations trying to assess the importance of vortex pairing in the generation of noise. But Hussain [20] argued that this mechanism could not be dominant source of sound in practical jets. Since, for an initially laminar jet, most of the vortex pairing takes place in the shear layer near the lip of the jet, being complete within one diameter from the exit, while several studies (e.g. Juve et al [21]) show very clearly that most noise originates from the region near the end of the potential core (see Fig.2), it is suggested that vortex pairing can not be the dominant source. This view is reinforced by the fact that vortex pairing is almost absent in practical jet, which are turbulent at the exit. This initially turbulent mixing layer rolls up, tipically at the jet column mode, bypassing the shear layer mode.

Anyway since the role played by coherent structures in sound generation is felt to be crucial, and because of these structures are identified by coherent vorticity, which is the spatially phase-correlated component of vorticity underlying the random vorticity fluctuations of turbulent flows, some mechanism involving these coherent vorticity should be responsible for most of the sound generated. Bridges and Hussain [22] suggested to recall Möhring's formula ([9] p.689) for the far field pressure due to vorticity in low Mach number flow, because it is linear in vorticity. This formula is rearranged to give

$$p(\vec{x}) = \frac{1}{12\pi c_o^3 x^2} \rho_o \vec{x} \cdot [\frac{\partial^3}{\partial t^3} \int_v \vec{y}(\vec{y} \wedge \vec{\omega}) \, d^3\vec{y}] \cdot \vec{x}$$

(6.1)

Taking into account the linear decomposition of $\vec{\omega}$ in coherent, $\langle \vec{\omega} \rangle$, and incoherent, $\vec{\omega}_1$, parts, $\vec{\omega}$ is replaced in (6.1) by $\langle \vec{\omega} \rangle$ to get the sound due to coherent structures. Summarizing, what is important is the tensor $\langle \vec{Q} \rangle$ defined by (see Bridges and Hussain [22]).

$$\langle \vec{Q} \rangle = \frac{\partial^3}{\partial t^3} \langle \vec{Q} \rangle = \frac{\partial^3}{\partial t^3} \int_v \vec{y}(\vec{y} \wedge \vec{\omega}) \, d^3\vec{y} \quad (6.2)$$

Therefore coherent motions which generate a large $\langle \vec{Q} \rangle$ appears to be important sources of sound. It seems this is not the case for vortex pairing in practical jets.

Hussain [20] proposed that the breakdown process of the initial toroidal structures into substructures near the end of the potential core (see Fig.3) and their interaction is the process which produce most noise. He suggested too that this process involves the so called cut-and-connect mechanism as responsible of the generation of substructures from the toroidal structures. The cut-and-connect mechanism consists in the process during which two adjoining vortex filaments are cut and connected after switching. Some researchers have reported this phenomenum, which, as far as we know, remains unexplained. Theoretical treatment of this mechanism is rather complicated because it is three dimensional and involves vorticity. Though some investigation about the influence of this process on the generation of turbulent jet noise has been carried out, it is still soon to draw realistic conclussions and more research on this topic is needed.

7. CONCLUSSIONS

Much effort has been devoted to understand the physical mechanisms of the sound generation by turbulent jets, since the time of the first commercial jet aircraft. Perhaps the first theory which gave a rather full description of the sound generated aerodinamically, namely "the acoustic analogy approach" of M.J. Lighthill, has been the most succesful. Lighthill established an analogy between the nonlinear problem of the turbulent flow and the linear theory of classical acoustics and suggested to split the

turbulent flow into independent quadrupole distributions (energy bearing eddies). The results achieved by the theory when applied to jet noise have been, in general, impressive, specially the famous "law" of the jet sound power scaling on the eighth power of the jet velocity.

Nevertheless, effects of various phenomena like source convection, absorption diffraction and scattering of sound are explicitly absent of the theory. Some of these can be considered in the light of the theory like both the effects of source convection and temperature (i.e. hot jets), while it seems very complex to include in the mathematical formulation of the theory the other effects referred to.

Other theories have been devised so far to take explicitly into account some of these effects as well as to gain insight on the mechanism of sound generation. Among them the so called Powell-Howe one and that of Möhring are the most succesful, specially when applied to flows with concentrated vorticity known in analytical form. In fact, according to these theories the sources of sound are those regions of the flow with vorticity and entropy gradient.

The former assert is not very helpful when one tries to look for an explanation for the generation of sound and some qualitative models of mechanisms of sound generation by jets have been proposed. The pairing of

vortex rings in jets is the mechanism which has deserved more attention, but no clear reason in its support has been yet presented. Experiments have shown that most noise comes from the region near the end of the jet potential core, while vortex pairing takes place far away upstream. Moreover in practical jets, which are turbulent at the exit, vortex pairing is almost absent. Recently other process has been suggested as the most important for noise generation, namely the breakdown of the initial toroidal structures, which appear in the jet, into substructures near the end of the potential core. It has been stressed moreover that the so called cut and connect mechanism is the responsible for the generation of such substructures. This mechanism is the process during which two adjoining vortex filaments are cut and connected after switching. The role played by the cut and connect mechanism in the process of sound generation is believed to be important, but this must be supported by deeper studies.

REFERENCES

[1] Lighthill, M.J., "On Sound Generated Aerodinamically. I: General Theory", Proc. Roy. Soc. A, 211, 1952, pp 564-587.

[2] Lighthill, M.J., "On Sound Generated Aerodinamically. II: Turbulence as a Source of Sound", Proc. Roy. Soc. A, 222, 1954, pp 1-32.

[3] Lighthill, M.J., "Sound Generated Aerodinamically. The Bakerian Lecture", Proc. Roy. Soc. A, 267, 1962, pp 147-182.

[4] Lighthill, M.J., "Jet Noise", AIAA J.,7, 1963, PP 1057-1517.

[5] Phillips, O.M., "On the Generation of Sound by Supersonic Turbulent Shear Layers", J. Fluid Mech, 9, 1960, pp 1-28.

[6] Lilley, G.M., "On the Noise from Jets", in "Noise Mechanisms", AGARD-CP-131, 1973, Paper 13.

[7] Powell, A., "Theory of Vortex Sound", J. Acoust. Soc. Am., 16, 1964, pp 177-195.

[8] Howe, M.S., "Contributions to the Theory of Aerodynamic Sound, with Application to Excess Jet Noise and the theory of the Flute", J. Fluid Mech, 71, part 4, 1975, pp 625-673.

[9] Möhring, W., "On Vortex Sound at Low Mach Number", J. Fluid Mech, 85, part 4, 1978, pp 685-691.

[10] Ffowcs Williams, J.E., "Some Thoughts on the Effects of Aircraft Motion and Eddy Convection on the Noise from Air Jets", Univ. Southampton Aero. Astr. Rep. n° 155, 1960.

[11] Crighton, D.G., "Basic Principles of Aerodynamic Noise Generation", Prog. Aerospace, Sci, Vol 16, N° 1 Pergamon Press, 1975, pp 31-96.

[12] Ffowcs Williams, J.E., "The Noise of Turbulence Convected at High Speed", Phil. Trans. Roy. Soc. A 255, 1963, pp 469-503.

[13] Hoch, R.G., Duponchel, J.P., Cocking, B.J. and Bryce, W.D., "Studies of the Influence of Density on Jet Noise", J.Sound Vib. 18, 1973, pp 649-668.

[14] Lush, P.A. and Fisher, M.J., "Noise from Hot Jets", in "Noise Mechanisms", AGARD-CP-131, 1973, Paper 12.

[15] Ribner, H.S., "The Generation of Sound by Turbulent Jets" in Advances in Applied Mechanics 8, Academic Press, 1964, pp 103-182.

[16] Morfey, C.L., "Amplification of Aerodinamic Noise by Convected Flow Inhomogeneities". J.Sound. Vib. 31, 1973, pp 391-397.

[17] Laufer, J., Kaplan, R.E., and Chu, W.T., "On the Generation of Jet Noise" in "Noise Mechanisms", AGARD-CP-131, 1973, Paper 21.

[18] Moore, C.J., "The Role of Shear-Layer Instability Waves in Jet Exhaust Noise", J. Fluid Mech. 80, 1977, pp 321-367.shear layer mode.

[19] Ffowcs Williams, J.E., and Kempton, A.J., "The Noise from the Large-scale Structure of a Jet", J. Fluid Mech., 84, part 4, 1978, pp 673-694.

[20] Hussain, A.K.M.F., "Coherent Structures and Turbulence", J. Fluid Mech, 173, 1986, pp 303-356.

[21] Juve, D., Sunyach, M., Comte-Bellot, G., "Intermittency of the Noise Emission in Subsonic Cold Jets", J. Sound. Vib., 71, 1983, pp 319-332.

[22] Bridges, J.E. and Hussain, A.K.M.F., "Roles of Initial Condition and Vortex Pairing in Jet Noise", J. Sound Vib., 117 (2), 1987, pp 289-311.

Vortices form pairs and so increase axial spacing.

Vortices form.

Air becomes entrained.
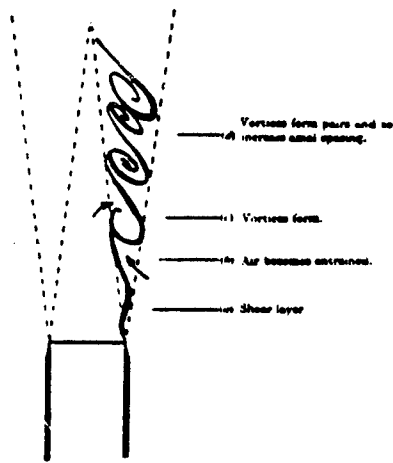
Shear layer

FIG.1. Schematic diagram of development of a jet shear layer (Moore [18])

Entrainment

U_0

Potential core

X = 4D   X = 8D

Mixing shear layer

Adjustment region

Fully developed self-preserving jet flow

u ~ U₀
l ~ X
A ~ DX

u ~ U₀D/X
l ~ X
A ~ X²
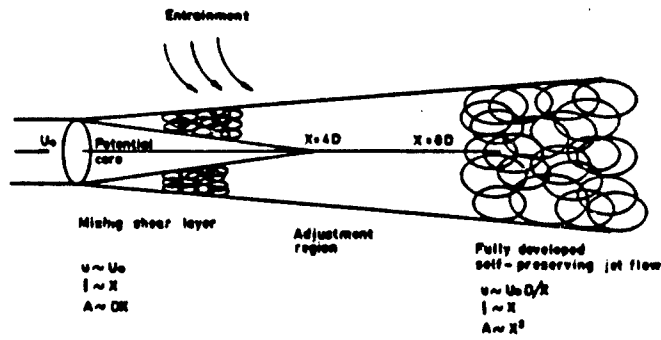
FIG.2. Downstream development of axisymmetric jet flow (Crighton [11])
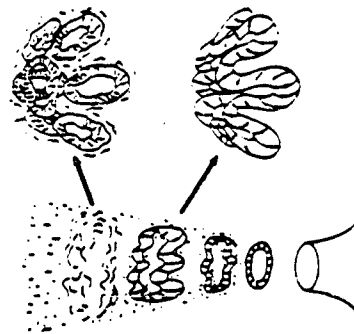
FIG.3. Idealization of the breakdown process in the circular jet (Hussain [20])

AD-P007 530

‖‖‖‖‖‖‖‖‖‖‖‖‖‖‖
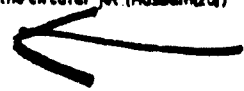
COMBAT AIRCRAFT NOISE REDUCTION BY TECHNICAL MEASURES

M. Wegner

F. Kennepohl

K. Heinig

MTU Motoren und Turbinen Union München GmbH
Dachauerstraße 665
8000 Munich 50
Federal Republic of Germany

92-17433

‖‖‖‖‖‖‖‖‖‖‖‖

SUMMARY

The noise of combat aircraft during low level flight is domi-
nated by the jet. Technical noise reduction measures must
therefore reduce the specific thrust of the engine. This can be
achieved by altering the engine cycle or by using secondary
air to increase the mass flow through the nozzle.

In the first part the influence of nozzle area, bypass ratio and
variable cycle features on the specific thrust of modern fighter
engines is shown. The effects on noise, thrust and fuel con-
sumption are discussed. In the second part ejector-mixer noz-
zles and the aft-fan are considered. Both reduce the jet veloc-
ity by entraining air through secondary inlets and expelling it
together with the engine's exhaust flow through a common
nozzle.

NOTATION

A	area
BPR	bypass ratio
D	diameter
$EPNL$	effective perceived noise level
h	height
m	velocity exponent
$\dot{m}$	mass flow
M	Mach number
n	rotational speed
$OAPWL$	overall sound power level
$OASPL$	overall sound pressure level
p	static pressure
P	total pressure, sound power
r	distance to microphone
SFC	specific fuel consumption
SOT	turbine rotor entry temperature
SPL	sound pressure level
T	thrust
v	velocity
θ	angle to inlet axis
π	nozzle pressure ratio
η	efficiency

Suffixes

corr	corrected
crit.	critical
d	design
f	flight
i	ideal
j	fully expanded jet
L	low pressure system
max.	maximum
nom.	nominal
ref.	reference
rel.	relative
0	engine intake
161	bypass exit (flame stabilizers)
8	nozzle throat
9	engine exit

1 INTRODUCTION

Due to Germany's dense population a significant number of
people are affected by noise of low flying combat aircraft. To
reduce the annoyance to the community, the German Luft-
waffe has introduced a number of operational measures. For
example, pilots are no longer allowed to fly below 1000 ft
(300 m) and above 420 kt ($M_f = 0.64$), and the total time at
low-level flying has been reduced.

The noise impact on the population may be further reduced by
complementing these operational restrictions by technical
measures, which reduce the noise directly at the source. Sev-
eral technical measures have been investigated and their effect
on weight, engine performance and aerodynamic performance
of the aircraft determined. They focus on the noise generated
during low level sorties flown by the German Air-Force and
it's NATO allies' Tornados and in future by new fighter air-
craft.

2 NOISE SOURCES

Combat aircraft are required to fly at high speeds and therefore
require an engine cycle that will provide a high specific thrust.
Additionaly, to minimize the aircraft's drag, the engine should
have a low frontal area. These and the requirement for after-
burning to augment thrust during combat demand an engine
cycle which is either a straight jet or a low bypass ratio turbo-
jet. The exhaust velocity of these engines is well over 600 m/s
and may be reheated to even higher velocities.

In a flight test program conducted by the German Bundes-
wehr (Erprobungsstelle 91 in Meppen), in-flight acoustic data
was obtained for the F-16, Alpha-Jet, Tornado and Phantom.
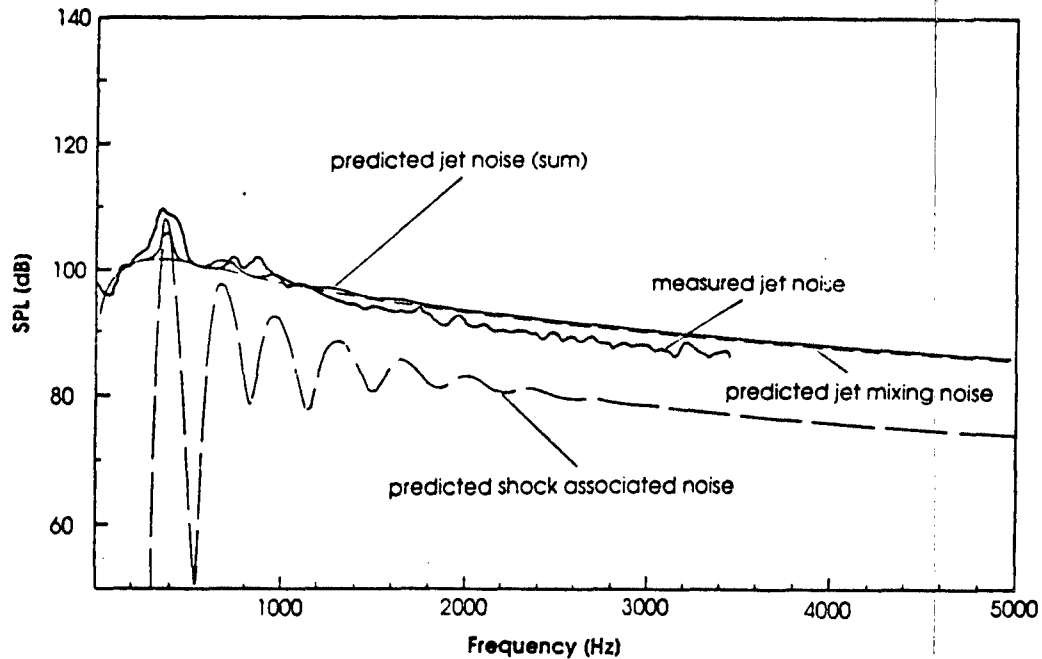
Fig. 1 Narrow-band spectrum of a Tornado at 30° to
the inlet axis at a flight velocity of 480 kt [3]

The narrow band spectrum at an angle of 30° to the inlet axis is shown in Fig.1 for a Tornado flying at 480 kt. The absence of any tonal content (fan and turbine noise) in the spectrum suggests that jet noise is the dominant source. In addition, the measured noise is predicted well by jet noise prediction methods [1 and 2].

3 JET NOISE

Jet noise describes the sum of all noise components generated by the jet. Jet mixing noise is due to the turbulent mixing of the jet with the surrounding atmosphere. In jets with a super-critical pressure ratio which are incorrectly expanded, the interaction between the pattern of oblique shocks and rarefaction waves with the turbulent jet leads to a further source termed shock associated noise. Of these, jet mixing noise is the most fundamental component and the most difficult to reduce.

3.1 Jet Mixing Noise

The source depends primarily on the shear force between the jet and the surrounding environment, and hence on the relative jet velocity. Fig.2 illustrates the dependence of the relative acoustic power output on jet velocity and temperature of a static jet with constant thrust. At constant thrust the nozzle area decreases with increasing jet velocity and increases with increasing temperature. As illustrated in Fig.2, reducing the jet velocity is the most powerful tool to control jet mixing noise.

The effect of increasing the temperature is to increase the noise radiation at low jet velocities, while at higher jet velocities the converse is true. However, the jet temperature is closely linked to the engine cycle, and therefore, altering the jet temperature to control noise is impractical.

3.2 Shock Associated Noise

The interaction between the shock cells and the turbulence generates a broadband signal with distinct spectral peaks. Since the shock associated noise depends on the existence of the shock structures, it follows that shock associated noise can be controlled or even eliminated by correctly expanding the jet to the surrounding atmospheric pressure. This can be accomplished by close control of the nozzle aerodynamics. Convergent nozzles should be used for nozzles operating at up to and slightly beyond the critical pressure ratio. At pressure ratios clearly above the critical pressure ratio convergent-divergent nozzles with the correct exit to throat area ratio should be employed. In addition, a correctly expanded jet provides for minimum thrust losses.
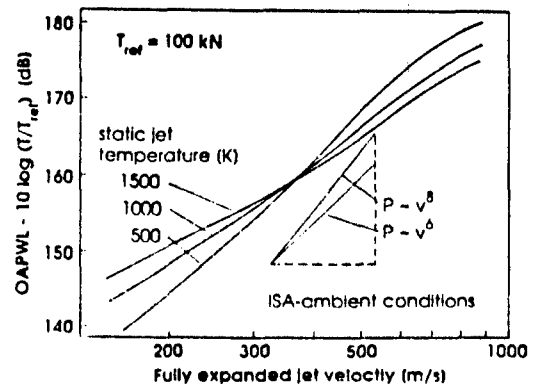
Fig.2 Variation of jet mixing noise with jet velocity and
temperature

3.3 Flight Velocity

With increasing flight velocity, reducing the jet noise becomes increasingly difficult. The net thrust of a jet engine in forward motion with a correctly expanded nozzle flow is given by:

$$T = \dot{m}(v_j - v_f)$$

In order to reduce the relative velocity between the jet and the surrounding environment $(v_j - v_f)$, mass flow must be increased inversely proportional to the relative velocity, if the thrust is to be maintained constant. This leads to large mass flow rises if the jet velocity is reduced at high flight velocities.

Further, since jet mixing noise should depend on the relative velocity, it might be expected that the noise reduction due to forward velocity would roughly vary according to the eighth power law of Lighthill's theory [5]:

$$\Delta OASPL \approx 10 \log_{10} \left(\frac{v_j}{v_j - v_f} \right)^8$$

However, due to the convective amplification of a moving source, the noise reduction due to flight is much less. In fact the maximum flyover jet noise correlates more closely with the absolute rather than the relative jet velocity. This adds to the difficulty of reducing the noise at high flight velocities.

3.4 Jet Noise Prediction

The jet mixing noise is predicted using an improved method by Michel and Böttcher [2]. Shock associated noise is computed using a modified form of Tam's method [1,3]. The predictions also account for the attenuation due to atmospheric absorption of sound at 50 % relative humidity.
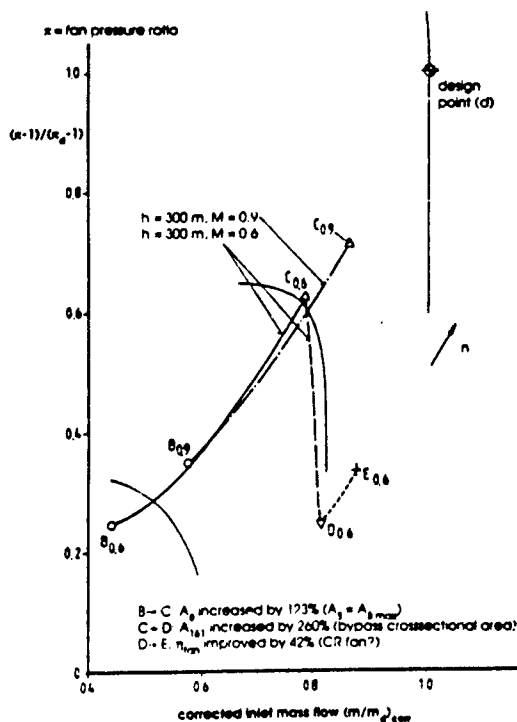
Fig.3 Fan-performance map

4 INCREASING THE NOZZLE AREA

A variable nozzle exit area provides for a constant corrected mass flow during afterburner operation and can be used to reduce the jet mixing noise during normal operation.

During low level flight the engines of a typical combat aircraft normally operate at partial of the available thrust, with mass flow through the engine well under the design mass flow. The mass flow through the engine is limited by the nozzle throat area. Increasing the nozzle area will therefore increase the mass flow and decrease the jet velocity. The increased power output of the low pressure turbine (LPT) is passed on to the fan. The effect of increasing the nozzle area on engine performance and noise was investigated on the basis of two combat aircraft engines:

- an engine for a typical fighter aircraft with a bypass ratio of 0.4, and
- the RB199 with a bypass ratio of 1.1 installed in the multi-role combat aircraft Tornado.

4.1 Engine with Bypass Ratio 0.4

4.1.1 Engine Cycle

Fig.3 shows the effect of increasing the nozzle area on the operating point in the fan-performance map.

Increasing the nozzle throat area from the nominal position (minimum fuel consumption) to the maximum area, moves the operating point to the desired higher corrected mass flow rate (B-->C), but to the contrary of what was expected, the fan pressure ratio also increases. This is due to a sharp rise in the total pressure losses in the bypass duct. Increasing the mass flow through the engine increases the bypass ratio, which rapidly leads to critical flow conditions in the bypass duct of this low bypass-ratio combat aircraft engine, especially near the afterburner fuel manifolds and the flame stabilizers.

Fig.4 illustrates the variation of some parameters of interest as the nozzle throat area is increased from the nominal position to the maximum, geometric area (usually selected during afterburner operation) for a typical combat aircraft during low level flight at $M_f = 0.6$. The top diagram (Fig.4.a) shows the variation of the Mach number at the narrowest point in the bypass duct: the flame stabilizers. As the Mach number increases, the total pressure losses at the flame stabilizers (Fig.4.b) and in the bypass duct rise sharply, and although the fan efficiency improves (see Fig.3) the specific fuel consumption of the engine increases by 50 % (Fig.4.c).

Fig.4.d shows the variation of the mean jet velocity v_9 at the exit of the convergent-divergent nozzle and the ideal fully expanded jet velocity v_{9i}. The jet will attain a velocity close to the ideal fully expanded jet at some distance downstream of the nozzle and jet noise prediction methods (e.g. [2] and [4]) use *this* velocity as input. Therefore, a reduction in jet mixing noise is apparent as the ideal fully expanded jet velocity v_{9i} recedes from the value at the nominal nozzle throat area to the value at the maximum nozzle throat area. (The next section will comment on the behavior of the nozzle exit velocity v_9.)

If the noise reduction at the maximum nozzle area is compared to a 50 % rise in specific fuel consumption, then this case is of little practical interest. A nozzle schedule could be devised, where the nozzle area is increased until critical flow conditions are *just* reached in the bypass duct. This would be a good compromise between noise reduction and losses in the bypass duct.
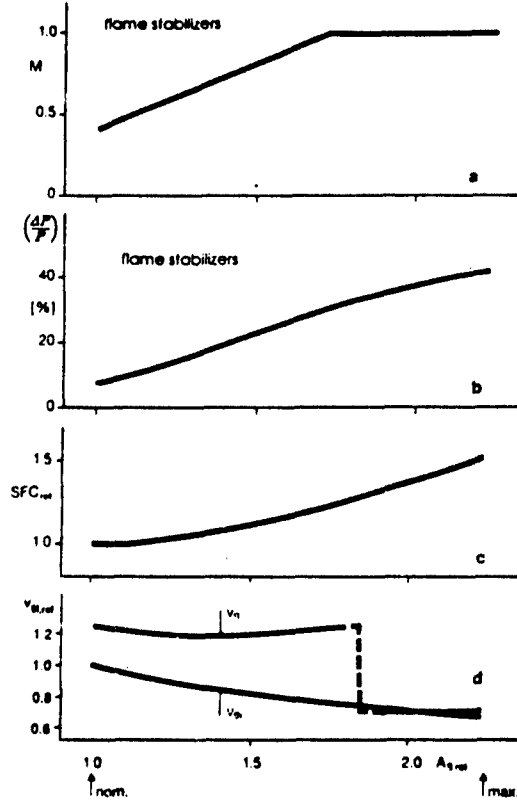
Fig.4 Variation of parameters as the nozzle area is increased from the nominal position to the maximum geometric area.
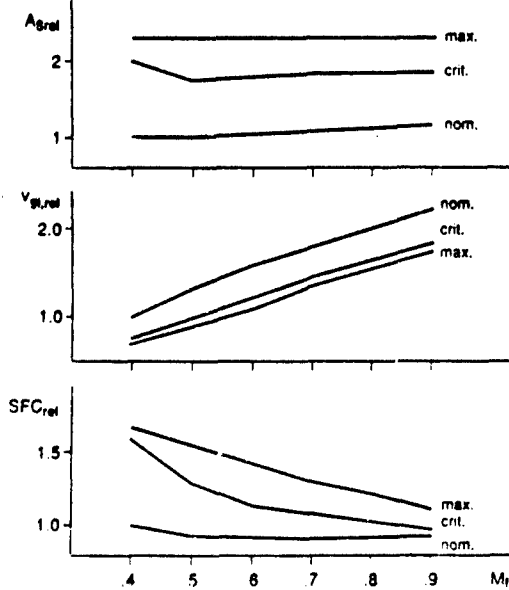
Fig.5 Variation of exit area, fully expanded jet velocity and specific fuel consumption with flight Mach number

Fig.5 illustrates the variation of the exit area, the ideal fully expanded jet velocity and the specific fuel consumption for a typical combat aircraft for :

- the nominal nozzle area (nom.),

- the nozzle area v.'iere critical flow conditions are just reached in the bypass duct (crit.), and

- the maximum nozzle area (max.)

as a function of the flight Mach number.

The afterbody drag and spillage drag of an engine are also influenced by the nozzle exit area. Increasing the area reduces the afterbody drag. As a result of the increased mass flow, spillage drag is reduced. Both effects will improve the specific fuel consumption to some extend, but cannot compensate for the losses in the bypass duct.

4.1.2 Nozzle Aerodynamics

To minimize thrust losses due to an incorrectly expanded jet and to minimize shock associated noise, nozzle aerodynamics must be controlled carefully. Some modern combat aircraft engines operate at very high nozzle pressure ratios and often require a convergent-divergent nozzle. Fig.6 shows the static pressure variation in a convergent-divergent nozzle as the pressure ratio across the nozzle is increased.

The ratio of exit to throat area should always match the nozzle pressure ratio, i.e. the static pressure of the jet at the exit should equal the surrounding static pressure (cases 1, 2, 3 and 7). If this is not so, pressure equilibrium at the exit is established over a series of shocks either within (case 4) or outside of the nozzle (cases 6 and 8).
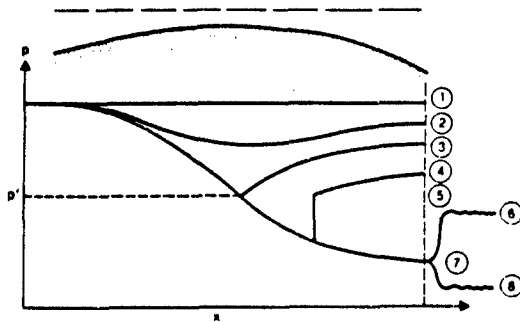
Fig.6 Static Pressure variation in a convergent-divergent nozzle

A convergent-divergent nozzle can be adapted to provide shock-free jet flow under all conditions by varying the area of the throat and the exit independently, as opposed to varying the throat area and linking the exit area to the throat area, but this so called two-parameter nozzle adds complexity and weight to the exhaust system.

In this study, only a single-parameter nozzle is considered. Due to mechanical constraints increasing the nozzle throat area increases the ratio of the exit to throat area. The concern with this nozzle is that this leads to an extreme overexpansion of the nozzle flow at partially increased nozzle throat area (case 6 in Fig.6) with exit velocities much higher than the fully expanded jet velocity (see Fig.4). At this condition high thrust losses and shock associated noise occur. This condition, however, could be avoided with a two-parameter nozzle or possi-

bly with a modified single-parameter nozzle. At the operating condition corresponding to the fully opened nozzle throat area shown in Fig.4, the nozzle pressure ratio has dropped sufficiently to provide for a subsonic flow at the nozzle exit.

4.1.3 Noise Reduction

The calculated EPNL is shown in Fig.7 for the combat aircraft flying at 100 m as a function of flight Mach number. The total noise (i.e. jet mixing noise and shock associated noise) and jet mixing noise only have been computed separately:

* for the nominal engine,

* for the engine with an increased nozzle throat area where critical conditions are just reached in the bypass duct, and

* for the engine with the maximum possible geometric nozzle throat area.

As the flight Mach number increases, shock associated noise becomes increasingly dominant and the total noise reaches the level of the reference aircraft with the nominal nozzle area above a flight Mach number of approx. 0.8. Noise reduction by increasing the nozzle area must therefore be coupled with a two-parameter nozzle. The resulting computed reduction in jet noise would be slightly lower than the jet mixing noise only curves, due to reduced thrust losses in the nozzle, and therefore reduced engine rating. At $M_f = 0.6$ the reduction would be about 6 EPNdB.
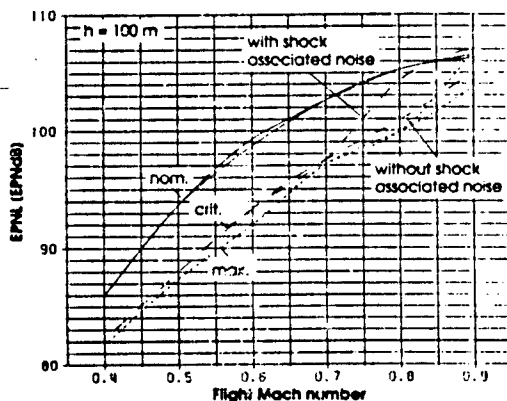
Fig.7 Predicted EPNL for a fighter aircraft at 100 m with an increased nozzle throat area for noise reduction

Fig.8 shows the 1/3-octave spectrum at 60° for a flyover at 100 m and $M_f = 0.8$. Shock associated noise can be clearly seen in the 1/3-octave spectrum at a frequency of 2 kHz.

4.2 Engine with Bypass Ratio 1.1

During low level steady flight the engines of the Tornado operate at a much higher thrust rating than the engines installed in the typical fighter aircraft described in section 4.1. In addition, the thrust rating of the Tornado depends heavily on the aircraft configuration and load.

The larger design bypass ratio of this engine prevents the critical flow conditions in the bypass duct as the nozzle area is increased up to the maximum possible area. But this can not be fully exploited, since the engine rapidly reaches its mechanical limits at some operating points as the nozzle area is increased.
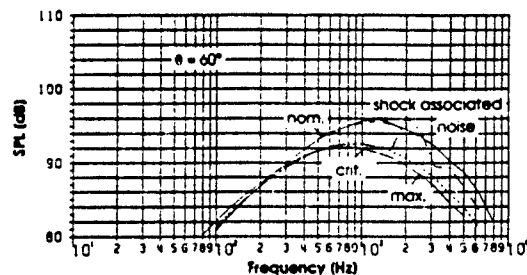
Fig.8 1/3-Octave Spectrum at 60° to the inlet axis for a flyover at 100 m and M=0.8 with various nozzle throat areas

4.2.1 Engine Cycle

To investigate the effect of increasing the nozzle exit area on the engine cycle two aircraft loads were considered:

* clean aircraft, and

* heavy wing aircraft.

Figs.9 and 10 show the variation of some parameters of interest with the nozzle exit area for the clean aircraft and the heavy wing aircraft, respectively, at a flight Mach number of 0.7.
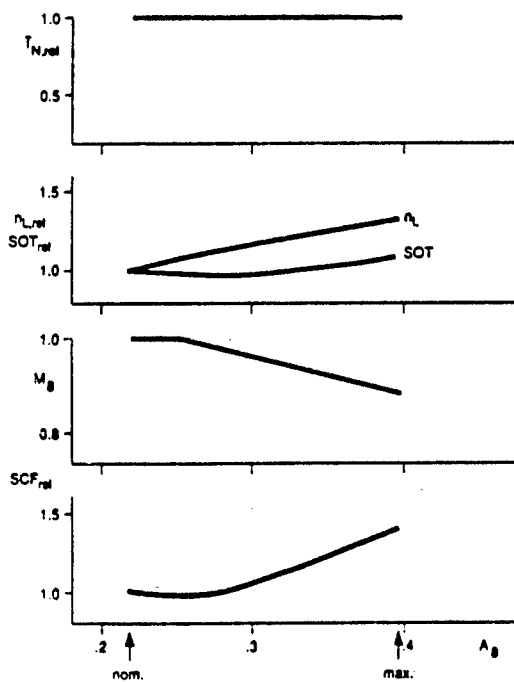
Fig.9 Variation of the relative thrust, the relative low pressure system r.p.m, the relative turbine entry temperature, the exit Mach number and the specific fuel consumption with the nozzle exit area for the clean Tornado at $M_f = 0.7$.
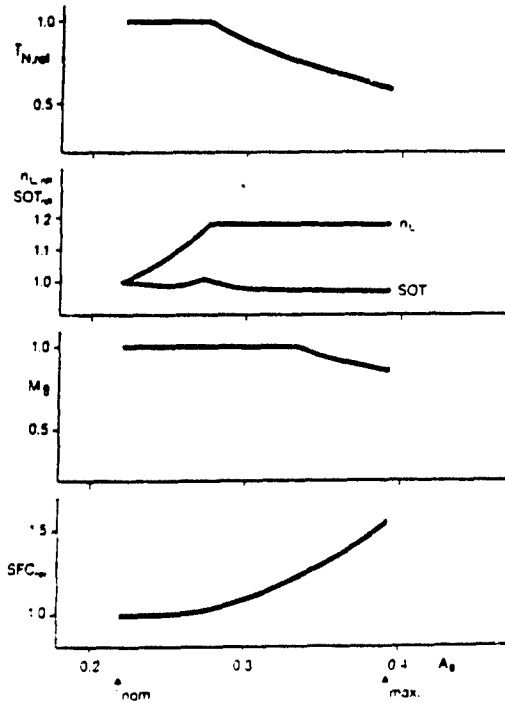
Fig. 10 Variation of the relative thrust, the relative low
pressure system r.p.m, the relative turbine entry
temperature, the exit Mach number and the spe-
cific fuel consumption with the nozzle exit area for
the heavy wing Tornado at $M_f = 0.7$.

For the clean aircraft (Fig.9) the rotational speed of the low
pressure system and the turbine entry temperature increase
within their mechanical limits. Thrust can be maintained up to
the maximum nozzle exit area, but the corresponding specific
fuel consumption increases by almost 50 %. (The effect of in-
creasing the nozzle exit area on the spillage drag and afterbody
drag have been included in the thrust calculation.) Due to the
reduction of the nozzle pressure ratio the nozzle exit Mach
number recedes from unity.

The higher thrust requirements of the heavy wing aircraft
drive the engine to its mechanical limits as the nozzle exit area
is increased. This can be seen in Fig.10 where the rotational
speed of the low pressure system and the turbine entry tem-
perature reach their maximum permissible values. The pre-
scribed thrust can no longer be maintained and falls off.

For the purpose of noise reduction a nozzle schedule is pro-
posed which avoids these mechanical limits, with the implica-
tions that the nozzle exit area can be opened wider for low
thrust ratings (i.e. clean aircraft and low flight Mach number)
than for high thrust ratings (i.e. heavy wing aircraft and high
flight Mach numbers).

4.2.2 Nozzle Aerodynamics

The engine of the Tornado has a variable area convergent noz-
zle. As can be seen in Figs.9 and 10 the nozzle exit Mach
number falls below unity for the clean aircraft, implying that
the nozzle pressure ratio has fallen below the critical value.
However, the exit Mach number of the heavy wing aircraft re-
mains one, implying that the nozzle pressure ratio is equal to,
or above the critical value.

If the nozzle flow is underexpanded, shock associated noise
must be taken into consideration.

4.2.3 Noise Reduction and Specific Fuel Consumption for the Proposed Nozzle Schedule

Fig.11 shows the predicted EPNL for a Tornado flying at
100 m as a function of flight Mach number. Total jet noise and
jet mixing noise only have been computed separately. It can be
seen that shock associated noise may become important at
high flight Mach numbers especially for the heavy wing air-
craft. At $M_f = 0.6$ the calculated jet noise reduction is 4.0 and
5.0 EPNdB for the clean aircraft and the heavy wing aircraft,
respectively.
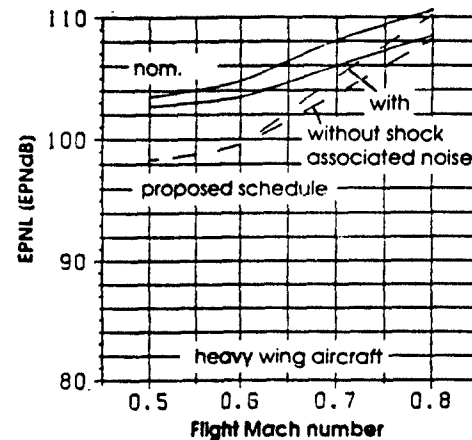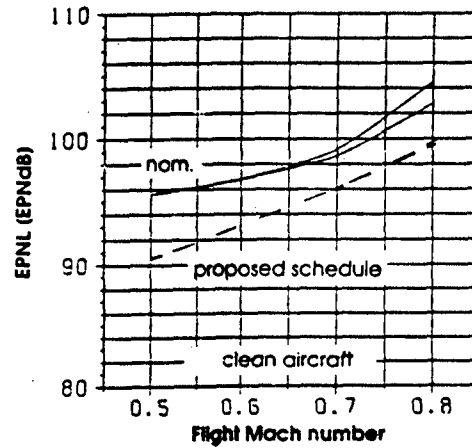
Fig. 11 Predicted EPNL as a function of flight Mach num-
ber for Tornado at 100 m with the proposed noz-
zle schedule

The effect of the proposed nozzle schedule on the specific fuel
consumption is shown in Fig.12. The specific fuel consump-
tion rises by up to 20 %.

5 EFFECT OF DESIGN BYPASS RATIO ON NOISE

Increasing the bypass ratio increases the mass flow through
the engine, and jet noise may therefore be reduced. To investi-
gate this in more detail, the design bypass ratio of a modern
combat aircraft engine was varied between 0.25 and 0.8 on the

basis of constant take-off thrust.
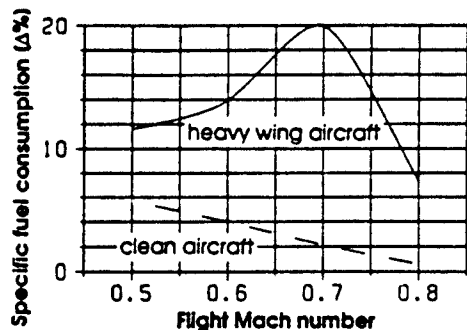
Fig. 12 Specific fuel consumption as a function of flight Mach number

The effect of the bypass ratio on some engine parameters of interest of this engine when installed in a modern combat aircraft during low level flight at Mach numbers between 0.4 and 0.9 is shown in Fig.13 for 3 nozzle positions:

- the nominal (minimum fuel consumption) nozzle exit area (nom.),

- the nozzle exit area where critical flow conditions in the bypass duct are just reached (crit.), and

- the maximum nozzle area (max.).
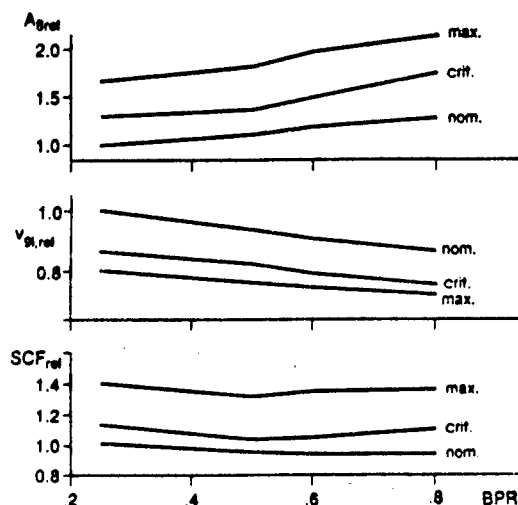
Fig. 13 Variation of the nozzle exit area, the fully expanded jet velocity and the specific fuel consumption with bypass ratio

It can be seen that the fully expanded jet velocity falls with increasing bypass ratio, corresponding to a reduction in jet noise shown in Fig.14. Only the jet mixing noise curves are shown and the corresponding noise reduction would apply to an engine with a correctly expanded nozzle flow (i.e. no shock associated noise).

The variation of some important dimensions are shown in Fig.15. The outer diameter and the total length of the engine with bypass ratio 0.8 is 9.6 % and 5.3 %, larger, respectively than the corresponding dimensions of the engine with bypass

ratio 0.25. Engine weight varies only slightly with bypass ratio.
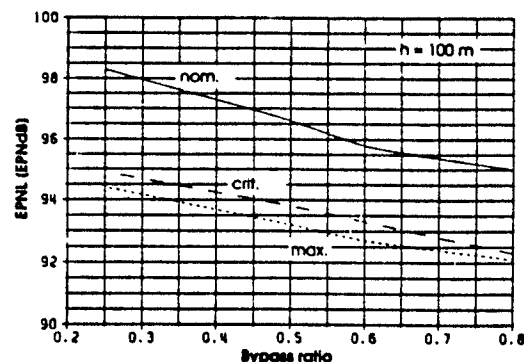
Fig. 14 Predicted EPNL for a modern combat aircraft at 100 m for various bypass ratios and nozzle throat areas
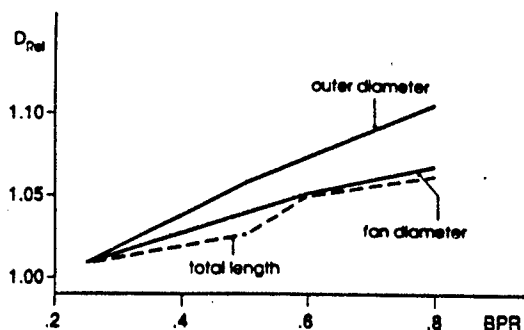
Fig. 15 Some engine dimensions as a function of the bypass ratio

In addition to dimensional and weight aspects, the choice of a fighter aircraft engine is influenced by the maximum achievable thrust and fuel consumption at the relevant operating conditions. A high bypass ratio engine, for example, normally has a lower thrust at transonic and supersonic flight at dry conditions and an increased fuel consumption at afterburning conditions, compared to a low bypass ratio engine of the same combat thrust at sea level static conditions.

6 VARIABLE CYCLE ENGINES

Variable cycle engines (VCE) can actively alter the geometry of the engine to modify the engine cycle to suit requirements. For the 0.4 bypass ratio engine mentioned earlier, variable geometry can be used to partially compensate for the losses incurred in the bypass duct as the nozzle area is increased.

As described in the section 4 jet noise may be reduced by increasing the nozzle throat area. Referring back to the fan performance map in Fig.3 it can be seen that as the nozzle throat area is increased, both the pressure ratio and corrected mass flow increase from B to C. Fig.16 shows some additional parameters of interest, together with the effect of additional changes to the engine, as:

- the nozzle throat area is increased from the nominal to the maximum position (B-->C),

- the area of the bypass duct near the flame stabilizers (where critical flow conditions are reached first) is in-
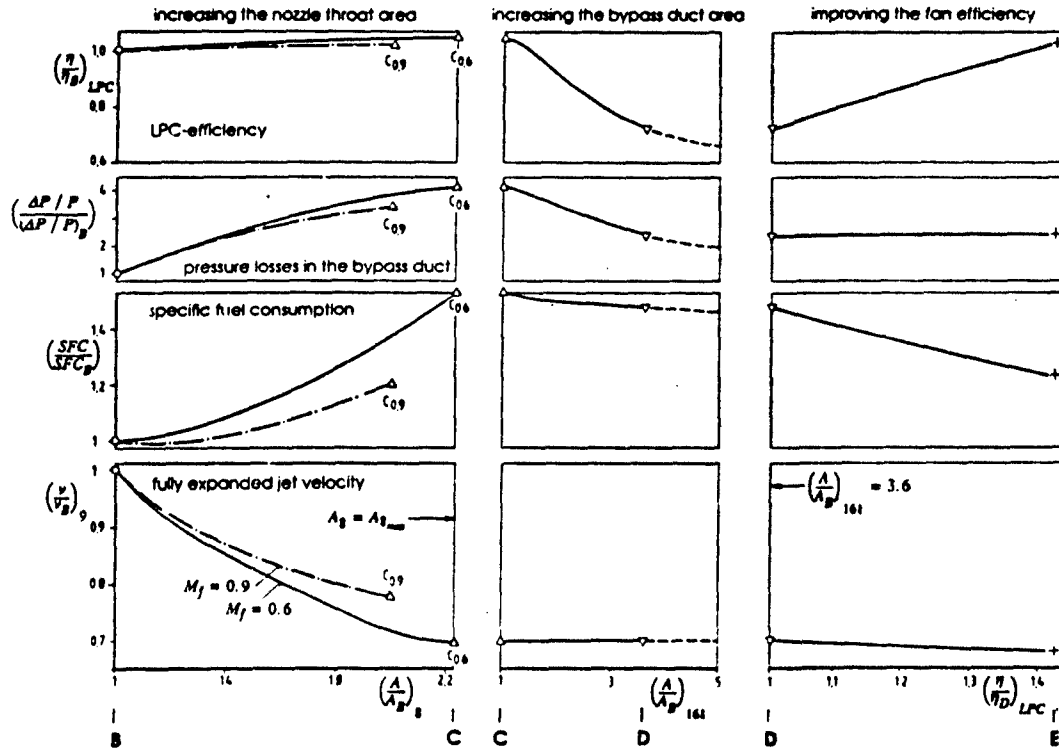
Fig. 16 Variation of some engine parameters
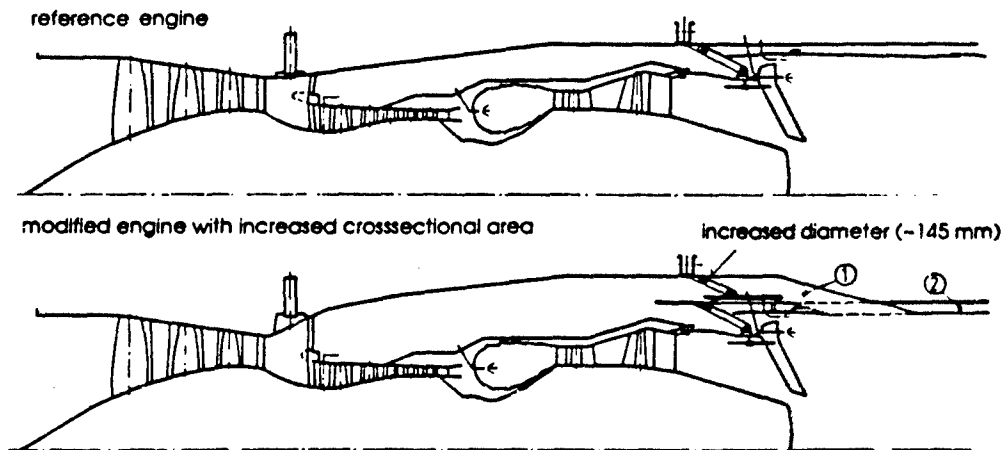
*Fig. 17 Variable cycle engine: Increased bypass duct
area*

creased (C-->D), and

- the efficiency of the fan is improved, say by a variable geometry counter rotating fan (D-->E).

The high losses in the bypass duct can be reduced if its cross-sectional area is increased. The effect of this is shown in the

fan performance map (Fig.3): line C to D. The pressure ratio across the fan falls consistent with the reduced pressure losses in the bypass duct. Unfortunately the fan efficiency also drops. Increasing the cross-sectional area only partially restores the value of the specific fuel consumption but still falls far short of the original value at B. It has no effect on jet velocity and mass flow and therefore on jet noise.

The fuel consumption can be further improved by replacing the conventional LPC by a more efficient variable geometry (e.g. counter rotating) fan. Specific fuel consumption improves considerably but is still 20 % higher than that of the reference engine (at B).

The required modifications to the bypass duct are illustrated in Fig.17. The critical area of the bypass duct near the flame stabilizers can be increased by 260 % and the area of the remaining bypass duct by 100 %. This will require an increase in engine diameter of 15 cm and therefore major modifications to the aircraft.

The computed EPNLs of the variable cycle engine are similar to the engine with an increased nozzle area (Fig.7).

7 MIXER-EJECTOR NOZZLES

In the following section noise reduction measures are presented that do not willingly alter the engine cycle. The afterburner of the Tornado engine could be modified to operate as a variable geometry ejector nozzle as illustrated in Fig.18.

Secondary intakes in the aircraft and the engine allow ambient air to enter the afterburner and mix with the primary exhaust flow. During afterburner operation the intakes are closed and the chutes retracted and stored between the engine and the fuselage of the aircraft. Access to the afterburner is only possible over part of the circumference due to the elevator to one side of the engine and due to the second engine to the other side of the engine.

Mass flow is increased at the expense of jet velocity and associated jet mixing noise while maintaining thrust. To allow for the extra mass flow the nozzle exit area is increased to the maximum position (usually selected during afterburner operation), which also reduces the afterbody drag.

The performance of the ejector depends on the efficiency of the turbulent mixing between the primary and secondary streams. If the length to diameter ratio of the mixing chamber is of the order 6 to 8, then ejector performance is good, and a uniform velocity profile will leave the nozzle. However, the ratio for the afterburner of RB199 is much shorter, which makes it necessary to use a multiple chute nozzle as shown in Fig.18. The number of "primary chutes" is 8 to give a relative length to diameter ratio of about 6. The associated reduction in mixing length is the principle advantage of the mixer-ejector.

Another important factor for the ejector performance are the two forward facing intakes on the top and bottom of the aft section of the aircraft. They each distribute the secondary airflow to the 3 chutes on the top and bottom of the mixer-ejector nozzle. The oncoming flow must turn sharply into the ejector and is retarded as it enters the intake, but the associated pressure losses for a forward facing intake are less than for a flush intake.
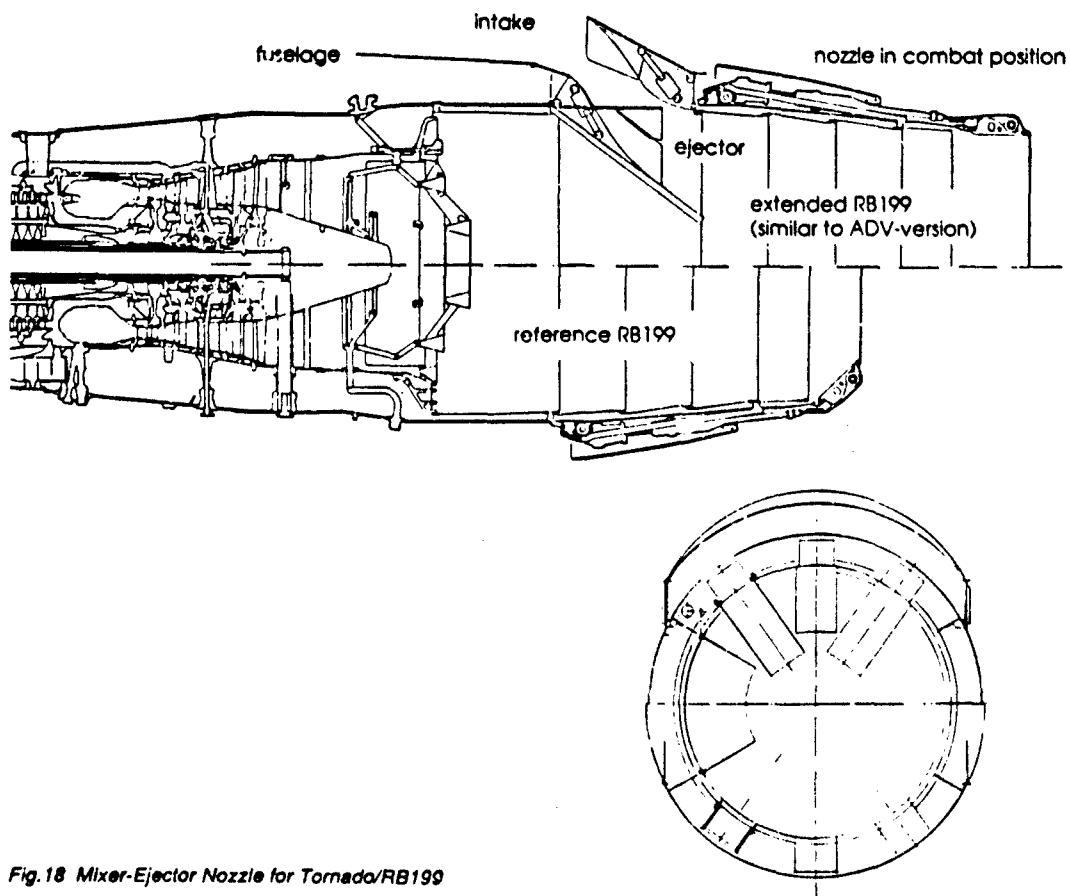
Fig.18 Mixer-Ejector Nozzle for Tornado/RB199

7.1 One Dimensional Aerodynamic Calculation

To investigate the performance of the ejector a one dimensional routine to solve the conservation laws for mass, momentum and energy within a cylindrical mixing control volume was developed. To account for all losses due to incomplete mixing and skin friction a momentum loss factor of 0.9 was used. According to [6] this value is within the range for an optimum ejector design.

Nozzle pressure ratio and jet total temperature for the aircraft at a flight Mach number 0.6 are of the order 2.25 and 620 K, respectively. The corresponding fully expanded jet velocity is 520 m/s. The ejector secondary to primary mass flow ratio is 0.6 and the mean jet velocity is reduced to 405 m/s. The predicted in-flight noise reduction for a 100 m direct flyover of a heavy wing aircraft is 7.0 EPNdB. The EPNL and the specific fuel consumption as a function of Mach number are shown in Fig.19 and Fig.20, respectively, for the two Tornado configurations with different weight and drag. It should be noted, that it is assumed that high frequency mixing noise generated inside the ejector can be absorbed by allowing the heat shield of the afterburner to function as an acoustic liner.

7.2 Two-dimensional viscous CFD computation

To investigate the external flow about the ejector shroud and
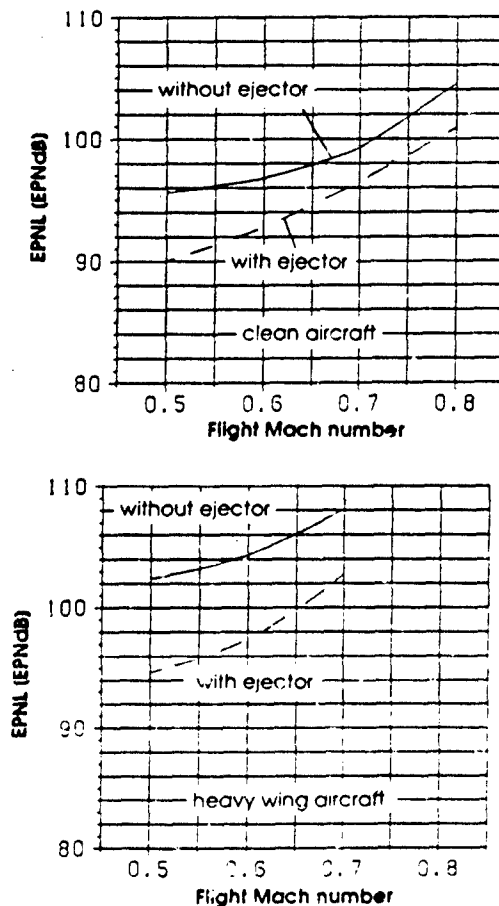
Fig.19 Predicted EPNL of a Tornado at 100 m with and without an ejector for noise reduction
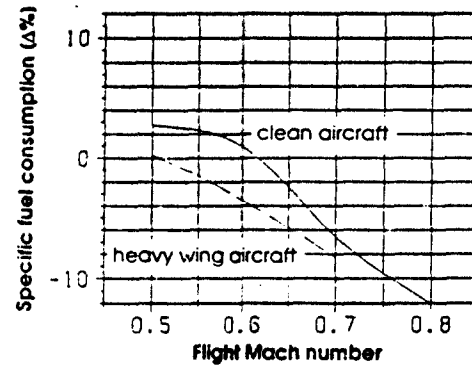
Fig.20 Change in specific fuel consumption of a Tornado due to an ejector

into the inlet a viscous 2D CFD simulation of the mixer-ejector at $M_f = 0.7$ was carried out. Fig.21 shows the contour fitted mesh around the mixer-ejector configuration. The figure does not show the final configuration, nevertheless the results are considered to be worthy to be included.

The basic ejector performance of the viscous CFD calculation was in quite good agreement with the simple one-dimensional ejector routine.

The velocity vectors illustrated in Fig.22 show that the flow separates from the lip of the forward facing intake. A large separation bubble forms and the flow does not reattach. The associated pressure drag would be high. However, the 2D computation is by definition symmetric around the axis of the engine and the resulting intake area —with the intake height being the same —is therefore twice as large as for the real ejector. If the flow were to be modelled by a 3D computation fully resolving the geometry of the ejector, spillage would be less and more encouraging results would be expected.

8 AFT-FAN

Gulfstream Aerospace has proposed an aft-fan to reduce the jet mixing noise of civil jet engines [7]. A similar concept has been devised for a combat aircraft engine, where the afterburner can be temporarily (training aircraft) or permanently replaced by a duct housing an aft-fan as illustrated in Fig.23. An additional turbine extracts energy from the exhaust flow and powers a fan attached to the outside of the turbine. The fan draws in additional ambient air and expels it together with the turbine flow through the common nozzle. For structural and aerodynamic reasons stators are positioned upstream of the fan/turbine rotors.

The aft-fan reduces the total pressure and temperature of the primary flow. Analogous to the ejector mass flow is increased at the expense of jet velocity and consequently jet mixing noise is reduced.

Due to thermal constraints afterburner operation is not possible, but interestingly the thrust performance of the aft-fan is better than for the ejector. In fact the aft-fan produces a thrust gain of 30 % at take-off, which may make the afterburner redundant if the aircraft is used for low-level flying only. The performance of the aft-fan was determined by applying the power balance between the fan and the turbine and making reasonable assumptions for the fan and turbine pressure ratios and efficiencies. At $M_f = 0.6$ fan to turbine mass flow ratio is 0.8 (secondary to primary mass flow ratio for the ejector was 0.6). Assuming that turbine and fan flows will not mix along
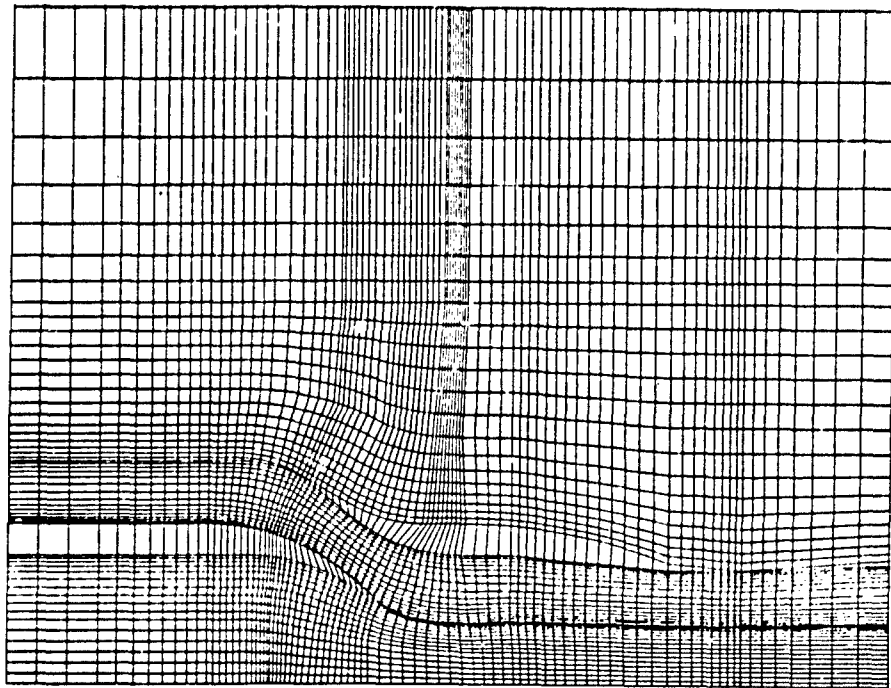
Fig.21 Contour-fitted mesh for 2D viscous CFD compu-
tation
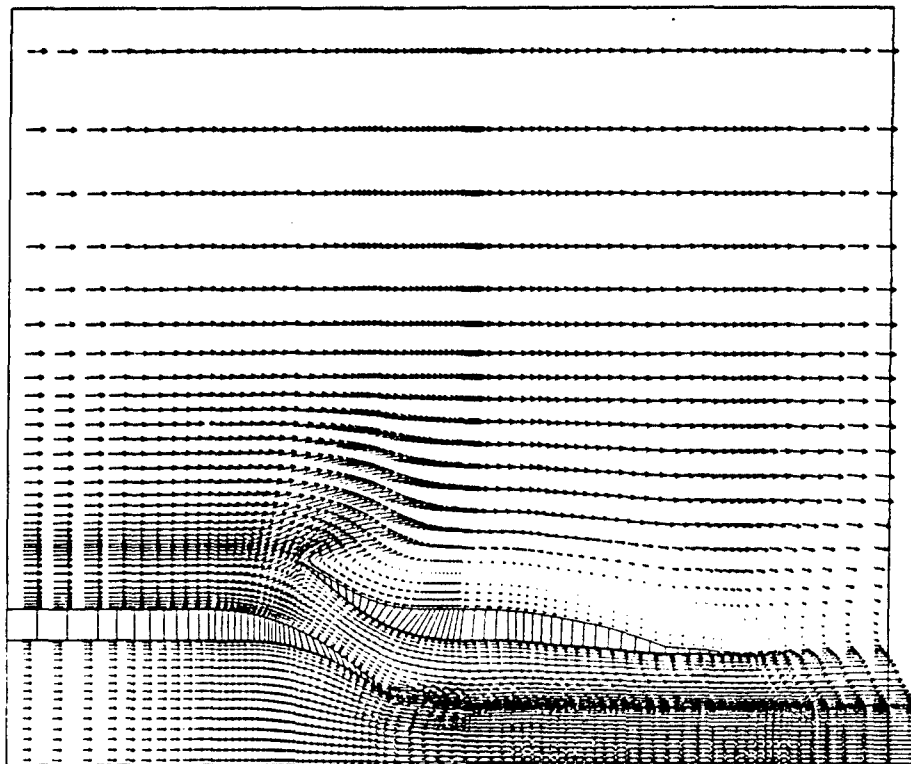
Fig.22 Velocity vectors around and through the mixer-
ejector CFD model
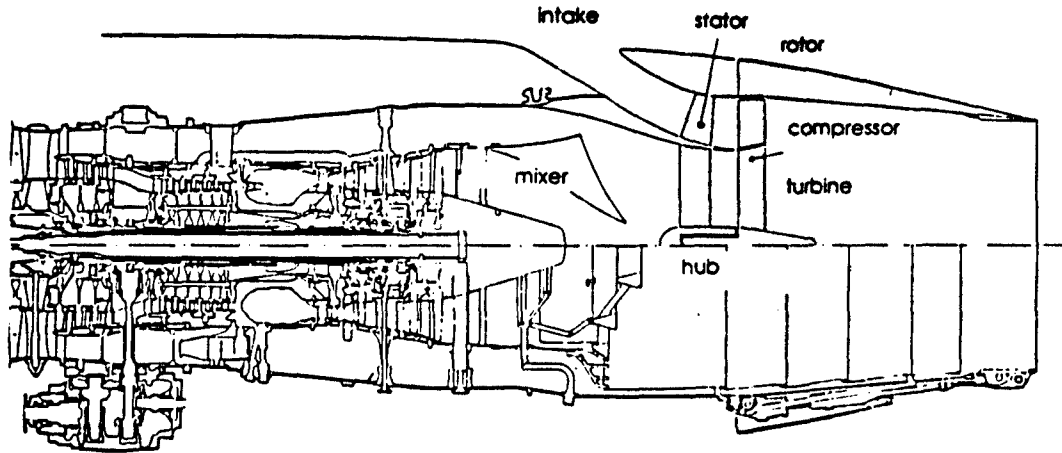
Fig.23 Aft-fan for Tornado/RB199
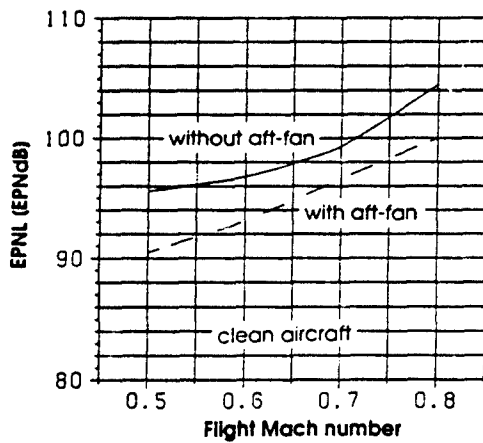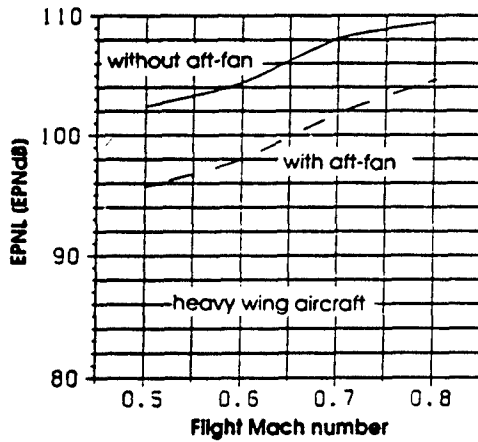
Fig.24 Predicted EPNL for a Tornado at 100 m with an aft-fan for noise reduction

the short distance to the nozzle exit, then the flow will leave the nozzle with a coaxial velocity profile. Jet velocities of the turbine and fan flow are 410 m/s and 350 m/s, respectively. The corresponding jet noise reduction is 6.4 EPNdB. Fig.24. shows the EPNL as a function of flight Mach number.

To enhance the analysis an aerodynamic layout using a streamline geometry program was carried out. The computational domain and the resulting streamlines are shown in Fig.25. The pressure ratio of 1.6 across the fan is considered to be quite high but should be within accepted limits. The small hub of the turbine, however, poses an aerodynamic as well as a structural challenge. The low angular velocity of the turbine near the hub implies a low energy extraction from the exhaust flow. The reduction in jet velocity will therefore be somewhat less than the ideal one dimensional reduction.
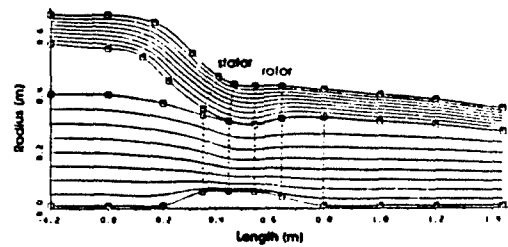
Fig.25 Computational domain and computed streamlines

9 CONCLUSION

The technical measures for the reduction of jet noise range from simple modifications to the nozzle schedule to replacing the complete exhaust system. Variable cycle engines, mixer-ejectors and aft-fans add considerable complexity and weight to the exhaust system but merit this by an improved fuel consumption when compared to increasing the nozzle area.

The results obtained in this study should be considered suffi-

ciently encouraging to warrant continued development and implementation of some of these technical measures for the reduction of jet noise.

10 ACKNOWLEDGEMENTS

11 REFERENCES

[1] Böttcher, J.; Michel, U.
Comparison of Flyover Noise Data from Aircraft at High Subsonic Speeds with Prediction
DLR (SM-EA), Germany, AGARD 78th-B Specialists' Meeting in Bonn, 21, 23-25 October, 1991

[2] Michel, U.; Böttcher, J.
Prediction of Jet Mixing Noise for High Subsonic Flight Speeds

DLR (SM-EA), Germany, AGARD 78th-B Specialists' Meeting in Bonn, 8, 23-25 October, 1991

[3] Böttcher, J.
Untersuchung zur Verminderung des Triebwerkslärms von Kampfflugzeugen.
3. Teil: Erweiterte Auswertung von Überflugmessungen und Vergleich mit Lärmvorhersageverfahren.
DLR Braunschweig, IB 129-89/18, 1990

[4] SAE APR 876 C
Gas Turbine Jet Exhaust Noise Prediction
Society of Automotive Engineers, Inc., 1985

[5] Lighthill, M. J.
On sound generated aerodynamically I: General theory.
Proc. Roy. Soc. A., 211, p.564-587, 1952

[6] ESDU 84029
Ejectors and Jet Pumps, Design and Performance for Compressible Flow
Engineering Science Data, 1984

[7] Daly, K.
Gulfstream patents 'bolt-on' hushkit device
Flight International, 13-19 June 1990

Discussion

QUESTION BY: A. Koc, MBB, Germany
If you take the mixer-ejector nozzle type, what is happening with the aerodynamic drag? Because with increasing drag, you need more thrust and so the SFC increases also.

AUTHOR'S RESPONSE:
With the ejector the thrust of the engine is increased, when the engine power setting is held constant, even at high flight speeds. Spillage drag at the secondary air inlets can be minimized by careful choice of the inlet cross-sectional area.

AD-P007 531
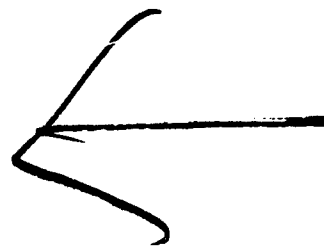
TECHNICAL MEASURES FOR THE ATTENUATION OF AIRCRAFT NOISE
AND THEIR APPLICABILITY TO GAF COMBAT AIRCRAFT

H. Tönskötter
S. Bläck
R. Richter

Industrieanlagen-Betriebsgesellschaft mbH
Einsteinstraße 20
8012 Ottobrunn
Germany

92-17434

SUMMARY

Possible technical measures for the reduction of
aircraft engine noise are evaluated with respect
to the noise attenuation potential at take-off,
low level flight and landing and their applicabi-
lity to the combat aircraft of the German Air-
force (GAF) is discussed.

Based on this analysis short and mid term solu-
tions for Tornado are proposed and investigated
with respect to noise attenuation, integration,
weight, flight performance, operational impact
and safety.
The design concept of a "Low Noise Training-Tor-
nado" with reheatless RB199 engines and ejector
nozzles is described.

LIST OF SYMBOLS

A/C	aircraft
A_N	nozzle area
A_P	primary mixer area, exhaust gas
A_S	secondary mixer area, air
BME	basic mass empty
F_N	net thrust
M	flight Mach number
m_S/m_P	secondary to primary mass flow ratio
SFC	specific fuel consumption
S.L.	sea level
SOT	turbine inlet temperature

1. INTRODUCTION

Aircraft noise is primarily related to engine
noise. Due to the introduction of high bypass
turbofan engines the noise of civil aircraft was
drastically reduced in the last twenty years. The
high bypass air flow decreases jet noise and the
fan, compressor and turbine noise is attenuated
by design measures and sound absorbing material
in the intake, bypass and exhaust duct.

To meet the required weapon system performance
most military combat aircraft have to provide su-
personic flight/cruise capability and high maneu-
verability. This led to the development of zero
or low bypass ratio afterburning engines with
high thrust-to-weight ratio and small diameter to
reduce supersonic aircraft drag. For these en-
gines the main source of noise is the high energy
exhaust jet. The turbo component noise (e. g. fan
noise) is of much lower order.

Therefore, noise attenuation of combat aircraft
has to be concentrated on the reduction of jet
noise.

2. LOW LEVEL FLIGHT NOISE OF GAF COMBAT AIRCRAFT

Since at least 10 years the noise of low flying
combat aircraft is a continuous matter of com-
plaints in Germany. Therefore, in 1984 a test
campaign was carried out by the German Ministry
of Defence (Ref. 1) to establish the noise level
of all relevant military aircraft of the GAF and
the Allied Forces operated in the area of the Fe-
deral Republic of Germany.
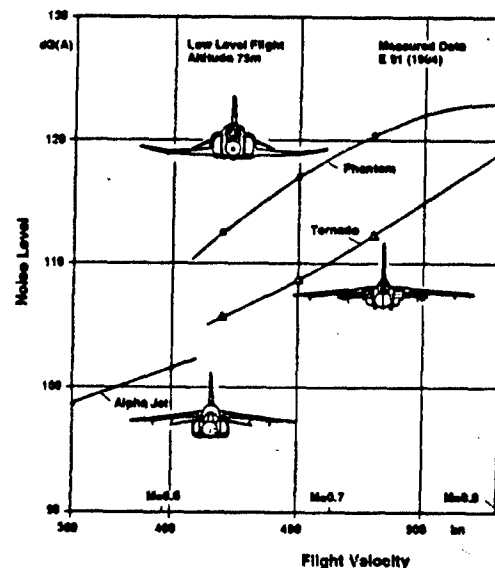
Fig. 1 Impact of Flight Velocity on Noise
Emission

Fig. 1 shows the results for three most relevant
GAF aircraft. The flyover noise is mainly a func-
tion of flight velocity. The noise level of the
Tornado is about 8 dB(A) lower compared with the
Phantom as the Tornado engine has a bypass ratio
of about 1 whereas the Phantom engine is of the
turbojet type (bypass ratio "zero").

Besides the noise level the gradient of noise in-
crease *(Fig. 2)* also causes annoyance to people
due to the shock effect. In *Fig. 3* the measured
impact of flight altitude and velocity on noise
level and gradient is shown for the Tornado air-
craft. Doubling the flight altitude decreases the
noise level by about 6 dB(A) but has only a minor
impact on the gradient of noise increase. Hence,
the most important parameter for low flying air-
craft noise is flight velocity.
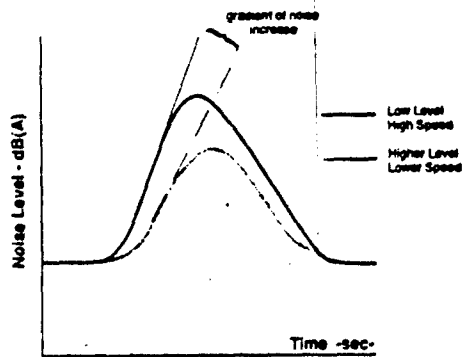
Fig. 2 Typical Flyover Noise Profile
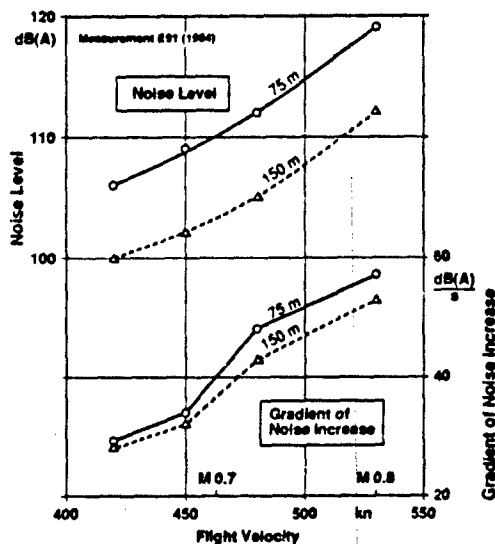
Fig. 3 Tornado Low Level Flight Noise

3. OPERATIONAL NOISE REDUCTION MEASURES

The operational measures to reduce the nuisance to people resulting from combat aircraft noise can roughly be summarized as follows:

- Increase of low level flight altitude (e. g. from 75 m to 150 m ==> ≈ 6 dB(A))

- Reduction of flight velocity (e. g. by 50 kn ==> 5-7 dB(A))

- Removal of external stores (≈ 3 dB(A))

- Low level intercept training at higher altitude (e. g. from 150 m to 300 m ==> ≈ 6 dB(A))

- Reduction of low level flying time (e. g.from 28 min to 15 min)

- Flight path planning to avoid areas with dense population, hospitals etc.

- Transfer of low level flight training into foreign countries with large unpopulated areas

- Use of low level flight training simulators (not yet available)

It should be noted that although the increase of flight altitude, e. g. from 75 m to 150 m, reduces flyover noise by about 6 dB(A), the sideline noise e. g. beyond 240 m may be increased. This is because of the noise absorption of the ground. Fig. 4 shows the calculated noise distribution as a function of flight altitude. The demonstrated impact of flight altitude on flyover noise as well as on sideline noise could be verified by the measurements in Ref. 1.

In many cases the introduction of operational measures as listed above has a detrimental impact on the level of pilot training and therefore needs to be evaluated carefully. Nevertheless, some of these measures have already been introduced by the German Airforce in 1989.
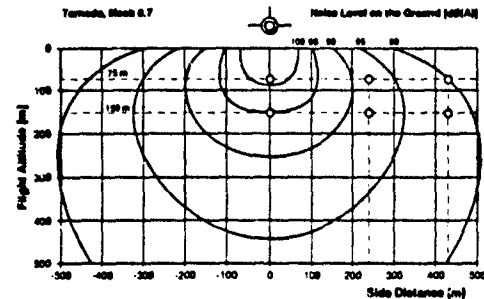
Fig. 4 Impact of Flight Altitude on Ground-Noise Distribution

4. TECHNICAL MEASURES

As the operational measures in many cases adversely affect the pilot training effectiveness if a meaningful noise attenuation is to be achieved, the potential and applicability of technical measures - taking into account integration aspects and the impact on engine and flight performance - are discussed in this paper and proposals for short term as well as mid term solutions for Tornado are presented.

4.1 Survey and Applicability of Technical Measures

Table 1 summarizes the technical measures which may reduce engine and especially jet noise of military aircraft. They are evaluated with respect to their noise attenuation potential during take-off, landing and low level flight and to their applicability to GAF combat aircraft.

Reduction of Jet Velocity

Reducing exhaust jet velocity of the engine is the most effective measure for jet noise attenuation. This can be achieved by opening the exhaust nozzle at part load operating conditions (increase of air mass flow at constant thrust) and by ejector nozzles.

Noise optimized nozzle control provides noise attenuation at part load only, as for max. thrust the nozzle needs to be closed. It is applicable to aircraft with engines with variable exhaust nozzles, like Tornado and Phantom.

A much greater noise reduction potential is offered by the installation of exhaust ejectors, as a higher increase in air mass flow can be realized. Noise attenuation is achieved at all

Table 1 Possible Engine-/Aircraft Modifications for Noise Attenuation

Noise Reduction Measure	Technical Solution	Noise Reduction			Applicability to GAF Combat Aircraft		
		Takeoff	Landing	Low Level Flight	Tornado	Phantom	Alpha Jet
Reduction of Jet Velocity	Part Load Needs Cooled	·	●	·	●●	·	●
	Ejector	●●	·	●●	·	●	·
	Mixer (within the engine)	·	●	●	●	·	●●
Frequency Shift	Multitube Nozzle	·	·	·	·	·	○
	Mixing Nozzle (lobe & corrugated Type)	·	·	·	·	·	·
Jet Profile	Asymmetric Nozzle	·	○	●	·	·	·
	Inverted Jet	·	·	·	·	·	●
	Swirl Generator	●	●	●	·	·	·
Absorption	Absorbing Material Helmholtz-Resonator	·	·	·	●	●	·
	Porous Plug Nozzle	·	·	·	·	·	●
Shielding	Mechanical Shielding	●	●	·	·	·	·
	Jet Shielding	●	●	·	·	·	·
	Engine Installation	●	●	·	·	·	·
Anti Sound Method (Interference)	Anti Sound Generation Interference Tubes (helium, hydrogen)	●●	●●	●●	·	·	·
		·	·	●●	·	·	·
Component Optimization	Adapt. Nozzle (var. area)	·	·	·	●	·	·
	Opt. Nozzle-Kontur	●	●	●	·	·	●
	Optimal Intake	·	●	·	·	·	·
	Low Noise Fan	·	●	·	·	·	·
	Low Noise Combustor and Turbine	·	●	·	·	·	·

Noise Reduction:
●● 5 - 10 dB(A)
● 3 - 5 dB(A)
· 2 - 3 dB(A)
· < 2 dB(A)

Applicability:
●● recommendable, low effort
● recommendable, mean effort
· not recommendable, high effort
· not applicable

flight conditions but its realization for reheat engines necessitates the development of complex folding nozzles and adds considerable weight to the end of the aircraft. Therefore, the application can only be recommended for aircraft with nonafterburning engines or for modified aircraft, which will be used for special training tasks only, like low level flight training, and which do not need the afterburner. For the Phantom the ejector is not advisable as a modification of the rear fuselage would be necessary.

Mixing of core and bypass flow offers some noise reduction and can be recommended for the Alpha -t with its unmixed flow engines.

Frequency Shift

Multitube, lobe and corrugated nozzles increase the frequency of the jet noise and reduce the length of the free exhaust gas stream. As atmospheric absorption capability increases with frequency the jet noise is attenuated. This type of nozzle is well known as hushkits for the late civil aircraft with low bypass engines but cannot be applied to combat aircraft with variable exhaust nozzle engines (reheat engines).

Jet Profile

A nonconcentric arrangement of the primary and the bypass stream provides - according to Ref. 2 - a noise reduction potential, but it decreases with forward flight velocity.

An inversion of the hot (fast) and cold exhaust stream, such that the faster stream is outside and surrounding the cold stream with lower velocity, reduces - according to Ref. 3 - the free stream length and by this the jet noise. An application to combat aircraft with mixed flow reheat engines is not possible.

The introduction of swirl generators into the exhaust jet to reduce free stream length and hence noise is not a practical measure for combat aircraft, as its integration is difficult, the thrust loss is high and the effectiveness has not been demonstrated as far as known.

Absorption

Noise absorbing materials and devices (e. g. Helmholtz resonators) can be used in ducts (e. g. intake, bypass, ejector etc.) to reduce the noise of the internal sources (turbo component and mixing noise) where necessary. They can not be used to reduce jet noise, as jet noise is generated outside the confines of the engine.

The porous plug nozzle features a porous surface of the plug which will suppress the shock cell noise of underexpanding convergent nozzles (Ref. 4). This type of nozzle is only applicable to dry engines, as for reheat engines the integration and cooling of a variable area plug nozzle is very difficult.

Shielding

Mechanical shielding and jet shielding are based on the reflexion and deflection of the noise waves generated by the exhaust jet. Mechanical shielding increases the length of the aircraft drastically and adversely affects the handling of the aircraft.

Jet shielding necessitates additional hot gas generators and/or additional gas/fluid on board and therefore is only suited for short time operation.

An embedded engine arrangement or the installation of the engine above the wing can only be considered for new aircraft.

Anti Sound Method

The technology for anti sound generation is not yet available. Furthermore, due to the high energy of the jet noise the anti sound generators would have a high power consumption.

The technology of interference tubes which would be located below the jet and through which gas with different density (e. g. helium or hydrogen) flows, is also not available. As these tubes are to be retracted during take-off and landing no noise attenuation is provided at these flight conditions.

Component Optimization

As for combat aircraft engines turbo component noise is much lower than jet noise, noise optimization of the components (except the nozzle) is not a prime task. With respect to noise an underexpanding convergent nozzle has to be avoided and fully adaptive convergent/divergent nozzles are to be preferred.

4.2 Short Term Solution for Tornado

In section 4.1 it was shown that the most effective way to reduce jet noise is decreasing exhaust jet velocity by increasing the nozzle mass flow rate. This can be achieved to some extent by opening the exhaust nozzle at dry part load operation of the engine.

Fig. 5 shows the actual RB199 nozzle area schedule versus power lever setting and the modified

schedule for noise optimized nozzle control. Opening the nozzle is limited by choked flow conditions at colander exit (afterburner inlet). In this case the flow in the bypass duct upstream of the colander is still subsonic.

Increasing the exhaust nozzle area at constant installed cruise thrust reduces jet velocity by the increase of engine air mass flow and the reduction of intake spillage and afterbody drag. *Fig. 6* shows the impact of nozzle area on specific fuel consumption of the Tornado engine at different flight Mach numbers. Due to the decrease of intake and afterbody drag SFC is nearly constant (solid lines, "installed").
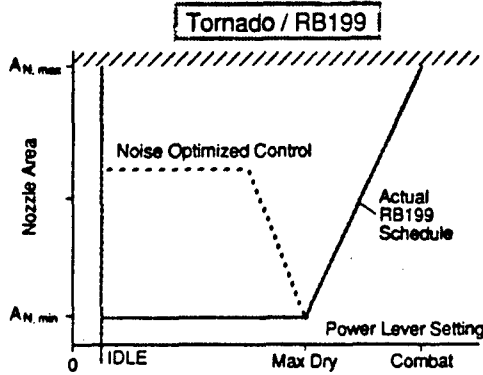
Fig. 5 Noise Optimized Exhaust Nozzle Control
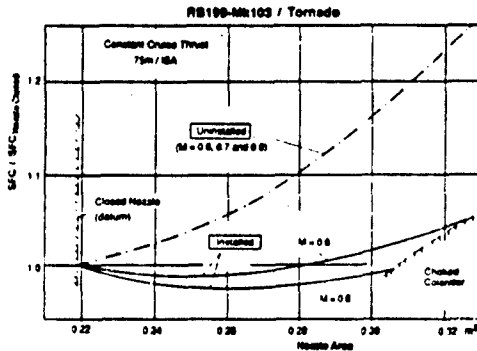
Fig. 6 Impact of Nozzle Area on Specific Fuel Consumption

The realization of the noise optimized nozzle control can be achieved in a short time, as only a software change of the digital engine control unit, which is in service since some years, is necessary.

The attenuation of low level flight noise is shown in *Fig. 14*. At max. dry and reheat power no noise reduction is provided, as at these power settings the engine has to be controlled to the original nozzle schedule.

4.3 Mid Term Solution for Tornado

Based on the results of the survey of technical measures of section 4.1 a "clean" Low Noise Training-Tornado version with "dry" engines and exhaust ejectors installed instead of the afterburner and the variable nozzle is proposed. The air-

craft can be returned to a standard Tornado with reheat engines in no more than 24 hours, as only an engine change and the reinstallation of gun and pylons are necessary.

This Tornado training version is designated for low level flight training and other subsonic training tasks which do not require external stores (or only minimum stores) and reheat thrust.

Within the ejector the exhaust gas of the engine is mixed with secondary air, which increases the nozzle mass flow by 100 - 200 % and effectively decreases jet velocity and noise.

The integration of an ejector into the afterburner of the RB199 was rejected due to the following reasons:

- the amount of secondary air which can be added to the exhaust gas of the engine is limited by the size of the afterburner and the nozzle

- the development of a complex folding mixer nozzle within the afterburner and the resulting afterburner modifications need several years and are very expensive

- secondary air doors would have to be integrated into the rear fuselage

- the increased propulsion system weight at the rear of the aircraft needs to be balanced by additional mass in the front to avoid a shift of the center of gravity.

For the assessment of the noise attenuation potential and the impact on engine mass and aircraft performance a project design and detailed performance calculations were carried out.

To avoid unacceptable thrust losses at high subsonic flight Mach numbers the intake of the ejector needs to be designed carefully. *Fig. 7* shows the impact of the intake type on thrust versus flight Mach number. Without taking into account the reduction of afterbody drag due to the increased nozzle area of the ejector, the thrust continuously decreases with flight Mach number (dashed curve "Flush, uninstalled").
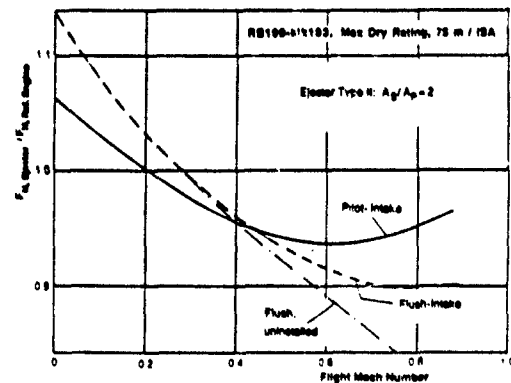
Fig. 7 Impact of Ejector Inlet Design on Installed Net Thrust

As the difference in thrust at Mach 0.3 (critical take-off and climb phase for one engine failed)

is small the pitot intake was chosen. With this intake high subsonic flight velocity and and high maneuver performance (clean aircraft) is provided.

The size (type II, $A_S/A_P = 2$) of the ejector was chosen based on a compromise between noise attenuation and thrust loss *(Fig. 8)* taking into account installation constraints due to the location of the taileron. The mass flow ratio (m_S/m_P) of this ejector is 1.1. to 1.3 depending on flight Mach number.
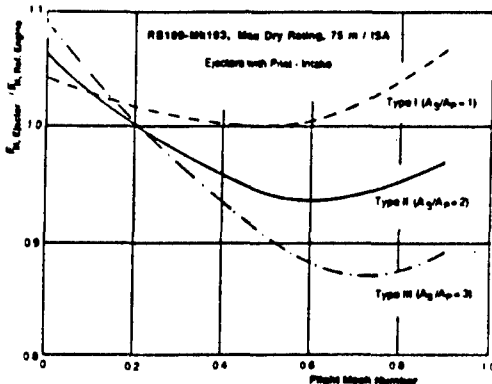
Fig. 8 Impact of Ejector Size on Installed Net Thrust
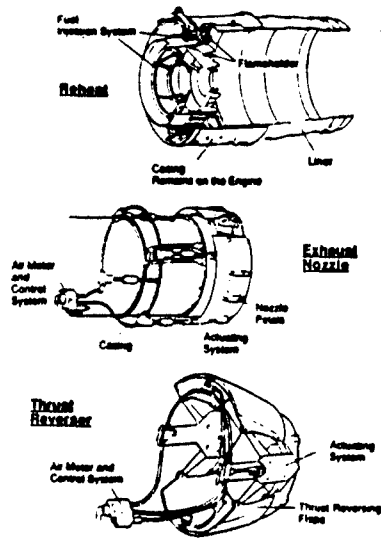
Fig. 9 Engine Components to be removed for the Ejector Version (RB199-Mk103)

To change the RB199-Mk103 Tornado engine into a non-afterburning ejector version the following work is necessary *(Fig. 9)*.

- removal of thrust reverser, exhaust nozzle (incl. actuation system) and afterburner (the front part of the afterburner casing remains on the engine)

- installation of the ejector module with the fixed lobe type mixing nozzle

- replacement of the DECU or software change only

- replacement of the Mk103 fan by the Mk105 fan to increase max. dry and emergency thrust (if the engine is changed back to the standard reheat version the Mk105 fan remains on the engine)

As no modification of the fuselage is necessary, the ejector engine can be replaced by the original reheat engine by a simple engine change.

The DECU of the ejector engine has the same hardware as the original DECU, only the software is changed to enable reheatless operation of the engine and to provide the proposed engine rerating (take-off rating at combat SOT and emergency rating).
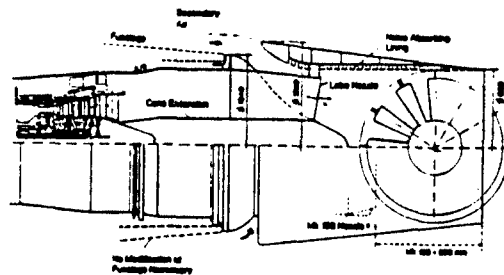
Fig. 10 Reheatless RB199 Engine with Ejector Nozzle (Type II, $A_S/A_P = 2$, Design Point M = 0.8)

Fig. 10 shows a cross section of the rear part of the RB199 engine and the installed ejector. The lobe nozzle with the cone extension and the ejector casing with the noise absorbing lining are one module. The length of the ejector is such that the area were maximum mixing noise occures is within the ejector.
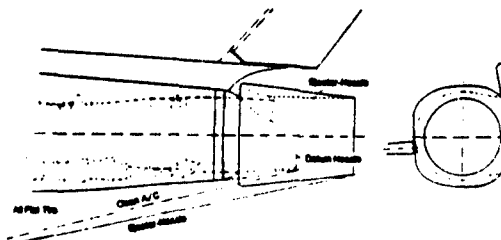
Fig. 11 Low Noise Training-Tornado with Ejector Nozzle (rear A/C section)

The mass of the ejector engine is 190 kg lower compared with the original reheat engine with thrust reverser. The lower engine mass at the rear of the aircraft (380 kg total) allows the removal of the gun in the front section and hence an additional aircraft weight reduction.

The shape of the ejector is designed such that its fits very well in the overall design of the rear Tornado fuselage *(Fig. 11)*. Although the length of the aircraft is increased by 530 mm *(Fig. 10)*, the rotation capability of the aircraft at take-off is reduced relative to the clean Tornado by only 2 degrees.

To reduce the A/C drag and weight the Low Noise Training-Tornado is operated without external stores, without the gun and with the pylons removed. Compared with the Reference Tornado defined below the A/C weight is reduced by more than 20%.
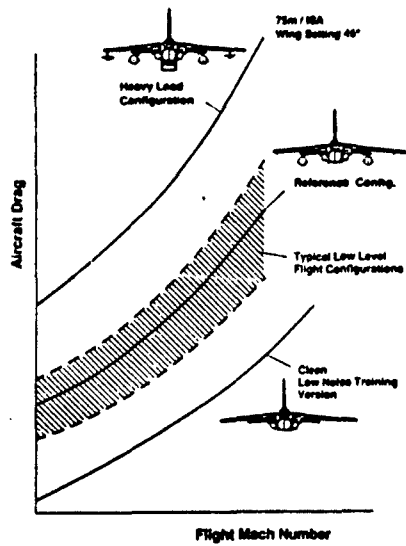
Fig. 12 Tornado Drag Characteristics at Low Level Flight

The analysis of the Tornado configurations for low level flight training of the GAF showed that no standard configuration can be identified. As illustrated in *Fig 12*, the variation in A/C drag is such that the definition of a Reference Tornado configuration ((2) external tanks, (1) ATM-9L, 50 % ext. fuel) for the evaluation of A/C performance was necessary. Furthermore, in *Fig. 12* the drag versus flight Mach number characteristic of the Low Noise Training-Tornado is shown relative to the Reference Tornado and to a heavy load configuration.

5. NOISE ATTENUATION AND IMPACT ON FLIGHT PERFORMANCE

During take-off and low level flight of combat aircraft the jet noise is the predominant noise source. Engine fan and turbine noise are of much lower order. Therfore, only the jet noise attenuation was calculated.

5.1 Jet Noise Calculation

Jet noise calcualation was carried out according to SAE ARP 876 C. In *Fig. 13* the measured and calculated flyover noise of the Tornado at low level flight condition (75 m altitude) is compared at different flight Mach numbers. It becomes evident that the shock cell noise calculated with the SAE method is too high.

Therefore, all noise attenuation results in this paper are based on the calculation of jet mixing noise only without taking into account the reduction of shock cell noise. In consequence, the real noise reduction potential of the proposed technical measures is higher than shown in *Fig. 14*.

5.2 Low Level Flyover Noise Attenuation

In *Fig. 14* the flyover noise attenuation for Tornado is summarized. At Mach 0.7 the removal of external stores and pylons ("clean" Tornado) reduces the noise by about 3 dB(A). Opening the exhaust nozzle provides an additional attenuation of 5 dB(A). The flyover noise of the Low Noise Training-Tornado is - depending on the ejector

size - 13 to 19 dB(A) lower as compared to the Reference Tornado. The chosen ejector type II provides 17 dB(A) noise reduction. Due to the thrust loss caused by the ejector the noise reduction potential decreases with increasing flight Mach number.
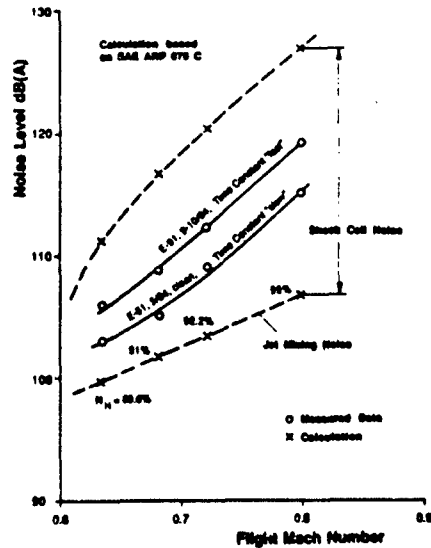
Fig. 13 Comparison of Calculated and Measured Tornado Flyover Noise at 75 m
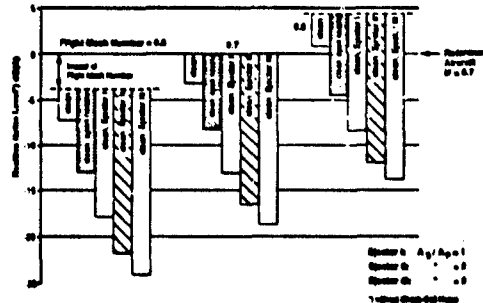
Fig. 14 Impact of Tornado Noise Reduction Measures on Flyover Noise at 75 m Flight Altitude

5.3 Take-off and Climb Noise Reduction

Fig. 15 shows the noise distribution on the ground for the Low Noise Training-Tornado at take-off power compared with the Reference Tornado (dashed curve) at max. reheat power. The difference in noise depends on the direction and distance of the observer. At 130 degree and a distance of about 800 m, for instance, the noise reduction is 30 dB(A).

Although the rate of climb of the Low Noise Training-Tornado is lower compared with the Refernce Tornado, the area with a noise level of greater 90 dB(A) during take-off and initial climb is much smaller than the equivalent area of the Reference Tornado *(Fig. 16)*. Hence, annoyance to the population living near the military air field is drastically reduced.
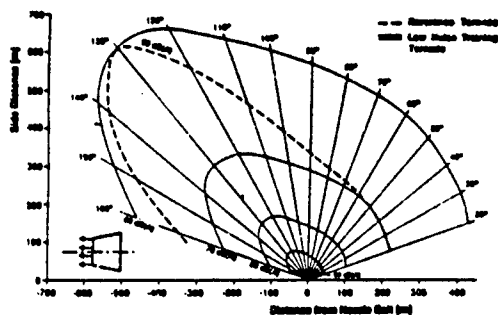
Fig. 15 Noise Contours of the Low Noise Training-
Tornado with Ejector and of the Reference
Aircraft
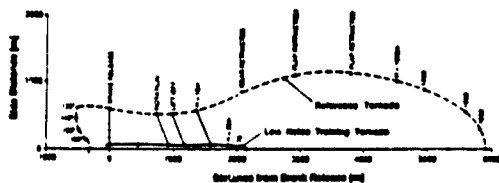
Fig. 16 90 dB(A) Noise Contours of Reference and
Low Noise Training-Tornado during Take-
off and Initial Climb

5.4 Impact on Flight Performance

As the reheat system of the RB199 engine is re-
moved to install the exhaust ejector the thrust
rating of the engine needs to be revised for the
Low Noise Training-Tornado in order to minimize
flight performance losses.

Instead of "max. reheat" a dry "take-off" rating
at combat SOT and instead of "combat" a dry
"emergency" rating are proposed. The "emergency"
rating is a short time rating to be used if one
engine fails during take-off and initial climb.
Two emergency ratings with an increase in SOT by
50 K and 100 K have been considered.

Fig. 17 shows that even for an altitude of 2000ft
and hot day conditions (ISA + 15 K) the reduced
emergency rating provides a single engine climb
performance of the A/C which is greater than the
minimum required. The lower weight of the Trai-
ning-Tornado allows a maneuver flap setting - in-
stead of the standard mid flap setting - which
improves the climb performance but adversely af-
fects the take-off distance. Nevertheless, even
at 2000 ft/ISA + 15 K the take-off distance of
the Training-Tornado with maneuver flaps setting
is about 20 % shorter than the shortest runway of
the relevant military air fields in Germany.

Although the Training-Tornado has no external
tanks the low level flight time is only reduced
by about 22 % compared with the Reference Tornado
which is equipped with two external tanks.

For low level flight training the maneuverabi-
lity, which can be described by the sustained
turn rates, is of outstanding importance. Al-
though the max. thrust of the dry ejector engine
of the Tornado training version is much lower
than the max. reheat thrust of the Reference Tor-
nado the sustained turn rates of both aircraft
are quite similar *(Fig. 18)*. This is due to the
lower weight and lower drag (no external stores)
of the Low Noise Training-Tornado.

- RB199 with Ejector, Emergency Rating, Min. Eng.
- Landing Gear Extended
- Free Air Data
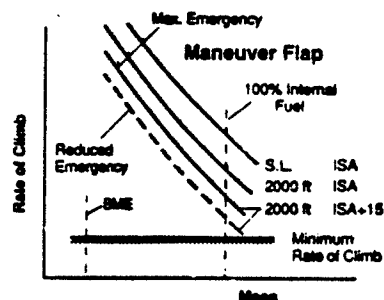
Fig. 17 Single Engine Climb Performance of Low
Noise Training-Tornado with Ejector
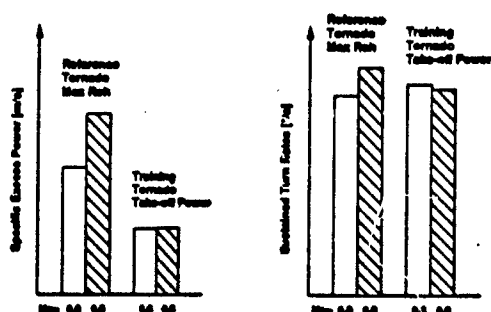
Fig. 18 Flight Performance of Reference and
Training-Tornado (ISA, sea level)

The acceleration capability of the Tornado trai-
ning version is only about 50 % of the Reference
Tornado as shown in *Fig. 18* in terms of specific
excess power. This is considered to be accep-
table, as for low level flight training specific
excess power is of lower importance than sustai-
ned turn rates.

CONCLUSION

Based on a survey of technical measures to reduce
the noise of combat aircraft two solutions are
proposed for Tornado

- as a short term solution the noise optimized
nozzle control and

- as a mid term solution a Low Noise Trai-
ning-Tornado with dry engines and ejector
nozzles which can be returned to a stan-
dard Tornado within 24 hours.

Detailed analysis showed that the Low Noise Trai-
ning-Tornado with nonafterburning ejector engines
fulfills the single engine rate of climb require-
ment and provides sufficient maneuver capability.
If the gust sensitivity of the low weight Trai-
ning-Tornado is too different compared with the
original Tornado in a typical low level flight
configuration with external stores, wing sweep
can be increased (lower lift slope) to compensate
this effect.

An ejector developed for the Tornado can be
modified such that it can also be installed on
the future EFA aircraft if the need would arise.

REFERENCES

1. *Hellmann, H.*, "Schallpegelmessungen bei Standardtiefflügen", BWB-WTD 91, Ministry of Defence, Germany, 13 November 1985.

2. *O'Keefe, J. V., Mangiarotty, R. A. and Pickup, N.*, "Current Status and the Future of Advanced Supersonic Transport Noise", AIAA 80-1056, J. Aircraft, Vol. 18, No. 7, July 1981, pp 576 - 581.

3. *Ribner, H. S.*, "Perspectives on Jet Noise", AIAA 81-0428, AIAA Journal, Vol 19, No. 12, December 1982.

4. *Maestrello, L.*, "Initial Results of a Porous Plug Nozzle for Supersonic Jet Noise Suppression", NASA TM 78802, Nov. 1978.

Discussion

QUESTION BY: AVM G. Williams, AGARD AAS-34

1. Comment on operational measures: Flying higher and slower will greatly reduce the training value of missions.
2. Having two different engine types for one aircraft type will lead to considerable extra operational and logistic costs. Also, development costs would be very high so the practicality of this development is questionable.
3. Your method addresses jet related noise effects; could you indicate how your results would be modified in the light of the UK findings on the importance of airframe noise (paper 22)?

AUTHOR'S RESPONSE:

1. As most operational measures adversely affect the training value, this paper primarily deals with technical measures which will allow noise attenuation without reducing the training level.
2. The engine for the Low Noise Training Tornado is a standard RB199 engine. Only the rear part of the engine is modified. Instead of the afterburner and the variable exhaust nozzle the ejector nozzle is installed such that the engine can be changed back to a standard RB199 within a few hours. Hence, the additional operational and logistic costs can be expected to be not very high. The development costs have to be related to the level of noise reduction. Without costs no noise attenuation by technical measures can be achieved.
3. The proposed Low Noise Training Tornado incorporates both aspects. The airframe noise will be attenuated by the release of the external stores and of the pylons (reduction of aircraft weight and drag). The jet noise will be reduced due to the lower required thrust and due to the ejector nozzle. Unfortunately the UK measurements do not cover a noise breakdown for the clean aircraft. It's agreed that the technical measures for jet noise reduction have to be evaluated with respect to their contribution to the overall noise attenuation of the aircraft. Nevertheless, whatever the findings on the importance of airframe noise for a clean aircraft will be, the ejector nozzle will considerably reduce the noise in the max. power mission phases like takeoff, climb, acceleration and low level flight manoeuvres.
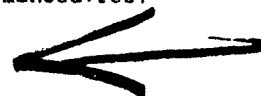
STUDY RESULTS ON COMBAT AIRCRAFT SOURCE NOISE REDUCTION

I.U. Borchers
H.J. Hackstein
P. Bartels

Dornier Luftfahrt GmbH
Postfach 1303
W-7990 Friedrichshafen
Germany

92-17435

SUMMARY

For use in combat aircraft noise control, important results of extensive studies on jet noise reduction are presented. The studies covered low-noise nozzle designs such as linear arrays of circular nozzles, inverted profile jets as well as special shape mixing nozzles and coaxial bypass flow configurations. In addition interesting results of systematic research on special acoustic absorbers for propulsion system internal noise reduction and of initial theoretical and experimental studies on promising ejector flow systems are reported. The results of the different investigations are in detail explained and discussed. Furthermore, practical applications, including examples of performed and possible future integrations of the considered noise control measures into aircraft, are presented. It is noted that the implementation of these methods could significantly reduce combat aircraft engine noise. For substantial noise reductions, of the order of 20 dB or more as obtained for civil jet transport aircraft, the integration of advanced ejector flow systems is suggested which are capable of effectively lowering the jet exhaust speed as required and with this strongly reduce the jet noise generation. It is concluded that extensive information and an advanced technology basis for jet engine noise reduction exist. Applying this, by given the needed noise control equal importance and priority as other critical aircraft aspects, may strongly help resolving the related noise problem.

1. INTRODUCTION

The fly-over noise of high performance combat aircraft (fighters/bombers) is extremely intense, especially at low altitude flights. For certain aircraft and flight heights of about 75 m to 300 m, the noise levels on the ground may assume peak values of about 120 dB(A) to 110 dB(A). Although combat-readiness flying at such altitudes is frequently needed to maintain required defense strength, this intense noise impact has caused increasingly adverse public reactions in the more densely populated countries of Western Europe, particularly in Germany over recent years. With this a difficult noise problem exist for which technical and/or operational solutions need to be urgently developed and/or introduced.

The intense noise of these aircraft is generated primarily by their powerful propulsion systems and in most cases is fully dominated by the strong low frequency jet exhaust noise of these systems. The jet noise is created by the intense turbulent mixing of the high velocity exhaust gases with the ambient air. Thus, this noise is generated outside and downstream of the jet engine and with this is the most difficult noise to control. For example, it is not amenable to sound absorption measures in the engine or nacelle as is generally the case for engine fan and combustion noise. In order to re-

duce combat aircraft jet noise, therefore, significant effort is needed and all possible methods have to be considered for effective noise control including new more noise controlling integrations of the engines into the overall aircraft design for future aircraft configurations.

For the first generation of civil jet transport aircraft, introduced in the 1950's, also jet noise was the most dominant aircraft noise source and needed to be strongly reduced, for lowering noise annoyance and achieving public acceptance of this new higher performance aircraft type. Since this time, extensive experimental and theoretical research on jet noise reduction and on the suppression of other engine noise components such as fan and combustion noise have been performed. For jet noise the most effective noise reduction measure was found to be the reduction of the jet exhaust speed as the sound power of free exhausting jets is according to Lighthill's well known law [1] proportional to the eighth power of this speed. In addition, extensive results of a large number of mixing nozzles, ejector systems and various other devices for jet noise reduction have been established and could now also be used for related noise control, if feasible and required.

The noise problem of civil jet transport aircraft was to a large extent resolved by applying the effective principle of reducing the jet exhaust velocity. The reduced velocities resulted from the development and application of increasingly high bypass ratio engines having now bypass ratios up to about 1:7. In conjuction with careful fan design and the installation of noise absorbing liners in the engine inlet and exhaust section, significant noise reductions followed reaching values of as high as approximately 20 dB.

For future high performance combat aircraft, also a lowering of the jet exhaust velocity seems to be required, if substantial noise reductions, similar to those of civil transport aircraft, should be obtained. For this typ of aircraft, however, the application of engines with relatively high bypass ratios appears to be not feasible as they are related, for example, with larger engine dimensions and higher weight and drag, which could significantly reduce flight performance. As an alternative, the development and use of variable cycle engines and/or the application of ejector flow systems offering also a high potential of jet exhaust velocity reductions and thus of jet noise reduction may be considered. While variable cycle engines could be related with additional rather extensive development costs, ejector flow systems may be fully integrated into future aircraft designs and could be based on existing engine configurations.

The principle of ejector systems bases on secondary air which is entrained into the ejector channel and mixes there with the jet engine primary flow. Thus, the ejector generates a jet of larger cross-

sectional area but with substantially reduced exhaust velocities and, what is more important, with significantly reduced jet noise levels. For higher altitude and supersonic flights as well as combat missions the ejector geometry could be varied in such a way that unacceptable performance losses for these operation conditions might be avoided. In conjuction with optimized special mixing nozzles, effective noise absorbing liners attached to the inner ejector surfaces and possible other noise control measures such as shielding surfaces, the required ejector length may be kept sufficiently short and rather high noise reduction values comparable to those achieved for civil transport aircraft could be obtained.

If a lowering of the noise-important jet exhaust velocity and a more noise controlling aircraft propulsion system integration for future aircraft is not possible, only a moderate jet noise reduction may be expected based on technical measures and current technology. However, also such noise reductions might be of interest as in conjunction with effective operational measures an interestingly high overall noise relief for the public may result. In this case also ejector systems, but more designed as add-on configuration, special mixing nozzles and optimized jet exhaust velocity profiles as well as jet noise shielding and noise absorption measures and combination of these methods could be considered and produce noise reductions of say approximately 6 to 10 dB. To a certain extent, these techniques could also be realized as add-on devices to existing combat aircraft and for this application may establish noise reductions of similar levels as mentioned before. With such add-on devices and effective operational measures, therefore, also an interesting noise control on a short term basis could be achieved.

For possible guidance of the required combat aircraft noise control and for supporting needed near to long term decisions on this subject, at present a review and discussion of interesting results on jet noise reduction measures which may be realized in practical applications seems to be of great importance. In the present paper, therefore, related selected results on this topic are presented. The results refer to the noise control methods mentioned before and concern the following subtopics

* noise characteristics of linear arrays of mixing circular jets

* flow and noise data of inverted profile jets

* selected results of special shape mixing nozzles and coaxial bypass jets

* data on special acoustic absorbers for engine and ejector acoustic liners

* initial theoretical and experimental results on ejector flow systems

The presented results have been partially published already previously. If more detailed information is required, reference can be made to these publications and/or reports noted in the following sections and listed at the end of this paper.

2. NOISE CHARACTERISTICS OF LINEAR ARRAYS OF MIXING CIRCULAR JETS

In this section interesting results on the noise radiation and related jet interference effects are presented, for linear nozzle arrays consisting of several circular nozzles equally spaced along a straight line.

Previous experimental studies have indicated that free jets may constitute an effective acoustic shield for jet noise radiation [2, 3] and that the mixing of adjacent jets could produce an interesting jet sound power reduction [4]. Therefore, in the plane through the nozzle axes of the considered nozzle arrays, a high degree of noise shielding and also a reduced overall sound power of these nozzles may be expected, giving them an interesting noise reduction potential. In addition, these nozzle designs seem to be well suited for implementation into even more effective noise reduction ejector systems, so that their basic noise characteristics need to be known also for such applications.

The shielding of the considered nozzle arrays may be expected to be a result of reflections of sound waves by the adjacent jet streams. In addition, as illustrated in Figure 1, the shielding could be related with a possible coherent or partially coherent noise radiation of the elemental jets, resulting from regular interactions of possible large scale turbulence structures in the jet flow field. The sound power reduction of mixing adjacent jets may be assumed as previously done [4] to be due to reduced turbulence intensities in their common mixing regions, but could also be effected by possible coherent or partially coherent noise radiation of the separate but mixing jet streams.
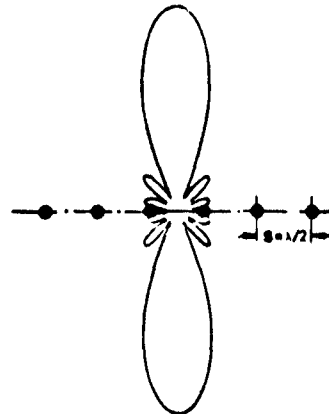
Figure 1: Directional sound field of six linearly arranged coherent noise sources (after Ref. [5])

In the following, results of free field directivity measurements and sound power measurements are reported describing the sound field of the considered nozzle configuration for two to five parallel jets with different nozzle center spacing. In addition, some results of hot film measurements and spark shadowgraphs are discussed, which were taken to investigate flow characteristics associated with the noise radiation. Additional result and information are given in References [6, 7].

2.1 Remarks on Test Equipment and Test Procedures

2.1.1 Multinozzle model design

The model nozzle used for testing the linear nozzle arrays is shown in Figure 2. The nozzle design enabled an easy change of the nozzle number, N, and the spacing ratio, SR = S/D (S = distance between center of nozzles, D = nozzle diameter). The nozzle number could be varied from N = 1 to 5 and the spa-
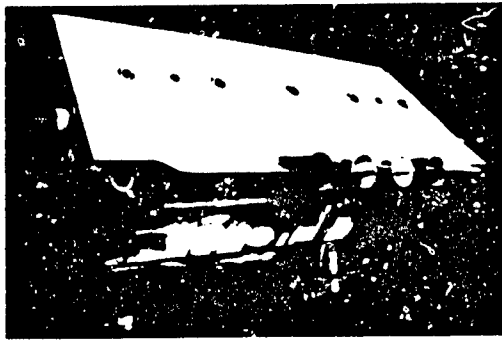
Figure 2: Multinozzle model design

cing ratio, for example, from SR = 1.25 to 9.0 for N = 2. The exhaust diameter of the individual nozzles was constant, D = 2.12 cm.

The testing of the nozzle arrays was performed with cold air and an exhaust Mach number M_e = 0.9, except for the hot film measurements, which were conducted for M_e = 0.7.

2.1.2 Experimental techniques

Acoustic test. The free field directivity measurements were performed using a free field test facility with the stilling chamber of the test stand inclined at an angle of 35°. The nozzle exit was located about 4.5 m above ground. Three microphone sweep arms could be used for performing simultaneous measurements within the nozzle prinicple planes XY, XZ and YZ. For testing, spherical coordinates, θ, φ, and R, were introduced based on the facility coordinate system as explained in Figure 3. The matrix of Figure 3 summarizes the locations at which measurements were performed. The sound power measurements were conducted in a reverberation room with a volume V = 10.3 r^3 and a lower cutoff frequency of approximately 0.6 kHz. The reverberation time, T_R, ranged from 1.1 sec at 0.5 kHz to about 0.4 sec at the high end of the audible spectrum.

The acoustic results are compared in the following with corresponding results of a single nozzle of the nozzle arrays adjusted by adding the constant
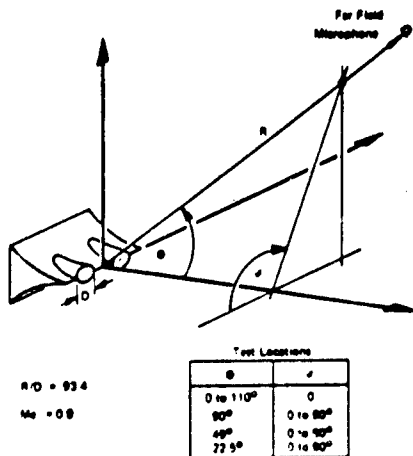
Figure 3: Coordinates and test locations of free field measurements

$$C = 10 \log (N) \qquad [dB]$$

to these data. The adjusted results can be interpreted as results of N equal jets operating independently and are used to identify the effect of the jet interference on the radiated sound field. The adjusted data are denoted "single nozzle + C dB" where C = 3, 4.8, 6 and 7 for N = 2, 3, 4 and 5, respectively.

Flow measurements. The hot film measurements included turbulence intensity and mean velocity traverses in the plane through the jet axes at the downstream locations X/D = 3, 5, 8 and 12. For the shadowgraphs, the photographic film plate was located parallel to the plane given by the jet axes so that the common mixing zone could be photographed.

2.2 Results and Discussion

2.2.1 Directivity measurements

Effect of emission angle θ. Initial tests were performed to study the effect of jet interference or noise shielding in sideline direction, φ = 0, as function of the angle θ. A typical result for the 2-nozzle array is shown in Figure 4. Comparing these results with the data given for the single
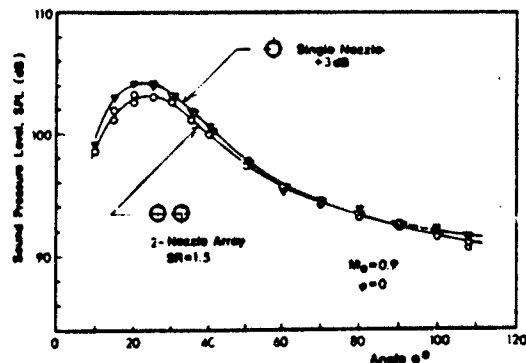
Figure 4: Directivity of 2-nozzle array with SR = 1.5 for φ = 0

nozzle +3 dB it appears that the jet noise shielding or any other jet interference effect is restricted to angles θ < 60°. For this range the tested two adjacent jets result in a reduction of the radiated noise with a maximum reduction of about 2 dB around the peak of the directivity.

Effect of spacing ratio SR. The majority of the tests were conducted at the constant angles θ = 22.5°, 45° and 90° for varying angles φ. The 2-nozzle array was tested in this manner for spacing ratios SR = 1.25 to 8 to obtain some reliable information on the effect of the adjacent jets on the sound field directivity. The results of these tests are shown in Figure 5 in comparison with data from a single nozzle +3 dB tested several times during the same experiments. The basic features of these results may be summarized as follows

* the jets radiate a rotationally asymmetric sound field with less intense noise levels in sideline direction, but not for all θ and SR

* for both θ = 22.5° and 45° the asymmetry of the sound field is strongly pronounced, increases with increasing SR and includes for

θ = 22.5°

θ = 45°

M₀ = 0.9 appears as $M_0 = 0.9$

θ = 90°

Sound Pressure Level, SPL (dB)

Angle ψ°
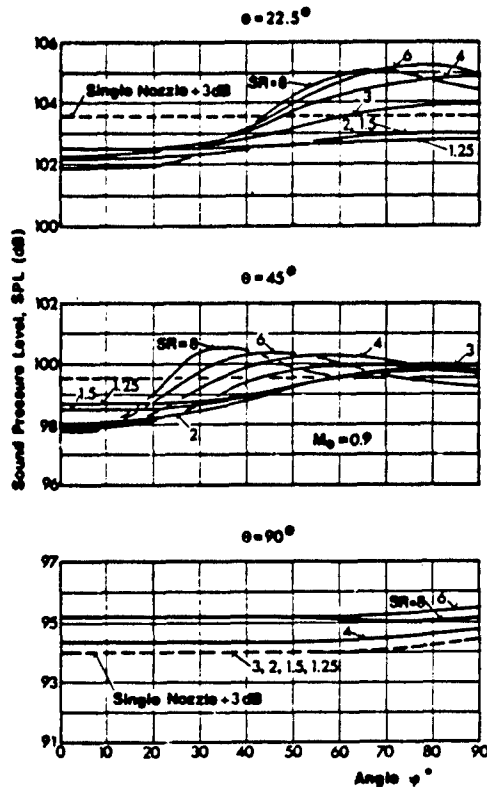
Figure 5: Directivity of 2-nozzle array as function of spacing ratio, SR

larger SR also noise amplifications compared to independent jets

* in contrast, for $\theta = 90°$, the sound field is nearly equal to that of two independent jets and has a circular directivity for most SR

* for spacing ratios SR = 1.25 to 2.0 the directivity is in general nearly circular but for $\theta = 22.5°$ and partially $\theta = 45°$ less noise is radiated compared with independent jets

* for large spacing ratios, SR > 4, and $\theta = 22.5°$ and 45° the peak of the directivity with noise levels larger than those of independent jets rotates from $\psi = 90°$ to $\psi < 90°$.

The sideline noise reduction of Figure 5 for angles $\psi \approx 0$ and $\theta = 22.5°$ and 45° is about 1.5 dB for all spacing ratios SR > 2, indicating that only a portion of the noise of the adjacent jets is shielded. For small spacing ratios the shielding effect slightly decreases which may be a result of the mixing of the jets. At $\theta = 22.5°$ the measured sideline noise reduction is relatively uniform and occurs between $\psi = 0$ and 30°. At $\theta = 45°$ the range of ψ associated with this reduction tends to decrease with increasing SR, which is related with the rather evident rotation of the peak of the directivity for this emission angle. Another interesting feature of Figure 5 is that the noise radiated at $\theta = 22.5°$ and $\psi = 90°$ depends strongly on .R in the range 2 < SR < 4. For SR < 2 this noise is

approximately constant and similar as for $\psi = 0$ less intense than that of independent jets.

Effect of nozzle number N. This effect was studied by keeping the spacing ratio SR approximately constant and varying the nozzle number N between N = 1 and 5. For N = 2, 3 and 4 the spacing ratio was SR = 2, and for N = 5, SR = 2.25. Selected results of these measurements are summarized in Figure 6. The results in this figure have been adjusted by the constant $-C = -10 \log (N)$, so that a comparison with N independent jets is possible.

It follows from these results that for $\theta = 22.5°$ and 45° increasing the nozzle number significantly decreases the sideline noise radiated at small angles ψ but that this does practically not change the noise radiated at these angles θ at large angles ψ compared with independent jets. For $\theta = 90°$ the measured radiated sound fields shown in Figure 6 are nearly equal to those of independent or incoherent jets similar as observed before.

The sideline noise reduction reflected by Figure 6 decreases nearly linearly with the nozzle number N. For both $\theta = 22.5°$ and 45° this reduction is about 1.5 dB for N = 2, and assumes a value of about 4 dB for N = 5. Based on the previous results it may be expected that similar reductions occur for spacing ratios SR > 2.

θ = 22.5°

θ = 45°

SPL – 10 log N, (dB)

$M_0 = 0.9$
SR = 2.0 (2.25)

θ = 90°

Angle ψ°
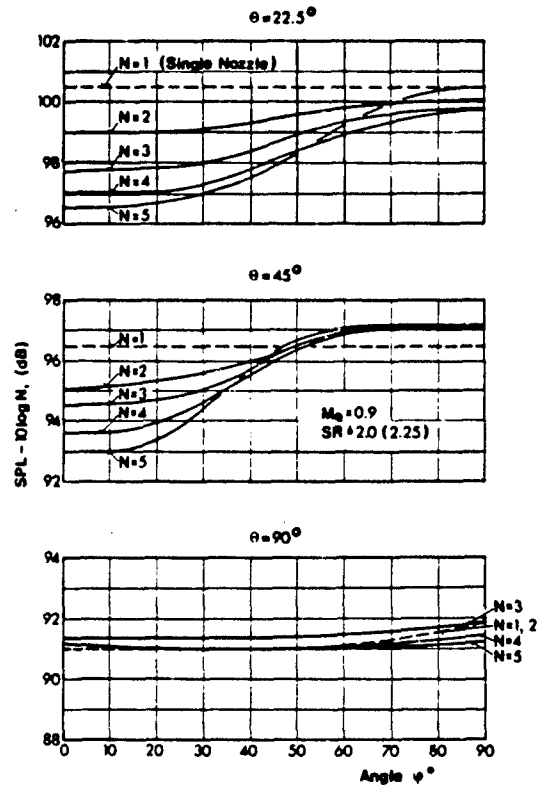
Figure 6: Directivity of nozzle arrays as function of nozzle number, N

1/3 octave SPL-spectra. The selected 1/3 octave
SPL-spectra in Figure 7 indicate that the sideline
noise reduction is exclusively due to a reduction
in the high frequency range of the noise spectra.
For $\Theta = 22.5°$, this range includes frequencies a-
bove 2.5 kHz corresponding to wavelengths $\lambda/D < 6.5$,
and for $\Theta = 45°$, frequencies above 5 kHz correspon-
ding to $\lambda/D < 3.2$. The reductions in these fre-
quency ranges are nearly constant and of the order
of 2.5 to 6 dB, depending on the nozzle number N.

Figure 8: Sound power reduction of linear nozzle
arrays

Figure 7: Sideline noise spectra of linear nozzle
arrays

Figure 9: Sound power spectrum of 4-nozzle array

1 and 10 kHz. The maximum reduction takes place
around the peak of the noise spectrum located for
all nozzles at about 2.5 kHz.

2.2.3 Hot film measurements

Some of the measured turbulence intensity data are
reproduced in Figure 10 showing the maximum turbu-
lence intensity midway between the jets, I_M, as
function of the downstream location X/D. I_M is re-
ferred in Figure 10 to the maximum turbulence in-
tensities, I_{max}, in the outer mixing region of the
adjacent jets, which were found to be equal to that
of the single reference nozzle.

2.2.2 Sound power measurements

The results of the sound power measurements are
summarized in Figure 8 showing the sound power re-
duction ΔPWL_N of the different nozzle arrays com-
pared with independent jets as a function of the
spacing ratio SR.

The data of Figure 8 suggest that the sound power
of the adjacent jets approaches the values of in-
dependent jets around SR = 4. In the direction of
smaller spacing ratios the sound power decreases
continuously until about SR = 2 and then remains
approximately constant. The maximum sound power
reduction for SR = 2.0 is about 1 to 1.5 dB depen-
ding in the nozzle number. It may be noted that
the sound power of the 2-nozzle array shows the
same dependence on the spacing ratio SR as the
noise radiated by this nozzle at $\Theta = 22.5°$ and
$\psi > 60°$ (compare Figures 5 and 7). Therefore, the
corresponding noise reductions may be expected to
be strongly related.

Figure 9 shows typical sound power spectra mea-
sured during the experiments. These results, as
well as several others, show that the total sound
power reduction of the interfering jets compared
with independent jets is due to a reduction within
the medium-to-high frequency range, between about

Figure 10: Turbulence intensity ratio, I_M/I_{max}, in
common mixing zone of 2-nozzle array

The results of Figure 10 show that the interference of the adjacent jets, depending on SR and X/D, reduces the turbulence intensity in the common mixing zone. For large spacing ratios the turbulence intensity is comparatively little reduced, but it decreases significantly when SR approaches values SR < 2. For SR between SR = 1.25 and 1.5, I_M is for most test locations about 20 to 30 percent smaller than I_{max}.

2.2.4 Results of shadowgraphs

The shadowgraphs were taken of the 2-nozzle array jets with SR = 1.25, 1.5, and 1.75 at an exhaust Mach number of M_e = 0.9. Some of the shadowgraphs are reproduced in Reference [7]. For the small spacing ratio SR = 1.25 an intense mixing was indicated by the shadowgraphs with large turbulence structures passing from one jet to the other. The mixing occured at downstream locations X/D = 4 to 6 corresponding to the region where the turbulence intensity, I_M, is maximally reduced.

In the shadowgraphs for SR = 1.5 the jets appeared to be separated by a wavy layer. In addition, in several photographs longish large-scale structures could be observed in the adjacent mixing regions which were in general spaced out of phase, suggesting a mutual interference between these structures. It is possible that these regular interactions are related with so-called orderly structures in the turbulence, although the shadowgraphs failed to clearly show these structures.

2.3 Examination of Acoustic Results

2.3.1 General far field characteristics

For larger spacing ratios, SR, the rotational asymmetry of the sound field of the nozzle arrays appears to be due to reflections of sound waves by the adjacent jet streams rather than due to a coherent noise radiation. The jets tend to behave similar as two-dimensional shear layers, which also almost completely transmit noise at 90° but reflect this noise for smaller angles of incidence, especially if total reflection occurs.

Since only wavelengths small compared to the size of the jets may be expected to be appreciably reflected by the jet flow, there should be a certain wavelength, say λ_c, above which noise is radiated independent of the adjacent jets. The measured 1/3 octave spectra suggest that this critical wavelength is λ_c/D = 6.5 for Θ = 22.5° and λ_c/D = 3.2 for Θ = 45°, which are of the order of the jet stream dimension. The dependence of λ_c on Θ may be explained by the fact that sound rays radiated at different Θ "see" different dimensions of the adjacent jet.

2.3.2 Sideline noise reduction

The capability of a single jet to reflect or transmit incident sound waves may be expressed by a certain transmission coefficient, say α_t. Assuming incoherent noise radiation and equal jets with equal α_t's, the sideline noise reduction of a N-nozzle array compared with independent jets, say ΔSPL_{O_N}, may be easily shown to follow

$$\Delta SPL_{O_N} = -10 \log \left[\frac{1}{N} \frac{\alpha_t^N - 1}{\alpha_t - 1} \right]$$

In Figure 11 this relationship is compared with present measurement results of the high frequency noise reduction in the range 2.5 to 40 kHz, where most of the sideline shielding occurs, and of the
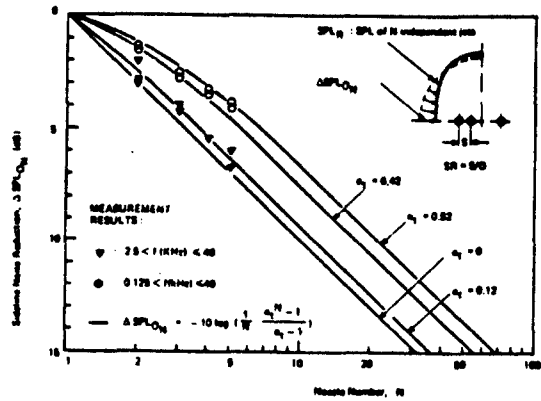
Figure 11: Sideline noise reduction of linear nozzle arrays

overall noise reduction including frequencies between 0.125 and 40 kHz, both for Θ = 22.5°. The experimental data of the high frequency noise reductions are in good agreement with the theoretical curve for α_t = 0.12 corresponding almost to ideal noise reductions. The data of the overall noise reduction correspond to larger transmission coefficients, α_t = 0.42 to 0.52, and tend to decrease somewhat less than given by the theoretical curve, because of the more or less completely transmitted low frequency noise.

2.3.3 Critical angle φ_c

If the rotational asymmetry of the sound field of the linear nozzle arrays is primarily due to reflection effects, a relationship may be expected between the geometry of the flow field and the far field noise patterns. This relation may be identified by defining a "critical angle" φ_c, see Figure 12, dividing the sound field into two regions, one above the jets which can be reached by direct
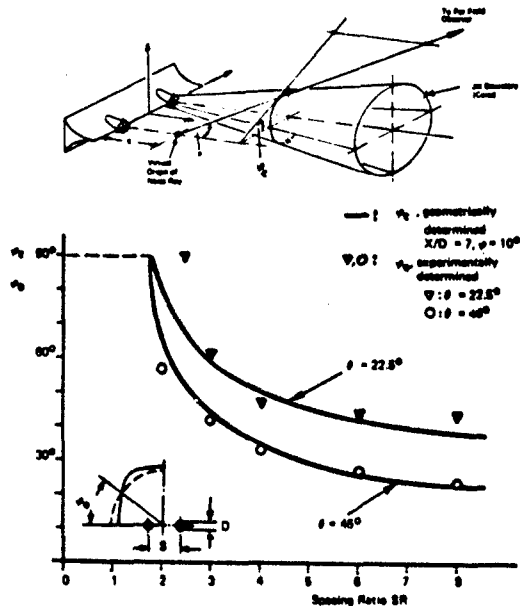
Figure 12: Comparison of critical angle φ_c with measurements

sound rays radiated from all jets, and one in side-line direction which cannot be reached by reflected rays.

Based on this definition, φ_c, may be expected to be strongly related to an angle, say φ_0, given by the condition that the sound pressure level radiated from the jets of the nozzle array is equal to that of corresponding independent jets, see Figure 12. To check whether this relation indeed exists, φ_0 was obtained from the measured directivity patterns, and φ_c was determined graphically assuming jets spreading at an angle of 10° and having a virtual noise origin located at about X/D = 7, based on the hot film measurement data and results reported by Grosche [8], respectively.

As can be seen in Figure 12 the general trend of φ_c and φ_0 agree very good. With this several of the free field noise characteristic observed and mentioned before may be explained.

2.3.4 Sound power reduction

For spacing ratios SR ≥ 2.0 the measured sound power reductions where found to follow approximately the simple relationship

$$\Delta PWL_N = -10 \log \left[1 - \frac{N-1}{N} \cdot \frac{\Delta V}{V} \right]$$

(V = noise generating volume of single jet, ΔV = noise generating volume of common mixing zone), which assumes, as often done, that the sound power is proportional to the jet volume where most of the noise is generated and that each common mixing zone reduces the sound power by the same amount. For a reasonable jet extension of 20 diameter downstream of the nozzle exit and a jet spreading angle of 6° corresponding results for N = 2 and 4 are shown in Figure 8, which are in good agreement with the test data. For SR < 2.0 this relationship tends to overpredict the sound power reduction suggesting that for these smaller spacing ratios other mechanisms are involved, as may be expected.

3. FLOW AND NOISE DATA OF INVERTED PROFILE JETS

A further interesting measure for jet noise reduction is the application of inverted profile jets. During the last years, a number of investigations showed that jets of this kind may lead to remarkable noise reductions compared to normal coaxial jets as produced by typical two-cycle jet engines.

For jets with inverted profiles the high-speed hot turbine exhaust flow covers the outer jet area where normally the low-speed cold fan bypass jet is produced and the cold fan jet occupies the inner jet area where by conventional profile jets the hot turbine jet is generated.

Because of the relocation of the high-speed jet to the outer circumferential region of the overall jet flow, the radial dimension of the high-speed jet is always much smaller as a corresponding inner diameter of a conventional profil jet would be by equal exhaust area and mass flow rate. Based on this, a significantly enhanced mixing of inverted profile jets and consequently also largly reduced noise levels of these jets may be expected. In addition, primarily because of the enhanced mixing, these jet configurations may be also very well suited for implementation into ejector flow systems with possibly even more jet noise reduction.

In order to obtain more detailed information on these interesting features of inverted profile jets, an extensive experimental and theoretical study was performed on these jet configurations, covering both systematic flow and noise measurements as well as jet flow calculations. In the following selected results of these topics are presented and discussed. More detailed description of the performed study is given in Reference [9].

3.1 Test Set-Up and Measurement Techniques

The test set-up used in the measurements for generating different coaxial jets with inverted and conventional profiles consisted in principle of two coaxial tubes which could be provided alternatively with hot or cold air. At the end of the tubes a coaxial pair of nozzles was installed which can be seen in Figure 13. The inner nozzle of this pair was exchangeable for variation of the nozzle area ratio AR = A_a/A_i (A_a = area of outer jet ring, A_i = area of inner jet) and had a wall thickness of 0.5 mm. Area ratios of AR = 2.00, 0.94 and 0.48 could be realised. For adjustments of velocities and temperatures the test set-up was equipped with pressure and temperature probes. Velocity and turbulence profiles of the coaxial jets were measured by pitot tubes, hot-film probes and by laser-doppler-anemometry. The temperature profiles of the jets were measured by thermo-elements.

D$_i$ variable: ϕ 17, 21, 24 mm
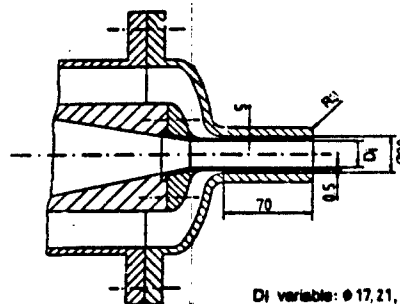
Figure 13: Design of coaxial nozzles used for experiments

The acoustic measurements included far field test which were performed in an anechoic chamber with a rotating 1/4 inch microphone mounted far away from the source. The acoustic data evaluation included narrow band spectra and directivity patterns. A more detailed description of the test set-ups and the measurement techniques is given in Reference [9].

3.2 Results of Flow Investigations

3.2.1 Jet flow geometry

The flow geometry of a typical coaxial jet is shown in Figure 14. In general, this geometry can be devided as indicated in this figure in the following three regions:

Region 1: From the nozzle exit to the end of the outer potential core. This region can be further divided into the inner and outer mixing zone.

Region 2: From the end of the outer potential core to the end of the inner potential core.

Region 3: From the end of the inner potential core further downstream. In this region the mixing zone is equal to the jet width.
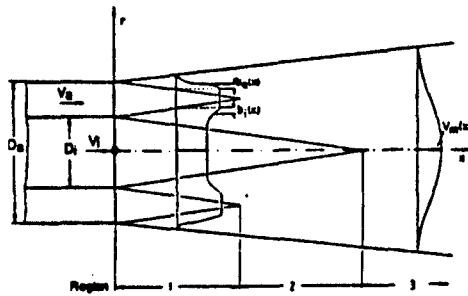
Figure 14: Geometry of the flow field of typical coaxial jets

For conventional coaxial jet the velocity ratio, V_a/V_i and the total temperature ratio, T_{Oa}/T_{Oi}, are in general smaller than one, while for inverted profile jets generally the reverse is true, $V_a/V_i > 1$ and $T_{Oa}/T_{Oi} > 1$.

If a conventional coaxial jet is converted into an inverted profil jet by keeping the primary and secondary mass flow rates and velocities and with this the total thrust constant, the outer diameter, D_a' does in general not change, since the total flow area must also be constant. The inner diameter, however, generally increases because the bypass ratio and with this the area ratio of the initial jet are in general larger than one. In addition, for this case the area ratio, velocity ratio and temperature ratio of the inverted profile jet must be the reciprocals of the corresponding values of the conventional jet.

3.2.2 Flow Measurements

In Figure 15 two sets of measured velocity profiles are shown, one for a typical convential coaxial jet and one for a related inverted profile jet. Both jets have nearly the same maximum velocity and maximum temperature, as well as nearly reciprocal area ratios, velocity ratios and temperature ratios. Both jets, therefore, generate approximately the same thrust.

Comparing the velocity decay for the jets shown in Figure 15, it follows that for both jets the velocity reduction of the first reduced outer jet is approximately proportional to the velocity gradient. This results in a much quicker reduction of the maximum velocity for the inverted profile jet. Thus these kind of jets have in the noise important region $X/D_a < 15$ much lower velocities than the conventional profile jets and therefore should also generate significantly less noise.

Additional tests with parameter variations showed that the area ratio and velocity ratio have a great influence on the reduction of the maximum nozzle velocity in downstream direction for the inverted profile jets. A reduction of the area ratio AR and an increase of the velocity ratio V_a/V_i was found for example to accelerate the decay of the maximum velocity. The temperature of the jets was identified to have only a small effect on the reduction of the maximum nozzle exit velocity. In contrast, for conventional profile jets the effect of all these parameters was found to be rather insignificant for the considered velocity decay.
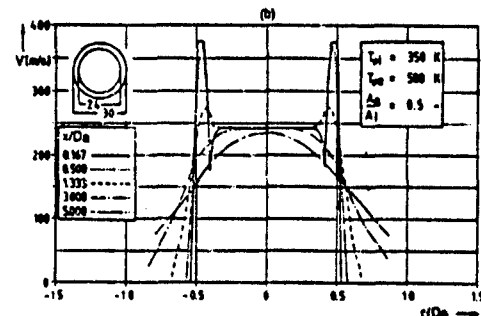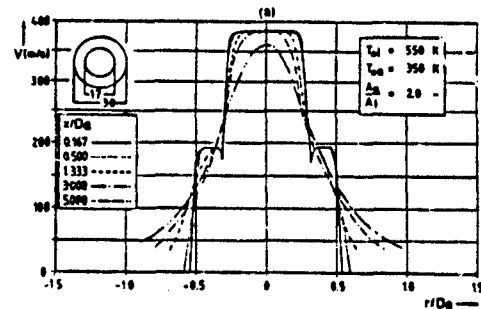
Figure 15: Comparison of measured velocity profiles of a conventional coaxial jet (a) and a related inverted profile jet (b)

Furthermore, the process of mixing of both conventional and inverted profile jets was investigated by measurements of the mean velocities and turbulent velocity fluctuations at several sections X/D_a downstream of the nozzle exit. These investigations showed, that the velocity fluctuations very near the nozzle are higher for inverted profile jets than for conventional jets, because of their higher velocity gradients in the outer shear layer. More downstream however, for $X/D_a > 1$ the velocity fluctuations for the inverted profile jets are smaller than for conventional profile jets, especially for larger distances X/D_a. This can be seen in Figure 16 showing the maximum RMS turbulent velocity fluctuations of several different jet configurations tested.
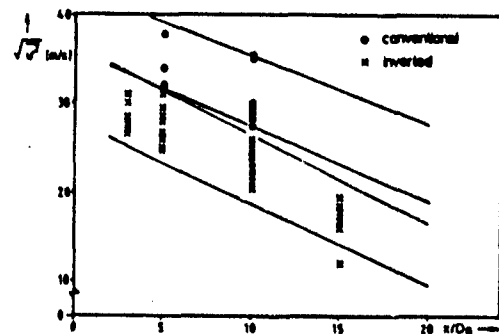
Figure 16: Maximum RMS turbulent velocity fluctuations of several tested conventional and inverted profile jets

3.2.3 Flow calculations

In addition to the flow measurements extensive calculations were performed, in particular to predict the decay of the velocity profiles in downstream direction of the considered jets. The calculation codes were based on simplified equations of conservation of mass, momentum and energy which were solved by applying alternatively the following three different turbulence-models

* mixing length hypothesis after Prandtl [10]
* simplified mixing length hypothesis after Prandtl [11]
* two-equation model after Jones and Launder [12]

The results of these calculations show good agreement with the test data, especially if the wake due to the wall thickness of the inner nozzle is implemented in the starting velocity profile. As an example, Figure 17 shows the comparison between measurements and calculations of the decay of the maximum velocity for an inverted profile jet with an area ratio of AR = 0.5. The calculated results shown were obtained using two different computer program versions, the program FLODH considering the wake mentioned above and the program FLOH not considering this wake. For both programs the simplified mixing length hypothesis after Prandtl [11] was applied.
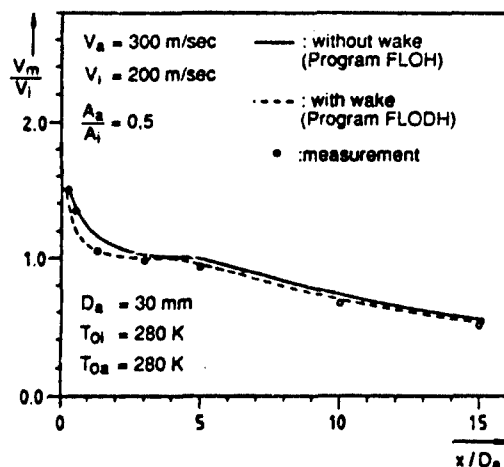
Figure 17: Calculated velocity decay in comparison with measurement data

3.3 Results of Acoustic Measurements

3.3.1 General results

The acoustic measurements provided a large number of interesting general results. The sound levels of conventional coaxial jets were found to depend mainly on the maximum nozzle exit velocity and only relatively little on the exit velocity profile. However, using inverted profiles, noise reductions of up to 11 dB were identified compared to conventional jets with the same nozzle exit velocity and thrust, which would be of great advantage in practical applications.

A variation of the nozzle area ratio A_a/A_i and velocity ratio V_a/V_i was found to have only a small influence on the noise of conventional profile jets

but a great influence for inverted profile jets. A reduction of A_a/A_i and an increase of V_a/V_i led, for example, to a significantly reduced noise emission, because of the much quicker decay of the maximum velocity as identified in the flow investigation discussed before.

3.3.2 Localization of sound sources

The localization of the sound sources of the considered jets was carried out with the correlation technique after Evertz [13]. For the present investigation the source localization was made for the frequency range of maximum spectral level and a radiation angle of $\Theta = 25°$ (angle between jet axis and position of microphone). For a conventional profile jet a rather peaked and limited main source region was found at about $X/D_a = 7$ to 10 downstream of the nozzle exit. The source region of inverted profile jets was identified to be not that peaked and limited. Following the test data it ranges from $X/D_a = 3$ to 10 downstream of the nozzle exit with a flat maximum at about $X/D_a = 8$.

3.3.3 Narrow band noise spectra

Narrow band noise spectra of conventional and inverted coaxial jets were recorded in the frequency range between 50 Hz and 20 kHz for different radiation angles Θ. Figure 18 shows the spectra for the two jet configurations of which flow data are given in Figure 15. For this example the general behavior shall be discussed. Both jets produce broadband noise with flat spectrum maxima. The shape of the spectra can be explained as being formed by the superposition of noise from 'disordered' turbulence and noise of the periodic vortices in the shear layers. The frequencies of the maximum spectrum levels are lower for the inverted profile jet than for the conventional jet. For these results, the maximum level for the inverted jet is at about 2 kHz and for the conventional jet at about 4 kHz.

In the direction of lower frequencies the spectrum levels decrease rapidly. The noise sources generating these levels can be found downstream of the source location of maximum noise radiation. The source locations for the higher frequency noise levels of the spectra are located at smaller distances from the nozzle exit, because of turbulent velocity fluctuations of higher frequencies at these locations. As mentioned before, the velocity fluctuations in this area are higher but the source area is small, because of the thin shear layers in the initial region of the jet. Thus the levels at higher frequencies are lower.

In addition, Figure 18 shows that the levels of the inverted profile jet are lower especially in the frequency range with maximum levels. Towards higher frequencies the difference between the two jets becomes smaller and for radiation angles of $\Theta = 120°$ the levels of the inverted profile jets are even higher. This is due to the observed higher velocity fluctuations of inverted profile jets near the nozzle exit, but has only a very small effect on the overall total noise radiation.

3.3.4 Directivity pattern

Figure 19 shows the comparison of the directivity pattern for the two coaxial jets of which flow data and noise spectra are given in Figures 15 and 18, respectively. As noted before, both jets produce about the same nozzle exit thrust.

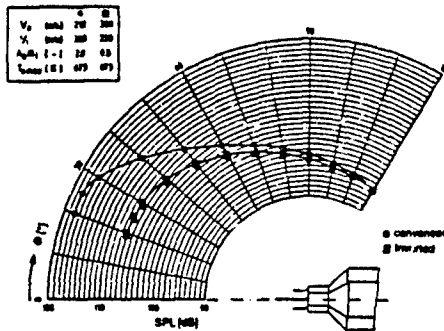As follows from Figure 19, the maximum levels of both jet configurations are radiated between angles

Figure 19: Comparison of directivity pattern of a conventional and a inverted profile jet

Figure 20: Comparison of fly-over noise characteristics of a conventional and a inverted profile jet
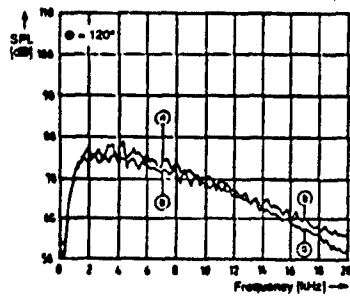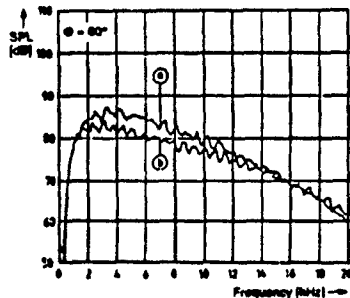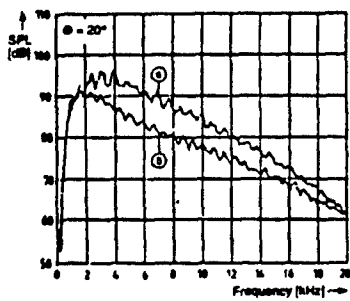
Figure 18: Comparison of narrow band noise spectra of a conventional and a inverted profile jet

of $\theta = 20°$ to 25°. However, for the inverted profile jet a remarkable noise reduction of about 11 dB can be seen at these angles. For higher angles the level difference between both kinds of jets decreases as could be expected based on the noise spectra shown before.

3.3.5 Fly-over noise characteristics

Figure 20 shows a comparison of the fly-over noise characteristics of the different profile jets is considered before, which were derived from the directivity pattern shown in Figure 19. It follows from these result that when the aircraft approaches the observer the noise levels for both jet configurations are nearly the same. For the fly-over point,

the noise of the inverted profile jet is about 1.5 dB quieter than the noise of the conventional profile jet. When the aircraft leaves the observer, however, the levels strongly diverge. The maximum noise for the inverted profile jet is reached earlier and is about 9.5 dB lower than that of the conventional profiled jet.

To get information of real engines, the measured spectra can be scaled down with the Strouhal number. If these scaled spectra are being A-weighted, additional 4 to 5 dB noise reduction can be expected. Based on this, fly-over jet noise reductions of more than 13 dB(A) appear possible using the inverted profile method.

4. SELECTED RESULTS OF SPECIAL SHAPE MIXING NOZZLES AND COAXIAL BYPASS JETS

In addition to the studies reported in the previous sections, a large variety of experimental and theoretical investigations was performed on special shape mixing nozzles and typical coaxial bypass jets. The goal of these investigations was in particular the development of effective jet noise reductions measures for VSTOL transport aircraft such as the Dornier Do 31, as this was identified to be one of the most important factors for the in-service operation of this type of aircraft [14]. Also, with these studies a supporting data base should be established for jet noise control of future combat and/or other jet aircraft.

As generally known, due to special shaping of the nozzle exit geometry the turbulent mixing with the ambient air and the corresponding turbulence intensities of the free jet may significantly change.

Based on this also changes in the radiated noise spectra may be expected, which as often previously observed can be related with interesting noise reductions. In addition, coaxial bypass nozzles have a high jet noise reduction potential as the maximum exhaust velocity may be reduced by increasing the related bypass ratio for keeping the nozzle thrust constant. For the performed investigations the establishment of more detail information on these subjects was one of the main objectives.

The experimental part of the conducted investigations included the design and provision of a relatively big test set-up within the Dornier large acoustically treated test room for hot gas and cold air nozzle testing. The test set-up permitted noise directivity as well as flow and even thrust measurements. A large number of different special shape mixing nozzles and a variable bypass flow coaxial nozzle was manufactured and in detail tested. The theoretical part of the investigation covered the development and application of extensive jet noise prediction software suitable for different nozzle configurations and noise contour calculations. Also various smaller jet noise theories were developed and tested.

In the present paper selected interesting test results of the measurements on different special mixing nozzles and on the coaxial bypass nozzle are reported. Further information including a detail description of the test set-up used is reported, for example, in References [15, 16, 17].

4.1 Special Shape Mixing Nozzles

4.1.1 Selected nozzle configurations and test cases

The special shape mixing nozzles of which acoustic test data are reported are summarized in Figure 21 and are denoted by No. 3.3, 3.6 and 4. Also shown is a circular nozzle with center body denoted by No. 2, which was used as reference nozzle in the experiments. The exhaust area of the different nozzles is denoted by A_e, and D_0 is the diameter corresponding to this area. As can be seen, all nozzles have about the same exhaust area ranging only from 72 to 81 cm^2 and corresponding to approximately $D_0 = 10$ cm.

In addition, Table 1 summarizes the total exit temperature, T_{Oe}, the maximum exhaust velocity, $V_{e\,max}$, and the corrected nozzle thrust, T_N, of the nozzles and test cases selected for this paper. It follows that only hot gas tests with approximately $T_{Oe} = 773$ K are considered and that for all cases $V_{e\,max}$ and T_N are nearly equal.

4.1.2 Measured directivity patterns

Figure 22 shows as an example the measured overall sound pressure level directivity patterns of the special shape mixing nozzles and the circular reference nozzle as summarized in Figure 21 and Table 1. It follows from these data that for radiation angles $\theta \geq 60°$ the overall noise level of the mixing nozzles is about the same as that of the circular reference case. In the direction of about $\theta = 30°$, however, the noise level of the 3/6-spoke nozzle is about 7 dB less intense compared to the reference nozzle.

The next good nozzle is the 9-lobe nozzle with also about 7 dB noise reduction at $\theta = 30°$ but with no noise reduction at about $\theta = 45°$ compared to the reference case. The circular multiple nozzle shows around $\theta = 30°$ and 45° also no significant improvement with respect to the reference nozzle.
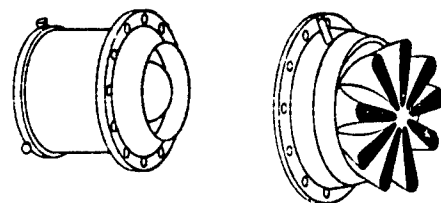
No. 2 (●)
$D_0 = 98$ mm
$A_e = 75.5\ cm^2$

No. 4 (✳)
$D_0 = 101.4$ mm
$A_e = 81.0\ cm^2$
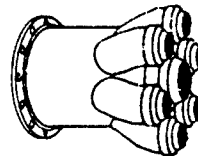
No. 3.3 (◌)
$D_0 = 98.8$ mm
$A_e = 76.8\ cm^2$
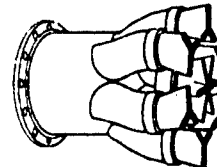
No. 3.6 (◌)
$D_0 = 95.5$ mm
$A_e = 71.9\ cm^2$

Figure 21: Special shape mixing nozzles (No. 4, 3.3 and 3.6) and circular nozzle (No. 2) used for experiments

Nozzle No.	Nozzle Type	D_0 [cm]	A_e [cm^2]	T_{Oe} [K]	$V_{e\,max}$ [m/s]	T_N [kp]
2	circular with center body	9.80	75.5	773	468	94
3.3	circular multiple nozzle	9.88	76.8		470	92
3.6	3/6-spoke multiple nozzle	9.55	71.9		470	94
4	9-lobe nozzle	10.14	81.0		467	94

Table 1: Test values of special shape mixing nozzles

Since the maximum noise levels of the different nozzles are radiated for each case in the range $\theta = 15°$ to 60°, the observed noise reductions in the directivity pattern may be expected to correspond to similar reductions in the sound power radiated by these nozzles.

4.1.3 Measured 1/3 octave SPL-spectra

More interesting than the overall noise reductions of the different nozzle configurations shown in Figure 22 are the shifts in the related 1/3 octave sound pressure level spectra as presented in Figure 23. Especially the 6/9-spoke multiple nozzle and the 9-lobe nozzle show for $\theta = 30°$ and 45° noise maxima at frequencies around 8 kHz compared to the reference nozzle noise level peak located around 1.25 kHz. For $\theta = 60°$ the noise levels of these two mixing nozzles peak also around 8 kHz but the peak of the noise of the reference nozzle is very broad and ranges from 1 kHz to 8 kHz. The noise spectrum of the circular multiple nozzle is above 5 kHz for all θ approximately equal to those of the other two mixing nozzles. At lower frequencies, however, this nozzle radiates significantly more noise than the other two.

Ve_{max} = 468 to 487 m/s
Toe = 773 K
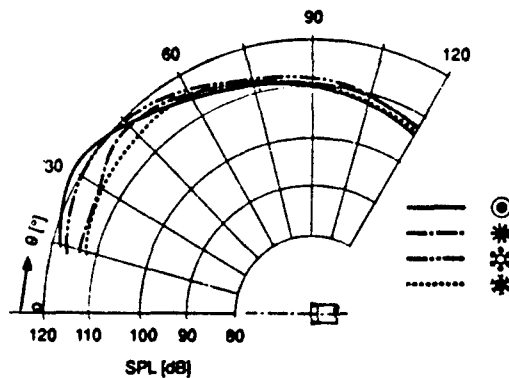A_e = 72 to 81 cm²
T_N = 82 to 84 kp

Figure 22: Comparison of directivity patterns of special shape mixing nozzles and circular nozzle

The shift of the spectrum maxima of the mixing nozzles to higher frequencies is due to the smaller sectional dimensions of these nozzles producing a larger number of smaller vortices generating more high frequency instead of low frequency noise. This may have an additional positive effect on the noise reduction, since higher frequencies are in general always more absorbed by atmospheric absorption than lower frequencies although this absorption depends strongly on the air humidity and temperature.

4.2 Coaxial Bypass Nozzles

4.2.1 Nozzle configuration and test conditions

The coaxial bypass nozzle used in these experiments and a section of the related test set-up are shown in Figure 24. The inner diameter of this nozzle was constant, D_i = 5.6 cm, while the outer diameter could be changed to have values of D_a = 13.5, 15.5, 18.0, 22.5 and about 24 cm.

The test flow conditions of the different nozzle configurations during the acoustic measurements are summarized in Table 2. As may be seen, the inner nozzle area A_i, the densities ρ_i and ρ_a (i = inner jet, a = outer jet), and for the tests No. II, III, IV the bypass ratio $\mu = \dot{m}_i/\dot{m}_a$ were kept constant during the measurement, while the nozzle exhaust velocities V_i and V_a as well as the outer exhaust area A_a were varied.

4.2.2 Determined sound power results

The acoustic measurements performed on the different nozzle configurations included overall sound pressure level directivity measurements similar as for the special shape mixing nozzles, from which sound power values were determined considering the important radiation angle range $11° < \theta < 139°$. The results of this evaluation are plotted in Figure 25 versus the nozzle thrust, T_N, which was estimated based on the velocity and mass flow rate data given in Table 2.
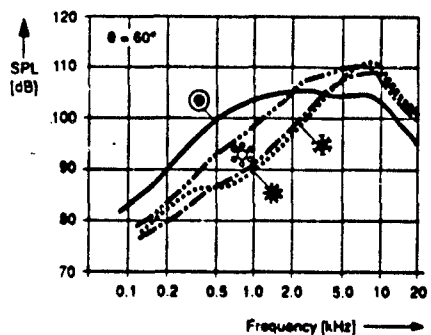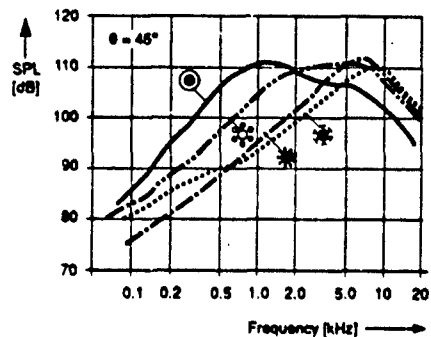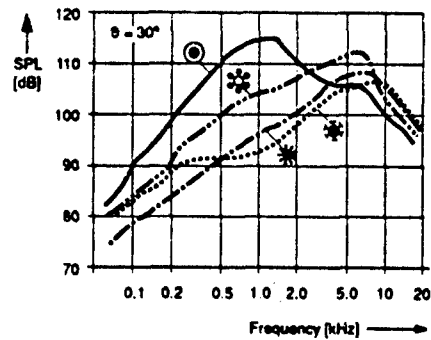
Ve_{max} = 468 to 487 m/s
Toe = 773 °K
A_e = 72 to 81 cm²
T_e = 82 to 84 kp
(see table 1)

Figure 23: Comparison of 1/3 octave noise spectra of special shape mixing nozzles and circular nozzle

Figure 25 confirms, for example, that a significant thrust increase may be obtained with no large change in the radiated sound power by only increasing the bypass flow area A_a but leaving the velocities V_i and V_a approximately equal (see tests No. II, VI, VII, case①). In addition it follows, as expected, that a large noise reduction can be obtained by nearly equal thrust if the inner jet velocity, V_i, is reduced and the resulting lack of thrust is compensated by increasing the outer jet velocity, V_a (see tests No. I, V, case②). As already mentioned in Section 3, this indicates again
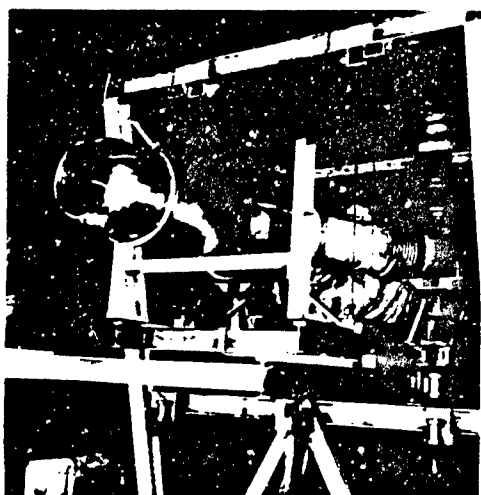
Figure 24: Test setup of coaxial bypass nozzles (D_i = 5.6 cm)

Test No	V_i (m/s)	ρ_i (kg/m³)	A_i (cm²)	V_a (m/s)	ρ_a (kg/m³)	A_a (m²)10^{-4}	$\dot{m}_i$ (kg/s)	$\dot{m}_a$ (kg/s)	$\mu = \dot{m}_i/\dot{m}_a$
I	507.7	0.5	24.6	142.8	1.06	118.5	0.625	1.795	2.87
II	491.6	0.5		150.6	1.13	229.9	0.605	3.91	6.46
III	492.9	0.5		96.4	1.11	373.4	0.606	3.995	6.69
IV	427.5	0.46		170.8	1.15	164.4	0.485	3.23	6.66
V	359.1	0.47		186	1.08	118.5	0.415	2.405	5.8
VI	490.6	0.5		149	1.1	373.4	0.604	6.11	10.1
VII	490.6	0.5		149	1.1	420	0.604	6.86	11.4

Table 2: Test values of coaxial bypass nozzles
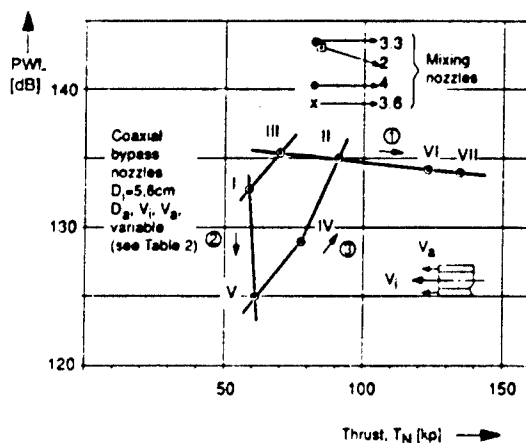
Figure 25: Sound power of coaxial bypass nozzles and special shape mixing nozzles versus thrust, T_N

that the most important noise parameter of this nozzle type is the relatively high inner jet velocity V_i and not so much the outer nozzle values A_a and V_a. The data of tests No. V, IV and II in Figure 25 (see case ③) demonstrate this further although in this case V_a decreases and A_a largely increases.

In addition, Figure 25 shows the sound power levels of the special shape mixing nozzles and circular reference nozzles summarized in Figure 21, which were determined similarly as described above. The levels of these nozzles are up to about 10 dB higher than those of the coaxial bypass nozzles by about equal thrust, indicating for the bypass nozzles a clear acoustical advantage. However, since these test have been performed in different test campagnes at quite different times, this result has to be taken with certain precaution.

5. DATA ON SPECIAL ACOUSTIC ABSORBERS FOR ENGINE AND EJECTOR ACOUSTIC LINERS

The use of acoustic liners is of particular interest for engine inlet and engine bypass exhaust sections for reducing intense fan noise components, if these noticeably effect the aircraft overall noise. In addition, high temperature resistive liner designs may be implemented into the primary exhaust nozzle for combustion noise and turbine noise reduction. Also, acoustic liners are needed for treatments of the inner surface of ejector flow systems for reduction of the intense jet mixing noise underneath the ejector shroud.

Because of this broad range of application and the special need for military aircraft engine noise reductions, a large number of investigations of the acoustic and structural properties of a variety of conventional flow resistive type of acoustic absorbers was carried out. Two selected reports partially documenting this work are given in the list of References [18, 19]. Based on these investigations and further publications [20], an extensive theoretical and experimental work program on special acoustic absorbers applicable for aircraft acoustic liners was set-up and conducted. As an example, References [21, 22] name for information two reports related to this program.

A main feature of the considered special acoustic absorbers, which may be termed also special Helmholtz type absorbers, is their capability to extend the absorption properties of acoustic liners into the important low frequency range and with this requiring only about 1/3 of the height of resistive resonator type absorbers (conventional absorbers), which is important for aircraft application. The special absorbers consist of a conical or exponential horn covered by a resistive permeable sheet and surrounded by a closed supporting cell. The volume of the horn and the surrounding cell are coupled by a slot of certain size in the horn neck. Due to this coupling an absorption peak could be achieved at much lower frequencies than predictable for comparable conventional absorbers based on the generally used quarter wavelength rule. In addition a high frequency absorption peak exists, which may be related to the effect of the resistive permeable sheet and the covered horn volume. Therefore, in combination with conventional absorbers a relatively broadband absorption may be established, which is also of great practical importance.

In the following, selected test results on these special absorber studies are presented including normal incidence absorption data of only special acoustic absorbers and data obtained for an Alpha

Jet engine inlet treated with these absorbers in combination with conventional ones. The result were taken from References [21, 22] mentioned already before. Further details can be found in these reports.

5.1 Normal Incidence Absorption Data

Two sets of measured normal incidence absorption data of only special absorbers are shown in Figures 26 and 27. The absorbers are denoted in these figures and in the following by Kx/y and Ex/y where K and E indicate absorbers with a conical or exponential horn, and x and y stand for the dimensionless contraction ratios of these horns and the horn slot heigh in mm, respectively. In addition, in Figure 27 the term WRA is used for conventional resistive resonator type absorbers.

Figure 26 presents data of conical horn absorbers K 5/2 with different support cell volumes and support cell cross-sectional shapes. From these data the characteristic feature of the special acoustic absorbers, can be identified, having two absorption maxima, one in the relatively low and one in the higher frequency range. In addition, it follows that the frequency of the low frequency absorption peak may be strongly effected by the total absorber volume as may be expected. Changing for example the volume from 16.5 cm^3 to 24.4 cm^3, this frequency shifts from about 1.0 kHz to approximately 0.75 kHz.

In Figure 27 the frequency ranges with absorption values of $\geq$ 80 % are given for several special acoustic absorbers with an exponential horn with contraction ratios of 2, 3, 4 and 5 (see E 2 to E 5) and an absorber with a conical horn with contraction ratio 5 (see K 5). For all absorbers, data are presented for slot heights of 1, 2, 3, 4 and 5 mm as indicated. In addition one result for a conventional resistive resonator type absorber is given (see WRA).

From Figure 27 follows that the frequency of especially the low frequency absorption is strongly influenced by the horn contraction ratio and the horn slot height. In addition, the result for the conventional absorber indicates that the gap between the two absorption peaks can be filled by conventional absorber designs. Thus, for the optimum low frequency absorber E 5/1, a frequency range with optimum absorption values ranging from as much as 0.63 to 6.3 kHz appear to be possible in practical applications.

5.2 Results of Alpha Jet Inlet Tests

For obtaining first practical results on the special acoustic absorbers, two 1:1 scale Alpha Jet engine inlet section models were build, one without and one with acoustic liners consisting of 50 % special acoustic absorbers and of 50 % conventional absorbers. As partially shown by Figure 28, the inlet sections were later mounted into the test window separating the Dornier reverberation chamber and anechoic room and were then acoustically excited with a typical engine noise spectra at the engine side located in the reverberation chamber.

The results of these tests, the noise radiated from the test model inlet sides, are presented in Figure 29. The data indicate noise reductions up to about 25 dB and confirm the remarkable broadband noise reduction capability of the special acoustic absorbers investigated. For future applications, therefore, also those absorbers should be considered.
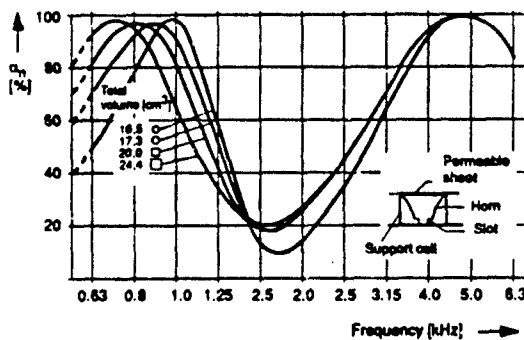
Figure 26: Normal incidence absorption of conical horn type absorbers K5/2 in four different support cells
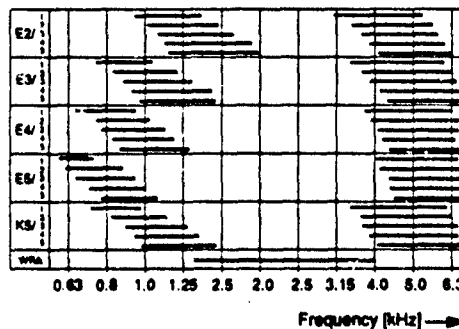
Figure 27: Frequency range of normal incidence absorption $\alpha_n \geq$ 80° of different special absorber samples (E 2/1 to K 5/5) and a conventional resistive resonator type absorber (WRA)

Figure 28: Test set-up with acoustically treated Alpha Jet inlet
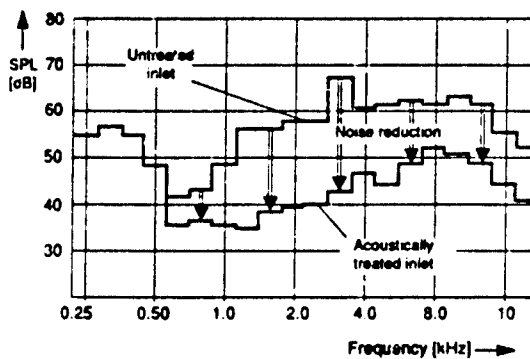
Figure 29: Measured noise reduction of Alpha Jet inlet with special acoustic absorber treatment

6. INITIAL THEORETICAL AND EXPERIMENTAL RESULTS ON EJECTOR FLOW SYSTEMS

As already mentioned in Section 1, a very attractive mean for the reduction of jet exhaust noise seems to be the use of ejector systems, which have also a great potential of increasing the static thrust compared to normal jet engine nozzles.

In principle an ejector system consists of the aircraft jet engine and a shroud placed around and downstream from the engine exhaust exit. Because of the ejector effect, a flow of secondary ambient air, $\dot{m}_s$, is entrained into the shroud and mixes there with the primary jet flow, $\dot{m}_p$. The result is an augmented airflow, $\dot{m}_p + \dot{m}_s$, exhausting from the downstream end of the shroud with a velocity, which may be quite smaller than that of the primary high-speed engine jet. Based on Lighthill's V^8-Law, therefore, this jet flow may be expected to produce significantly less noise than the primary jet without ejector shroud. In addition, if friction losses are kept small within the shroud and shroud inlet, the effect of the augmented flow is also to enhance the static thrust of the initially unshrouded jet.

The relatively quiet external ejector jet is the most important acoustic feature of ejector systems. In addition, it can be expected that the internal ejector noise, generated underneath the shroud by the intense mixing of the primary and secondary ejector flows, is also less intense than the noise of corresponding unshrouded nozzles, since the primary ejector jet mixes not with air at rest or flight speed, but with the secondary airflow having always an at least somewhat higher velocity. Also, the internal ejector noise may be channeled or shielded by the ejector shroud, so that possibly only reduced levels of this noise can be radiated to the ground. Hence, if the shroud is sufficiently long so that the internal mixing process can be completed within the shroud and assuming that some noise channeling or shielding takes place, the noise of ejector systems may be expected to be greatly reduced compared to unshrouded jets.

For practical applications and if higher noise reductions are required, however, it appears to be necessary to further reduce the internal ejector noise, as it may strongly dominate the total ejector noise, at least in certain frequency bands. Since this noise is now generated underneath the shroud, this is compared to the noise reduction of

free jets no longer a very difficult problem. Similar as for fan and combustion noise control, acoustic liners may now be used attached to the inner surface of the shroud. This is another great advantage of ejector systems, which can be and certainly should be used for further noise reductions.

In addition, effective ejector systems with single circular primary jets may require rather long shrouds, probably more than 10 jet diameters long, which certainly could cause design difficulties. This problem may be also relatively easily overcome, namely by acceleration of the mixing process within the shroud. For example, to enhance this mixing, optimized multiple nozzles and/or special shape mixing nozzles may be used in the ejector design significantly reducing the required shroud length and lowering the jet noise already by itself. In addition, if a real breakthrough in combat aircraft jet noise reduction is desired and put forward with required high priority, ejector systems may be fully integrated into future aircraft designs so that longer shroud lengths could be used. If this would be the case, together with optimized ejector mixing nozzles and acoustic liners, noise reductions of the order as achieved for civil jet aircraft, say up to about 20 dB or more, appear possible at present, reflecting clearly a significant noise reduction potential of these systems not given by any other currently known jet noise suppressor design.

To explore the ejector system noise reduction potential in somewhat more detail, an initial theoretical and experimental study on these systems was performed in conjunction with the investigation on linear arrays of mixing circular jets reported in Section 2. The theoretical part of the study included one-dimensional first ejector calculations for ejectors with constant-area shrouds. For the initial experiments, ejector configurations were used consisting of the 2-nozzle array described in Section 2 and rectangular shrouds with parallel side walls and of different lengths. The test performed with these configurations covered sound power measurements using the reverberation chamber technique and mass flow recordings for static thrust estimates, besides typical pressure and temperature measurements.

In the following, selected interesting results of the performed theoretical and experimental studies are presented and outlined, after some brief explaining general remarks on this work. More detailed information can be found in References [7, 23].

6.1. Selected Ejector Models, Notations and Ejector Reference Nozzle

6.1.1 Ejector models and notations

A sketch of the ejector models and some notations used for the experimental and theoretical study, respectively, are shown in Figure 30.

For characterizing the shroud inlet geometry and mass flow rate conditions at Station 1, an area ratio, AR, and a mass flow ratio, k_m, were defined given by

$$AR = \frac{A_s}{A_p} \quad , \quad km = \frac{\dot{m}_s}{\dot{m}_p}$$

where A_s and A_p are the secondary and primary nozzle exit areas.

$D = 2.12$ cm
$H/D = 2.0$
$W/D = 4.0$
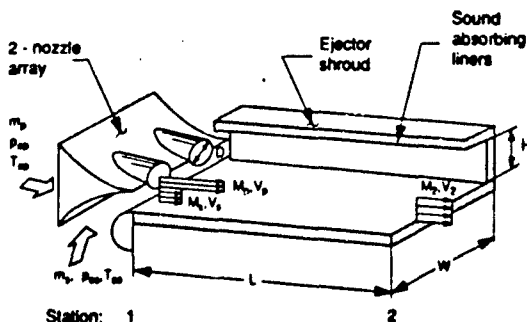$L/D = 10; 20; 30$

$AR = \dfrac{A_s}{A_p} = 4.09$

Figure 30: Ejector model with 2-nozzle array and selected notations used for experimental and theoretical study, respectively

6.1.2 Ejector reference nozzle

In order to correctly compare and judge the noise radiation and thrust performance of ejector systems a corresponding unshrouded reference nozzle need to be clearly defined.

For the present study it was assumed that the reference nozzle, if attached to the ejector jet engine, should permit operation of this engine at the same operating point. Therefore, the reference nozzle was defined as being in principle the primary ejector nozzle having the same total flow conditions $p'_{op} = p_{op}$ and $T'_{op} = T_{op}$ but also the same mass flow rate $\dot{m}'_p = \dot{m}_p$, where the primes (') denote unshrouded reference conditions. In addition the atmospheres surrounding both the reference nozzle and the ejector were assumed to be the same so that $p'_a = p_a = p_{os}$ and $T'_a = T_a = T_{os}$.

The exhaust Mach number of the selected reference nozzle, termed "reference Mach number" in the following, is thus $M'_p = f(p_a/p_{op})$ while the Mach number of the primary ejector jet is $M_p = f(p_1/p_{op})$. Since $p_1 < p_a$, because of the ejector effect, it follows that $M'_p < M_p$ and, to keep the mass flow rates, equal, that $A'_p > A_p$.

It may be noted that this definition of the selected reference nozzle is from an acoustic point of view conservative and leads to somewhat smaller noise reduction values than for a reference nozzle with equal Mach number and equal mass flow rate but reduced total pressure (equal Mach number reference nozzle). For area ratios $AR = 2$ to 12 and test data for a reference Mach number $M'_p = 0.90$, the corresponding differences were estimated to be about 4 dB to 1 dB. These values should be taken into account by interpreting the present results and/or by comparing them with other study data.

6.2 Ejector Analysis and Related Results

6.2.1 Assumptions and analysis outline

The purpose of the analysis was to first estimate the performance characteristics of ejector systems operating under static and more or less ideal conditions. Of primary interest was the jet noise reduction and thrust augmentation of these systems,

as well as the determination of optimum shroud configurations. In addition the analysis was needed to support and guide the initial experimental study and to help judging the test results.

The calculations were restricted to cold primary and secondary airflows of equal total temperatures, $T_{op} = T_{os} = T_0$, and assumed that the surrounding atmosphere and the ejectors are at rest. In addition it was assumed that the internal ejector noise is sufficiently absorbed, so that the total noise is governed only by the external ejector jet. Also, friction losses within the ejector nozzles and along the inner shroud surfaces were neglected and isentropic flows within the nozzles were assumed. At the inlet and exhaust of the ejector shroud, Sections 1 and 2, uniform velocity profiles were postulated also. Hence the shroud was assumed to be sufficiently long so that the mixing of the primary and secondary jet could take place fully within the shroud.

The noise reductions calculated for the different ejector systems correspond to sound power reductions, Δ PWL, compared to the selected unshrouded reference nozzle. Based on the assumption of uniform velocity profiles also for the reference jet and using Lighthill's V^8-Law with the same constant of proportionality for both external ejector jet and reference nozzle, it follows that

$$\Delta \text{ PWL} = 10 \log \left[\frac{A'_p}{A_p} \cdot \left(\frac{V'_p}{V_2} \right)^8 \right]$$

For describing the static thrust augmentation of the ejector systems, a static thrust ratio, TR, was defined given by

$$\text{TR} = \frac{F_2}{F'_p} = \left(1 + k_m \right) \cdot \frac{V_2}{V'_p}$$

where F_2 and F'_p are the thrust values of the external ejector jet and the reference nozzle, respectively.

6.2.2 Selected analysis results and discussion

Sound power reduction, Δ PWL. As an example, Figure 31 shows the sound power reduction Δ PWL of an ejector with a constant-area shroud versus the reference Mach number, M'_p, for constant area ratios ranging between AR = 2 and 12. At higher values of M'_p the primary ejector nozzle is choked ($M_p = 1$) and the calculations were stopped at this point, indicated in Figure 31 by the dashed line.

As can be seen, Δ PWL, depends only slightly on M'_p but varies strongly with AR. With increasing M'_p, Δ PWL decreases by about 1.0 to 2.0 dB depending on AR. This decrease corresponds to an increase in the velocity ratio V_2/V'_p with M'_p and suggests that V_s/V'_p increases somewhat faster towards larger values of M'_p.

With increasing area ratio AR, Δ PWL increases rapidly. For AR = 2, 4, 8 and 12, and reference Mach numbers around Mp = 0.90, it assumes values, for example, of about Δ PWL = 9, 14, 20 and 24 dB. It may be noted that this indicates a significant jet noise reduction potential and that these values would be even higher if another reference nozzle would have been used. For the equal Mach number reference nozzle described before, for example, corresponding noise reductions of even approximately Δ PWL = 13, 17, 22 and 25 dB would have been predicted.
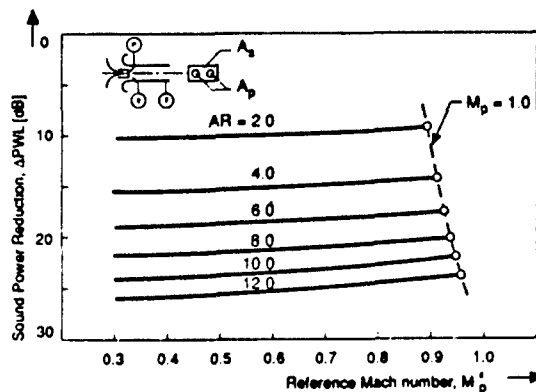
Figure 31: Predicted ejector sound power reduction, Δ PWL, versus reference Mach number, M_p'

Effect of area ratio, AR. Figure 32 is a graph showing the sound power reduction, Δ PWL, and the static thrust ratio, TR, plotted as a function of the area ratio, AR. The results correspond to the particular case $M_p' = 0.90$, which was selected for the ejector experiments.

The effort in building and integrating practical ejector systems increases more than likely with AR. The results in Figure 31 suggest an optimal area ratio around AR = 4 to 8. Based on the previously discussed results, for such ejectors sound power reductions up to about 17 to 22 dB appear possible making the ejector system to a rather attractive jet noise control measure.
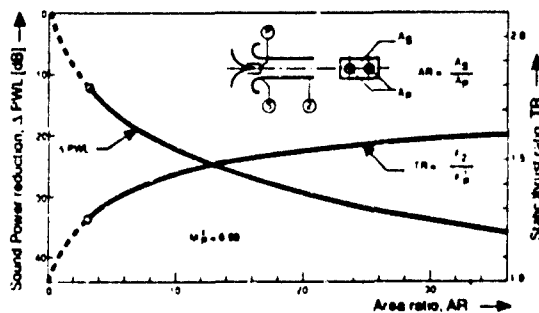
Figure 32: Predicted ejector sound power reduction, Δ PWL, and static thrust ratio, TR, versus area ratio AR ($M_p' = 0.90$)

6.3 Ejector Model Tests

6.3.1 Remarks on test set-up and test performance

The 2-nozzle array used for the model ejectors had a spacing ratio SR = S/D = 2.0 (S = distance between nozzle centers, D = diameter of single primary nozzle). With this, each primary nozzle was equally centered in one half of the inner shroud cross-sectional area and the area ratio of the ejector models was AR = 4.09

Three equal constant-area shroud sections of length ratio L/D = 10 were available, which could be connected, so that tests with shrouds of length ratios L/D = 10, 20 and 30 could be performed. The inner surfaces of all shroud sections were equipped with acoustic liners. The latter consisted of a double layer of honeycomb each covered with a resistive permeable wire cloth facing and was designed to achieve a reasonably broadband absorption. By putting suitable thin solid metal channels into the shroud sections the liners could be made completely inoperative. With this also tests on shrouds with acoustically hard inner surfaces (tests without liners) were possible.

For testing the different model ejectors a coaxial two-stilling chamber set-up was used with the primary nozzle mounted to the inner stilling chamber and the ejector shroud attached to the outer one. Each stilling chamber was fed by a separate duct system, which further upstream combined to connect the test set-up via a single pipe with the air supply system. This permitted separate and relatively easy and accurate measurements of the mass flow rates $\dot{m}_p$ and $\dot{m}_s$. In addition the total mass flow rate $\dot{m}_p + \dot{m}_s$ could be measured in the single duct leading to the air supply system. Since the ambient temperature, T_a, of the ejector models was during all experiments nearly equal to the stilling chamber temperatures, $T_{op} = T_{os} = T_0$, actual ejector condition, corresponding to entrained secondary air from the surrounding, could be readily simulated with this test set-up by adjusting the secondary mass flow rate, $\dot{m}_s$, such that $p_{os} = p_a$. In addition, the test set-up permitted variations in $\dot{m}_s$ independently of $\dot{m}_p$ for additional investigations.

The sound power measurements on the different model ejectors were performed in the same reverberation chamber as used for the linear nozzle array tests described in Section 2. During the tests, the pressure ratio p_{op}/p_{os} was kept constant and preselected to correspond to $M_p' = 0.90$. The variable parameter during the tests was the mass flow ratio k_m which was changed in such a way to included cases with $p_{os} > p_a$, $p_{os} = p_a$ and $p_{os} < p_a$. The data for $p_{os} = p_a$ correspond to actual ejector conditions.

The sound power levels, PWL, of the different model ejectors as determined from the reverberation chamber measurements were compared with the corresponding levels of the selected ejector reference nozzle, PWL_p', giving the measured ejector sound power reduction

$$PWL = PWL_p' - PWL \quad [dB]$$

as defined in the ejector analysis. The values of PWL_p' were obtained from sound power data of the tested 2-nozzle array with $M_s = 0.90$ and SR = 2.0, and by correcting these data according to the V^8-Law with regard to the ejector system conditions measured. The resulting corrections did not exceed + 0.6 and - 0.2 dB.

In addition sound power density spectra were obtained for the different model ejectors and test points considered. Since the corrections mentioned above turned out to be rather small they could be compared directly with corresponding spectra of the 2-nozzle array for $M_s = 0.90$, without any correction.

In addition to the ejector tests, noise measurements on only the external ejector jet were conducted to identify its sound power and sound power density spectrum for the purpose of ejector data interpretation. To enable these tests, the primary

ejector nozzle was removed from the inner stilling chamber and the corresponding airflow control valve was closed.

6.3.2 Test data for ejectors without acoustic liners

The selected test data for the ejectors without acoustic liners are given in Figures 33 to 35. All data shown correspond to actual ejector conditions as the stilling chamber and atmospheric pressure were nearly equal for these tests, $p_{os} = p_a$.

Sound power reduction versus length ratio, L/D. It follows from Figure 33 that the short ejector, L/D = 10 shows no sound power reduction nor does it produce any sound power amplification. For increasing values of L/D, however, this noise reduction significantly increases and assumes a level of about 5 dB for L/D = 20. If L/D further increases, the increase in the noise reduction is smaller leading to a value of about 7 dB for L/D = 30.

Also shown in Figure 33 are data reported by Middleton [24] for ejectors with a single circular primary jet with diameter D_0. The corresponding data curve given in Figure 33 is plotted versus the length ratio L/D_0 and is the mean line through Middleton's results with the range of slatter indicated. Both L/D and L/D_0 are related in Figure 33 by $L/D = \sqrt{2} \, L/D_0$, based on the interpretation that for multiple circular nozzles D_0 is the exit diameter of an area-wise equivalent single nozzle so that for the present case $D_0 = \sqrt{2} \, D$.

Considering the two data sets in Figure 33, it follows that they agree very well, if a comparison is made on the bases of only the number at their related length ratio rather than on the bases of absolute lengths values. This suggest that for multiple nozzles and ejectors without acoustic liners, the length of the shrouds required for a certain sound power reduction reduces significantly by the factor $1/\sqrt{N}$, where N = number of individual nozzles. Also, Figure 33 suggests that for optimum noise attenuation of ejectors without acoustic liners, this length may be about 20 to 30 times the individual nozzle diameter. Therefore, using, for example, linear arrays of mixing circular jets instead of a single circular jet could significantly reduce this required length.

Sound power spectra. The sound power spectra shown in Figure 34 give some explanations of the sound power reduction behaviour observed and discussed before, especially if compared with the spectra of their related unshrouded reference jet.

As can be seen, the ejector with L/D = 10 produces up to about 5 dB less noise than the unshrouded primary nozzles for the high frequency range above approximately 4.0 kHz. However, at medium and low frequencies, between about 0.50 to 4 kHz and below 0.5 kHz, respectively, this configuration generates significantly more noise than the reference nozzle. Both of these noise components evidently cancel so that no total noise reduction or amplification can occur.

If the ejector shroud length increases to L/D = 20, a significant noise reduction takes place, primarily in the medium frequency range and up to about 7 dB, compared to the short ejector L/D = 10. In addition the noise in the low and high frequency ranges reduces somewhat, say by about 3 dB. As a result this ejector generates a sound power spectrum which in the high frequency range is about 8 dB less intense than that of the unshrouded reference nozzle. In the direction of lower frequencies, this attenuation de-
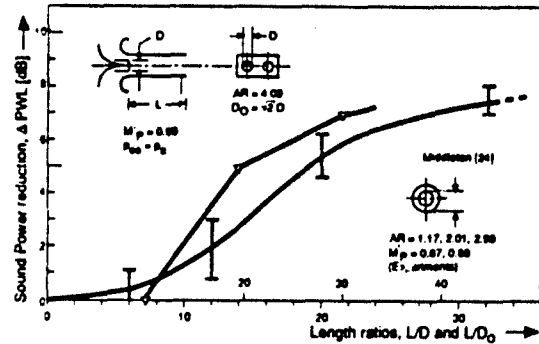
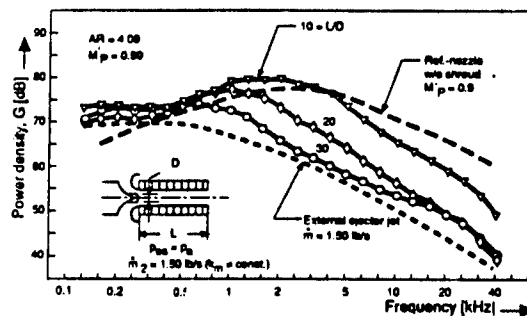Figure 33: Measured ejector sound power reduction, Δ PWL, versus length ratios, L/D and L/D_0 ($M_p' = 0.9$, no acoustic liners)
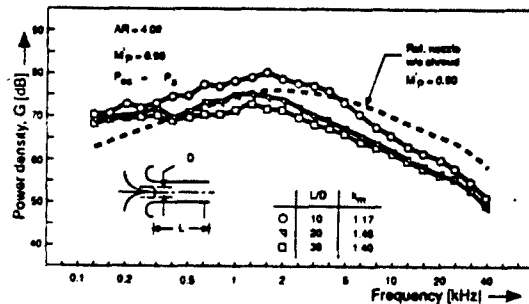
Figure 34: Effect of ejector length ratio, L/D, on sound power spectrum ($M_p' = 0.90$, no acoustic liners)
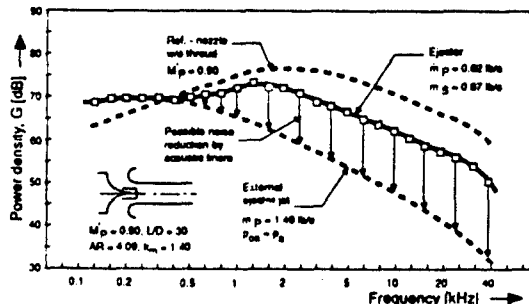
Figure 35: Measured sound power spectrum of model ejector in comparison with spectrum of external ejector jet and unshrouded reference nozzle ($M_p' = 0.90$, L/D = 30, no acoustic liners)

creases. Between about 1.0 kHz and 0.40 kHz this ejector is as loud as the reference nozzle and below 0.40 kHz even somewhat more noise is generated.

For the long ejector L/D = 30 a further sound power reduction of about 2 dB occurs compared to the ejector L/D = 20. According to Figure 34 this is due to a corresponding reduction in also primarily the medium frequency range.

Examination of results. As can be seen in Figure 35, the spectrum of the external ejector jet peaks in the low frequency range f < 0.50 kHz and has in this range spectral density levels approximately equal to those of the ejector model with L/D = 30. This explains the high content of low frequency noise of the ejectors tested, and suggests that the noise in the low frequency range is mainly noise generated externally. In the direction of higher frequencies, both the spectra of the ejector L/D = 30 and of the external ejector jet deviate more and more, and for frequencies f > 1.2 kHz differ by about 10 to 17 dB, depending on the frequency. Hence, for frequencies above 0.5 kHz the noise of the considered ejector is evidently governed by the internal ejector noise, particularly for f > 1.2 kHz, which propagates through the ejector shroud and radiates at its end into the surrounding atmosphere. The high frequency content of this noise strongly suggests the use of acoustically lined shrouds, which should be rather effective in this range of frequencies. Based on the test data and theoretical results, the potential of further sound power reduction of such liners may be estimated to be about 7 dB for this ejector.

The spectrum of the medium long ejector, L/D = 20, was found before to be very similarly to that of the long ejector, L/D = 30, considered above. The slightly more intense noise of this ejector in the medium frequency range is possibly due to nonuniformities in the exhaust velocity profile of this configuration and/or due to a possible incomplete mixing process in the ejector shroud. Because of the latter, intense turbulence could be present at the downstream end of the shroud, radiating additional noise into the free atmosphere.

For the short ejector system, L/D = 10, the incomplete mixing appears to be the main reason for the intense medium frequency noise radiation. This is expected, since the peak frequency of the sound power spectrum of this configuration is of the order of that of the unshrouded ejector reference nozzle. However, also nonuniformities in the exit velocity profile, which may be present for this configuration, could contribute to the comparatively intense noise levels of this ejector system.

6.3.3 Results of ejectors with acoustic liners

The results of the tests on the different ejectors with acoustically lined shrouds selected for this papers are shown in Figures 36 and 37. They correspond to the data presented previously for the ejectors without liners. Similar as before, all data correspond nearly to actual ejector conditions, as the stilling chamber and atmospheric pressure were approximately equal for these tests, $p_{os} = p_a$.

Sound power reduction versus length ratio, L/D, of acoustically lined ejectors. As can be seen in Figure 36, the effect of the acoustic liner for the ejector with L/D = 10 is comparatively small and increases the sound power reduction of this ejector only from about zero to approximately 1 dB. Towards larger length ratios, L/D, however, the increase of the sound power reduction due to the liners improves and assumes for the ejectors with L/D = 20 and 30 values of about 2 and 5 dB, respectively. With this, these ejectors have correspondingly total sound power reductions of about 7 dB and 12 dB.

The large sound power reduction of about 12 dB of the lined ejector with L/D = 30 is very promising and comes very close to the noise reduction of about 14 dB predicted for this ejector for $M'_p = 0.9$. For a selected equal Mach number reference nozzle as des-
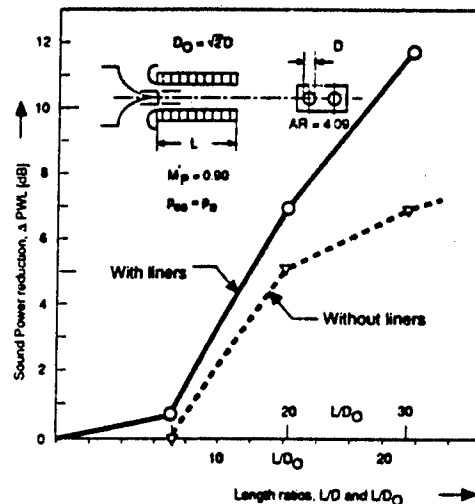
Figure 36: Measured ejector sound power reduction, Δ PWL, with and without acoustic liners versus ejector length ratios, L/D and L/D₀ ($M'_p = 0.90$)

Figure 37: Effect of ejector length ratio, L/D, on sound power spectrum ($M'_p = 0.90$, with acoustic liners)

cribed before, the measured noise reduction would be even about 15 dB, while the correspondingly predicted reduction would be about 17 dB.

These data also indicate that the selected noise attenuating liners performed evidently very good for the ejector L/D = 30. Only a limited further noise reduction of about 2 dB can be possibly achieved for this ejector by improving the liners and/or the corresponding shroud design. In addition this result confirms, that the noise of the unlined ejector with L/D = 30 is as expected strongly dominated by internal ejector noise, which in the present test could be significantly absorbed by the shroud liner treatment.

For the ejector L/D = 20 the relatively small effect of the acoustic liners on the sound power reduction suggests that the noise of this ejector is more than for the ejector with L/D = 30 due to the external ejector jet. In addition, it also could be possible that for this ejector the selected liners were not optimal. Thus, using improved liners or simply installing more liners into the corresponding ejector shroud could possibly produce a further noise reduction for this ejector.

For the ejector with L/D = 10, the total noise is about equal to that of the corresponding unlined version. This is more than likely due to the evidently strong external noise generation of this ejector configuration, but possibly also for this ejector an improved noise reduction might result if other or more liners would be used.

Sound power spectra of acoustically lined ejectors. The differences in the sound power spectra of the ejectors with acoustically lined shrouds shown in Figure 37 are a result of two effects, the effect of the acoustic liners and the effect of the associated different shroud length ratios, L/D.

Comparison of the spectra of the acoustically lined ejectors of Figure 37 with those given in Figure 34 for the ejectors without acoustic liners shows, for example, that the selected acoustic liners effect the spectrum for the ejector with L/D = 10 only very little. Practically, the spectra of these ejectors with and without acoustic liners are equal, in spite of a small noticeable noise reduction of about 1 to 2 dB above 16 kHz. For the ejectors with L/D = 20 this comparison yields noise reductions due to the liners starting at a frequency of about 1.6 kHz. Towards higher frequencies the noise reduction continuously increases until reaching a constant value of approximately 10 dB for f > 20 kHz. The largest effect of the acoustic liners can be seen by this comparison for the long ejector with L/D = 30. The corresponding noise reduction starts at about f = 1.0 kHz and rapidly increase towards higher frequencies. For frequencies f > 2.5 kHz the noise reduction is about constant and has a value of about 10 dB.

The differences in the spectra of Figure 37 for the ejectors with L/D = 10 and 20 are, therefore, above approximately 4 kHz primarily due to the selected acoustic liners, while the noise reduction below this frequency is evidently mainly due to trapping more of the turbulent mixing of the primary and secondary jet into the shroud by increasing its length. Similarily, the differences in the spectra for the ejectors with L/D = 20 and 30 are above about 1.6 kHz primarily due to the liners and below this frequency a result of the different shroud length.

The spectrum in Figure 37 of the long ejector with L/D = 30 approaches very closely the spectrum of the external ejector jet. Between f = 2.0 kHz and 10 kHz the corresponding spectral density levels differ by only approximately 2.0 dB. This shows again that the selected liners worked for this ejector evidently rather well, so that as discussed before noise reductions close to the predicted ones could be obtained.

7. POSSIBLE INTEGRATION OF NOISE CONTROL MEASURES INTO COMBAT AIRCRAFT

7.1 General Remarks

The different noise control measures investigated and described before may be integrated into both existing and currently developed combat aircraft as well as certainly into corresponding future aircraft designs.

For existing and currently developed aircraft, add-on noise control reduction kits could be designed based on these measures, which may be summarized as follows

* add-on ejector systems with acoustically lined shrouds

* application of multiple nozzles and special shape mixing nozzles

* use of optimum velocity profile jets including inverted profile jets

* implementation of special acoustic absorbers for effective acoustic liners

* application of jet noise shielding measures

Certainly, these measures can be also combined and in certain cases as, for example, for ejector systems should be combined. Also, for each possible application a careful selection of the measures to be used needs to be made. The latter, in any case, must include detailed trade-off studies, considering noise, flight performance and special operational requirements, for overall performance penalty minimization.

The development of such add-on noise reduction kits can at present fortunately be based on a rather extensive and advanced technical basis born out of now nearly four decades jet aircraft noise control research. Hence, the development of these noise reduction devices covering practical design and noise control work could start comparatively soon.

Based on available results, the application of such noise control reduction kits may be expected to result into noise reductions values of about, say 6 to 10 dB, perhaps also somewhat more. The latter certainly depends strongly on the applicable and selected noise reduction measures and their degree of integration into the selected aircraft, which is important for noise control optimization. It may be noted that noise reductions of this order are comparatively high as, for example, 10 dB corresponds in general already to a reduction of the noise nuisance by a factor of two. Therefore, using this approach and adding, for example, effective noise control operational measures may result into a rather interestingly high overall noise relief for the public.

For future aircraft designs the same noise reduction methods as summarized before may be applied. However, if for these aircraft a more noise controlling integration of these methods compared to that for existing and currently developed aircraft is not possible, not very much higher noise reduction values than those mentioned before may be expected. Perhaps if somewhat more care is taken for integrating these measures, noise reductions of 8 to 12 dB may be obtained.

For obtaining additional and substantial noise reductions for future combat aircraft of values similar to those established for civil transport aircraft over the past three to four decades, say 20 dB or more, an effective lowering of the jet engine exhaust velocity seems to be mandatory as mentioned already before. At present, using existing engine configurations, this is fortunately possible, but only with effective ejector flow systems. As born out by the study results presented before, the size of the ejector shroud may be of the order of that of the jet engine and the ejector should be carefully integrated into the overall aircraft design for obtaining optimum noise reductions by minimum flight performance losses. Hence,

technology is available to establish high noise
reductions of about 20 dB or more, also for combat
aircraft, but a more fully noise controlling air-
craft propulsion system integration including ejec-
tor system seems to be required. In order to reach
this goal, equal importance and priority as to
other critical aircraft aspects must be given to
combat aircraft noise considerations in the future.

7.2 Selected Examples of Noise Control Applications

The acoustic advantages and details of the radia-
ted sound field of linear arrays of mixing circu-
lar jets are reported in Section 2. The most re-
cently published example of a nozzle configuration
which could be modified into a nozzle generating a
jet flow of this type, is the slot type nozzle
producing 12 closely spaced square jets as used in
the Lockheed F-117 A and shown in Figure 38 [25].
Based on the results in Section 2, this nozzle may
be expected to generate significant less sideline
noise than, for example, a single nozzle of equal
total exhaust area. In addition, since the indivi-
dual nozzle spacing ratio is very small, also some
fly-over noise reduction may be expected, although
the exhausting total jet stream is not shielded by
an ejector shroud. As shown by this example, noz-
zles of this type with acceptable weight may be
evidently designed now as well as manufactured and
are being used already in important military ap-
plications. Hence, also for the application in
low-noise effective ejector systems nozzles of
this type certainly may be used.

The use of inverted profile jets is as described
in Section 3 another interesting measure promising
a large jet noise reduction potential of about
10 dB. A strong advantage of this technique is
that for its application special changes to the
aircraft structure are not necessarily needed.
Furthermore, the weight impact may be about zero
and the thrust losses could be small. In principle,
all required main modifications may be retained to
the area of the jet engine and only the existing

Figure 39: Design sketch of a possible engine
producing inverted profile jets

engines have to be exchanged into engines gener-
ating inverted profile jets. As an example, a de-
sign sketch of such an engine is shown in Figure
39 [26]. This particular design is based on a con-
ventional engine which can remain unchanged up to
the section of the turbine exit. Downstream of the
turbine, flow change passages have to be implemen-
ted to cross the hot and the cold flow. In addi-
tion, even this partial engine change appears to
be not necessarily required as also special nozz-
les may be designed and applied for taking care of
the velocity profile inversion. Thus, it appears
that also this technique may be used in conjunc-
tion with unchanged existing jet engines and thus
may be also considered for short to medium term
applications including possible installations into
ejector systems.

An example of a possible aircraft application of
special shape mixing nozzles as described in Sec-
tion 4 is given in Figure 40. The figure shows a
nozzle of this type attached to one of the lift
producing engines of the Dornier Do 31 VTOL trans-
port aircraft [14]. The engine is installed into a
planned wing mounted lift engine ejector nacelle
as can be seen. Similar designs may be used for
effective noise control measures for future combat
aircraft but certainly in a more advanced high
speed and low performance loss version.

Figure 38: Slot type nozzle configuration used for
the Lockheed F-117 A stealth aircraft
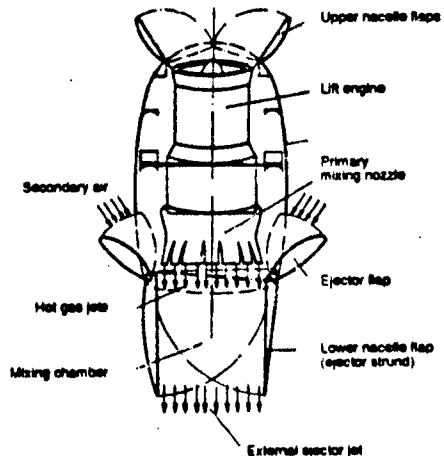
Figure 40: Special shape mixing nozzle used in
Dornier Do 31 ejector lift engine na-
celle design

The detailed investigation on special acoustic absorbers described in Section 5 showed rather promising results, so that also preliminary designs for its practical applications were carried out. Figure 41 shows as an example, a design application of these special acoustic absorbers combined with conventional absorbers for the Alpha Jet partially taken from References [22, 27]. As can be

Inlet acoustic liner

Exhaust nozzle acoustic liner
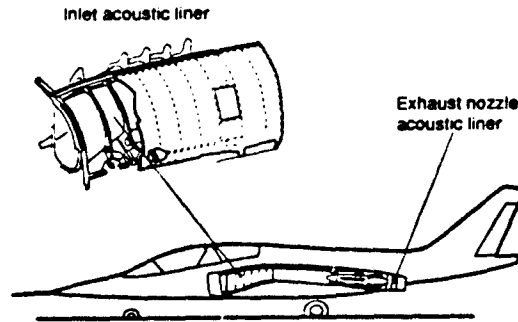
Figure 41: Alpha Jet with possible integration of special acoustic absorbers within engine inlet duct

seen, the special acoustic absorbers were planned to be used for both the inlet channel of the engine as well as for the bypass engine exhaust nozzles for optimum noise reduction. In order to realize integrations like this for practical application, a large number of requirements have to be considered and their fulfilment has to be proven in addition to the noise reduction capability, e.g. load carrying properties, bird impact resistance, corrosion, drainage, reparability and others.

Ejector systems in conjunction with special mixing nozzles also have been planned or even used already in aircraft applications and/or flight tests. One example is the ejector engine/nacelle project for the Dornier Do 31 mentioned before and shown in Figure 40. Other examples are the well known ejector system used for the DC 8 aircraft which was commercially applied [28] as well as interesting ejector systems used in flight tests fitted to a RR Viper engine on an HS-125 executive jet [29, 30]. In most of the previous examples, however, the ejectors were designed as add-on devices and thus where comparatively small so that it appears that not the full potential of these systems could be realized.

For future combat aircraft based on existing engine technology, at present the use of fully integrated ejector systems seems to be the only possibility to arrive at substantial noise reductions of the order of 20 dB or more as described before. In such applications the ejector system must be acoustically optimized in geometry, and equipped with effective special multiple mixing nozzle designs and advanced special absorbers. Also, the engine should be acoustically optimized. In addition, certainly, the ejector system must be de-

signed and integrated in such a manner that unacceptable flight performance losses can be avoided.

Figure 42 shows an idea of a concept for a fighter/bomber aircraft with advanced low-noise ejector system integration for obtaining the substantial noise reductions mentioned above. In this particular example the ejector is installed in the rear part of the aircraft and a linear nozzle array is used surrounded by a rectangular shroud.

It may be noted that for the type of ejector shown in Figure 42 the upper and lower shroud parts could be designed to consist of 3 to 4 or more adjustable sections. With this, for example, for supersonic flight the shroud might be changed into a convergent/divergent nozzle for improving overall thrust performance. In addition, the end of the shrouds could be equipped with jet flaps for thrust vectoring.

Since the exhaust temperature at the shroud end would be relatively low, the jet flaps could be realized comparatively easy and made of composite material. Because of the entrained secondary airflow, also the entire shroud would be relatively low temperature loaded. Thus, also these parts might be designed as low weight structures based on these advanced material.

Hence, there are sufficient information and an advanced technology basis available for lowering combat aircraft engine noise by rather interesting and even substantial noise reduction values. Applying this, by giving the noise control of these aircraft equal importance and priority as other critical aircraft aspects, may strongly help resolving the related noise problem.

Engine inlets with acoustic liners

Multiple mixing nozzles

Engines acoustically optimized

Ejector with acoustic liners and variable geometry
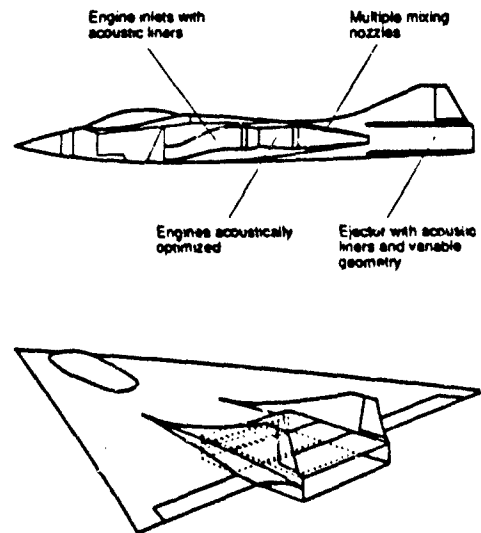
Figure 42: Idea of concept of fighter/bomber low-noise ejector system integration

REFERENCES

[1] Lighthill, M.J., "On Sound Generated Aerodynamically, I. General Theory", Proc. Roy Soc., A211, pp. 564-587 (1952)

[2] Cowan, S.J., and R.W. Crouch, "Transmission of Sound Through a Two-Dimensional Shielding Jet", AIAA Paper No. 73-1002 (1973)

[3] Gray, V.H., O.A. Gutierrez, and D.Q. Walker, "Assessment of Jets as Acoustic Shields by Comparison of Single and Multitube Suppressor Nozzle Data", AIAA Paper No. 73-1001 (1973)

[4] Middleton, D., and P.J.F. Clark, "Assessment and Development of Methods of Acoustic Performance Prediction for Jet Noise Suppressors". University of Toronto Institute for Aerospace Studies Technical Note No. 134 (1969)

[5] Stenzel, H., and O. Brosze, Leitfaden zur Berechnung von Schallvorgängen, Second edition, Springer-Verlag (1958)

[6] Borchers, I.U., and B.H. Goethert, "An Experimental Study of the Noise Radiation of Interfering Free Jets", AIAA Paper No. 77-1285 (1977)

[7] Borchers, I.U., "Noise and Flow Characteristics of Linear Arrays of Circular Jets and Ejector Flow Systems", PhD Dissertation, The University of Tennessee Space Institute, Tullahoma (1976)

[8] Grosche, F.R., J.H. Jones, and G.A. Wilhold, "Measurements of the Distribution of Sound Source Intensities in Turbulent Jets", AIAA Paper No. 73-989 (1973)

[9] Hackstein, H.J., "Strömungsmechanische und akustische Untersuchungen an Koaxialstrahlen unterschiedlicher Profilierung", Fortschr.-Ber. VDI Reihe 15 Nr. 48, Düsseldorf, VDI-Verlag (1987)

[10] Prandtl, L., "Bericht über Untersuchungen zur ausgebildeten Turbulenz", Zeitschr. f. angewandte Mechanik, Bd. 5, S. 136ff (1925)

[11] Prandtl, L., "Bemerkungen zur Theorie der freien Turbulenz", Zeitschr. f. angewandte Mathematik u. Mechanik, Bd. 22, S. 16 ff (1942)

[12] Jones, E.P., and B.E. Launder, "The Prediction of Laminerization with Two-Equation Model of Turbulence", Int. Journal of Heat and Mass Transfer, Bd. 15, S. 301ff (1972)

[13] Evertz, E., "Aerodynamische und akustische Interferenz eines axialsymmetrischen Luftstrahls mit einer tangential angeströmten ebenen Platte", Dissertation, RWTH Aachen, ILR (1979)

[14] Bartels, P., "Schallabstrahlung im Nah- und Fernfeld des VSTOL-Strahltransporters Do 31 und Lärmminderungsmöglichkeiten bei zukünftigen VSTOL-Entwicklungen", Forschungsbericht aus der Wehrtechnik, BMVg-FBWT 72-23 (1972)

[15] Eckert, Moddemann, Prechter and Winscher, "Verminderung von Abgaslärm und Bodenerosion durch intensivierte Strahlmischung bei Hub- und Reisetriebwerken", ZTL-FAG 4, Dornier/MTU-Bericht 16/69 A (1969)

[16] Bartels, Lautenbach, Winscher and Zink, "Verminderung von Abgaslärm durch intensivierte Strahlmischung bei Hub- und Reisetriebwerken", ZTL-FAG 4, Teilaufgabe DO 4.01a, Dornier-Bericht 70/23 B (1970)

[17] Bartels, Eckert, Lautenbach, Münch and Zink, "Untersuchungen zum Strahllärm bei Zweikreistriebwerken", ZTL-FAG 4, Endbericht Do 4.11 (1971)

[18] Bartels, P., H. Burkhart, and R. Daschler, "Untersuchungen zur Reduzierung der Fan-Lärm durch zellenseitige, schallabsorbierende Maßnahmen und abschließende Arbeiten zur Fan-Lärm-Abstrahlung", ZTL-FAG 4, Aufgabe Do 4.10/4, Endbericht (1972)

[19] Bartels, P., W. Kreder, H. Straßner, and W. Uhse, "Untersuchungen zur Auslegung schallabsorbierender Strukturen des LSK und Aerodyne", ZTL-FAG 2, Aufgabe Do 2.17/2, Endbericht (1974)

[20] Wirt, L.W., "Sound-absorptive Materials to Meet Special Requirements", JASA 57, S. 126-143 (1975)

[21] Laube, L., and H. Straßner, "Mittragende Schallabsorber", ZTL-FAG 2, Aufgabe Do 2.17/4, Endbericht (1976)

[22] Laube, L., R. Deschler, H. Straßner, and W. Uhse, "Untersuchung zur praxisnahen Anwendung von neuartigen Absorbern, Teil 1: Absorber zur Minderung von Triebwerkslärm", ZTL-FAG 2, Aufgabe Do 2.17/5 (1977)

[23] Goethert, B.H., and I.U. Borchers, "Noise and Thrust Characteristics of Shrouded Multi-Nozzles of Circular Cross Section", Journal of Aircraft, Vol. 12, No. 3, pp. 188-189, (1975)

[24] Middleton, D., "Theoretical and Experimental Investigations into the Acoustic Output from Ejector Flows", Journal of Sound and Vibration, Vol. 11, No. 4, 1970

[25] Aviation Week & Space Technology, McGraw-Hill Publication, June 24 (1991)

[26] General Electric "Design sketch for an engine with inverted profile jet"

[27] Laube, L., "Untersuchung zur praxisnahen Anwendung von neuartigen Absorbern", ZTL-FAG 2 Aufgabe Do 2.17-7, Endbericht (1979)

[28] Smith, Michael J.T., Aircraft Noise, Cambridge Aerospace Series, Cambridge University Press (1989)

[29] Brooks, J.R., R.A. McKinnon, and E.S. Johnson, "Results from Flight Noise Tests on a Viper Turbojet Fitted with Ejector-Suppressor Nozzle Systems", AIAA Paper No. 80-1028 (1980)

[30] Fitzsimmons, R.D., R.A. McKinnon, and E.S. Johnson, "Flight Test and Tunnel Test Results of the MDC Mechanical Jet Noise Suppressor", NASA CP-2108 (1979)

Discussion

QUESTION BY: L.W. Illston, BAe, UK

Although some attenuations at low angles to the jet axis haven been encouraging statically for multi lobed nozzles and inverted velocity profile nozzles, the attenuations measured in flight have been considerably reduced. It is therefore very important to evaluate such devices with forward speed effects. Have you evaluated in flight-noise reductions?

The multi lobed nozzle plus ejector has good potential for in-flight noise reduction, but it also introduces weight and performance penalties, and these must be included in any evaluation.

AUTHOR'S RESPONSE:

The comments were agreed. It is important to consider flight effects. However, weight and performance penalties depend on the ejector design. In future fully integrated designs these penalties can be minimized if not avoided. In addition, it must be noted that, depending on the design, even performance improvements could be achieved.

QUESTION BY: H.J. Lichtfuss, MTU, Germany

You have shown a noise reduction due to ejectors which shows an effect only if you have a length of the ejector of L/D > 10. If this is used for the ejector concepts of the last two papers then there can be no effect at all.

AUTHOR'S RESPONSE:

Please recall, that the data, which were shown, correspond to sound power reduction values and are therefore conservative. Due to channeling and directivity effects of the internal ejector noise larger noise reductions, also for shorter ejectors, may be possible.

In addition, Mr. Tönskötter, IABG, noted that the previous papers made use of mixing nozzles leading to effective ejectors with shorter length.

REDUCTION OF PROPELLER NOISE BY ACTIVE NOISE CONTROL

O. Bschorr / D. Kubanke
Messerschmitt-Bölkow-Blohm GmbH
ZTT2 / Aeroacoustics
P.O.Box 80 11 09
8000 München 80
Federal Republic of Germany
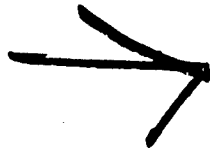
SUMMARY

Active noise control, a method of cancelling noise by means of interference with a secondary anti-noise source, is now in full development. The first commercial application of this technique is in the case of active electronically controlled head sets. The next step will be the active noise cancellation in air ducts and in passenger cabins. The aim of this paper is to assess the possibilities of the anti-noise technique for reducing propeller noise. First, by a mathematical simulation the theoretical noise reduction on the ground was calculated and found to be promising for further investigations. In the case of the periodic engine and propeller noise, for example, with only a single anti-noise source the noise foot prints of the lower propeller harmonics can be reduced by up to 10 dB. In laboratory tests the theoretical values will be confirmed experimentally. For cancellation of the periodic noise one can use synchronous anti-noise generators. Compared with the engine and propeller noise the reduction of jet noise by the anti-noise technique is much more difficult. Therefore a sensor and controlling units are necessary because of the stochastic nature of jet noise. Since aircraft noise is a severe problem all methods are to be considered.

LIST OF SYMBOLS

c	sound velocity
H	altitude
J	Bessel function
k	$k = \omega/c$ wave number
L	noise level
m	number of propeller blades
Ma	Mach number
n	number of propeller harmonics
N	sound power output
p	sound pressure
Q	source strength
R	effective radius of the propeller
s	distance
t	time
v	particle velocity
e	cone angle
λ	wave-length
ω	angular frequency of the propeller
ϕ	velocity potential
γ	angle
ρ	density (radius of curvature 3.2)
τ	tangent angle
x,y	cartesian coordinates
ϕ,θ,r	spherical coordinates

1. INTRODUCTION

1.1 Situation

Aircraft noise is a substantial environmental problem. The increasing number of protests against aircraft noise also base on the idea that the noise problem is not inevitable, but solvable by laws and technical methods. Concerning the legislature the Federal Republic of Germany is very advanced. Already since 1971 there is a 'Law for Protection from Aircraft Noise' [1]. Based on the 'Aircraft Noise Report' (Report 10/5029) [2] the 10 civil and 30 military airport managements had to pay noise compensations of 755 million DM up to 1985. A bill from Feb. 26.1988 (Report of the Bundesrat 545/87) [3] intended to further intensify the 'Law for Protecion from Aircraft Noise'. Concerning the jurisdiction, there is the Ense-basic ruling, where the Federal supreme court in a final jurisdiction ruled that 'noise pollution is equivalent expropriation' [4].

Those laws relate to the noise immission. Since the essential point for environmental protection is the reduction of noise emission, there are also legal noise limitations for aircraft. The maximum admissible noise levels for civil jet aeroplanes are determined in the 'ICAO – International Standards & Recommended Practices, Annex 16'. For propeller airplanes there are national regulations which for example in the FRG were intensified by about 4 dB(A) [5].

What is the technical potential to reduce aircraft noise? The best are primary methods to avoid noise directly at the source. For jet engines the noise emission increases by the power of eight of the jet stream velocity. By increasing the by-pass-ratio the jet-stream velocity and therefore the noise emission can be decreased eminently for the same thrust level. At a by-pass-ratio of 4 the noise of the Airbus is about 30 dB (A) lower than the jet engines at the beginning of the jet age. (30 dB are equivalent to a power reduction of 1000 to 1.) But this method is nearly exhausted for civil airplanes. For propeller engines the relation between thrust and noise production is stronger. The propeller thrust radiates like an acoustical dipole. A further problem of the propeller noise is its pulse and tone contents which results for the same sound level in a 10 dB higher annoyance.

At present the potential of noise reduction by controlled interference cancellation is recognized but not used beyond test applications. Though anti-sound methods are no longer considered outsiders and are expected to be successful in one dimensional ducts and in car interior noise reduction. Concerning the reduction of aircraft noise there still is reluctance regarding techniques and economy. E.g.: Within the Euromart-program (initiated by the EC) it was proposed to perform a feasibility study for rotor noise cancellation which was given lower priority and was therefore not included in the program [6].

1.2 State of the art (anti-sound)

In 1933 the Berlin physicist Paul Lueg suggested to superpose on a noise field an antiphased sound-field for obtaining an interference cancellation [7]. His patented 'Cancellation System' made of microphone, controller and speaker still is the basis for modern systems. His suggestion fell into oblivion and 20 years later this method was invented again. O'son [8] even made experiments with it. Despite the efforts for the electronic system the achieved reduction rates were technically not interesting and so the work was not pursued further. After a break of nearly 20 years Jessel [9] and Bschorr [10 - 14] took up the idea. Among the latter references are two patents for sectorial and omnidirectional rotor noise cancellation.

At that time the concerns regarding economy and technical practicability of the anti-sound method were justified. But it was dismaying that there were fundamental doubts against the physical principle, especially regarding the energy balance. The few publications up to 1980 show that this method, while not not forgotten, was still of low interest. Only when micro-electronics were developed and made rapid progress did this have positive effects on the concept of anti-sound. One mile-stone was the 'Inter Noise Congress 1985' [15] with a continuous session 'Active noise cancellation' and a total of 20 reports. According to the bibliography of Guicking [16] the number of publications about 'anti-sound' increases exponentially.

The first commercial anti-sound products are active, electronically controlled earmuffs. Technically that's the most promising case. There is a null dimensional volume, because the length of the cancelled wave is large compared to the volume of the ear. Concerning the power output the conventional headsets are sufficient actuators. In addition, the passive noise isolation of the ear muffs decreases the problem of the acoustic feedback. The next more complicated case is noise cancellation in one-dimensional ducts, e.g. ventilation shafts and airconditioning systems. Nearly all car manufacturers work on controlled interference cancellation inside vehicles. Concerning the cancellation of the periodic part of the noise, there is the possibility of triggering the control system synchronous with the engine.

All mentioned cases are for interior noise. The main problem is the exterior noise caused by aircraft and traffic. Here a three-dimensional noise cancellation is required. Since exhaust noise is a point-like noise source, one can obtain a three-dimensional cancellation by pointlike nearby anti-sound sources. Using conventional speakers Chaplin et al [17] achieved a total reduction of 2 dB(A). Kallergis [18] suggested a very elegant method for reducing propeller noise: He uses the exhaust noise of the engine as an anti-sound source for cancelling the propeller noise. So he could demonstrate a 3 - 4 dB noise reduction in flight with a wing-tip installed microphone. Kallergis expects a further possible noise reduction.

1.3 Task

In terms of air traffic and noise level the jet engines are the dominant noise sources. Compared to that propeller aircraft are not so relevant. Anti-noise systems for jet engines are very complicated and still out of discussion. Compared to that active propeller noise control is probably more successful: Interference cancellation of the periodic rotor noise requires only a synchronised repetition of the anti-sound signal. On the other hand the periodicity and the lower noise emission of the propeller reduce the demands for an anti-sound generator.

For these reasons the following study is limited to cancellation of the periodic part of the propeller noise. The base is the un-ducted propeller engine. From numerical simulations the noise reduction over ground with a single aircraft mounted antisound source is determined. From the results the expenditure can be compared with noise reduction. To allow a type-independent comparison the individual propeller harmonics are regarded separately.

2. INTERFERENCE CANCELLATION

2.1 Conditions for cancellation [14]

A sound-field can be described by the velocity potential $\phi(r,t)$. ϕ obeys the wave equation ($\delta/\delta t$ = partial derivative)

$$\delta^2\phi/\delta t^2 - c^2\nabla^2\phi = c^2 q(r,t) + \delta v/\delta t .$$

The left part of the equation describes the propagation, the right part stands for the source terms (acoustical monopole, dipole). The sound pressure p and particle velocity v result from

$$p = \rho\,\delta\phi/\delta t \quad ; \quad v = -\,grad\,\phi .$$

Subsequently a sound-field ϕ^*, designed for cancelling an unwelcome noise-field ϕ is called anti-sound field. The anti-sound field ϕ^* for destructive interference is

$$\phi^*(r,t) = -\phi(r,t) .$$

If, in general, the anti-sound signal is not exactly cancelling the noise signal, because of a phase error $\Delta\phi$ and an ampli-

tude error $\Delta p/p$, then the possible noise reduction ΔL [dB] can be

$$\Delta L = 20 \lg [(1 + \Delta p/p)^2$$
$$+ 1 - 2 (1 + \Delta p/p) \cos \Delta \phi] .$$

For example, with a phase error of $\Delta \phi = \pm 15°$ and an amplitude error of $\pm 30\%$ there is a level reduction of 10 dB (Fig. 1).

2.2 Acoustical neutralisation [14]

The most obvious way to cancel a noise source is to place an anti-sound source, which is opposite in phase, as close as possible. Due to the pressure equalization between noise source and anti-sound source less energy is radiated. This effect is verified for a monopole noise source:
The noise source with the strength Q at the origin of the coordinates radiates with the angular velocity ω. The position of the n-th anti-sound source is s_n, its strength is Q_n. The sound-field ϕ_L of the single noise source is

$$\phi_L = \frac{1}{4} \frac{Q}{\pi} \frac{1}{r} \sin(\omega t - kr) .$$

The resulting sound-field ϕ_{L+A} of noise source plus anti-sound source is

$$\phi_{L+A} = \frac{1}{4} \frac{Q}{\pi} \frac{1}{r} \sin(\omega t - kr)$$
$$- \sum_{n=1} \frac{Q_n \sin(\omega t - k |r - s_n|)}{4\pi |r - s_n|} .$$

The sound power output N_L of the noise source and the output N_{L+A} of the combination of noise source L and anti-sound source A can be obtained by integrating the intensity on the surface of the surrounding control sphere. The ratio N_{L+A}/N_L is a measure for noise reduction.

Noise reduction is better the higher the degree of the combination ϕ_{L+A} is. To cancel the radiation part of the nullth degree it is required that

$$Q - \sum_{n=1} Q_n = 0 .$$

To cancel the dipole part of two or more anti-sound sources it is required that

$$\sum_{n=1} s_n Q_n = 0 \qquad s \ll \lambda .$$

There are optimizing conditions for groups of anti-sound sources to cancel the quadrupole part.

The so called 'acoustical neutralisation' could be interpreted as transforming the noise source into a radiator with a degree as high as possible.

Figure 2 shows the power output reduction for various combinations of noise and anti-sound sources in relation to the distance s. The simplest combination is using a single anti-sound source, which results in a dipole radiator. By using two collinear anti-sound sources the combined radiation has a quadrupole characteristic.

2.3 Sectorial cancellation [14]

If it is not possible to meet the condition $s \ll \lambda$, there is no omnidirectional cancellation, but still there is sectorial noise cancellation in the shadow angle of the anti-sound source. For cancellation in the far-field where the distance to the immission point is large compared to the distance s between noise source and anti-sound source the noise reduction is

$$\Delta L_c = 20 \lg [2 \sin (2\pi(s/\lambda) \sin^2\alpha/2)] .$$

Here α is the angular deflection from the center line. This relation is shown in Figure 3. At a distance relation $s/\lambda = 1$ there is a noise reduction of 20 dB in a cone with angle $\alpha = \pm 10°$.

3. CANCELLATION OF PROPELLER NOISE

3.1 Propeller noise

There are two causes for the periodic part of the propeller noise: Thrust by a rotor is acoustically a dipole radiator. By separating this dipole into its three-dimensional components, one sees that the axial, thrust-based component is dominant. In addition there is a tangential and a radial component which result from frictional and centrifugal forces. A second cause for noise is the blade-thickness noise (volume displacement). Primarily it is an acoustical monopole with a volume source at the front and a sink at the rear of the blade. If the distance between source and sink is small compared to the wave-length, this is as well an acoustic dipole source.

The fundamental theory of propeller noise is based on Gutin [19]. Additional pioneering work was done by Merbt and Billing [20] and Lowson [23]. A theory of noise radiation from moving surfaces originates from Ffowcs-Williams and Hawking [24]. In the following a simplified derivation of the propeller sound-field is used. It is especially aimed at the question of interference cancellation. For the model used here speakers are distributed over the propeller area. The volume displacement of the rotating propeller is simulated by an equivalent action of the speaker's membrane. In the same way the propeller-thrust induced acoustical dipole can be simulated by pairs of speakers. Each pair has the same loudness level but opposite phase. For this model the phase surface and the directional diagram of the propeller sound-field can be calculated. For the description the spherical coordinates r, ϕ, θ are introduced. The origin is at the center of the propeller. r is the distance from the origin to the point of immission. θ is the angle to the propeller plane and ϕ is the meridian angle.

For the problem here treated an annular cut of the sound-emitting propeller plane with radius R is considered. With the annular angle Y the motion of the 'membrane' of the n-th harmonic wave of a m-bladed propeller, rotating with the angular frequency ω, is

$$Q = Q_0 \sin nm(\omega t - \psi) .$$

With this annular distribution of sound sources the sound pressure p in the far-field ($r \gg R$) is ($k = \omega/c$)

$$p = Q_0 \int_{\psi = 0}^{2\pi} \sin nm(\omega t - kr - k\cos\theta) \cdot$$
$$\cdot \sin(\psi - \theta) \, d\psi/r$$

$$= p_{nm} J_{nm}(nm \, kR \cos\theta) \cdot$$
$$\cdot \sin nm(\omega t - kr + \phi)/r .$$

The sound-field p_T of the dominant axial dipole caused by thrust is represented by a superposition of two antiphased circles of speakers, which are shifted by an axial distance

$$p_T = p_{nm} \sin\theta \, J_{nm}(nm \, k \, R \cos\theta) \cdot$$
$$\cdot \sin nm(\omega t - kr + \phi)/r .$$

Analogously the blade-thickness-noise p_B is represented by two circles of emitters, shifted by the angle $\Delta\gamma$.

$$p_B = p_{nm} J_{nm}(nm \, k \, R \cos\theta) \cdot$$
$$\cdot \sin nm(\omega t - kr + \phi)/r .$$

The phase of both the dipole p_- and the blade thickness noise p_B is described by

$$\sin nm(\omega t - kr + \theta) .$$

For a discrete time $t = t_0$ the condition for the location of constant phase is

$$- kr + \phi = const.$$

That is the equation for a spherical Archimedian spiral.

3. Interference cancellation

For propeller airplanes it is sufficient to cancel the ground directed noise field. Therefore in principle the arrangement of anti-sound sources is simpler. In the following the area for which noise can be cancelled by a single anti-sound source is calculated.

With [14] a constantly rotating propeller produces a spirally formed sound-field. In the far field the lines of equal phase are on Archimedian spirals with the rotor axis at the centre. Independent of the design of the propeller, in the plane of the propeller the spiral is represented by

$$r = c\phi/\omega .$$

The sound-field of a propeller with m blades is composed of m spirals, revolved into each other. For large distances r the spiral has the tangent

$$tg \, \tau = c/r\omega$$

and the radius of curvature is

$$\rho = \sqrt{r^2 + (c/\omega)^2} .$$

An aircraft mounted anti-noise source creates a spherical phase surface. Fixing the anti-sound source at a horizontal distance c/ω from the propeller axis, there is the same tangent and radius of curvature for the spiral and the sphere in the vertical direction (Fig. 4). If the anti-sound source signal is antiphased to the propeller sound, there is cancellation.

The degree of cancellation decreases on both sides, because spiral and circle differ from the 3rd degree on. The distance difference Δr is

$$\Delta r = (\phi - \sin\phi) c/\omega .$$

For the n-th harmonic wave the cancellation decreases as

$$\Delta L = 20 \, lg \, 2 \sin \pi \, \Delta r/\lambda_n .$$

In Fig. 5 the achievable level reductions in the propeller plane ($\theta = 0$) for each propeller harmonics of a 2-bladed propeller are shown.

Fig. 6 shows the effect of an anti-sound source on the noise footprint of the blade-thickness noise. A 2-bladed propeller ($m = 2$) is located at the origin ($x = y = 0$) and at an altitude $H = 100m$. The propeller axis is in the x-direction. On y the right ($y>0$) and on the left ($y<0$) side are the noise foot prints with and without the anti-sound source respectivly. The anti-sound source has a monopole characteristic and is fixed to the airplane. Its position is in the propeller plane at a distance $a = c/\omega$ from the propeller axis. Amplitude and phase of the anti-sound source are adjusted for absolute cancellation in the vertical direction $\theta=\phi=0$. For that configuration blade-thickness noise and anti-sound source have the sound-fields p_B and p_A

$$p_B = \hat{p}_B \sin nm(\omega t - kr + \phi)$$

$$p_A = \hat{p}_A \sin nm(\omega t - kr') .$$

With $\hat{p}_B$ and $\hat{p}_A$ denoting the pressure amplitudes of blade-thickness noise and anti-sound

$$\hat{p}_B = p_{nm} J_{nm}(n \, m \, k \, R \cos\theta)/r$$

$$\hat{p}_A = p_{nm} J_{nm}(n \, m \, k \, R)/r$$

the resulting amplitude $\hat{p}_{AB}$ is

$$\hat{p}_{AB} = \sqrt{\hat{p}_A^2 + \hat{p}_B^2 - 2\hat{p}_A \hat{p}_B \cos nm(\phi - k(r - r'))}$$

In the neighbourhood of the cancellation direction $\theta = \phi = 0$ there is also sufficient cancellation. Far from this region and for the higher harmonics the superposition of the blade-thickness noise and the anti-noise source causes an amplification. Likewise this amplification effect can be reduced by another cancellation direction. In Fig. 7, f.e. the direction $\phi = 0$ and $\theta = 45°$ for absolute cancellation was chosen.

Fig. 8 shows the noise foot prints for the thrust noise with and without an anti-sound source. Likewise the propeller is at an altitude $H = 100$ m above the origin of

the coordinates. The anti-sound source has a dipole characteristic. The anti-sound source is designed for absolute cancellation in the direction $\phi=0$ and $\theta=30°$.

ACKNOWLEDGEMENT

We thank Dr. Bölkow for his kind and continuous interest in the acoustic laboratory, especially in our anti-noise activities.

4. REFERENCES

[1] "Gesetz zum Schutz gegen Fluglärm".
Bundesgesetzblatt. Jahrgang 1971,
Teil 1, Nr. 28, S. 282 - 287.

[2] "Novellierung des Fluglärm-
gesetzes".
Bundestag-Drucksache 10/5029
vom 14.02.86.

[3] Entwurf eines Gesetzes zur Änderung
des Gesetzes zum Schutz gegen Flug-
lärm.
Bundesrat-Drucksache 545/87
vom 26.02.88.

[4] Urteil des Bundesgerichtshofs
III ZR 34/85 (Ense-Urteil)
vom 30.01.86.

[5] Bekanntmachung einer Herabsetzung
der Lärmgrenzwerte für Propeller-
flugzeuge. Nachrichten für Luft-
fahrer. Teil II.
Herausgegeben von der Bundesanstalt
für Flugsicherung. NfL - 51/87
vom 16.07.87.

[6] Commission of the European
Communities. Directorate
Stimulation of Scientific and
Technological Development.
Information Package for the
1989 Call for Proposal (Area 5).

[7] P. Lueg : "Verfahren zur Dämpfung
von Schallschwingungen".
Dt. Reichspatent 655 508
vom 28.01.33.

[8] H.S. Olson; E.G. May : "Electronic
Sound Absorber"
Journ. Acoust. Soc. Am. 25 (1953).

[9] M.J. Jessel : "Procede electro-
acoustique d'absorption des sons
et bruits genants dans des zones
etendues".
Frans. Patent 1 494 967 (1966).

[10] O. Bschorr : "Schallreduktion durch
Antischallgeber".
Dt. Patent 1918 437 vom 11.04.69.

[11] O. Bschorr : "Lärminderung bei
Propellertriebwerken".
Dt. Patent 2 009 105 vom 26.02.70.

[12] O. Bschorr : "Lärminderung bei
Rotoren".
Dt. Patent 2 133 378 vom 05.07.71.

[13] O. Bschorr : "Verminderung des
Fluglärms durch gesteuerte Inter-
ferenz".
DGLR-Tagung 11. - 13.10.71,
Baden-Baden.

[14] O. Bschorr : "Lärmverminderung
durch Antischall".
Jahrbuch 1970 der DGLR.

[15] Proceedings "Inter Noise 1985",
Edinbourgh.

[16] D. Guicking : "Active Noise and
Vibration Control".
III. Physik. Institut Universi-
tät Göttingen, Januar 1986.

[17] M.C. Trinder, G.B. Chaplin,
P.M. Nelson : "Active Control
of Commercial Vehicle Exhaust
Noise".
Inter Noise Proceedings 1986,
Cambridge.

[18] M. Kallergis : "Möglichkeit einer
aktiven Propellergeräusch-Dämpfung
bei kolbenmotorgetriebenen Flug-
zeugen durch Änderung der Phasen-
beziehung Propeller/Motorauslaß-
signal".
J. Acoustique 2 (1989),
S.401 - 406.

[19] R. Gutin : "On the sound-field
of a rotating propeller".
NASA Techn. Memorandum No. 1195
(Translation), (1948).

[20] M. Herbt, M. Billing : "Der Pro-
peller als rotierende Schall-
quelle".
Z. Angew. Math. v. Mech. 25 (1945).

[21] F. Farassat : "Linear Acoustic
Formulas for Calculation of
Rotating Blade Noise".
AIAA Journ. Vol. 19, Nr. 9 (1981),
S. 1122 - 1130.

[22] Shenoy, Rajarama K. : "NASA/AHS
Rotorcraft Noise Reduction
Programs".
NASA IAA Journ. Vol. 35,
Jan/Febr. 1989, S. 68 - 73.

[23] Lowson, R.V. : "The Sound-Field
of Singularities in Motion".
Proc. Roy. Soc. London,
Vol. A 286 (1965), S. 559 - 57"

[24] Ffowcs Williams, J.E. and
Hawkings, D.L. : "Sound Generated
by Turbulence and Surfaces in
Arbitrary Motion".
Transaction Roy. Soc. London,
Vol. A 264 (1969), S. 321 - 342.
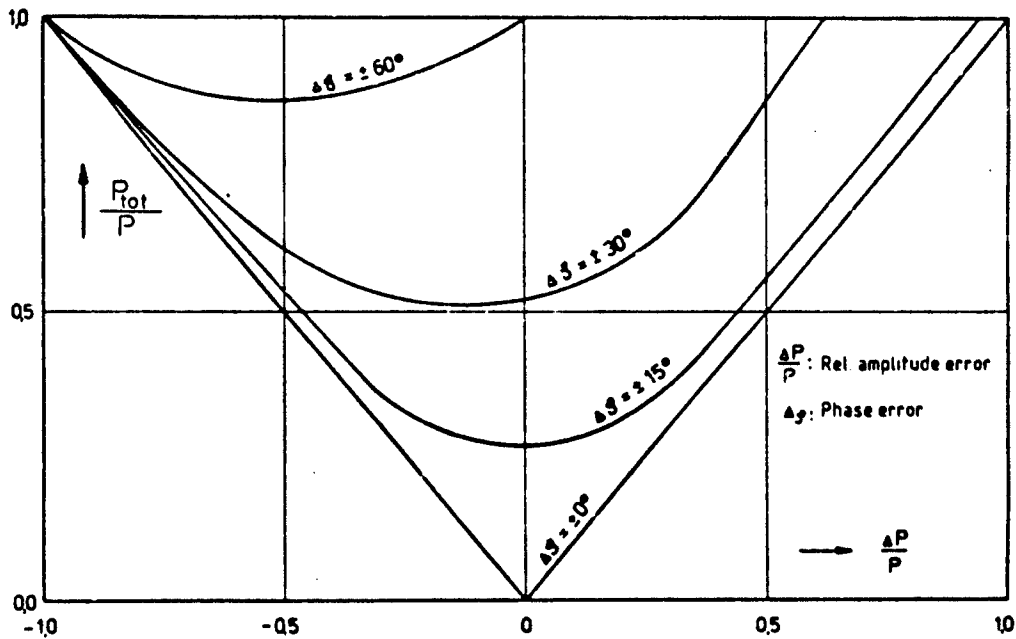
Fig. 1 Demands on the exactness.
Achievable cancellation p_{tot}/p for an anti-sound signal
with an amplitude error Δp and a phase error $\Delta\phi$.
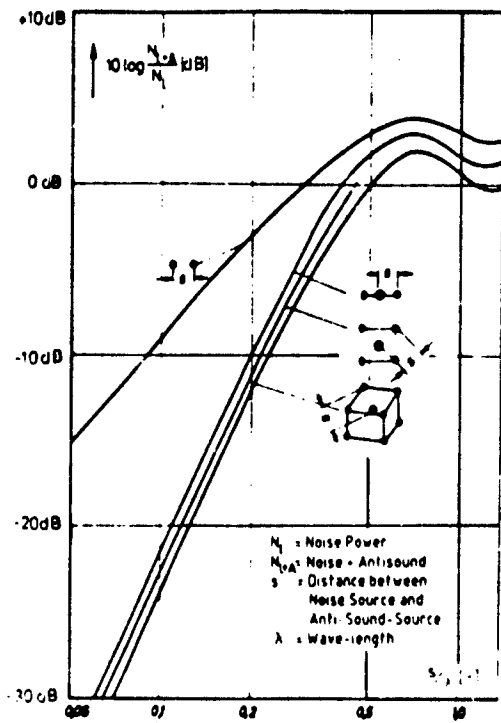
Fig. 2 Acoustical cancellation.
Reduction of noise emission by using
anti-sound sources located at a dis-
tance s (λ = wave-length).
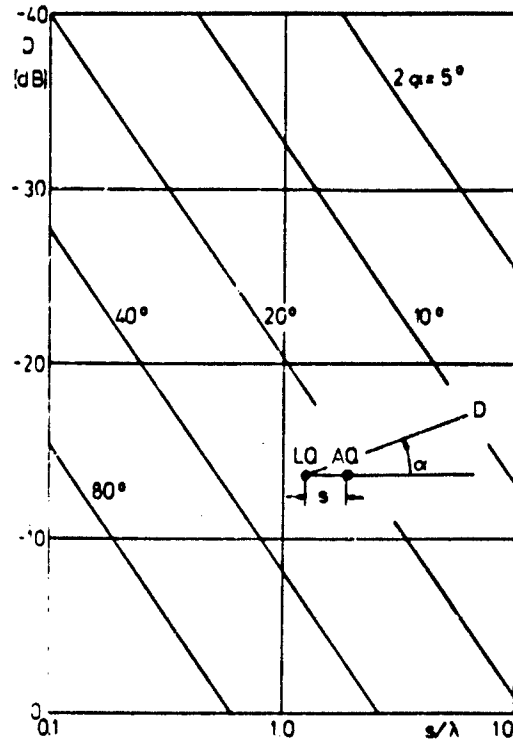
Fig. 3 Sectorial cancellation.
Noise reduction D related to the cone
angle α. LQ = Noise source.
AQ = anti-sound source. λ = wave-length.
s = distance from LQ to AQ.

$$a = c/\omega$$

$$\phi = \text{arc tg } y/_H$$

$$\theta = \text{arc sin } x/_r$$

$$r = \sqrt{x^2 + y^2 + H^2}$$

$$r' = \sqrt{x^2 + (y-a)^2 + H^2}$$
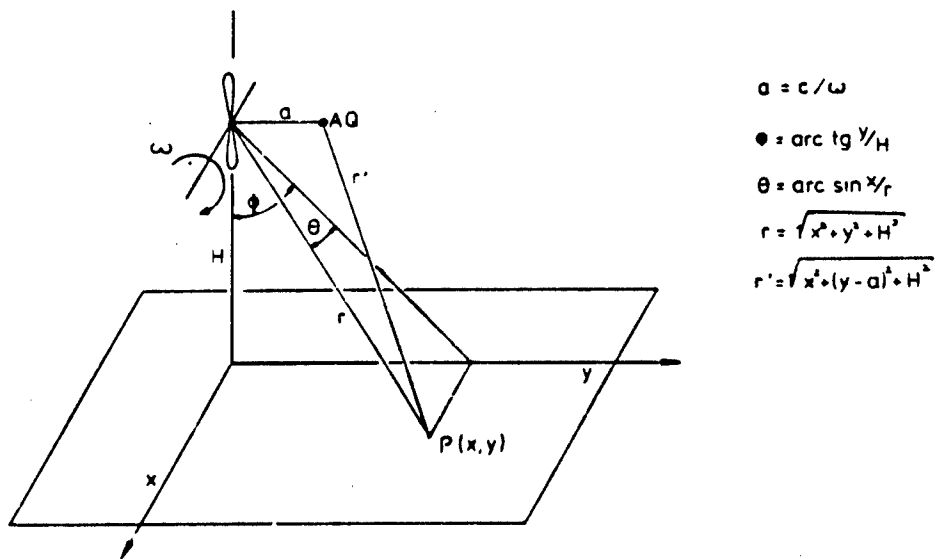
Fig. 4 Definition of the coordinates.
AQ = anti-sound source,
P = Immission point in the x,y-ground plane
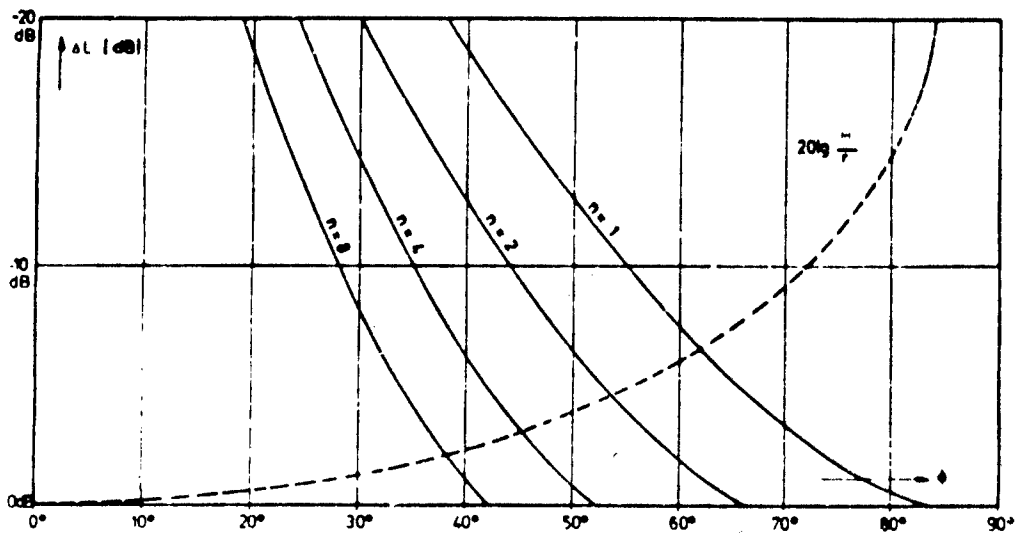
Fig. 5 Noise cancellation ΔL **in the propeller plane** $\theta = 0$
for the n-th propeller harmonic by an anti-sound source lo-
cated in the propeller plane at a distance $a = c/\omega$ to the
propeller axis.

n = 1
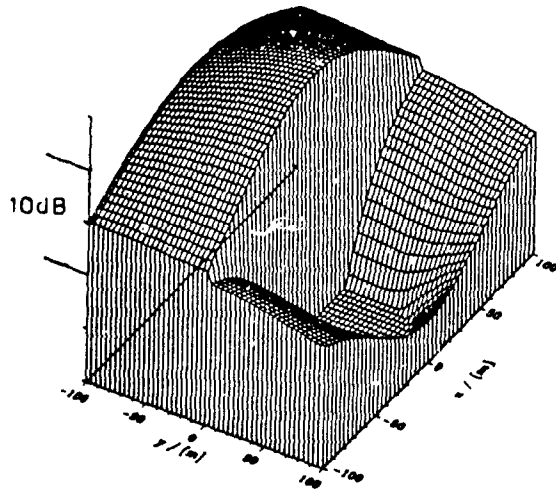
n = 2
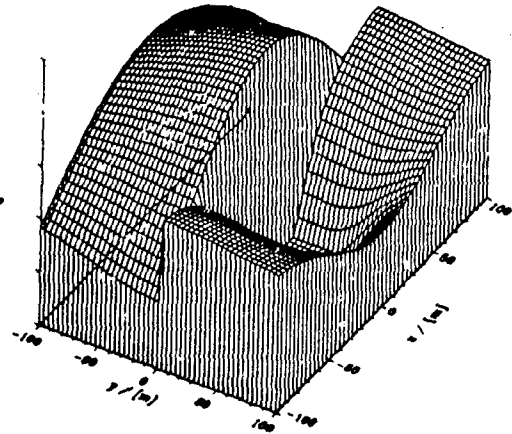
n = 3
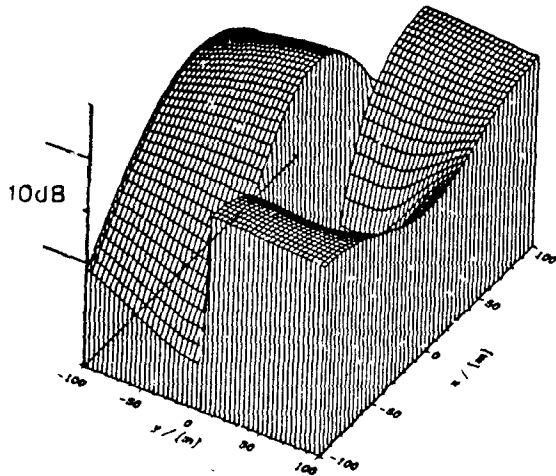
n = 4
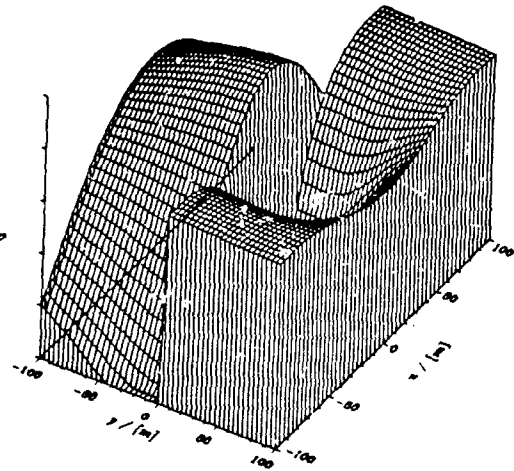
Fig. 6 Foot print of the blade thickness noise of a 2-bladed propeller (m = 2) for the propeller harmonics n = 1 - 4. The left side (y < 0) shows the sound-field without and the right side (y > 0) shows it with an anti-sound source. The anti-sound source is adjusted for absolute cancellation in the centre passing over (x = y = 0).

n = 1

n = 2

n = 3

n = 4
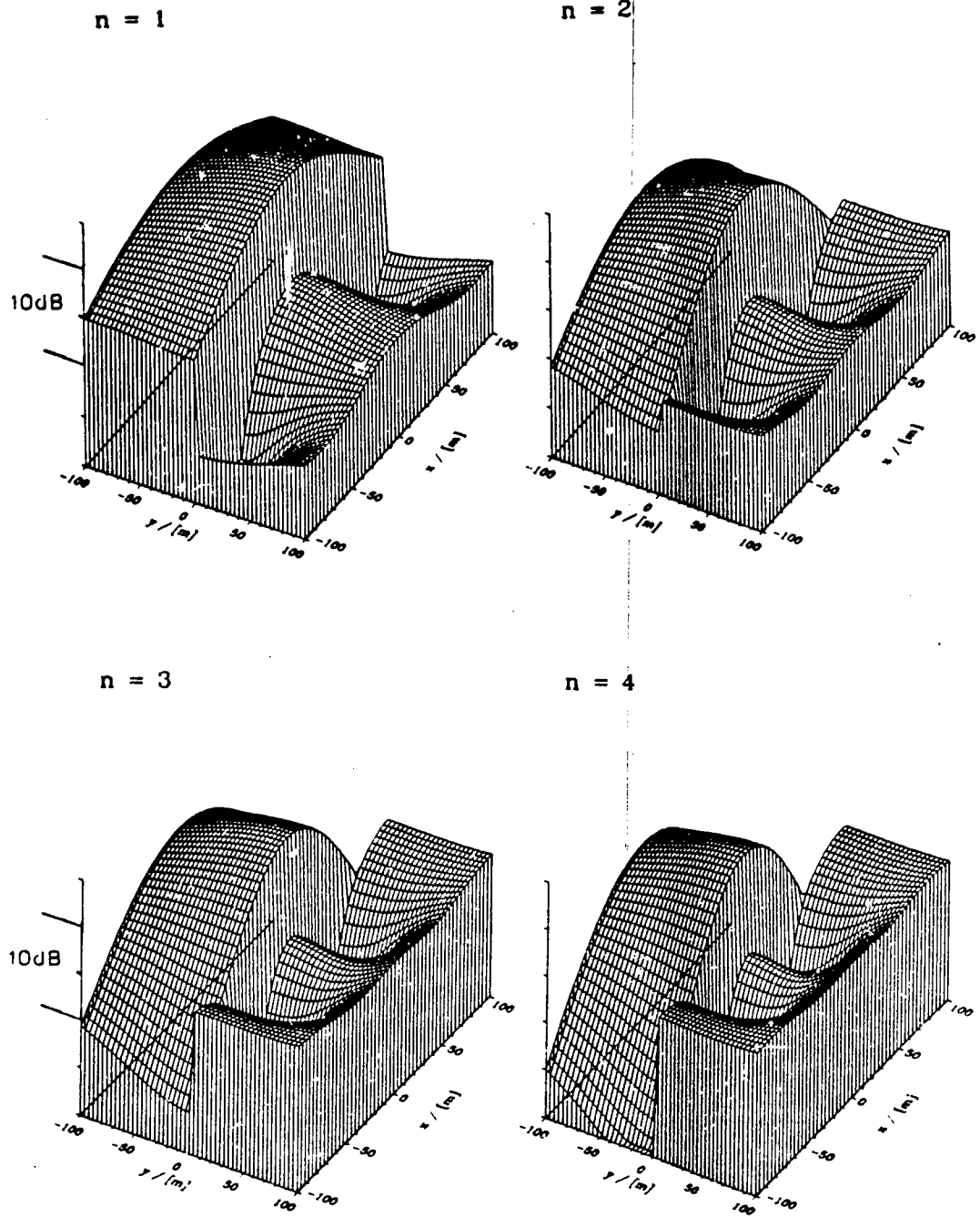
Fig. 7 Foot print of the blade-thickness noise of a 2-bladed propeller (m = 2) for the propeller harmonics n = 1 - 4.
The left side (y < 0) shows the sound-field without and the right side (y > 0) shows it with an anti-sound source.
The anti-sound source is designed for a 10 dB cancellation in the centre passing over (x = y = 0).

n = 1   n = 2

10dB

n = 3   n = 4

10dB
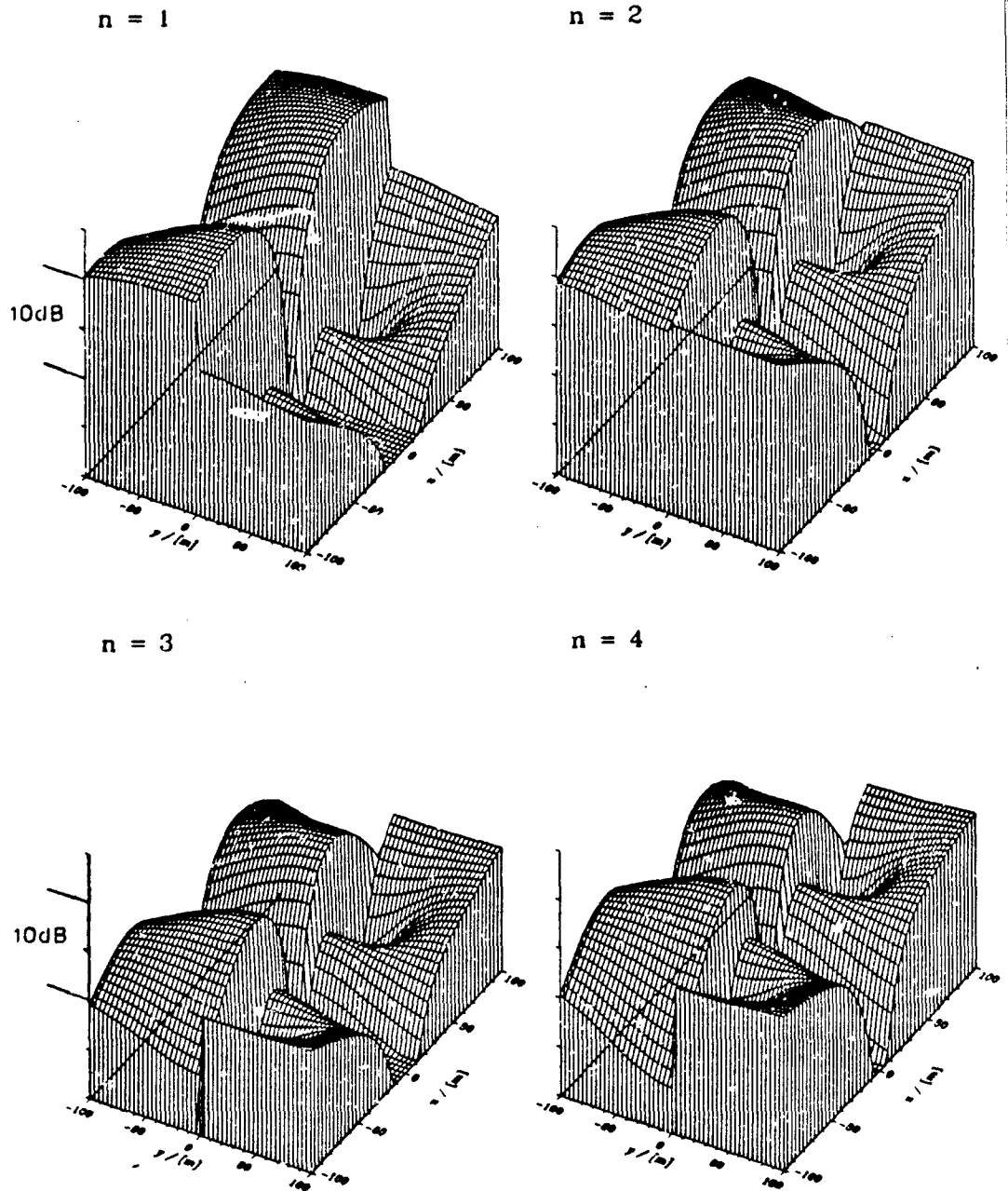
Fig. 8 Foot print of the thrust noise of a 2-bladed propeller (m = 2) for the propeller harmonics n = 1 - 4.
The left side (y < 0) shows the sound-field without and the right side (y > 0) shows it with an anti-sound source.
The anti-sound source is adjusted for absolute cancellation in the direction $\phi = 0$ and $\theta = 30°$.
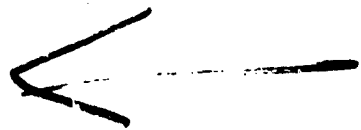
REPORT DOCUMENTATION PAGE

1. Recipient's Reference	2. Originator's Reference	3. Further Reference	4. Security Classification of Document
	AGARD-CP-512	ISBN 92-835-0667-7	UNCLASSIFIED

5. Originator	Advisory Group for Aerospace Research and Development North Atlantic Treaty Organization 7 rue Ancelle, 92200 Neuilly sur Seine, France

6. Title	COMBAT AIRCRAFT NOISE

7. Presented at	the Propulsion and Energetics Panel 78th B Specialists' Meeting held in Bonn, Germany, 23rd—25th October 1991.

8. Author(s)/Editor(s)	9. Date
Various	April 1992

10. Author's/Editor's Address	11. Pages
Various	372

12. Distribution Statement	This document is distributed in accordance with AGARD policies and regulations, which are outlined on the back covers of all AGARD publications.

13. Keywords/Descriptors

Active noise control	Low altitude
Aerodynamic noise	Noise
Aircraft noise	Noise criteria
Combustion noise	Noise measurement
Engine noise	Noise reduction
Jet noise	Noise source

14. Abstract

The Conference Proceedings contain 26 papers presented at the Propulsion and Energetics Panel 78B Specialists' Meeting on "Combat Aircraft Noise" which was held 23rd—25th October 1991 in Bonn, Germany.

Noise emission from combat aircraft at low altitude, high-speed training missions over populated areas has led to massive complaints. The purpose of the Meeting was to offer a forum for specialists to discuss the latest state of the technology concerned and — if possible — to find solutions for overcoming the problems.

The Specialists' Meeting was composed of the following sessions: User's Demand, Experience of Noise Effects (11); Mechanisms of Noise Generation (5); Noise Measurements, Predictions Methods (6); Noise Reduction (4). Questions and answers of the discussions follow each paper in the Proceedings.

As a result, there were numerous possibilities in discussion for moderate noise reductions, while for significant noise reductions the prospects are unclear.

AGARD Conference Proceedings 512
Advisory Group for Aerospace Research and Development, NATO
COMBAT AIRCRAFT NOISE
Published April 1992
372 pages

The Conference Proceedings contain 26 papers presented at the Propulsion and Energetics Panel 78B Specialists' Meeting on "Combat Aircraft Noise" which was held 23rd—25th October 1991 in Bonn, Germany.

Noise emission from combat aircraft at low altitude, high-speed training missions over populated areas has led to massive complaints. The purpose of the Meeting was to offer a forum for specialists to discuss the latest state of the

P.T.O.

AGARD-CP-512

Active noise control
Aerodynamic noise
Aircraft noise
Combustion noise
Engine noise
Jet noise
Low altitude
Noise
Noise criteria
Noise measurement
Noise reduction
Noise source

technology concerned and — if possible — to find solutions for overcoming the problems.

The Specialists' Meeting was composed of the following sessions: User's Demand, Experience of Noise Effects (11); Mechanisms of Noise Generation (5); Noise Measurements, Predictions Methods (6); Noise Reduction (4). Questions and answers of the discussions follow each paper in the Proceedings.

As a result, there were numerous possibilities in discussion for moderate noise reductions, while for significant noise reductions the prospects are unclear.

ISBN 92-835-0667-7

AGARD

NATO ⊕ OTAN

7 RUE ANCELLE · 92200 NEUILLY-SUR-SEINE
FRANCE

Téléphone (1)47.38.57.00 · Télex 610 176
Télécopie (1)47.38.57.99

DIFFUSION DES PUBLICATIONS
AGARD NON CLASSIFIEES

L'AGARD ne détient pas de stocks de ses publications, dans un but de distribution générale à l'adresse ci-dessus. La diffusion initiale des publications de l'AGARD est effectuée auprès des pays membres de cette organisation par l'intermédiaire des Centres Nationaux de Distribution suivants. A l'exception des Etats-Unis, ces centres disposent parfois d'exemplaires additionnels; dans les cas contraire, on peut se procurer ces exemplaires sous forme de microfiches ou de microcopies auprès des Agences de Vente dont la liste suite.

CENTRES DE DIFFUSION NATIONAUX

ALLEMAGNE
Fachinformationszentrum,
Karlsruhe
D-7514 Eggenstein-Leopoldshafen 2

BELGIQUE
Coordonnateur AGARD-VSL
Etat-Major de la Force Aerienne
Quartier Reine Elisabeth
Rue d'Evere, 1140 Bruxelles

CANADA
Directeur du Service des Renseignements Scientifiques
Ministère de la Défense Nationale
Ottawa, Ontario K1A 0K2

DANEMARK
Danish Defence Research Board
Ved Idractsparken 4
2100 Copenhagen Ø

ESPAGNE
INTA (AGARD Publications)
Pintor Rosales 34
28008 Madrid

ETATS-UNIS
National Aeronautics and Space Administration
Langley Research Center
M/S 180
Hampton, Virginia 23665

FRANCE
O.N.E.R.A. (Direction)
29, Avenue de la Division Leclerc
92322 Châtillon Cedex

GRECE
Hellenic Air Force
Air War College
Scientific and Technical Library
Dekelia Air Force Base
Dekelia, Athens TGA 1010

ISLANDE
Director of Aviation
c/o Flugrad
Reykjavik

ITALIE
Aeronautica Militare
Ufficio del Delegato Nazionale all'AGARD
Aeroporto Pratica di Mare
00040 Pomezia (Roma)

LUXEMBOURG
Voir Belgique

NORVEGE
Norwegian Defence Research Establishment
Attn: Biblioteket
P.O. Box 25
N-2007 Kjeller

PAYS-BAS
Netherlands Delegation to AGARD
National Aerospace Laboratory NLR
Kluyverweg 1
2629 HS Delft

PORTUGAL
Portuguese National Coordinator to AGARD
Gabinete de Estudos e Programas
CLAFA
Base de Alfragide
Alfragide
2700 Amadora

ROYAUME UNI
Defence Research Information Centre
Kentigern House
65 Brown Street
Glasgow G2 8EX

TURQUIE
Millî Savunma Başkanlığı (MSB)
ARGE Daire Başkanlığı (ARGE)
Ankara

LE CENTRE NATIONAL DE DISTRIBUTION DES ETATS-UNIS (NASA) NE DETIENT PAS DE STOCKS
DES PUBLICATIONS AGARD ET LES DEMANDES D'EXEMPLAIRES DOIVENT ETRE ADRESSEES DIRECTEMENT
AU SERVICE NATIONAL TECHNIQUE DE L'INFORMATION (NTIS) DONT L'ADRESSE SUIT.

AGENCES DE VENTE

National Technical Information Service
(NTIS)
5285 Port Royal Road
Springfield, Virginia 22161
Etats-Unis

ESA/Information Retrieval Service
European Space Agency
10, rue Mario Nikis
75015 Paris
France

The British Library
Document Supply Division
Boston Spa, Wetherby
West Yorkshire LS23 7BQ
Royaume Uni

Les demandes de microfiches ou de photocopies de documents AGARD (y compris les demandes faites auprès du NTIS) doivent comporter la dénomination AGARD, ainsi que le numero de serie de l'AGARD (par exemple AGARD-AG-315). Des informations analogues, telles que le titre et la date de publication sont souhaitables. Veuiller noter qu'il y a lieu de specifier AGARD-R-nnn et AGARD-AR-nnn lors de la commande de rapports AGARD et des rapports consultatifs AGARD respectivement. Des references bibliographiques completes ainsi que des resumes des publications AGARD figurent dans les journaux suivants:

Scientifique and Technical Aerospace Reports (STAR)
publié par la NASA Scientific and Technical
Information Division
NASA Headquarters (NTT)
Washington D.C. 20546
Etats-Unis

Government Reports Announcements and Index (GRA&I)
publié par le National Technical Information Service
Springfield
Virginia 22161
Etats-Unis

(accessible également en mode interactif dans la base de
donnees bibliographiques en ligne du NTIS, et sur CD-ROM)

AGARD

NATO ⊕ OTAN

7 RUE ANCELLE · 92200 NEUILLY-SUR-SEINE

FRANCE

Telephone (1)47.38.57.00 · Telex 610 176
Telefax (1)47.38.57.99

DISTRIBUTION OF UNCLASSIFIED
AGARD PUBLICATIONS

AGARD does NOT hold stocks of AGARD publications at the above address for general distribution. Initial distribution of AGARD publications is made to AGARD Member Nations through the following National Distribution Centres. Further copies are sometimes available from these Centres (except in the United States), but if not may be purchased in Microfiche or Photocopy form from the Sales Agencies listed below.

NATIONAL DISTRIBUTION CENTRES

BELGIUM
Coordonnateur AGARD — VSL
Etat-Major de la Force Aérienne
Quartier Reine Elisabeth
Rue d'Evere, 1140 Bruxelles

CANADA
Director Scientific Information Services
Dept of National Defence
Ottawa, Ontario K1A 0K2

DENMARK
Danish Defence Research Board
Ved Idraetsparken 4
2100 Copenhagen Ø

FRANCE
O.N.E.R.A. (Direction)
29 Avenue de la Division Leclerc
92322 Châtillon Cedex

GERMANY
Fachinformationszentrum
Karlsruhe
D-7514 Eggenstein-Leopoldshafen 2

GREECE
Hellenic Air Force
Air War College
Scientific and Technical Library
Dekelia Air Force Base
Dekelia, Athens TGA 1010

ICELAND
Director of Aviation
c/o Flugrad
Reykjavik

ITALY
Aeronautica Militare
Ufficio del Delegato Nazionale all'AGARD
Aeroporto Pratica di Mare
00040 Pomezia (Roma)

LUXEMBOURG
See Belgium

NETHERLANDS
Netherlands Delegation to AGARD
National Aerospace Laboratory, NLR
Kluyverweg 1
2629 HS Delft

NORWAY
Norwegian Defence Research Establishment
Attn: Biblioteket
P.O. Box 25
N-2007 Kjeller

PORTUGAL
Portuguese National Coordinator to AGARD
Gabinete de Estudos e Programas
CLAFA
Base de Alfragide
Alfragide
2700 Amadora

SPAIN
INTA (AGARD Publications)
Pintor Rosales 34
28008 Madrid

TURKEY
Milli Savunma Başkanlığı (MSB)
ARGE Daire Başkanlığı (ARGE)
Ankara

UNITED KINGDOM
Defence Research Information Centre
Kentigern House
65 Brown Street
Glasgow G2 8EX

UNITED STATES
National Aeronautics and Space Administration (NASA)
Langley Research Center
M/S 180
Hampton, Virginia 23665

THE UNITED STATES NATIONAL DISTRIBUTION CENTRE (NASA) DOES NOT HOLD
STOCKS OF AGARD PUBLICATIONS, AND APPLICATIONS FOR COPIES SHOULD BE MADE
DIRECT TO THE NATIONAL TECHNICAL INFORMATION SERVICE (NTIS) AT THE ADDRESS BELOW.

SALES AGENCIES

National Technical
Information Service (NTIS)
5285 Port Royal Road
Springfield, Virginia 22161
United States

ESA/Information Retrieval Service
European Space Agency
10, rue Mario Nikis
75015 Paris
France

The British Library
Document Supply Centre
Boston Spa, Wetherby
West Yorkshire LS23 7BQ
United Kingdom

Requests for microfiches or photocopies of AGARD documents (including requests to NTIS) should include the word 'AGARD' and the AGARD serial number (for example AGARD-AG-315). Collateral information such as title and publication date is desirable. Note that AGARD Reports and Advisory Reports should be specified as AGARD-R-nnn and AGARD-AR-nnn, respectively. Full bibliographical references and abstracts of AGARD publications are given in the following journals:

Scientific and Technical Aerospace Reports (STAR)
published by NASA Scientific and Technical
Information Division
NASA Headquarters (NTT)
Washington D.C. 20546
United States

Government Reports Announcements and Index (GRA&I)
published by the National Technical Information Service
Springfield
Virginia 22161
United States

(also available online in the NTIS Bibliographic
Database or on CD-ROM)

SPS

Printed by Specialised Printing Services Limited
40 Chigwell Lane, Loughton, Essex IG10 3TZ